

DISS. ETH NO. 31078

***NEW TOOLS, PROGRAMMING MODELS, AND SYSTEM SUPPORT FOR
PROCESSING-IN-MEMORY ARCHITECTURES***

A thesis submitted to attain the degree of

DOCTOR OF SCIENCES
(Dr. sc. ETH Zürich)

presented by

GERALDO FRANCISCO DE OLIVEIRA JUNIOR

born on *04.02.1994*

accepted on the recommendation of

Prof. Dr. Onur Mutlu, examiner

Dr. Christian Weis, co-examiner

Dr. Donghyuk Lee, co-examiner

Prof. Dr. Reetuparna Das, co-examiner

Prof. Dr. Tony Nowatzki, co-examiner

2025

To my loving parents, Simone and Geraldo.
(Aos meus amados pais, Simone e Geraldo).

Acknowledgments

This thesis marks the culmination of a transformative journey over the past several years, one made possible through the unwavering support, mentorship, and friendship of many individuals. I take this opportunity to express my deepest gratitude to those who have shaped, supported, and walked beside me along the way.

First and foremost, I thank my advisor, Prof. Dr. Onur Mutlu, for his invaluable guidance and support throughout my PhD. His deep insight, boundless enthusiasm, and high expectations continually pushed me to grow—not only as a researcher but also as a thinker and problem solver. I am immensely grateful for the opportunities he has given me and for believing in my potential, especially at times when I struggled to do so myself.

I owe a great debt of gratitude to my close collaborators and mentors, Juan Gómez-Luna and Saugata Ghose. Their technical mentorship and personal support were instrumental to this dissertation. In particular, I am especially thankful to Juan Gómez-Luna. We began our SAFARI journey at nearly the same time, and over the years, we have grown together—as researchers, as colleagues, and as friends. His dedication, patience, and insight were a constant source of strength throughout this journey.

I also extend my sincere thanks to my PhD committee members: Dr. Christian Weis, Dr. Donghyuk Lee, Prof. Dr. Reetuparna Das, and Prof. Dr. Tony Nowatzki. I am grateful for their time, constructive feedback, and thoughtful questions that helped improve this dissertation and refine my research.

The SAFARI Research Group provided a unique and intellectually stimulating environment that shaped my growth as a researcher. I thank all current and former members for their friendship, support, and countless discussions. I am especially thankful to Nika Mansouri Ghiasi, who welcomed me to Zürich with open arms and a generous heart, easing my transition to a new country and culture. My deepest thanks to Abdullah Giray Yağlıkçı and Can Firtına—my PhD brothers—who embarked on this path with me and finished alongside me. Their camaraderie, encouragement, and daily support—including our shared hunt for chicken at the university mensa—remain some of the most cherished memories of my PhD. I am deeply proud of what we have accomplished together and forever grateful for their presence. I also thank

Minesh Patel for his wise, calm mentorship and his quiet but steady friendship, which always offered clarity and perspective when I needed it most. I am further grateful to Ataberk Olgun, Ismail E. Yüksel, and Nisa Bostancı for their support and for enriching my time in SAFARI.

Beyond the lab, I was fortunate to have met incredible friends who became my chosen family. I thank Vesna, Marcella, Tomer, Nathalia, Barbara, António, Bruna, Larissa, Pedro, Betül, and Çiçek. Each of you left a mark on this journey, and your presence made every challenge more bearable and every joy more meaningful. Vesna, my best friend, has been a pillar of light, love, and unwavering support. Her wisdom and strength have lifted me countless times. Switzerland will never be the same without Marcella, whose companionship and care carried me through both the best and hardest times. I am forever grateful for her generosity and friendship. And Tom—thanks for the memories.

To my coaches and friends at CrossFit Zürich—thank you for keeping me grounded and helping me maintain physical and mental resilience. More than sport, you taught me that consistency breeds strength, and your unwavering positivity gave me the motivation to keep going.

I am also deeply grateful for the early mentorship I received in Brazil, which laid the foundation for this academic journey. I thank Prof. Ricardo dos Santos Ferreira and Prof. Luigi Carro, who first sparked my curiosity about computer architecture and patiently taught me the fundamentals. Their encouragement was critical to my decision to pursue graduate studies abroad. I acknowledge with sincere gratitude the public policies implemented under the administration of President Dilma Rousseff, which enabled access to international educational opportunities for students from all backgrounds. It was through these initiatives that I was able to study abroad in the United States, learn English, and broaden my understanding of the world beyond Brazil—despite coming from a very simple family. This opportunity fundamentally transformed my life and academic path.

Finally, I owe everything to my parents, Simone and Geraldo. Their love, support, and sacrifices form the foundation of everything I have achieved. Their belief in me, even across continents and time zones, gave me the courage to persevere and pursue my dreams.

Abstract

Continuously increasing data intensiveness of modern applications has led to high performance and energy costs for data movement in traditional processor-centric computing systems. To mitigate these costs, the processing-in-memory (PIM) paradigm moves computation closer to where the data resides, reducing (and sometimes eliminating) the need to move data between memory and the processor. There are two main approaches to PIM: (i) processing-near-memory (PNM), where PIM logic is added to the same die as memory or to the logic layer of 3D-stacked memory, and (ii) processing-using-memory (PUM), which uses the operational principles of memory cells and memory circuitry to perform computation. Many works from academia and industry have shown the benefits of PNM and PUM for a wide range of workloads from different domains. However, fully adopting PIM in commercial systems is still very challenging due to the lack of tools as well as programming and system support for PIM architectures across the computer architecture stack, which includes: (i) workload characterization methodologies and benchmark suites targeting PIM architectures; (ii) execution and programming models that can take advantage of the available application parallelism to maximize hardware utilization and throughput; (iii) compiler support and compiler optimizations targeting PUM architectures; (iv) data-aware runtime systems that can leverage key characteristics of data to improve overall PIM performance and energy efficiency.

Our *goal* in this dissertation is to provide tools, programming models, and system support for PIM architectures (with a focus on DRAM-based solutions), to ease the adoption of PIM in current and future systems. To this end, we make at least *four* new major contributions.

First, we introduce DAMOV, the first rigorous methodology to characterize memory-related data movement bottlenecks in modern workloads, and the first data movement benchmark suite. In DAMOV, we (i) perform the first large-scale characterization of hundreds of applications, (ii) develop a three-step workload characterization methodology that introduces and evaluates four key metrics to identify the sources of data movement bottlenecks in real applications, and (iii) study whether PIM architectures are a viable data movement mitigation mechanism for different classes of memory-bottlenecked applications.

Second, we introduce MIMDRAM, a new hardware/software co-designed substrate that addresses the major current programmability and flexibility limitations of the bulk bitwise execution model of processing-using-DRAM (PUD) architectures. MIMDRAM enables the allocation and control of only the needed computing resources inside DRAM for PUD computing. On the hardware side, MIMDRAM introduces simple modifications to the DRAM architecture

that enable the execution of (i) different PUD operations concurrently inside a single DRAM subarray in a multiple-instruction multiple-data (MIMD) fashion, and (ii) native vector reduction computation. On the software side, MIMDRAM implements a series of compiler passes that automatically identify and map code regions to the underlying PUD substrate, alongside system support for data mapping and allocation of PUD memory objects.

Third, we introduce *Proteus*, the first hardware framework that addresses the high execution latency of bulk bitwise PUD operations in state-of-the-art PUD architectures by implementing a data-aware runtime engine for PUD. *Proteus* reduces the latency of PUD operations in three different ways: (i) *Proteus concurrently executes* independent in-DRAM primitives belong to a *single* PUD operation across DRAM arrays. (ii) *Proteus dynamically* reduces the bit-precision (and consequentially the latency and energy consumption) of PUD operations by exploiting narrow values (i.e., values with many leading zeros or ones). (iii) *Proteus chooses and uses* the most appropriate data representation and arithmetic algorithm implementation for a given PUD instruction *transparently* to the programmer.

Fourth, we introduce DaPPA (data-parallel processing-in-memory architecture), a new programming framework that eases programmability for general-purpose PNM architectures by allowing the programmer to write efficient PIM-friendly code without the need to manage hardware resources explicitly. The key idea behind DaPPA is to remove the responsibility of managing hardware resources from the programmer by providing an intuitive data-parallel pattern-based programming interface that abstracts the hardware components of the PNM system. Using this key idea, DaPPA transforms a data-parallel pattern-based application code into the appropriate PNM-target code, including the required application programming interfaces (APIs) for data management and code partitioning, which can then be compiled into a PNM-based binary transparently from the programmer.

Overall, our four major contributions demonstrate that we can *effectively* exploit the inherent parallelism of PIM architectures and *facilitate* their adoption across a broad spectrum of workloads through end-to-end design of hardware and software support (i.e., workload characterization methodologies and benchmark suites, execution and programming models, compiler support and programming frameworks, and adaptive data-aware runtime mechanisms) for PIM, thereby enabling orders of magnitude improvements in performance and energy efficiency across a wide variety of modern workloads.

Zusammenfassung

Die stetig zunehmende Datenintensität moderner Anwendungen hat in herkömmlichen prozessorzentrierten Rechensystemen zu hohen Leistungs- und Energiekosten für die Datenbewegung geführt. Zur Minderung dieser Kosten verlagert das *Processing-in-Memory* (PIM)-Paradigma die Berechnung näher an den Ort der Daten, wodurch die Notwendigkeit, Daten zwischen Speicher und Prozessor zu bewegen, verringert (und mitunter ganz eliminiert) wird. Es gibt zwei Hauptansätze für PIM: (i) *Processing-Near-Memory* (PNM), bei dem PIM-Logik auf demselben Chip wie der Speicher oder in der Logikschicht von 3D-gestapeltem Speicher integriert wird, und (ii) *Processing-Using-Memory* (PUM), das die Funktionsprinzipien von Speicherzellen und Speicherschaltungen zur Durchführung von Berechnungen nutzt. Zahlreiche Arbeiten aus Wissenschaft und Industrie haben die Vorteile von PNM und PUM für eine breite Palette von Workloads aus unterschiedlichen Domänen aufgezeigt. Die vollständige Einführung von PIM in kommerziellen Systemen ist jedoch nach wie vor sehr herausfordernd, da es an Werkzeugen sowie an Programmier- und Systemunterstützung für PIM-Architekturen über den gesamten Computerarchitektur-Stack hinweg fehlt, einschließlich: (i) Methodiken zur Workload-Charakterisierung und Benchmark-Suiten, die auf PIM-Architekturen abzielen; (ii) Ausführungs- und Programmiermodellen, die die vorhandene Anwendungsparallelität ausnutzen, um Hardwareauslastung und Durchsatz zu maximieren; (iii) Compilerunterstützung und Compileroptimierungen für PUM-Architekturen; (iv) datenbewussten Laufzeitsystemen, die zentrale Datenmerkmale ausnutzen, um die PIM-Gesamtleistung und Energieeffizienz zu verbessern.

Ziel dieser Dissertation ist es, Werkzeuge, Programmiermodelle und Systemunterstützung für PIM-Architekturen (mit Fokus auf DRAM-basierte Lösungen) bereitzustellen, um die Einführung von PIM in aktuellen und künftigen Systemen zu erleichtern. Zu diesem Zweck leisten wir mindestens vier wesentliche neue Beiträge.

Erstens stellen wir DAMOV vor, die erste rigorose Methodik zur Charakterisierung speicherbezogener Datenbewegungs-Engpässe in modernen Workloads sowie die erste Benchmark-Suite für Datenbewegung. In DAMOV (i) führen wir die erste groß angelegte Charakterisierung von Hunderten von Anwendungen durch, (ii) entwickeln eine dreistu-

fige Workload-Charakterisierungsmethodik, die vier zentrale Metriken einführt und bewertet, um die Ursachen von Datenbewegungs-Engpässen in realen Anwendungen zu identifizieren, und (iii) untersuchen, ob PIM-Architekturen ein tauglicher Mechanismus zur Minderung von Datenbewegung für verschiedene Klassen speichergebundener Anwendungen sind.

Zweitens stellen wir MIMDRAM vor, ein neuartiges Hardware/Software-Codesign-Substrat, das die wesentlichen aktuellen Einschränkungen der Programmierbarkeit und Flexibilität des bitweisen Massenausführungsmodells von *Processing-Using-DRAM* (PUD)-Architekturen adressiert. MIMDRAM ermöglicht die Allokation und die Steuerung ausschließlich der jeweils benötigten Rechenressourcen innerhalb von DRAM für PUD-Berechnungen. Auf der Hardware-Seite führt MIMDRAM einfache Modifikationen der DRAM-Architektur ein, die (i) die gleichzeitige Ausführung verschiedener PUD-Operationen innerhalb eines einzelnen DRAM-Subarrays in *multiple-instruction multiple-data* (MIMD)-Manier und (ii) native Vektorreduktionsberechnungen ermöglichen. Auf der Software-Seite implementiert MIMDRAM eine Reihe von Compiler-Durchläufe, die Codeabschnitte automatisch identifizieren und auf das zugrunde liegende PUD-Substrat abbilden, zusammen mit Systemunterstützung für Datenabbildung und die Allokation von PUD-Speicherobjekten.

Drittens stellen wir *Proteus* vor, das erste Hardware-Framework, das die hohe Ausführungslatenz von Bulk-bitweisen PUD-Operationen in modernen PUD-Architekturen adressiert, indem es eine datenbewusste Runtime-Engine für PUD implementiert. *Proteus* reduziert die Latenz von PUD-Operationen auf drei Arten: (i) *Proteus* führt unabhängige *In-DRAM-Primitive*, die zu einer einzelnen PUD-Operation gehören, über DRAM-Arrays hinweg gleichzeitig aus. (ii) *Proteus* reduziert die Bitpräzision (und damit Latenz und Energieverbrauch) von PUD-Operationen dynamisch, indem es „narrow values“ ausnutzt (d. h. Werte mit vielen führenden Nullen oder Einsen). (iii) *Proteus* wählt und verwendet für eine gegebene PUD-Instruktion die jeweils geeignetste Datenrepräsentation und Implementierung des arithmetischen Algorithmus – für die Programmierenden transparent.

Viertens stellen wir DaPPA (*data-parallel processing-in-memory architecture*) vor, ein neues Programmier-Framework, das die Programmierbarkeit für allgemeine PNM-Architekturen erleichtert, indem es Programmierenden erlaubt, effizienten PIM-freundlichen Code zu schreiben, ohne Hardware-Ressourcen explizit verwalten zu müssen. Der zentrale Gedanke von DaPPA ist es, die Verantwortung für das Ressourcenmanagement von den Programmierenden zu nehmen, indem eine intuitive, datenparallele, musterbasierte Programmierschnittstelle bereitgestellt wird, die die Hardwarekomponenten des PNM-Systems abstrahiert. Auf Basis dieses Kerngedankens transformiert DaPPA einen datenparallelen, musterbasierenden Anwendungscode in den geeigneten PNM-Zielcode – einschließlich der notwendigen *Application Programming Interfaces* (APIs) für Datenmanagement und Code-Partitionierung –,

der anschließend für eine PNM-basierte Binärdatei kompiliert werden kann, ohne dass die Programmierenden dies explizit wahrnehmen.

Insgesamt zeigen unsere vier Hauptbeiträge, dass sich die inhärente Parallelität von PIM-Architekturen effektiv ausnutzen und ihre Einführung über ein breites Spektrum von Workloads hinweg erleichtern lässt – durch ein ganzheitliches End-to-End-Design von Hardware- und Software-Unterstützung (d. h. Workload-Charakterisierungsmethodiken und Benchmark-Suiten, Ausführungs- und Programmiermodelle, Compiler-Unterstützung und Programmier-Frameworks sowie adaptive, datenbewusste Runtime-Mechanismen) für PIM. Dadurch werden Leistungs- und Energieeffizienzsteigerungen um Größenordnungen über eine Vielzahl moderner Workloads hinweg ermöglicht.

Contents

Acknowledgments	iii
Abstract	v
Zusammenfassung	vii
List of Figures	xv
List of Tables	xix
1 Introduction	1
1.1 Problem Definition	3
1.2 Our Goal	4
1.3 Thesis Statement	4
1.4 Our Approach	5
1.4.1 A Methodology and Benchmark Suite for Understanding and Mitigating Data Movement Bottlenecks	5
1.4.2 Enabling Efficient and Programmable MIMD Execution in Processing-Using-DRAM (PUD) Architectures	6
1.4.3 Enabling High-Performance PUD Execution via Dynamic Precision PUD Arithmetic	7
1.4.4 A Data-Parallel Programming Framework for Easing Programmability and Enabling High-Performance PNM Execution	9
1.5 Contributions	10
1.6 Outline	12
2 Background	13
2.1 DRAM Organization & Operation	13
2.1.1 DRAM Organization	13
2.1.2 DRAM Operation	14

2.2	Processing-in-Memory Architectures	16
2.2.1	A Brief PIM Taxonomy	16
2.2.2	Early PIM Proposals	19
2.2.3	Major Trends Affecting Main Memory & PIM Resurgence	19
2.2.4	Real-World PIM Architectures	20
2.2.5	DRAM-Based PUM Architectures	25
3	Related Work	28
3.1	Processing-Near-Memory (PNM) Architectures	28
3.2	Processing-Using-Memory (PUM) Architectures	34
3.2.1	SRAM-Based PUM Architectures	34
3.2.2	DRAM-Based PUM Architectures	36
3.2.3	NVM-Based PUM Architectures	41
3.2.4	NAND Flash-Based PUM Architectures	44
3.3	System Support for PIM Architectures	45
3.3.1	Data Movement Bottlenecks: Identification, Workload Characteriza- tion, and Benchmark Suites	45
3.3.2	Identification of PIM Suitability	47
3.3.3	Compiler Support for PIM	48
3.3.4	Memory Management Support for PIM	49
3.3.5	Programming Frameworks and High-Level APIs for PIM	51
4	DAMOV: A New Methodology and Benchmark Suite for Evaluating Data Movement Bottlenecks	53
4.1	Motivation & Goal	53
4.2	Methodology Overview	57
4.2.1	Experimental Evaluation Framework	57
4.2.2	Step 1: Memory-Bound Function Identification	58
4.2.3	Step 2: Locality-Based Clustering	58
4.2.4	Step 3: Bottleneck Classification	60
4.3	Characterizing Memory Bottlenecks	63
4.3.1	Step 1: Memory-Bound Function Identification	64
4.3.2	Step 2: Locality-Based Clustering	66
4.3.3	Step 3: Bottleneck Classification	66
4.3.4	Effect of the Last-Level Cache Size	75

4.3.5	Validation and Summary of Our Workload Characterization Methodology	80
4.3.6	Limitations of Our Methodology	84
4.4	DAMOV: The Data Movement Benchmark Suite	85
4.4.1	Benchmark Diversity	85
4.5	Case Studies	87
4.5.1	Case Study 1: Impact of Load Balance and Inter-Vault Communication on NDP Systems	87
4.5.2	Case Study 2: Impact of NDP Accelerators on Our Memory Bottleneck Analysis	88
4.5.3	Case Study 3: Impact of Different Core Models on NDP Architectures	90
4.5.4	Case Study 4: Impact of Fine-Grained Offloading to NDP on Performance	91
4.6	Key Takeaways	92
4.6.1	Shaping Future Research with DAMOV	94
4.7	Summary	96
5	MIMDRAM: An End-to-End Processing-Using-DRAM System for High-Throughput, Energy-Efficient, and Programmer-Transparent Multiple-Instruction Multiple-Data Computing	97
5.1	Motivation	97
5.2	MIMDRAM: A MIMD PUD Architecture	99
5.2.1	MIMDRAM: Hardware Overview	99
5.2.2	MIMDRAM: Control & Execution	104
5.3	MIMDRAM: Software Support	107
5.4	System Support for MIMDRAM	109
5.4.1	Instruction-Set Architecture	110
5.4.2	Execution & Data Transposition	111
5.4.3	Operating System Support	111
5.5	Methodology	114
5.6	Evaluation	116
5.6.1	Single-Application Results	116
5.6.2	Multi-Programmed Workload Results	118
5.6.3	Comparison to Other PIM Architectures	120
5.6.4	MIMDRAM with subarray-level parallelism (SALP) & BLP	121
5.6.5	Hardware Area Analysis	124
5.7	Summary	125

6	Proteus: Achieving High-Performance Processing-Using-DRAM with Dynamic Bit-Precision, Adaptive Data Representation, and Flexible Arithmetic	126
6.1	Motivation & Goal	126
6.2	<i>Proteus</i> Overview	130
6.2.1	Main Components of <i>Proteus</i>	130
6.2.2	Execution Flow	131
6.3	<i>Proteus</i> Implementation	132
6.3.1	Subarray Organization	132
6.3.2	Parallelism-Aware μ Program Library	134
6.3.3	Dynamic Bit-Precision Engine	140
6.3.4	μ Program Select Unit	141
6.3.5	Other Considerations	142
6.4	Methodology	144
6.5	Evaluation	145
6.5.1	Real-World Application Analysis	145
6.5.2	Data Mapping and Representation Format Conversion Overheads	147
6.5.3	Performance of Floating-Point Operations	148
6.5.4	<i>Proteus</i> vs. Tensor Cores in GPUs	149
6.5.5	Area Analysis	150
6.6	Summary	151
7	DaPPA: A Data-Parallel Programming Framework for Processing-in-Memory Architectures	152
7.1	Motivation & Goal	152
7.2	DaPPA Overview	153
7.3	DaPPA Implementation	155
7.3.1	Data-Parallel Pattern APIs	155
7.3.2	Dataflow Programming Interface	159
7.3.3	Dynamic Template-Based Compilation	163
7.3.4	Handling Invalid Pipeline Implementations	167
7.4	Methodology	167
7.4.1	Implementation	167
7.4.2	Workloads	167
7.5	Evaluation	168
7.5.1	Productivity Improvement	168
7.5.2	Performance Analysis	169

7.5.3	DaPPA Execution Time Overheads	171
7.6	Summary	171
8	Conclusions and Future Directions	172
8.1	Future Research Directions	173
8.1.1	Extending the DAMOV Methodology & Benchmark Suite	174
8.1.2	Improving MIMDRAM & <i>Proteus</i> Execution Model	175
8.1.3	Enhancing the DaPPA Programming Framework	176
8.2	Concluding Remarks	177
A	Other Works of the Author	179
A.1	Other Works Lead by the Author	179
A.1.1	Extending Memory Capacity in Modern Consumer Systems with Emerging Non-Volatile Memory: Experimental Analysis and Charac- terization Using the Intel Optane SSD	179
A.1.2	Surveys & Summary Works on PIM	181
A.2	Other Works the Author Contributed to as Co-Author	182
B	Complete List of the Author's Contributions	185
B.1	Major Contributions Led by the Author	185
B.2	Other Contributions	186
C	Complete List of Application Functions, Representative Functions, and Evaluated Applications in DAMOV	190
C.1	Application Functions in the DAMOV Benchmark Suite	190
C.2	Representative Application Functions	196
C.3	Complete List of Evaluated Applications	197
	Bibliography	199

List of Figures

2.1	Overview of DRAM organization.	14
2.2	Overview of DRAM operation. Reproduced from [1].	15
2.3	UPMEM system organization.	21
2.4	Full adder operation in SIMDRAM.	27
4.1	Roofline (left) and last-level cache MPKI vs. NDP speedup (right) for 44 memory-bound applications. Applications are classified into four categories: (1) those that experience performance degradation due to NDP (blue; Faster on CPU), (2) those that experience performance improvement due to NDP (yellow; Faster on NDP), (3) those where the host CPU and NDP performance are similar (red; Similar on CPU/NDP), (4) those that experience either performance degradation or performance improvement due to NDP depending on the microarchitectural configuration (green; Depends).	54
4.2	Overview of our three-step workload characterization methodology.	57
4.3	Locality-based clustering of 44 representative functions.	65
4.4	L3 Cache Misses per Kilo-Instruction (MPKI) and Last-to-First Miss Ratio (LFMR) for 44 representative functions.	66
4.5	Performance of 12 representative functions on three systems: host CPU, host CPU with prefetcher, and NDP, normalized to one host CPU core.	68
4.6	Host CPU system IPC vs. utilized DRAM Bandwidth for representative Class 1a functions.	69
4.7	Cache and DRAM energy breakdown for representative Class 1a functions at 1, 4, 16, 64, and 256 cores.	69
4.8	Average Memory Access Time (Average Memory Access Time (AMAT)) for representative Class 1b functions.	70
4.9	Energy breakdown for representative Class 1b functions.	70
4.10	Energy breakdown for representative Class 1c functions.	72
4.11	Memory request breakdown for representative Class 2a functions.	73
4.12	Energy breakdown for representative Class 2a functions.	73

4.13	AMAT for representative Class 2b functions.	74
4.14	Energy breakdown for representative Class 2b functions.	74
4.15	Energy breakdown for representative Class 2c functions.	75
4.16	Performance of the host and the NDP system as we vary the LLC size, normalized to one host core with a fixed 8MB LLC size.	76
4.17	Energy of the host and the NDP system as we vary the LLC size. <i>Host</i> refers to the host system with a fixed 8MB LLC size; <i>Host NUCA</i> refers to the host system with 2MB/Core LLC.	78
4.18	Summary of our characterization for all 144 memory-bound functions. Each box is lower-bounded by the first quartile and upper-bounded by the third quartile. The median falls within the box. The inter-quartile range (IQR) is the distance between the first and third quartiles (i.e., box size). Whiskers extend to the minimum and maximum data point values on either sides of the box. . .	82
4.19	Hierarchical clustering of 44 representative functions.	86
4.20	Interconnection network performance overhead in our NDP system.	88
4.21	Distribution of NoC hops traveled per memory request.	88
4.22	Speedup of the NDP Accelerators over the Compute-Centric Accelerators for three functions from Classes 1a, 1b, and 2c.	89
4.23	Speedup of NDP architectures over 4 out-of-order host CPU cores for two NDP configurations: using 128 in-order NDP cores (<i>NDP+in-order</i>) and 6 out-of-order NDP cores (<i>NDP+out-of-order</i>) for representative functions from Classes 1a, 1b, and 2b.	91
4.24	Distribution of unique basic blocks (x-axis) and the percentage of last-level cache misses they produce (y-axis) for three representative functions from Classes 1a (LIGKcrEms), 1b (HSJPRH), and 1c (DRKRes).	92
4.25	Speedup of offloading to NDP the <i>hottest</i> basic block in each function versus the entire function.	92
4.26	Summary of our memory bottleneck classification.	93
5.1	Distribution of maximum vectorization factor across all vectorized loops. Whiskers extend to the minimum and maximum data points on either side of the box. Bubbles depict average values.	98
5.2	MIMDRAM subarray and bank organization. Green-colored boxes represent newly added hardware components.	100
5.3	MIMDRAM intra-mat interconnect.	102
5.4	An example of a PUD vector reduction in MIMDRAM.	104

5.5	MIMDRAM control unit in the memory controller.	106
5.6	MIMDRAM's compilation flow.	107
5.7	Overview of the MIMDRAM's memory allocation routine.	113
5.8	Single-application results for processor-centric (i.e., CPU and GPU) and memory-centric (i.e., SIMD RAM and MIMDRAM) architectures executing twelve real-world applications.	117
5.9	Multi-programmed workload results for three types of application mixes: (a) low VF, (b) medium VF, and (c) high VF. VF stands for vectorization factor. <i>SIMDRAM:X</i> uses <i>X</i> DRAM banks for computation. Values are normalized to <i>SIMDRAM:1</i> . Whiskers extend to the minimum and maximum observed data point values.	119
5.10	Multi-programmed workload results for ten application mixes. Values are normalized to the baseline CPU.	120
5.11	Single-application results for different state-of-the-art PIM architectures. . . .	121
5.12	Multi-programmed workload results for different PIM architectures and three types of application mixes. VF stands for vectorization factor. <i>DRISA:X/MIMDRAM:X (Fulcrum:X)</i> uses <i>X</i> DRAM banks (subarrays) for computation. Values are normalized to <i>DRISA:1</i> . Whiskers extend to the minimum and maximum observed data points.	122
5.13	Distribution of single-application performance across all twelve applications when varying the number of DRAM subarrays and banks for SIMD RAM and MIMDRAM. Values are normalized to the baseline CPU. Whiskers extend to the minimum and maximum observed data points on either side of the box. Bubbles depict average values.	123
5.14	GPU, SIMD RAM, and MIMDRAM performance (a), energy (b), and performance per Watt (c) for twelve real-world applications when using 16 DRAM banks and 64 DRAM subarrays per bank for in-DRAM computing. Values are normalized to the baseline CPU.	124
6.1	Required bit-precision distribution for input/output data arrays of auto-vectorized arithmetic instructions in loops across 12 applications. The box represents the 25th to 75th percentiles, with whiskers extending to the smallest/largest precision (with a diamond at the largest precision and a bubble at the mean precision).	127
6.2	Simplified bit-serial PUD addition of two input arrays <i>A</i> and <i>B</i> , each of which with two-bit data elements using (a) one and (b) two DRAM subarrays. . . .	129

6.3	Overview of the <i>Proteus</i> framework.	130
6.4	<i>Proteus</i> ' subarray organization.	133
6.5	Three data mappings for bit-serial computing.	134
6.6	<i>Proteus</i> ' implementation of different adders. Bits A_i and B_i are stored <i>vertically</i> in the same DRAM bitline of subarray i using the one-bit per-subarray (OBPS) data mapping.	136
6.7	<i>Proteus</i> ' Cost Model Logic.	138
6.8	Pareto analysis for throughput (top) and energy efficiency (bottom) for PUD addition operations. Dotted lines represent all-bits in one-subarray (ABOS); dashed lines represent all-bits per-subarray (APBS); straight lines represent OBPS data mapping.	140
6.9	Pareto analysis for throughput (top) and energy efficiency (bottom) for multiplication. Straight lines represent the Booth's multiplication method [2]; dashed lines represent the Karatsuba [3] multiplication method.	141
6.10	CPU-normalized performance per mm^2 for twelve real-world applications. Phoenix [4] and SPEC2017 [5] do <i>not</i> provide GPU implementations of <i>pca</i> and <i>x264</i>	147
6.11	End-to-end energy reduction compared to the baseline CPU for twelve applications.	147
6.12	Latency overheads of data mapping and representation format conversion. . .	148
6.13	Performance per mm^2 (top) and performance per Watt (bottom) of GEMM-intensive real-world applications using <i>int8</i> and <i>int4</i> , normalized to the same metric measured on 432 NVIDIA A100 tensor cores.	150
7.1	Overview of the DaPPA programming framework.	154
7.2	DaPPA's dataflow programming interface.	159
7.3	DaPPA's template-based compilation flow.	163
7.4	End-to-end execution time for six workloads using PrIM [6] hand-tuned and DaPPA implementations.	170
7.5	DPU kernel performance comparison for six workloads using PrIM [6] and DaPPA implementations.	171

List of Tables

4.1	Evaluated Host CPU and NDP system configurations.	63
5.1	MIMDRAM ISA extensions.	110
5.2	Evaluated system configurations.	115
5.3	Evaluated applications and their characteristics.	115
6.1	Conversion from two's complement to RBR.	143
6.2	Evaluated system configurations.	145
6.3	Evaluated applications. We measure peak GPU utilization and total memory footprint on a real system.	146
7.1	Lines-of-code (LOC) comparison.	169
C.1	List of application functions in Class 1a.	192
C.2	List of application functions in Class 1b.	193
C.3	List of application functions in Class 1c.	193
C.4	List of application functions in Class 2a.	194
C.5	List of application functions in Class 2b.	194
C.6	List of application functions in Class 2c.	195
C.7	44 representative application functions studied in detail in this work.	196
C.8	List of the evaluated 345 applications.	197

Chapter 1

Introduction

Modern computing systems, including servers, cloud platforms, supercomputers, mobile/embedded devices, and sensor systems, are designed following a *processor-centric* approach, where the system is divided between computation, communication, and storage/memory elements and computation is performed only in the computation engines (e.g., either a host CPU, GPU, FPGA, or accelerator). In contrast, data storage (including main memory) and communication units are treated as unintelligent workers that are incapable of computation. As a direct result of this processor-centric design model, data needs to be *constantly* moved back and forth between computation and communication/storage units, so that computation can be performed, which frequently leads to *data movement bottlenecks* that greatly reduce performance and increase energy consumption. Data movement bottlenecks can be observed across a wide variety of computing systems and application domains, including machine learning, databases, graph analytics, genome analysis, high-performance computing, security, data manipulation, and a wide variety of mobile and server-class workloads [7–53], directly and largely degrading the performance and energy efficiency of modern processor-centric systems since data movement from storage/memory to computing engines incurs long latency and consumes a large amount of energy [13–15, 54–58].

High-performance systems have evolved to include mechanisms that aim to alleviate data movement’s impact on system performance and energy consumption, such as large-capacity and multi-level cache hierarchies [59–68], aggressive prefetchers [55, 69–116], sophisticated out-of-order execution techniques [117–124], and many levels of multi-threading [120, 125–139]. As a result, most of the hardware real estate within a single compute node (e.g., large caches, memory controllers, interconnects, communication interfaces and associated circuitry, main memory, and solid-state drives) is dedicated to structures that to handle data movement and storage [140–145]. Unfortunately, such mechanisms not only come with significant hardware cost and complexity, but also often fail to hide the latency and energy costs of ac-

cessing off-chip main memory—which consists mostly of dynamic random access memory (DRAM) [7, 146–149], the *de-facto* main memory technology—in many modern and emerging applications [7, 10, 13, 35, 150, 151]. One primary reason behind the ineffectiveness of such processor-centric data movement mitigation mechanisms is that modern applications’ memory behavior can differ significantly from more traditional applications from decades ago (for which many of the aforementioned mechanisms were designed) since modern applications often have lower memory locality, more irregular access patterns, and much larger working sets [19, 21, 55, 56, 93, 116, 152–157]. For example, recent works [13–15] show that (i) more than 62% of the entire system energy of a mobile device is spent on data movement between the processor and the memory hierarchy for widely-used mobile workloads [13]; and (ii) more than 90% of the entire system energy is spent on memory when executing large commercial edge neural network models on modern edge machine learning accelerators [14, 15]. At the same time, as memory manufacturing process technology node continues to shrink, further scaling memory capacity, energy, cost, and performance has become increasingly difficult—especially in the past decade—leading to new reliability and robustness challenges such as DRAM read disturbance [1, 7, 8, 53, 151, 152, 158–199], including RowHammer [160] and RowPress [190], and reduced data retention capabilities [163, 194, 200–236].

One promising solution to fundamentally mitigate (and even eliminate) data movement bottlenecks in modern and emerging applications is to move from a *processor-centric* design paradigm, where computation is performed *only* in processing-using, to a *memory-centric* design paradigm, where computation is performed where data resides. A primary example of the memory-centric system design paradigm is *processing-in-memory* (PIM) [6, 13, 14, 21, 56, 57, 150, 154–157, 237–415], where the cost of data movement to/from storage/memory is reduced by placing computation capability inside or close to memory structures. In PIM, the computational logic inside or close to memory structures has access to data that resides in memory arrays with significantly higher memory bandwidth, lower latency, and lower energy consumption than the CPU (or GPU, FPGA, or any other processor-centric accelerator) has in existing systems.

There are two main approaches to PIM [7, 8, 16, 17, 19, 24, 145, 416–422]. The first approach, called *processing-near-memory* (PNM) [6, 13, 14, 21, 56, 57, 150, 154–157, 237–311, 382], exploits the ability to implement a wide variety of processing logic (i.e., computation capabilities) *near* the memory arrays (e.g., in a DRAM chip, next to each memory bank or sub-array, at the logic layer of 3D-stacked memory [423–425], in the memory controllers, near cache memory arrays, inside a flash memory chip) and thus leveraging the high internal bandwidth and low latency available inside the memory chip (e.g., between the logic layer and the memory layers of 3D-stacked memory). The second approach, called *processing-using-*

memory (PUM) [280, 312–381, 383, 389, 426–429], exploits the existing memory structures and the analog operational principles of the memory circuitry to enable (bulk) computation operations within the memory arrays. On the one hand, PNM designs are often a more general approach to PIM, where the logic implemented near the memory arrays can be powerful and customized, and thus can benefit a wide variety of applications. On the other hand, PUM designs (i) *fundamentally eliminate* data movement by performing computation *in situ* and (ii) exploit the large internal bandwidth and large bit-level and array-level parallelism available *inside* the memory arrays. Since both approaches offer different tradeoffs, they should be viewed as *complementary* to each other and can be combined to exploit the maximum potential of a PIM system [416, 422]. Both PNM and PUM architectures can be implemented using different memory technologies, including static random access memory (SRAM) [324, 325, 365–375], DRAM [280, 314–320, 323, 327–330, 332, 333, 339, 342, 343, 345, 346], emerging non-volatile memory [312, 313, 321, 322, 331, 334, 337, 338, 351, 376] or NAND flash memory [336, 353–364].

1.1 Problem Definition

Many works from academia [6, 13, 14, 21, 56, 57, 150, 154–157, 237, 238, 240–244, 247–282, 286–396, 430–434] and industry [239, 245, 246, 283–285, 397–401] have shown the benefits of PNM and PUM for a wide range of workloads from different domains, including machine learning [14, 15, 249, 267, 268, 276, 277, 283, 294, 312, 313, 319, 324, 334, 354, 358, 360, 362, 364, 365, 368, 371, 379, 384, 388, 389, 392, 397, 400, 400, 435–439], genome analytics [21, 240, 367, 389, 394, 395, 440], databases [238, 255, 266, 278, 388, 398, 441], graph analytics [56, 57, 154, 257, 280, 292, 293, 303, 304, 321, 345, 442, 443], high-performance computing [444], and a wide variety of mobile [13, 277, 445, 446] and server-class [447, 448] workloads. These past PIM approaches improve system performance and energy efficiency by reducing costly data movement between memory and compute units while exploiting the massive internal parallelism inherent in modern memory architectures. However, adopting PIM as a mainstream architecture *holistically*, i.e., in a seamless manner that does *not* place a heavy burden on the vast majority of programmers, and *efficiently*, i.e., where PIM drawbacks (such as limited computation power, stringent design constraints, and data layout restriction) can be avoided while its benefits (such as access to data with low latency, high bandwidth, and low energy cots) can be enhanced, is still very challenging due to the lack of tools, programming, and system support for PIM across the computer architecture stack.

First, there is a lack of **workload characterization methodologies and benchmark suites** targeting PIM architectures, making it difficult to *systematically* identify application-specific data movement bottlenecks that can be potentially mitigated by PIM, compare alternative processor-centric and memory-centric data movement mitigation solutions, and quantify

performance and energy efficiency gains. Developing standardized benchmarks and clear metrics is critical to drive adoption in both academic research and industry settings. Second, current processor-centric **execution models** often fail to fully harness the abundant parallelism available in PIM-enabled systems. New, specialized memory-centric execution paradigms need to be designed to map applications effectively onto PIM hardware resources, ensuring high PIM utilization and throughput. Third, **compiler support** and **programming frameworks** to aid PIM programmability are severely underdeveloped. Conventional compiler frameworks are *not* designed to (i) generate code that effectively leverages the main characteristics of PIM systems, such as abundant bit-level and array-level memory and compute parallelism, and (ii) schedule and orchestrate PIM operations in ways that can maximize data locality and minimize data movement. Consequently, effective programming of PIM systems frequently places significant demands on the programmer, who must acquire an in-depth understanding of the underlying hardware substrate to accurately and efficiently map the target application onto the PIM architecture. Fourth, **adaptive data-aware runtime** mechanisms are essential to fully harness the benefits of PIM architectures. Besides adopting a *data-centric* design (by co-locating computation near/in memory), an efficient PIM system should also be *data-aware*, where the intrinsic properties of the data are used to make informed decisions during execution. By dynamically adapting PIM resources and execution parameters based on the observed data characteristics at runtime, such data-centric and a data-aware PIM system can significantly reduce latency and improve overall system performance, throughput, and energy efficiency. The dynamic nature of data requires the development of dynamic runtime mechanisms, to adapt PIM execution to the characteristics of the target workload (and its dataset).

1.2 Our Goal

Our *goal* in this dissertation is to provide tools, programming, and system support for PIM architectures (with a focus on DRAM-based solutions), to ease the adoption of such architectures in current and future systems.

1.3 Thesis Statement

The following thesis statement encompasses our approach:

We can effectively exploit the inherent parallelism of PIM architectures and facilitate their adoption across a broad spectrum of workloads through end-to-end design of hardware and software support for PIM, including benchmark suites and workload analysis methodologies, compiler/programming frameworks, and data-aware runtime systems, thereby enabling large (e.g., factors or orders of magnitude) improvements in performance and energy efficiency.

1.4 Our Approach

In line with our thesis statement, we investigate four major directions that enable us to ease PIM adoption and effectiveness in current and future systems: (i) identifying and characterizing potential sources of data movement bottlenecks over a broad set of applications, (ii) providing programming/compilation and system support for end-to-end PUM execution while maximizing hardware utilization and attained throughput, (iii) enabling data-aware optimizations for efficient PUM execution, and (iv) designing programming frameworks to aid PIM programmability. Toward these four major directions, we make four key contributions:

1.4.1 A Methodology and Benchmark Suite for Understanding and Mitigating Data Movement Bottlenecks

The *goals* of our first contribution are twofold. First, we aim to methodically identify potential sources of data movement bottlenecks over a broad set of applications and to comprehensively compare traditional processor-centric data movement mitigation techniques (e.g., caching and prefetching) to memory-centric techniques (e.g., PIM), thereby developing a rigorous understanding of the best techniques to mitigate each source of data movement. Second, we aim to develop a benchmark suite for data movement that captures the previously-characterized sources of data movement bottlenecks across many applications.

With these goals in mind, we perform the first large-scale characterization of a wide variety of applications, across a wide range of application domains, to identify *fundamental* program properties that lead to data movement to/from main memory. We develop the first systematic methodology to classify applications based on the sources contributing to data movement bottlenecks. From our large-scale characterization of 77K functions across 345 applications, we select 144 functions to form the first open-source benchmark suite for main memory data movement studies (called DAMOV). We select a diverse range of functions that (i) represent different types of data movement bottlenecks, and (ii) come from a wide range of application domains. We identify new insights about the different data movement bottlenecks and use these insights to determine the most suitable data movement mitigation mechanism (from processor-centric to memory-centric solutions) for a particular application. We show how our DAMOV benchmark suite can aid the study of open research problems for PIM architectures, via four case studies, where we evaluate: (i) the performance impact of load balance and inter-PIM communication in PIM systems, (ii) the impact of PIM accelerators on our memory workload analysis, (iii) the impact of different core models on PIM architecture performance, and (iv) the potential benefits of identifying simple PIM instructions for offloading. We conclude that our benchmark suite and methodology can be employed to address many different open research and develop-

ment questions on data movement mitigation mechanisms, particularly topics related to PIM systems and architectures. We open-source DAMOV and the complete source code for our new characterization methodology at <https://github.com/CMU-SAFARI/DAMOV>. Chapter 4 describes this work in more detail.

1.4.2 Enabling Efficient and Programmable MIMD Execution in Processing-Using-DRAM (PUD) Architectures

Our second contribution aims to design a flexible processing-using-DRAM (PUD) system that overcomes the limitations caused by the large and rigid granularity of PUD execution. PUD is a PIM approach that uses a DRAM array’s massive internal parallelism to execute very-wide (e.g., 16,384–262,144-bit-wide) data-parallel operations, in a single-instruction multiple-data (SIMD) fashion. However, DRAM rows’ large and rigid granularity limit the effectiveness and applicability of PUD in three ways. First, since applications have varying degrees of SIMD parallelism (which is often smaller than the DRAM row granularity), PUD execution often leads to under-utilization, throughput loss, and energy waste. Second, due to the high area cost of implementing interconnects that connect columns in a wide DRAM row, most PUD architectures are limited to the execution of parallel *map* operations, where a single operation is performed over equally-sized input and output arrays. Third, the need to feed the wide DRAM row with tens of thousands of data elements combined with the lack of adequate compiler support for PUD systems create a programmability barrier, since programmers need to manually extract SIMD parallelism from an application and map computation to the PUD hardware.

To tackle the three limitations caused by the large and rigid granularity of PUD execution, we propose MIMDRAM, a hardware/software co-designed PUD system that introduces new mechanisms to allocate and control only the necessary resources for a given PUD operation. The *key idea* of MIMDRAM is to leverage fine-grained DRAM [449–457] (i.e., the ability to independently access smaller segments of a large DRAM row) for PUD computation. MIMDRAM exploits this key idea to enable a multiple-instruction multiple-data (MIMD) execution model in each DRAM subarray (and SIMD execution within each DRAM row segment). MIMDRAM leverages fine-grained DRAM for PUD in hardware and software. On the hardware side, MIMDRAM proposes simple modifications to the DRAM subarray and includes new mechanisms in the memory controller that (i) allow the execution of independent PUD operations across the DRAM mats in a single subarray; and (ii) enable communication across columns of a DRAM row at varying granularities for the execution of vector-to-scalar reduction in DRAM at low hardware cost. On the software side, MIMDRAM implements compiler passes to (i) automatically vectorize code regions that can benefit from PUD execution (called PUD-friendly regions); (ii) for such regions, generate PUD operations with the most appropriate SIMD gran-

ularity; and (iii) schedule the concurrent execution of independent PUD operations in different DRAM row segments. We discuss how to integrate MIMDRAM in a real system, including how MIMDRAM deals with (i) data allocation within a DRAM subarray and (ii) mapping of a PUD’s operands to guarantee high utilization of the PUD substrate.

We evaluate MIMDRAM using twelve real-world applications and 495 multi-programmed application mixes. When using 64 DRAM subarrays per bank and 16 banks for PuD computation in a DRAM chip, MIMDRAM provides (i) $13.2\times/0.22\times/173\times$ the performance, (ii) $0.0017\times/0.00007\times/0.004\times$ the energy consumption, (iii) $582.4\times/13612\times/272\times$ the performance per Watt of the CPU [458]/GPU [459]/SIMDRAM [378] (the prior state-of-the-art PUD framework) baselines and (iv) when using a single DRAM subarray, $15.6\times$ the SIMD utilization of SIMDRAM. MIMDRAM adds small area cost to a DRAM chip (1.11%) and CPU die (0.6%). We open-source MIMDRAM workloads and evaluation framework at <https://github.com/CMU-SAFARI/MIMDRAM>. Chapter 5 describes this work in more detail.

1.4.3 Enabling High-Performance PUD Execution via Dynamic Precision PUD Arithmetic

Our third contribution aims to overcome three major limitations of PUD architectures caused by the naive use of a bit-serial execution model in such architectures. While PUD promises high throughput at low energy and area cost, we uncover three limitations of existing PUD approaches that lead to significant performance and energy inefficiencies. First, they employ a **rigid and static data representation**, which is *inefficient* for bit-serial execution. Existing PUD engines typically employ a fixed bit-precision, statically defined data representation (commonly two’s complement) for all PUD operations. This rigid and static data format introduces inefficiencies in a bit-serial execution model, where bits of a data word are *individually* and *sequentially* processed. Since many applications store data in data representation formats that exceed the necessary precision [460–467] (e.g., 8-bit values stored in a 32-bit integer), a significant fraction of PUD computation is wasted on inconsequential bits, such as leading zeros or sign-extended bits, causing significant latency and energy overhead. Second, PUD architectures *only* favor a **throughput-oriented execution with limited latency tolerance**. PUD operations are composed of high-latency in-DRAM primitives (e.g., in-DRAM row copy [317] and in-DRAM majority-of-three [314]), making individual PUD operations inherently slow. To compensate for this latency, PUD architectures adopt a *throughput-oriented execution model* that distributes large amounts of data across multiple DRAM subarrays and DRAM banks, enabling a massively parallel execution. However, this approach is *only* effective when sufficient data-level parallelism is available to amortize the high latency of individual PUD primitives. In scenarios where data-level parallelism is limited, this throughput-oriented

execution model fails to hide the latency of individual in-DRAM primitives, potentially leading to performance degradation. Third, bit-serial PUD architectures face **scalability challenges for high-precision operations**. PUD systems suffer from increased latency as the target bit-precision grows. Due to their bit-serial nature, the latency of arithmetic PUD operations scales linearly [378] (for operations such as addition/subtraction) or quadratically [378] (for operations such as multiplication/division) with the target bit-precision. This scaling behavior arises from the inherently serial structure of these operations, which often requires long carry-propagation chains across the individual bits of a data word. As a result, high-precision computations (e.g., beyond 32-bit) become prohibitively slow.

To address these issues, we propose *Proteus*, an adaptive *data-representation* and *operation-implementation* framework, which builds on three *key ideas*. To solve the **first limitation** (i.e., rigid and static data representation), *Proteus* reduces the bit-precision for PUD operations by leveraging *narrow values* (i.e., values with many leading zeros). As several works observe [460–467], programmers often over-provision the bit-precision used to store operands, using large data types (e.g., a 32-bit or 64-bit integer) to store small (i.e., narrow) values. Based on this observation, *Proteus* can exploit narrow values to reduce the bit-precision of a PUD operation to that of the best-fitting number of bits; thus performing costly in-DRAM operations *only* over consequential bits, which improves overall performance and energy efficiency. To solve the **second limitation** (i.e., throughput-oriented execution with limited latency tolerance), *Proteus* *parallelizes* the execution of *independent* in-DRAM primitives in a PUD operation by leveraging DRAM’s internal organization combined with *bit-level parallelism*. We make the key observation that many in-DRAM primitives that compose a PUD operation (e.g., an in-DRAM addition) can be executed *concurrently* across different bits of a data word. For example, executing an n -bit in-DRAM addition (i.e., $A_{n-1}, \dots, A_0 + B_{n-1}, \dots, B_0$) in a bit-serial manner requires performing at least three majority-of-three (MAJ3) operations per bit i to compute the *sum* and propagate the carry to bit $i+1$. However, only one of these operation (i.e., the carry propagation from bit i to bit $i+1$) needs to be serialized across the n bit positions of a data word, while the other two MAJ3 operations for bit positions i and $i+1$ can be *concurrently executed*. To exploit this observation, *Proteus* scatters the n bits of a data word across multiple DRAM subarrays (i.e., $\text{subarray}_i \leftarrow \{A_i, B_i\}$) and employs subarray-level parallelism (SALP) [161] to enable each subarray i to *concurrently* execute the in-DRAM primitive associated with its respective bit i , thus hiding the high latency of individual in-DRAM primitives in a PUD operation over the many bits of the target data word. To solve the **third limitation** (i.e., scalability challenges for high-precision operations), *Proteus* exploits an alternative data representation for high-precision computation. Concretely, we investigate an alternative data representation, i.e., the redundant binary representation (RBR) [468–472] (where multiple-

digit combinations represent the same value), for high-precision computation. PUD execution can take advantage of two properties of RBR-based arithmetic: (i) the operations no longer need to propagate carry bits through the full width of the data (e.g., RBR-based addition limits carry propagation to at most two places [473]), and (iii) the operation latency is *independent* of the bit-precision.

Based on these two three key ideas ideas, we design *Proteus* as a three-component hardware framework for high-performance PUD computation that *transparently* (from the user/programmer) selects (i) the most efficient data format (e.g., 2's complement, redundant binary [468–470]), (ii) the exact bit-precision for a workload, and (iii) the fastest arithmetic algorithm for latency- or throughput-oriented PUD execution.

We compare *Proteus* to different state-of-the-art computing platforms (CPU, GPU, and the SIMDRAM PUD architecture) for twelve real-world applications. Using only a single DRAM bank, *Proteus* provides (i) 17 \times , 7.3 \times , and 10.2 \times the performance per mm²; and (ii) 90.3 \times , 21 \times , and 8.1 \times lower energy consumption than that of the CPU, GPU, and SIMDRAM, respectively, on average across twelve real-world applications. *Proteus* incurs low area cost on top of a DRAM chip (1.6%) and CPU die (0.03%). Chapter 6 describes this work in more detail.

1.4.4 A Data-Parallel Programming Framework for Easing Programmability and Enabling High-Performance PNM Execution

Our fourth contribution aims to ease programmability for the general-purpose PNM architectures, allowing a programmer to write efficient PIM-friendly code *without* the need to manage hardware resources explicitly. We use the UPMEM PIM architecture [6, 241, 474–476], the first publicly-available real-world PIM architecture, as a case study for the implementation of our programming framework. The UPMEM PIM architecture is a many-core system consisting of *UPMEM modules*, which are standard DDR4-2400 DIMMs with multithreaded general-purpose in-order processors (called DRAM Processing Units, i.e., DPUs) coupled together with DRAM banks (called *MRAM*). A programmer needs to follow four main steps to implement a given application targeting the UPMEM system. The programmer needs to: (i) partition the computation (and input data) across the DPUs in the system, *manually* exposing thread-level parallelism (TLP); (ii) distribute (copy) the appropriate input data from the CPU's main memory into the DPU's memory space; (iii) launch the computation kernel that the DPUs will execute; and (iv) gather (copy) output data from the DPUs to the CPU main memory once the DPUs execute the kernel. Even though UPMEM's programming model resembles that of widely employed architectures, such as GPUs, it requires the programmer to (i) have detailed knowledge of the underlying UPMEM hardware and its idiosyncrasy and (ii) *manually* manage data movement at a fine granularity (e.g., guarantee that memory accesses are byte-aligned, orches-

trating data reading/writing from DPUs’ local scratchpad memory). Such limitations and the requirement of introduce knowledge of underlying hardware by the programmer can greatly limit the adoption of PNM systems as general-purpose systems.

To solve this major adoption and programming problem, we introduce DaPPA (data parallel processing-in-memory architecture), a programming and compilation framework that eases the programmability of general-purpose PNM systems by automatically managing data movement, memory allocation, and workload distribution. The *key idea* behind DaPPA is to leverage a high-level data-parallel pattern-based [477, 478] programming interface to abstract hardware complexities away from the programmer. DaPPA comprises three main components: (i) *data-parallel pattern APIs*, a collection of five primary data-parallel pattern primitives that allows the programmer to express data transformations within an application at an abstract level; (ii) *dataflow programming interface*, which allows the programmer to define how data moves across data-parallel patterns; and (iii) a *dynamic template-based compilation*, which leverages code skeletons and dynamic code transformations to convert data-parallel patterns implemented via the dataflow programming interface into an optimized binary for the target PNM architecture.

We evaluate DaPPA using six workloads from the PrIM benchmark suite [479] on a real UPMEM system. Compared to hand-tuned implementations, DaPPA improves end-to-end performance by 2.1 \times , on average, and reduces programming complexity (measured in lines-of-code) by 94%. Our results demonstrate that DaPPA is an effective programming framework for efficient and user-friendly programming on UPMEM systems. DaPPA is also a general PNM programming framework that can be deployed for any PNM architecture. Chapter 7 describes this work in more detail.

1.5 Contributions

In this dissertation, we make the following contributions:

- We propose the first methodology to characterize data-intensive workloads based on the sources of their data movement bottlenecks. This methodology is driven by insights obtained from a large-scale experimental characterization of 345 applications from 37 different benchmark suites and an evaluation of the performance of memory-bound functions from these applications with three data-movement mitigation mechanisms.
- We introduce DAMOV, the first open-source benchmark suite for main memory data movement-related studies, based on our systematic characterization methodology. This suite consists of 144 functions representing different sources of data movement bottlenecks and can be used as a baseline benchmark set for future data-movement mitigation research. In

fact, multiple works have already used DAMOV [281, 454, 457, 480–489] since its initial release in 2021.

- We show how the DAMOV benchmark suite and methodology to identify data movement bottlenecks can aid the study of open research problems for PIM architectures, via four case studies. In particular, we evaluate (i) the performance impact of load balance and inter-PIM communication in PIM systems, (ii) the impact of PIM accelerators on our workload analysis, (iii) the impact of different core models on PIM architecture performance, and (iv) the potential benefits of identifying simple PIM instructions for offloading. We conclude that our benchmark suite and methodology can be employed to address many different open research and development questions on data movement mitigation mechanisms, particularly topics related to PIM systems and architectures.
- We propose MIMDRAM, an end-to-end processing-using-DRAM (PUD) system for general-purpose applications, which executes operations in a multiple-instruction multiple-data (MIMD) fashion. MIMDRAM makes low-cost modifications to the DRAM subarray design that enable the *concurrent* execution of multiple independent PUD operations in a single DRAM subarray.
- We propose compiler passes that take as input unmodified C/C++ applications and, transparently to the programmer, (i) identify loops that are suitable for PUD execution, (ii) transform the source code to use PUD operations, and (iii) schedule independent PUD operations for concurrent execution in each DRAM subarray, maximizing utilization of the underlying PUD architecture.
- We propose *Proteus*, a novel PUD framework that overcomes three major inefficiencies in existing bit-serial PUD architectures: static data representation, lack of support for latency-oriented execution, and high-latency for high-precision PUD operations. *Proteus* exploits DRAM’s internal parallelism to hide the latency of individual in-DRAM primitives (i.e., row copy, majority-of-three), and introduces mechanisms to scatter bits of a data word across multiple DRAM subarrays. This bit-level distribution enables *concurrent* execution of independent in-DRAM primitives, and allows *Proteus* to leverage both bit-serial and bit-parallel algorithms for PUD arithmetic.
- We introduce a three-component adaptive data-aware runtime mechanism that transparently (from the user/programmer) selects the most suitable data representation, bit-precision, and arithmetic algorithm (bit-serial or bit-parallel) for each PUD instruction, enabling high-performance and energy-efficient PUD execution.
- We propose DaPPA (data-parallel processing-in-memory architecture), a data-parallel pattern-based programming framework that abstracts *both* computation and communication requirements while *automatically* generating code for general-purpose PIM architectures.

We equip DaPPA with a series of code optimizations that greatly improve the performance of workloads running on general-purpose PNM systems.

- We demonstrate that DaPPA’s data-parallel pattern-based programming significantly improves both performance and programming efficiency for real-world UPMEM-based PNM architectures. The results highlight DaPPA’s broad applicability to different workloads and indicate that adopting a data-parallel pattern-based, high-level programming approach can lead to performance improvements while minimizing programmers’ effort.

1.6 Outline

This dissertation is organized into eight chapters.

Chapter 2 gives relevant background information about DRAM organization, operation, and the PIM architectures we build on top of in this dissertation. Chapter 3 provides a comprehensive overview of related prior work in (i) PUM architectures (§3.2), including SRAM-based (§3.2.1), DRAM-based (§3.2.2), non-volatile memory (NVM)-based (§3.2.3), and NAND flash-based (§3.2.4) PUM architectures; and (ii) system support for PIM (§3.3), including data movement bottleneck characterization (§3.3.1), PIM suitability (§3.3.2), compiler support for PIM (§3.3.3), memory management support for PIM (§3.3.4), and programming frameworks and high-level application programming interfaces (APIs) for PIM (§3.3.5). Chapter 4 presents DAMOV, our workload characterization methodology and benchmark suite for data movement bottlenecks. Chapter 5 presents the design of MIMDRAM, our end-of-end hardware/-software co-designed PUD system. Chapter 6 presents *Proteus*, our runtime solution for dynamic precision bit-serial PUD computation. Chapter 7 discusses DaPPA, our programming framework that abstracts hardware components away from the programmer, thus facilitating code development for general-purpose PNM architectures. Chapter 8 provides a summary of this dissertation, along with promising future research directions and concluding remarks.

Chapter 2

Background

This chapter provides an overview of the background material necessary to understand our discussions, analyses, and contributions. Section 2.1 reviews DRAM organization and DRAM operation. Section 2.2 provides background material about PIM architectures (both PNM and PUM) relevant for this dissertation.

2.1 DRAM Organization & Operation

2.1.1 DRAM Organization

A DRAM [146, 147] system (Figure 2.1a) comprises of a hierarchy of components. A *DRAM module* (Figure 2.1b) has several (e.g., 8–16) DRAM chips. A *DRAM chip* (Figure 2.1c) has multiple DRAM banks (e.g., 8–16). A *DRAM bank* (Figure 2.1d) has multiple (e.g., 64–128) 2D arrays of DRAM cells known as *DRAM mats*. Several DRAM mats (e.g., 8–16) are grouped in a *DRAM subarray* [161, 172, 173, 224, 317]. In a DRAM bank, there are three global components that are used to access the DRAM mats (as Figure 2.1d depicts): (i) a *global row decoder* that selects a row of DRAM cells *across* multiple mats in a subarray, (ii) a *column select logic* (CSL) that selects portions of the DRAM row based on the column address, and (iii) a *global sense amplifier* (also sometimes called global row buffer) that transfers the selected fraction of the data from the selected DRAM row through the *global bitlines*.

A *DRAM mat* (Figure 2.1e) consists of a 2D array of DRAM cells organized into multiple rows (e.g., 512–1024) and multiple *columns* (e.g., 512–1024) [175, 183, 490]. Each mat contains (i) a *local row decoder* that drives the local wordlines to the appropriate voltage levels to open (activate) a row, (ii) a row of sense amplifiers (also called a *local row buffer*; ❶ in Figure 2.1e) that sense and latch data from the activated row, and (iii) *helper flip-flops* (HFFs) that drive a portion (e.g., 4 bit) of the data in the local row buffer to the global bitlines. A *DRAM cell* (❷) consists of an *access transistor* and a *storage capacitor*. The source nodes of the access

transistors of all the DRAM cells in the same column connect the cells' storage capacitors to the same *local bitline*. The gate nodes of the access transistors of all the DRAM cells in the same row connect the cells' access transistors to the same *local wordline*. To achieve high density, modern DRAM designs employ an *open bitline architecture* [491–493], fitting only enough sense amplifiers in a local row buffer to sense half a row of cells. To sense the entire row of cells, each subarray has local bitlines connecting to two rows of local sense amplifiers—one above and one below the cell array (③). For more detail on DRAM organization, we refer the reader to prior literature [1, 146, 152, 153, 158, 161, 163, 165, 171–174, 179, 181, 182, 190, 194, 195, 224, 314, 315, 317, 377, 425, 449, 451, 455, 456, 494–508], especially [315].

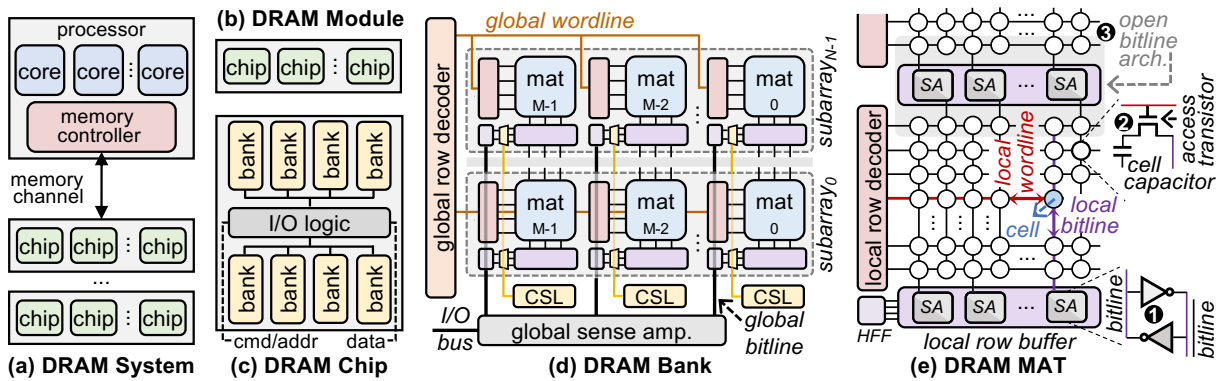


Figure 2.1: Overview of DRAM organization.

2.1.2 DRAM Operation

The memory controller (Figure 2.1a) can issue three commands to service a DRAM request, in four main steps: (i) **row activation & sense amplification**: opening a row to transfer its data to the row buffer, (ii) **read/write**: accessing the target column in the row buffer, (iii) **charge restoration**: recharging the capacitor in the DRAM cell to its original voltage level after the sense amplification, and (iv) **precharge**: closing the row and the row buffer. We use Figure 2.2 to explain these four steps in detail. The top part of the figure shows the phase of the cells within the row that is being accessed. The bottom part shows both the DRAM command and data bus timelines, and demonstrates the associated timing parameters.

Initial State. Initially, the DRAM bank is in the precharged state (step 4 in Figure 2.2), where all of the components are ready for activation, i.e., the local bitlines are set at a reference voltage ($\frac{V_{DD}}{2}$), the local wordline is disabled, and the local sense amplifiers is *off* without any data latched in it.

Row Activation & Sense Amplification Phases. To open a row, the memory controller sends an ACTIVATE (ACT) command to raise the local wordline of the corresponding DRAM

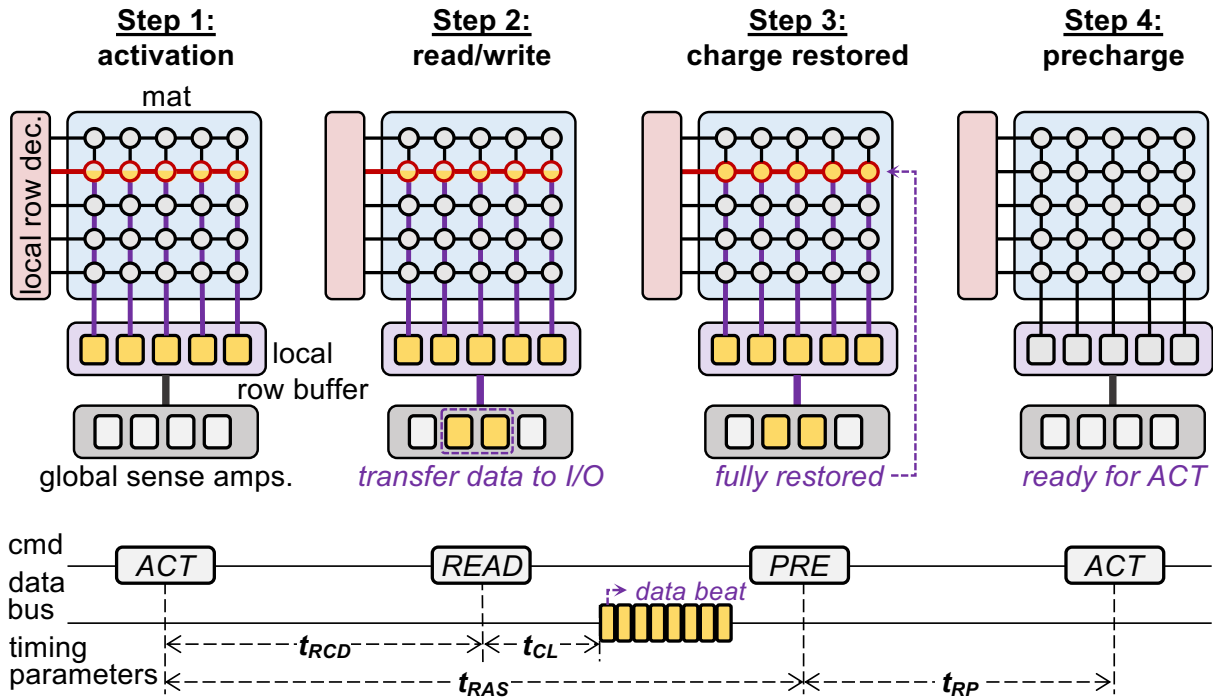


Figure 2.2: Overview of DRAM operation. Reproduced from [1].

row, which connects the row to the local bitlines (step 1 in Figure 2.2). This triggers an activation, where charge starts to flow from the DRAM cell to the local bitline (or the other way around, depending on the initial charge level in the cell) via a process called *charge sharing*. This process perturbs the voltage level on the corresponding local bitline by a small amount. If the DRAM cell is initially charged (which we assume for the rest of this explanation, without loss of generality), the local bitline voltage is perturbed *upwards*. Note that this causes the DRAM cell itself to discharge, losing its data temporarily (hence the partial filling color of the accessed row), but this charge will be restored as we will describe below. After the activation phase, the sense amplifier senses and amplifies the voltage perturbation on the local bitline. When the local bitline is amplified to a certain voltage level (e.g., $0.8V_{DD}$), the sense amplifier latches in the cell's data, which transforms it into binary data, i.e., a logical '1' or '0'. At this point in time, the data can be read from the local sense amplifier. The latency of these two phases (activation and sense amplification) is called the *activation latency*, and is defined as t_{RCD} in the standard DDR interface [509–511]. This activation latency specifies the latency from the time an ACT command is issued to the time the data is ready to be accessed in the local sense amplifiers.

Read/Write & Restoration Phases. Once the local sense amplifiers (row buffer) latches in the data, the memory controller can send a READ (RD) or WRITE (WR) command to access the corresponding column of data within the row buffer (step 2 in Figure 2.2). The column access time to read the cache line data is called t_{CL} (t_{CWL} for writes). These parameters define the

time between the column command and the appearance of the first *beat* of data on the data bus, shown at the bottom of Figure 2.2. A data beat is a 64-bit data transfer from the DRAM to the processor. In a typical DRAM [509–511], a column RD command reads out 8 data beats.

After the DRAM bank becomes activated and the local sense amplifier latches in the binary data of a cell, it starts to restore the connected cell’s charge back to its original fully-charged state (step 3 in Figure 2.2). This phase is known as *charge restoration*, and can happen in parallel with column accesses. The timing parameter that defines the restoration latency (from issuing an ACT command to fully restoring a row of DRAM cells) is called t_{RAS} .

Precharge Phase. In order to access data from a different DRAM row, the DRAM bank needs to be re-initialized back to the precharged state (step 4 in Figure 2.2). To achieve this, the memory controller sends a PRECHARGE (PRE) command, which (i) disables the local wordline of the corresponding DRAM row, disconnecting the DRAM row from the local sense amplifiers, and (ii) resets the voltage level on the bitline back to the initialized state. The timing parameter that defines the precharge latency is called t_{RP} .

For more detail on DRAM operation, commands, and latency, we refer the reader to prior literature [1, 146, 152, 153, 158, 161, 163, 165, 171–174, 179, 181, 182, 190, 194, 195, 224, 314, 315, 317, 377, 425, 449, 451, 455, 456, 494–508].

2.2 Processing-in-Memory Architectures

2.2.1 A Brief PIM Taxonomy

PIM aims to reduce the impact that data movement between memory and CPU has on the overall system’s performance and energy by (i) adding computation logic to the same die as memory [6, 237–261], memory controllers [54, 55, 153, 165, 244], or to the logic layer of 3D-stacked memory [13, 14, 21, 56, 57, 150, 154–157, 262–311] (i.e., PNM); or (ii) exploiting the analog operational properties of the memory circuitry (i.e., PUM [280, 312–381, 383, 389, 426–429]).

In the literature, the term PNM (also processing-in-memory, near-data computing/processing, or near-memory computing/processing) has come to refer to a wide range of architectures. We categorize these different architectures into three general approaches where PIM logic can be integrated into the system. Each of the three approaches has different trade offs.

The first approach adds PIM logic to the memory controller, enabling the memory controller to perform more complex functions than scheduling reads/writes without the need for CPU involvement. For example, several works [54, 55, 153, 165, 244] add computation logic to the memory controller to reduce the round-trip cost of data movement, avoiding the latency of moving data within the cache hierarchy until it reaches to the host CPU core. A key advantage of such an approach is that it can work with conventional memory technologies such as DDRx

memories. Unfortunately, this approach does *not* eliminate unnecessary data movement, as the memory controller typically sits on-chip with the CPU cores and still requires data to move back-and-forth between the pin-limited and power-hungry main memory channel and the memory controller.

Beyond reducing data movement overhead, a promising direction enabled by computation-capable memory controllers is the design of *intelligent memory controllers* that actively manage and mitigate reliability and robustness issues in DRAM. For example, by integrating specialized logic, the memory controller can detect and respond to phenomena such as read disturbance (e.g., RowHammer [160] and RowPress [190]) and data retention failures more effectively and at lower overhead compared to traditional, reactive system-level techniques. Several recent works demonstrate that such intelligent mechanisms can proactively identify vulnerable rows [160, 181, 192–194, 503, 512–585] or dynamically adjust refresh policies [163, 184, 586] to maintain data integrity, security, and overall system robustness. Embedding this functionality within a programmable or specialized in-controller PIM substrate allows for fine-grained, real-time memory management that adapts to the dynamic behavior of DRAM devices, thereby improving reliability without incurring significant performance or energy penalties. Several recent works demonstrate that such intelligent mechanisms can implement different read disturbance mitigation mechanisms [160, 181, 192–194, 503, 512–585] or perform online profiling of DRAM cell retention times and online adjustment of refresh rate on a per-row basis [163, 180, 222, 497, 508, 586–593] to maintain data integrity, security, and overall system robustness.

The second approach adds PIM logic close physical to (but *not* within) the memory chip, enabling near-data processing without requiring modifications to the memory chip itself. Such designs typically exploit one of two integration strategies: (i) 2.5D integration, where PIM logic is integrated alongside high-bandwidth memory chips on a silicon interposer, enabling low-latency, high-bandwidth communication between logic and memory dies [594]; (ii) module-level integration, where PIM logic is embedded on the same printed circuit board (PCB) as memory chips. One notable example of the latter is the use of the buffer chips in load-reduced DIMMs (LRDIMMs) as hosts for PIM logic [246, 251, 256, 595], although similar concepts can extend to PIM chips co-packaged with standard DRAM devices on a DRAM module. These approaches have the advantage of avoiding data transfers over the off-chip memory channel between the host processor and main memory, thereby reducing memory latency and memory bandwidth pressure. However, because data movement still occurs to/from the memory chip to the computation chip(s), and such data movement consumes more energy than data movement that happens *only* inside the memory chip.

The third approach adds PIM logic inside the memory chip, allowing the PIM logic to

access the abundant internal bandwidth inside the memory chip directly at the lowest energy costs. Recent advances in memory manufacturing have enabled adding PIM logic inside the memory chip in two ways. First, PIM logic can be added to the *logic layer* of 3D-stacked memories [13, 14, 21, 56, 57, 150, 154–157, 262–311]. In a 3D-stacked memory, multiple layers of memory (typically DRAM in already-existing systems) are stacked on top of each other. These layers are connected together using vertical through-silicon vias (TSVs) [425, 596]. Using current manufacturing process technologies, thousands of TSVs can be placed within a single 3D-stacked memory chip. As such, the TSVs provide much greater internal memory bandwidth than the narrow memory channel. Examples of 3D-stacked DRAM available commercially include Hybrid Bandwidth Memory (HBM) [424, 425, 597], Wide I/O [598], Wide I/O 2 [599], and the Hybrid Memory Cube (HMC) [600]. Emerging die-stacking and packaging technologies, like *hybrid bonding* [601–603] and *monolithic 3D integration* [604–611], can further amplify the benefits of conventional TSV-based 3D-stacked memory chips by greatly improving internal bandwidth across layers using *high-density* inter-layer vias (ILVs) [604, 610] or *direct* wafer-to-wafer connections via Cu–Cu bonding [601–603, 612], respectively. In addition to the multiple layers of DRAM, a number of prominent 3D-stacked DRAM architectures, including HBM and HMC, incorporate a logic layer inside the chip [56, 424, 425, 596, 597, 600]. The logic layer is typically the bottommost layer of the chip, and is connected to the same TSVs as the memory layers.¹ The logic layer provides area inside the 3D-stacked DRAM system where architects can implement functionality that interacts with both the processor and the DRAM cells. Currently, manufacturers make limited use of the logic layer and there is significant amount of area the logic layer can provide, especially when manufactured with a high-quality logic fabrication process. This presents a promising opportunity for architects to implement new and efficient PIM logic in the available area of the logic layer. We can potentially add a wide range of computational logic (e.g., general-purpose cores [13, 56, 265, 273, 282, 287, 288, 615], accelerators [14, 21, 263, 266–268, 272, 277, 279, 281, 291, 616], reconfigurable logic [237, 264], special-purpose functional units [13, 57, 154, 156, 283, 284], or a combination of different such types of logic) in the logic layer, as long as the added logic meets area, energy, and thermal dissipation constraints, which are important and potentially limiting constraints in 3D-stacked systems [13, 56]. Second, PIM logic can be added near memory banks by leveraging DRAM manufacturing processes that support mixing logic and memory [6, 239, 241, 242, 245, 283, 284]. The main drawbacks of integrating PIM logic inside the memory chip are high manufacturing costs, limited area budget inside 3D-stacked memories, and difficulties tight to thermal dissipation.

¹Logic layer(s) in monolithic 3D architectures can also be added *between* memory layers [613, 614].

2.2.2 Early PIM Proposals

PIM is not a new idea: the first works that foresaw the need to bring computation closer to memory dates from 1969 [617] and 1970 [420]. In the 70s and 80s, many works [618–632] investigate the implementation of PIM architectures using different memory technologies (e.g., hard disks, content-addressable memories) for key applications (e.g., databases, production systems, computer vision, knowledge base management) and kernels (e.g., sorting) at the time. In the 1990s, another wave of works [252, 253, 258, 259, 421, 633–638] focused on exploiting the difference between internal and external bandwidth in DDRx memories with PNM by integrating computational modules in the same PCB as DRAM chips. However, these early PNM works were not adopted into real systems in part due to the challenges of manufacturing logic and memory (particularly DRAM) into a single, high-performance, and high-area-efficient chip [639, 640].

2.2.3 Major Trends Affecting Main Memory & PIM Resurgence

Recently, PIM (particularly PNM) has seen a resurgence due to three main reasons. First, due to the maturation of 3D manufacturing and advances in the CMOS manufacturing process, integrating memory and computation is now possible [56, 424, 425, 596, 597, 600, 641–643] and becoming increasingly effective and cheaper with better packaging, technology nodes, and integration. Second, data movement has become a very large cause of performance and energy bottleneck in today’s systems [7–53] due to a combination of factors. (i) From a *technology point of view*, the memory subsystem has long been optimized *primarily* for cost per bit and capacity. However, memory access latency has remained almost constant over the past two decades (i.e., main memory access latency, measured by the row cycling time [161, 172], reduced by only 30%) [171, 508], making it a significant performance and energy bottleneck for many modern workloads. As low-latency computing is becoming ever more important [7–9, 20, 21, 278, 644–647], e.g., due to the ever-increasing need to process large amounts of data at real time, and predictable performance continues to be a critical concern in the design of modern computing systems [8, 165, 648–657], it is increasingly important to design low-latency main memory chips. (ii) From the *application point of view*, the growing data working set sizes of modern applications [7–15, 658–662] impose an ever-increasing demand for higher main memory capacity and performance. For example, memory capacity requirements of large machine learning models increased by more than 10,000 times in the past five years [37]. Unfortunately, DRAM technology scaling is becoming increasingly challenging: it is increasingly difficult to enlarge DRAM chip capacity at low cost while also maintaining DRAM performance, energy efficiency, and reliability [1, 7–24, 26–53, 151, 158–194, 497, 503, 535, 538, 663, 664].

Third, main memory (i.e., DRAM) technology scaling to smaller nodes adversely affects DRAM reliability and robustness. For a DRAM cell to operate correctly, both the capacitor and the access transistor (as well as the peripheral circuitry) need to operate reliably. As the size of the DRAM cell reduces, both the capacitor and the access transistor become less reliable, more leaky, and generally more vulnerable to electrical noise and disturbance. As a result, reducing the size of the DRAM cell increases the difficulty of correctly storing and detecting the desired original value in the DRAM, as shown in various recent works that study DRAM reliability by analyzing data retention and other reliability issues of modern DRAM chips cell [7, 160, 163, 164, 178, 180, 181, 184, 185, 190–194, 222, 497, 503, 535, 538, 586–592, 663, 665]. Hence, memory technology scaling causes memory errors to appear more frequently, even leading to new robustness-related (including security and safety problems) vulnerabilities. For instance, many works demonstrated that the *read disturbance* phenomenon in DRAM can be exploited to cause security and safety problems that enable attackers to take over a system [503, 543, 666–682], read data they do *not* have access to [503, 668, 671, 673, 683–689], break out of virtual machine sandboxes [690, 691], corrupt important data (even rendering machine learning inference useless) [160, 503, 538, 665, 671, 680, 690, 692–699], steal secret data (e.g., cryptographic keys [503, 583, 668, 683–687, 690, 700–707] and steal or alter machine learning model parameters [693, 694, 708–715]).

In summary, the resurgence of PIM is fueled by three fundamental and converging trends: (i) the increasing feasibility and affordability of memory–compute integration enabled by advances in 3D integration and CMOS scaling, (ii) the growing inefficiency and cost of data movement driven by stagnant memory latency and rapidly expanding application data demands, and (iii) the declining reliability and security of DRAM due to aggressive technology scaling. These trends expose the *fundamental* limitations of traditional processor-centric architectures and motivate a paradigm shift toward architectures that minimize data movement, improve energy efficiency, and enhance system robustness. PIM is a promising direction to overcome these limitations by enabling computation capability close to or within memory, thereby directly addressing the key bottlenecks in performance, energy, scalability, and reliability faced by modern processor-centric systems.

2.2.4 Real-World PIM Architectures

In this section, we describe several DRAM-based real-world PIM architectures that have been introduced by industry in recent years. First, we provide details on the general-purpose UP-MEM PIM architecture, which we use as a baseline PIM architecture in Chapter 7. Second, we briefly describe several application-specific PIM architectures introduced by Samsung, SK hynix, and Alibaba.

2.2.4.1. General-Purpose Real-World PIM Architecture: The UPMEM PIM

In 2019, UPMEM introduced UPMEM PIM [6, 241, 474–476], the first real-world general-purpose PIM architecture that is commercially available. Figure 2.3 illustrates the main components of a UPMEM-enabled system [6, 241, 474–476]. An UPMEM-enabled system consists of a host CPU (Figure 2.3a) equipped with regular DRAM as its main memory (Figure 2.3b) and specialized UPMEM DRAM dual in-line memory modules (DIMMs) (PIM-enabled memory in Figure 2.3c). An UPMEM module is a standard DDR4-2400 DIMM (module) with 8 (1-rank) or 16 (2-rank) PIM chips. Inside each UPMEM PIM chip (Figure 2.3d), there are 8 small general-purpose in-order *PIM cores*, called *DPUs*. Each DPU is placed next to a DRAM bank. Each DPU is fine-grained multithreaded. Each DPU (Figure 2.3e) has exclusive access to (i) a 64 MB DRAM bank, called *MRAM*; (ii) a 24 kB instruction memory, called *IRAM*; and (iii) a 64 kB scratchpad memory, called *WRAM*. The PIM cores in an UPMEM system operate at 450 MHz and feature a 14-stage pipeline, enabling them to execute one integer addition or subtraction per cycle. Integer multiplication and division require up to 32 cycles when the pipeline is fully utilized. However, floating-point operations incur significantly higher latencies, ranging from tens to 2,000 cycles [476] because they are emulated in software due to the lack of native hardware support in DPUs. A standard UPMEM-based PIM system is composed of 20 UPMEM DIMMs, thus containing up to 2,560 DPUs and 160 GB of PIM-capable memory, achieving a peak compute throughput exceeding 1 TOPS.

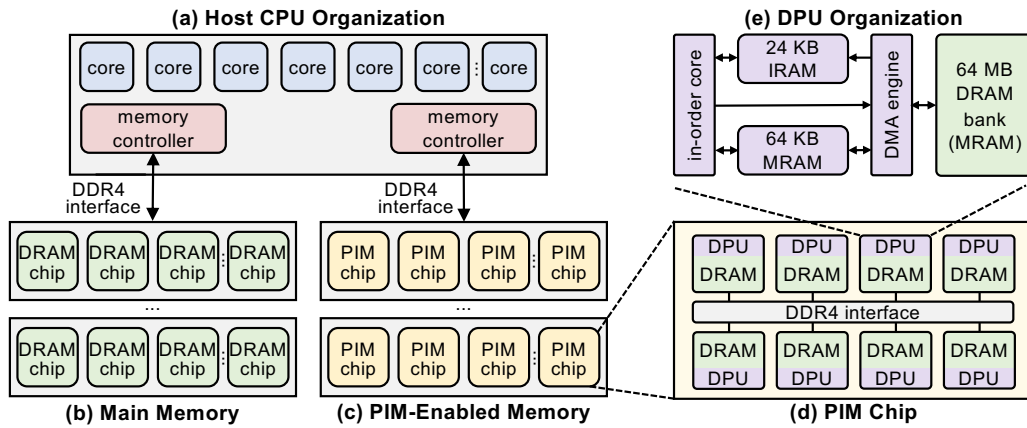


Figure 2.3: UPMEM system organization.

Gómez-Luna *et al.* [6, 241, 476] have conducted the first experimental characterization of the UPMEM PIM system. First, they implement and deploy various microbenchmarks to assess the microarchitectural limitations (such as compute throughput, memory bandwidth) and potential benefits of the UPMEM PIM system. All these works demonstrate that the UPMEM PIM system can provide substantial performance improvements compared to processor-centric architectures when executing such workloads. We highlight three key new insights from their

analyses. (i) The UPMEM PIM architecture is *fundamentally compute bound*. As a result, the most suitable workloads are memory-bound in processor-centric systems (i.e., CPU, GPU). (ii) The most well-suited workloads for the UPMEM PIM architecture use *no arithmetic operations* or use *only simple operations* (e.g., bitwise operations and integer addition/subtraction). The primary reason is that each DPU in the UPMEM PIM system is a very lightweight processor, featuring native hardware support *only* for 32-bit integer addition/subtraction and 8-bit multiplication while emulating the implementation of complex (e.g., 32-bit integer multiplication/division) and floating-point operations. (iii) The most well-suited workloads for the UPMEM PIM architecture require *little or no communication across DPUs*. This is due to the fact that there is *no* direct inter-DPU communication mechanism in the current UPMEM PIM system; instead, all communication between PIM cores occurs through memory transfers between host main memory and PIM-enabled memory. Second, Gómez-Luna *et al.* present the *PrIM* benchmarks (*Processing-In-Memory benchmarks*) [479], a benchmark suite of 16 workloads from different application domains (e.g., dense/sparse linear algebra, databases, data analytics, graph processing, neural networks, bioinformatics, image processing) targeting the UPMEM PIM system. Their experimental evaluation results show that the UPMEM PIM systems outperform modern CPUs in terms of performance and energy efficiency on most of *PrIM* benchmarks and outperform modern GPUs on a majority (10 out of 16) of *PrIM* benchmarks.

Many recent works [247, 392, 394, 437, 716–735] have explored in depth the suitability of the UPMEM PIM system for important application domains, including bioinformatics workloads (e.g., RNA-seq qualification [723], variant calling [724], BLAST [725]), analytics & databases [726–731], image processing [732], and machine learning (ML) workloads (e.g., deep neural networks [733] and recommendation models [734]). To illustrate, we briefly discuss some of such works below. First, [247] introduces *SparseP* [717], the first sparse matrix-vector multiplication (SpMV) library for real PIM architectures, which covers a wide variety of sparse matrices with diverse sparsity patterns. Second, [394] (i) evaluates the suitability of the UPMEM PIM system to accelerate sequence alignment algorithms (such as *Needleman-Wunsch* [736], *Smith-Waterman-Gotoh* [737], GenASM [21], and *wavefront algorithm* [738]) and (ii) introduces a framework for PIM-based sequence alignment, called *Alignment-in-Memory (AiM)* [719], where the host CPU dispatches sequence pairs across the DPUs available in the UPMEM PIM system.

Third, works such as [392, 437, 720–722] comprehensively study the potential of the UPMEM PIM architecture to accelerate ML training. (i) [392, 720] implements and optimizes several representative classical ML algorithms (namely, linear regression [739, 740], logistic regression [741], decision tree [742], k-means clustering [743, 744]) on the UPMEM PIM system. (ii) [721] proposes *PIM-Opt*, where the authors implement, optimize, and rigorously evaluate

12 representative distributed stochastic gradient algorithms [745] on a real-world PIM architecture. (iii) [437] proposes *PyGim*, a software library that efficiently maps graph neural networks [746–749] to the UPMEM PIM system. (iv) [722] proposes *SwiftRL*, which accelerates reinforcement learning [750] algorithms and their training phases on the UPMEM PIM system.

Some other works [751–754] propose improvements over the UPMEM PIM system, focusing especially on benchmarking and communication mechanisms between processing units.

2.2.4.2 Application-Specific Real-World PIM Architectures

Samsung Function-In-Memory DRAM (FIMDRAM). In 2021, Samsung introduced FIMDRAM [283, 284, 399] (also known as HBM-PIM [284] or Aquabolt-XL [399]), a PNM architecture targeted for accelerating matrix multiplication operations, commonly used during machine learning inference. FIMDRAM embeds one 16-bit floating-point SIMD unit with 16 lanes, called *Programmable Compute Unit (PCU)*, next to two DRAM banks in HBM2 layers [597]. Each PCU supports a small instruction set (FP16 add, multiply, multiply-accumulate, multiply-and-add). In 2023, Samsung introduced two main extensions of the FIMDRAM architecture [400] targeting generative artificial intelligence (AI) [755–757] applications, e.g., large language models (LLMs) such as GPT-4 [758], GPT-J [759], T5 [760], BERT [761, 762], and Llama-2 [763]. The extended architectures are: (i) LPDDR-PIM, which adds FIMDRAM’s PCU to LPDDR_x [764] memories and targets on-device generative AI inference, and (ii) CXL-PNM, which adds PNM engines to the compute express link (CXL) [765] memory expander.

Samsung CXL-PNM. Samsung presented two different implementations of their CXL-PNM architecture [397, 400]. The first architecture adds PNM engines to the CXL controller [765], while the second architecture adds PNM engines (similar to the FIMDRAM architecture) to the memory chip itself [400]. The PNM engines are composed of a processing element (PE) array (targeting the acceleration of general matrix multiplication operations) and an adder tree (targeting the acceleration of general matrix vector multiplication operations). The CXL-PNM architecture can provide a capacity of 512 GB and a memory bandwidth of 1.1 TB/s. Samsung provides further details on their CXL-PNM architecture in their HPCA 2024 paper [397], where they describe their current realization of the CXL-PNM architecture using LPDDR5X-based CXL memory. The paper shows that the proposed architecture (equipped with eight CXL-PNM devices) achieves 23% lower latency, 31% higher throughput, and 2.8× higher energy efficiency at 30% lower hardware cost compared to a modern GPU-based architecture (with eight A100 NVIDIA GPUs [459]) on LLM inference tasks.

Samsung Acceleration DIMM (AxDIMM). AxDIMM [246, 398, 399], also from Samsung, is a DIMM-based solution which places an field-programmable gate array (FPGA) fabric in the

buffer chip of registered DIMMs (RDIMMs). A RDIMM [766–768] is a commonly used DRAM module architecture in server-class systems, where extra buffer chips are added to the DRAM module to decouple I/O signals, improving signal integrity and scalability. This enables scaling the RDIMM DRAM devices to higher memory capacities and frequencies compared to unbuffered DIMMs [769]. Several prior works [246, 251, 256, 398, 399, 595, 770–795], including AxDIMM, augment the buffer chip with computation in order to implement PNM architectures, without modifying the DRAM interface. AxDIMM has been tested for deep learning recommendation model (DLRM) inference [246, 796] and for database operations [398]. In the context of DLRM acceleration [246] inference, AxDIMM offloads the execution of sparse embedding computations (particularly the element-wise summation of multiple embedding table entries), since embedding operations are a major performance bottleneck in DLRMs [246, 595, 797]. AxDIMM implements two near-memory accelerators (one per rank) within the FPGA, which operate in parallel to perform the summation, thus reducing data movement and improving inference throughput by up to $1.5\times$ that of the baseline CPU.

Accelerator-in-Memory (AiM). Another major DRAM vendor, SK hynix, introduced their own PNM called Accelerator-in-Memory (AiM) [245], a GDDR6 [798] PIM architecture with specialized units for multiply-and-accumulate and lookup-table-based activation functions for deep learning applications. In AiM, next to each DRAM bank in a DRAM chip, there is a *processing unit (PU)* that is composed of an array of 16 16-bit floating-point multipliers, an adder tree, an accumulator, and the necessary logic for activation functions. The chip also adds in the peripheral circuitry of each DRAM bank a 2 kB SRAM buffer, called *global buffer (GB)*, which can store input vectors or serve as an intermediate buffer for copy operations between DRAM banks. This inter-bank copy operation is a limited form of a RowClone-like operation [317] (which we describe next in Section 2.2.5).

SK hynix CXL-Memory Solution (CMS). SK hynix later introduced a CXL [765]-based PIM architecture, called CXL-memory solution (CMS) [401]. The CMS architecture [401] comprises of a CXL controller, internal DDR4 memory chips, a custom load balancer, and a PIM engine tailored for k-nearest neighbors (kNN) execution. CMS has been prototyped using a Xilinx Alveo U250 FPGA board [799]. The custom load balancer is designed to, transparently from the host CPU, maximize memory bandwidth utilization by interleaving data across each channel at multiples of the DDR access granularity (i.e., 64 B). The PIM engine comprises of three custom logic units (i.e., dot product, kNN calculator, and top-K unit) targeting the acceleration of kNN application kernels. Their experimental results show that the CMS architecture achieves up to $1.9\times$ the performance/power of the baseline CPU system.

Alibaba Logic-to-DRAM Hybrid Bonding with PNM (HB-PNM). Alibaba presented HB-

PNM [285], a PNM system with specialized engines for recommendation systems, which is composed of a DRAM die and a logic die vertically integrated via hybrid bonding (HB) [612]. The DRAM die contains 36 1 Gbit DRAM cores (organized in a 6×6 2D-array of DRAM cores) with 8 banks each. The logic die contains multiple processing elements called *match* and *neural engines* that perform, respectively, matching and ranking in a recommendation system. HB-PNM achieves $9.78\times$ the throughput and $317.43\times$ the energy efficiency of the baseline CPU.

2.2.5 DRAM-Based PUM Architectures

In-DRAM-Row Copy. RowClone [317] enables copying a row A to a row B in the *same* subarray by issuing two consecutive ACT commands to these two rows, followed by a PRE command. This command sequence is called AAP [314] (ACT-ACT-PRE). The first ACT copies the contents of the source row A into the local row buffer. The second ACT connects the DRAM cells in the destination row B to the local bitlines. Because the sense amplifiers have already sensed and amplified the source data by the time row B is activated, the data in each cell of row B is overwritten by the data stored in the row buffer (i.e., row A 's data). LISA [377] expands RowClone functionally to enable the execution of in-DRAM row copy operations across DRAM rows in *different* subarrays of a DRAM chip by connecting local row buffers of neighbors subarrays using isolation transistors. Recent works [323,343] experimentally demonstrate the feasibility of executing in-DRAM row copy operations in unmodified off-the-shelf DRAM chips.

In-DRAM Data Relocation. FIGARO [800] is a mechanism that enables data relocation in DRAM. It is built upon the key observation that the local row buffers inside a subarray in a bank are connected to a single shared global row buffer. FIGARO takes advantage of this connectivity to perform column-granularity data relocation across subarray without using the off-chip memory channel. To relocate data, FIGARO introduces a new DRAM command called RELOC (*relocate column*). The RELOC command moves a column A (i.e., 64 B data) stored in subarray S_A to another column B stored in subarray S_B by: (i) activating the DRAM row that contains column A in S_A , which latches the DRAM row to subarray S_A 's local row buffer; (ii) selecting column A from subarray S_A 's local row buffer, which loads the column into the global row buffer; (iii) simultaneously connecting the global row buffer to subarray S_B using subarray's S_B 's column decoder, which effectively places column A from subarray S_A into column B of subarray S_B ; (iv) activating subarray S_B , which overwrites column B in the activated row with column A , since the global row buffer has a higher drive strength of the local row buffer [800,801]; and (v) precharging the entire bank for future accesses.

In-DRAM AND/OR/NOT. Ambit [314,315,318,327,328,330] shows that simultaneously activating *three* DRAM rows, via a DRAM operation called *triple row activation* (TRA), can perform

in-DRAM bitwise AND and OR operations. Upon sensing the perturbation of the three simultaneously activated rows, the sense amplifier amplifies the local bitline voltage to V_{DD} or 0 if at least two of the capacitors of the three DRAM cells are charged or discharged, respectively. As such, a TRA results in a Boolean majority operation (*MAJ*). A majority operation *MAJ* outputs a 1 (0) only if more than half of its inputs are 1 (0). In terms of AND (\cdot) and OR ($+$) operations, a 3-input majority operation can be expressed as $MAJ(A, B, C) = A \cdot B + A \cdot C + B \cdot C$. To achieve functional completeness, Ambit implements NOT operations by exploiting the differential design of DRAM sense amplifiers. As Section 2.1 explains, the sense amplifier already generates the complement of the sensed value as part of the activation process. Therefore, Ambit simply forwards the complement of the sensed value to a special DRAM row in the subarray that consists of DRAM cells with *two* access transistors, called *dual-contact cells* (DCCs). Each access transistor is connected to one side of the sense amplifier and is controlled by a separate wordline (*d-wordline* or *n-wordline*). By activating either the d-wordline or the n-wordline, the row of DCCs can provide the true or negated value stored in the row's cells, respectively. Ambit defines a new command called AP that issues a TRA to compute a *MAJ*, followed by a PRE to close all three rows.² Since TRA operations are destructive, Ambit divides DRAM rows into *three groups* for PUD computing: (i) the **Data** group, which contains regular data rows; (ii) the **Control** group, which consists of two rows (C0 and C1) with all-0 and all-1 values; and (iii) the **Bitwise** group, which contains six rows designated for computation (four regular rows, T0, T1, T2, T3; and two rows, DCC0 and DCC1, of dual-contact cells for NOT). The B-group rows are designated to perform bitwise operations. They are all connected to a special local row decoder that can simultaneously activate three rows using a single address (i.e., perform a TRA).

Generalizing In-DRAM Majority. SIMD RAM [378] proposes a three-step framework to implement PUD operations. In the first step, SIMD RAM converts an AND/OR/NOT-based representation of the desired operation into an equivalent optimized MAJ/NOT-based representation. By doing so, SIMD RAM reduces the number of TRA operations required to implement the operation. In the second step, SIMD RAM generates the required sequence of DRAM commands to execute the desired operation. Specifically, this step translates the MAJ/NOT-based implementation of the operation into AAPs/APs. This step involves (i) allocating the designated compute rows in DRAM to the operands and (ii) determining the optimized sequence of AAPs/APs that are required to perform the operation. This step's output is a μ Program, i.e., the optimized sequence of AAPs/APs that will be used to execute the operation at runtime. Each

²Although the 'A' in AP refers to a TRA operation instead of a conventional ACT, we use this terminology to remain consistent with the Ambit paper [314], since an ACT can be internally translated to a TRA operation by the DRAM chip [314].

μ Program corresponds to a different *bbop* instruction, which is one of the CPU ISA extensions to allow programs to interact with the SIMDRAM framework. In the third step, SIMDRAM uses a control unit in the memory controller to execute the *bbop* instruction using the corresponding μ Program. SIMDRAM implements 16 *bbop* instructions, including *abs*, *add*, *bitcount*, *div*, *max*, *min*, *mult*, *ReLU*, *sub*, and *-/or-/xor-reduction*, *equal*, *greater*, *greater equal*, and *if-else*.

Figure 2.4 illustrates how SIMDRAM executes a one-bit full addition operation using the sequence of row copy (AAP) and majority (AP) operations in DRAM. The figure shows one iteration of the full adder computation that computes $Y_0 = A_0 + B_0 + C_{in}$.

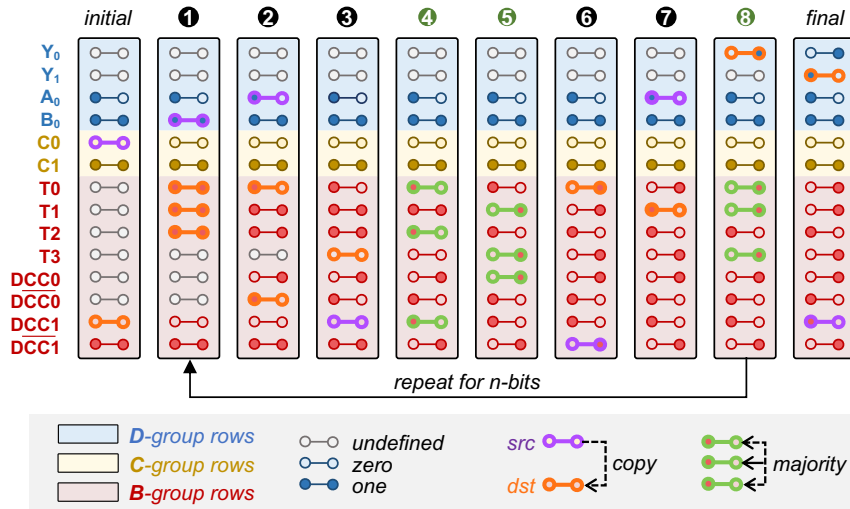


Figure 2.4: Full adder operation in SIMDRAM.

First, SIMDRAM uses a *vertical* data layout, where all bits of a data element are placed in a single DRAM column when performing PUD computation. Consequently, SIMDRAM employs a *bulk bit-serial SIMD* execution model, where each data element is mapped to a column of a DRAM row. This allows a DRAM subarray to operate as a *PUD SIMD engine*, where a single bit-serial operation is performed over a large number of independent data elements (i.e., as many data elements as the size of a logical DRAM row, for example, 65,536) at once. Second, as shown in the figure, each iteration of the full adder requires five AAPs (1, 2, 3, 6, 7) and three APs (4, 5, 8). A bit-serial addition of n -bit operands needs n iterations, thus $(8n + 2)$ APs and AAPs [378].

Chapter 3

Related Work

This chapter provides an overview of the broader literature related to PIM architectures. First, in Section 3.1, we give an overview of the design space of PNM architectures. Second, in Section 3.2, we discuss the implementation of PUM using various memory technologies, including SRAM (Section 3.2.1), DRAM (Section 3.2.2), NVM (Section 3.2.3), and flash (Section 3.2.4). Third, in Section 3.3, we discuss closely related works that aim to address system challenges for PIM architectures, including (i) workload characterization & benchmark suites (Section 3.3.1), (ii) application suitability (Section 3.3.2), (iii) compiler support (Section 3.3.3), (iv) memory management (Section 3.3.4), and (v) programming frameworks & high-level APIs (Section 3.3.4).

3.1 Processing-Near-Memory (PNM) Architectures

PNM architectures integrates computation capabilities (via accelerators, simple processing cores, reconfigurable logic, for example) closer to memory (either within the memory chips themselves or in close physical proximity) [6, 13, 14, 21, 56, 57, 150, 154–157, 237–311, 382]. Despite this physical proximity, PIM logic and memory elements in a PNM architecture typically maintain a logical and architectural separation, allowing the memory to retain its main role as a storage substrate and the PIM logic to be designed independently to match specific performance, area, and energy targets. As a result, PNM exposes a broad design space in which compute and memory can be co-designed but still optimized separately. Hence, the PNM design space can be systematically described along three key dimensions: (i) *memory technology*, i.e., the memory technology (e.g., SRAM, DRAM, flash, disk) with which the logic is integrated; (ii) *offloading granularity*, i.e., the granularity of computation offloaded from the host processor to near-memory logic (e.g., a single instruction, an application kernel, or an entire application); and (iii) *computation type*, i.e., the nature of the PIM logic embedded near or within the

memory arrays (e.g., general-purpose, fixed-function unit, or specialized accelerator). Next, we briefly describe how each one of these dimensions impacts the design of PNM architectures.

Memory Technology. PNM systems have been explored across a spectrum of memory technologies, including SRAM (e.g., [250, 261, 374, 802–811]), DRAM (e.g., [6, 13, 14, 21, 56, 57, 150, 154–156, 237–239, 241–249, 251–256, 259, 260, 262–268, 271–275, 277–294, 296–311, 352]), and non-volatile memories, including NAND flash [44, 812–836] and magnetic disks [636, 837–839]. The choice of memory technology for PNM is heavily influenced by the characteristics of the target application (e.g., the degree of spatial and temporal locality, data reuse, and memory footprint). These characteristics determine not only the suitability of a memory technology in terms of capacity and performance, but also the feasibility and efficiency of performing computation near it. Moreover, since PNM logic operates within or near the memory hierarchy, it is subject to the latency and energy-per-access constraints of the underlying memory substrate. For instance, SRAM provides fast and energy-efficient access, but its low density and high leakage make it less suitable for large-scale data processing. In contrast, DRAM and NAND flash offer higher storage densities but exhibit higher access latencies and energy costs, with additional constraints imposed by their respective manufacturing processes.

The feasibility of manufacturing PNM logic is closely tied to the fabrication process used for the target memory technology. For example, integrating logic near SRAM arrays is relatively straightforward, as both memory and logic can be fabricated using standard CMOS processes, enabling tight integration without requiring process specialization. Similarly, NAND flash systems already incorporate logic, such as simple programmable microcontrollers, for purposes such as wear leveling, garbage collection, and address translation [840–851]. PNM systems targeting NAND flash often repurpose these existing controllers for specialized data processing tasks, such as filtering [240, 821, 822] or aggregation [852, 853], thus avoiding the need for major fabrication changes.

In contrast, integrating PIM logic with DRAM presents significant challenges due to DRAM’s specialized manufacturing process targeting high-density and low cost. Logic transistors fabricated in a DRAM process suffer from limited performance due to thicker gate oxides, longer channel lengths, and lower drive strengths, making them less energy-efficient and slower than transistors fabricated in standard logic processes [639]. In addition, DRAM chips are built with a limited number of metal layers, which significantly constrains the area available for interconnect and limits the complexity of the logic that can be integrated [239]. Thermal constraints are also critical, as DRAM is sensitive to temperature increases that can affect data retention times and increase refresh frequency [163, 180, 497, 587, 854], thereby further complicating logic integration. These limitations impose tight area and power budgets on

any logic embedded directly within DRAM die. To address these integration barriers, recent advances in 3D integration technologies, such as HBM [424, 597] and HMC [423, 600, 642], enable the stacking of logic and memory dies using Through-Silicon Vias (TSVs) and hybrid bonding techniques [612]. These approaches allow logic to be fabricated in a more suitable process node, separate from the DRAM die, while maintaining high-bandwidth, low-latency connectivity between logic and memory. By partially decoupling the conflicting fabrication constraints of logic and memory, these integration techniques provide a practical path forward for building more capable PNM systems, especially for DRAM-based architectures.

Offloading Granularity. PNM systems can vary in terms of their offloading granularity, i.e., in the granularity with which computation is offloaded to PIM logic. At the finest granularity, PNM systems that implement *instruction-level offloading* (e.g., [57, 154, 258, 300, 310, 442, 855–861]) allow the execution of individual instructions or fine-grained operations directly within memory. This fine-grained approach can have significant benefits in terms of potential adoption, since existing processor-centric execution models already operate (i.e., perform computation) at the granularity of individual instructions, and all such machinery can be reused to aid offloading to be as seamless as possible with existing programming models and system mechanisms (such as data coherency). For example, the authors of [57] propose *PIM-Enabled Instructions* (PEI), a collection of simple instructions, generated by the compiler or programmer to indicate potentially PIM-offloadable operations in the program, that can be executed either on a traditional host CPU (that fetches and decodes them) or on the PIM logic in 3D-stacked memory. PEI simplifies system integration by defining PIM instructions that are cache-coherent, virtually addressed by the host processor, and operate on only a single cache block. It requires no changes to the sequential execution and programming model, no changes to virtual memory, minimal changes to cache coherence, and no need for special data mapping to take advantage of PIM (because each PEI is restricted to a single memory module due to the single cache block restriction it has). Such system-level simplifications allow PEI to implement a *locality-aware execution* runtime mechanism that dynamically decides where to execute a PEI (that is, the host processor or PIM logic) based on simple locality characteristics and simple hardware predictors. This runtime mechanism executes the PEI at the location that maximizes performance. In summary, PIM-Enabled Instructions provide the illusion that PIM operations are executed as if they were host instructions: the programmer may not even be aware that the code is executing on a PIM-capable system, and the exact same program containing PEIs can be executed on conventional systems that do not implement PIM. Other works [154, 300, 310, 442, 856, 860, 861] built on top of the HMC 2.0 architecture [423], which implements a fixed set of atomic-like near-memory instructions that perform simple read-

modify-write operations close to memory. Despite its simplicity and coherence advantages, instruction-level offloading often incurs increased traffic between the host CPU and PIM logic due to the fine granularity of the offloaded instructions and associated control metadata.

At a coarser level, PNM systems that implement *function-level offloading* (e.g., [13, 14, 21, 156, 244, 277, 281, 288, 301, 405, 595, 862–871]) move portions of an application (e.g., an application function) to PIM logic. This design can better partition the compute load, allowing the host CPU to focus on compute-intensive tasks while the PIM logic accelerates data-intensive operations, thereby reducing instruction traffic between the CPU and memory. However, function-level offloading introduces two key challenges in system integration. First, determining the *appropriate granularity* for function-level offloading is non-trivial, since the semantic definition of a function in software does *not* always align with uniform execution characteristics (i.e., a single software-defined function may interleave memory-bound and compute-bound regions). This issue can be addressed in two primary ways. In the first way, the programmer can *manually* identify memory-bound functions by performing application profiling during development and then selectively transfer them to PIM. This methodology is widely used in the literature [13, 14, 21, 156, 244, 277, 281, 288, 301, 405, 595, 862–871]. For example, the authors of [13] manually profile key consumer workloads (i.e., Chrome web browser [872], TensorFlow Mobile [873], video playback [874], and video capturing [875]) and identify memory-bound kernels (such as texture tiling, color blitting, and page compression/decompression in Chrome web browser; quantization and packing in TensorFlow Mobile; and sub-pixel interpolation, deblocking filter, motion estimation in video playback/capturing) as suitable offloading targets. In bioinformatics workloads, prior works such as GRIM-Filter [156, 301] target memory-intensive bitmap filtering operations in sequence alignment, while GenASM [21] accelerates the memory-bound dynamic programming steps in genome assembly. These works demonstrate that coupled static profiling is effective in identifying offloadable units of computation in various application domains. Second, an alternative approach is to use dynamic profiling and segmentation, in which the system itself analyzes runtime behavior to automatically partition code into offloadable segments.

In the second way, compiler and/or hardware runtime mechanisms aim to identify group of instructions belonging to high-level software constructs (e.g., loops, software-defined functions, warps) that can be suitable for PIM offloading [272, 855, 876–883]. For example, TOM (Transparent Offloading and Mapping) [272] introduces new compiler analysis techniques to identify code blocks (in the *wrap* granularity) in GPU kernels that can benefit from offloading to PIM engines. The compiler estimates the potential memory bandwidth savings for each code block. To this end, the compiler compares the bandwidth consumption of the code block, when executed on the regular GPU cores, to the bandwidth cost of transmitting/receiving input/out-

put registers, when offloading to the GPU cores in the logic layer of a 3D-stacked memory. At runtime, a final offloading decision is made based on dynamic system conditions, such as contention for processing resources in the logic layer. Another work, ALP [876], addresses this by introducing the notion of *segments* (a sequence of instructions), and different segments can execute either in CPU cores or PIM cores. Such an execution model introduces inter-segment data movement overhead [884, 885], i.e., performance and energy overheads due to the cost of moving data between segments of an application that executes in different types of hardware (i.e., CPU cores and PIM cores). ALP alleviates the inter-segment data movement overhead by *proactively and accurately* transferring the required data between the segments mapped onto CPU cores and PIM cores. ALP uses a compiler pass to identify these instructions and uses specialized hardware support to transfer data between the CPU cores and PIM cores at runtime. Using both the compiler and runtime information, ALP efficiently maps application segments to either CPU or PIM cores.

Second, maintaining coherence between PIM logic and host CPU during function-level execution is challenging due to the longer-lived and more stateful nature of offloaded functions. Traditional coherence protocols, such as MESI [886, 887], often impose high overhead when applied to PIM systems [262, 302, 615]. To mitigate this, mechanisms such as CoNDA [615] and LazyPIM [262, 302] propose lazy coherence approaches that allow the speculative execution of offloaded kernels without immediate coherence enforcement. ConDA defers coherence validation until the end of the execution of the offloaded function, reducing coherence-related delays and synchronization overhead. Such designs strike a balance between correctness and performance by ensuring that coherence violations are detected and resolved in a deferred, lightweight manner.

In summary, function-level offloading provides significant performance and energy benefits while amortizing the offloading cost introduced by instruction-level offloading. As expected, the benefits are not as high as full offloading and customization of the application level PNM system, as we discuss next. This is expected since function-level offloading makes much fewer changes to the system and the programming model than application-level offloading, customization, and rethinking of the system. As such, function-level offloading is likely easier to adopt in the short-term for a wide variety of workloads and systems.

At the coarsest granularity, PNM that implement *application-level offloading* (e.g., [56, 281, 293, 303, 304, 888, 889]) delegates the execution of entire applications to dedicated PIM cores. In such approach, an entire application is re-written to completely execute on the PNM substrate, potentially using a specialized programming model and specialized architecture/hardware. This approach is especially promising because it can provide the maximum performance and energy benefits achievable from PNM acceleration of a given application, since it enables the

customization of the *entire* PNM system for the application. This approach can be especially promising for widely-used data-intensive applications, such as machine learning (including neural networks and large language models), databases, graph analytics, genome analysis, high-performance computing, security, data manipulation, and a wide variety of mobile and server-class workloads.

Tesseract [56,888] exemplifies this model by running entire graph applications directly on memory-side processors, with host CPUs serving primarily as orchestrators. Tesseract adopts a message-passing programming model that obviates the need for conventional cache coherence by decoupling PIM cores from the host memory hierarchy. Tesseract consists of (i) new hardware architecture that effectively utilizes the available memory bandwidth in 3D-stacked memory by placing simple in-order processing cores in the logic layer and enabling each core to manipulate data only on the memory partition it is assigned to control, (ii) an efficient method of communication between different in-order cores within a 3D-stacked memory to enable each core to request computation on data elements that reside in the memory partition controlled by another core, and (iii) a message-passing based programming interface, similar to how modern distributed systems are programmed, which enables remote function calls on data that resides in each memory partition. The Tesseract design moves functions (i.e., computations and temporary values) to data that is to be updated rather than moving data elements across different memory partitions and cores. It also includes two hardware prefetchers specialized for memory access patterns of graph processing, which operate based on the hints provided by our programming model.

Using the Tesseract-based PNM approach to accelerate graph processing can lead to more than two orders of magnitude improvements both in performance and in energy efficiency compared to a conventional processor-centric system with high bandwidth memory. This demonstrates the potential promise of designing an entire PNM system completely from the ground up for important data-intensive applications.

However, application-level offloading comes with its own challenges, most notably underutilization of system resources when the workload’s memory access patterns or compute phases do not map cleanly to the PIM cores. Moreover, this model often requires re-architecting applications for the PIM execution environment, making it less amenable to incremental adoption in general-purpose systems.

In summary, the choice of offloading granularity in PNM systems influences not only performance but also the complexity of system integration, programming models, and coherence mechanisms. While finer-grained offloading offers greater transparency and compatibility with existing software stacks, coarser-grained approaches provide higher potential performance gains but require deeper software and hardware co-design.

Computation Type. The nature of integrated near-memory compute logic ranges from fixed function accelerators [57, 245, 246, 266–268, 281, 284, 285, 398, 399, 595, 890] designed to support narrow, high-throughput operations (e.g., data copy, bitwise logic, vector operations) to general-purpose processor cores capable of executing arbitrary code [6, 56, 239, 247, 252, 263, 265, 287, 303, 306, 393, 474, 876, 891, 892]. Fixed-function designs typically offer higher energy efficiency and lower area cost, while general-purpose PNM cores provide programmability and flexibility, often at the cost of increased design and runtime complexity. Some designs employ a hybrid model that combines programmable engines with specialized accelerators to strike a balance between efficiency and generality [278].

A commonality across this diverse space is the higher data access efficiency that PNM logic enjoys relative to conventional off-chip compute units. By being co-located with memory, PNM logic can exploit higher bandwidth, lower latency, and lower energy per access, which is especially beneficial for data-intensive workloads. However, these benefits come at the cost of reduced memory density and increased system complexity, requiring careful hardware-software co-design.

3.2 Processing-Using-Memory (PUM) Architectures

Many prior works propose to leverage the operational principles of the memory circuitry to enable operations within memory arrays, hence implementing PUM architectures. Such works demonstrate that PUM is possible using different memory technologies, including (i) SRAM [324–326, 370], (ii) DRAM [314, 315, 317, 318, 327, 328, 330, 332, 343, 345, 377, 378, 893–895], (iii) emerging NVM (such as magnetoresistive random access memory (MRAM) [896–898], resistive random access memory (ReRAM) [313, 337, 338, 869, 899–910], and ferroelectric random access memory (FeRAM) [911–913]), and (iv) NAND flash [336, 353–364]. In summary, such PUM architectures enable a wide range of different functions, such as bulk as well as finer-grained data copy/initialization [317, 325, 343, 352, 377, 800, 895], bulk bitwise operations (e.g., a complete set of Boolean logic operations) [171, 185, 314–316, 320, 323, 325, 327, 330, 331, 343, 346, 896–898, 914, 915], simple arithmetic operations (e.g., addition, multiplication, implication) [313, 316, 319, 324–326, 345, 370, 899–908], and lookup table queries [332]. In this section, we provide an overview of PUM such architectures.

3.2.1 SRAM-Based PUM Architectures

SRAM arrays can be used to implement bitwise Boolean operations [324–326, 365–375, 916, 917]. Similarly to processing-using-DRAM (described in Section 2), a Boolean operation is realized by simultaneously activating multiple rows, specifically two rows containing the input operands and exploiting the parasitic bitline capacitance produced when sensing the produced

bitline voltage level. If *both* the activated rows store a logic-‘1’ value, the bitline voltage stays high and thus the sense amplifier senses ‘1’. However, if either one of the activated rows store a logic-‘0’ value, the bitline voltage goes below the reference sensing voltage V_{ref} , and the sense amplifier will sense a ‘0’. A similar process occurs when sensing the complementary bitline, i.e., the sense amplifier connecting the complementary bitline outputs ‘1’ *only* when both activated rows store a logic-‘0’ value. Therefore, a multiple row activation operation in SRAM array leads to the computation of logic AND and NOR operations.

One promising direction for SRAM-based PUM is to leverage the SRAM arrays already present in the cache hierarchy of modern computers for *in-situ* computation. We illustrate such an approach to SRAM-based PUM with three examples from recent scientific literature: (i) Compute Caches [325], (ii) Neural Cache [324], and (iii) Duality Cache [326]. Compute Caches [325] exploits the ability to implement bitwise Boolean operations in SRAM by turning the last-level cache (LLC) of a processor into an in-memory SIMD engine, where each bitline of SRAM subarray becomes a SIMD lane. It also extends the functionalities of SRAM-based PUM to other operations, including NOR, compare, search, copy, and carryless multiplication operations. Neural Cache [324] and Duality Cache [326] build on top of Compute Caches by implementing bit-serial arithmetic inside LLC slices. The Neural Cache architecture [324] targets accelerating neural network (NN) inference by re-purposing LLC slices into a SIMD engine capable of performing bit-serial arithmetic operations over integer or fixed-point data. Similar to SIMDRAM [378], Neural Cache stores and processes data vertically across the cache rows, with bits from multiple data elements distributed across different wordlines, allowing massive parallelism to be exploited: for example, a 35 MB LLC re-purposed as a bit-serial SIMD engine can execute an arithmetic operation over up to 1,146,880 1-bit input elements *simultaneously* while incurring only 2% area overhead when in computation mode [324].

Duality Cache [326] further enhances Neural Cache by targeting the execution of general-purpose data-parallel program in a Single Instruction Multiple Threads (SIMT) execution model. In Duality Cache’s execution model, an LLC slice is divided into (i) control blocks, each capable of executing 1,024 threads simultaneously; (ii) each control block is further subdivided into thread blocks; (iv) each thread block consists of 256 threads; and (v) each thread maps to a bitline in the cache slice. Each bitline in the cache slice represents a thread lane, with multiple threads executing the same bit-serial instruction *simultaneously*. Duality Cache further extends the computing capabilities of Compute Caches and Neural Cache by supporting floating-point and transcendental operations using bit-serial computation and CORDIC algorithms [918, 919] for functions such as sine and cosine.

SRAM-based PUM architectures are quite attractive solutions, since differently from DRAM-based and NVM-based PUM, they can be manufactured and tested using standard-

ized and commercially-available CMOS-based electronic design automation tools and library cells. However, the much lower density and much higher cost-per-bit of SRAM compared to DRAM and NVM are the major drawbacks of processing-using-SRAM architectures for two main reasons. First, they limit the applicability of SRAM-based PUM architectures to workloads with relatively small datasets that can fit within megabyte-sized SRAM arrays. Otherwise, the SRAM-based PUM architecture needs to bring data in/out the memory hierarchy, requiring extra data movement compared to DRAM and NVM-based PUM architectures. Second, they lead to a design that provides lower computation density. For example, while a 35 MB LLC can be deployed as a processing-using-cache SIMD engine with 1,146,880 SIMD lanes, an 8 GB DRAM chip deployed as a processing-using-DRAM SIMD engine has up to 67,108,864 SIMD lanes.¹

3.2.2 DRAM-Based PUM Architectures

Extending & Improving Bulk Bitwise In-DRAM Operations. Many works have extended Ambit’s approach to PUD to accelerate various application domains. GraphiDe [345] and [344] leverage quintuple-row activation (QRA) to implement in-DRAM addition operations. Even though such implementation is more performant than SIMDRAM’s TRA-based implementation for in-DRAM addition, [378] shows that TRA is more scalable and variation-tolerant than QRA operations. SpDRAM [920] proposes a framework for the implementation of SpMV operations using Ambit-style TRA operations. DrAcc [319] introduces subarray-level modifications to enable in-DRAM computation of ternary-weight neural network operations, particularly bitwise logic and accumulation. It extends Ambit’s architecture by repurposing one NOT row into a shift (SHF) row, enabling carry propagation essential for a carry-lookahead adder (CLA). To support this functionality, DrAcc adds three transistors per column to facilitate signal control and logic operations, and enhances the sense amplifier (SA) with two additional transistors for conditional activation based on intermediate results. A minor wire reconfiguration within the DRAM cell array allows the specialized rows to flexibly support both logic inversion and carry shifting.

Prior works [346, 921] use stochastic-based computing to reduce the latency of executing in-DRAM bit-serial multiplication operations. To do so, they approximate multiplication operations using bitwise AND operations on unary bitstreams (i.e., sequences of bits used to represent numbers probabilistically rather than in traditional binary encoding). In stochastic computing, operations such as multiplication are simplified: to compute $x \times y$, such works

¹Assuming that a DRAM row is 8 kB, and the DRAM module has 16 DRAM banks, each of which with 64 DRAM subarrays.

generate two unary bitstreams representing and performs a bitwise AND between them. The result is another unary bitstream where the proportion of ‘1’s approximates $x \times y$.

Enabling PUD via Enhanced DRAM Cell or Sense Amplifier (SA) Designs. DRISA [316] performs in-situ computing using either 3T1C (3 transistors–1 capacitor) or 1T1C (1 transistor–1 capacitor) designs. In the 3T1C approach, DRISA modifies standard DRAM cells to include two read/write access transistors and an additional transistor that ties the cell onto a bitline in a NOR style, hence allowing the 3T1C design to natively implement a bitwise NOR in a single cycle. In the 1T1C approach, DRISA augments sense amplifiers (SAs) with external logic gates and latches to support operations such as AND, OR, and NOT. DRISA uses these bitwise operations (NOR, AND, OR, XOR), alongside with an in-DRAM inter-lane shifting network, to implement complex PUD operations such as multiplication, max, and selection.

ReDRAM [922] enables in-situ DRAM operations using a dual-row activation (DRA) mechanism coupled with a reconfigurable SA design, which integrates additional logic elements (i.e., three inverters with distinct voltage transfer characteristics, a NAND gate, and a multiplexer). These enhancements allow the SA to exploit charge-sharing between two simultaneously activated DRAM rows, enabling the execution of bulk bitwise logic operations, including NOT, AND, OR, and XOR, directly on the bitlines in a single memory cycle. Similar to ReDRAM, Flex-iDRAM [923] implements in-situ DRAM operations by introducing a reconfigurable SA design that enables native support for complex logic functions, specifically XOR2 and MAJ3, using TRA. The modified SA integrates additional skewed inverters, transistors, and a multiplexer, controlled by four enable signals, allowing it to perform charge-based analog NAND/NOR logic in a single cycle. Sieve [924] also modifies the SAs by including a XNOR gate, an AND gate, and a one-bit latch, which is used to perform k-mer matching.

ROC [925] implements in-situ DRAM operations by introducing a computing unit (CU) within a DRAM array. Different than Ambit and DRISA, which leverage charge-sharing methods for in-DRAM computing, ROC instead utilizes diode-connected transistors between DRAM cells to enable bitwise logic within the DRAM array. The modification to the DRAM subarray lies in augmenting each CU with two DRAM cells and an additional diode-connected transistor to realize AND and OR operations via sequential data transfers: writing to one cell influences the state of the other based on logical semantics. For instance, to perform an OR operation, data is copied to both cells such that if either operand is ‘1’, the resulting cell becomes ‘1’. Additionally, a newly added transistor enables the NOT operation. To extend functionality, ROC introduces an enhanced SA equipped with additional transistors to support propagation and shift operations, enabling word-level operations like compare and increment.

ELP²IM [320] executes bulk bitwise in-DRAM operations by introducing a pseudo-

precharge-based mechanism that enables in-place logic using modified SA control sequences. Instead of relying on TRA (as in Ambit), ELP²IM exploits stable, non-traditional DRAM states: by regulating only one side of the bitline pair, ELP²IM creates a *pseudo-precharge* state that preserves or alters the bitline voltage based on operand values. This voltage state is then used to selectively overwrite the destination cell in the following access cycle, thereby realizing basic AND and OR logic operations over two such cycles (an APP-AP sequence). ELP²IM proposes modifying the precharge unit to decouple equalizer (EQ) signals and adding a single dual-contact row for NOT operations (similar to Ambit).

Compared to such approaches, an Ambit-style PUD *minimally* modifies the DRAM subarray to efficiently implement in-situ bulk bitwise operations. Such design principal provides an edge in adoption Ambit-style PUD in future systems, since DRAM's manufacturing process is highly sensitive to the area occupied by the DRAM core array.

PUD for True Random Number Generation. Intentionally violating DRAM access timing parameters can also be used to generate true random numbers inside DRAM. The technique proposed in [340] decreases the DRAM row activation latency below the datasheet specifications to induce read errors, or activation failures. As a result, some DRAM cells, called true random number generator (TRNG) cells, fail truly randomly. By aggregating the resulting data from multiple such TRNG cells, a technique called D-RaNGe, provides a high-throughput and low-latency TRNG. Extensive characterization and analysis of the DRAM latency TRNG on real commodity off-the-shelf (COTS) DRAM chips is provided in [340].

The authors of QUAC-TRNG [339] exploit the observation that a carefully-engineered sequence of DRAM commands activates four consecutive DRAM rows in rapid succession to generate random numbers. This QUadruple ACTivation (QUAC) causes the bitline sense amplifiers to non-deterministically converge to random values when four rows that store conflicting data are activated because the net deviation in bitline voltage fails to meet reliable sensing margins. QUAC-TRNG reads the result of the QUAC operation from the sense amplifiers and performs the SHA-256 cryptographic hash function [916] to post-process the result and output random numbers.

Another recent work proposes DR-STRaNGe [342], an end-to-end system design for DRAM-based TRNGs that mitigates three key system integration challenges: (i) generating random numbers with DRAM-based TRNGs can degrade overall system performance by slowing down concurrently-running applications due to the interference between RNG and regular memory operations in the memory controller (i.e., RNG interference), (ii) this RNG interference can degrade system fairness by causing unfair prioritization of applications that intensively use random numbers (i.e., RNG applications), and (iii) RNG applications can experience

significant slowdown due to the high latency of DRAM-based TRNGs. DR-STRaNGe proposes an *RNG-aware scheduler* and a *buffering mechanism* in the memory controller to tackle these challenges.

PUD for Physically Unclonable Functions. Physically unclonable functions (PUFs) are commonly used in cryptography to identify devices based on the uniqueness of their physical microstructures. DRAM-based PUFs have two key advantages: (i) DRAM is present in many modern computing systems, and (ii) DRAM has high capacity and thus can provide many unique identifiers. However, traditional DRAM PUFs exhibit unacceptably high latencies and are not runtime-accessible. The authors of [926] propose a new class of fast, reliable DRAM PUFs that are runtime-accessible, i.e., that can be used during online operation with low latency. The key idea is to reduce DRAM read access latency below the reliable datasheet specifications using software-only system calls. Doing so results in error patterns that reflect the compound effects of manufacturing variations in various DRAM structures (e.g., capacitors, wires, sense amplifiers). Some DRAM cells fail always after repeated accesses with violated timing parameters and some others never fail at all. A combination of a set of such consistently failing or never failing cells can be used to generate a unique identifier for the device. The DRAM latency PUF does *not* require any modification to existing DRAM chips – it only requires an intelligent memory controller that can change timing parameters and identify DRAM regions and cells that can be reliably used as PUFs. An extensive characterization and analysis of the DRAM latency PUF on real COTS DRAM chips is provided in [926].

PUD for Lookup Tables (LUT) Operations. LUT-based PUD [332,333,379,380,927–930] enables efficient implementation of complex operations, such as transcendental functions, that are costly to implement using arithmetic or bulk bitwise Boolean operations in-DRAM. By directly mapping inputs to precomputed outputs, LUT-based PUD can improve performance and enhance flexibility of PUD system. To illustrate how a LUT-based PUD operations, we highlight pLUTo [333], processing-using-memory with lookup table (LUT) operations, a DRAM-based PUM architecture that leverages LUT-based computing via bulk querying of LUTs to perform complex operations beyond the scope of prior PUD proposals (i.e., Ambit and SIM-DRAM). pLUTo introduces a LUT-querying mechanism, the *pLUTo LUT Query*, which enables the simultaneous querying of multiple LUTs stored in a single DRAM subarray. In pLUTo, the number of elements stored in each LUT may be as large as the number of rows in each DRAM subarray (e.g., 512–1024 rows [161,183,495]).

pLUTo executes seven main steps to perform a *pLUTo LUT Query*. First, the *source subarray* stores the *LUT query input vector*, which consists of a set of N -bit LUT indices associated with LUT elements. Second, the *pLUTo Match Logic* comprises a set of comparators that identify

matches between (i) the row index of the currently activated row in the pLUTo-enabled subarray, and (ii) each LUT index in the LUT query input vector (i.e., the source subarray's row buffer). Third, the *pLUTo-enabled row decoder* enables the successive activation of consecutive DRAM rows in the pLUTo-enabled subarray with a single DRAM command. It also outputs the row index of the currently activated row as input to the pLUTo Match Logic. Fourth, the *pLUTo-enabled subarray* stores multiple vertical copies of a given LUT, which consists of M -bit LUT elements. Fifth, the *pLUTo-enabled row buffer* allows the reading of individual LUT elements from the activated row in the *pLUTo-enabled subarray*. This is possible by extending the DRAM sense amplifier design of the pLUTo-enabled row buffer with switches controlled by the pLUTo Match Logic (using the *matchline* signal). Sixth, the *flip-flop (FF) buffer* enables pLUTo to temporarily store select LUT elements by copying them from the pLUTo-enabled row buffer, conditioned on the output of the pLUTo Match Logic following each row activation. Seventh, a LISA [377] operation (described in Section 2) copies the entire contents of the FF buffer (i.e., the LUT query output vector) into the destination row buffer, i.e., the row buffer of the *destination subarray*.

In contrast to the bit-serial paradigm employed by prior PUD architectures (e.g., SIM-DRAM [378]), pLUTo operates in a *bit-parallel* manner; in other words, the bits that make up each LUT element (e.g., A) are stored *horizontally* (i.e., in adjacent bitlines), and all the copies of each LUT element (i.e., $\{A, A, \dots, A\}$) take up *one whole row* in the depicted pLUTo-enabled subarray.

PUD Using Commodity Off-the-Shelf DRAM. ComputeDRAM [323] shows that one can mimic the effect of RowClone's back-to-back activation mechanism in off-the-shelf DRAM chips by violating the timing parameters such that two wordlines in a subarray are activated back-to-back as in RowClone. This work shows that such a version of RowClone can operate reliably in a variety of COTS DRAM chips tested using the SoftMC infrastructure [178, 931]. More recent works [894, 895] experimentally demonstrate the PUM capabilities of hundred COTS DRAM chips using DRAM Bender [932, 933], an FPGA-based DDR4 testing infrastructure that provides precise control of DDR4 commands issued to a DRAM module. These works demonstrate that COTS DRAM chips are capable of (i) performing functionally-complete bulk-bitwise Boolean operations: NOT, NAND, and NOR, (ii) executing up to 16-input AND, NAND, OR, and NOR operations, and (iii) copying the contents of a DRAM row (concurrently) into up to 31 other DRAM rows with $>99.98\%$ reliability. The authors evaluate the robustness of these operations across data patterns, temperature, and voltage levels, showing that COTS DRAM chips can perform these operations at high success rates ($>94\%$). These fascinating findings demonstrate the fundamental computation capability of DRAM, even when DRAM chips are

not designed for this purpose, and provide a solid foundation for building new and robust PUD mechanisms into future DRAM chips and standards.

3.2.3 NVM-Based PUM Architectures

Bitwise Operations in NVMs. Several works [331, 900–903, 934–941] investigate the implementation of *stateful* [900–902, 934–940] and *non-stateful* [331, 903, 941] bitwise Boolean operations in emerging NVM technologies. When implementing stateful Boolean bitwise operations, all input operands and the produced result are stored in terms of the resistance state variable. Hence, many Boolean bitwise operations can be executed back-to-back, at the expense of consuming the limited write cycles (i.e., endurance) of the emerging NVM device. In contrast, when implementing non-stateful Boolean bitwise operations, the input operands are stored as resistance state variables while the output value is represented as a voltage level. Such implementation avoids write cycles, since the produced output value is not directly written back into the NVM cells, but requires additional sensing circuitry when cascading consecutive operations. As examples, we highlight the implementation of stateful (e.g., MAGIC [900]) and non-stateful (e.g., Pinatubo [331]) NVM-based PUM architectures.

In memresistive devices, memory cells use resistance levels to represent logic-‘1’ (e.g., using a low resistance level R_{low}) and logic-‘0’ (e.g., using a high resistance level R_{high}). As in DRAM, NVM arrays organize memory cells in rows and columns, and a sense amplifier is used to convert resistance difference of memory cells into voltage levels or current signals based on a reference resistance level R_{ref} , determining the result between ‘0’ and ‘1’. MAGIC [900] implements a Boolean NOR operations as follows. Initially, a NOR logic gate is constructed using two input memristors (in_1 and in_2) connected in parallel and an output memristor (out) connected in series. First, the output memristor out is initialized with a logic-‘1’ value (i.e., $R_{out} = R_{low}$). Second, a voltage pulse V_0 is applied to the gateway of the NOR logic gate. Third, V_0 produces a current that passes through the circuit. The logical state of the output memristor out switches from the initial logic-‘1’ value to a logic-‘0’ value when *either* in_1 or in_2 has a low resistance value (i.e., $in_1 = R_{low}$ or $in_2 = R_{low}$), since the voltage/current will be greater than the memristor threshold voltage/current. MAGIC implements other Boolean operations (i.e., OR, NAND, and AND) by changing the connections between in_1 , in_2 , and out : (i) a Boolean OR operation is implemented by connecting in_1 , in_2 , and out as in a Boolean NOR, but initializing out with a logic-‘0’ value, i.e., $R_{out} = R_{high}$; (ii) a Boolean NAND (AND) operation is implemented by connecting in_1 , in_2 , and out in series, and initializing out with a logic-‘1’ (logic-‘0’) value, i.e., $R_{out} = R_{low}$ ($R_{out} = R_{high}$). A Boolean NOT operation is implemented by constructing an inverted logic gate using an input memristor (in) and an output memristor (out), which is initialized with a logic-‘1’ value, connected in series.

Pinatubo [331] implements bulk bitwise Boolean operations by (i) performing *multiple row activation*, similarly to Ambit [314], and (ii) modifying the array's sense amplifier by adding new reference resistance levels that are used during PUM execution to enable different Boolean operations. For example, to compute bulk bitwise A OR B of rows A and B, Pinatubo simultaneously activates the rows containing both input operands. The newly-added reference resistance level for a Boolean OR operation (i.e., R_{ref-or}) then allows the sense amplifier to output '0' only when $R_A = R_B = R_{ref-or}$. Pinatubo follows a similar approach to implement other Boolean operations, such as OR, AND, XOR, and INV operations.

NVM-based PUM architectures [443, 898, 900, 942–946] can implement complex arithmetic operations by decomposing such operations into a series of simple bitwise Boolean operations (e.g., AND, NOR, XOR) that are executed bit-serially over vertically-layout-out input operands. The authors of [942] use such an approach to accelerate an important data-intensive application, i.e., time series analysis (TSA) [947].

In-Memory Crossbar Array Matrix-Vector Multiplication (MVM) Operations. Crossbar array based NVM architectures can natively execute MVM operations based on analog operational principles [312, 313, 321, 322, 334, 376, 948, 949, 949–985], specifically Kirchhoff's Law [986–988]. A crossbar array based NVM architecture performs a MVM operation between the input vector V and the input matrix M , producing an output vector O (i.e., $O = V \times M$) as follows [312]. Before execution, the input matrix M is stored in the crossbar array as resistance levels, where each matrix element $M_{i,j}$ is represented as a resistance level corresponding to the value of the element i.e., $M_{i,j} = \frac{1}{R_{i,j}}$. Then, the crossbar array performs a *in-situ* MVM operation by applying (i) a voltage level V_i , which represents the input vector, on the wordlines of the array that stores the matrix M and (ii) sensing the output vector O on the bitlines. Based on Kirchhoff's Law [986–988], the current level sensed on the bitlines will be equal to $O_i = \sum_j V_j \times M_{i,j} = \sum_j V_j \times \frac{1}{R_{i,j}}$. Using a crossbar array based NVM, an MVM operation can be performed in nearly a single NVM read cycle (as long as the matrix fits in the crossbar array).

A large number of works leverage crossbar array based NVM's ability to natively perform MVM operations to accelerate different applications [312, 313, 321, 322, 334, 376, 948–985, 989–997], in particular, NN inference and training [312, 313, 322, 334, 949, 951–985, 994, 997]. Even though such proposals are intellectually promising, NVM-based acceleration of MVM operations needs to take into account inherent device non-idealities (e.g., non-ideal analog-to-digital and digital-to-analog converters, write resistance due to imperfect writes, non-ideal sensing circuits), architectural limitations (e.g., limited write endurance), and cost & latency considerations (e.g., due to analog-to-digital and digital-to-analog conversion and sensing circuitry)

that might impact the accuracy and robustness of the target application [389, 971] as well as the cost and scalability of the system.

In-Memory Crossbar Array String Matching Operations. Crossbar array based NVM architectures can also perform *in-situ* string matching operations. To enable these operations, the crossbar array is operated as a content addressable memory (CAM). The CAM array consists of $m \times n$ CAM cells that house m reference strings, each of which is n -bit long. Each CAM cell stores *one* bit and has two programmable resistors, R_l and R_r , and two transistors, M_l and M_r . To store ‘1’ (or ‘0’) in a CAM cell, R_l and R_r are programmed to high and low (or low and high) resistance levels, respectively. The NVM-based CAM array is able to query the existence of an n -bit string in parallel across all m rows in four steps. First, the CAM array precharges the matchline signals to *high* voltage. Second, each bit in the input string and its complement drive the gate voltages of M_l and M_r transistors of the CAM cells in the corresponding column, respectively. Third, each CAM cell compares its stored bit to the corresponding bit in the input string. If these two bits are different, the pull down network in the CAM cell is turned on and the matchline becomes ‘0’. Otherwise, the matchline keeps its precharged *high* voltage. Fourth, if all bits of the input string match with all corresponding CAM cells in a row, the matchline remains high, indicating an *exact match* between the input string and the reference string stored in the CAM array.

The authors of [395] leverage NVM’s ability to perform in-situ MVM and string matching operations to accelerate genome analysis, where a state-of-the-art NVM-based PUM array [998] is used to implement basecalling (by performing NN inference using the NVM array in-situ MVM operations) and chaining [999] (by performing the dynamic programming algorithm using the NVM array as a CAM for string matching operations). The authors of [389] developed a hardware/software framework to accelerate DNN-based genomic basecallers while taking into account the possible adverse effects of inherent NVM device non-idealities, which can greatly degrade basecalling accuracy.

We conclude that PUM architectures with emerging non-volatile memories offer a promising approach for accelerating different classes of data-intensive workloads by minimizing data movement overhead and enabling *in-situ* matrix-vector multiplication and bitwise operations. This approach demonstrates significant potential for performance and energy efficiency improvements, yet further work is needed to address the NVM devices’ non-idealities, improve overall robustness & cost efficiency, and investigate applicability to a wider variety of workloads.

3.2.4 NAND Flash-Based PUM Architectures

A recent work, ParaBit [353], proposes using NAND flash chips for bulk bitwise operations. However, ParaBit has two major limitations. First, it falls short of maximally exploiting the bit-level parallelism of bulk bitwise operations that could be enabled by leveraging the unique cell-array architecture and operating principles of NAND flash memory. Second, it is unreliable because it is not designed to take into account the highly error-prone nature of NAND flash memory.

Flash-Cosmos (Flash Computation with One-Shot Multi-Operand Sensing) [336] further enhances NAND flash-based bulk bitwise operations while providing high reliability with two key mechanisms: (i) Multi-Wordline Sensing (MWS), which enables bulk bitwise operations on a large number of operands (tens of operands) with a *single* sensing operation, and (ii) Enhanced SLC-mode Programming (ESP), which enables reliable computation inside NAND flash memory.

MWS leverages the two fundamental cell-array structures of NAND flash memory to perform in-flash bulk bitwise operations on a large number of operands with a *single* sensing operation: (i) a number of flash cells (e.g., 24–176 cells) are serially connected to form a NAND string (similar to digital NAND logic); (ii) thousands of NAND strings are connected to the same bitline (similar to digital NOR logic). Under these cell-array structures, simultaneously sensing *multiple* wordlines automatically results in (i) bitwise AND of *all* the sensed wordlines if they are in the same NAND string or (ii) bitwise OR of *all* the wordlines if they are in different NAND strings. ESP effectively avoids raw bit errors in stored data via more precise programming-voltage control using the NAND flash controller. A flash cell stores bit data as a function of the level of its threshold-voltage (V_{TH}). Reading a cell incurs an error if the cell's V_{TH} level moves to another V_{TH} range that corresponds to a different bit value than the stored value, due to various reasons, such as program interference [851, 1000–1002], data retention loss [841, 844, 846, 851, 1003], read disturbance [851, 1004, 1005], and cell-to-cell interference [851, 1001]. ESP maximizes the margin between different V_{TH} ranges by carefully leveraging two existing approaches. First, to store data for in-flash processing, it uses the single-level cell (SLC)-mode programming scheme [840, 1006]. Doing so guarantees a large V_{TH} margin by forming only two V_{TH} ranges (for encoding '1' and '0') within the fixed V_{TH} window. Second, ESP enhances the SLC-mode programming scheme by using (i) a higher programming voltage to increase the distance between the two V_{TH} ranges and (ii) more programming steps to narrow the high V_{TH} range. Using ESP makes bulk bitwise computation operations using flash memory completely reliable (i.e., no errors) on tested real NAND flash [336].

Enabling computation using flash memory to become more capable and programmable

is a promising direction future research can take. Compared to processing-using-DRAM, we believe processing-using-flash is still in its infancy. More work is needed to demonstrate the possibility of more complex computations, improve processing-using-flash programmability, and address system integration challenges. The good news is that in flash memory, the memory controller can have much more sophisticated capabilities to make computation reliable, as existing flash controllers already use many mechanisms to greatly enhance robustness and avoid errors [847, 848, 851]. For example, existing flash memory controllers perform data randomization, wear leveling, adaptive refresh, block remapping, garbage collection, careful tuning of read reference voltage, and sophisticated error correction [812–827, 827–830, 840, 844–847, 851, 865, 1000–1004, 1007–1009]. The ESP (enhanced SLC-mode programming) technique proposed in Flash-Cosmos [336] is a great example of using already supported mechanisms in flash memory controllers to improve the reliability of processing-using-flash techniques. We believe there is significant opportunity for creating novel and robust processing-using-flash techniques by exploiting and enhancing the sophisticated capabilities of flash memory controllers.

3.3 System Support for PIM Architectures

3.3.1 Data Movement Bottlenecks: Identification, Workload Characterization, and Benchmark Suites

Identifying Data Movement Bottlenecks. Many past works investigate how to reduce data movement cost using a range of different compute-centric, e.g., prefetchers [75–81, 83, 89–93, 1010–1020] (by proactively loading data into faster memory closer to the compute units before it is explicitly requested, thus reducing access latency and improving memory bandwidth utilization), speculative execution [55, 80, 114–116, 1021] (by preemptively executing instructions and fetching required data ahead of time, overlapping computation with memory access to hide latency and improve throughput), value-prediction [80, 1011, 1022–1038] (by speculatively supplying predicted data values, reducing the need to fetch them from memory and thereby decreasing latency and memory bandwidth pressure), data compression [460, 461, 659, 1039–1053] (by reducing the volume of data transferred across the memory hierarchy), approximate computing [22, 1022, 1054, 1055] (by enabling the use of lower-precision or lossy data representations, which reduce data size and consequently the bandwidth and energy required for memory requests), and memory-centric techniques [13, 18, 57, 136, 154, 238, 260, 262–264, 290, 787, 1056–1067] (by moving computation to where the data resides). These works evaluate the impact of data movement on different systems, including

mobile systems [13, 33, 1068–1070], data centers [10, 11, 34, 45, 797, 1010, 1071, 1072], accelerator-based systems [13, 20, 21, 156, 282, 797, 1073], and desktop computers [1074–1076]. They use very different profiling frameworks and methodologies to identify the root cause of data movement for a small set of applications. Two common approaches to identify data movement bottlenecks in applications is to use profiling tools, such as the roofline model [1077] for the application–system [6, 244, 277, 281, 288, 595, 863–871], or use simple metrics (such as last-level CPU cache Misses per Kilo-Instruction (MPKI)) as indication of memory pressure [13, 19, 150, 154, 155, 305, 442, 444, 1078–1080]. However, as we show in Chapter 4, even though both the roofline model and MPKI can identify some specific sources of memory bottlenecks, they alone cannot comprehensively identify different possible sources of memory bottlenecks in a system.

Workload Characterization Targeting PIM. Many works [13, 14, 157, 242, 244, 250, 278, 279, 281, 301, 385, 413, 437, 482, 595, 718, 722, 942, 1081–1085] perform ad-hoc workload characterization (where they perform in-depth profiling of an application) in order to determine whether an application suffers from memory bottlenecks, and hence would potentially benefit from a PIM design. However, such profiling approaches are closely tight to the target application under analysis, making it hard to generalize their application profiling methodology and observed findings to a broader set of applications.

Benchmark Suites Targeting PIM Architectures. First, in [1073], the authors provide the first work that characterizes workloads for PIM. They analyze five applications (FFT, ray tracing, method of moments, image understanding, data management). The PIM organization [1073] targets is similar to [252], where vector processing compute units are integrated into the DDRx memory modules. Even though [1073] has a similar goal to our work, it understandably does not provide insights into modern data-intensive applications and PIM architectures as it dates from 2001. Also, [1073] focuses its analysis only on a few workloads, whereas we aim to conduct a broader workload analysis starting from 345 applications. Therefore, a new, more comprehensive and rigorous analysis methodology of data movement bottlenecks in modern workloads and modern PIM systems is necessary. Second, in [476], the authors present the *PrIM* benchmark suite (*Processing-In-Memory benchmarks*) [479], a benchmark suite of 16 workloads from different application domains (e.g., dense/sparse linear algebra, databases, data analytics, graph processing, neural networks, bioinformatics, image processing) designed for evaluating the UPMEM PIM architecture [474, 475]. Using *PrIM*, the authors of [476] conduct an extensive evaluation on two real UPMEM-based PIM systems with 640 and 2556 DPUs, providing new insights about suitability of different workloads to the PIM system, programming recommendations for software designers, and suggestions and hints for

hardware and architecture designers of future PIM systems. Compared to our work, the PrIM benchmark suite is limited to a particular PIM system (i.e., the UPMEM PIM), while we aim to broadly encompass PIM architectures in our analyses.

3.3.2 Identification of PIM Suitability

In this section, we discuss works that aim to identify whether an application, kernel, or instruction might benefit from PIM execution. We call such portions *PIM offloading candidates*. While PIM offloading candidates can be identified manually by a programmer, the identification would require significant programmer effort along with a detailed understanding of the hardware trade-offs between CPU cores and PIM cores. For architects who are adding custom PIM logic (e.g., fixed-function accelerators, which we call PIM accelerators) to memory, the trade-offs between CPU cores and PIM accelerators may not be known before determining which portions of the application are PIM offloading candidates, since the PIM accelerators are tailored for the PIM offloading candidates. To alleviate the burden of manually identifying PIM offloading candidates, many prior works [13, 57, 272, 274, 310, 855, 857, 861, 876, 878–881, 883, 1086–1088] propose systematic approaches for identifying PIM offloading candidates in an application. We classify PIM suitability approaches into three classes: (i) static-based [13, 855, 861, 878–880], where PIM suitability is determinate based on characteristics of an application that can be obtained offline (e.g., via previous application profiling or compiler analysis), (ii) dynamic-based [57, 857, 876], where PIM suitability is determinate by probing the hardware state during application execution, (iii) hybrid-based [272, 274, 310, 881, 883, 1086–1088], where PIM suitability is determinate using a combination of the static and dynamic solutions.

Static-Based PIM Suitability Identification Approaches. In [13], to identify PIM suitability, the authors execute an offline profiling analysis of the target application. Using hardware performance counters and an energy model, they identify that a function is a PIM offloading candidate if it meets the following conditions: (i) it consumes a significant fraction (e.g., more than 30%) of the overall workload energy consumption; (ii) its data movement consumes a significant fraction (e.g., more than 30%) of the total workload energy, (iii) it is memory-intensive (e.g., its last-level cache misses per kilo instruction, or MPKI, is greater than 10 [223, 655, 1089, 1090]), (iv) data movement is the single largest component of the function’s energy consumption. In [861], the authors develop compiler analyses that statically identify candidate instructions for PIM offloading based on memory access patterns, data locality, and operation types, leveraging affine analysis and control/data flow properties to ensure correctness and offloading benefit. In [855], the authors implement a compiler-based PIM suitability solution that decides whether to offload a kernel to PIM using a latency-guided instruction-

level offloading model. To avoid expensive per-input profiling, it employs an offline-trained regression predictor to estimate performance benefits based on dataset features, such as expected cache misses.

Dynamic-Based PIM Suitability Identification Approaches. Many works propose runtime mechanisms for *dynamic scheduling* of PIM offloading candidates, i.e., mechanisms that decide whether or not to actually offload code that is marked to be potentially offloaded to PIM engines. In [57], the authors develop a locality-aware scheduling mechanism for PIM-enabled instructions. In [876], the authors add (i) an *Offload Management Unit* to the host chip to handle the offload of code segments to PIM cores and (ii) a *Monitor Unit* in both the PIM and CPU cores to collect the necessary runtime information (e.g., L1 cache misses, LLC misses) to feed the *Offload Management Unit*. In [857], the authors propose SAPIVe, a hardware binary translator that dynamically identifies patterns of AVX vector instructions during execution and speculatively converts them into PIM vector instructions. Offloading occurs if enough loop iterations match a recognized pattern, memory accesses are contiguous, and execution can be validated without disrupting the CPU pipeline.

Hybrid-Based PIM Suitability Identification Approaches. In [310], the authors introduce CAIRO, a fine-grained compiler-assisted approach that identifies PIM-offloadable instructions using static control flow analysis and memory access disambiguation. CAIRO further refines candidate selection using runtime information to guide offloading decisions dynamically, improving adaptability to program behavior. In [881], the authors propose A³PIM, a hybrid static-dynamic framework for PIM offloading that analytically estimates the performance impact of offloading candidate code regions. A³PIM leverages offline profiling to extract dynamic information and uses a cost model to predict the trade-offs between PIM execution and CPU execution. In [1088], the authors first instrument loop regions offline using LLVM to mark them as PIM offloadable candidates. Then, at runtime, it decides whether to offload each region by comparing the expected execution time on the host versus the PIM, using runtime profiling of data locality (specifically, the number of dirty cache blocks in the LLC). For GPU-based systems [272,274], the authors of [272,274] explore the combination of compile-time and runtime mechanisms for identification and dynamic scheduling of PIM offloading candidates.

3.3.3 Compiler Support for PIM

In this section, we describe previous efforts to implement compiler support for code generation, transformation, and optimization for PIM architectures.

Prior works propose programming models for different types of PUM architectures, as (i) CUDA/OpenAcc [1091, 1092] for in-cache computing [326]; (ii) tensor dataflow graphs for

in-ReRAM computing [349]. By enabling fine-grained DRAM, we believe such programming models can be now easily ported to PUD computing (for example, by assuming that each DRAM mat executes a different CUDA thread block).

CHOPPER [383] improves SIMD RAM’s programming model by leveraging bit-slicing compilers and employing optimizations to reduce the latency of a μ Program. Even though CHOPPER simplifies programmability compared to SIMD RAM, it still requires the programmer to re-write applications using the bit-slicing compiler’s syntax. Compared to CHOPPER, MIMDRAM has two main advantages. First, MIMDRAM *automatically* generates code for the PUD engine without any code refactoring. Second, since CHOPPER maintains the very-wide SIMD programming model of SIMD RAM, it also suffers from SIMD underutilization. Compared to CHOPPER, *Proteus* has two main advantages. First, *Proteus* improves a μ Program performance by *fully* leveraging the DRAM parallelism within a single DRAM bank. Second, although bit-slicing compilers can naturally adapt to different bit-precision values, they require the programmer to specify the target bit-precision manually. In contrast, *Proteus* dynamically identifies the most suitable bit-precision transparently from the programmer. Some other prior works (e.g., [441, 1093]) propose techniques to realize early termination of PUM operations for different memory technologies. Compared to these, *Proteus*’s main novelty lies in realizing early termination of bit-serial operation in the context of DRAM/majority-based PUD systems.

The authors of [882] propose CINM, a compiler based on MLIR [1094] (multi-level intermediate representation) for both UPMEM-like PIM systems and analog-based PIM architectures. Its main limitation is the fact that it only supports linear algebra-related kernels.

3.3.4 Memory Management Support for PIM

When an application needs to access its data inside the main memory, the CPU core must first perform an *address translation*, which converts the data’s virtual address into a *physical* address within main memory. If the translation metadata is not available in the CPU’s translation lookaside buffer (TLB), the CPU must invoke the page table walker in order to perform a long-latency page table walk that involves multiple *sequential* reads to the main memory and lowers the application’s performance [1095–1103]. In modern systems, the virtual memory system also provides access protection mechanisms.

Enabling a unified virtual address space between PIM cores and host cores, where the memory address space is shared across all computing elements in the system, is key for enabling a more flexible programming model (i.e., “*a point is a pointer*” semantics [1104]), with increased utilization of memory capacity and throughput. However, developing a high-performance and scalable unified virtual memory address space for both conventional host systems and PIM architectures can be challenging, since it requires a distributed memory management approach

where different components of the system are able to perform address translation while guaranteeing access protection mechanisms for every memory access.

One naive solution to the unified Host–PIM virtual memory address space issue is to make PIM cores reliant on existing CPU-side address translation mechanisms. However, in this approach, any performance gains from performing in-/near-memory operations could easily be nullified, as the PIM cores need to send a long-latency translation request to the CPU via the off-chip channel for each memory access. The translation can sometimes require a page table walk that issues multiple memory requests back to the memory, thereby leading to increased memory traffic on the main memory channels.

To improve over such a naive solution and reduce the overhead of page walks, one could utilize PIM engines to perform page table walks. This can be done by duplicating the content of the TLB and moving the page walker to the PIM processing logic in main memory. Unfortunately, this is either difficult or expensive for three reasons. First, coherence has to be maintained between the CPU’s TLBs and the memory-side TLBs. This introduces extra complexity and off-chip requests. Second, duplicating the TLBs increases the storage and complexity overheads on the memory side, which should be carefully contained. Third, if main memory is shared across CPUs with different types of architectures, page table structures and the implementation of address translations can be different across the different architectures. Ensuring compatibility between the in-memory TLB/page walker and all possible types of virtual memory architecture designs can be complicated and often not even practically feasible.

To address these concerns and reduce the overhead of virtual memory, the authors of [155] explore a tractable solution for PIM address translation as part of their in-memory pointer chasing accelerator, IMPICA [155]. IMPICA exploits the high bandwidth available within 3D-stacked memory to traverse a chain of virtual memory pointers within DRAM, *without* having to look up virtual-to-physical address translations in the CPU translation lookaside buffer (TLB) and without using the page walkers within the CPU. IMPICA’s key ideas are (i) to use a region-based page table, which is optimized for PIM acceleration, and (ii) to decouple address calculation and memory access with two specialized engines.

Beyond pointer chasing operations that are tackled by IMPICA [155], providing efficient mechanisms for PIM-based virtual-to-physical address translation (as well as access protection) remains a challenge for the generality of applications, especially those that access large amounts of virtual memory [1095–1097, 1101–1103].

In [1105], the authors present a detailed memory management scheme tailored for PIM systems. It introduces a segmented memory model that distinguishes between local and global segments, with PIM cores accessing both types based on locality and sharing needs. Address translation is handled differently for local and remote accesses, relying on a global naming

mechanism and parcel-based communication for remote data retrieval. Virtual memory management is extended to support fine-grained allocation and mapping of objects across multiple PIM cores, while a global segment table facilitates object sharing and consistency. The system also supports paging and context switching, enabling robust multi-programming and dynamic memory management across distributed PIM nodes.

In [1106], the authors propose DIPTA (distributed inverted page table) for near-memory address translation tailored for PIM architectures. DIPTA enables parallel and independent address translation and data fetch by restricting virtual-to-physical address mapping associativity, which allows PIM cores to avoid expensive page walks. The system also supports page faults, TLB coherence, multiprogramming, and unified virtual memory between CPUs and PIM cores, with minimal OS changes.

In [1063], the authors implement memory management for PIM hardware by introducing a *zero-copy memory virtualization* scheme that enables direct data sharing between the host processor and the PIM cores, avoiding costly data duplication. It employs a *slice-table* mechanism to manage the mapping between virtual and physical memory, supporting fine-grained memory access and enabling merged pages for efficient utilization. The system includes TLB support within the PIM to minimize translation overhead and improve efficiency.

In PiDRAM [343,915], the authors handle memory management for PIM by implementing a custom memory allocation mechanism in its supervisor software to meet the data alignment and allocation constraints of PUD operations. Concretely, it uses a subarray mapping table (SAMT) to ensure allocated pages reside in the same DRAM subarray, and an allocation ID table (AIT) to group allocations with shared constraints. For initialization, it maintains an initializer rows table (IRT) to find zero-initialized rows. These mechanisms are integrated into the PiDRAM framework to enable efficient end-to-end support for commodity DRAM-based PUM techniques.

3.3.5 Programming Frameworks and High-Level APIs for PIM

Several prior works [390,393,437] propose different programming frameworks or APIs to ease programmability in UPMEM-based PIM systems. First, SimplePIM [390] proposes a high-level programming framework that encapsulate management, computation, and communication primitives into software APIs. Similarly to DaPPA, SimplePIM uses a MapReduce-like programming model [1107], with support for three execution parallel patterns (i.e., map, reduce, and zip). DaPPA builds on top of SimplePIM by (i) further extending the programming model to allow for native implementation of more parallel patterns, (ii) *completely* eliminating the need for the user to handle data communication between CPU and DPUs and across DPUs, and (iii) allowing for *automatic* cooperative execution between CPU and DPUs for a given

kernel. By doing so, DaPPA further improves programming productivity compared to SimplePIM. Second, other works, such as TransPimLib [393] and PyGim [437], provide implementation support for key computation kernels, such as transcendental functions and graph neural networks. Even though such works also aid UPMEM programmability, they are limited to a narrow application scope.

Chapter 4

DAMOV: A New Methodology and Benchmark Suite for Evaluating Data Movement Bottlenecks

4.1 Motivation & Goal

Many recent works explore how near-data processing (NDP)¹ can benefit various application domains, such as graph processing [56, 57, 154, 257, 262, 271, 303, 304, 321, 345, 443], machine learning [13, 157, 268, 269, 277, 312, 313], bioinformatics [21, 156, 267], databases [155, 157, 262, 265, 266, 271, 279, 314], security [270, 340, 341], data manipulation [314, 316, 317, 330, 331, 352, 377, 800], and mobile workloads [13, 157]. These works demonstrate that simple metrics such as last-level CPU cache MPKI and arithmetic intensity (AI) are useful metrics that serve as a proxy for the amount of data movement an application experiences. These metrics can be used as a potential guide for choosing when to apply data movement mitigation mechanisms such as NDP. However, such metrics (and the corresponding insights) are often extracted from a small set of applications, with similar or not-rigorously-analyzed data movement characteristics. Therefore, it is difficult to generalize the metrics and insights these works provide to a broader set of applications, making it unclear what different metrics can reveal about a new (i.e., previously uncharacterized) application’s data movement behavior (and how to mitigate its associated data movement costs).

We illustrate this issue by highlighting the limitations of two different methodologies commonly used to identify memory bottlenecks and often used as a guide to justify the use of NDP architectures for an application: (a) analyzing a roofline model [1077] of the application, and (b) using last-level CPU cache MPKI as an indicator of NDP suitability of the application. The

¹Particularly in this chapter, we use the term NDP to refer to PNM architectures.

roofline model correlates the computation requirements of an application with its memory requirements under a given system. The model contains two *roofs*: (1) a diagonal line ($y = \text{Peak Memory Bandwidth} \times \text{Arithmetic Intensity}$) called the *memory roof*, and (2) a horizontal line ($y = \text{Peak System Throughput}$) called the *compute roof* [1077]. If an application lies under the memory roof, the application is classified as *memory-bound*; if an application lies under the compute roof, it is classified as *compute-bound*. Many prior works [6, 244, 277, 281, 288, 595, 863–871] employ this roofline model to identify memory-bound applications that can benefit from NDP architectures. Likewise, many prior works [13, 19, 150, 154, 155, 305, 442, 444, 1078–1080] observe that applications with high last-level cache MPKI² are good candidates for NDP.

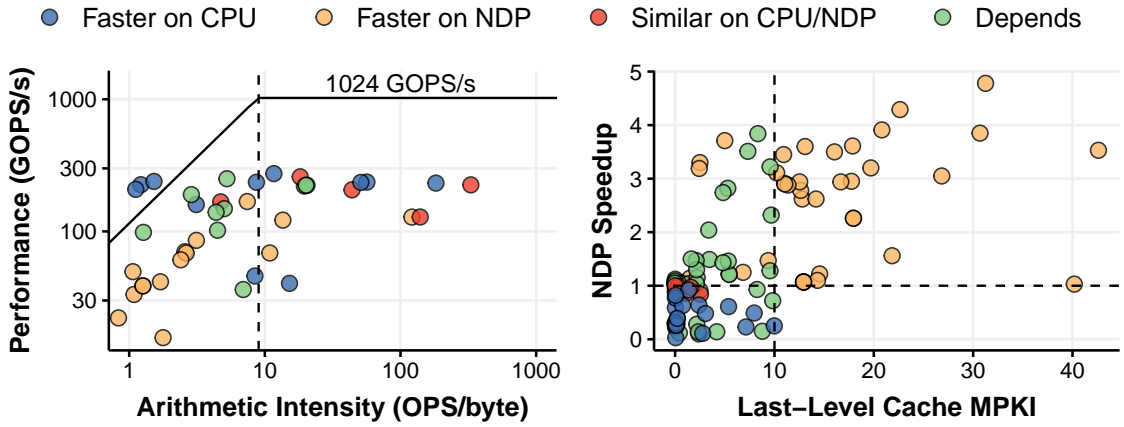


Figure 4.1: Roofline (left) and last-level cache MPKI vs. NDP speedup (right) for 44 memory-bound applications. Applications are classified into four categories: (1) those that experience performance degradation due to NDP (blue; Faster on CPU), (2) those that experience performance improvement due to NDP (yellow; Faster on NDP), (3) those where the host CPU and NDP performance are similar (red; Similar on CPU/NDP), (4) those that experience either performance degradation or performance improvement due to NDP depending on the microarchitectural configuration (green; Depends).

Figure 4.1 shows the roofline model (left) and a plot of MPKI vs. speedup (right) of a system with general-purpose NDP support over a baseline system without NDP for a diverse set of 44 applications (see Table C.7). In the MPKI vs. speedup plot, the MPKI corresponds to a baseline host CPU system. The speedup represents the performance improvement of a general-purpose NDP system over the baseline (see Section 4.2.4 for our methodology). We make the following observations. First, analyzing the roofline model (Figure 4.1, left), we observe that most of the memory-bound applications (yellow dots) benefit from NDP, as foreseen by prior works. We later observe (in Section 4.3.3) that such applications are DRAM bandwidth-bound and are a natural fit for NDP. However, the roofline model does *not* accurately account for the NDP suitability of memory-bound applications that (i) benefit from NDP only under particular microarchitectural configurations, e.g., either at low or high core counts (green dots, which are

²Typically, an MPKI value greater than 10 is considered *high* by prior works [54, 223, 653, 655, 1089, 1090, 1108].

applications that are either bottlenecked by DRAM latency or suffer from L3 cache contention; see Sections 4.3.3 and 4.3.3); or (ii) experience performance degradation when executed using NDP (blue dots, which are applications that suffer from the lack of a deep cache hierarchy in NDP architectures; see Section 4.3.3). Second, analyzing the MPKI vs. speedup plot (Figure 4.1, right), we observe that while all applications with high MPKI benefit from NDP (yellow dots with MPKI higher than 10), some applications with *low* MPKI can *also* benefit from NDP in all of the NDP microarchitecture configurations we evaluate (yellow dots with MPKI lower than 10) or under specific NDP microarchitecture configurations (green dots with MPKI lower than 10). Thus, even though both the roofline model and MPKI can identify some specific sources of memory bottlenecks and can sometimes be used as a proxy for NDP suitability, they alone cannot definitively determine NDP suitability because they cannot comprehensively identify different possible sources of memory bottlenecks in a system.

Our *goal* in this work is (1) to understand the major sources of inefficiency that lead to data movement bottlenecks by observing and identifying relevant metrics and (2) to develop a benchmark suite for data movement that captures each of these sources. To this end, we develop a new three-step methodology to correlate application characteristics with the *primary* sources of data movement bottlenecks and to determine the potential benefits of three example data movement mitigation mechanisms: (1) a deep cache hierarchy, (2) a hardware prefetcher, and (3) a general-purpose NDP architecture.³ We use two main profiling strategies to gather key metrics from applications: (i) an architecture-independent profiling tool and (ii) an architecture-dependent profiling tool. The architecture-independent profiling tool provides metrics that characterize the application memory behavior independently of the underlying hardware. In contrast, the architecture-dependent profiling tool evaluates the impact of the system configuration (e.g., cache hierarchy) on the memory behavior. Our methodology has three steps. In *Step 1*, we use a hardware profiling tool to identify memory-bound functions across many applications. This step allows for a quick first-level identification of many applications that suffer from memory bottlenecks and functions that cause these bottlenecks. In *Step 2*, we use the architecture-independent profiling tool to collect metrics that provide insights about the memory access behavior of the memory-bottlenecked functions. In *Step 3*, we collect architecture-dependent metrics and analyze the performance and energy of each function in an application when each of our three candidate data movement mitigation mechanisms is applied to the system. By combining the data obtained from all three steps, we can

³We focus on these three data movement mitigation mechanisms for two different reasons: (1) deep cache hierarchies and hardware prefetchers are standard mechanisms in almost all modern systems, and (2) NDP represents a promising paradigm shift for many modern data-intensive applications.

systematically classify the leading causes of data movement bottlenecks in an application or function into different bottleneck classes.

Using this new methodology, we characterize a large, heterogeneous set of applications (345 applications from 37 different workload suites) across a wide range of domains. Within these applications, we analyze 77K functions and find a subset of 144 functions from 74 different applications that are memory-bound (and that consume a significant fraction of the overall execution time). We fully characterize this set of 144 representative functions to serve as a core set of application kernel benchmarks, which we release as the open-source DAMOV (DAtA MOvEment) Benchmark Suite [1109]. Our analyses reveal six new insights about the sources of memory bottlenecks and their relation to NDP:

1. Applications with high last-level cache MPKI and low temporal locality are *DRAM bandwidth-bound*. These applications benefit from the large memory bandwidth available to the NDP system (Section 4.3.3).
2. Applications with low last-level cache MPKI and low temporal locality are *DRAM latency-bound*. These applications do *not* benefit from L2/L3 caches. The NDP system improves performance and energy efficiency by sending L1 misses directly to DRAM (Section 4.3.3).
3. A second group of applications with low LLC MPKI and low temporal locality are *bottlenecked by L1/L2 cache capacity*. These applications benefit from the NDP system at low core counts. However, at high core counts (and thus larger L1/L2 cache space), the caches capture most of the data locality in these applications, decreasing the benefits the NDP system provides (Section 4.3.3). We make this observation using a *new* metric that we develop, called *last-to-first miss-ratio (LFMR)*, which we define as the ratio between the number of LLC misses and the total number of L1 cache misses. We find that this metric accurately identifies how efficient the cache hierarchy is in reducing data movement.
4. Applications with high temporal locality and low LLC MPKI are *bottlenecked by L3 cache contention* at high core counts. In such cases, the NDP system provides a cost-effective way to alleviate cache contention over increasing the L3 cache capacity (Section 4.3.3).
5. Applications with high temporal locality, low LLC MPKI, and low AI are bottlenecked by the *L1 cache capacity*. The three candidate data movement mitigation mechanisms achieve similar performance and energy consumption for these applications (Section 4.3.3).
6. Applications with high temporal locality, low LLC MPKI, and high AI are *compute-bound*. These applications benefit from a deep cache hierarchy and hardware prefetchers, but the NDP system degrades their performance (Section 4.3.3).

We publicly release our 144 representative data movement bottlenecked functions from 74 applications as the first open-source benchmark suite for data movement, called DAMOV

Benchmark Suite, along with the complete source code for our new characterization methodology [1109].

4.2 Methodology Overview

We develop a new workload characterization methodology to analyze data movement bottlenecks and the suitability of different data movement mitigation mechanisms for these bottlenecks, with a focus on near-data processing (NDP). Our methodology consists of three main steps, as Figure 4.2 depicts: (1) *memory-bound function identification* using application profiling; (2) *locality-based clustering* to analyze spatial and temporal locality in an architecture-independent manner; and (3) *memory bottleneck classification* using a scalability analysis to nail down the sources of memory boundedness, including architecture-dependent characterization. Our methodology takes as input an application’s source code and its input datasets, and produces as output a classification of the primary source of memory bottleneck of important functions in an application (i.e., bottleneck class of each key application function). We illustrate the applicability of this methodology with a detailed characterization of 144 functions that we select from among 77K analyzed functions of 345 characterized applications. In this section, we give an overview of our workload characterization methodology. We use this methodology to drive the analyses we perform in Section 4.3.

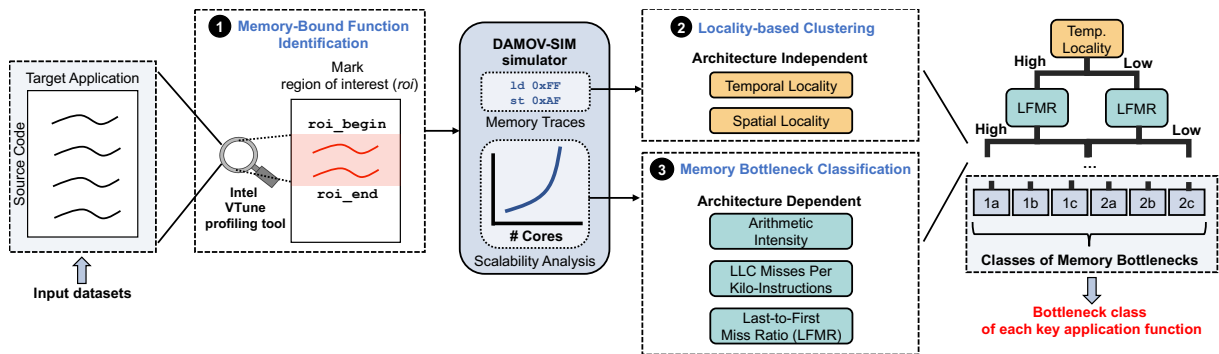


Figure 4.2: Overview of our three-step workload characterization methodology.

4.2.1 Experimental Evaluation Framework

As our scalability analysis depends on the hardware architecture, we need a hardware platform that can allow us to replicate and control all of our configuration parameters. Unfortunately, such an analysis cannot be performed practically using real hardware, as (1) there are very few available NDP hardware platforms, and the ones that currently exist do not allow us to comprehensively analyze our general-purpose NDP configuration in a controllable way (as existing platforms are specialized and non-configurable); and (2) the configurations of real CPUs can vary significantly across the range of core counts that we want to analyze, eliminating

the possibility of a carefully controlled study. As a result, we must rely on accurate simulation platforms to perform an accurate comparison across different configurations. To this end, we build a framework that integrates the ZSim CPU simulator [1110] with the Ramulator memory simulator [494] to produce a fast, scalable, and cycle-accurate open-source simulator called DAMOV-SIM [1109]. We use ZSim to simulate the core microarchitecture, cache hierarchy, coherence protocol, and prefetchers. We use Ramulator to simulate the DRAM architecture, memory controllers, and memory accesses. To compute spatial and temporal locality, we modify ZSim to generate a single-thread memory trace for each application, which we use as input for the locality analysis algorithm described in Section 4.2.3 (which statically computes the temporal and spatial locality at word-level granularity).

4.2.2 Step 1: Memory-Bound Function Identification

The first step (labeled ❶ in Figure 4.2) aims to identify the functions of an application that are *memory-bound* (i.e., functions that suffer from data movement bottlenecks). These bottlenecks might be caused at any level of the memory hierarchy. There are various potential sources of memory boundedness, such as cache misses, cache coherence traffic, and long queuing latencies. Therefore, we need to take all such potential causes into account. This step is optional if the application’s memory-bound functions (i.e., regions of interest, *roi*, in Figure 4.2) are already known *a priori*.

Hardware profiling tools, both open-source and proprietary, are available to obtain hardware counters and metrics that characterize the application behavior on a computing system. In this work, we use the Intel VTune Profiler [1111], which implements the well-known *top-down analysis* [1112]. Top-down analysis uses the available CPU hardware counters to hierarchically identify different sources of CPU system bottlenecks for an application. Among the various metrics measured by top-down analysis, there is a relevant one called *Memory Bound* [1113] that measures the percentage of CPU pipeline slots that are *not* utilized due to any issue related to data access. We employ this metric to identify functions that suffer from data movement bottlenecks (which we define as functions where *Memory Bound* is greater than 30%).

4.2.3 Step 2: Locality-Based Clustering

Two key properties of an application’s memory access pattern are its inherent spatial locality (i.e., the likelihood of accessing nearby memory locations in the near future) and temporal locality (i.e., the likelihood of accessing a memory location again in the near future). These properties are closely related to how well the application can exploit the memory hierarchy in computing systems and how accurate hardware prefetchers can be. Therefore, to understand

the sources of memory bottlenecks for an application, we should analyze how much spatial and temporal locality its memory accesses inherently exhibit. However, we should isolate these properties from particular configurations of the memory subsystem. Otherwise, it would be unclear if memory bottlenecks are due to the nature of the memory accesses or due to the characteristics and limitations of the memory subsystem (e.g., limited cache size, too simple or inaccurate prefetching policies). As a result, in this step (labeled ② in Figure 4.2), we use *architecture-independent* static analysis to obtain spatial and temporal locality metrics for the functions selected in the previous step (Section 4.2.2). Past works [1114–1123] propose different ways of analyzing spatial and temporal locality in an architecture-independent manner. In this work, we use the definition of spatial and temporal metrics presented in [1116, 1117].

The spatial locality metric is calculated for a window of memory references⁴ of length W using Equation 4.1. First, for every W memory references, we calculate the minimum distance between any two addresses (*stride*). Second, we create a histogram called the *stride profile*, where each bin i stores how many times each *stride* appears. Third, to calculate the spatial locality, we divide the *percentage* of times stride i is referenced (*stride profile*(i)) by the stride length i and sum the resulting value across all instances of i .

$$\text{Spatial Locality} = \sum_{i=1}^{\#bins} \frac{\text{stride profile}(i)}{i} \quad (4.1)$$

A spatial locality value close to 0 is caused by large *stride* values (e.g., regular accesses with large strides) or random accesses, while a value equal to 1 is caused by a completely sequential access pattern.

The temporal locality metric is calculated by using a histogram of reused addresses. First, we count the number of times each memory address is repeated in a window of L memory references. Second, we create a histogram called *reuse profile*, where each bin i represents the number of times a memory address is reused, expressed as a power of 2. For each memory address, we increment the bin that represents the corresponding number of repetitions. For example, *reuse profile*(0) represents memory addresses that are reused only once. *reuse profile*(1) represents memory addresses that are reused twice. Thus, if a memory address is reused N times, we increment *reuse profile*($\lfloor \log_2 N \rfloor$) by one. Third, we obtain the temporal locality metric with Equation 4.2.

$$\text{Temporal Locality} = \sum_{i=0}^{\#bins} \frac{2^i \times \text{reuse profile}(i)}{\text{total memory accesses}} \quad (4.2)$$

⁴We compute both the spatial and temporal locality metrics at the word granularity. In this way, we keep our locality analysis architecture-independent, using *only* properties of the application under study.

A temporal locality value of 0 indicates no data reuse, while a value close to 1 indicates very high data reuse (i.e., a value equal to 1 means that the application accesses a single memory address continuously).

To calculate these metrics, we empirically select window lengths W and L to 32. We find that different values chosen for W and L do not significantly change the conclusions of our analysis. We observe that our conclusions remain the same when we set both values to 8, 16, 32, 64, and 128.

4.2.4 Step 3: Bottleneck Classification

While Step 2 allows us to understand inherent application sources for memory boundedness, it is important to understand how hardware architectural features can also result in memory bottlenecks. As a result, in our third step (③ in Figure 4.2), we perform a scalability analysis of the functions selected in *Step 1*, where we evaluate performance and energy scaling for three different system configurations. The scalability analysis makes use of three *architecture-dependent* metrics: (1) *arithmetic intensity* (AI), (2) *Misses per Kilo-Instruction* (MPKI), and (3) a new metric called *Last-to-First Miss-Ratio* (LFMR). We select these metrics for the following reasons. First, AI can measure the compute intensity of an application. Intuitively, we expect an application with high compute intensity to not suffer from severe data movement bottlenecks, as demonstrated by prior work [1124]. Second, MPKI serves as a proxy for the memory intensity of an application. It can also indicate the memory pressure experienced by the main memory system [54, 55, 57, 152, 272, 649, 650, 1089, 1108, 1125]. Third, LFMR, a new metric we introduce and is described in detail later in this subsection, indicates how efficient the cache hierarchy is in reducing data movement.

As part of our methodology development, we evaluate other metrics related to data movement, including raw cache misses, coherence traffic, and DRAM row misses/hits/conflicts. We observe that even though such metrics are useful for further characterizing an application (as we do in some of our later analyses in Section 4.3.3), they do not necessarily characterize a specific type of data movement bottleneck. We show in Section 4.4.1 that the three architecture-dependent and two architecture-independent metrics we select for our classification are enough to accurately characterize and cluster the different types of data movement bottlenecks in a wide variety of applications.

Definition of Metrics.

We define Arithmetic Intensity (AI) as the number of arithmetic and logic operations performed per L1 cache line accessed.⁵ This metric indicates how much computation there is per memory request. Intuitively, applications with high AI are likely to be computationally intensive, while applications with low AI tend to be memory intensive. We use MPKI at the last-level cache (LLC), i.e., the number of LLC misses per one thousand instructions. This metric is considered to be a good indicator of NDP suitability by several prior works [13, 19, 150, 154, 155, 305, 442, 444, 1078, 1079]. We define the LFMR of an application as the ratio between the number of LLC misses and the total number of L1 cache misses. We find that this metric accurately identifies how much an application benefits from the deep cache hierarchy of a contemporary CPU. An LFMR value close to 0 means that the number of LLC misses is very small compared to the number of L1 misses, i.e., the L1 misses are likely to hit in the L2 or L3 caches. However, an LFMR value close to 1 means that very few L1 misses hit in L2 or L3 caches, i.e., the application does not benefit much from the deep cache hierarchy, and most L1 misses need to be serviced by main memory.

Scalability Analysis and System Configuration.

The goal of the scalability analysis we perform is to nail down the specific sources of data movement bottlenecks in the application. In this analysis, we (i) evaluate the performance and energy scaling of an application in three different system configurations; and (ii) collect the key metrics for our bottleneck classification (i.e., AI, MPKI, and LFMR). During scalability analysis, we simulate three system configurations of a general-purpose multicore processor:

- A host CPU with a deep cache hierarchy (i.e., private L1 (32 kB) and L2 (256 kB) caches, and a shared L3 (8 MB) cache with 16 banks). We call this configuration *Host CPU*.
- A host CPU with a deep cache hierarchy (same cache configurations as in *Host CPU*), augmented with a stream prefetcher [1126]. We call this configuration *Host CPU with prefetcher*.
- An NDP CPU with a single level of cache (only a private read-only⁶ L1 cache (32 kB), as assumed in many prior NDP works [13, 56, 150, 243, 262, 265, 271, 281, 282, 306]) and no hardware prefetcher. We call this configuration *NDP*.

The remaining components of the processor configuration are kept the same (e.g., number of cores, instruction window size, branch predictor) to isolate the impact of only the caches,

⁵We consider AI to be architecture-dependent since we consider the number of cache lines accessed by the application (and hence the hardware cache block size) to compute the metric. This is the same definition of AI used by the hardware profiling tool we employ in *Step 1* (i.e., the Intel VTune Profiler [1111]).

⁶We use read-only L1 caches to simplify the cache coherence model of the NDP system. Enabling efficient synchronization and cache coherence in NDP architectures is an open-research problem, as we discuss in Section 4.3.6.

prefetchers, and NDP. This way, we expect that the performance and energy differences between the three configurations to come *exclusively* from the different data movement requirements. For the three configurations, we sweep the number of CPU cores in our analysis from 1 to 256, as previous works [56, 265, 1127] show that large core counts are necessary to saturate the bandwidth provided by modern high-bandwidth memories, and because modern CPUs and NDP proposals can have varying core counts. The core count sweep allows us to observe (1) how an application’s performance changes when increasing the pressure on the memory subsystem, (2) how much Memory-Level Parallelism (MLP) [114, 115, 650, 1128, 1129] the application has, and (3) how much the cores leverage the cache hierarchy and the available memory bandwidth. We proportionally increase the size of the CPU’s private L1 and L2 caches when increasing the number of CPU cores in our analysis (e.g., when scaling the CPU core count from 1 to 4, we also scale the aggregated L1/L2 cache size by a factor of 4). We use out-of-order and in-order CPU cores in our analysis for all three configurations. In this way, we build confidence that our trends and findings are independent of a specific underlying general-purpose core microarchitecture. We simulate a memory architecture similar to the Hybrid Memory Cube (HMC) [423], where (1) the host CPU accesses memory through a high-speed off-chip link, and (2) the NDP logic resides in the logic layer of the memory chip and has direct access to the DRAM banks (thus taking advantage of higher memory bandwidth and lower memory latency). Table 6.2 lists the parameters of our host CPU, host CPU with prefetcher, and NDP baseline configurations.

Choosing an NDP Architecture.

We note that across the proposed NDP architectures in literature, there is a lack of consensus on whether the architectures should make use of general-purpose NDP cores or specialized NDP accelerators [19, 416]. In this work, we focus on general-purpose NDP cores for two major reasons. First, many prior works (e.g., [13, 56, 150, 243, 261, 262, 265, 273, 281, 282, 290, 305, 306, 309, 1133]) suggest that general-purpose cores (especially simple in-order cores) can successfully accelerate memory-bound applications in NDP architectures. In fact, UPMEM [239], a start-up building some of the first commercial in-DRAM NDP systems, utilizes simple in-order cores in their NDP units inside DRAM chips [6, 239]. Therefore, we believe that general-purpose NDP cores are a promising candidate for future NDP architectures. Second, the goal of our work is not to perform a design space exploration of different NDP architectures, but rather to understand the key properties of applications that lead to memory bottlenecks that can be mitigated by a simple NDP engine. While we expect that each application could potentially benefit further from an NDP accelerator tailored to its computational and memory requirements, such customized architectures open many challenges for a methodical characterization, such as the

Table 4.1: Evaluated Host CPU and NDP system configurations.

Host CPU Configuration	
Host CPU Processor	1, 4, 16, 64, and 256 cores @2.4 GHz, 32 nm; 4-wide out-of-order 1, 4, 16, 64, and 256 cores @2.4 GHz, 32 nm; 4-wide in-order Buffers: 128-entry ROB; 32-entry LSQ (each) Branch predictor: Two-level GAs [1130]. 2,048 entry BTB; 1 branch per fetch
Private L1 Cache	32 KB, 8-way, 4-cycle; 64 B line; LRU policy Energy: 15/33 pJ per hit/miss [150, 1131]
Private L2 Cache	256 KB, 8-way, 7-cycle; 64 B line; LRU policy MSHR size: 20-request, 20-write, 10-eviction Energy: 46/93 pJ per hit/miss [150, 1131]
Shared L3 Cache	8 MB (16-banks), 0.5 MB per bank, 16-way, 27-cycle 64 B line; LRU policy; Bi-directional ring [1132]; Inclusive; MESI protocol [887] MSHR size: 64-request, 64-write, 64-eviction Energy: 945/1904 pJ per hit/miss [150, 1131]
Host CPU with Prefetcher Configuration	
Processor, Private L1 Cache, Private L2 Cache, and Share L3 Cache	Same as in Host CPU Configuration
L2 Cache Prefetcher	Stream prefetcher [92, 1126]; 2-degree; 16 stream buffers; 64 entries
NDP Configuration	
NDP CPU Processor	1, 4, 16, 64, and 256 cores @2.4 GHz, 32 nm; 4-wide out-of-order 1, 4, 16, 64, and 256 cores @ 2.4 GHz, 32 nm; 4-wide in-order Buffers: 128-entry ROB; 32-entry LSQ (each) Branch predictor: Two-level GAs [1130]. 2,048 entry BTB; 1 branch per fetch
Private L1 Cache	32 KB, 8-way, 4-cycle; 64 B line; LRU policy; Read-only Data Cache Energy: 15/33 pJ per hit/miss [150, 1131]
Common	
Main Memory	HMC v2.0 Module [423] 32 vaults, 8 DRAM banks/vault, 256 B row buffer 8 GB total size; DRAM@166 MHz; 4-links@8 GHz 8 B burst width at 2:1 core-to-bus freq. ratio; Open-page policy; HMC default interleaving [152, 423] ¹⁰ Energy: 2 pJ/bit internal, 8 pJ/bit logic layer [150, 263, 1133], 2 pJ/bit links [150, 273, 1134]

need for significant code refactoring, changes in data mapping, and code partitioning between NDP accelerators and host CPUs.^{7,8}

4.3 Characterizing Memory Bottlenecks

In this section, we apply our three-step workload characterization methodology to characterize the sources of memory bottlenecks across a wide range of applications. First, we apply *Step 1* to identify memory-bound functions within an application (Section 4.3.1). Second, we apply *Step 2* and cluster the identified functions using two architecture-independent metrics (spatial and temporal locality) (Section 4.3.2). Third, we apply *Step 3* and combine the architecture-dependent and architecture-independent metrics to classify the different sources of memory bottlenecks we observe (Section 4.3.3).

We also evaluate various other aspects of our three-step workload characterization methodology. We investigate the effect of increasing the last-level cache on our memory bottleneck classification in Section 4.3.4. We provide a validation of our memory bottleneck clas-

⁷We show in Section 4.5.2 that our DAMOV benchmark suite is useful to rigorously study NDP accelerators.

⁸The development of a new methodology or extension of our methodology to perform analysis targeting function-specific, customized, or reconfigurable NDP accelerators is a good direction for future work.

sification in Section 4.3.5. We discuss the limitations of our proposed methodology in Section 4.3.6.

4.3.1 Step 1: Memory-Bound Function Identification

We first apply Step 1 of our methodology across 345 applications (listed in Appendix C.3) to identify functions whose performance is significantly affected by data movement. We use the previously-proposed top-down analysis methodology [1112] that has been used by several recent workload characterization studies [10, 1135, 1136]. As discussed in Section 4.2.2, we use the Intel VTune Profiler [1111], which we run on an Intel Xeon E3-1240 processor [1137] with four cores. We disable hyper-threading for more accurate profiling results, as recommended by the VTune documentation [1138]. For the applications that we analyze, we select functions (1) that take at least 3% of the clock cycles, and (2) that have a Memory Bound percentage that is greater than 30%. We choose 30% as the threshold for this metric because, in preliminary simulation experiments, we do not observe significant performance improvement or energy savings with data movement mitigation mechanisms for functions whose Memory Bound percentage is less than 30%.

The applications we analyze come from a variety of sources, such as popular workload suites (Chai [1139], CORAL [1140], Parboil [1141], PARSEC [1075], Rodinia [1142], SD-VBS [1143], SPLASH-2 [1144]), benchmarking (STREAM [1145], HPCC [1146], HPCG [1147]), bioinformatics [1148], databases [1149, 1150], graph processing frameworks (GraphMat [1151], Ligra [1152]), a map-reduce framework (Phoenix [4]), and neural networks (AlexNet [1153], Darknet [1154]). We explore different input dataset sizes for the applications and choose real-world input datasets that impose high pressure on the memory subsystem (as we expect that such real-world inputs are best suited for stressing the memory hierarchy). We also use different inputs for applications whose performance is tightly related to the input dataset properties. For example, we use two different graphs with varying connectivity degrees (rMat [1155] and USA [1156]) to evaluate graph processing applications and two different read sequences to evaluate read alignment algorithms [20, 21, 645].

In total, our application analysis covers more than 77K functions. To date, this is the most extensive analysis of data movement bottlenecks in real-world applications. We find a set of 144 functions that take at least 3% of the total clock cycles and have a value of the Memory Bound metric greater or equal to 30%, which forms the basis of DAMOV, our new data movement benchmark suite. We provide a list of all 144 functions selected based on our analysis and their major characteristics in Appendix C.1.

⁹The default HMC interleaving scheme (Row:Column:Bank:Vault [423]) interleaves consecutive cache lines across vaults, and then across banks [1157].

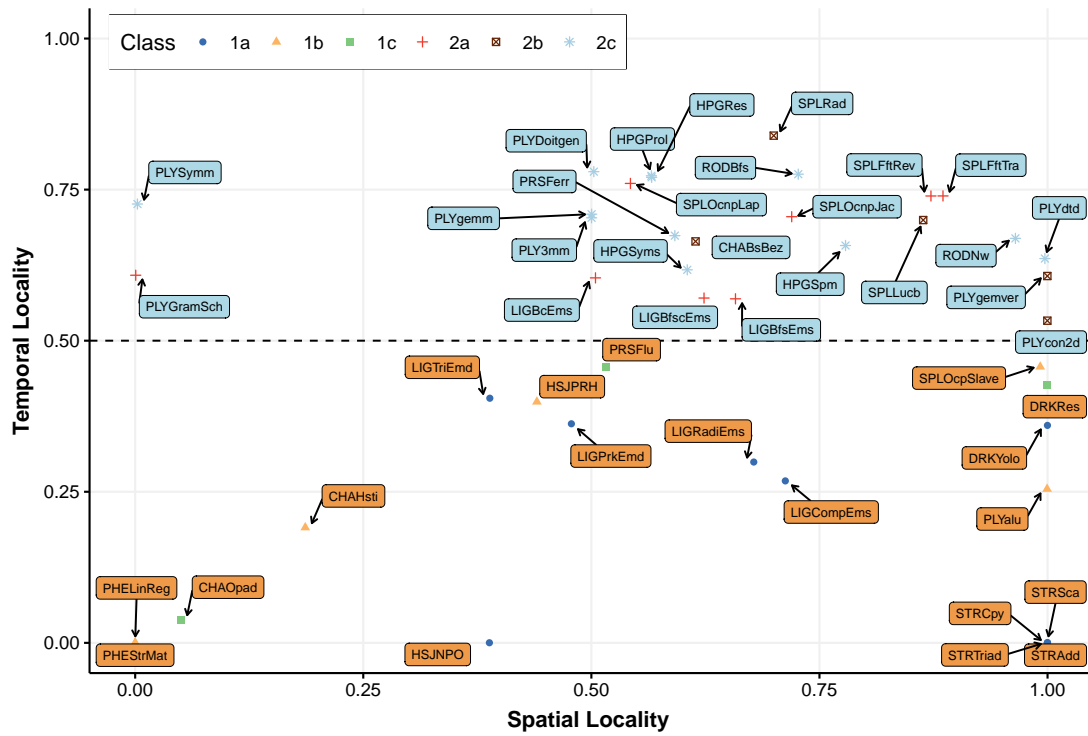


Figure 4.3: Locality-based clustering of 44 representative functions.

After identifying memory-bound functions over a wide range of applications, we apply Steps 2 and 3 of our methodology to classify the primary sources of memory bottlenecks for our selected functions. We evaluate a total of 144 functions out of the 77K functions we analyze in Step 1. These functions span across 74 different applications, belonging to 16 different widely-used benchmark suites or frameworks.

From the 144 functions that we analyze further, we select a subset of 44 representative functions to explore in-depth in Sections 4.3.2 and 4.3.3 and to drive our bottleneck classification analysis. We use the 44 representative functions to ease our explanations and make figures more easily readable. Table C.7 in Appendix C.1 lists the 44 representative functions that we select. The table includes one column that indicates the class of data movement bottleneck experienced by each function (we discuss the classes in Section 4.3.3), and another column representing the percentage of clock cycles of the selected function in the whole application. We select representative functions that belong to a variety of domains: benchmarking, bioinformatics, data analytics, databases, data mining, data reorganization, graph processing, neural networks, physics, and signal processing. In Section 4.3.5, we validate our classification using the remaining 100 functions and provide a summary of the results of our methodology when applied to all 144 functions.

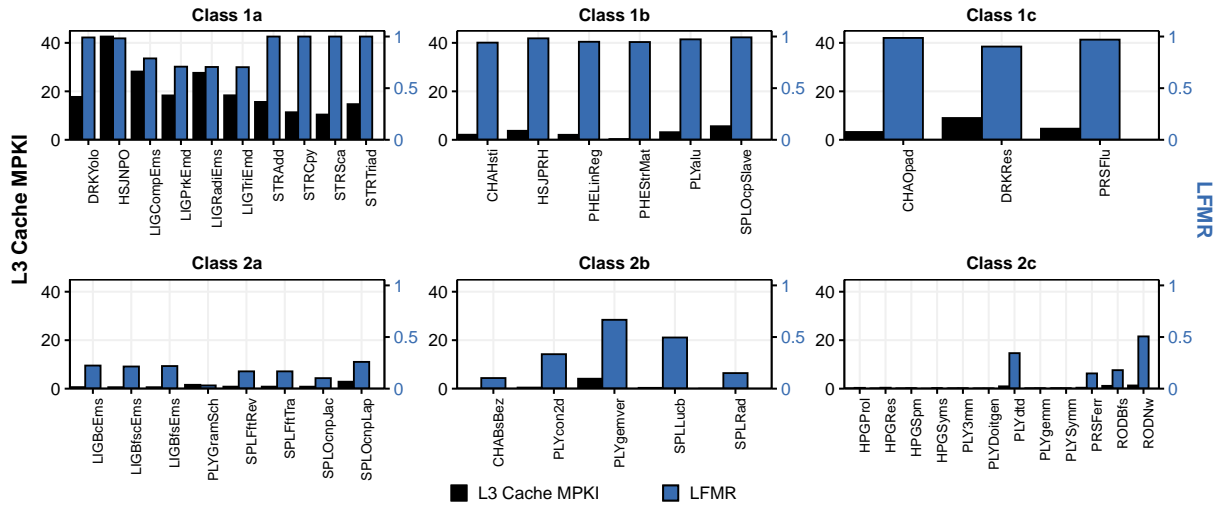


Figure 4.4: L3 Cache MPKI and Last-to-First Miss Ratio (LFMR) for 44 representative functions.

4.3.2 Step 2: Locality-Based Clustering

We cluster the 44 representative functions across both spatial and temporal locality using the K-means clustering algorithm [1158]. Figure 4.3 shows how each function is grouped. We find that two groups emerge from the clustering: (1) low temporal locality functions (orange boxes in Figure 4.3), and (2) high temporal locality functions (blue boxes in Figure 4.3). Intuitively, the closer a function is to the bottom-left corner of the figure, the less likely it is to take advantage of a multi-level cache hierarchy. These functions are more likely to be good candidates for NDP. However, as we see in Section 4.3.3, the NDP suitability of a function also depends on a number of other factors.

4.3.3 Step 3: Bottleneck Classification

Within the two groups of functions identified in Section 4.3.2, we use three key metrics (AI, MPKI, and LFM) to classify the memory bottlenecks. We observe that the AI of the analyzed low temporal locality functions is low (i.e., always less than 2.2 ops/cache line, with an average of 1.3 ops/cache line). Among the high temporal locality functions, there are some with low AI (minimum of 0.3 ops/cache line) and others with high AI (maximum of 44 ops/cache line). LFM indicates whether a function benefits from a deeper cache hierarchy. When LFM is low (i.e., less than 0.1), then a function benefits significantly from a deeper cache hierarchy, as most misses from the L1 cache hit in either the L2 or L3 caches. When LFM is high (i.e., greater than 0.7), then most L1 misses are not serviced by the the L2 or L3 caches, and must go to memory. A medium LFM (0.1–0.7) indicates that a deeper cache hierarchy can mitigate some, but not a very large fraction of L1 cache misses. MPKI indicates the memory intensity of a function (i.e., the rate at which requests are issued to DRAM). We say that a function is

memory-intensive (i.e., it has a high MPKI) when the MPKI is greater than 10, which is the same threshold used by prior works [54, 223, 653, 655, 1089, 1090, 1108].

We find that six classes of functions emerge, based on their temporal locality, AI, MPKI, and LFMR values, as we observe from Figures 4.3 and 4.4. We observe that spatial locality is not a key metric for our classification (i.e., it does not define a bottleneck class) because the L1 cache, which is present in both host CPU and NDP system configurations, can capture most of the spatial locality for a function. Figure 4.4 shows the LFMR and MPKI values for each class. Note that we do not have classes of functions for all possible combinations of metrics. In our analysis, we obtain the temporal locality, AI, MPKI, and LFMR values and their combinations empirically. Fundamentally, not all value combinations of different metrics are possible. We list some of the combinations we do *not* observe in our analysis of 144 functions:

- A function with high LLC MPKI does *not* display low LFMR. This is because a low LFMR happens when most L1 misses hit the L2/L3 caches. Thus, it becomes highly unlikely for the L3 cache to suffer many misses when the L2/L3 caches do a good job in fulfilling L1 cache misses.
- A function with high temporal locality does *not* display both high LFMR and high MPKI. This is because a function with high temporal locality will likely issue repeated memory requests to few memory addresses, which will likely be serviced by the cache hierarchy.
- A function with low temporal locality does *not* display low LFMR since there is little data locality to be captured by the cache hierarchy.

We discuss each class in detail below, identifying the memory bottlenecks for each class and whether the NDP system can alleviate these bottlenecks. To simplify our explanations, we focus on a smaller set of 12 representative functions (out of the 44 representative functions) for this part of the analysis. Figure 4.5 shows how each of the 12 functions scales in terms of performance for the *host CPU*, *host CPU with prefetcher*, and *NDP* system configurations.

Class 1a: Low Temporal Locality, Low AI, High LFMR, and High MPKI (DRAM Bandwidth-Bound Functions)

Functions in this class exert high main memory pressure since they are highly memory intensive and have low data reuse. To understand how this affects a function’s suitability for NDP, we study how performance scales as we increase the number of cores available to a function, for the host CPU, host CPU with prefetcher, and NDP system configurations. Figure 4.5(a) depicts performance¹⁰ as we increase the core count, normalized to the performance of one host CPU core, for two representative functions from Class 1a (HSJNP0 and LIGPrkEmd; we see similar trends for all functions in the class).

¹⁰Performance is the inverse of application execution time.

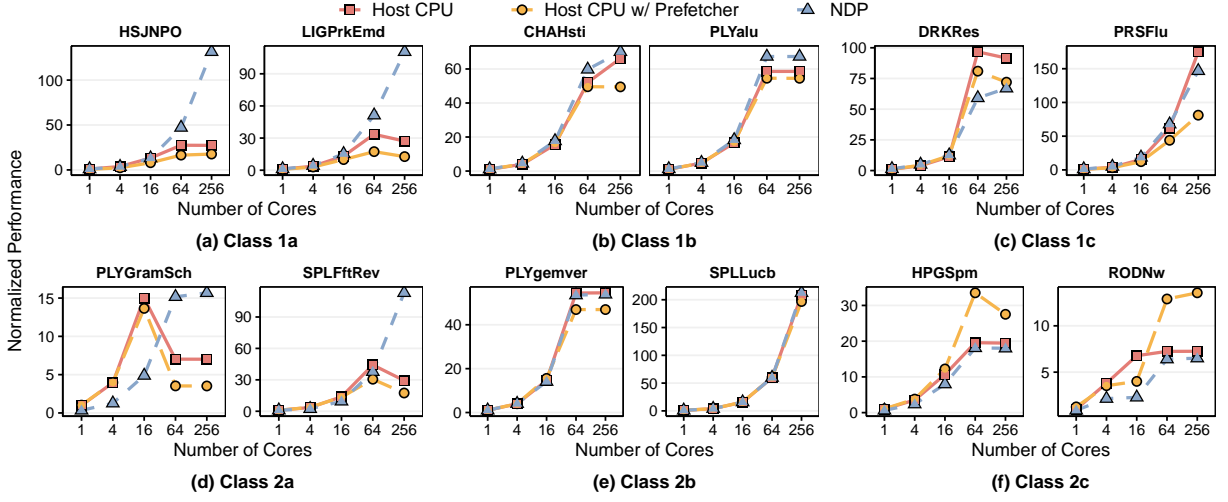


Figure 4.5: Performance of 12 representative functions on three systems: host CPU, host CPU with prefetcher, and NDP, normalized to one host CPU core.

We make three observations from the figure. First, as the number of host CPU cores increases, performance eventually stops increasing significantly. For HSJNPO, host CPU performance increases by $27.5\times$ going from 1 to 64 host CPU cores but only 27% going from 64 host CPU cores to 256 host CPU cores. For LIGPrkEmd, host CPU performance increases by $33\times$ going from 1 to 64 host CPU cores but *decreases* by 20% going from 64 to 256 host CPU cores. We find that the lack of performance improvement at large host CPU core counts is due to main memory bandwidth saturation, as shown in Figure 4.6. Given the limited DRAM bandwidth available across the off-chip memory channel, we find that Class 1a functions saturate the DRAM bandwidth once enough host CPU cores (e.g., 64) are used, and thus these functions are *bottlenecked by the DRAM bandwidth*. Second, the host CPU system with prefetcher slows down the execution of the HSJNPO (LIGPrkEmd) function compared with the host CPU system without prefetcher by 43% (38%), on average across all core counts. The prefetcher is ineffective since these functions have low temporal and spatial locality. Third, when running on the NDP system, the functions see continued performance improvements as the number of NDP cores increases. By providing the functions with access to the much higher bandwidth available inside memory, the NDP system can greatly outperform the host CPU system at a high enough core count. For example, at 64/256 cores, the NDP system outperforms the host CPU system by $1.7\times/4.8\times$ for HSJNPO, and by $1.5\times/4.1\times$ for LIGPrkEmd.

Figure 4.7 depicts the energy breakdown for our two representative functions. We make two observations from the figure. First, for HSJNPO, the energy spent on DRAM for both host CPU system and NDP system are similar. This is due to the function’s poor locality, as 98% of its memory requests miss in the L1 cache. Since LFMR is near 1, L1 miss requests almost always miss in the L2 and L3 caches and go to DRAM in the host CPU system for all core counts

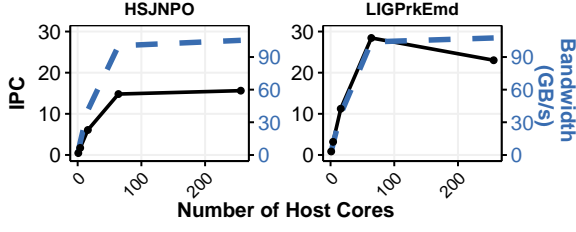


Figure 4.6: Host CPU system IPC vs. utilized DRAM Bandwidth for representative Class 1a functions.

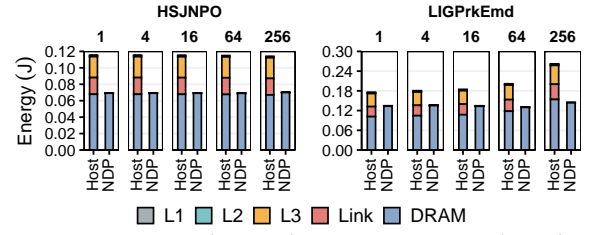


Figure 4.7: Cache and DRAM energy breakdown for representative Class 1a functions at 1, 4, 16, 64, and 256 cores.

we evaluate, which requires significant energy to query the large caches and then to perform off-chip data transfers. The NDP system does not access L2, L3, and off-chip links, leading to large system energy reduction. Second, for LIGPrkEmd, the DRAM energy is higher in the NDP system than in the host CPU system. Since the function’s LFMR is 0.7, some memory requests that would be cache hits in the host CPU’s L2 and L3 caches are instead sent directly to DRAM in the NDP system. However, the total energy consumption on the host CPU system is still larger than that on the NDP system, again because the NDP system eliminates the L2, L3 and off-chip link energy.

DRAM bandwidth-bound applications such as those in Class 1a have been the primary focus of a large number of proposed NDP architectures (e.g., [13, 56, 154, 268, 273, 288, 309, 595, 1062, 1063]), as they benefit from increased main memory bandwidth and do not have high AI (and, thus, do not benefit from complex cores on the host CPU system). An NDP architecture for a function in Class 1a needs to extract enough MLP [114–116, 135, 650, 1128, 1129, 1159–1163] to maximize the usage of the available internal memory bandwidth. However, prior work has shown that this can be challenging due to the area and power constraints in the logic layer of a 3D-stacked DRAM [13, 56]. To exploit the high memory bandwidth while satisfying these area and power constraints, the NDP architecture should leverage application memory access patterns to efficiently maximize main memory bandwidth utilization.

We find that there are two dominant types of memory access patterns among our Class 1a functions. First, functions with regular access patterns (DRKYolo, STRAdd, STRCpy, STRSca, STRTriad) can take advantage of specialized accelerators or single-instruction multiple-data (SIMD) architectures [13, 265], which can exploit the regular access patterns to issue many memory requests concurrently. Such accelerators or SIMD architectures have hardware area and thermal dissipation that fall well within the constraints of 3D-stacked DRAM [13, 56, 263, 1164]. Second, functions with irregular access patterns (HSJNPO, LIGCompEms, LIGPrkEmd, LIGRadiEms) require techniques to extract MLP while still fitting within the design constraints. This requires techniques that cater to the irregular memory access patterns, such as prefetching algorithms designed for graph processing [56, 86–88, 1165, 1166], pre-execution of difficult

access patterns [54, 55, 85, 113–116, 1167–1172] or hardware accelerators for pointer chasing [84, 90, 93, 155, 261, 311, 1079].

Class 1b: Low Temporal Locality, Low AI, High LFMR, and Low MPKI (DRAM Latency-Bound Functions)

While functions in this class do not effectively use the host CPU caches, they do *not* exert high pressure on the main memory due to their low MPKI. Across all Class 1b functions, the average DRAM bandwidth consumption is only 0.5 GB/s. However, all the functions have very high LFMR values (the minimum is 0.94 for CHAHsti), indicating that the host CPU L2 and L3 caches are ineffective. Because the functions cannot exploit significant MLP but still incur long-latency requests to DRAM, the DRAM requests fall on the critical path of execution and stall forward progress [54, 55, 116, 650, 1173]. Thus, Class 1b functions are *bottlenecked by DRAM latency*. Figure 4.5(b) shows performance of both the host CPU system and the NDP system for two representative functions from Class 1b (CHAHsti and PLYalu). We observe that while performance of both the host CPU system and the NDP system scale well as the core count increases, NDP system performance is always higher than the host CPU system performance for the same core count. The maximum (average) speedup with NDP over host CPU at the same core count is $1.15\times$ ($1.12\times$) for CHAHsti and $1.23\times$ ($1.13\times$) for PLYalu.

We find that the NDP system’s improved performance is due to a reduction in the Average Memory Access Time (AMAT) [1174]. Figure 4.8 shows the AMAT for our two representative functions. Memory accesses take significantly longer in the host CPU system than in the NDP system due to the additional latency of looking up requests in the L2 and L3 caches, even though data is rarely present in those caches, and going through the off-chip links.

Figure 4.9 shows the energy breakdown for Class 1b representative functions. Similar to Class 1a, we observe that the L2/L3 caches and off-chip links are a large source of energy usage in the host CPU system. While DRAM energy increases in the NDP system, as L2/L3 hits in the host CPU system become DRAM lookups with NDP, the overall energy consumption in the NDP system is greatly smaller (by 69% maximum and 39% on average) due to the lack of L2 and L3 caches.

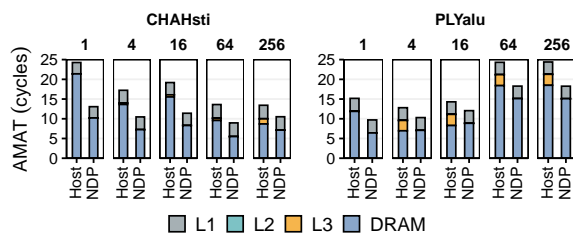


Figure 4.8: Average Memory Access Time (AMAT) for representative Class 1b functions.

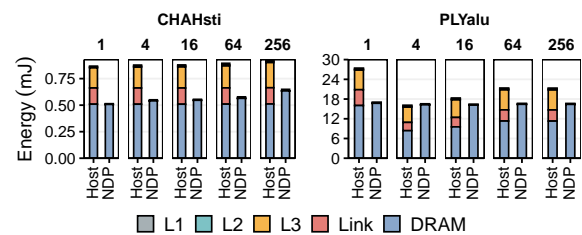


Figure 4.9: Energy breakdown for representative Class 1b functions.

Class 1b functions benefit from the NDP system, but primarily because of the lower memory access latency (and energy) that the NDP system provides for memory requests that need to be serviced by DRAM. These functions could benefit from other latency and energy reduction techniques, such as L2/L3 cache bypassing [150, 1059, 1064, 1175–1184], low-latency DRAM [1, 163, 171–175, 178, 179, 181, 183, 186, 224, 225, 317, 350, 377, 493, 495, 1185–1189], and better memory access scheduling [498, 649, 650, 652–655, 1089, 1090, 1108, 1125, 1173, 1190–1200]. However, they generally do *not* benefit significantly from prefetching (as seen in Figure 4.5(b)), since infrequent memory requests make it difficult for the prefetcher to successfully train on an access pattern.

Class 1c: Low Temporal Locality, Low AI, Decreasing LFMR with Core Count, and Low MPKI (*L1/L2 Cache Capacity Bottlenecked Functions*)

We find that the behavior of functions in this class depends on the number of cores they are using. Figure 4.5(c) shows the host CPU system and the NDP system performance as we increase the core count for two representative functions (DRKRes and PRSFlu). We make two observations from the figure. First, at low core counts, the NDP system outperforms the host CPU system. With a low number of cores, the functions have medium to high LFMR (0.5 for DRKRes at 1 and 4 host CPU cores; 0.97 at 1 host CPU core and 0.91 at 4 host CPU cores for PRSFlu), and behave like Class 1b functions, where they are DRAM latency-sensitive. Second, as the core count increases, the host CPU system begins to outperform the NDP system. For example, beyond 16 (64) cores, the host CPU system outperforms the NDP system for DRKRes (PRSFlu). This is because as the core count increases, the aggregate L1 and L2 cache size available at the host CPU system grows, which reduces the miss rates of both L2 and L3 caches. As a result, the LFMR decreases significantly (e.g., at 256 cores, LFMR is 0.09 for DRKRes and 0.35 for PRSFlu). This indicates that the *available L1/L2 cache capacity* bottlenecks Class 1c functions.

Figure 4.10 shows the energy breakdown for Class 1c functions. We make three observations from the figure. First, for functions with larger LFMR values (PRSFlu), the NDP system provides energy savings over the host CPU system at lower core counts, since the NDP system eliminates the energy consumed due to L3 and off-chip link accesses. Second, for functions with smaller LFMR values (DRKRes), the NDP system does not provide energy savings even for low core counts. Due to the medium LFMR, enough requests still hit in the host CPU system L2/L3 caches, and these cache hits become DRAM accesses in the NDP system, which consume more energy than the cache hits. Third, at high-enough core counts, the NDP system consumes more energy than the host CPU system for all Class 1c functions. As the LFMR decreases, the functions effectively utilize the caches in the host CPU system, reducing the off-

chip traffic and, consequently, the energy Class 1c functions spend on accessing DRAM. The NDP system, which does not have L2 and L3 caches, pays the larger energy cost of a DRAM access for all L2/L3 hits in the host CPU system.

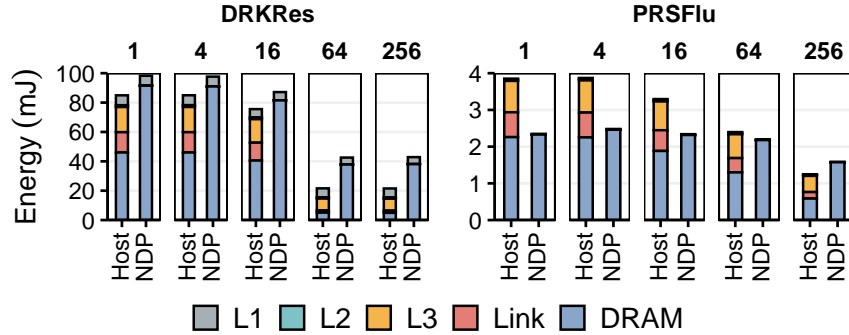


Figure 4.10: Energy breakdown for representative Class 1c functions.

We find that the primary source of the memory bottleneck in Class 1c functions is limited L1/L2 cache capacity. Therefore, while the NDP system improves performance and energy of some Class 1c functions at low core counts (with lower associated L1/L2 cache capacity), the NDP system does not provide performance and energy benefits across all core counts for Class 1c functions.

Class 2a: High Temporal Locality, Low AI, Increasing LFMR with Core Count, and Low MPKI (L3 Cache Contention Bottlenecked Functions)

Like Class 1c functions, the behavior of the functions in this class depends on the number of cores that they use. Figure 4.5(d) shows the host CPU system and the NDP system performance as we increase the core count for two representative functions (PLYGramSch and SPLFftRev). We make two observations from the figure. First, at low core counts, the functions do *not* benefit from the NDP system. In fact, for a single core (16 cores), PLYGramSch *slows down* by 67% (3 \times) when running on the NDP system, compared to running on the host CPU system. This is because, at low core counts, these functions make reasonably good use of the cache hierarchy, with LFMR values of 0.03 for PLYGramSch and lower than 0.44 for SPLFftRev until 16 host CPU cores. We confirm this in Figure 4.11, where we see that very few memory requests for PLYGramSch and SPLFftRev go to DRAM (5% for PLYGramSch, and at most 13% for SPLFftRev) at core counts lower than 16. Second, at high core counts (i.e., 64 for PLYGramSch and 256 for SPLFftRev), the host CPU system performance starts to *decrease*. This is because Class 2a functions are *bottlenecked by cache contention*. At 256 cores, this contention undermines the cache effectiveness and causes the LFMR to increase to 0.97 for PLYGramSch and 0.93 for SPLFftRev. With the last-level cache rendered essentially ineffective, the NDP system greatly improves performance over the host CPU system: by 2.23 \times for PLYGramSch and 3.85 \times for SPLFftRev at 256 cores.

One impact of the increased cache contention is that it converts these high-temporal-locality functions into memory latency-bound functions. We find that with the increased number of requests going to DRAM due to cache contention, the AMAT increases significantly, in large part due to queuing at the memory controller. At 256 cores, the queuing becomes so severe that a large fraction of requests (24% for PLYGramSch and 67% for SPLFftRev) must be reissued because the memory controller queues are full. The increased main memory bandwidth available to the NDP cores allows the NDP system to issue many more requests concurrently, which reduces the average length of the queue and, thus, the main memory latency. The NDP system also reduces memory access latency by getting rid of L2/L3 cache lookup and interconnect latencies.

Figure 4.12 shows the energy breakdown for the two representative Class 2a functions. We make two observations. First, the host CPU system is more energy-efficient than the NDP system at low core counts, as most of the memory requests are served by on-chip caches in the host CPU system. Second, the NDP system provides large energy savings over the host CPU system at high core counts. This is due to the increased cache contention, which increases the number of off-chip requests that the host CPU system must make, increasing the L3 and off-chip link energy.

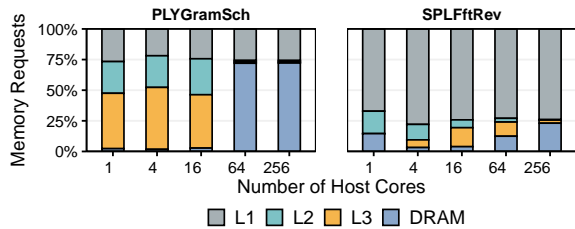


Figure 4.11: Memory request breakdown for representative Class 2a functions.

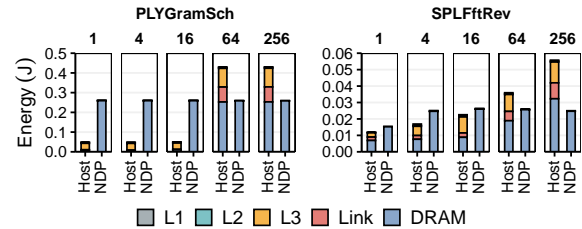


Figure 4.12: Energy breakdown for representative Class 2a functions.

We conclude that cache contention is the primary scalability bottleneck for Class 2a functions, and the NDP system can provide an effective way of mitigating this cache contention bottleneck without incurring the high area and energy overheads of providing additional cache capacity in the host CPU system, thereby improving the scalability of these applications to high core counts.

Class 2b: High Temporal Locality, Low AI, Low/Medium LFMR, and Low MPKI (*L1 Cache Capacity Bottlenecked Functions*)

Figure 4.5(e) shows the host CPU system and the NDP system performance for PLYgemver and SPLLucb. We make two observations from the figure. First, as the number of cores increases, performance of the host CPU system and the NDP system scale in a very similar fashion. The NDP system and the host CPU system perform essentially on par with (i.e., within 1% of)

each other at all core counts. Second, even though the NDP system does not provide any performance improvement for Class 2b functions, it also does not hurt performance. Figure 4.13 shows the AMAT for our two representative functions. When PLYgemver executes on the host CPU system, up to 77% of the memory latency comes from accessing L3 and DRAM, which can be explained by the function’s medium LFMR (0.5). For SPLLucb, even though up to 73% of memory latency comes from L1 accesses, some requests still hit in the L3 cache (its LFMR is 0.2), translating to around 10% of the memory latency. However, the latency that comes from L3 + DRAM for the host CPU system is similar to the latency to access DRAM in the NDP system, resulting in similar performance between the host CPU system and the NDP system.

We make a similar observation for the energy consumption for the host CPU system and the NDP system (Figure 4.14). Even though a small number of memory requests hit in L3, the total energy consumption for both the host CPU system and the NDP system is similar due to L3 and off-chip link energy. For some functions in Class 2b, we observe that the NDP system slightly reduces energy consumption compared to the host CPU system. For example, the NDP system provides an 12% average reduction in energy consumption, across all core counts, compared to the host CPU system for PLYgemver.

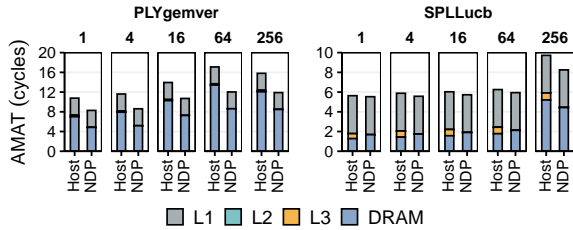


Figure 4.13: AMAT for representative Class 2b functions.

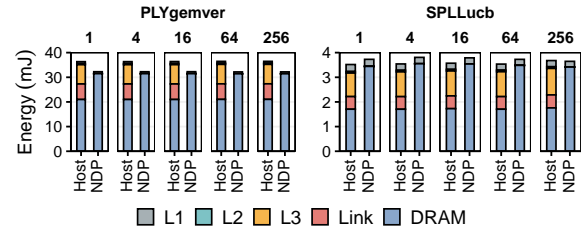


Figure 4.14: Energy breakdown for representative Class 2b functions.

We conclude that while the NDP system does not solve any memory bottlenecks for Class 2b functions, it can be used to reduce the overall SRAM area in the system without any performance or energy penalty (and sometimes with energy savings).

Class 2c: High Temporal Locality, High AI, Low LFMR, and Low MPKI (*Compute-Bound Functions*).

Aside from one exception (PLYSymm), all of the 11 functions in this class exhibit high temporal locality. When combined with the high AI and low memory intensity, we find that these characteristics significantly impact how the NDP system performance scales for this class. Figure 4.5(f) shows the host CPU system and the NDP system performance for HPGSpm and RODNw, two representative functions from the class. We make two observations from the figure. First, the host CPU system performance is *always* greater than the NDP system performance (by 44% for HPGSpm and 54% for RODNw, on average). The high AI (more than 12 ops per cache line), combined with the high temporal locality and low MPKI, enables these functions to make

excellent use of the host CPU system resources. Second, both of the functions benefit greatly from prefetching in the host CPU system. This is a direct result of these functions' high spatial locality, which allows the prefetcher to be highly accurate and effective in predicting which lines to retrieve from main memory.

Figure 4.15 shows the energy breakdown consumption for the two representative Class 2c functions. We make two observations. First, the host CPU system is 77% more energy-efficient than the NDP system for HPGSpm, on average across all core counts. Second, the NDP system provides energy savings over the host CPU system at high core counts for RODNw (up to 65% at 256 cores). When the core count increases, the aggregate L1 cache capacity across all cores increases as well, which in turn decreases the number of L1 cache misses. Compared to executing on a single core, executing on 256 cores decreases the L1 cache miss count by 43%, reducing the memory subsystem energy consumption by 40%. However, due to RODNw's medium LFMR of 0.5, the host CPU system still suffers from L2 and L3 cache misses at high core counts, which require the large L3 and off-chip link energy. In contrast, the NDP system eliminates the energy of accessing the L3 cache and the off-chip link energy by directly sending L1 cache misses to DRAM, which, at high core counts, leads to lower energy consumption than the host CPU system.

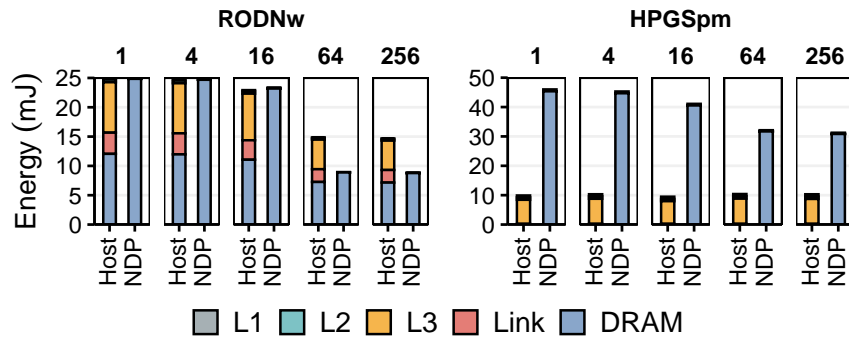


Figure 4.15: Energy breakdown for representative Class 2c functions.

We conclude that Class 2c functions do not experience large memory bottlenecks and are not a good fit for the NDP system in terms of performance. However, the NDP system can sometimes provide energy savings for functions that experience medium LFMR.

4.3.4 Effect of the Last-Level Cache Size

The bottleneck classification we present in Section 4.3.3 depends on two key architecture-dependent metrics (LFMR and MPKI) that are directly affected by the parameters and the organization of the cache hierarchy. Our analysis in Section 4.3.3 partially evaluates the effect of caching by scaling the aggregated size of the private (L1/L2) caches with the number of cores in the system while maintaining the size of the L3 cache fixed at 8 MB for the host CPU sys-

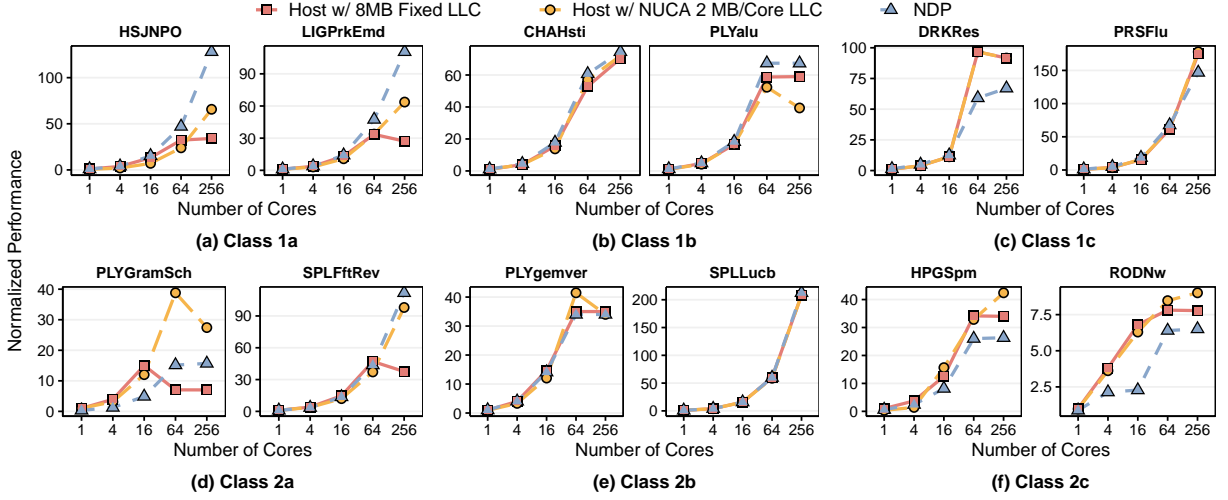


Figure 4.16: Performance of the host and the NDP system as we vary the LLC size, normalized to one host core with a fixed 8MB LLC size.

tem. However, we also need to understand the impact of the L3 cache size on our bottleneck classification analysis. To this end, this section evaluates the effects on our bottleneck classification analysis of using an alternative cache hierarchy configuration, where we employ a Non-Uniform Cache Architecture (NUCA) [490] model to scale the size of the L3 cache with the number of cores in the host CPU system.

In this configuration, we maintain the sizes of the private L1 and L2 caches (32 kB and 256 kB per core, respectively) while increasing the shared L3 cache size with the core count (we use 2 MB/core) in the host CPU system. The cores, shared L3 caches, and DRAM memory controller are interconnected using a 2D-mesh Network-on-Chip (NoC) [1201–1208] of size $(n + 1) \times (n + 1)$ (an extra interconnection dimension is added to place the DRAM memory controllers). To faithfully simulate the NUCA model (e.g., including network contention in our simulations), we integrate the M/D/1 network model proposed by ZSim++ [1209] in our DAMOV simulator [1109]. We use a latency of 3 cycles per hop in our analysis, as suggested by prior work [811]. We adapt our energy model to account for the energy consumption of the NoC in the NUCA system. We consider router energy consumption of 63 pJ per request and energy consumed per link traversal of 71 pJ, same as previous work [1064].

Figure 4.16 shows the performance scalability curves for representative functions from each one of our bottleneck classes presented in Section 4.3.3 for the baseline host CPU system (*Host with 8MB Fixed LLC*), the host CPU NUCA system (*Host with NUCA 2MB/Core LLC*), and the NDP system. We make two observations. First, the observations we make for our bottleneck classification (Section 4.3.3) are *not* affected by increasing the L3 cache size for Classes 1a, 1b, 1c, 2b, and 2c. We observe that Class 1a functions benefit from a large L3 cache size (by up to $1.9\times/2.3\times$ for HSJNPO/LIGPrkEmd at 256 cores). However, the NDP system still

provides performance benefits compared to the host CPU NUCA system. We observe that increasing the L3 size reduces some of the pressure on main memory but cannot fully reduce the DRAM bandwidth bottleneck for Class 1a functions. Functions in Class 1b do *not* benefit from extra L3 capacity (we do not observe a decrease in LFMR or MPKI). Functions in Class 1c do *not* benefit from extra L3 cache capacity. We observe that the private L1 and L2 caches capture most of their data locality, as mentioned in Section 4.3.3, and thus, these functions do *not* benefit from increasing the L3 size. Functions in Class 2b do *not* benefit from extra L3 cache capacity, which can even lead to a decrease in performance at high core counts for the host CPU NUCA system in some Class 2b functions due to long NUCA L3 access latencies. For example, we observe that PLYgemver’s performance drops 18% when increasing the core count from 64 to 256 in the host CPU NUCA system. We do *not* observe such a performance drop for the host CPU system with fixed LLC size. The performance drop in the host CPU NUCA system is due to the increase in the number of hops that L3 requests need to travel in the NoC at high core counts, which increase the function’s AMAT. Class 2c functions benefit from a larger last-level cache. We observe that their performance improves by $1.3\times/1.2\times$ for HPGSpm/RODNw compared to the host CPU system with 8MB fixed LLC at 256 cores.

Second, we observe two different types of behavior for functions in Class 2a. Since cache conflicts are the major bottleneck for functions in this class, we observe that increasing the L3 cache size can mitigate this bottleneck. In Figure 4.16, we observe that for both PLYGramSch and SPLFftRev, the host system with NUCA 2MB/Core LLC provides better performance than the host system with 8MB fixed LLC. However, the NDP system can still provide performance benefits in case of contention on the L3 NoC (e.g., in SPLFftRev). For example, the NDP system provides 14% performance improvement for SPLFftRev compared to the NUCA system (with 512 MB L3 cache) for 256 cores.

In summary, we conclude that the key takeaways and observations we present in our bottleneck classification in Section 4.3.3 are also valid for a host system with a shared last-level cache whose size scales with core count. In particular, different workload classes get affected by an increase in L3 cache size as expected by their characteristics distilled by our classification.

Figure 4.17 shows the energy consumption for representative functions from each one of our bottleneck classes presented in Section 4.3.3. We observe that the NDP system can provide substantial energy savings for functions in different bottleneck classes, even compared against a system with very large (e.g., 512 MB) cache sizes. We make the following observations for each bottleneck class:

- *Class 1a*: First, for both representative functions in this bottleneck class, the host CPU NUCA system and the NDP system reduce energy consumption compared to the baseline host CPU

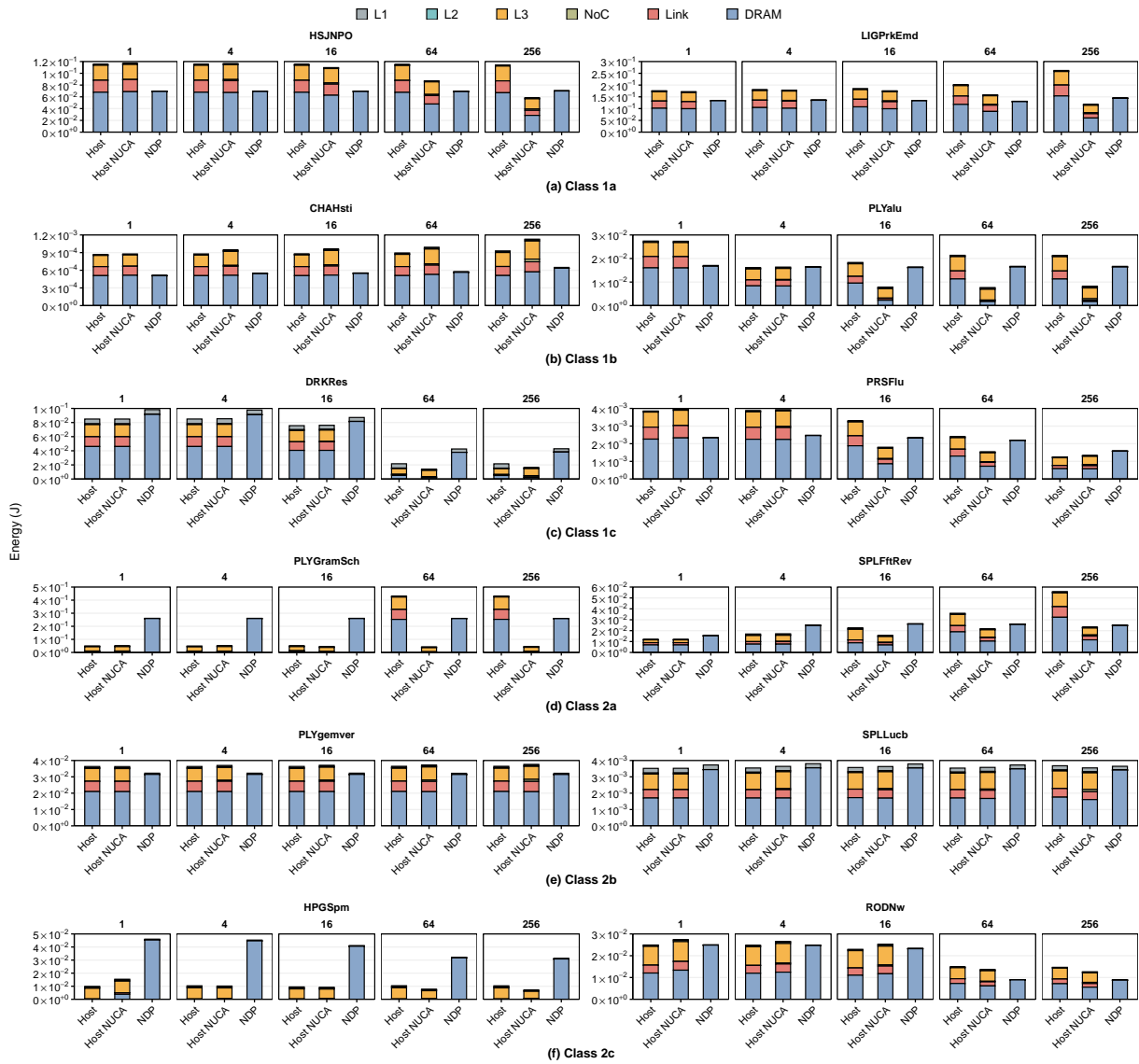


Figure 4.17: Energy of the host and the NDP system as we vary the LLC size. *Host* refers to the host system with a fixed 8MB LLC size; *Host NUCA* refers to the host system with 2MB/Core LLC.

system. However, we observe that the NDP system provides larger energy savings than the host CPU NUCA system. On average, across all core counts, the NDP system and the host CPU NUCA system reduce energy consumption compared to the host CPU system for HSNPO/LIGPrkEmd by 46%/65% and 25%/22%, respectively. Second, at 256 cores, the host CPU NUCA system provides larger energy savings than the NDP system for both representative functions. This happens because at 256 cores, the large L3 cache (i.e., 512 MB) captures a large portion of the dataset for these functions, reducing costly DRAM traffic. The host CPU NUCA system reduces energy consumption compared to the host CPU system for HSNPO/LIGPrkEmd at 256 cores by 2.0×/2.2× while the NDP system reduces energy consumption by 1.6×/1.8×. The L3 cache capacity needed to make the host CPU NUCA sys-

tem more energy efficient than the NDP system is *very* large (512 MB SRAM), which is likely not cost-effective.

- *Class 1b*: First, for CHA_{Hst}i, the host CPU NUCA system *increases* energy consumption compared to the host CPU system by 9%, on average across all core counts. In contrast, the NDP system *reduces* energy consumption by 57%. Due to its low spatial and temporal locality (Figure 4.3), this function does not benefit from a deep cache hierarchy. In the host CPU NUCA system, the extra energy from the large amount of NoC traffic further increases the cache hierarchy's overall energy consumption. Second, for PLY_{alu}, the host CPU NUCA system and the NDP system reduce energy consumption compared to the host CPU system by 76% and 23%, on average across all core counts. Even though the increase in LLC size does not translate to performance improvements, the large LLC sizes in the host CPU NUCA system aid to reduce DRAM traffic, thereby providing energy savings compared to the baseline host CPU system.
- *Class 1c*: First, for DRK_{Res}, the host CPU NUCA system reduces energy consumption compared to the host CPU system by 15%, on average across all core counts. In contrast, the NDP system increases energy consumption by 30%, which is due to the function's medium LFMR (Section 4.3.3). Second, for PRS_{F1u}, we observe that the NDP system provides large energy savings than the host CPU NUCA system. The host CPU NUCA system reduces energy consumption compared to the host CPU system by 21%, while the NDP system reduces energy consumption by 25%, on average across all core counts. However, the energy savings of both host CPU NUCA and NDP systems compared to the host CPU system reduces at high-enough core counts (the energy consumption of the host CPU NUCA system (NDP system) is $0.6\times$ ($0.9\times$) that of the host CPU system at 64 cores and $1.1\times$ ($1.3\times$) that of the host CPU system at 256 cores). This result is expected for Class 1c functions since the functions in this class have decreasing LFMR, i.e., the functions effectively utilize the private L1/L2 caches in the host CPU system at high-enough core counts.
- *Class 2a*: First, for PLY_{GramSch}, compared to the host CPU system the host CPU NUCA system reduces energy consumption by $2.53\times$ and the NDP system increases energy consumption by 55%, on average across all core counts. Even though at high core counts (64 and 256 cores) the host CPU NUCA system provides larger energy savings than the NDP system compared to the host CPU system (the host CPU NUCA system and the NDP system reduce energy consumption compare to the host CPU system by $9\times$ and 65% respectively, averaged across 64 and 256 cores), such large energy savings come at the cost of very large (e.g., 512 MB) cache sizes. Second, for SPL_{FftRev}, the host CPU NUCA system and the NDP system reduce energy consumption compared to the host CPU system by 42% and 7%, on average across all core counts. The NDP system increases energy consumption compared

to the host CPU system at low core counts (an increase of 33%, averaged across 1, 4, and 16 cores). However, it provides similar energy savings as the host CPU NUCA system for large core counts (99% and 75% energy reduction compare to the host CPU system for the host CPU NUCA system and the NDP system, respectively, averaged across 64 and 256 cores counts). Since the function suffers from high network contention, the increase in core count increases NoC traffic, which in turn increases energy consumption for the host CPU NUCA system. We conclude that the NDP system provides energy savings for Class 2a applications compared to the host CPU system at lower cost than the host CPU NUCA system.

- *Class 2b*: First, for PLYgemver, the host CPU NUCA system increases energy consumption compared to the host CPU system by 2%, on average across all core counts. In contrast, the NDP system reduces energy consumption by 13%. This function does not benefit from large L3 cache sizes since Class 2b functions are bottlenecked by L1 capacity. Thus, the NoC only adds extra static and dynamic energy consumption. Second, for SPLLucb, the host CPU NUCA system consumes the same energy as the host CPU system while the NDP system increases energy consumption by 5%, averaged across all core counts.
- *Class 2c*: For both representative functions in this class, the host CPU NUCA system reduces energy consumption compared to the host CPU system while the NDP system increases energy consumption. For HPGSpm/RODNw, the host CPU NUCA system reduces energy consumption by 6%/9% while the NDP system increases energy consumption by 74%/22%, averaged across all core counts. This result is expected since Class 2c functions are compute-bound and highly benefit from a deep cache hierarchy.

In conclusion, the NDP system can provide substantial energy savings for functions in different bottleneck classes, even compared against a system with very large (e.g., 512 MB) cache sizes.

4.3.5 Validation and Summary of Our Workload Characterization Methodology

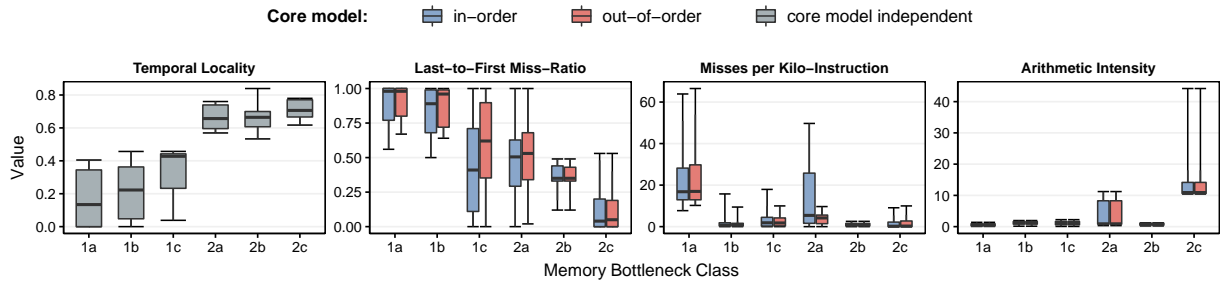
In this section, we present the validation and a summary of our new workload characterization methodology. First, we use the remaining 100 memory-bound functions we obtain from *Step 1* (see Section 4.3.1) to validate our workload characterization methodology. To do so, we calculate the accuracy of our workload classification by using the remaining 100 memory-bound functions, which were not used to identify the six classes we found and described in Section 4.3.3. Second, we present a summary of the key metrics we obtain for all 144 memory-bound functions, including our analysis of the host CPU system and the NDP system using two types of cores (in-order and out-of-order).

Validation of Our Workload Characterization Methodology

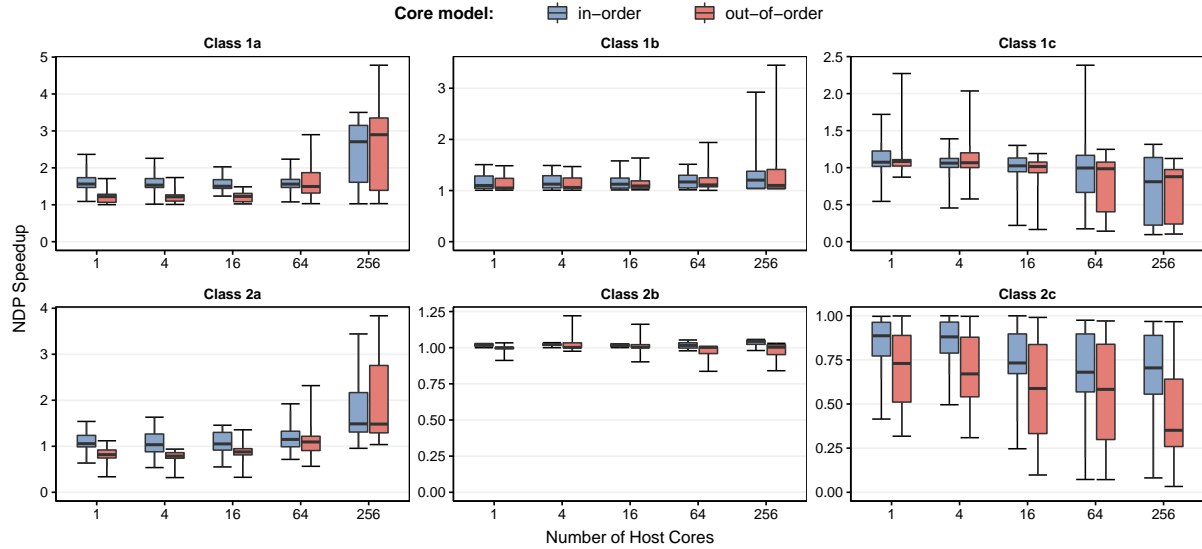
Our goal is to evaluate the accuracy of our workload characterization methodically on a large set of functions. To this end, we apply *Step 2* and *Step 3* of our memory bottleneck classification methodology (as described in Sections 4.2.3 and 4.2.4) to the remaining 100 memory-bound functions we obtain from *Step 1* (in Section 4.3.1). Then, we perform a two-phase validation to calculate the accuracy of our workload characterization.

In *phase 1* of our validation, we calculate the threshold values that define the low/high boundaries of each of the four metrics we use to cluster the initial 44 functions in the six memory bottleneck classes in Section 4.3.3 (i.e., temporal locality, LFMR, LLC MPKI, and AI). We also include the LFMR curve slope to indicate when the LFMR increases, decreases or stays constant as we scale the core count. We calculate the threshold values for a metric *M* by computing the middle point between (i) the average value of *M* across the memory bottleneck classes with *low* values of *M* and (ii) the average value of *M* across the memory bottleneck classes with *high* values of *M* values out of the 44 functions. In *phase 2* of our validation, we calculate the accuracy of our workload characterization by classifying the remaining 100 memory-bound functions using the threshold values obtained from *phase 1* and the LFMR curve slope. After *phase 2*, a function is considered to be *accurately* classified into a correct memory bottleneck class if and only if it (1) fits the definition of the assigned class using the threshold values obtained from *phase 1* and (2) follows the expected performance trends of the assigned class when the function is executed in the host CPU system and the NDP system. For example, a function is correctly classified into Class 1a *if and only if* it (1) displays low temporal locality, low AI, high LFMR, high MPKI and (2) the NDP system outperforms the host CPU system as we scale the core count when executing the function. The final *accuracy of our workload characterization methodology* is calculated by computing the percentage of the functions that are *accurately* classified into one of the six memory bottleneck classes.

First, by applying *phase 1* of our two-phase validation, we obtain that the threshold values are: 0.48 for *temporal locality*, 0.56 for *LFMR*, 11.0 for *MPKI*, and 8.5 for *AI*. Second, by applying *phase 2* of our two-phase validation, we find that we can accurately classify 97% of the 100 memory-bound functions into one of our six memory bottleneck classes (i.e., the accuracy of our workload characterization methodology is 97%). We observe that three functions (*Ligra:ConnectedComponents:compute:rMat*, *Ligra:MaximalIndependentSet:edgeMapDense:USA*, and *SPLASH-2:Oceanncp:relax*) could not be accurately classified into their correct memory bottleneck class (Class 1a). We observe that these functions have LLC MPKI values *lower* than the MPKI threshold expected for Class 1a functions. We expect that the accuracy of our



(a) Summary of the key metrics for each memory bottleneck class.



(b) Summary of NDP speedup for each memory bottleneck class at 1, 4, 16, 64, and 256 cores.

Figure 4.18: Summary of our characterization for all 144 memory-bound functions. Each box is lower-bounded by the first quartile and upper-bounded by the third quartile. The median falls within the box. The inter-quartile range (IQR) is the distance between the first and third quartiles (i.e., box size). Whiskers extend to the minimum and maximum data point values on either sides of the box.

methodology can be further improved by incorporating more workloads into our workload suite and fine-tuning each metric to encompass an even larger set of applications.

We conclude that our workload characterization methodology can accurately classify a given new application/function into its appropriate memory bottleneck class.

Summary of Our Workload Characterization Results.

Figure 4.18a summarizes the metrics we collect for all 144 functions across all core counts (i.e., from 1 to 256 cores) and different core microarchitectures (i.e., out-of-order and in-order cores). The figure shows the distribution of the key metrics we use during our workload characterization for each memory bottleneck class in Section 4.3.3, including architecture-independent metrics (i.e., temporal locality) and architecture-dependent metrics (i.e., AI, LFM, and LLC MPKI). We report the architecture-dependent metrics for two core models: (i) in-order and (ii)

out-of-order cores.¹¹ Together with the out-of-order core model that we use in Section 4.3.3, we incorporate an in-order core model to our analysis, so as to show that our memory bottleneck classification methodology focuses on data movement requirements and works independently of the core microarchitecture. Figure 4.18b shows the distribution of speedups we observe for when we offload the function to our general-purpose NDP cores, while employing the same core type as the host CPU system.

We make two key observations from Figure 4.18. First, we observe similar values for each architecture-dependent key metric (i.e., LFMR, MPKI, AI) regardless of core type for all 144 functions (in Figure 4.18a). Second, we observe that the NDP system achieves similar speedups over the host CPU system, when using both in-order and out-of-order core configurations (in Figure 4.18b). The speedup provided by the NDP system compared to the host CPU system when both systems use out-of-order (in-order) cores for Classes 1a, 1b, 1c, 2a, 2b, and 2c is 1.59 (1.77), 1.22 (1.15), 0.96 (0.95), 1.04 (1.22), 0.94 (1.01), and 0.56 (0.76), respectively, on average across all core counts and functions within a memory bottleneck class. The NDP system greatly outperforms the host CPU system across *all core counts* for Class 1a and 1b functions, with a maximum speedup for the out-of-order (in-order) core model of 4.8 (3.5) and 3.4 (2.9), respectively. The NDP system greatly outperforms the host CPU system at *low core counts* for Class 1c functions and at *high core counts* for Class 2a functions, with a maximum speedup for the out-of-order (in-order) core model of 2.3 (2.4) and 3.8 (3.4), respectively. The NDP system provides a modest speedup compared to the host CPU system across *all core counts* for Class 2b functions and slowdown for Class 2c functions, with a maximum speedup for the out-of-order (in-order) core model of 1.2 (1.1) and 1.0 (1.0), respectively. We observe that, averaged across all classes and core types, the average speedup provided by the NDP system using in-order cores is 11% higher than the average speedup offered by the NDP system using out-of-order cores. This is because the host CPU system with out-of-order cores can hide the performance impact of memory access latency to some degree (e.g., using dynamic instruction scheduling) [55, 113–116, 1210]. On the other hand, the host CPU system using in-order cores has little tolerance to hide memory access latency [55, 113–116, 1210].

We conclude that our methodology to classify memory bottlenecks of applications is *robust* and *effective* since we observe similar trends for the six memory bottleneck classes across a large range of (144) functions and two very different core models.

¹¹In Section 4.3.3, we collect and report the values of the architecture-independent metrics and architecture-dependent metrics for a subset of 44 representative functions out of the 144 memory-bound functions we identify in *Step 1* of our workload characterization methodology. In Section 4.3.5, we report values for the *complete set* of 144 memory-bound functions.

4.3.6 Limitations of Our Methodology

We identify three limitations to our workload characterization methodology. We discuss each limitation next.

NDP Architecture Design Space. Our methodology uses the same type and number of cores in the host CPU and the NDP system configurations for our scalability analysis (Section 4.3.3) because our main goal is to highlight the performance and energy differences between the host CPU system and the NDP system that are caused by data movement. We do not consider practical limitations related to area or thermal dissipation that could affect the type and the maximum number of cores in the NDP system, because our goal is **not** to propose NDP architectures but to characterize data movement and understand the different data movement bottlenecks in modern workloads. Proposing NDP architectures for the workload classes that our methodology identifies as suitable for NDP is a promising topic for future work.

Function-level Analysis. We choose to conduct our analysis at a function granularity rather than at the application granularity for two major reasons. First, general-purpose NDP architectures are typically leveraged as accelerators to which only *parts* of the application or specific functions are offloaded [13, 57, 154, 156, 239, 251, 261, 263, 264, 272, 279, 297, 309, 310, 314, 317, 320, 326, 378, 595, 1211, 1212], rather than the entire application. Functions typically form natural boundaries for parts of algorithms/applications that can potentially be offloaded. Second, it is well-known that applications go through distinct phases during execution. Each phase may have different characteristics (e.g., a phase might be more compute-bound, while another one might be more memory-bound) and thus fall into different classes in our analysis. A fine-grained analysis at the function level enables us to identify each of those phases and hence, identify more fine-grained opportunities for NDP offloading. However, the main drawback of function-level analysis is that it does not take into account data movement across function boundaries, which affects the performance and energy benefits the NDP system provides over the host CPU system. For example, the NDP system might hurt overall system performance and energy consumption when a large amount of data needs to be continuously moved between a function executing on the NDP cores and another executing on the host CPU cores [262, 271].

Overestimating NDP Potential. Offloading kernels to NDP cores incurs overheads that our analysis does not account for (e.g., maintaining coherence between the host CPU and the NDP cores [262, 271], efficiently synchronizing computation across NDP cores [6, 243], providing virtual memory support for the NDP system [57, 155, 1106], and dynamic offloading support for NDP-friendly functions [272]). Such overheads can impact the performance benefits NDP can provide when considering the end-to-end application. However, deciding how to and whether or not to offload computation to NDP is an open research topic, which involves several

architecture-dependent components in the system, such as the following two examples. First, maintaining coherence between the host CPU and the NDP cores is a challenging task that recent works tackle [262, 271]. Second, enabling efficient synchronization across NDP cores is challenging due to the lack of shared caches and hardware cache coherence protocols in NDP systems. Recent works, such as [243, 1213], provide solutions to the NDP synchronization problem. Therefore, to focus our analysis on the data movement characteristics of workloads and the broad benefits of NDP, we minimize our assumptions about our target NDP architecture, making our evaluation as broadly applicable as possible.

4.4 DAMOV: The Data Movement Benchmark Suite

In this section, we present DAMOV, the DAta MOVement Benchmark Suite. DAMOV is the collection of the 144 functions we use to drive our memory bottleneck classification in Section 4.3. The benchmark suite is divided into each one of the six classes of memory bottlenecks presented in Section 4.3. DAMOV is the first benchmark suite that encompasses *real* applications from a diverse set of application domains tailored to stress different memory bottlenecks in a system. We present the complete description of the functions in DAMOV in Appendix A. We highlight the benchmark diversity of the functions in DAMOV in Section 4.4.1. We open source DAMOV [1109] to facilitate further rigorous research in mitigating data movement bottlenecks, including in near data processing.

4.4.1 Benchmark Diversity

We perform a hierarchical clustering algorithm with the 44 representative functions we employ in Section 4.3.3.¹² Our goal is to showcase our benchmark suite’s diversity and observe whether a clustering algorithm produces a noticeable difference from the application clustering presented Section 4.3. The hierarchical clustering algorithm [1214] takes as input a dataset containing features that define each object in the dataset. The algorithm works by incrementally grouping objects in the dataset that are similar to each other in terms of some distance metric (called *linkage distance*), which is calculated based on the features’ values. Two objects with a short linkage distance have more affinity to each other than two objects with a large linkage distance. To apply the hierarchical clustering algorithm, we create a dataset where each object is one of the 44 representative functions from DAMOV. We use as features the same metrics we use for our analysis, i.e., temporal locality, MPKI, LFMR, and AI. We also include the LFMR curve slope to indicate when the LFMR increases, decreases or stays con-

¹²In Section 4.4.1, we use the same 44 representative functions that we use during our bottleneck classification instead of the entire set of 144 functions in DAMOV, in order to visualize better the clustering produced by the hierarchical clustering algorithm.

stant when scaling the core count. We use Euclidean distance [1214] to calculate the linkage distance across features in our dataset. We evaluate other linkage distance metrics (such as Manhattan distance [1214]), and we observe similar clustering results.

Figure 4.19 shows the dendrogram that the hierarchical clustering algorithm produces for our 44 representative functions. We indicate in the figure the application class each function belongs to, according to our classification. We make three observations from the figure.

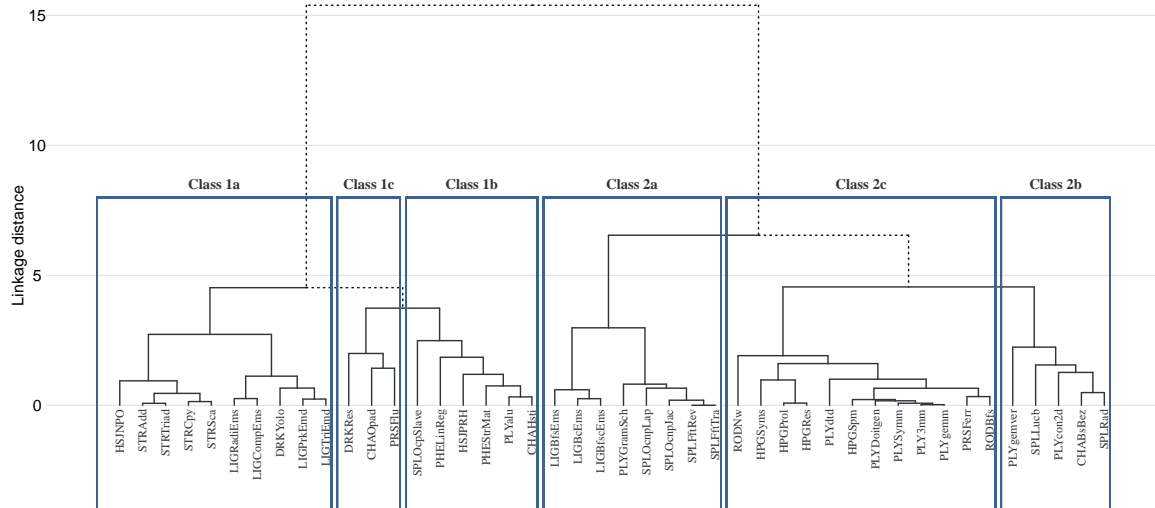


Figure 4.19: Hierarchical clustering of 44 representative functions.

First, our benchmarks exhibit a wide range of behavior diversity, even among those belonging to the same class. For example, we observe that the functions from Class 1a are divided into two groups, with a linkage distance of 3. Intuitively, functions in the first group (HSJNPO, STRAdd, STRCpy, STRSca, STRTriad) have regular access patterns while functions in the second group (DRKYolo, LIGCompEms, LIGPrkEms, LIGRadEms) have irregular access patterns. We observe a similar clustering in Section 4.3.3.

Second, we observe that our application clustering (Section 4.3.3) matches the clustering that the hierarchical clustering algorithm provides (Figure 4.19). From the dendrogram root, we observe that the right part of the dendrogram consists of functions with high temporal locality (from Classes 2a, 2b, and 2c). Conversely, the left part of the dendrogram consists of functions with low temporal locality (from Classes 1a, 1b, and 1c). The functions in the right and left part of the dendrogram have a high linkage distance (higher than 15), which implies that the metrics we use for our clustering are significantly different from each other for these functions. Third, we observe that functions within the same class are clustered into groups with a linkage distance lower than 5. This grouping matches the six classes of data movement bottlenecks present in DAMOV. Therefore, we conclude that our methodology can successfully cluster functions into distinct classes, each one representing a different memory bottleneck.

We conclude that (i) DAMOV provides a heterogeneous and diverse set of functions to study data movement bottlenecks and (ii) our memory bottleneck clustering methodology matches the clustering provided by a hierarchical clustering algorithm (this section; Figure 4.19).

4.5 Case Studies

In this section, we demonstrate how our benchmark suite is useful to study open questions related to NDP system designs. We provide four case studies. The first study analyzes the impact of load balance and communication on NDP execution. The second study assesses the impact of tailored NDP accelerators on our memory bottleneck analysis. The third study evaluates the effect of different core designs on NDP system performance. The fourth study analyzes the impact of fine-grained offloading (i.e., offloading small blocks of instructions to NDP cores) on performance.

4.5.1 Case Study 1: Impact of Load Balance and Inter-Vault Communication on NDP Systems

Communication between NDP cores is one of the key challenges for future NDP system designs, especially for NDP architectures based on 3D-stacked memories, where accessing a remote vault incurs extra latency overhead due to network traffic [56,243,1215]. This case study aims to evaluate the load imbalance and inter-vault communication that the NDP cores experience when executing functions from the DAMOV benchmark suite. We statically map a function to an NDP core, and we assume that NDP cores are connected using a 6x6 2D-mesh Network-on-Chip (NoC), similar to previous works [265,269,293,438,1216]. Figure 4.20 shows the performance overhead that the interconnection network imposes to NDP cores when running several functions from our benchmark suite. We report performance overheads of functions from different bottleneck classes (i.e., from Classes 1a, 1b, 2a, and 2b) that experience at least 5% of performance overhead due to the interconnection network. We calculate the interconnection network performance overhead by comparing performance with the 2D-mesh versus that with an ideal zero-latency interconnection network. We observe that the interconnection network performance overhead varies across functions, with a minimum overhead of 5% for SPL0cpSlave and a maximum overhead of 26% for SPLLucb.

We further characterize the traffic of memory requests injected into the interconnection network for these functions, aiming to understand the communication patterns across NDP cores. Figure 4.21 shows the distribution of all memory requests (y-axis) in terms of how many hops they need to travel in the NoC between NDP cores (x-axis) for each function. We make the following observations. First, we observe that, on average, 40% of all memory requests

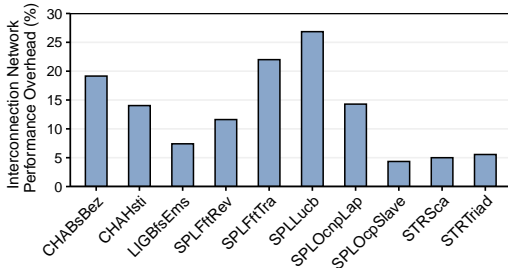


Figure 4.20: Interconnection network performance overhead in our NDP system.

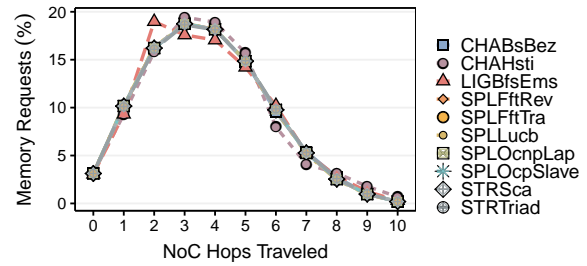


Figure 4.21: Distribution of NoC hops traveled per memory request.

need to travel 3 to 4 hops in the NoC, and less than 5% of all requests are issued to a local vault (0 hops). Even though the functions follow different memory access patterns, they all inject similar network traffic into the NoC.¹³ Therefore, we conclude that the NDP design can be further optimized by (i) employing more intelligent data mapping and scheduling mechanisms that can efficiently allocate data nearby the NDP core that accesses the data (thereby reducing inter-vault communication and improving data locality) and (ii) designing interconnection networks that can better fit the traffic patterns that NDP workloads produce. The DAMOV benchmark suite can be used to develop new ideas as well as evaluate existing ideas in both directions.

4.5.2 Case Study 2: Impact of NDP Accelerators on Our Memory Bottleneck Analysis

In our second case study, we aim to leverage our memory bottleneck classification to evaluate the benefits an NDP accelerator provides compared to the same accelerator accessing memory externally. We use the Aladdin accelerator simulator [1217] to tailor an accelerator for an application function. Aladdin works by estimating the performance of a custom accelerator based on the data-flow graph of the application. The main difference between an NDP accelerator and a regular accelerator (i.e., compute-centric accelerator) is that the former is placed in the logic layer of a 3D-stacked memory device and thus can leverage larger memory bandwidth, shorter memory access latency, and lower memory access energy, compared to the compute-centric accelerator that is exemplary of existing compute-centric accelerator designs.

To evaluate the benefits of NDP accelerators, we select three functions from our benchmark suite for this case study: DRKYolo (from Class 1a), PLYalu (from Class 1b), and PLY3mm (from Class 2c). We select these functions and memory bottleneck classes because we expect them to benefit the most (or to show no benefit) from the near-memory placement of an accelerator. According to our memory bottleneck analysis, we expect that the functions we select to (i)

¹³We use the default HMC data interleaving scheme in our experiments (Table 6.2).

benefit from NDP due to its high DRAM bandwidth (Class 1a), (ii) benefit from NDP due to its shorter DRAM access latency (Class 1b), or (iii) do *not* benefit from NDP in any way (Class 2c).

Figure 4.22 shows the speedup that the NDP accelerator provides for the different functions compared to the compute-centric accelerator. We make four observations. First, as expected based on our classification, the NDP accelerator provides performance benefits compared to the compute-centric accelerator for functions in Classes 1a and 1b. It does not provide performance improvement for the function in Class 2c. Second, the NDP accelerator for DRKYolo shows the largest performance benefits ($1.9\times$ performance improvement compared to the compute-centric accelerator). Since this function is DRAM bandwidth-bound (Class 1a, Section 4.3.3), the NDP accelerator can leverage the larger memory bandwidth available in the logic layer of the 3D-stacked memory device. Third, we observe that the NDP accelerator also provides speedup ($1.25\times$) for the PLYalu function compared to the compute-centric accelerator, since the NDP accelerator provides shorter memory access latency to the function, which is latency-bound (Class 1b, Section 4.3.3). Fourth, the NDP accelerator does not provide performance improvement for the PLY3mm function since this function is compute-bound (Class 2c, Section 4.3.3).

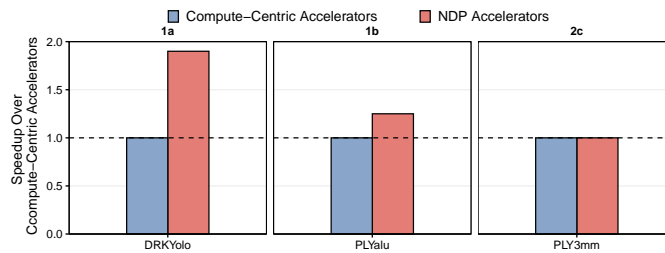


Figure 4.22: Speedup of the NDP Accelerators over the Compute-Centric Accelerators for three functions from Classes 1a, 1b, and 2c.

In conclusion, our observations for the performance of NDP accelerators are in line with the characteristics of the three memory bottleneck classes we evaluate in this case study. Therefore, our memory bottleneck classification can be applied to study other types of system configurations, e.g., the accelerators used in this section. However, since NDP accelerators are often employed under restricted area and power constraints (e.g., limited area available in the logic layer of a 3D-stacked memory [262, 271]), the core model of the compute-centric and NDP accelerators cannot always be the same. We leave a thorough analysis that takes area and power constraints in the study of NDP accelerators into consideration for future research.

4.5.3 Case Study 3: Impact of Different Core Models on NDP Architectures

This case study aims to analyze when a workload can benefit from different core models and numbers of cores while respecting the area and power envelope of the logic layer of a 3D-stacked memory. Many prior works employ 3D-stacked memories as the substrate to implement NDP architectures [13, 21, 56, 57, 154–157, 237, 243, 262–269, 271–275, 277, 279, 281, 286, 289, 290, 298, 299, 308, 309, 382, 440, 442, 616, 866, 1211, 1218, 1219]. However, 3D-stacked memories impose severe area and power restrictions on NDP architectures. For example, the area and power budget of the logic layer of a single HMC vault are 4.4 mm^2 and 312 mW , respectively [13, 262].

In the case study, we perform an iso-area and iso-power performance evaluation of three functions from our benchmark suite. We configure the host CPU system and the NDP system to guarantee an iso-area and iso-power evaluation, considering the area and power budget for a 32-vault HMC device [13, 262]. We use four out-of-order cores with a deep cache hierarchy for the host system configuration and two different NDP configurations: (1) one using six out-of-order NDP cores (*NDP+out-of-order*) and (2) using 128 in-order NDP cores (*NDP+in-order*), without a deep cache hierarchy. We choose functions from Classes 1a, 1b, and 2b for this case study since the major effects distinct microarchitectures have on the memory system are: (a) how much DRAM bandwidth they can sustain, and (b) how much DRAM latency they can hide. Classes 1a, 1b, and 2b are the most affected by memory bandwidth and access latency (as shown in Section 4.3). We choose two representative functions from each of these classes.

Figure 4.23 shows the speedup provided by the two NDP system configurations compared to the baseline host system. We make two observations. First, in all cases, the *NDP+in-order* system provides higher speedup than the *NDP+out-of-order* system, both compared to the host system. On average across all six functions, the *NDP+in-order* system provides 4× the speedup of the *NDP+out-of-order* system. The larger speedup the *NDP+in-order* system provides is due to the high number of NDP cores in the *NDP+in-order* system. We can fit 128 in-order cores in the logic layer of the 3D-stacked memory as opposed to only six out-of-order cores in the same area/power budget. Second, we observe that the speedup the *NDP+in-order* system provides compared to the *NDP+out-of-order* system does not scale with the number of cores. For example, the *NDP+in-order* system provides *only* 2× the performance of the *NDP+out-of-order* system for DRKYolo and PLYalu, even though the *NDP+in-order* system has 21× the number of NDP cores of the *NDP+out-of-order* system. This implies that even though the functions benefit from a large number of NDP cores available in the *NDP+in-order* system, static instruction scheduling limits performance on the *NDP+in-order* system.

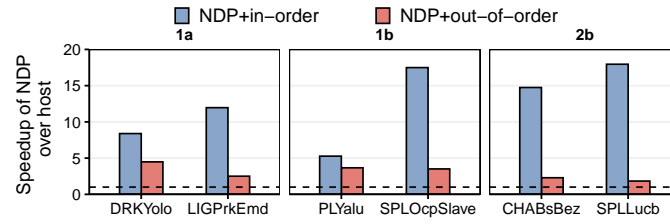


Figure 4.23: Speedup of NDP architectures over 4 out-of-order host CPU cores for two NDP configurations: using 128 in-order NDP cores (*NDP+in-order*) and 6 out-of-order NDP cores (*NDP+out-of-order*) for representative functions from Classes 1a, 1b, and 2b.

We believe, and our previous observations suggest, that an efficient NDP architecture can be achieved by leveraging mechanisms that can exploit both dynamic instruction scheduling and many-core design while fitting in the area and power budget of 3D-stacked memories. For example, past works [55, 114–116, 136–138, 884, 1159, 1220–1234] propose techniques that enable the benefits of simple and complex cores at the same time, via heterogeneous or adaptive architectures. These ideas can be examined to enable better core and system designs for NDP systems, and DAMOV can facilitate their proper design, exploration, and evaluation.

4.5.4 Case Study 4: Impact of Fine-Grained Offloading to NDP on Performance

Several prior works on NDP (e.g., [57, 154, 300, 310, 314, 317, 378, 442, 861, 1087, 1212]) propose to identify and offload to the NDP system simple primitives (e.g., instructions, atomic operations). We refer to this NDP offloading scheme as a *fine-grained NDP offloading*, in contrast to a *coarse-grained NDP offloading scheme* that offloads whole functions and applications to NDP systems. A fine-grained NDP offloading scheme provides two main benefits compared to a coarse-grained NDP offloading scheme. First, a fine-grained NDP offloading scheme allows for a reduction in the complexity of the processing elements used as NDP logic, since the NDP logic can consist of simple processing elements (e.g., arithmetic units, fixed function units) instead of entire in-order or out-of-order cores often utilized when employing a coarse-grained NDP offloading scheme. Second, a fine-grained NDP offloading scheme can help developing simple coherence mechanism needed to allow shared host and NDP execution [57]. However, identifying arbitrary NDP instructions can be a daunting task since there is no comprehensive methodology that indicates what types of instructions are good offloading candidates.

As the first step in this direction, we exploit the key insight provided by [54, 1235] to identify potential regions of code that can be candidates for fine-grained NDP offloading. [54, 94, 1235] show that few instructions are responsible for generating most of the cache misses during program execution in memory-intensive applications. Thus, these instructions are naturally good candidates for fine-grained NDP offloading. Figure 4.24 shows the distribu-

tion of unique basic blocks (x-axis) and the percentage of last-level cache misses (y-axis) the basic block produces for three representative functions from our benchmark suite. We select functions from Classes 1a (LIGKcrEms), 1b (HSJPRH), and 1c (DRKRes) since functions in these classes have higher L3 MPKI than functions in Classes 2a, 2b, and 2c. We observe from the figure that 1% to 10% of the basic blocks in each function are responsible for up to 95.3% of the LLC misses. We call these basic blocks the *hottest* basic blocks.¹⁴ We investigate the data-flow of each basic block and observe that these basic blocks often execute simple read-modify-write operations, with few arithmetic operations. Therefore, we believe that such basic blocks are good candidates for fine-grained offloading. Figure 4.25 shows the speedup obtained by offloading (i) the hottest basic block we identified for the three representative functions and (ii) the entire function to the NDP system, compared to the host system. Our initial evaluations show that offloading the hottest basic block of each function to the NDP system can provide up to $1.25\times$ speedup compared to the host CPU, which is half of the $1.5\times$ speedup achieved when offloading the entire function. Therefore, we believe that methodically identifying simple NDP instructions can be a promising research direction for future NDP system designs, which our DAMOV Benchmark Suite can help with.

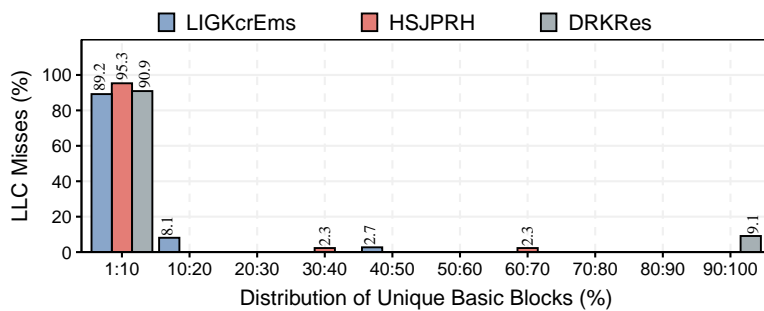


Figure 4.24: Distribution of unique basic blocks (x-axis) and the percentage of last-level cache misses they produce (y-axis) for three representative functions from Classes 1a (LIGKcrEms), 1b (HSJPRH), and 1c (DRKRes).

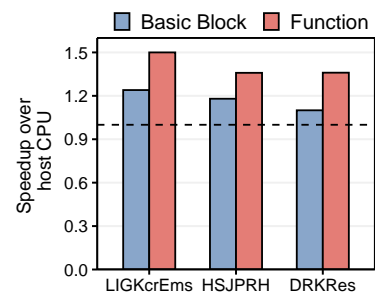


Figure 4.25: Speedup of offloading to NDP the *hottest* basic block in each function versus the entire function.

4.6 Key Takeaways

We summarize the key takeaways from our extensive characterization of 144 functions using our new three-step methodology to identify data movement bottlenecks. We also highlight when NDP is a good architectural choice to mitigate a particular memory bottleneck.

Figure 4.26 pictorially represents the key takeaways we obtain from our memory bottleneck classification. Based on four key metrics, we classify workloads into six classes of memory bottlenecks. We provide the following key takeaways:

¹⁴We observe for the 44 functions we evaluate in Section 4.3 that in many cases (for 65% of the evaluated workloads), a single basic block is responsible for 90% to 100% of the LLC misses during the function’s execution.

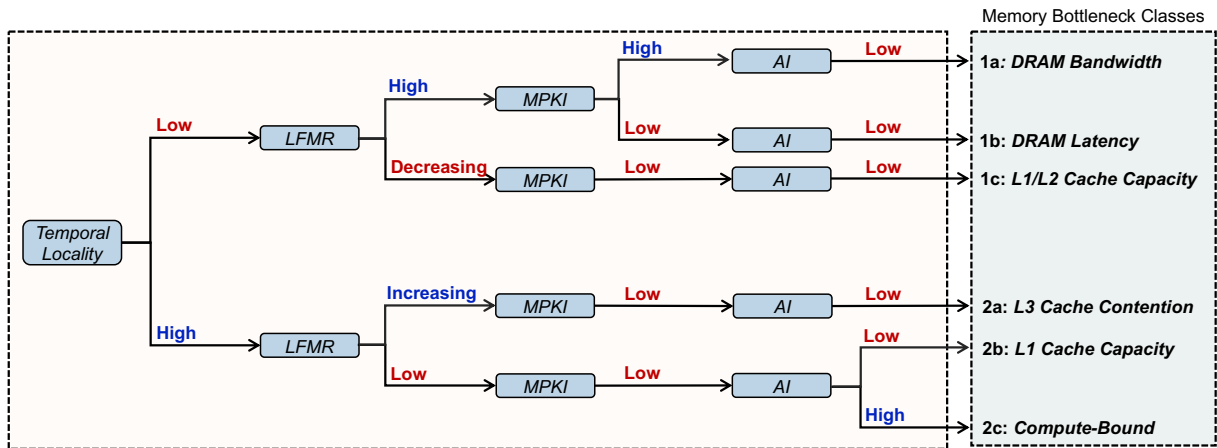


Figure 4.26: Summary of our memory bottleneck classification.

1. Applications with low temporal locality, high LFMR, high MPKI, and low AI are *DRAM bandwidth-bound* (Class 1a, Section 4.3.3). They are bottlenecked by the limited off-chip memory bandwidth as they exert high pressure on main memory. We make three observations for Class 1a applications. First, these applications do benefit from prefetching since they display a low degree of spatial locality. Second, these applications highly benefit from NDP architectures because they take advantage of the high memory bandwidth available within the memory device. Third, NDP architectures significantly improve energy for these applications since they eliminate the off-chip I/O traffic between the CPU and the main memory.
2. Applications with low temporal locality, high LFMR, low MPKI, and low AI are *DRAM latency-bound* (Class 1b, Section 4.3.3). We make three observations for Class 1b applications. First, these applications do not significantly benefit from prefetching since infrequent memory requests make it difficult for the prefetcher to train successfully on an access pattern. Second, these applications benefit from NDP architectures since they take advantage of NDP's lower memory access latency and the elimination of deep L2/L3 cache hierarchies, which fail to capture data locality for these workloads. Third, NDP architectures significantly improve energy for these applications since they eliminate costly (and unnecessary) L3 cache look-ups and the off-chip I/O traffic between the CPU and the main memory.
3. Applications with low temporal locality, decreasing LFMR with core count, low MPKI, and low AI are *bottlenecked by the available L1/L2 cache capacity* (Class 1c, Section 4.3.3). We make three observations for Class 1c applications. First, these applications are DRAM latency-bound at low core counts, thus taking advantage of NDP architectures, both in terms of performance improvement and energy reduction. Second, NDP's benefits

reduce when core count becomes larger, which consequently allows the working sets of such applications to fit inside the cache hierarchy at high core counts. Third, NDP architectures can be a good design choice for such workloads in systems with limited area budget since NDP architectures do not require large L2/L3 caches to outperform or perform similarly to the host CPU (in terms of both system throughput and energy) for these workloads.

4. Applications with high temporal locality, increasing LFMR with core count, low MPKI, and low AI are *bottlenecked by L3 cache contention* (Class 2a, Section 4.3.3). We make three observations for Class 2a applications. First, these applications benefit from a deep cache hierarchy and do not take advantage of NDP architectures at low core counts. Second, the number of cache conflicts increases when the number of cores in the system increases, leading to more pressure on main memory. We observe that NDP can effectively mitigate such cache contention for these applications without incurring the high area and energy overheads of providing additional cache capacity in the host. Third, NDP can improve energy for these workloads at high core counts, since it eliminates the costly data movement between the last-level cache and the main memory.
5. Applications with high temporal locality, low LFMR, low MPKI, and low AI are *bottlenecked by L1 cache capacity* (Class 2b, Section 4.3.3). We make two observations for Class 2b applications. First, NDP can provide similar performance and energy consumption than the host system by leveraging lower memory access latency and avoiding off-chip energy consumption for these applications. Second, NDP can be used to reduce the overall SRAM area (by eliminating L2/L3 caches) in the system without a performance or energy penalty.
6. Applications with high temporal locality, low LFMR, low MPKI, and high AI are *compute-bound* (Class 2c, Section 4.3.3). We make three observations for Class 2c applications. First, these applications suffer performance and energy penalties due to the lack of a deep L2/L3 cache hierarchy when executed on the NDP architecture. Second, these applications highly benefit from prefetching due to their high temporal and spatial locality. Third, these applications are not good candidates to execute on NDP architectures.

4.6.1 Shaping Future Research with DAMOV

A key contribution of our work is DAMOV, the first benchmark suite for main memory data movement studies. DAMOV is the collection of 144 functions from 74 different applications, belonging to 16 different benchmark suites or frameworks, classified into six different classes of data movement bottlenecks.

We believe that DAMOV can be used to explore a wide range of research directions on the study of data movement bottlenecks, appropriate mitigation mechanisms, and open research topics on NDP architectures. We highlight DAMOV's usability and potential benefits with four brief case studies, which we summarize below:

- In the first case study (Section 4.5.1), we use DAMOV to evaluate the interconnection network overheads that NDP cores placed in different vaults of a 3D-stacked memory suffer from. We observe that a large portion of the memory requests an NDP core issues go to remote vaults, which increases the memory access latency for the NDP core. We believe that DAMOV can be employed to study better data mapping techniques and interconnection network designs that aim to minimize (i) the number of remote memory accesses the NDP cores execute and (ii) the interconnection network latency overheads.
- In the second case study (Section 4.5.2), we evaluate the benefits that NDP accelerators can provide for three applications from our benchmark suite. We compare the performance improvements an NDP accelerator provides against the compute-centric version of the same accelerator. We observe that the NDP accelerator provides significant performance benefits compared to the compute-centric accelerator for applications in Classes 1a and 1b. At the same time, it does not improve performance for an application in Class 2c. We believe that DAMOV can aid the design of NDP accelerators that target different memory bottlenecks in the system.
- In the third case study (Section 4.5.3), we perform an iso-area/-power performance evaluation to compare NDP systems using in-order and out-of-order cores. We observe that the in-order cores' performance benefits for some applications are limited by the cores' static instruction scheduling mechanism. We believe that better NDP systems can be built by leveraging techniques that enable dynamic instruction scheduling without incurring the large area and power overheads of out-of-order cores. DAMOV can help in the analysis and development of such NDP architectures.
- In the fourth case study (Section 4.5.4), we evaluate the benefits of offloading small portions of code (i.e., a basic block) to NDP, which simplifies the design of NDP systems. We observe that for many applications, a small percentage of basic blocks is responsible for most of the last-level cache misses. By offloading these basic blocks to an NDP core, we observe a performance improvement of up to 1.25 \times . We believe that DAMOV can be used to identify simple NDP instructions that enable building efficient NDP systems in the future.

4.7 Summary

We introduce the first rigorous methodology to characterize memory-related data movement bottlenecks in modern workloads and the first data movement benchmark suite, called DAMOV. We perform the first large-scale characterization of applications to develop a three-step workload characterization methodology that introduces and evaluates four key metrics to identify the sources of data movement bottlenecks in real applications. We use our new methodology to classify the primary sources of memory bottlenecks of a broad range of applications into six different classes of memory bottlenecks. We highlight the benefits of our benchmark suite with four case studies, which showcase how representative workloads in DAMOV can be used to explore open-research topics on NDP systems and reach architectural as well as workload-level insights and conclusions. We open-source our benchmark suite and our bottleneck analysis toolchain [1109]. We hope that our work enables further studies and research on hardware and software solutions for data movement bottlenecks, including near-data processing.

Chapter 5

MIMDRAM: An End-to-End Processing-Using-DRAM System for High-Throughput, Energy-Efficient, and Programmer-Transparent Multiple-Instruction Multiple-Data Computing

5.1 Motivation

The efficiency of state-of-the-art processing-using-DRAM (PUD) substrates can be subpar when the SIMD parallelism that exists in an application is smaller than or not a multiple of the size of a DRAM row. To quantify the SIMD parallelism some real-world applications inherently possess, we profile the *maximum vectorization factor* of twelve real-world applications. The vectorization factor of a loop is the number of scalar operands that fit into a SIMD register [1236, 1237]. We calculate the maximum vectorization factor by multiplying the vectorization factor of a single loop iteration and the loop’s trip count [858]. We leverage modern compilers’ loop auto-vectorization engines, which allows us to have an initial understanding of the SIMD parallelism that a large number of applications possesses.

For our analysis, we use (i) the LLVM compiler toolchain [1238] (version 12.0.0) to *automatically* vectorize loops in the application, and (ii) an LLVM pass [1239–1241] that instruments each application’s loop to, during execution, gather *dynamic* information about each vectorized loop, i.e., the loop trip count, execution count, execution time, and instruction

breakdown [1242]. We compile each application using the clang compiler [1238], using the appropriate flags to enable the loop auto-vectorization engine and its loop vectorization report (i.e., `-O3 -Rpass-analysis=loop-vectorize -Rpass=loop-vectorize`).¹ We assume SIMDram [378] as the target PUD architecture.

Figure 5.1 shows the distribution of maximum vectorization factors (y-axis) of all the vectorizable loops in an application (x-axis). We indicate different amounts of SIMD parallelism with horizontal dashed lines for reference. We make two observations. First, the maximum vectorization factor varies both within an application and across different applications. Our analysis shows maximum vectorization factors as low as 8 and as high as 134,217,729. Second, only a small fraction of vectorized loops have enough maximum vectorization factor (i.e., values above the green horizontal dashed line) to fully exploit the SIMD parallelism of SIMDram. On average, only 0.11% of all vectorized loops have a maximum vectorization factor equal to or greater than a DRAM row (i.e., greater than 65,536 data elements). We conclude that (i) real-world applications have varying degrees of SIMD parallelism; and (ii) these varying degrees of SIMD parallelism rarely take full advantage of the very-wide SIMD width of state-of-the-art PUD substrates.

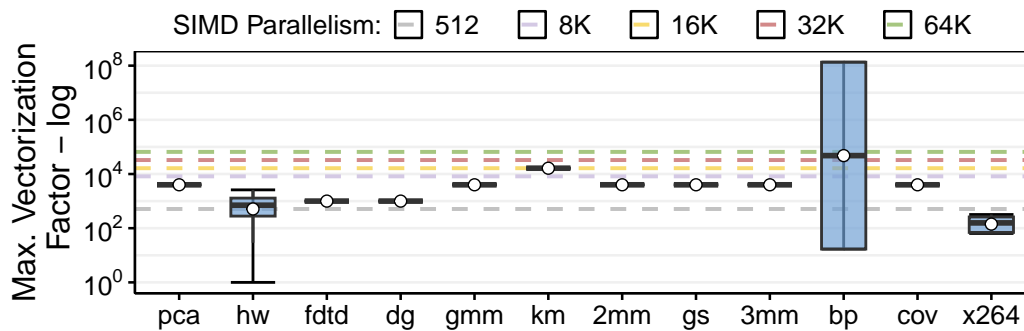


Figure 5.1: Distribution of maximum vectorization factor across all vectorized loops. Whiskers extend to the minimum and maximum data points on either side of the box. Bubbles depict average values.

Problem & Goal. We observe that the rigid granularity of PUD architectures limits their efficiency (and thus their *effective* applicability) for many applications. Such applications would benefit from a variable-size SIMD substrate that can dynamically adapt to the varying levels of SIMD parallelism (i.e., different vectorization factors) an application exhibits during its execution. Therefore, our *goal* is to design a flexible PUD substrate that (i) adapts to the varying levels of SIMD parallelism present in an application, and (ii) maximizes the utilization of the very-wide PUD engine by concurrently exploiting parallelism across *different* PUD operations (potentially from different applications).

¹See §7.4 for the description of our applications and their dataset.

5.2 MIMDRAM: A MIMD PUD Architecture

MIMDRAM is a hardware/software co-designed PUD system that enables fine-grained PUD computation at low cost and low programming effort. The *key idea* of MIMDRAM is to leverage fine-grained DRAM activation for PUD, which provides three benefits. First, it enables MIMDRAM to allocate *only* the appropriate computation resources (based on the maximum vectorization factor of a loop) for a target loop, thereby reducing underutilization and energy waste. Second, MIMDRAM can currently execute multiple independent operations inside a single DRAM subarray *independently* in separate DRAM mats. This allows MIMDRAM to operate as a multiple-instruction multiple-data (MIMD) PUD substrate, increasing overall throughput. Third, MIMDRAM implements low-cost interconnects that enable moving data across DRAM columns *across* and *within* DRAM mats by combining fine-grained DRAM activation with simple modifications to the DRAM I/O circuitry. This enables MIMDRAM to implement reduction operations in DRAM without any intervention of the host CPU cores.

5.2.1 MIMDRAM: Hardware Overview

Figure 5.2 shows an overview of the DRAM organization of MIMDRAM. Compared to the baseline Ambit subarray organization, MIMDRAM adds four new components (colored in green) to a DRAM subarray and DRAM bank, which enable (i) fine-grained PUD execution; (ii) global I/O data movement; and (iii) local I/O data movement.

Fine-Grained PUD Execution. To enable fine-grained PUD execution, MIMDRAM modifies Ambit’s subarray and the DRAM bank with three new hardware structures: the *mat isolation transistor*, the *row decoder latch*, and the *mat selector*. At a high level, the *mat isolation transistor* allows for the independent access and operation of DRAM mats within a subarray while the *row decoder latch* enables the execution of a PUD operation in a range of DRAM mats that the *mat selector* defines.

First, the *mat isolation transistor* (① in Figure 5.2) segments the global wordline connected to the local row decoder in *each* DRAM mat in a subarray. Second, the *row decoder latch* (②) stores the bits from the global wordline used to address the local row decoder. Third, the *mat selector* (③), shared across all DRAM mats in a subarray, asserts one or more mat isolation transistors. The *mat selector* enables the connection between the global wordline and the *row decoder latches* belonging to a range of DRAM mats. When issuing PUD operations, the memory controller specifies the *logical* address of the *first* and *last* DRAM mats that the PUD operation targets (called *logical mat range*). Internally, each DRAM chip (i) identifies whether *any* of its DRAM mats belong to the logical mat range and (ii) translates the logical mat range

into the appropriate *physical mat range*, which is used as input for the *mat selector*. With these structures, *different* PUD operations can execute in *different* ranges of DRAM mats.

For example, to execute a triple row activation (TRA) in only mat_0 , MIMDRAM performs four steps: (i) when issuing a TRA, the memory controller sends, alongside the row address information, the *logical mat range* $[mat\ begin, mat\ end] = [\#0, \#0]$ to address mat_0 (❶ in Figure 5.2); (ii) the *mat selector* (❷) receives the logical mat range, translates it to the appropriate *physical mat range*, and raises the *matline* corresponding to mat_0 , which asserts mat_0 's *mat isolation transistor* (❸) and connects the global wordline to mat_0 's row decoder latch; (iii) the bits of the global wordline used to drive mat_0 's local row decoder are stored in mat_0 's *row decoder latch* (❹); (iv) finally, mat_0 's local row decoder drives the appropriate rows in mat_0 's DRAM array based on the value stored in the row decoder latch. From here, the DRAM row activation (and thus, PUD computation) proceeds as described in §2.1, only involving the DRAM rows in mat_0 . Since the per-mat row decoder latch stores the local row address for a given row activation in a mat, the memory controller can issue a TRA to another DRAM mat while mat_0 is being activated (❺).

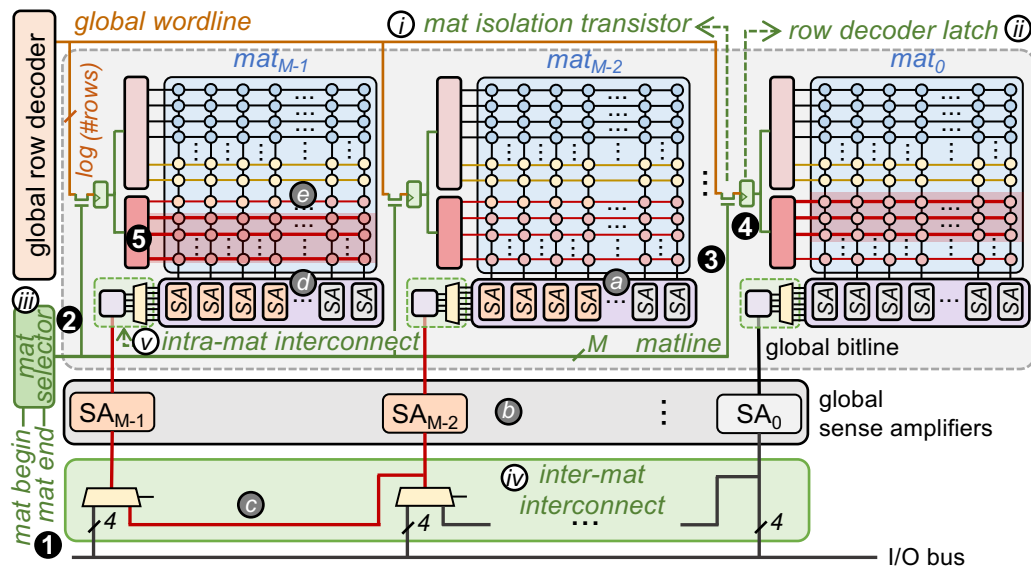


Figure 5.2: MIMDRAM subarray and bank organization. Green-colored boxes represent newly added hardware components.

Global I/O Data Movement. To enable data movement across different mats, MIMDRAM implements an *inter-mat interconnect* by slightly modifying the connection between the I/O bus and the global sense amplifiers (❺ in Figure 5.2). The inter-mat interconnect relies on the observation that the global sense amplifiers have *higher* drive than the sense amplifiers in the local row buffer [499, 800], allowing to directly drive data from the global sense amplifiers into the local row buffer.² To leverage this observation, MIMDRAM adds a 2:1 multiplexer to

²Prior work [800] leverages the same observation to copy DRAM columns from one subarray to another.

the input/output port of each set of *four* 1-bit global sense amplifiers. The multiplexer selects whether the data that is written to the sense amplifier set SA_i comes from the I/O bus or from the neighbor global sense amplifier set SA_{i-1} .

To manage inter-mat data movement, MIMDRAM exposes a new DRAM command to the memory controller called GB-MOV (global I/O move). The GB-MOV command takes as input: (i) the logical mat range $[mat\ begin, mat\ end]$, row address, and column address of the *source* DRAM row and column; and (ii) the logical mat range $[mat\ begin, mat\ end]$, row address, and column address of the *destination* DRAM row and column. With the inter-mat interconnect and new DRAM command, MIMDRAM can move *four* bits³ of data from a source row and column ($row_{src}, column_{src}$) in mat_{M-2} to a destination row and column ($row_{dst}, column_{dst}$) in mat_{M-1} , in a DRAM subarray with M DRAM mats. Once the memory controller receives a GB-MOV command, it performs three steps. First, the memory controller issues an ACT to the source row in mat_{M-2} , which loads the target DRAM row_{src} to mat_{M-2} 's local sense amplifiers (Ⓐ in Figure 5.2). Concurrently, the memory controller issues an ACT to the destination row in mat_{M-1} , which connects row_{dst} to mat_{M-1} 's local sense amplifiers. Second, the memory controller issues a RD with the address of the four-bit *source* column to mat_{M-2} . The column select command loads the four-bit $column_{src}$ from mat_{M-2} 's local sense amplifiers to its HFFs, and mat_{M-2} 's HFFs drive the corresponding set of four one-bit global sense amplifiers SA_{M-2} (Ⓑ). Third, the memory controller issues a WR with the address of the four-bit *destination* column to mat_{M-1} . Since the WR corresponds to a GB-MOV command, the multiplexer that connects mat_{M-1} 's HFFs to the global sense amplifiers takes as input the added datapath coming from SA_{M-2} instead of the conventional datapath coming from the I/O bus (Ⓒ). As a result, the data stored in SA_{M-2} is loaded into SA_{M-1} , which in turn drives mat_{M-1} 's HFFs and local sense amplifiers (Ⓓ). Once the four-bit column coming from row_{src} is written into mat_{M-1} 's local sense amplifiers, the local sense amplifiers finish the WR by restoring the local bitlines in mat_{M-1} to VDD or GND, thereby storing the four-bit column coming from $column_{src}$ as a column of row_{dst} (Ⓔ).

The *conservative worst-case latency* of a GB-MOV command (i.e., where the addresses of the source and the destination rows differ) is equal to $t_{RAS} + t_{RELOC} + t_{WR} + t_{RP}$; where t_{RAS} is latency from the start of row activation until the completion of the DRAM cell's charge restoration, t_{RELOC} [800] is the latency of turning on the connection between the source and destination local sense amplifiers; t_{WR} is the minimum time interval between a WR and a PRE command,

³The number of bits the inter-mat interconnect can move at once depends on the number of helper flip-flops (HFFs) *already present* in a DRAM mat. We assume that each mat has four HFFs, as prior works suggest [451, 452, 456].

which allows the sense amplifiers to restore the data to the DRAM cells; t_{RP} is the latency between issuing a PRE and when the DRAM bank is ready for a new row activation.

Local I/O Data Movement. To enable data movement across columns *within* a DRAM mat, MIMDRAM implements an *intra-mat interconnect* (⑤ in Figure 5.2), which does *not* require any hardware modifications. Instead, it modifies the sequence of steps DRAM executes during a column access operation. There are two *key observations* that enable the intra-mat interconnect. First, we observe that the local bitlines of a DRAM mat *already* share an interconnection path via the HFFs and column select logic (as Figure 5.3 illustrates). Second, the HFFs in a DRAM mat can latch and *amplify* the local row buffer’s data [455, 499].

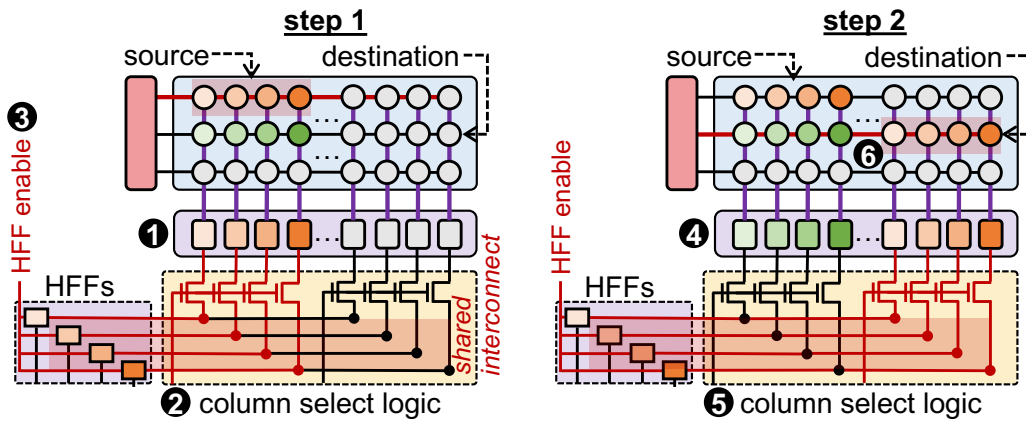


Figure 5.3: MIMDRAM intra-mat interconnect.

To manage intra-mat data movement, MIMDRAM exposes a new DRAM command to the memory controller called LC-MOV (local I/O move). The LC-MOV command takes as input: (i) the logical mat range [mat_{begin} , mat_{end}] of the target row, (ii) the row and column addresses of the *source* DRAM row and column; and (iii) the row and column addresses of the *destination* DRAM row and column. With the intra-mat interconnect and new DRAM command, MIMDRAM can move *four* bits of data from a source row and column (row_{src} , $column_{src}$) to a destination row and column (row_{dst} , $column_{dst}$) in mat_M . Once the memory controller receives an LC-MOV command, it performs two steps, which Figure 5.3 illustrates. In the *first step*, the memory controller performs an ACT-RD-PRE targeting row_{src} , $column_{src}$ in mat_M . The ACT loads row_{src} to mat_M ’s local sense amplifier (1 in Figure 5.3). The RD moves four bits from row_{src} , as indexed by $column_{src}$, into the mat’s HFFs by enabling the appropriate transistors in the column select logic (2). The HFFs are then enabled by transitioning the *HFF enable* signal from low to high. This allows the HFFs to *latch* and *amplify* the selected four-bit data column from the local sense amplifier (3). The PRE closes row_{src} . Until here, the LC-MOV command operates exactly as a regular ACT-RD-PRE command sequence. However, differently from a regular ACT-RD-PRE, the LC-MOV command does *not* lower the *HFF enable* signal when the

RD finishes. This allows the four-bit data from column_{src} to reside in the mat's HFFs. In the *second step*, the memory controller performs an ACT-WR-PRE targeting row_{dst} , column_{dst} in mat_M . The ACT loads row_{dst} into the mat's local row buffer (④), and the WR asserts the column select logic to column_{dst} , creating a path between the HFFs and the local row buffer (⑤). Since the *HFF enable* signal is kept high, the HFFs will *not* sense and latch the data from column_{dst} . Instead, the HFFs overwrite the data stored in the local sense amplifier with the previously four-bit data latched from column_{src} . The new data stored in the mat's local sense amplifier propagates through the local bitlines and is written to the destination DRAM cells (⑥).

The *conservative worst-case latency* of an LC-MOV command (i.e., where the addresses of the source and the destination rows differ) is equal to $2 \times (t_{RAS} + t_{RP}) + t_{RELOC} + t_{WR}$.

PUD Vector Reduction

We describe how MIMDRAM uses the inter-mat and intra-mat interconnects to implement PUD vector reduction. To do so, we use a simple example, where MIMDRAM executes a vector addition followed by a vector reduction, i.e., $\text{out} += (\text{A}[\text{i}] + \text{B}[\text{i}])$. We assume that DRAM has only two mats, and the data elements of the input arrays A and B are evenly distributed across the two DRAM mats, as Figure 5.4 illustrates. MIMDRAM executes a vector reduction in three steps. In the first step, MIMDRAM executes a PUD addition operation over the data in the two DRAM mats (①), storing the temporary output data C into the same mats where the computation takes place (i.e., $C = \{C[9:5]_{mat1}, C[4:0]_{mat0}\}$). In the second step, MIMDRAM issues a GB-MOV to move part of the temporary output $C[4:0]$ stored in mat_0 to a temporary row tmp in mat_1 ($\text{tmp}[9:5]_{mat1} \leftarrow C[4:0]_{mat0}$) via the inter-mat interconnect (②–③), four bits (i.e., four data elements) at a time. MIMDRAM *iteratively* executes step 2 until *all* data elements of $C[4:0]$ are copied to mat_1 . In the third step, once the GB-MOV finishes, MIMDRAM executes the final addition operation, i.e. $\text{tmp} + C[1]$, in mat_1 . The final output of the vector reduction operation is stored in the destination row out in mat_1 (④).

Once the vector reduction operation finishes, the temporary output array stored in mat_1 holds as many data elements as the number of DRAM columns in a mat (e.g., 512 data elements). MIMDRAM allows reducing the temporary output vector further to an output vector with *four* data elements using the intra-mat interconnect. The process is analogous to that employed during the 512-element vector reduction: MIMDRAM uses the intra-mat interconnect and the LC-MOV command to implement an adder tree inside a single DRAM mat.⁴

⁴The number of GB-MOV and LC-MOV commands issued depends on the bit-precision of the input operands [378].

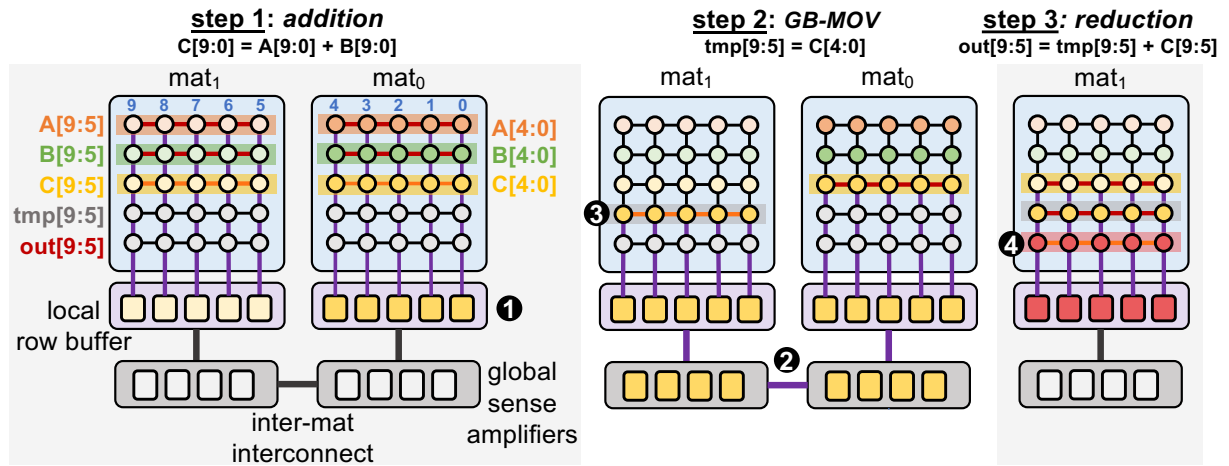


Figure 5.4: An example of a PUD vector reduction in MIMDRAM.

5.2.2 MIMDRAM: Control & Execution

To enable MIMDRAM to execute in a MIMD fashion, we need to efficiently (i) *encode* and *communicate* information regarding the target DRAM mats (i.e., the target mat range) in a *timely* manner (i.e., respecting DRAM timing parameters) while (ii) *orchestrating* the execution of independent PUD operations across the DRAM mats of a DRAM subarray. To do so, we take a *conservative* design approach: we aim to integrate MIMDRAM in commodity DRAM chips by providing an implementation (i) *compatible* with existing DRAM standards and (ii) that does *not* add new pins to a DRAM chips.

Encoding MAT Information. MIMDRAM needs a compact way to encode the target mat information, since a DRAM module often contains many DRAM mats. To solve this issue, MIMDRAM only allows a PUD operation to be executed in a *physically contiguous* set of DRAM mats.⁵ In this way, when executing the DRAM commands (i.e., ACTs and PREs) that realize a PUD operation, the memory controller only needs to provide the *first* and *last* (logical) mats an ACT target. Then, MIMDRAM internally decides which (physical) mats fit into the provided mat range. To do so, MIMDRAM implements a simple *chip select logic* and *mat identifier logic* inside the I/O circuitry of each DRAM chip. The *chip select logic* and *mat identifier logic* take as input the *logical mat range* and output (i) if DRAM mats placed in a chip belong to the mat range, and (ii) the physical mat range. In case a DRAM mat placed in a chip belongs to the mat range, the DRAM chip queues the physical mat range in the *mat queue* (which we describe later in this section). The *physical mat range* is used as input for the *mat selector* (see Figure 5.2). Since there are up to 128 DRAM mats in a DDR4 module [1243], MIMDRAM uses 14 bits to encode the logical mat range (7 bits each for *mat begin* and *mat end*, each), from which (i) the three most significant bits are used to identify the target DRAM chip and (ii) the four least

⁵In §5.4.3, we describe how we enforce physically contiguous mat allocation.

significant bits are used to identify individual mats. The *chip select logic* and *mat identifier logic* comprise simple hardware elements: four comparators, two 2-input AND gates, two 2:1 multiplexers, and a 3-bit *chip id register* in each DRAM chip.

Communicating MAT Information. MIMDRAM needs to communicate to the DRAM chip information regarding the target mats during a PUD operation. However, it is challenging to communicate the mat information alongside an ACT due to the narrow DRAM command/address (C/A) bus interface, since the memory controller uses most of the available pins during a row activation for row address and command communication.⁶ Our *key idea* to solve this issue is to overlap the latency of communicating the mat information to DRAM with the latency of DRAM commands in a μ Program in two ways: (i) ACT–ACT overlap, and (ii) PRE–ACT overlap. The first case (ACT–ACT overlap) happens when issuing a row copy operation (AAP). In this case, the mat information required by the second ACT is transmitted immediately *after* issuing the first ACT, exploiting the delay between two activations. The mat information is buffered once it reaches DRAM. The second case (PRE–ACT overlap) happens when issuing the first ACT in a row copy operation or the ACT in a TRA. We notice that (i) the first ACT command in an AAP/AP is *always* preceded by a PRE (due to a previous AAP/AP, or due to a previous DRAM request), and (ii) a PRE does *not* use the row address pins, since it targets a DRAM bank (not a DRAM row). Thus, MIMDRAM uses the row address pins during a PRE that immediately precedes the first ACT in an AAP/AP command sequence to communicate the mat information.⁷

Timing of MAT Information. MIMDRAM needs to communicate the mat information *before* a respective ACT in a μ Program. Communicating the mat information immediately *after* the memory controller issues the ACT would open the *entire* DRAM row (instead of only the relevant portion of the DRAM row). To solve this issue, we devise a simple queuing-based mechanism for partial row activation. Our mechanism relies on the fact that the execution order of ACTs and PREs in a μ Program is *deterministic*.⁸ Thus, we can add to each DRAM command in an AAP/AP the information about when the DRAM circuitry should propagate the mat information. MIMDRAM leverages this key idea by adding a *mat queue* to the I/O logic of each DRAM chip and adding extra functionality to the existing ACT and PRE commands to

⁶There are 27 C/A pins in a DDR4 chip [510], from which only three pins are *not* used during an ACT command.

⁷If there are insufficient pins in the DDRx interface to communicate mat information (e.g., as in DDR5 [511]), MIMDRAM utilizes multiple DRAM C/A cycles to propagate the mat information. For example, in DDR5, MIMDRAM still performs PRE–ACT overlap, communicating the mat information in two cycles. Note that an extra cycle does *not* impact MIMDRAM’s performance, since in a PRE–ACT command sequence, the PRE still needs to wait for the completion of the ACT for more than two DRAM C/A cycles.

⁸To realize a PUD operation, the memory controller *must* respect the order in which ACT and PRE commands are specified in the μ Program. Therefore, during PUD execution, ACTs and PREs in a μ Program cannot be reordered, and the behavior of the μ Program is thus deterministic. If the memory controller is performing maintenance operation to a DRAM bank, the AAP/AP commands of a PUD operation wait until the maintenance operation finishes.

control the mat queue: (i) ACT-enqueue issues an ACT to row_addr in the first DRAM clock cycle and enqueues [mat_begin, mat_end] in the second DRAM clock cycle; (ii) PRE-enqueue issues a PRE to bank_id and enqueues [mat_begin, mat_end]; (iii) ACT-dequeue issues an ACT to row_addr and dequeues from the mat queue.

Orchestrating MAT Information. MIMDRAM needs to execute different PUD operations concurrently. To this end, we implement a control unit inside the memory controller on the CPU die, which Figure 5.5 illustrates. MIMDRAM leverages SIMD RAM control unit to translate each *bbop* instruction into its corresponding μ Program and adds extra circuitry to (i) schedule each μ Program based on its target mats and (ii) maintain multiple μ Program contexts. MIMDRAM control unit consists of four main components. First, *bbop buffer*, which stores *bbops* dispatched by the host CPU. Second, *mat scheduler*, which schedules the most appropriate *bbop* to execute depending on the *bbop*'s mat range and current mat utilization. Third, *mat scoreboard*, which tracks whether a given mat is being used by a *bbop* instruction. The *mat scoreboard* stores an M -bit *mat bitmap* that keeps track of which mats are currently in use, where M is the number of mats in the DRAM module. The *mat scoreboard* can index a range of positions in the *mat bitmap* using a *mat index*. Fourth, several (e.g., eight) μ Program processing engines, each of which translates a *bbop* into its respective μ Program and controls the *bbop*'s execution.

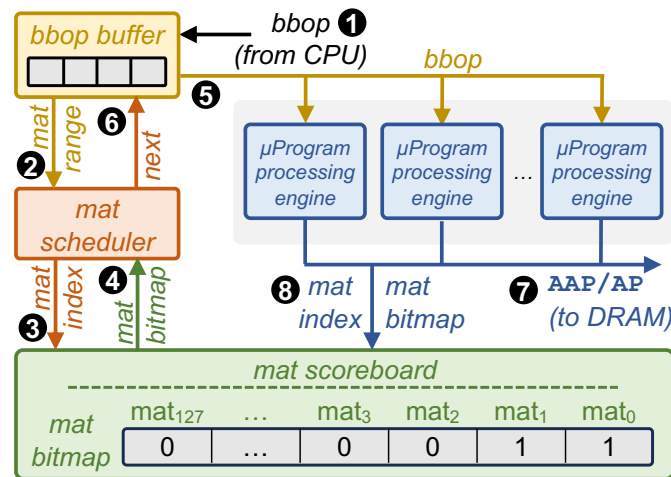


Figure 5.5: MIMDRAM control unit in the memory controller.

MIMDRAM control unit works in four steps. In the first step, MIMDRAM control unit enqueues an incoming *bbop* instruction dispatched by the host CPU (❶ in Figure 5.5) in the *bbop* buffer. In the second step, the *mat scheduler* scans the *bbop* buffer from the oldest to the newest element. Then, the *mat scheduler* employs an online first fit algorithm [1244] to select a *bbop* to be executed. For each *bbop* in the *bbop* buffer, the algorithm: (i) extracts the *mat range* information encoded in the *bbop* (❷), which is used to index the *mat scoreboard* (❸); (ii) reads

the mat bitmap to identify whether the mats belonging to the *bbop*'s mat range are currently free or busy (④); (iii) in case the mats are free, the mat scheduler writes a new mat bitmap to the mat scoreboard, indicating that the given mat range is now busy, selects the current *bbop* to be executed by allocating and copying the *bbop* to a free μ Program processing engine (⑤), and removes the current *bbop* from the *bbop* buffer (⑥); (iv) in case the mats belonging to the *bbop*'s range are busy, the mat scheduler reads the next available *bbop* from the *bbop* buffer and repeats (i)–(iii). In the third step, one or multiple μ Program processing engines execute their allocated *bbop*, issuing AAPs/APs to the DRAM chips (⑦). The μ Program processing engine is responsible for maintaining the timing of AAP/AP commands. In our design, we avoid the need to maintain state for *all* DRAM mats in a DRAM module *individually* by: (i) only allowing a PUD operation to address a contiguous range of DRAM mats, which share state as they execute the same sequence of ACT–PRE commands and (ii) limiting the number of concurrent PUD operations to the number of μ Program processing engines available in the control unit. In the fourth step, when a μ Program processing engine finishes executing, it frees its allocated mats by correspondingly updating the mat bitmap in the mat scoreboard (⑧) and notifies the CPU that the execution of the *bbop* instruction is done.

5.3 MIMDRAM: Software Support

To ease MIMDRAM's programmability, we provide compiler support to transparently map SIMD operations to MIMDRAM. Figure 5.6 illustrates MIMDRAM's compilation flow, which we implement using LLVM [1238]: we take a C/C++ application's source code as input, perform three transformations passes, and output a binary with a mix of CPU and PUD instructions.

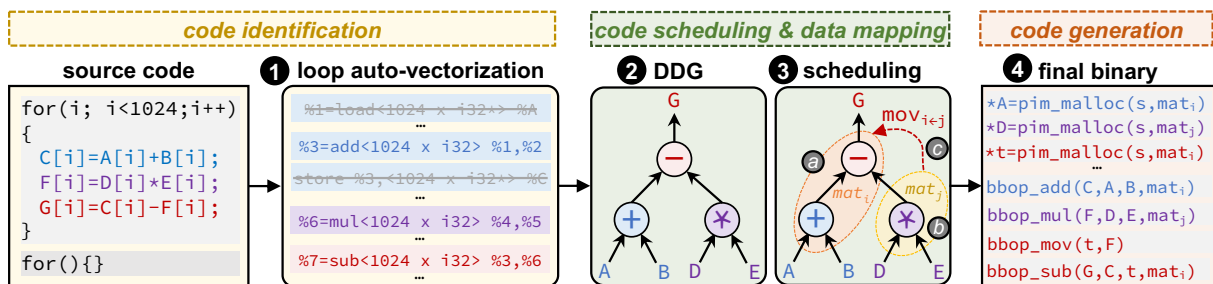


Figure 5.6: MIMDRAM's compilation flow.

Pass 1: Code Identification. The first pass is responsible for *code identification*. Its goal is to identify (i) loops that can be successfully auto-vectorized and (ii) the appropriate vectorization factor of a given vectorized loop. The code identification pass takes as input the application's LLVM intermediate representation (IR) generated by the compiler's front-end. It produces as output an optimized IR containing SIMD instructions that will be translated to *bbop* instructions. We leverage the native LLVM's loop auto-vectorization pass [1245] to identify and trans-

form loops into their vectorized form (❶ in Figure 5.6).⁹ We apply two modifications to LLVM’s loop auto-vectorization pass. First, instead of using a cost model to choose the vectorization factor that leads to the highest performance improvement compared to a scalar version of the same loop, we *always* select the *maximum* vectorization factor for the loop. This is important because the native cost model takes into account the hardware characteristics of a target CPU SIMD engine (i.e., number of available vector registers, SIMD width of the target execution engine, the latency of different SIMD instructions), which are not representative of our MIMDRAM engine with a variable SIMD width. Second, we modify the code generation routine for a given vectorized loop. Concretely, for a given vectorized loop, we identify and remove memory instructions related to each arithmetic SIMD operation (i.e., load/store instructions that manipulate vector registers) since PUD operations directly manipulate the data stored in DRAM; thus, there is no need to *explicitly* move data into/out SIMD registers.

Pass 2: Code Scheduling & Data Mapping. The second pass is responsible for *code scheduling and data mapping*. Its goal is to improve overall SIMD utilization by allowing the distribution of independent PUD instructions across DRAM mats. Since PUD instructions operate directly on the data stored in DRAM, the DRAM mat where the data is allocated determines the efficiency and utilization of the PUD SIMD engine. If operands of independent instructions are distributed across different DRAM mats, such instructions can be executed concurrently. Likewise, operands of dependent instructions are mapped to the same DRAM mat. In that case, intermediate data that one instruction produces and the next instruction consumes do *not* need to be moved across different DRAM mats, improving energy efficiency. Leveraging these observations, the code scheduling pass takes as input all *bbop* instructions the code identification pass generates and outputs new *bbop* instructions containing metadata regarding their mat location (i.e., *mat label*). The code scheduling pass works in two steps.

In the first step, the code scheduling pass creates a data-dependency graph (DDG) of the vectorized instructions (❷). Each node represents a *bbop* instruction, incoming edges represent input, and outgoing edges represent output of the *bbop*. In the second step, the code scheduling pass takes as input the DDG and employs a data scheduling algorithm to distribute *bbop* instructions across DRAM mats (❸). The data scheduling algorithm traverses the DDG in *topological order* to respect dependencies between *bbop* instructions using a depth-first search (DFS) kernel, which is a common algorithm for topological ordering [1246, 1247], and performs three operations. First, the algorithm traverses the *left* nodes in the DDG, assigning a single *mat label* *i* to nodes in the *left* path (❸-ⓐ). Second, when the algorithm reaches a leaf node, it traverses the *right* sub-tree in the DDG. In this case, the algorithm assigns a new *mat label*

⁹Prior works [861, 892] also leverage modern compilers’ loop auto-vectorization engines to generate instructions to processing-near-memory (processing-near-memory (PNM)) architectures equipped with SIMD engines.

j to the nodes in the *right* path in the sub-tree (③-⑥). Third, once the algorithm visits all the nodes in the *right* sub-tree, it returns to the parent node of the sub-tree. Since the parent node has already been visited when descending into the left path, the left and right sub-tree nodes will be assigned to different mats while having data dependencies across them (as indicated by the parent node). In this case, the algorithm creates a data movement *bbop* instruction (see §5.4.1) to move the output produced by the right sub-tree from *mat label j* to *mat label i* (③-⑥). This process repeats until the algorithm visits all nodes in the DDG.

Pass 3: Code Generation. The third pass is responsible for (i) *data allocation* and (ii) *code generation*. It takes as input the LLVM IR containing both CPU and *bbop* instructions (with metadata) and produces a binary to the target ISA (④). To implement data allocation, the code generation pass first identifies calls for memory allocation routines (e.g., `malloc`) associated with operands of *bbops* and replaces such memory allocation routines with a specialized processing-in-memory (PIM) memory allocation routine (i.e., `pim_malloc`, see §5.4.3). `pim_malloc` receives as input the *mat label* assigned to its associated *bbop* instruction. Second, the pass inserts a `bbop_trsp_init` instruction right after each `pim_malloc` call for each memory object that is an input/output of a *bbop* instruction. This instruction registers the memory object in MIMDRAM’s transposition unit (§5.4.2). Similar to the `pim_malloc` call, the `bbop_trsp_init` instruction receives as input the *mat label* assigned to its associated *bbop* instruction. To implement code generation, we modify LLVM’s X86 back-end to identify *bbop* instructions and generate the appropriate assembly code. In case the application uses parallel primitives (e.g., OpenMP pragmas [1248]) to parallelize outermost loops, the code generation pass interacts with the underlying runtime system to statically distribute *bbop* instructions from innermost loops across the available DRAM mats in a subarray, i.e., mats with unsigned *mat labels*. This allows MIMDRAM to execute in a Single Instruction Multiple Threads (SIMT) [1249, 1250] fashion for manually parallelized applications.

5.4 System Support for MIMDRAM

We envision MIMDRAM as a tightly-coupled accelerator for the host processor. As such, MIMDRAM relies on the host processor for its system integration, which includes ISA support (§5.4.1), instruction execution & data transposition (§5.4.2), and operating system support for address translation and data allocation & alignment (§5.4.3).

5.4.1 Instruction-Set Architecture

Table 5.1 shows the CPU ISA extensions that MIMDRAM exposes to the compiler.¹⁰ There are five types of instructions: (i) object initialization instructions, (ii) 1-input arithmetic instructions, (iii) 2-input arithmetic instructions, (iv) predication instructions, and (v) data movement instructions. The first three types of MIMDRAM instructions are inherited from the SIMD RAM ISA [378]. These instructions can be further divided into two categories: (i) operations with one input operand (e.g., bitcount, ReLU), and (ii) operations with two input operands (e.g., addition, division, equal, maximum). To enable predication, MIMDRAM uses the `bbop_if_else` instruction that SIMD RAM introduces, which takes as input three operands: two input arrays (`src1` and `src2`) and one predicate array (`select`). We modify such instructions by including two new fields: (i) *mat label* (ML), which identifies groups of instructions that must execute inside the same DRAM mat, and (ii) *vectorization factor* (VF), which dictates how many scalar operands are packed within the vector instruction. These two new fields are automatically generated by MIMDRAM’s compiler passes (§5.3).

Table 5.1: MIMDRAM ISA extensions.

Type	ISA Format
Initialization	<code>bbop_trsp_init</code> <code>addr</code> , <code>size</code> , <code>n</code> , <code>ML</code>
1-Input Arith.	<code>bbop_op</code> <code>dst</code> , <code>src</code> , <code>size</code> , <code>n</code> , <code>ML</code> , <code>VF</code>
2-Input Arith.	<code>bbop_op</code> <code>dst</code> , <code>src₁</code> , <code>src₂</code> , <code>size</code> , <code>n</code> , <code>ML</code> , <code>VF</code>
Predication	<code>bbop_if_else</code> <code>dst</code> , <code>src₁</code> , <code>src₂</code> , <code>sel</code> , <code>size</code> , <code>n</code> , <code>ML</code> , <code>VF</code>
Data Move	<code>bbop_mov</code> <code>dst</code> , <code>dst_idx</code> , <code>src</code> , <code>src_idx</code> , <code>size</code> , <code>n</code>

Data movement instructions allow the compiler to trigger inter-mat and intra-mat data movement operations. In a data movement instruction, `dst` and `src` represent the source and destination *arrays*; `dst_idx` and `src_idx` represent the first position of the first element inside the source and destination arrays to be moved; `size` represents the number of elements to move from source to the destination array; `n` represents the number of bits in each array element. MIMDRAM control unit automatically identifies the *mat range* the data movement instruction targets by calculating the distance between the source and destination arrays, taking into account the indexes and number of elements to move. In case the source and destination mats are the same, MIMDRAM control unit translates the data movement instruction into an LC-MOV command; otherwise, a GB-MOV command.

¹⁰MIMDRAM ISA extensions are vector-oriented by design. We did *not* use an existing ISA because we needed to define new fields for MIMDRAM that do *not* exist in current vector ISAs (e.g., mat label information). Instead, we propose to extend the baseline CPU ISA with MIMDRAM instructions since there is usually more than enough unused opcode space to support the extra opcodes that MIMDRAM requires [1251, 1252]. Extending the CPU ISA to interface with accelerators is a common approach [57, 314, 378, 1253, 1254].

5.4.2 Execution & Data Transposition

Instruction Fetch and Dispatch. MIMDRAM relies on the host CPU to offload *bbop* instructions to DRAM since they are part of the CPU ISA. Assuming that the host CPU consists of one or more out-of-order cores, MIMDRAM leverages the host processor's front-end to (i) identify and (ii) dispatch to MIMDRAM control unit *only* independent *bbops*. This simplifies the design of MIMDRAM control unit since no in-flight *bbop* instructions will have data dependencies. As a result, MIMDRAM control unit can freely schedule μ Programs to the PUD SIMD engine as they arrive.

Data Coherence. Input arrays to MIMDRAM may be generated or modified by the CPU, and the data updates may reside only in the cache (e.g., because the updates have not yet been written back to DRAM). To ensure that MIMDRAM does not operate on stale data, programmers are responsible for flushing cache lines [1255, 1256] modified by the CPU. MIMDRAM can leverage coherence optimizations tailored to PIM to improve overall performance [262, 271].

MIMDRAM Transposition Unit. MIMDRAM transposition unit shares the same hardware components and functionalities as the SIMDRAM transposition unit [378], which includes: (i) *object tracker*, a small cache that keeps track of the memory objects used by *bbop* instructions; (ii) an *horizontal to vertical transpose* unit, which converts cache lines of memory objects stored in the object tracker from a horizontal to vertical data layout during a LLC writeback; (iii) a *vertical to horizontal transpose* unit, which converts cache lines of memory objects stored in the object tracker from a vertical to horizontal data layout during an LLC read request; (iv) *store* and *fetch* units, which generate memory read/write requests using the transpose units' output data. One main limitation of the SIMDRAM transposition unit is that it needs to fill *at least* an entire DRAM row with vertically-laid out data before the execution of a *bbop*. Instead, MIMDRAM transposes only as much data as required to fill the segment of the DRAM row that the *bbop* instruction operates over. To do so, the MIMDRAM transposition unit adds information regarding the mat range a memory object operates to the object tracker.

5.4.3 Operating System Support

Address Translation. As SIMDRAM, MIMDRAM operates directly on physical addresses. When the CPU issues a *bbop* instruction, the instruction's virtual memory addresses are translated into their corresponding physical addresses using the same translation lookaside buffer (TLB) lookup mechanisms used by regular load/store operations.

Data Allocation & Alignment. MIMDRAM (as other PUD architectures [314, 315, 317, 318, 327–330, 333, 343]) requires OS support to guarantee that data is properly mapped and aligned

within the boundaries of the bank/subarray/mat that will perform computation. Particularly, since PUD operations are executed in-situ, it is essential to enforce that memory objects belonging to the same *bbop* (and their dependent instructions) are placed together in the same DRAM mats. To achieve this functionality, we propose the implementation of a new data allocation API called `pim_malloc`. The main idea is to allow the compiler to inform the OS memory allocator about the memory objects that must be allocated inside the same set of DRAM mats. The `pim_malloc` API takes as input the *size* of the memory region to allocate (as a regular `malloc` instruction) and the *mat label* that the compiler generates (§5.3). Then, it ensures that *all* memory objects with the same *mat label* are placed together within a set of DRAM mats that satisfies the target memory allocation size.

To allow the `pim_malloc` API to influence the OS memory allocator and ensure that memory objects are placed within specific DRAM mats, we propose a new *lazy data allocation routine* (in the kernel) for `pim_malloc` objects, which Figure 5.7 illustrates. This routine has three main components: (i) information about the DRAM organization (e.g., row, column, and mat sizes), (ii) the DRAM interleaving scheme, which the memory controller provides via an open firmware device tree [1257];¹¹ and (iii) a huge page pool for `pim_malloc` objects (configured during boot time), which guarantees that virtual addresses assigned to a `pim_malloc` object are contiguous in the physical address space and that DRAM mats are free whenever a `pim_malloc` object is allocated. The allocation routine uses the DRAM address mapping knowledge to split the huge pages into different memory regions. Then, when an application calls the `pim_malloc` API, the allocation routine selects the appropriate memory region that satisfies `pim_malloc`. Internally, the `pim_malloc` API operates using three main sub-tasks, depending on the order of the data allocation: (i) `pim_preallocate`, for data pre-allocation; (ii) `pim_alloc`, for the first data allocation; and (iii) `pim_alloc_align`, for subsequent aligned allocations.

(i) Pre-Allocation. The first sub-task’s role is to indicate the number of huge pages available for PUD allocations (❶ in Figure 5.7). We leave it to the user to provide the number of huge pages used for PUD operations (❷ in Figure 5.7) because huge pages are scarce in the system.

(ii) First Allocation. The second sub-task uses the *worst-fit allocation scheme* [1260] to manage the allocation of memory regions in the huge page pool. The *key idea* behind this placement

¹¹The DRAM interleaving scheme can be obtained by reverse engineering the bit locations of memory addresses [184, 663, 1258, 1259]. Even though typical DRAM interleaving does *not* take mats into account, it is relatively straightforward to reverse-engineer how a memory address is distributed across the DRAM mats in a DRAM module, since the mat interleaving is a function of the DRAM chip’s organization. For example, in a DDR4 module with 8 chips, 16 mats per chip, and 4 HFFs per mat, a 64 B cache line is evenly distributed across all 128 total mats; i.e., the four least-significant bits of the cache line are placed in mat 0, chip 0, and the four most-significant bits of the cache line are placed in mat 15, chip 7. Our `pim_malloc` API takes into account such mat interleaving.

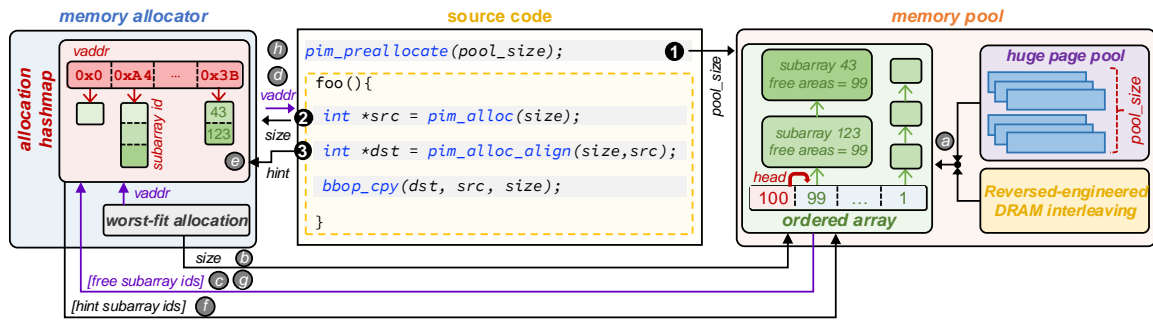


Figure 5.7: Overview of the MIMDRAM's memory allocation routine.

strategy is to optimize the remaining memory space after allocations to increase the chances of accommodating another process in the remaining space. For the first PUD memory allocation, the `pim_alloc` sub-task (②) simply scans an *ordered array* data structure (similar to the one used in the Linux Kernel buddy allocator algorithm [1261], where each entry represents the number of memory regions in a single subarray) to select the subarray with the *largest* amount of memory regions available (⑥). If the requested memory allocation requires more than one memory region, MIMDRAM iteratively scans the *ordered array*, searching for the next largest memory region until the memory allocation is fully satisfied. Once enough space is allocated (③), `pim_alloc` sub-task creates a new allocation object and inserts it in an *allocation hashmap*, which is indexed by the allocation's virtual address (④). The sub-task needs to keep track of allocations since it might need to find a memory region from the *same* subarray/mat when performing future *aligned allocations*.

(iii) Aligned Allocation. After allocating a memory region for the first operand in a PUD operation, the user can use this memory region as a regular memory object. However, when allocating the remaining operands for a PUD operation, the `pim_malloc` API needs to guarantee data alignment for all memory objects within the same DRAM subarray/mat. To this end, the third sub-task (`pim_malloc_align`; ⑤) identifies a previously allocated memory region to which the current memory allocation must be aligned (based on the compiler-generated *mat labels*). The `pim_malloc_align` sub-task works in five main steps. First, it searches the *allocation hashmap* using the *mat label* as a *hint* for a match with previously allocated memory regions (⑦). If a match is not found, the allocation fails. Second, if a match is found, the `pim_malloc_align` sub-task iterates through the identified previously-allocated memory regions (⑧). Third, for each memory region, the sub-task identifies its source subarray/mat address and tries to allocate another memory region in the same subarray/mat for the new allocation (⑨). Fourth, if the subarray/mat of a given memory region has no free region, the sub-task allocates a new memory region from another subarray/mat following the worst-fit allocation scheme (⑩). Since we use a worst-fit allocation scheme that always selects the *largest* number of memory regions available during memory allocation for the *first* operand of a PUD

operation, we have a good chance of having a single subarray/mat holding memory regions for the remaining operands of a PUD operation. Fifth, since memory regions might come from different huge pages, we must perform `re-mmap` to map such memory regions into contiguous virtual addresses.

Mat Label Translation. To keep track of the mapping between *mat labels* and allocated *mat ranges*, MIMDRAM adds a small *mat translation table* alongside the page table. The table is indexed by hashing the *mat label* with the *process ID*. It stores in each entry the associated *mat range* that the memory allocator assigned to that particular *mat label*. When the CPU dispatches a *bbop*, the CPU (i) accesses the *mat translation table* to obtain the *mat range* assigned to the given *bbop*, and (ii) replaces the *mat label* with the *mat range*.

5.5 Methodology

We implement MIMDRAM using the `gem5` simulator [1262] and compare it to a real multicore CPU (Intel Skylake [458]), a real high-end GPU (NVIDIA A100 [459]), and a state-of-the-art PUD framework (SIMDRAM [378]). In all our evaluations, the CPU code is optimized to leverage AVX-512 instructions [1263]. Table 6.2 shows the system parameters we use. To measure CPU energy consumption, we use Intel RAPL [1264]. We capture GPU kernel execution time that excludes data initialization/transfer time. To measure GPU energy consumption, we use the `nvml` API [1265]. We implement SIMDRAM on `gem5`, taking into account that the latency of executing the back-to-back ACTs is only $1.1\times$ the latency of t_{RAS} [314,315,318,327,328,330], and validate our implementation rigorously with the results reported in [378]. We use CACTI [1266] to evaluate MIMDRAM and SIMDRAM energy consumption, where we take into account that each additional simultaneous row activation increases energy consumption by 22% [314,378]. Our simulation accounts for the additional latency imposed by MIMDRAM’s mat isolation transistors and row decoder latches (i.e., measured (using CACTI [1131, 1266]) to incur less than 0.5% extra latency for an ACT). We open-source our simulation infrastructure at <https://github.com/CMUSAFARI/MIMDRAM>.

Real-World Applications. We analyze 117 applications from seven benchmark suites (SPEC 2017 [5], SPEC 2006 [1267], Parboil [1141], Phoenix [4], Polybench [1268], Rodinia [1142], and SPLASH-2 [1144]) to select applications that (i) are memory-bound, and (ii) the most time-consuming loop can be auto-vectorized. From this analysis, we collect 12 multi-threaded CPU applications (as Table 6.3 describes) from different domains (i.e., video compression, data mining, pattern recognition, medical imaging, stencil computation), and their respective GPU implementations, when available. Our evaluated applications are: (i) `525.x264_r` (`x264`) from SPEC 2017; (ii) `heartwall` (`hw`), `kmeans` (`km`), and `backprop` (`bs`) from Rodinia; (iii) `pca` from

Table 5.2: Evaluated system configurations.

Real Intel Skylake CPU [458]	x86 [1255], 16 cores, 8-wide, out-of-order, 4 GHz; <i>L1 Data + Inst. Private Cache</i> : 256 kB, 8-way, 64 B line; <i>L2 Private Cache</i> : 2 kB, 4-way, 64 B line; <i>L3 Shared Cache</i> : 16 MB, 16-way, 64 B line; <i>Main Memory</i> : 64 GB DDR4-2133, 4 channels, 4 ranks
Real NVIDIA A100 GPU [459]	7 nm technology node; 6912 CUDA Cores; 108 streaming multiprocessors, 1.4 GHz base clock; <i>L2 Cache</i> : 40 MB L2 Cache; <i>Main Memory</i> : 40 GB HBM2 [424, 425]
Simulated SIMDram [378] & MIMDRAM	gem5 system emulation; x86 [1255], 1-core, out-of-order, 4 GHz; <i>L1 Data + Inst. Cache</i> : 32 kB, 8-way, 64 B line; <i>L2 Cache</i> : 256 kB, 4-way, 64 B line; <i>Memory Controller</i> : 8 kB row size, FR-FCFS [649, 1194] <i>Main Memory</i> : DDR4-2400, 1 channel, 8 chips, 4 rank 16 banks/rank, 16 mats/chip, 1 K rows/mat, 512 columns/mat <i>MIMDRAM's Setup</i> : 8 entries mat queue, 2 kB <i>bbop</i> buffer 8 μ Program processing engines, 2 kB <i>mat translation table</i>

Phoenix; and (iv) 2mm, 3mm, covariance (cov), doitgen (dg), fdtd-apml (fdtd), gemm (gmm), and gramschmidt (gm) from Polybench.¹² Since our base PUD substrate (SIMDRAM) does *not* support floating-point, we manually modify the selected floating-point-heavy auto-vectorized loops to operate on fixed-point data arrays.¹³ We use the largest input dataset available and execute each application *end-to-end* in our evaluations.

Table 5.3: Evaluated applications and their characteristics.

Benchmark Suite	Application (Short Name)	Dataset Size	# Vector Loops	VF {min, max}	PUD Ops. [†]
Phoenix [4]	[‡] pca (pca)	reference	2	{4000, 4000}	D, S, M, R
Polybench [1268]	2mm (2mm)	NI = NJ = NK = NL = 4000	6	{4000, 4000}	M, R
	[‡] 3mm (3mm)	NI = NJ = NK = NL = NM = 4000	7	{4000, 4000}	M, R
	covariance (cov)	N = M = 4000	2	{4000, 4000}	D, S, R
	doitgen (dg)	NQ = NR = NP = 1000	5	{1000, 1000}	M, C, R
	[‡] fdtd-apml (fdtd)	CZ = CYM = CXM = 1000	3	{1000, 1000}	D, M, S, A
	gemm (gmm)	NI = NJ = NK = 4000	4	{4000, 4000}	M, R
	gramschmidt (gs)	NI = NJ = 4000	5	{4000, 4000}	M, D, R
Rodinia [1142]	backprop (bs)	134217729 input elm.	1	{17, 134217729}	M, R
	heartwall (hw)	reference	4	{1, 2601}	M, R
	kmeans (km)	16384 data points	2	{16384, 16384}	S, M, R
SPEC 2017 [5]	525.x64_r (x264)	reference input	2	{64, 320}	A

[†]: D = division, S = subtraction, M = multiplication, A = addition, R = reduction, C = copy

[‡]: application with independent PUD operations

Multi-Programmed Application Mixes. To measure system throughput and fairness, we *manually* create 495 application mixes by randomly selecting eight applications (from our group of 12 applications) for execution co-location. We classify each application mix into one of three categories: *low*, *medium*, and *high* vectorization factor (VF) mixes based on Figure 5.1.

¹²Several prior works [274, 326, 349, 482, 878, 892, 1109] show that our selected twelve workloads can benefit from different types of PIM architectures.

¹³We only modify the three applications from the Rodinia benchmark suite to use fixed-point operations. Prior works [349, 1269, 1270] also employ fixed-point for the same three Rodinia applications. The applications from Polybench can be configured to use integers; the auto-vectorized loops in 525.x264_r use `uint8_t`; pca uses integers. We do *not* observe an output quality degradation when employing fixed-point for the selected loops.

In the *low* mix, the maximum VF of *all* eight applications is lower than 16K; in the *medium* mix, *at least* one application has a maximum vectorization factor between 16K (inclusive) and 64K; and in the *large* mix, *at least* one application has a maximum VF larger than 64K (inclusive).

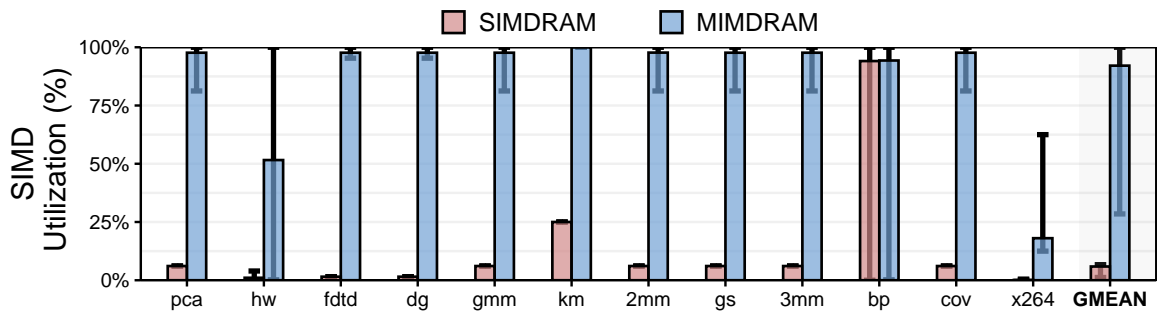
Comparison to State-of-the-Art PIM Architectures. We compare MIMDRAM to two other state-of-the-art PIM architectures: DRISA [316] and Fulcrum [382]. DRISA is a combined processing-using-memory (PUM) and PNM architecture that *significantly* modifies the DRAM microarchitecture and organization to enable bulk in-DRAM computation (e.g., by using 3T1C DRAM cells to execute in-situ bitwise NOR operations and by adding logic gates *near* the subarray’s sense amplifiers). Fulcrum is a PNM architecture that adds computation logic *near* subarrays. Fulcrum’s primary components are a series of shift registers (called walkers) that latch input/output DRAM rows and a narrow scalar ALU that executes arithmetic and logic operations. We model the DRISA 3T1C implementation and Fulcrum (i) using a DRAM module of equal dimensions (i.e., number of DRAM ranks, chips, banks, mats, rows, and columns) as the baseline DDR4 DRAM we use for SIMD RAM and MIMDRAM (see Table 6.2) and (ii) including all the changes that the DRISA 3T1C and Fulcrum architectures propose to the DRAM cell array and DRAM subarray.

5.6 Evaluation

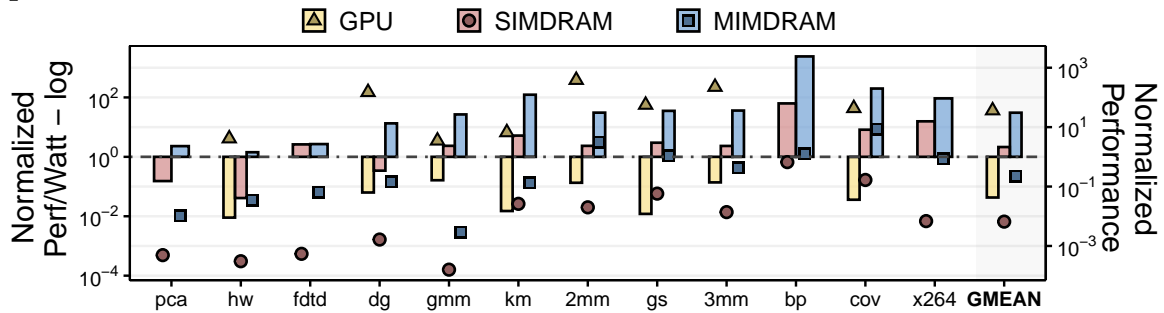
We demonstrate the advantages of MIMDRAM by evaluating (i) SIMD utilization and energy efficiency (i.e., performance per Watt) for single applications (§5.6.1); (ii) system throughput (in terms of weighted speedup [1271–1273]), job turnaround time (in terms of harmonic speedup [1272, 1274]), and fairness (in terms of maximum slowdown [649, 652, 654, 655, 1018, 1089, 1108, 1125, 1191, 1202, 1275]) for multi-programmed application mixes in comparison to the baseline CPU, GPU, and a state-of-the-art PUD architecture, i.e., SIMD RAM [378] (§5.6.2); (ii) area-normalized performance analysis for single applications and throughput analysis for multi-programmed application mixes in comparison to state-of-the-art PIM architectures, i.e., DRISA [316] and Fulcrum [382] (§5.6.3). In most of our analyses (§5.6.1–§5.6.2), to keep our analyses pure, we very *conservatively* allow MIMDRAM to use only a *single* DRAM subarray in a *single* DRAM bank for PUD computation. In §5.6.4, we perform a scalability analysis to evaluate MIMDRAM’s performance when enabling *multiple* DRAM subarrays and banks for PUD computation, which reflects a more accurate evaluation of the true benefits of MIMDRAM and PUD. Finally, we evaluate MIMDRAM’s DRAM and CPU area cost (§6.5.5).

5.6.1 Single-Application Results

Figure 5.8 shows MIMDRAM’s SIMD utilization and normalized energy efficiency (in performance per Watt) for all 12 applications. Values are normalized to the baseline CPU.



(a) SIMD utilization. Whiskers extend to the minimum and maximum observed data point values.



(b) CPU-normalized performance per Watt (left y-axis; bars) and performance (right y-axis; dots).

Figure 5.8: Single-application results for processor-centric (i.e., CPU and GPU) and memory-centric (i.e., SIMDDRAM and MIMDRAM) architectures executing twelve real-world applications.

SIMD Utilization. We make two observations from Figure 5.8a. First, MIMDRAM *significantly* improves SIMD utilization over SIMDDRAM. On average across all applications, MIMDRAM provides 15.6 \times the SIMD utilization of SIMDDRAM. This is because MIMDRAM matches the available SIMD parallelism in an application with the underlying PUD resources (i.e., PUD SIMD lanes) by using *only* as many DRAM mats as the maximum vectorization factor of a given application’s loop. In contrast, SIMDDRAM always occupies *all* available PUD SIMD lanes (i.e., entire subarrays) for a given operation, resulting in low SIMD utilization for applications without a very-wide vectorization factor. Second, we observe that SIMD utilization can vary considerably within an application. For example, MIMDRAM’s SIMD utilization for hw and bp goes from as low as 0.2% to as high as 100%. This happens because the SIMD parallelism for each vectorized loop in these applications changes at different execution phases. MIMDRAM can better adjust to the variation in SIMD parallelism (than SIMDDRAM) due to its flexible design. We conclude that MIMDRAM greatly improves overall SIMD utilization for many applications.

Performance & Energy Efficiency. We make three observations from Figure 5.8b. First, MIMDRAM *significantly* improves energy efficiency and performance over SIMDDRAM. On

average across all applications, MIMDRAM provides $14.3\times$ the energy efficiency and $34\times$ the performance of SIMD RAM. MIMDRAM's higher energy efficiency is due to three main reasons. (i) MIMDRAM parallelizes the computation of independent *bbops* in a single application loop across different mats, improving overall performance. MIMDRAM reduces execution time by $2.8\times$ compared with SIMD RAM, on average across applications with independent *bbops* (i.e., *pca*, *3mm*, and *fdtd*). (ii) MIMDRAM implements in-situ PUD vector reduction operations, while SIMD RAM requires the assistance of the CPU for vector reduction, increasing latency and energy consumption. MIMDRAM reduces execution time and energy consumption by $1.6\times$ and $266\times$ over SIMD RAM, on average across the applications with vector reduction operations (from our twelve applications, only *fdtd* and *x264* do *not* require vector reduction operations). (iii) MIMDRAM activates only the necessary PUD SIMD lanes during an application loop's execution, significantly saving energy when the application has low SIMD utilization. MIMDRAM reduces energy consumption by $325\times$ over SIMD RAM, on average across applications with a maximum vectorization factor lower than 65,536 (from our twelve applications, only *bs* exhibits a vectorization factor *higher* than 65,536). Second, MIMDRAM provides $30.6\times/6.8\times$ the energy efficiency of CPU/GPU baselines. MIMDRAM's higher energy efficiency is due to its inherent ability to avoid costly data movement operations for memory-bound applications. Third, even though MIMDRAM improves performance (by $3.1\times$, $8.6\times$, $1.1\times$, and $1.3\times$) compared to the baseline CPU for some applications (i.e., *2mm*, *cov*, *gs*, and *bp*), it leads to performance loss compared to the baseline CPU and GPU on average across all applications. This is because, for some applications, the bulk parallelism available inside a *single* DRAM subarray and bank is insufficient to hide the latency of costly bit-serial operations (e.g., multiplication). We observe that enabling MIMDRAM in 16 DRAM banks and 64 subarrays (per bank) allows MIMDRAM to provide performance gains compared to the CPU and the GPU (see §5.6.4). We conclude that MIMDRAM is an energy-efficient and high-performance PUD system.

5.6.2 Multi-Programmed Workload Results

We evaluate SIMD RAM and MIMDRAM's impact on system throughput (in terms of weighted speedup [1271–1273]), job turnaround time (in terms of harmonic speedup [1272, 1274]), and fairness (in terms of maximum slowdown [649, 652, 654, 655, 1018, 1089, 1108, 1125, 1191, 1202, 1275]) when executing applications concurrently. To provide a fair comparison, we introduce MIMD parallelism in SIMD RAM with bank-level parallelism (BLP) [161, 494, 650, 655, 1019], where each SIMD RAM-capable DRAM bank can independently run an application. We evaluate four configurations of SIMD RAM where 1 (*SIMDRAM:1*), 2 (*SIMDRAM:2*), 4 (*SIMDRAM:4*), and 8 (*SIMDRAM:8*) banks have SIMD RAM computation capability. Figure 5.9 shows the system throughput, job turnaround time (which measures a balance of fairness and throughput),

and fairness that SIMD RAM and MIMDRAM provide on average across all application mixes. Values are normalized to *SIMDRAM:1*. We make three observations.

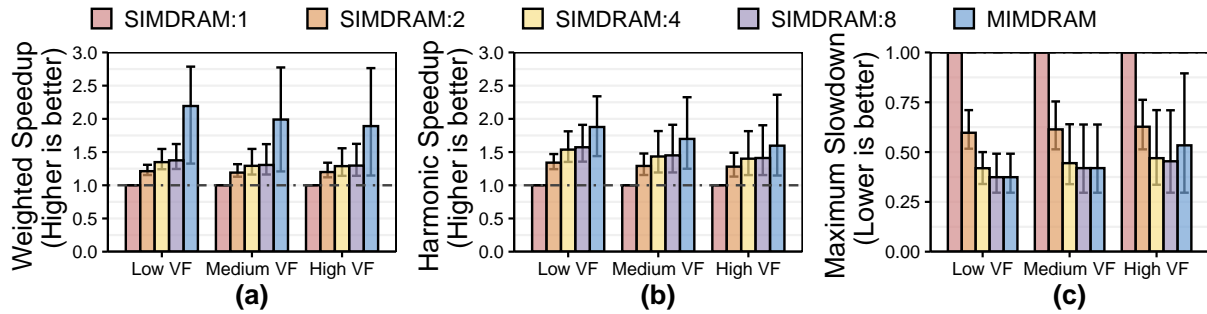


Figure 5.9: Multi-programmed workload results for three types of application mixes: (a) low VF, (b) medium VF, and (c) high VF. VF stands for vectorization factor. *SIMDRAM:X* uses *X* DRAM banks for computation. Values are normalized to *SIMDRAM:1*. Whiskers extend to the minimum and maximum observed data point values.

First, MIMDRAM *significantly* improves system throughput, job turnaround time, and fairness compared with SIMD RAM. On average, across all application groups, MIMDRAM achieves: (i) $1.68\times$ (min. $1.52\times$, max. $2.02\times$) *higher* weighted speedup, (ii) $1.33\times$ (min. $1.17\times$, max. $1.72\times$) *higher* harmonic speedup, and (iii) $1.32\times$ (min. $0.95\times$, max. $2.29\times$) *lower* maximum slowdown than SIMD RAM (averaged across all four configurations). Second, MIMDRAM using a single subarray and single bank for computation, provides $1.68\times$, $1.54\times$, and $1.52\times$ the system throughput of SIMD RAM using 2, 4, and 8 banks for computation, respectively. This happens because MIMDRAM (i) utilizes idle resources at DRAM mat granularity to execute computation as soon as a mat is available, thus reducing queuing time and improving parallelism; and (ii) reduces execution latency of a single application due to its concurrent execution of independent *bbop* instructions and support for PUD vector reduction. Third, even though MIMDRAM achieves similar fairness compared with *SIMDRAM:4* and *SIMDRAM:8* for application mixes with low and medium VF, MIMDRAM's maximum slowdown is 15% (12%) higher than *SIMDRAM:8* (*SIMDRAM:4*) for application mixes with high VF. This is because in MIMDRAM (i) applications share the DRAM mats available inside a single DRAM bank and (ii) *bbops* are dispatched to execution using an online *first fit* algorithm. In this way, an application in a mix with *high* occupancy and execution latency penalizes an application with *low* occupancy and execution time, negatively impacting fairness. In contrast, such interference does *not* happen in *SIMDRAM:8* since each application is assigned to a different DRAM bank to execute at the cost of occupying eight banks instead of one. MIMDRAM's fairness can be further improved by (i) employing better scheduling algorithms that target quality-of-service [650, 652, 1125, 1191, 1198, 1274] or (ii) using subarray-level parallelism (SALP) [161] and BLP [161, 494, 650, 655, 1019] in MIMDRAM, i.e., exploiting multiple subarrays and multi-

ple banks for MIMDRAM computation (§5.6.4).¹⁴ We conclude that MIMDRAM is an efficient and high-performance PUD substrate when the system concurrently executes several applications.

CPU Multi-Programmed Workload Results. We evaluate how MIMDRAM performance compares to that of a state-of-the-art CPU when executing multiple applications. To do so, we randomly generate ten different application mixes, each containing eight applications out of our 12 applications. Then, we run each application mix in our baseline CPU (using multi-threading) and in MIMDRAM and compute the achieved system throughput for each system (using weighted speedup). Figure 5.10 shows the system throughput MIMDRAM achieves compared to the baseline CPU. We observe that MIMDRAM improves overall throughput by 19%. This is because MIMDRAM can parallelize the execution of the applications in each application mix across the DRAM mats in a subarray. In contrast, when executing each application mix, the baseline CPU often suffers from contention in its shared resources (e.g., shared cache and DRAM bus). We conclude that MIMDRAM is an efficient substrate for highly-parallel environments.

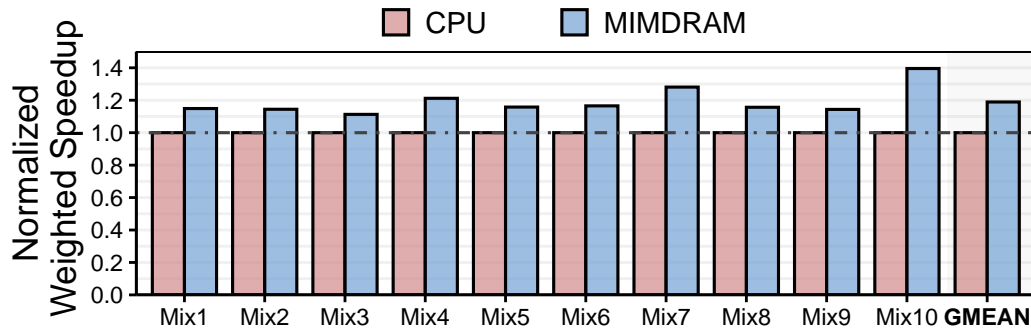


Figure 5.10: Multi-programmed workload results for ten application mixes. Values are normalized to the baseline CPU.

5.6.3 Comparison to Other PIM Architectures

Single-Application Results. We compare the performance of each PIM architecture and MIMDRAM. Since DRISA and Fulcrum use large additional area (i.e., 21% and 82% DRAM area overhead, respectively, over our baseline DDR4 DRAM chip) to implement PIM operations, we report area-normalized results (i.e., performance per area) for a fair comparison. We use the area values reported in both DRISA and Fulcrum’s papers, scaled to the baseline DDR4 DRAM device we employ. We allow each mechanism to leverage the data parallelism available in each application by dividing the work evenly across DRISA’s PIM-capable DRAM banks and Fulcrum’s PIM-capable subarrays. Figure 5.11 shows the normalized performance per area for

¹⁴In our extended version [893], we provide multi-programmed workload results while exploiting SALP and BLP for MIMDRAM computation.

all 12 applications. Values are normalized to MIMDRAM. We make two observations. First, MIMDRAM achieves the highest performance per area compared to DRISA and Fulcrum. On average across the 12 applications, MIMDRAM performance per area is $1.18\times/1.92\times$ that of DRISA and Fulcrum. This is because although DRISA and Fulcrum achieve higher absolute performance than MIMDRAM ($7.5\times$ and $3.0\times$, respectively), such performance benefits come at the expense of very large area overheads. While MIMDRAM incurs small area cost on top of a DRAM array (1.11% DRAM area overhead, see §6.5.5), DRISA and Fulcrum incur significantly larger area costs. Second, for some applications (namely hw, dg, km, and x264), DRISA and Fulcrum achieve higher performance per area than MIMDRAM. We observe that such applications are dominated by multiplication operations, which are costly to implement using MIMDRAM’s bit-serial approach. We conclude MIMDRAM is an area-efficient PIM architecture, which provides performance benefits compared to state-of-the-art PIM architectures for a fixed area budget.

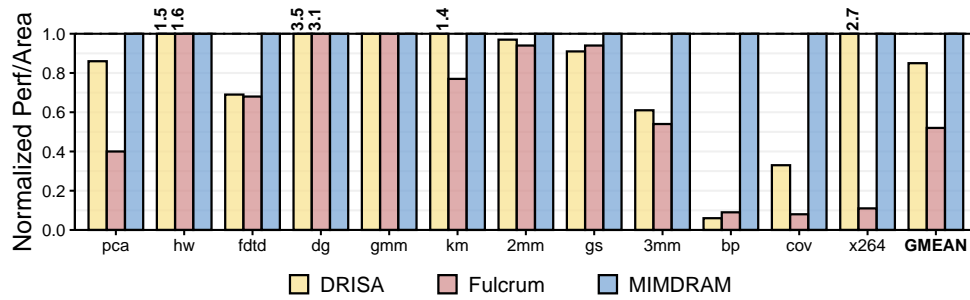


Figure 5.11: Single-application results for different state-of-the-art PIM architectures.

Multi-Programmed Workload Results. Figure 5.12 shows the system throughput, job turnaround time, and fairness that DRISA, Fulcrum, and MIMDRAM provide on average across all application mixes. We employ BLP in DRISA and MIMDRAM, and SALP [161] in Fulcrum to enable MIMD execution. We make two observations. First, all three PIM architectures achieve similar system throughput. On average across all application mixes and configurations, DRISA, Fulcrum, and MIMDRAM achieve $1.20\times$, $1.17\times$, and $1.19\times$ the system throughput of *DRISA:1*, respectively. Second, when considering a *single* DRAM subarray for computation, MIMDRAM achieves 8% and 11% *higher* fairness than DRISA and Fulcrum, respectively.

5.6.4 MIMDRAM with SALP & BLP

One of the main advantages of PUD architectures is the ability to exploit the large internal DRAM parallelism for computation. A PUD substrate can leverage SALP [161] and BLP [161, 494, 650, 655, 1019] techniques to operate *simultaneously* exploit the many DRAM subarrays (e.g., 8–64 per bank) and banks (e.g., 8–16 per rank) in a DRAM chip for PUD computation. To this end, we perform a sensitivity analysis of SIMDRAM and MIMDRAM’s performance

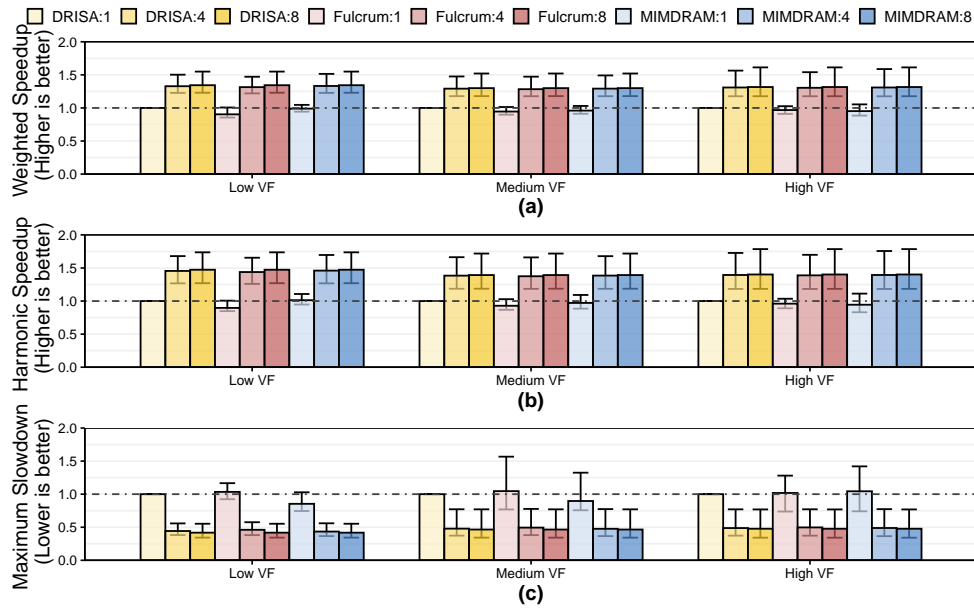


Figure 5.12: Multi-programmed workload results for different PIM architectures and three types of application mixes. VF stands for vectorization factor. *DRISA:X/MIMDRAM:X (Fulcrum:X)* uses *X* DRAM banks (subarrays) for computation. Values are normalized to *DRISA:1*. Whiskers extend to the minimum and maximum observed data points.

for our twelve applications when using multiple DRAM subarrays (1–64 per bank) and DRAM banks (1–16 per rank) for PUD computation, as Figure 5.13 depicts. We make two observations from the figure.

First, by *fully* leveraging the internal DRAM parallelism in a DRAM chip, MIMDRAM can provide *significant* performance gains compared to the baseline CPU. On average across all twelve applications, MIMDRAM (using 64 DRAM subarrays per bank and 16 banks for PUD computation) achieves $13.2\times$ the performance of the CPU. Second, in contrast, SIMDRAM *fails* to outperform the baseline CPU, even when fully utilizing the internal DRAM for computation ($0.08\times$ the performance of the CPU when using 64 DRAM subarrays per bank and 16 banks). This is because: (i) MIMDRAM unlocks further parallelism by leveraging idle DRAM mats for computation and (ii) MIMDRAM reduces the latency of costly vector reduction operations. Third, we observe that MIMDRAM can lead to performance loss compared to the baseline CPU for some workloads, even when using all available DRAM subarrays and banks for computation, for two main reasons: (i) quadratically-scaling PUD operations (i.e., multiplication and divisions) or (ii) PUD vector reduction operations dominate MIMDRAM’s execution time of the application. In the first case, MIMDRAM’s performance could be further improved by leveraging lower-latency algorithms for costly PUD operations (e.g., bit-parallel multiplication and division algorithms [946]) or performing such complex operations near memory (close to DRAM) [6, 13, 14, 21, 56, 57, 155, 156, 239–247, 250, 252, 253, 258, 259, 262, 263, 266, 267, 269, 271, 272, 277–282, 284, 301, 302, 311, 382]. In the second case, MIMDRAM would benefit from the as-

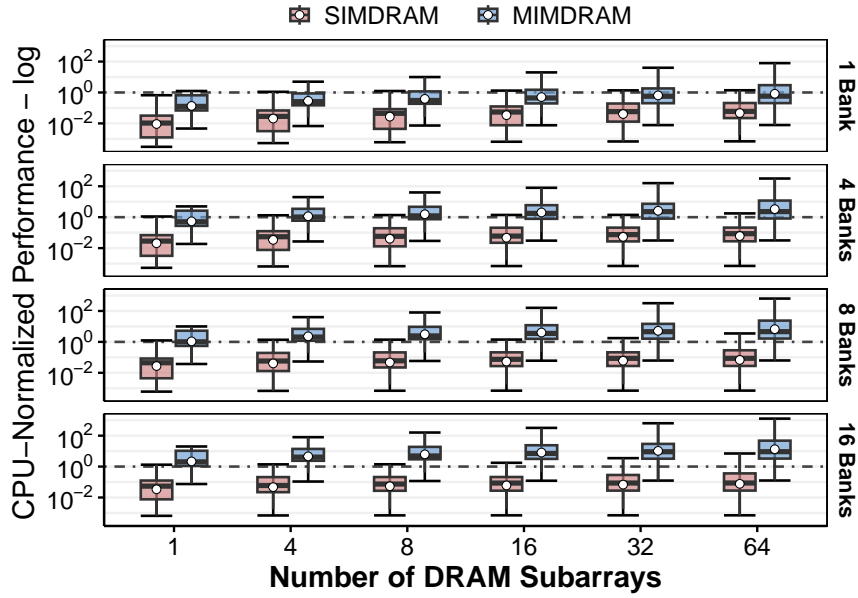


Figure 5.13: Distribution of single-application performance across all twelve applications when varying the number of DRAM subarrays and banks for SIMDram and MIMDRAM. Values are normalized to the baseline CPU. Whiskers extend to the minimum and maximum observed data points on either side of the box. Bubbles depict average values.

sistance of PNM architectures to perform faster vector reduction operations in DRAM, at the cost of an increase in area cost. We conclude that MIMDRAM highly benefits from exploiting SALP and BLP for PUD computation.

Performance & Energy Efficiency. Figure 5.14 shows the CPU-normalized performance (Figure 5.14a), CPU-normalized energy (Figure 5.14b), and CPU-normalized performance per Watt (Figure 5.14c) when allowing SIMDram and MIMDRAM to simultaneously issue in-DRAM operations across all 16 banks and 64 subarrays per bank in a DRAM rank. We make two key observations.

First, MIMDRAM provides (i) $13.2\times/0.22\times/173\times$ the performance, (ii) $0.0017\times/0.00007\times/0.004\times$ the energy consumption, and (iii) $582.4\times/13612\times/272\times$ the performance per Watt of the CPU/GPU/SIMDRAM baseline. Second, we observe that MIMDRAM’s end-to-end performance gains are limited by the throughput of the inter- and intra-mat interconnects, which are utilized during in-DRAM reduction operations. If we consider only MIMDRAM’s arithmetic throughput (i.e., no reduction operations), we observe that MIMDRAM provides $272\times$ and $11\times$ the performance of the CPU and GPU baselines, respectively. We believe that combining PUM and PNM holistically, where auxiliary logic placed within the logic layer of 3D-stacked memories is used for high-throughput in-DRAM reduction and DRAM cells are used for high-throughput in-DRAM bulk arithmetic, would be beneficial to improve MIMDRAM’s end-to-end performance. We conclude that

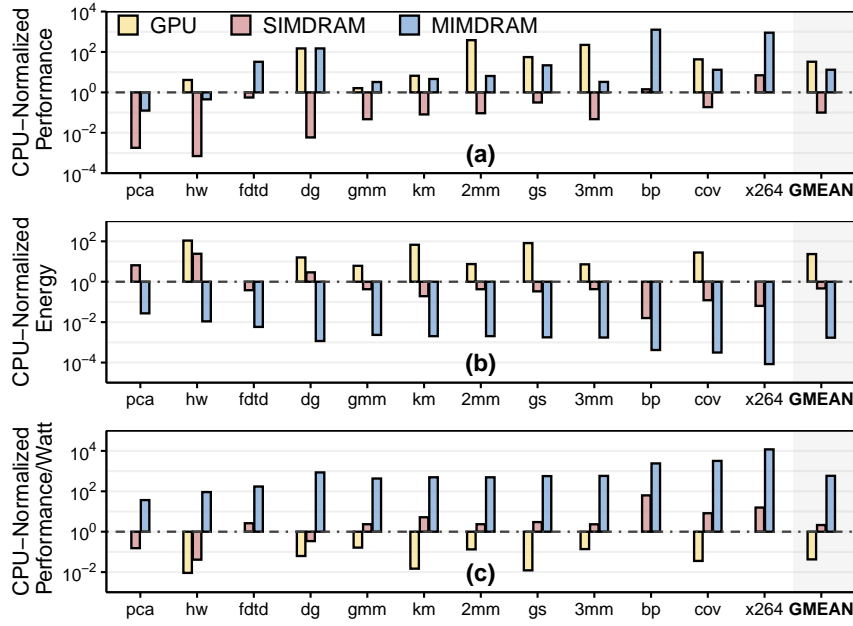


Figure 5.14: GPU, SIMD, and MIMD performance (a), energy (b), and performance per Watt (c) for twelve real-world applications when using 16 DRAM banks and 64 DRAM subarrays per bank for in-DRAM computing. Values are normalized to the baseline CPU.

MIMDRAM enables effective exploitation of DRAM bank-level and subarray-level parallelism for massively-parallel bulk bitwise execution.

5.6.5 Hardware Area Analysis

We use CACTI [1131, 1266] to model the area of a DRAM chip (Table 6.2) using a 22 nm technology node. We implement MIMDRAM’s chip select and mat identifier logic in Verilog HDL and synthesize the HDL using the Synopsys Design Compiler [1276] with a 65 nm process technology node.¹⁵

DRAM Bank Area. We evaluate the area overhead of (i) mat isolation transistors, (ii) row decoder latches, (iii) mat selectors, (iv) the wiring to propagate mat selector output to mat isolation transistors (matlines), and (v) multiplexers and wiring of the inter-mat interconnect. MIMDRAM incurs 1.15% area overhead over the baseline DRAM bank.

DRAM Chip I/O Area. The total area overhead for MIMDRAM’s chip select and mat identifier is *only* $825.7 \mu\text{m}^2$ at a 65 nm technology node. We estimate the equivalent area overhead at a 22 nm technology node to be $116.3 \mu\text{m}^2$ [1277].

Overall, MIMDRAM increases the area of the evaluated DRAM chip (16 banks and I/O) by only 1.11%.

¹⁵We use a 65 nm technology node since that is the best CMOS standard cell library we have access to in our environment. We scaled our design to a 22 nm technology node following prior works’ methodology [240, 776, 1277, 1278].

MIMDRAM Control Unit & Transposition Unit Area. The main components in the MIMDRAM control unit are the (i) *bbop* buffer, (ii) mat scoreboard, and (iii) μ Program processing engines. We set the size of the *bbop* buffer to 2 kB, which accommodates up to 1024 *bbops*. The mat scoreboard requires 128 bits of storage, one bit per DRAM mat per subarray. A single μ Program processing engine has an area of 0.03 mm^2 . We empirically include eight μ Program processing engines in our design. We estimate, using CACTI, that MIMDRAM control unit area is 0.253 mm^2 . MIMDRAM transposition unit has an area equal to the SIMD RAM transposition unit (of 0.06 mm^2). Considering the area of the control and transposition units, MIMDRAM has a low area overhead of 0.6% over the die area of a state-of-the-art Intel Xeon E5-2697 v3 CPU [326].

5.7 Summary

We introduce MIMDRAM, a hardware/software co-designed processing-using-DRAM (PUD) substrate that can allocate and control only the needed computing resources inside DRAM for PUD computing. On the hardware side, MIMDRAM introduces simple modifications to the DRAM architecture that enables the execution of (i) different PUD operations concurrently inside a single DRAM subarray in a multiple-instruction multiple-data (MIMD) fashion, and (ii) native vector reduction computation. On the software side, MIMDRAM implements a series of compiler passes that automatically identify and map code regions to the underlying PUD substrate. We experimentally demonstrate that MIMDRAM provides significant benefits over state-of-the-art CPU, GPU, and processing-using-memory (PUM) and processing-near-memory (PNM) systems. We hope and believe that our work can inspire more efficient and easy-to-program PUD systems. The source code of MIMDRAM is freely available at <https://github.com/CMU-SAFARI/MIMDRAM>.

Chapter 6

Proteus: Achieving High-Performance Processing-Using-DRAM with Dynamic Bit-Precision, Adaptive Data Representation, and Flexible Arithmetic

6.1 Motivation & Goal

We discuss three major shortcomings of prior PUD architectures: *static data representation*, *support for only throughput-oriented execution*, and *high latency for high-precision operands*.

Limitation 1: Static Data Representation. PUD architectures naively utilize conventional data formats (e.g., two’s complement) and fixed operand bit-precision (e.g., 32-bit integers) to implement bit-serial computation. However, because bit-serial latency directly increases with bit-precision, these architectures experience subpar performance since an application’s data with small dynamic range (i.e., narrow values) are often stored in large data formats [460–467] that waste most of the bit-precision. Note that data values often become narrow dynamically at runtime. Narrow values have been exploited in many scenarios, e.g., cache compression [460–462, 467, 1042, 1043, 1045, 1279–1282], register files [463, 465, 1283–1288], logic synthesis & circuit optimizations [1289–1293], neural network quantization [1294, 1295], error tolerance [463, 1296, 1297].

Opportunity 1: Narrow Values for PUD Computation. Narrow values can be exploited to reduce the bit-precision of a PUD operation to that of the best-fitting number of bits, thereby, improving overall performance. We quantify the required bit-precision in PUD-friendly real-world applications in Figure 6.1. We define as *required bit-precision* the minimum number of

bits required to represent the input operands of the PUD operation.¹ We collect the required bit-precision dynamically in three main steps: we (i) instrument loops in applications that can be auto-vectorized using LLVM’s loop auto-vectorization pass [1238–1241] (since prior work [893] shows that such loops are well-suited for PUD execution) to output the data values such loops use (i.e., we collect the data values of *each* data array that is used as input/output of an auto-vectorized arithmetic instruction across the auto-vectorized loops in an application), (ii) execute the application to completion, (iii) post-process the output file containing the loop information data to calculate the required bit-precision.

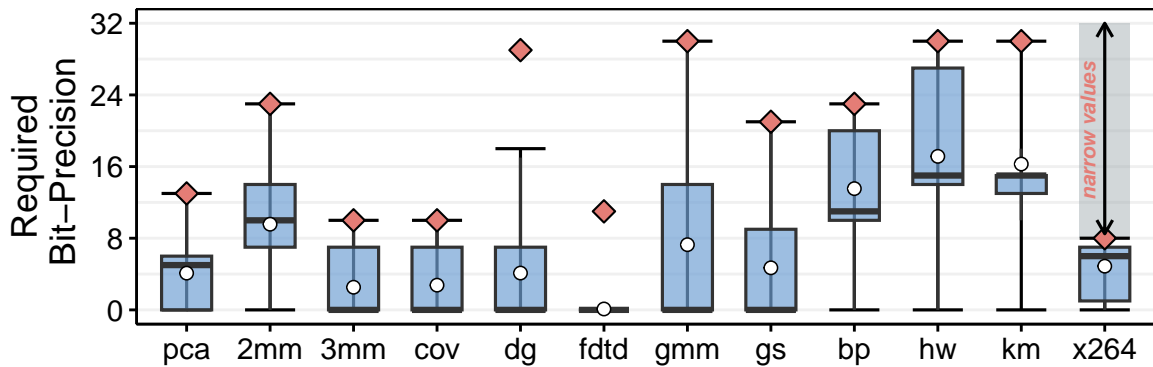


Figure 6.1: Required bit-precision distribution for input/output data arrays of auto-vectorized arithmetic instructions in loops across 12 applications. The box represents the 25th to 75th percentiles, with whiskers extending to the smallest/largest precision (with a diamond at the largest precision and a bubble at the mean precision).

We make two observations. First, all our real-world applications display a *significant* amount of narrow values. In such applications, the input bit-precision can be reduced from the native 32-bit to 20-bit (min. of 8-bit, max. of 30-bit) on average across *all* applications. By doing so, the performance of the underlying PUD architecture can improve by 1.6 \times , in case the application utilizes linearly-scaling PUD operations (such as addition [378]), or 2.6 \times , in case the application utilizes quadratically-scaling PUD operations (such as multiplication [378]). Second, the bit-precision significantly varies across data arrays within a given application. This indicates the need for a mechanism that can *dynamically* identify the target bit-precision for a given PUD operation (similar to prior works that leverage narrow values for tasks other than PUD [460–467, 1283, 1284, 1298, 1299]). As prior work points out [464], static compiler analyses *cannot* identify the bit-precision of dynamically allocated and initialized data arrays. We investigated several prior compiler works [1289, 1300–1303] that perform bit-width identification. However, such works are limited to identifying the bit-precision of statically-allocated variables.

¹For example, if the input operand is an integer storing the value ‘2’, the required bit-precision for such an input operand would be 3 bits (two bits to represent the data value and one bit to represent the sign).

Limitation 2: Throughput-Oriented Execution. Existing PUD architectures favor throughput-oriented execution as DRAM parallelism can partially hide the activation latency in a μ Program. To further improve throughput, prior works [378, 383, 893] use DRAM’s bank-level parallelism (BLP) to (i) distribute independent μ Programs across DRAM banks [378], or (ii) parallelize data writing and PUD computation of *different* μ Programs targeting *different* banks [383]. However, such approaches cannot reduce the latency of a *single* μ Program.

Opportunity 2: DRAM Parallelism for Latency-Oriented Execution. We make the *key observation* that several primitives in a μ Program (i.e., AAP/AP primitives that execute in-DRAM row copy or in-DRAM MAJ3/NOT operations) can be executed concurrently, as they are independent of one another. Figure 6.2 shows this opportunity for a two-bit addition. In conventional bit-serial execution (Figure 6.2a), *all* bits of the input arrays A and B are placed in a *single* DRAM subarray. Because of that, *all* in-DRAM primitives in a μ Program are *serialized*, enabling the execution of only a single bit-position at a time. In our example, (i) DRAM cycles ①–③ execute MAJ3/NOT operations over the *least-significant bits* (LSBs) of the input arrays A and B , i.e., A_0 and B_0 ; and afterwards (ii) DRAM cycles ④–⑥ execute MAJ3/NOT operations over the *most-significant bits* (MSBs) of the input arrays A and B , i.e., A_1 and B_1 .² However, the only *inter-bit* dependency in the μ Program is the *carry propagation* (Ⓢ in Figure 6.2a). In contrast, we can leverage *bit-level parallelism* to *concurrently* execute bit-independent in-DRAM primitives *across multiple* DRAM subarrays. In our example, we can reduce the overall latency of the bit-serial PUD addition operation by (i) *distributing* the individual bits of data-elements from arrays A and B across two DRAM subarrays (i.e., $subarray_0 \leftarrow \{A_0, B_0\}$; $subarray_1 \leftarrow \{A_1, B_1\}$), (ii) executing the required in-DRAM row copies (not shown) and MAJ3/NOT operations for the LSBs (DRAM cycles ①–③ in Figure 6.2b) and MSBs (DRAM cycles ②–④ in Figure 6.2b) *concurrently*, and (iii) serializing *only* the carry generated from the LSBs to the MSBs of the input arrays (Ⓢ in Figure 6.2b).

Besides reducing the latency of bit-serial PUD operations, carefully distributing individual bit positions across different DRAM subarrays within a DRAM bank enables the efficient realization of latency-friendly *bit-parallel* PUD arithmetic operations. By mapping each bit position of a data element to a distinct subarray, our PUD substrate can *concurrently* perform bitwise operations across all bits of the operand, thereby fully exploiting the parallelism inherent to bit-parallel arithmetic algorithms.

Limitation 3: High-Precision Computation. PUD suffers from high latency for high bit-precision operations. For example, even when employing multiple (i.e., 16) parallel DRAM banks, SIMDRAM’s throughput for 32-bit and 64-bit division is $0.8\times$ and $0.5\times$ that of a 16-core

²For simplicity, we do *not* depict DRAM cycles that perform in-DRAM row copy operations in Figure 6.2.

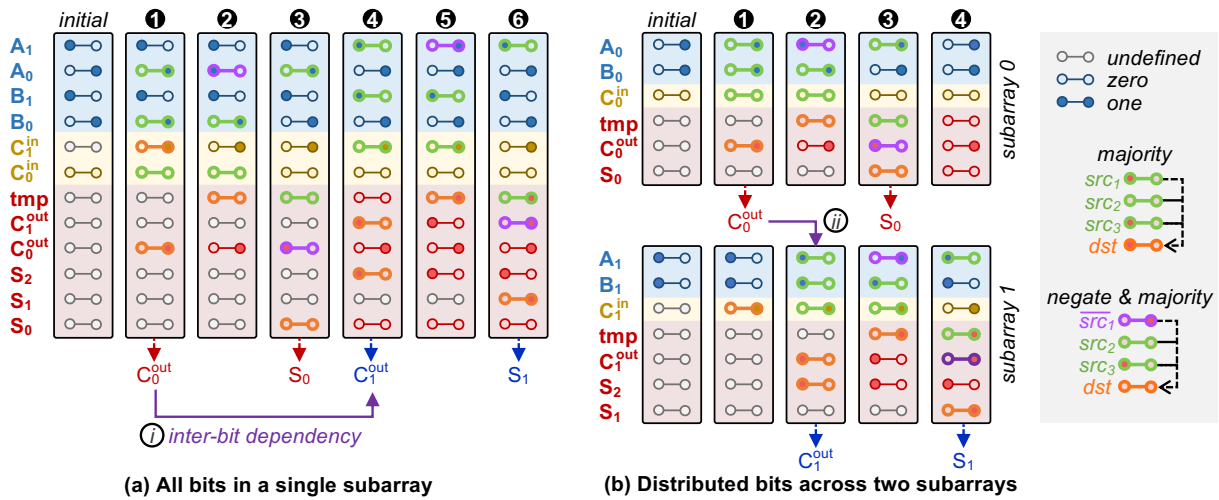


Figure 6.2: Simplified bit-serial PUD addition of two input arrays A and B , each of which with two-bit data elements using (a) one and (b) two DRAM subarrays.

CPU system [378]. This is because the latency of bit-serial multiplication and division scales *quadratically* with the bit-precision.

Opportunity 3: Alternative Data Representation for High-Precision Computation.

The high latency associated with high-precision computation is an *inherent* property of coupling the binary numeral system with bit-serial computation. We investigate an alternative data representation, i.e. the *redundant binary representation (RBR)* [468–472], for high-precision computation. redundant binary representation (RBR) is a positional number system where each bit-position i , which encodes 2^i , is represented by two bits that can take on a value $v \in \{-1, 0, 1\}$, such that the magnitude of bit-position i is $v \times 2^i$. For example, the 4-bit-position number $\langle 0, 1, 0, -1 \rangle$ represents $2^2 - 2^0 = 3$. PUD execution can take advantage of two key properties of RBR-based arithmetic: (i) the operations no longer need to propagate carry bits through the full width of the data (e.g., RBR-based addition limits carry propagation to *at most* two places [473]), and (ii) the operation latency is *independent* of the bit-precision.

Goal. Our *goal* in this work is to mitigate the three limitations of PUD architectures that arise due to the naive use of a bit-serial execution model. To do so, we aim to *fully* exploit the opportunities that DRAM’s internal parallelism and dynamic bit-precision can provide to reduce the latency and energy of PUD operations. Concretely, we aim to enable (i) adaptive data-representation formats (two’s complement and RBR) for PUD operands and (ii) flexible execution of different arithmetic algorithm implementations (bit-serial and bit-parallel) for PUD instructions.

Model Logic comprises of *Pre-Loaded Cost Model lookup tables (LUTs)*, which list the most-suitable μ Program for each bit-precision, and *Select Logic* to identify the target LUT for a *bbop* instruction. We *empirically* measure the throughput and energy efficiency of μ Programs in *Parallelism-Aware μ Program Library* while scaling the target bit-precision to populate the *Pre-Loaded Cost Model LUTs*.

Dynamic Bit-Precision Engine (§6.3.3). *Proteus' Dynamic Bit-Precision Engine* (Ⓐ in Figure 6.3) aims to identify the dynamic range of *memory objects* associated with a PUD operation. To do so, we dynamically identify (in hardware) the *largest* input operand a PUD's memory object stores. In state-of-the-art PUD architectures [323, 344, 345, 378, 383], cache lines belonging to a PUD's memory object need to be transposed from the traditional horizontal data layout to a vertical data layout *prior* to the execution of a PUD operation. To efficiently perform such data transformation, SIMDRAM [378] implements a *Data Transposition Unit*, which hides the data transposition latency by overlapping cache line evictions and data layout transformation. The *Data Transposition Unit* consists of an *Object Tracker* table (a small cache that keeps track of memory objects that are used by PUD operations) and *Data Transposition Engines*. The user/compiler informs the *Object Tracker* of PUD's memory objects (both inputs and outputs) using a specialized instruction called *bbop_trsp_init*. *Proteus* leverages such a *Data Transposition Unit* to dynamically identify in hardware the largest value in a PUD's memory object by adding: (i) a *new field* in the *Data Transposition Unit* called *maximum value*, which stores the largest value in a given memory object; and (ii) a *Dynamic Bit-Precision Engine*, which scans the data elements of evicted cache lines, identifies the largest data value across all data elements and updates the stored *maximum value* entry in the *Data Transposition Unit*.

μ Program Select Unit (§6.3.4). *Proteus' μ Program Select Unit* (Ⓑ in Figure 6.3) identifies the appropriate bit-precision for a PUD operation based on the operation's input data. The *μ Program Select Unit* has of a (i) *Bit-Precision Calculator Unit*, which evaluates the target bit-precision based on the input operands of the PUD operation and their associated maximum values, and (ii) buffers to store the selected μ Program.

6.2.2 Execution Flow

Proteus works in five main steps. In the first step (Ⓐ in Figure 6.3), the programmer/compiler utilizes specialized instructions (i.e., *bbop_trsp_init*) to (i) register in the *Object Tracker* the address, size, and initial bit-precision for each memory object used as an input, output, or temporary operand in a PUD operation; and (ii) execute a PUD operation over previously-registered memory objects. When issuing an arithmetic *bbop* instruction, the programmer/-compiler indicates whether or not dynamic bit-precision is enabled or disabled for that *bbop*

instruction. When dynamic bit-precision is disabled, *Proteus*' *Dynamic Bit-Precision Engine* is turned off, and the μ *Program Select Unit* utilizes the user-provided bit-precision for the upcoming PUD operation related to the issued *bbop* instruction. In the second step, if the *Dynamic Bit-Precision Engine* is enabled, it intercepts evicted cache lines belonging to previously registered memory objects (❷) and identifies the largest value stored in the cache line. If the identified value is *larger than* the current maximum value stored in the *Object Tracker*, the *Dynamic Bit-Precision Engine* updates the *Object Tracker* with the up-to-date value (❸). The second step is repeated for all cache lines belonging to the memory objects registered in the *Object Tracker*. As in SIMDRAM [378], our system employs lazy allocation and maintains data coherence for PUD memory objects through cache line flushing, using the *clflush* instruction [1255]. Thus, all memory objects initially reside within the CPU caches, and prior to PUD execution, all cache lines belonging to a PUD operation are evicted to DRAM, which allows *Proteus*' *Dynamic Bit-Precision Engine* to access *all* data elements of a PUD operation prior to computation.³ In the third step, the host CPU dispatches the arithmetic *bbop* instruction (❹) to *Proteus*' Control Unit. In the fourth step, *Proteus*' Control Unit receives the *bbop* instruction from the CPU and the maximum values from the *Dynamic Bit-Precision Engine* (❺), which are used as inputs to the μ *Program Select Unit*. Based on this information, the *Bit-Precision Calculator Unit* computes the target bit-precision and probes the *Parallelism-Aware μ Program Library* (❻), which returns the best-performing μ Program and data format representation for the target PUD operation and its associated bit-precision. In the fifth step, the μ *Program Select Unit* dispatches the sequence of AAPs/APs in the selected μ Program to DRAM (❼). When the host CPU reads back PUD memory objects (not shown in the figure), *Proteus* (i) performs the necessary data format conversions either from the reduced bit-precision to the user's specified bit-precision or from RBR to two's complement (thus maintaining system compatibility), and (ii) prepares the *Dynamic Bit-Precision Engine* for future accesses by resetting the current maximum data value stored in the *Object Tracker*.

6.3 *Proteus* Implementation

6.3.1 Subarray Organization

To efficiently perform PUD operations, *Proteus* uses a subarray organization that incorporates additional functionality to perform (i) in-DRAM logic primitives (i.e., AAPs/APs), (ii) inter-subarray data copy, and (iii) subarray-level parallelism (SALP) [161]. Figure 6.4 illustrates the

³Some real-world PNM architectures [6, 239, 241, 242, 392, 474] employ a similar execution model, where *all* inputs need to be copied to PNM cores *prior* to PNM execution.

internal organization of a subarray in *Proteus*, which is replicated across *all* subarrays in a *Proteus*-enabled DRAM bank.

Performing Logic Primitives with Ambit. *Proteus* reuses the subarray organization of Ambit [314] and SIMDRAM [378] (shown in Figure 6.4) to enable logic primitive execution with only small subarray modifications. DRAM rows are divided into three groups: (i) the **Data** group (D-group), containing regular rows that store program data; (ii) the **Control** group (C-group), containing two rows pre-initialized with all-‘0’ and all-‘1’ values; and (ii) the **Bitwise** group (B-group), containing six rows (called *compute rows*) to perform bitwise operations. The B-group rows are all connected to a special row decoder that can simultaneously activate three rows when performing an AP and two when performing an AAP (❶ in Figure 6.4).

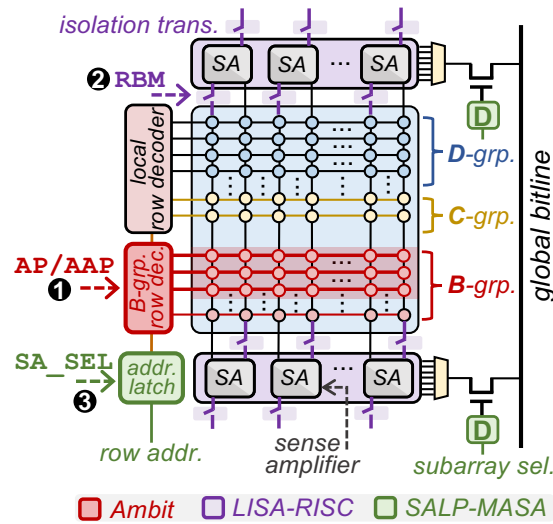


Figure 6.4: *Proteus*' subarray organization.

Inter-Subarray Data Copy with LISA. *Proteus* leverages LISA-RISC [377], which dynamically connects adjacent subarrays using isolation transistors, to propagate intermediate data across subarrays. LISA-RISC works in four steps: (i) activate the source row in the source subarray (latency: t_{RAS}); (ii) use the LISA row *buffer movement* command (RBM, ❷ in Figure 6.4) to turn on isolation transistors, which copies data from the source subarray's local row buffer (LRB) to the destination subarray's LRB (latency: t_{RBM} , 5 ns [377]); (iii) activate the destination row, to save the contents of the destination LRB into the destination row (latency: t_{RAS}); and (iv) precharge the bank (latency: t_{RP}). Due to DRAM's open bitline architecture [491,492], each LRB stores half of the row, so we must perform steps (ii)–(iv) twice to copy both halves of the row.

Enabling Subarray-Level Parallelism with SALP. To enable the concurrent execution of bit-independent primitives in a μ Program, *Proteus* leverages SALP [161]. SALP-MASA (*Multitude of Activated Subarrays*) allows multiple subarrays in a bank to be activated con-

currently by (i) pushing the global row-address latch to individual subarrays, (ii) adding a designated-bit latch (**D** in Figure 6.4) to each subarray to ensure that only a single subarray's row buffer is connected to the global bitline, and (iii) routing a new global wire (called *subarray select*), controlled by a new DRAM command (SA_SEL, **3** in Figure 6.4), allowing the memory controller to set/clear each designated-bit latch.

6.3.2 Parallelism-Aware μ Program Library

One-Bit Per-Subarray (OBPS) Data Mapping

To reduce the latency of PUD operations (§6.1), *Proteus* employs a specialized data mapping called *one-bit per-subarray* (OBPS). Bit-serial PUD architectures can employ three data mappings, as Figure 6.5 illustrates: (i) all-bits in one-subarray (ABOS), (ii) all-bits per-subarray (APBS), and (iii) OBPS. Assume an example DRAM bank with four subarrays, a DRAM row size of three and an input array A with six two-bit data elements.

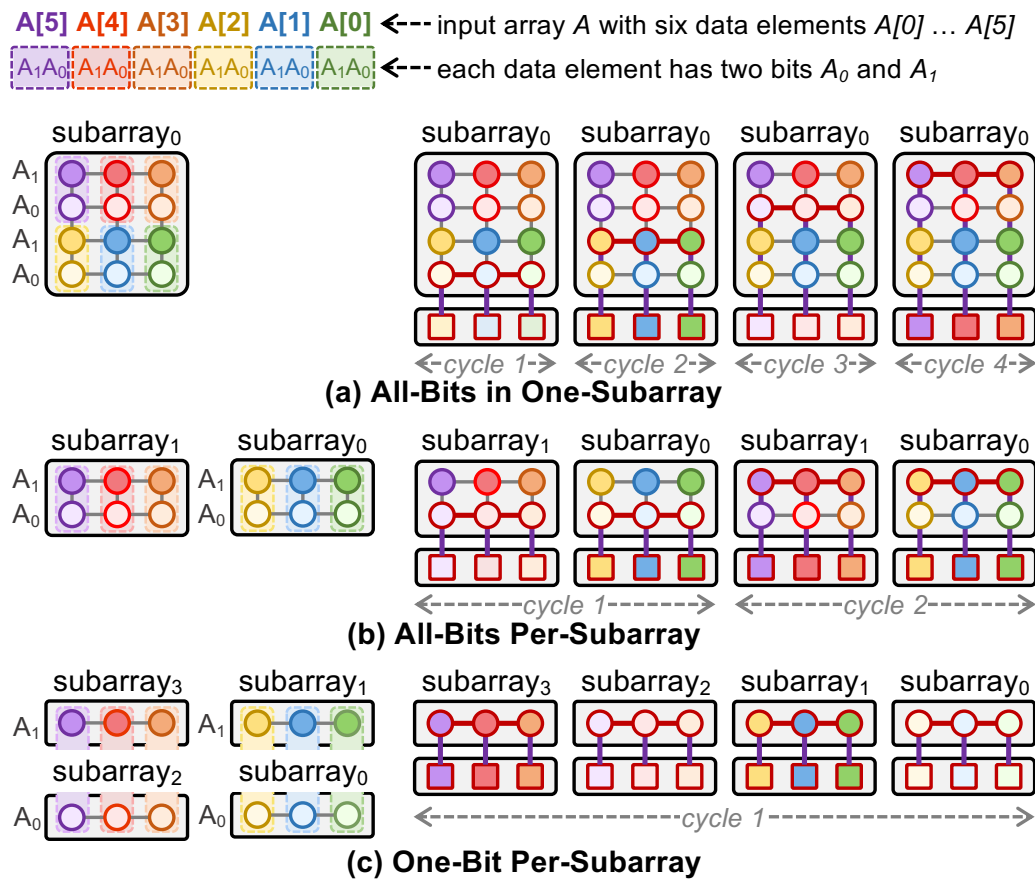


Figure 6.5: Three data mappings for bit-serial computing.

First, the ABOS data mapping stores *all* six two-bit data elements in *one* DRAM subarray (Figure 6.5a). This data mapping limits the parallelism available for PUD execution to that of a *single* DRAM subarray, i.e., the number of DRAM columns simultaneously activated by a

single PUD primitive (e.g., 65,536 DRAM columns per cycle in DDR4 memory chips [1304]). In our example, the latency of executing a single PUD primitive over *all* data elements of the input array A is four PUD cycles (as shown in Figure 6.5a).⁴ Second, the APBS data mapping distributes *all* bits of multiple sets of the input array across *multiple* DRAM subarrays (Figure 6.5b), allowing a PUD primitive to execute concurrently on different portions of the input data stored in each subarray by exploiting *data-level parallelism*. In our example, the latency of executing a single PUD primitive over *all* data elements of the input array A while employing the APBS data mapping is two PUD cycles (as shown in Figure 6.5b). This is because, although execution across data elements can be parallelized by distributing them across multiple DRAM subarrays, the PUD system must still serialize the execution of PUD primitives across different bit positions of each data element, since *all bits of a given data element* are co-located within a single DRAM subarray under APBS. Third, the OBPS data mapping distributes each of the m individual bits of a given data element of the input array to m DRAM subarrays (Figure 6.5c), i.e., $subarray_0 \leftarrow \{A_0\}, \dots, subarray_{m-1} \leftarrow \{A_{m-1}\}$, allowing a PUD primitive to execute concurrently on different bits of the input array stored in each subarray by exploiting *bit-level parallelism*.⁵ In our example, the latency of executing a single PUD primitive over *all* data elements of the input array A while employing the OBPS data mapping is *only* a single PUD cycle (as shown in Figure 6.5c).

μProgram Library Implementation

Proteus leverages the subarray organization illustrated in Figure 6.4 and our OBPS data mapping (Figure 6.5) to implement parallelism-aware μPrograms for key arithmetic operations (e.g., addition, multiplication). We implement three classes of algorithms for arithmetic PUD computations: *bit-serial*, *bit-parallel*, and *RBR-based algorithms*. In *Proteus*, each μProgram implementation (i) has an associated *μProgram_addr*, and (ii) is stored in a reserved memory space in DRAM (i.e., *μProgram Memory*).

Bit-Serial Algorithms. We optimize μPrograms for bit-serial arithmetic operations (i.e., addition, subtraction, division, and multiplication) by concurrently executing independent AAPs/APs across different DRAM subarrays. Figure 6.2b illustrates such a process for addition using the OBPS data mapping (the process is analogous for other arithmetic operations). *Proteus* implements a ripple-carry adder using majority gates in two main steps. First, *Proteus* utilizes SALP-MASA to concurrently execute the appropriate row copies and majority operations across N different subarrays. Second, *Proteus* utilizes LISA-RISC to pipeline the carry propagation process (⑦ in Figure 6.2b) from $subarray_i$ (e.g., C_{out}^0) to $subarray_{i+1}$ (e.g., C_{in}^1). This

⁴We refer to a *PUD cycle* as the end-to-end latency required to execute a single AAP/AP in-DRAM primitive.

⁵If the number of subarrays is smaller than the target bit-precision, OBPS *evenly* distributes the bits of input operands across the available subarrays.

process repeats for all N bits in the input operand. *Proteus* reduces the latency of executing an N -bit bit-serial addition from $8N + 1$ AAP/AP cycles [378] to $2N + 7$ AAP/AP cycles + $2(N - 1)$ RBM cycles.⁶

Bit-Parallel Algorithms. We implement bit-parallel variants of our μ Programs that leverage *carry-lookahead logic* to decouple the calculation of the carry bits and arithmetic logic (e.g., addition). Carry-lookahead logic can identify if any arithmetic on a bit will *generate* a carry (e.g., both operands bits are ‘1’ for an addition), or if it will *propagate* the carry value (e.g., only one operand bit for an addition is a ‘1’). For N -bit operands, this reduces time complexity compared to ripple-carry logic from $\mathcal{O}(N)$ to $\mathcal{O}(\log N)$, where N is the number of bits in the input operands. We implement several carry-lookahead algorithms in *Proteus*, including the carry-select [1306], Kogge–Stone [1307], Ladner–Fischer [1308], and Brent–Kung [1309] adders, as building blocks to implement subtraction, multiplication, and division. Figure 6.6a shows an example *Proteus* implementation of a Kogge–Stone adder.

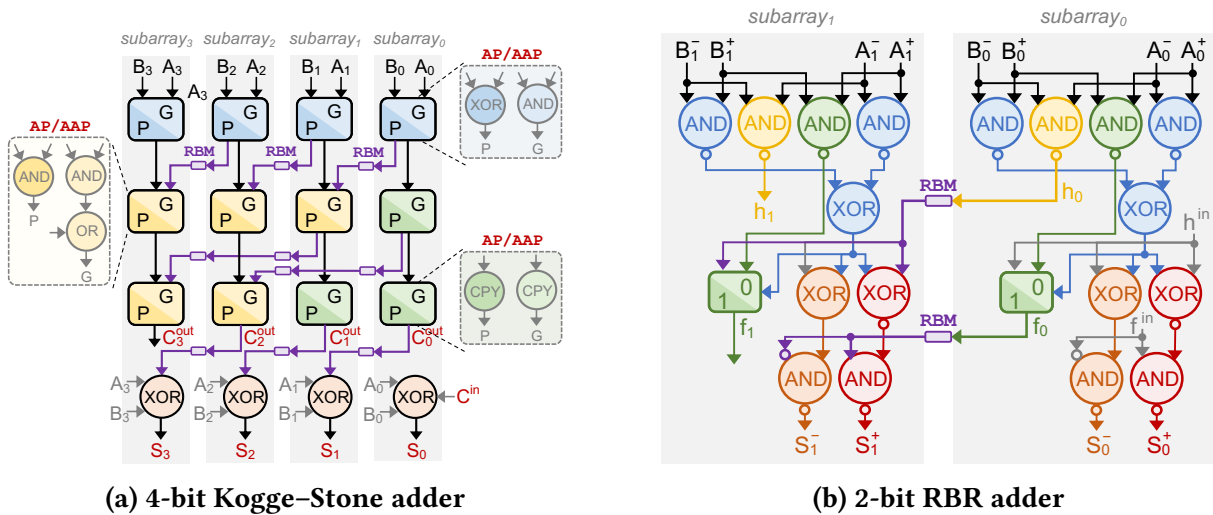


Figure 6.6: *Proteus*’ implementation of different adders. Bits A_i and B_i are stored *vertically* in the same DRAM bitline of subarray i using the OBPS data mapping.

In the first step, *Proteus* performs $2N + 4$ inter-subarray data copies (using LISA-RISC) to copy the *generate* and *propagate* bits from $subarray_i$ to $subarray_{i+1}$. In the second step, *Proteus* performs a series of Boolean operations (using AAPs/APs) to compute the next generate and propagate bits in parallel (using SALP-MASA) across *all* DRAM subarrays. These two steps repeat for $\log(N)$ iterations. The latency of executing an N -bit bit-parallel addition using *Proteus* is $3\log_2 N + 13$ AAP/AP cycles + $2N + 4$ RBM cycles. Even though the bit-parallel algorithms have a lower time complexity than the bit-serial algorithms, the former can require more inter-

⁶To compute the number of AAP/AP and RBM cycles in a μ Program, we implement each μ Program’s algorithm using our cycle-level data-accurate simulator (see §7.4; open sourced at [1305]). We verified the correctness of a μ Program by testing it against several randomly generated data set combinations.

subarray copies, i.e., $2N + 4$ RBM cycles for bit-parallel algorithms versus $2(N - 1)$ RBM cycles for bit-serial algorithms.

RBR-Based Algorithms. Figure 6.6b illustrates *Proteus*' implementation of a two-bit RBR-based adder [1310]. The adder operates in three steps. First, each digit i generates an intermediate value h_i , computed *only* from the corresponding input digit i . Second, the output value f_i at digit i is computed as a function of both the current digit and the preceding intermediate value h_{i-1} . Third, the *sum* at digit i depends on the current digit, h_{i-1} , and f_{i-1} . To propagate intermediate results between digits, *Proteus* uses RBM commands to transfer the values of h_i and f_i from *subarray_i* to *subarray_{i+1}*. The RBR-based addition executes with a constant latency of 34 AAPs/APs cycles and 8 RBM cycles. Beyond addition, *Proteus* reuses the same RBR-based adder design to support additional arithmetic operations, including subtraction and multiplication in the RBR format.

Cost Model Logic Implementation

Figure 6.7 depicts the hardware design of the *Cost Model Logic*. The *Cost Model Logic* has two main components: (i) one LUT per PUD operation, and (ii) *Select Logic*. Each LUT row represents a different bit-precision, and stores the index of the best-performing μ Program in the library for that operation–precision combination. We *empirically* sized each LUT to contain 64 eight-bit rows (i.e., supporting up to 64-bit computation, and indexing up to 64 different μ Program implementations per PUD operation). The *Cost Model Logic* works in four main CPU cycles. It receives as input the *bit-precision* (6 bits) and the *bbop_op* opcode (4 bits) of the target PUD operation. In the first cycle, the *bit-precision* indexes all the LUTs in parallel (❶ in Figure 6.7), selecting the best-performing μ Program_ *id* for the given bit-precision for all implemented PUD operations (❷). The *Cost Model Logic* can *quickly* query the LUTs since they consist of a few (i.e., 16) small (i.e., 64 B in size) SRAM arrays indexed in parallel. In the second cycle, based on the 4-bit *bbop_op* opcode, the *Select Logic* chooses the appropriate μ Program_ *id* (❸). In the third cycle, the μ Program_ *id* is concatenated with the *bbop_op* opcode to form the μ Program_ *addr* (❹). In the fourth cycle, the μ Program_ *addr* indexes and fetches the best-performing μ Program from the *μProgram Scratchpad* (❺). If the target μ Program is not loaded in the *μProgram Scratchpad*, the *Cost Model Logic* fetches it from the *μProgram Memory* (not shown). We estimate, using CACTI [1266], that the access latency and energy per access of the 64 B SRAM array (used in our *Cost Model Logic*) is of 0.07 ns (i.e., less than 1 CPU cycle) and 0.000 04 nJ.

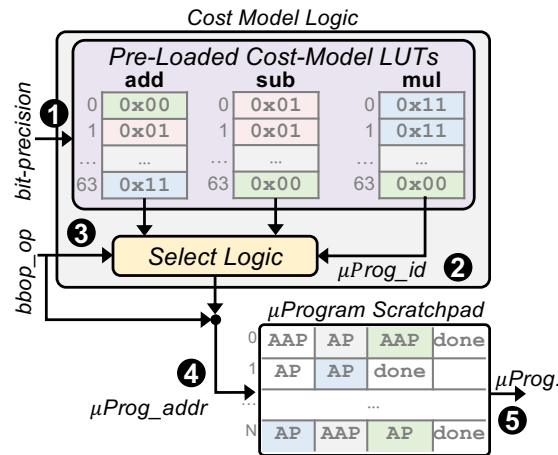


Figure 6.7: Proteus' Cost Model Logic.

Pareto Analysis

We conduct a performance and energy Pareto analysis to populate the *Pre-Loaded Cost Model LUTs*. We model each μ Program using an analytical cost model that takes as input the target bit-precision, the number of elements used during computation, and the number of DRAM subarrays available. The analytical cost model outputs the throughput (in GOPs/s) and energy efficiency (in throughput/Watt) for each μ Program in the *Parallelism-Aware μ Program Library*. We highlight our analyses for two main operations (i.e., addition and multiplication) since they represent linearly and quadratically-scaling PUD operations, respectively. The analyses for subtraction and division follow similar observations. In our analyses, we evaluate a SIMD-DRAM-like PUD architecture using the three data mapping schemes described in Figure 6.5. We assume a DRAM bank with 64 PUD-capable DRAM subarrays and a subarray with 65,536 columns. We vary the number of input elements as multiples of the number of DRAM columns per subarray (from 1 DRAM subarray with 64K input elements to 64 DRAM subarrays with 4M input elements) for our measurements.

Linearly-Scaling PUD Operations. Figure 6.8 shows the throughput (y -axis; top) and energy efficiency (y -axis; bottom) of six μ Program implementations for a linearly-scaling PUD operation (i.e., integer addition) for different bit-precision values (x -axis). Each subplot depicts the different input data sizes we use in our analysis. For this analysis, we implement the following addition algorithms: ripple-carry adder (RCA), carry-select adder (CSA) [1306], Brent-Kung adder [1309], Kogge–Stone adder [1307], Ladner-Fischer adder [1308], using (i) both two's complement and RBR data format representations; and (ii) ABOS, APBS, and OBPS data mappings. Note that the bit-parallel adder can *only* be implemented using the OBPS data mappings. We make two observations. First, in terms of throughput, the best-performing adder implementation varies depending on the target bit-precision and number of input elements. The

achievable throughput ultimately depends on a combination of the number of AAPs/APs that can be concurrently executed across DRAM subarrays and the number of inter-DRAM subarray operations required to implement the adder. In general, we empirically observe that as the input data size increases (see subplots' titles), the number of inter-DRAM subarray operations also increases and eventually dominates the overall execution time. For *small bit-precision* and *small input size* (i.e., bit-precision smaller than 8, and fewer than 256K input elements), the bit-serial RCA using the OBPS data mapping provides the highest throughput, while for *large bit-precision* and *small input size* (i.e., bit-precision larger than 8, and fewer than 256K input elements), the RBR adder using the OBPS data mapping provides the highest throughput. For large-enough input sizes (i.e., more than 1M input elements), employing the APBS data mapping leads to the highest throughput, independent of the bit-precision. This is because when more DRAM subarrays are involved in the execution of the target PUD operation, the inter-subarray data transfers dominate overall execution time in the OBPS implementations. Second, in terms of energy efficiency, the bit-serial implementation of RCA provides the best throughput/Watt for ABOS, APBS, and OBPS, independent of the bit-precision and input size. This is because (i) the number of AAPs/APs performed to execute RCA is the same *independent* of the data mapping, and (ii) the energy the bit-parallel algorithms consume is dominated by inter-subarray operations, which is *not* present in bit-serial implementations.

Quadratically-Scaling PUD Operations. Figure 6.9 shows the throughput (top) and energy efficiency (bottom) of six μ Program implementations for a quadratically-scaling PUD operation (i.e., integer multiplication). We implement PUD multiplication operations as a triplet composed of (i) the multiplication method (i.e., Booth's multiplication algorithm [2] or the divide-and-conquer Karatsuba [3] multiplication); (ii) different methods for addition (i.e., bit-serial RCA, bit-parallel Ladner-Fischer [1308], and RBR-based adder); and (iii) data mappings (i.e., ABOS, APBS, and OBPS). Note that PUD multiplication operations that use bit-parallel and RBR-based adders can *only* be implemented using the OBPS data mapping. We make two observations. First, in terms of throughput, the best-performing multiplier implementation varies depending on the bit-precision and number of input elements. For small bit-precision and small input size (i.e., bit-precision smaller than 8, and fewer than 64K input elements), Booth's bit-serial multiplication with ABOS data mapping provides the highest throughput, while for medium bit-precision and small input size (i.e., bit-precision from 8 to 16 and fewer than 64K input elements), Booth's bit-parallel multiplication with the OBPS data mapping provides the highest throughput. For high bit-precision and small-to-medium input size (i.e., bit-precision larger than 32 and fewer than 256K input elements), RBR-based multiplication using OBPS data mapping provides the highest throughput. For large-enough input sizes (i.e.,

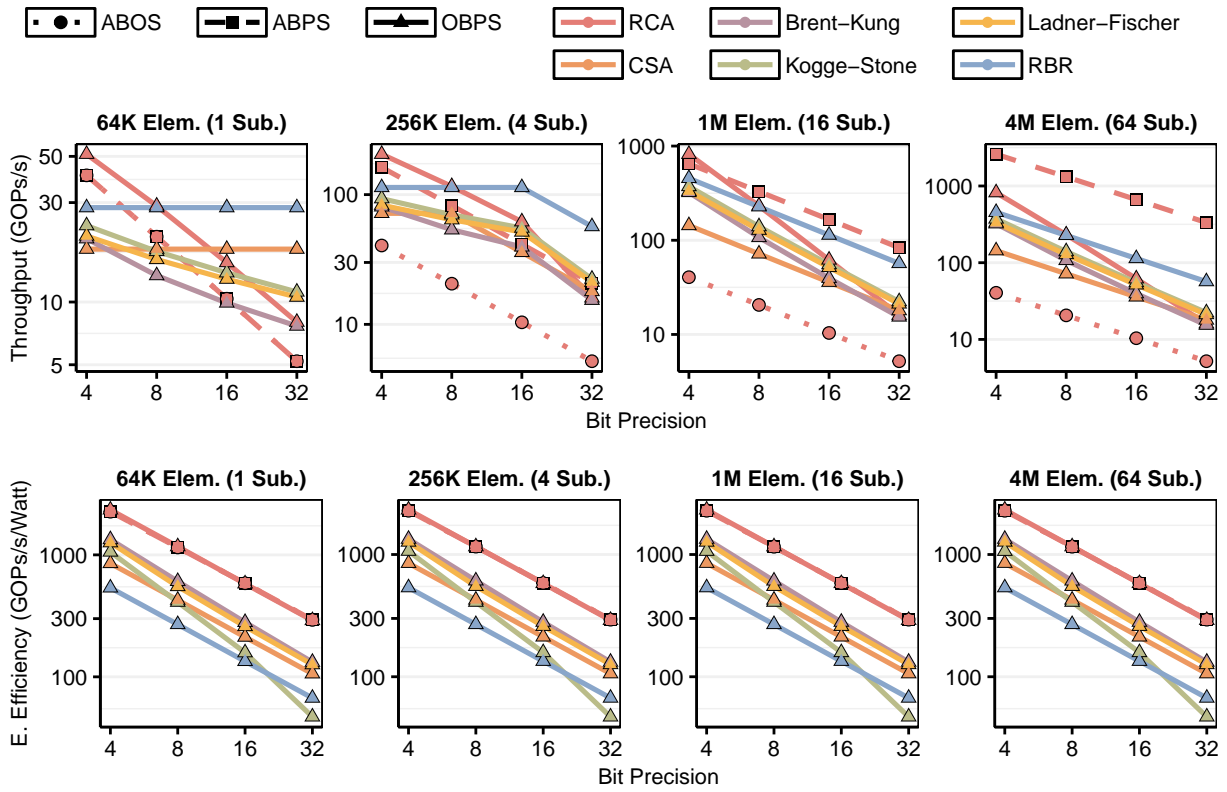


Figure 6.8: Pareto analysis for throughput (top) and energy efficiency (bottom) for PUD addition operations. Dotted lines represent ABOS; dashed lines represent APBS; straight lines represent OBPS data mapping.

larger than 1M input elements), employing Booth’s bit-serial RCA-based multiplication using APBS data mapping leads to the highest throughput, independent of the bit-precision. Second, in terms of energy efficiency, Booth’s bit-serial RCA-based multiplication implementation provides the best throughput/Watt for ABOS, APBS, and OBPS, independent of the bit-precision and input size, since (i) the number of AAPs/APs required to execute the addition step is the same regardless of the data mapping and (ii) the energy of the bit-parallel-based algorithms is dominated by the large number of inter-subarray operations they require.

Non-Arithmetic PUD Operations.

We also equip *Proteus’ Parallelism-Aware μ Program Library* with SIMDGRAM’s implementations of non-arithmetic PUD operations [378], including (i) N -bit logic operations (i.e., AND/OR/XOR of more than two input bits), (ii) relational operations (i.e., equality/inequality check, greater than, maximum, minimum), (iii) predication, and (iv) bitcount and ReLU [1311].

6.3.3 Dynamic Bit-Precision Engine

The *Dynamic Bit-Precision Engine* comprises a simple reconfigurable n -bit comparator and a finite state machine (FSM). For each evicted cache line, the FSM probes the *Object Tracker*

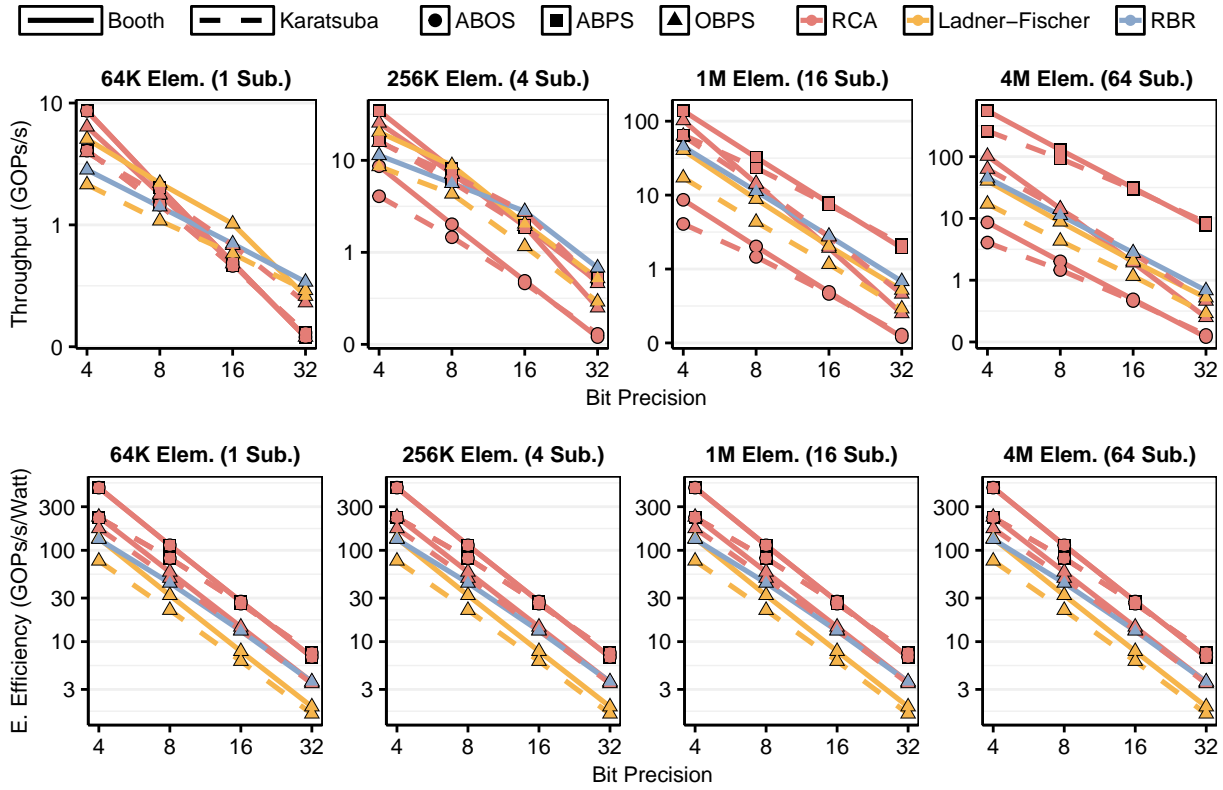


Figure 6.9: Pareto analysis for throughput (top) and energy efficiency (bottom) for multiplication. Straight lines represent the Booth’s multiplication method [2]; dashed lines represent the Karatsuba [3] multiplication method.

and identifies if the incoming evicted cache line belongs to a PUD’s memory object. If it does, the FSM executes four operations. First, it reads the bit-precision value (specified by the `bbop_trsp_init` instruction) and the current maximum value stored in the *Object Tracker* for the given memory object. Second, it uses the bit-precision value to configure the n -bit comparator. Third, it inputs to the n -bit comparator all n -bit values in the incoming cache line (one at a time) and the current maximum value. Fourth, after all the n -bit values are processed, if any value in the incoming cache line is larger than the current maximum value, the FSM sends an update signal to the *Object Tracker* alongside the new maximum value. The energy cost of identifying the largest element in a 64 B cache line is 0.0016 nJ [1312]. That represents an increase in 0.084% in the energy of an LLC eviction [150, 1109, 1131], which *needs* to happen prior to PUD execution regardless.

6.3.4 μ Program Select Unit

Calculating Bit-Precision. The *μ Program Select Unit* needs to address two scenarios when calculating the bit-precision for PUD operations: *vector-to-vector* PUD operations, and *vector-to-scalar* reduction PUD operations. In *vector-to-vector*, the target PUD operation implements a parallel *map* operation, in which inputs and outputs are data vectors. For such opera-

tions, the bit-precision can be computed *a priori*, using the maximum values the *Dynamic Bit-Precision Engine* provides, even in the presence of chains of PUD operations. In such a case, the *Bit-Precision Calculation Engine* updates the *Object Tracker* with the maximum possible output value for *each* PUD in the chain. For example, assume a kernel that executes $D[i] = (A[i] + B[i]) \times C[i]$ as follows:

```
bbop_add(tmp, A, B, 8k, 8, 1); // tmp ← A + B
bbop_mul(D, tmp, C, 8k, 8, 1); // D ← tmp × C
```

Assume that the maximum value of A, B, and C are 3, 6, and 2, respectively. In this case, the *μProgram Select Unit* (i) computes the bit-precision for the addition operation as $\lceil \log_2(3 + 6) \rceil = 4$ bits; (ii) updates the *Object Tracker* entry of tmp with the maximum value of the addition operation (i.e., 9); (iii) computes the bit-precision for the multiplication operation as $\lceil \log_2(9 \times 2) \rceil = 5$ bits using an *n*-bit scalar ALU; (iv) updates the *Object Tracker* entry of D with the maximum value of the multiplication (i.e., 18).

In *vector-to-scalar* reduction, the PUD operation implements a parallel *reduction* operation, where the inputs are vectors and the output is a scalar value. In this case, the bit-precision *cannot* be computed with *only* the maximum input operands without causing *overprovisioning*, since in a reduction, each element contributes to the bit-precision of the scalar output. Therefore, for *vector-to-scalar* reduction PUD operations, the *μProgram Select Unit* needs to (i) fetch from DRAM the row containing the carry-out bits produced during partial steps⁷ of the PUD reduction; (ii) evaluate if a partial step generated an overflow (i.e., check if any carry-out bit is '1'); and (iii) increment the bit-precision for the next partial step if overflow is detected.

Hardware Design. The *μProgram Select Unit* comprises of simple hardware units: (i) an *n*-bit ALU to compute the target bit-precision, (ii) a *Fetch Unit* to generate load instructions for carry re-evaluation, and (iii) a *μProgram Buffer* to store the currently running *μProgram*.

6.3.5 Other Considerations

Data Format Conversion. To distribute the bits of input operands to different DRAM subarrays, *Proteus* issues RBM commands from the DRAM row storing bit *i* in the source DRAM subarray to the target DRAM row in the destination DRAM subarray *i*, i.e., $row[dst]_{subarray_i} \leftarrow RBM(row[src]_i; i \in [1, bits])$. To convert the data stored in two's complement to its equivalent RBR (see §6.1), *Proteus* performs in-DRAM bitwise operations, as Table 6.1 describes.

System Integration. *Proteus* leverages the *same* system integration solutions as in prior PUD systems [378, 893], including: (i) ISA extensions included to the host CPU ISA that the programmer utilizes to launch *bbop* instructions; (ii) a hardware control unit, alongside the

⁷*Proteus* implements PUD reduction operations using *reduction trees* [893]. Thus, a partial step refers to a level of the reduction tree.

Table 6.1: Conversion from two's complement to RBR.

Input X → two's complement →	2 0 0 1 0	-1 1 1 1 1	-7 1 0 0 1
Steps to convert two's to RBR ↓	Output ↓		
Extract most-significant bit (MSB)	0	1	1
buffer1: broadcast MSB to all subarrays	0 0 0 0	1 1 1 1	1 1 1 1
buffer2: NOT(buffer1)	1 1 1 1	0 0 0 0	0 0 0 0
X + 1	1 1 1 0	0 0 0 1	0 1 1 1
X- = buffer1 & (X + 1)	0 0 0 0	0 0 0 1	0 1 1 1
X+ = buffer2 & (X)	0 0 1 0	0 0 0 0	0 0 0 0

memory controller, to control the execution of μ Programs; and (iii) a hardware transposition unit, placed between the LLC and the memory controller, to transpose data from the native horizontal data layout to the PUD-friendly vertical data layout.

Limitation of SALP. SALP is limited by the t_{FAW} DRAM timing constant [510, 1313, 1314], which corresponds to the time window during which at most four ACT commands can be issued per DRAM rank. This constraint protects against the deterioration of the DRAM reference voltage. DRAM manufacturers have been able to relax t_{FAW} substantially in commodity DRAM chips [1315], as well as to perform a targeted reduction of this parameter specifically for PIM architectures where it becomes a performance bottleneck [284, 435]. These advances suggest that t_{FAW} likely does *not* limit *Proteus*' scalability in commodity DRAM chips.

Proteus for Floating-Point Operations. *Proteus*' dynamic bit-precision computation can be employed in two different stages of floating-point arithmetic for PUD operations, during exponent and mantissa computation, using three steps. First, the *Dynamic Bit-Precision Engine* identifies the sign, exponent, and mantissa bits in floating-point numbers stored in the evicted cache lines of PUD memory objects. Second, the *Dynamic Bit-Precision Engine* updates the *Object Tracker* with the maximum exponent and the mantissa values for the PUD memory object, in case the identified maximum values are smaller than the values stored in the current evicted cache line. This process is analogous to the execution flow described in §6.2.2 for integer operands, with the addition of the fields for the maximum exponent and maximum mantissa values in the *Object Tracker*. Third, *Proteus* performs the target in-memory floating-point computation by issuing [326] (i) bit-serial subtraction (addition) PUD operations to calculate the resulting exponents, followed by (ii) bit-serial addition (multiplication) PUD operations to calculate the resulting mantissas for a vector addition (multiplication) instruction [326]. Note that the bit-serial PUD operations involved in (i)–(ii) are vector-to-vector PUD operations. As such, *Proteus* can leverage the maximum exponent and mantissa values stored in the *Ob-*

ject *Tracker* to set the required bit-precision for such bit-serial operations, following the same approach described in §6.3.4.

6.4 Methodology

We implement *Proteus* using an in-house cycle-level simulator (which we open-source at [1305]) and compare it to a real multicore CPU (Intel Comet Lake [458]), a real high-end GPU (NVIDIA A100 using CUDA and tensor cores [459]), and a simulated state-of-the-art PUD framework (SIMDRAM [378]). In our evaluations, the CPU code uses AVX-512 instructions [1263]. Our simulator is rigorously validated against SIMDRAM [378] and MIMDRAM [893]’s gem5 [1262] implementation [1316]. The simulator (i) is cycle-level accurate with regard to DRAM commands and (ii) accounts for the data movement cost of cache line eviction on a per-cycle basis. Our simulation accounts for the additional latency imposed by SALP [161] on ACT commands, i.e., the extra circuitry required to support SALP incurs an extra latency of 0.028 ns to an ACT [557], which is less than 0.11% extra latency of an AAP. To verify the functional correctness of our applications, our simulation infrastructure performs functional verification over application’s data when performing PUD operations. We did *not* observe any difference from the golden outputs. We open-source our simulation infrastructure at <https://github.com/CMU-SAFARI/Proteus>.

Table 6.2 shows the system parameters we use in our evaluations. To measure CPU energy consumption, we use Intel RAPL [1264]. We capture GPU kernel execution time that excludes data initialization/transfer time. We use the nvml API [1265] to measure GPU energy consumption. We use CACTI 7.0 [1266] to evaluate *Proteus* and SIMDRAM energy consumption, where we take into account that each additional simultaneous row activation increases energy consumption by 22% [314, 378]. We evaluate two SIMDRAM configurations: (i) SIMDRAM with SALP [161] and static bit-precision (*SIMDRAM-SP*), and (ii) SIMDRAM with SALP and *Proteus*’ *Dynamic Bit-Precision Engine* (*SIMDRAM-DP*). In both configurations, the system implements only the 16 μ Programs proposed in SIMDRAM (i.e., there is *no Parallelism-Aware μ Program Library* enabled). We evaluate four *Proteus* configurations: (i) *Proteus LT-SP* and (ii) *Proteus EN-SP*, where *Proteus* selects the *lowest latency* (LT) and *lowest energy* (EN) consuming μ Program, respectively, using the statically profiled bit-precision from Figure 6.1; (iii) *Proteus LT-DP* and (iv) *Proteus EN-DP*, where *Proteus* executes the *lowest latency* and *lowest energy* consuming μ Program with dynamically chosen bit-precision. We use 64 subarrays in *only one* DRAM bank for our PUD evaluations.⁸

Real-World Applications. We select twelve workloads from four popular benchmark suites

⁸The column/address (C/A) bus allows the simultaneously activation of up to 84 DRAM subarrays ($\frac{t_{RAS}}{t_{CK}} = \frac{32 \text{ ns}}{0.38 \text{ ns}} = 84$).

Table 6.2: Evaluated system configurations.

Intel Comet Lake CPU [1317] (Real System)	x86 [1255], 16 cores, 8-wide, out-of-order, 3.8 GHz; <i>L1 Data + Inst. Private Cache</i> : 256 kB, 8-way, 64 B line; <i>L2 Private Cache</i> : 2 MB, 4-way, 64 B line; <i>L3 Shared Cache</i> : 16 MB, 16-way, 64 B line; <i>Main Memory</i> : 64 GB DDR4-2133, 4 channels, 4 ranks
NVIDIA A100 GPU [459] (Real System)	7 nm technology node; 826 mm ² die area [459]; 6912 CUDA cores; 432 tensor cores, 108 streaming multiprocessors, 1.4 GHz base clock; <i>L2 Cache</i> : 40 MB L2 Cache; <i>Main Memory</i> : 40 GB HBM2 [424, 425]
SIMDRAM [378] & Proteus (Simulated)	gem5-based in-house simulator [1305, 1316]; x86 [1255]; 1 out-of-order core @ 4 GHz (<i>only</i> for instruction offloading); <i>L1 Data + Inst. Cache</i> : 32 kB, 8-way, 64 B line; <i>L2 Cache</i> : 256 kB, 4-way, 64 B line; <i>Memory Controller</i> : 8 kB row size, FR-FCFS [649, 1194] <i>Main Memory</i> : DDR5-5200 [511], 1 channel, 1 rank, 16 banks

in our real-workload analysis (as Table 6.3 describes). We manually modified each workload to (i) identify loops that can benefit from PUD computation, i.e., loops that are memory-bound and that can leverage SIMD parallelism and (ii) use the appropriate *bbop* instructions. To identify loops that can leverage SIMD parallelism, we use the MIMDRAM compiler [1316] for identification and generation of PUD instructions, which uses LLVM’s loop auto-vectorization engine [1238–1241] as a profiling tool that outputs SIMD-safe loops in an application. We use the clang compiler [1238] to compile each application while enabling the loop auto-vectorization engine and its loop vectorization report (i.e., `-O3 -Rpass-analysis=loop-vectorize -Rpass=loop-vectorize`). We observe that applications with regular and wide data parallelism (e.g., applications operating over large dense vectors) are better suited for SIMD-based PUD systems. We select applications from various domains, including linear algebra and stencil computing (i.e., 2mm, 3mm, doitgen, fdtd-apml, gemm, gramschmidt from Polybench [1268]), machine learning (i.e., pca from Phoenix [4], covariance from Polybench [1268], kmeans and backprop from Rodinia [1142]), and image/video processing (i.e., heartwall from Rodinia [1142] and 525.x264_r from SPEC 2017 [5]). Since our baseline PUD substrate (SIMDRAM) does *not* support floating-point, we manually modify the selected floating-point-heavy PUD-friendly loops to operate on fixed-point data arrays.⁹ We do *not* observe an output quality degradation when employing fixed-point. We use the largest input dataset available for each benchmark.

6.5 Evaluation

6.5.1 Real-World Application Analysis

Performance. Figure 6.10 shows the CPU, GPU, SIMDRAM, and *Proteus* performance for twelve real-world applications. As in prior works [316, 332, 333, 364, 1318], we report area-

⁹We only modify the three applications from Rodinia to use fixed-point, as done by prior works [349, 1269, 1270]. Polybench can be configured to use integers; the PUD-friendly loops in x264 and pca use integers.

Table 6.3: Evaluated applications. We measure peak GPU utilization and total memory footprint on a real system.

Benchmark Suite	Application (Short Name)	Peak GPU Util. (%)	Total Mem. Footprint (GB)	Bit-Precision {min, max}	PUD Instrs. [†]
Phoenix [4]	pca (pca)	–	1.91	{8, 8}	D, S, M, R
Polybench [1268]	2mm (2mm)	98	4.77	{13, 25}	M, R
	3mm (3mm)	100	26.7	{12, 12}	M, R
	covariance (cov)	100	7.63	{23, 23}	D, S, R
	doitgen (dg)	92	33.08	{10, 11}	M, C, R
	fdtd-apml (fdtd)	–	36.01	{11, 13}	D, M, S, A
	gemm (gmm)	98	22.89	{12, 24}	M, R
	gramschmidt (gs)	66	22.89	{12, 13}	M, D, R
Rodinia [1142]	backprop (bp)	–	22.50	{13, 13}	M, R
	heartwall (hw)	48	0.03	{17, 17}	M, R
	kmeans (km)	36	1.23	{17, 17}	S, M, R
SPEC 2017 [5]	525.x264_r (x264)	–	0.15	{1, 8}	A, R

[†] D = division, S = subtraction, M = multiplication, A = addition, R = reduction, C = copy

normalized results (i.e., performance per mm^2) for a fair comparison. We make four observations. First, *Proteus* significantly outperforms all three baseline systems. On average across all twelve applications, *Proteus LT-DP* (*Proteus EN-DP*) achieves $17\times$ ($11.2\times$), $7.3\times$ ($4.8\times$), and $10.2\times$ ($6.8\times$) the performance per mm^2 of the CPU, GPU, and SIMDRAM, respectively. Second, we observe that equipping SIMDRAM with *Proteus' Dynamic Bit-Precision Engine* to leverage narrow values for PUD execution significantly improves overall performance. On average, *SIMDRAM-DP* provides $6.3\times$ the performance per mm^2 of *SIMDRAM-SP*. Third, *Proteus'* ability to adapt the μ Program depending on the target bit-precision further improves overall performance by $1.6\times$ that of *SIMDRAM-DP*. Fourth, *Proteus' Dynamic Bit-Precision Engine* further increases performance by 46%, over *Proteus* with static bit-precision. This happens because for statically profiled bit-precision, we *must* round the bit-precision up to the nearest power-of-two, as high-level programming languages (e.g., C/C++) are *inherently* constrained by the two's complement data representation.

Energy. Figure 6.11 shows the end-to-end energy reduction the GPU, SIMDRAM, and *Proteus* provide compared to the baseline CPU for twelve applications. We make four observations. First, *Proteus* significantly reduces energy consumption compared to all three baseline systems. On average across all twelve applications, *Proteus EN-DP* (*Proteus LT-DP*) provides $90.3\times$ ($27\times$), $21\times$ ($6.3\times$), and $8.1\times$ ($2.5\times$) lower energy consumption than CPU, GPU, and *SIMDRAM-SP*, respectively. Second, enabling *Proteus' Dynamic Bit-Precision Engine* and *Parallelism-Aware μ Program Library* allows *Proteus* to reduce energy consumption by an average of $8\times$ and $1.02\times$ compared to PUD substrates with statically-defined bit-precision (*SIMDRAM-SP*) and bit-serial

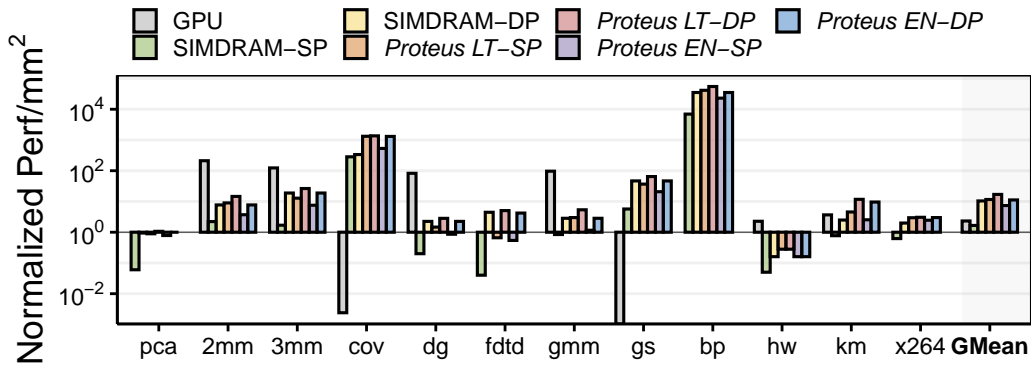


Figure 6.10: CPU-normalized performance per mm^2 for twelve real-world applications. Phoenix [4] and SPEC2017 [5] do not provide GPU implementations of *pca* and *x264*.

only arithmetic (*SIMDRAM-DP*), respectively. Third, compared to *SIMDRAM-DP*, *Proteus LT-DP* increases energy consumption by 3.3 \times , on average. This is because the highest performance implementation of a PUD operation often leads to an increase in the number of AAPs/APs required for PUD computing. In many cases, the energy associated with inter-subarray data copies (employed in RBR and bit-parallel algorithms) leads to an *increase* in energy consumption. Even though the inter-subarray data copy latency can be hidden by leveraging *Proteus*' OBPS data mapping, the extra power the DRAM subsystem requires to perform them impacts overall energy consumption. Fourth, the *Dynamic Bit-Precision Engine* further reduces *Proteus*' energy consumption by 58%, compared to *Proteus* with static bit-precision.

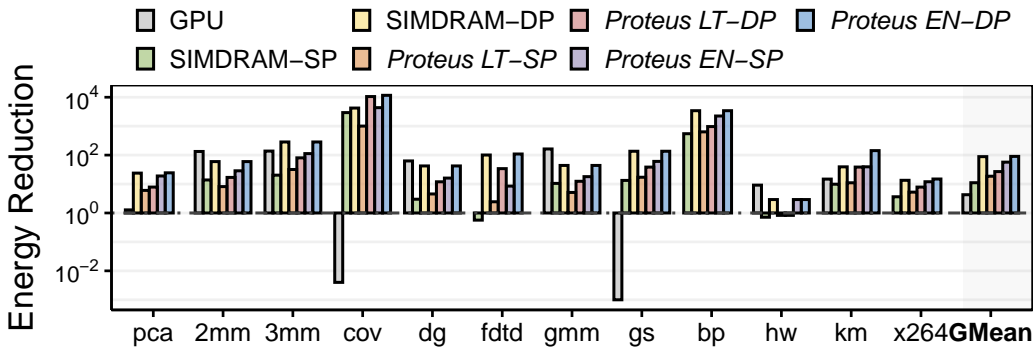


Figure 6.11: End-to-end energy reduction compared to the baseline CPU for twelve applications.

6.5.2 Data Mapping and Representation Format Conversion Overheads

We evaluate the worst-case latency associated with (i) data mapping conversion (from the conventional ABOS data mapping to our OBPS data mapping) and (ii) data representation format conversion (from ABOS to RBR) that *Proteus* might perform during the execution of a PUD operation. Figure 6.12 shows the worst-case data mapping and representation format

conversion latency overhead for linearly- and quadratically-scaling μ Programs. We make two observations.

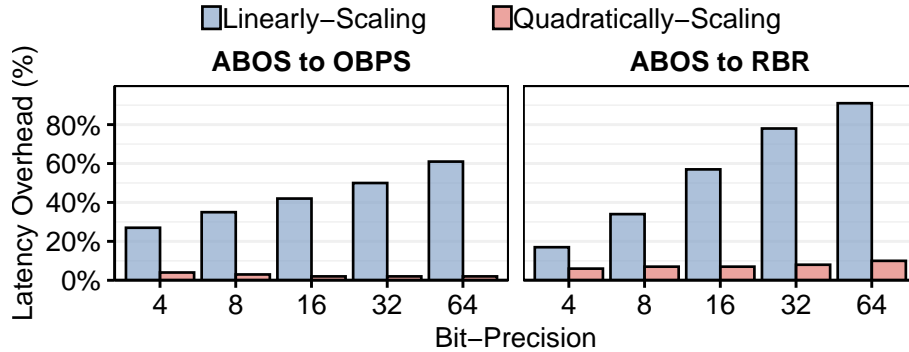


Figure 6.12: Latency overheads of data mapping and representation format conversion.

First, data mapping and representation format conversion can *significantly* impact linearly-scaling μ Programs, causing up to 60% and 91% latency overhead when converting from ABOS to OBPS and from ABOS to RBR, respectively. Second, in contrast, the impact of data mapping and representation format conversion in quadratically-scaling μ Programs is low (i.e., less than 10% latency overhead). This difference is because the number of in-DRAM operations required to perform data mapping and representation format conversion increases *linearly* with the bit-precision (§6.3.5). In most cases, the data mapping and representation format conversion is a one-time overhead that an application pays when executing a series of PUD operations. On average, across our 12 applications, data mapping and representation format conversion accounts for 7.2% of the total execution time.

6.5.3 Performance of Floating-Point Operations

We evaluate *Proteus*' throughput for floating-point arithmetic operations. Since our underlying PUD architecture, i.e., SIMDram, does *not* natively support floating-point operations, we demonstrate how *Proteus* can be leveraged in a different PUD architecture that can be modified to support floating-point data formats, i.e., DRISA [316]. The main limitation of SIMDram when supporting floating-point computation is the lack of interconnects across DRAM columns, which is required for exponent normalization during floating-point addition. Since the DRISA architecture includes a shifting network within a DRAM subarray, it can perform the required exponent normalization. We perform a synthetic throughput analysis of in-DRAM vector addition/subtraction and multiplication/division operations.¹⁰ We use 64M-element input arrays, with randomly initialized single-precision floating-point data. We evaluate two system configurations: (i) DRISA 3T1C [316] architecture, which performs

¹⁰We evaluate synthetic workloads instead of our twelve real-world applications since there is *no* publicly available tool-chain to map real-world applications to the baseline DRISA [316] architecture. A similar approach is followed in [378].

in-situ NOR computation; and (ii) DRISA 3T1C architecture coupled with *Proteus*. We make two observations. First, we observe that the DRISA 3T1C architecture coupled with *Proteus* achieves $1.17\times/1.15\times$ and $1.38\times/1.37\times$ the arithmetic throughput of the baseline DRISA 3T1C for floating-point addition/subtraction and multiplication/division operations, respectively. Second, *Proteus*' throughput gains are more prominent for multiplication/division operations, since it can reduce costly in-memory multiplication/division operations during mantissa computation by leveraging narrow mantissa values. We conclude that *Proteus*' key ideas apply to different underlying in-DRAM processing techniques and data types.

6.5.4 *Proteus* vs. Tensor Cores in GPUs

We compare the performance and energy efficiency of our real-world applications that perform general matrix-matrix multiplication (GEMM) operations while running on the tensor cores in the NVIDIA A100 GPU and *Proteus* for narrow data precision input operands (i.e. 4-bit and 8-bit integers). To do so, we (i) identify the subset of our real-world applications that mainly perform GEMM operations and therefore are suitable for the A100's tensor core engines; and (ii) re-implement such workloads using optimized instructions (from NVIDIA's CUTLASS [1319]) to perform tensor GEMM operations on the A100 GPU tensor cores. Re-implementing the GPU workloads is necessary since GPU tensor core instructions are *not* automatically produced via the standard CUDA code our workloads use and there is *no* reference implementation available from the original benchmark suites targeting tensor core GPUs. We employ A100's all 432 tensor cores during GPU execution.

Figure 6.13 shows the tensor cores, SIMD RAM, and *Proteus* performance per mm^2 (Figure 6.13, top) and energy efficiency (i.e., performance per Watt in Figure 6.13, bottom) for three GEMM-heavy real-world applications using 8-bit (int8) and 4-bit (int4) data types. Values are normalized to those obtained on real GPU tensor cores. We make two observations. First, *Proteus* significantly improves performance per mm^2 and energy efficiency compared to both tensor cores and SIMD RAM across all applications and data types. On average across the three applications, *Proteus* provides (i) $20\times/43\times$ and $8\times/21\times$ the performance per mm^2 and (ii) $484\times/767\times$ and $9.8\times/25\times$ the performance per Watt of the tensor cores and SIMD RAM, respectively, using int8/int4 data types. *Proteus* and SIMD RAM are capable of outperforming the tensor cores of the A100 GPU for narrow data precisions since both the throughput and the energy efficiency of bit-serial PUD architectures *increase* quadratically for multiplication operations as the bit-precision *decreases* [378]. Second, we observe that by employing dynamic bit-precision and adaptive arithmetic computation, *Proteus* further improves the performance and energy gains that SIMD RAM provides compared to the A100 GPU's tensor cores, even

improving performance compared to the tensor cores in cases where SIMD RAM fails to do so (i.e., for gmm).

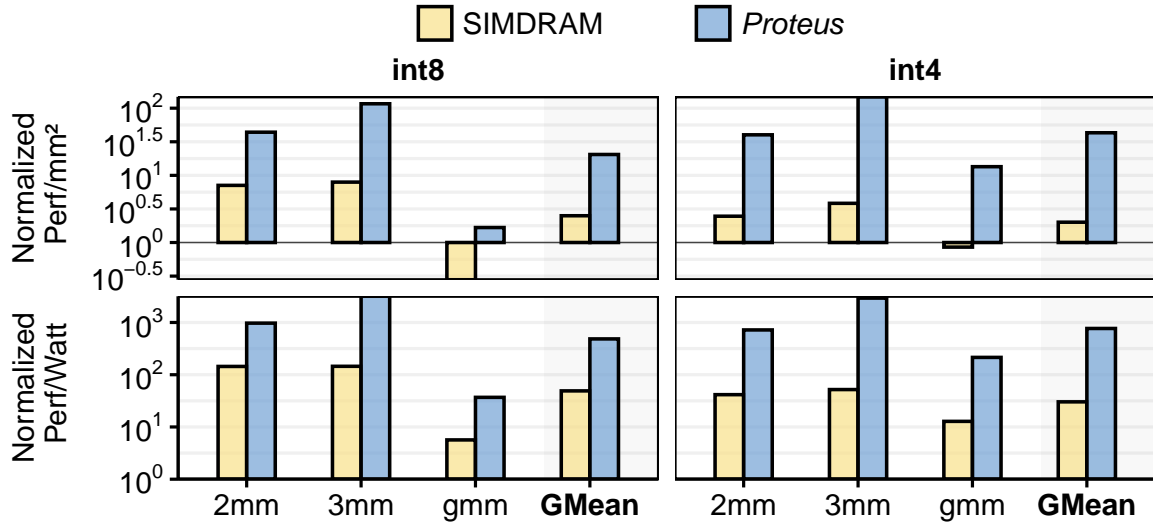


Figure 6.13: Performance per mm² (top) and performance per Watt (bottom) of GEMM-intensive real-world applications using int8 and int4, normalized to the same metric measured on 432 NVIDIA A100 tensor cores.

6.5.5 Area Analysis

DRAM Chip Area and Storage Overhead. We use CACTI 7.0 [1266] to evaluate the area overhead of the primary components in the *Proteus* design using a 22 nm technology node. *Proteus* does *not* introduce any modifications to the DRAM array circuitry other than those proposed by (i) Ambit, which has an area overhead of <1% in a commodity DRAM chip [314]; (ii) LISA, which has an area overhead of 0.6% in a commodity DRAM chip [377]; and (iii) SALP, which has an area overhead of 0.15% in a commodity DRAM chip [161]. We reserve less than 1 DRAM row (i.e., 6.25 kB in an 8 GB) to store our implemented μ Programs. In total, we implement 50 μ Programs, each of which takes 128 B of DRAM space.

CPU Area Overhead. We size the *Parallelism-Aware μ Program Library* to contain: (i) 16 64 B LUTs, each LUT holding a 8-bit μ Program_{id}; (ii) one 2 kB μ Program Scratchpad Memory. The size of the *Parallelism-Aware μ Program Library* is enough to hold one LUT per SIMD RAM PUD operations and address 2⁸ different μ Program implementations. The size of the μ Program Scratchpad is large enough to store the μ Programs for all 16 SIMD RAM operations. We use a 128 B scratchpad for the *Dynamic Bit-Precision Engine*. Using CACTI, we estimate that the *Proteus Control Unit* area is 0.03 mm². *Proteus' Data Transposition Unit* (one per DRAM channel) uses an 8 kB fully-associative cache with a 128-bit cache line size for the *Object Tracker*, and two 4 kB transposition buffers. Using CACTI, we estimate the *Data Transposition Unit* area

is 0.06 mm^2 . Considering the area of the control and transposition units, *Proteus* has an area overhead of only 0.03% compared to the die area of an Intel Xeon E5-2697 v3 CPU [326].

6.6 Summary

We introduce *Proteus*, an efficient PUD framework with adaptive data precision and dynamic arithmetic. *Proteus* fully leverages the internal parallelism inside a DRAM bank to accelerate the execution of various bit-serial and bit-parallel arithmetic operations and dynamically decides the best-performing bit-precision, data representation format, and algorithmic implementation of a PUD operation. We experimentally demonstrate that *Proteus* provides significant benefits over state-of-the-art CPU, GPU, and PUD systems.

Chapter 7

DaPPA: A Data-Parallel Programming Framework for Processing-in-Memory Architectures

7.1 Motivation & Goal

Programming general-purpose PNM systems (such as the UPMEM PIM system [474,475,1320]) require the programmer to follow three main steps.

Step 1: Distribute & Transfer Input Data Across DPUs. In the first step, the programmer distributes the input data across the multiple PIM cores in the PIM-enabled memory, and subsequently across the many threads within a single PIM core, by explicitly moving the input data from the host main memory to the PIM-enabled memory (❶ in Figure 2.3). To do so, particularly in the UPMEM PIM system, the programmer makes use of one of the three CPU–DPU data transfer primitives the UPMEM SDK [474] provides, which allow for: (i) *serial* CPU–DPU data transfer, where a *single* portion of data is moved from main memory to a *single* DPU (i.e., one MRAM bank); (ii) *parallel* CPU–DPU data transfer, where *multiple* portions of data from main memory are distributed across *multiple* DPUs (i.e., across many MRAM banks); and (iii) *broadcast* CPU–DPU data transfer, where a *single* portion of data from main memory is moved and replicated across *multiple* DPUs (i.e., multiple MRAM banks).

Step 2: Handle Caching in Local Scratchpad Memory. In the second step, after data is copied to the PIM memory, the PIM cores can start their computations. For a PIM core to process data, the programmer must carefully (and manually) orchestrate internal data movement between local DRAM banks and scratchpad memory, as well as communication and synchronization between PIM cores. In the UPMEM PIM system, the programmer needs to

orchestrate (i) data movement between the DRAM bank (MRAM) and the local scratchpad memory (WRAM) using the DPU engine direct memory access (DMA) (② in Figure 2.3), and (ii) inter-DPU communication & tasklet synchronization. For MRAM–WRAM data movement orchestration, the programmer must respect restrictive memory alignment requirements (i.e., both source addresses in WRAM and MRAM *must* be 8-byte aligned) and set the appropriate transfer size (which can vary from 8 to 2048 bytes). For inter-DPU communication, the programmer needs to identify programming patterns that require data transfers across DPUs (e.g., merging of partial results to obtain a final output) and explicitly perform DPU–CPU and CPU–DPU data transfers (since there is *no* direct communication across DPUs in the PIM-enabled memory) accordingly. For tasklet synchronization, the programmer needs to decide which synchronization primitive (e.g., mutex, handshake, barrier, or semaphore) is the most appropriate for the given task.

Step 3: Consolidating Results. In the third step, once the main kernel finishes its execution within the PIM cores, partial output values will be stored across the many DRAM banks in the PIM-enabled memory. For such output values to be visible to the host application, the programmer needs to perform DPU–CPU data transfers (③ in Figure 2.3), so that data is moved from the PIM-enabled memory to the main memory. After this transfer is complete, the host CPU might still have to perform some post-processing, depending on the target application (e.g., the host CPU might combine the partial results that each DPU produces).

Problem & Goal. Even though the programming model of general-purpose PNM systems resembles that of widely employed architectures, such as GPUs, it requires the programmer to (i) have prior knowledge of the underlying PIM hardware and (ii) manage data movement at a fine-grained granularity *manually*. Concretely, programming a PIM-enabled system requires the programmer to perform (i) efficient workload partitioning across the many PIM cores and PIM threads within the system; (ii) manual transfer of data between standard main memory and PIM banks, while ensuring that both host CPU and PIM cores have access to accurate and up-to-date copies of data; and (iii) orchestrate data movement between PIM banks local scratchpad memory. Such limitations can difficult the adoption of PIM architectures in general-purpose systems. Therefore, our **goal** in this work is to ease programmability for general-purpose PNM systems, allowing a programmer to write efficient PIM-friendly code *without* the need to manage hardware resources *explicitly*.

7.2 DaPPA Overview

To ease the programmability of PIM architectures, we propose DaPPA (data-parallel processing-in-memory architecture), a programming framework that can, for a given appli-

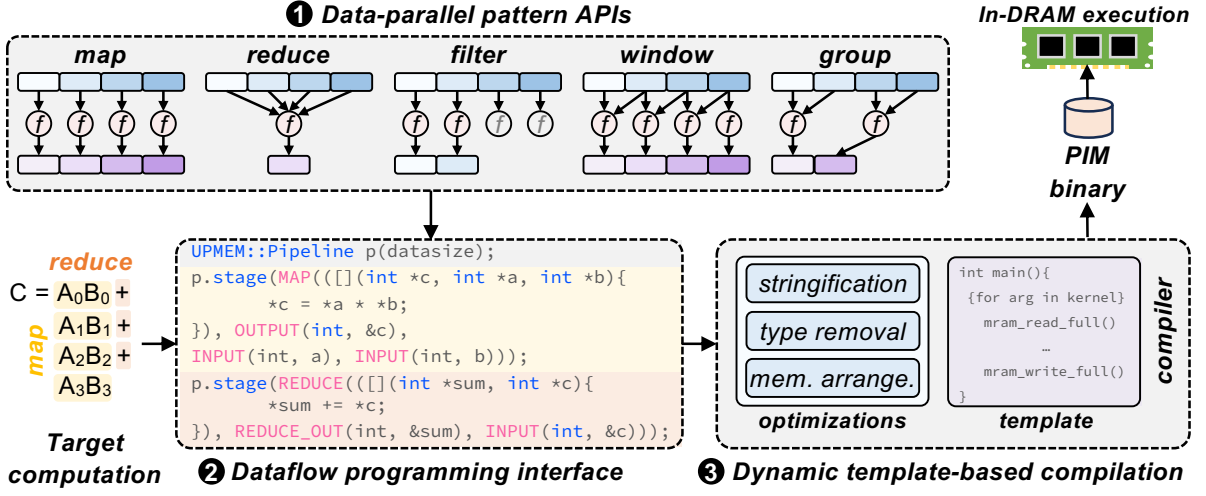


Figure 7.1: Overview of the DaPPA programming framework.

cation, *automatically* distribute input and gather output data, handle memory management, and parallelize work across the PIM cores. The *key idea* behind DaPPA is to remove the responsibility of managing hardware resources from the programmer by providing an intuitive data-parallel pattern-based programming interface [477,478] that abstracts the hardware components of the PNM system. Using this key idea, DaPPA transforms a data-parallel pattern-based application code into the appropriate PIM-target code, including the required APIs for data management and code partition, which can then be compiled into a PIM-based binary *transparently* from the programmer. While generating PIM-target code, DaPPA implements several code optimizations to improve performance.

Figure 7.1 shows an overview of our DaPPA programming framework. DaPPA takes as input C/C++ code, which describes the target computation using a collection of data-parallel patterns and DaPPA’s programming interface, and generates as output the requested computation. DaPPA consists of three main components: (i) DaPPA’s data-parallel pattern APIs, (ii) DaPPA’s dataflow programming interface, and (iii) DaPPA’s dynamic template-based compilation.

Data-Parallel Pattern APIs. DaPPA’s data-parallel pattern APIs (① in Figure 7.1) are a collection of pre-defined functions that implement high-level data-parallel pattern primitives. Each primitive allows the user to express how data is transformed during computation. DaPPA supports five primary data-parallel pattern primitives, including: (i) *map*, which applies a function f to each individual input element i , producing unique output elements $y_i = f(x_i)$; (ii) *reduce*, which reduces input vectors to a scalar; (iii) *filter*, which selects input elements based on a predicate; (iv) *window*, which *maps* and output element as the *reduction* of W *overlapping* input elements; (v) *group*, which *maps* and output element as the *reduction* of G *non-overlapping*

input elements. The user can combine these five data-parallel primitives to describe complex data transformations in an application.

Dataflow Programming Interface. DaPPA exposes a dataflow programming interface to the user (❷ in Figure 7.1). In this programming interface, the main component is the Pipeline class, which represents a sequence of data-parallel patterns that will be executed on the PIM cores. A given Pipeline has one or more stages. Each stage utilizes a given data-parallel pattern primitive to transform input operands following a user-defined computation sequence. Stages are executed in order, in a pipeline fashion.

Dynamic Template-Based Compilation. DaPPA uses a dynamic template-based compilation (❸ in Figure 7.1) to generate the PIM code in two main steps. In the first step, DaPPA creates an initial PIM code based on a skeleton of a PIM application. In the second step, DaPPA uses a series of transformations to (i) extract the required information that will be fed to the PIM code skeleton of the user program; (ii) calculate the appropriate offsets used to manage data across PIM banks and local PIM scratchpad memory; and (iii) divide computation between CPU and PIM cores.

Putting All Together. Using DaPPA’s data-parallel pattern APIs, dataflow programming interface, and dynamic template-based compilation, the user can quickly implement and deploy applications to the PNM system without any knowledge of the underlying architecture. Figure 7.1 showcases an example of implementing a simple vector dot-product application using DaPPA. In this example, the user defines a Pipeline with two stages: a map stage and a reduce stage. DaPPA generates the appropriate binary for the PNM system, executes the target computation on the PIM cores, and copies the final output from the PIM cores to the CPU.

7.3 DaPPA Implementation

7.3.1 Data-Parallel Pattern APIs

DaPPA exposes *data-parallel pattern APIs* that leverages skeleton-based programming and data-parallel patterns to allow users to define their algorithms using high-level abstractions [477, 478, 1321, 1322]. In skeleton-based programming, applications are composed of pre-defined *skeletons* (e.g., map, reduce, pipeline, farm), each encapsulating a common parallel computation pattern. In this way, programmers can focus on application logic rather than low-level concerns such as tasklet management, synchronization, or inter-DPU communication. Data-parallel patterns further enable concurrent execution of the same operation (or sequence of operations) across multiple data elements, thereby reducing boilerplate (i.e., re-

peated) code and errors associated with explicit tasklet or DPU management [1323, 1324]. This separation of *what* (algorithmic intent) from *how* (hardware-specific optimizations) eases code reuse, scalability, and maintainability for CPUs [1325–1327], GPUs [1325, 1326, 1328], special-purpose accelerators [1329], and distributed systems [1326, 1330]. Numerous skeleton-based frameworks (e.g., SkePU [1328], Skandium [1331], and Muesli [1325, 1326, 1332]) as well as libraries supporting data-parallel constructs (e.g., CUDA [1091], OpenCL [1333], Intel Threading Building Blocks [1334], and Apache Spark [1335, 1336]) exemplify the breadth and efficacy of these high-level parallel programming approaches. Therefore, we leverage such a programming paradigm to aid in programmability for general-purpose PNM systems.

Currently, DaPPA supports five primary data-parallel patterns (which Figure 7.1 illustrates), i.e., map, reduce, filter, window, and group. Each data-parallel pattern takes as input one or more one-dimensional (1D) vectors, and produces as output a single 1D vector or a scalar value. Non-vector arguments, such as scalar parameters, can also be supplied as arguments and are broadcast across all PIM cores involved in the computation. DaPPA implements each one of the five data-parallel patterns as follows:

- **map:** the map data-parallel pattern takes as input a 1D vector x of size N , a *pure* function f , and produces as output a 1D vector y of size N , where $y_i = f(x_i)$. A *pure* function consistently produces the same output for a given input (i.e., the pure function produces *deterministic* outputs) and does *not* induce side effects (i.e., the invocation of f does *not* modify any external state, such as global variables, files, or shared memory, and does *not* depend on any non-local state that may vary over time). As a result, no synchronization between PIM threads is required, and data sharing is unnecessary, making the map data-parallel pattern highly suitable for data-parallel execution on PNM architectures. In our implementation of the map data-parallel pattern, each PIM thread *independently* executes an instance of the function f , generating its corresponding output $f(x_i)$.
- **reduce:** The reduce data-parallel pattern takes as input a 1D vector x of size N , a reduction function f , and produces as output a single scalar value r . In its simplest form, the result r is computed by repeatedly applying f over all elements of x , for example: $r = f(x_1, f(x_2, \dots f(x_{N-1}, x_N) \dots))$. For efficient parallelization, f is commonly required to be *associative*, meaning that $f(a, f(b, c)) = f(f(a, b), c)$, for all valid operands a , b , and c . Associativity ensures that partial computations of f (i.e., partial “*reductions*”) can be combined in arbitrary groupings and orders without affecting the final result. In case f is pure *and* associative, the reduce data-parallel pattern allows for intermediate values to be processed in parallel and merged incrementally, reducing the need for extensive synchronization. In our implementation of the reduce data-parallel pattern, the input vector x is equally distributed across PIM cores, and then multiple PIM threads within a PIM core com-

pute partial reductions on each distinct subranges of the input vector. These partial results are then combined (in the host CPU), using the same function f , in a tree-based hierarchy until a single final result r remains. In case f is pure and associative, the order in which PIM threads combine intermediate results does *not* affect correctness, thereby enabling efficient parallel execution.

- **filter:** The filter data-parallel pattern takes as input a 1D vector x of size N and a *pure* predicate function f , and produces as output a new 1D vector y . The predicate f tests each element of x for a condition (returning true or false). The resulting vector y contains exactly those elements of x for which $f(x_i)$ is true, while preserving their original order. Formally, $y = [x_i \mid f(x_i) = \text{true}, 1 \leq i \leq N]$. A *pure* predicate function consistently produces the same result for a given input (i.e., deterministic output) and does *not* induce side effects. Purity ensures that each evaluation of $f(x_i)$ can be performed *independently* and in parallel, without synchronization or data sharing. Once the true/false decisions are computed, the filter data-parallel pattern gathers the qualifying elements to form the final output vector y .
- **window:** the window data-parallel pattern generalizes the map pattern to computations where each output element depends on a contiguous block (or “*window*”) of the input. Specifically, the window data-parallel pattern takes as input: (i) a 1D vector x of size N , (ii) a *window size* W , and (iii) a *pure* function f that operates on sub-vectors of length W . It produces as output a 1D vector y of size M , where M depends on how windows are defined and handled at the boundaries (e.g., M might be $N - W + 1$ if every complete window produces exactly one output). Formally, for each valid index i , $y_i = f(x_i, x_{i+1}, \dots, x_{i+W-1})$. Since f is assumed to be *pure*, each sub-vector (x_i, \dots, x_{i+W-1}) can be processed *independently*. The main distinction from map arises because consecutive outputs in a window may depend on overlapping input segments. Users often provide additional (or padding) elements for the end of the input to ensure that the last positions can form a complete window of size W . This data-parallel pattern is widely used in signal processing, sliding-window algorithms, and stencil computations, and it can be parallelized effectively on general-purpose PNM systems by distributing different sub-vectors to different PIM cores.
- **group:** the group data-parallel pattern partitions a 1D input vector x of size N into contiguous, *non-overlapping* sub-vectors (or “*groups*”) of size G . A *pure* function f is then applied to each sub-vector to produce one output element per group. Formally, assuming N is divisible by G , the vector x is segmented into $\frac{N}{G}$ sub-vectors: $(x_1, \dots, x_G), (x_{G+1}, \dots, x_{2G}), \dots, (x_{N-G+1}, \dots, x_N)$, and each group is independently processed by $y_i = f(x_{(i-1)G+1}, \dots, x_{iG})$ for $i = 1, 2, \dots, \frac{N}{G}$. Unlike the window, whose sub-vectors can overlap, the group data-parallel pattern advances its input index by G ele-

ments each step, thereby ensuring these sub-vectors are disjoint. Purity allows each group to be processed in *isolation*, making the group data-parallel pattern highly amenable to data-parallel execution. In some applications, group can also be viewed as a special case of a reduction over fixed-size chunks: each chunk is “*reduced*” into a single value by the function f , without overlapping the inputs of neighboring chunks.

DaPPA also allows the user to combine some of the five primary data-parallel patterns to implement more complex execution patterns. In our current implementation, DaPPA enables the combination of window, filter, and group data-parallel patterns into four new implementations: window+group, window+filter, group+filter, and window+group+filter. We describe each implementation below:

- **window+group**: the window+group data-parallel pattern combines the window and group data-parallel patterns. Like group, the input vector is divided into contiguous, non-overlapping sub-vectors of size G . However, for each sub-vector, the computation will depend not only on its own G elements but also on up to an additional W elements (forming a “*window*”). Formally, whereas the group data-parallel pattern would compute: $y_n = f(x_{(n-1)G+1}, \dots, x_{nG})$, the window+group data-parallel pattern extends the domain of f to: $y_n = f(x_{(n-1)G+1}, \dots, x_{nG+W})$, with W specifying how far beyond the current group the function may read. This expanded scope is useful for computations where nearby elements (beyond the immediate group boundary) influence the result. As with window and group, the window+group data-parallel pattern assumes a *pure* function f , ensuring that each sub-vector plus its “*window*” can be processed in parallel.
- **window+filter**: the window+filter data-parallel pattern combines the behavior of window (sliding or overlapping sub-vectors) with filter (selecting outputs based on a predicate). Like window, it processes an input vector x in overlapping segments (“*windows*”) of size W . However, rather than producing an output for every window, it applies a *pure* predicate function f to each window and includes that window’s contribution in the output only if f returns true. Formally, for each valid index i , consider the window $w_i = (x_i, x_{i+1}, \dots, x_{i+W-1})$. The pattern outputs w_i if $f(w_i) = \text{true}$, and omits it otherwise. As with both window and filter, the use of a pure predicate function f . This combined pattern is particularly useful when overlapping context is necessary for deciding which segments of the data should be preserved.
- **group+filter**: the group+filter data-parallel pattern partitions an input vector x into contiguous, non-overlapping sub-vectors (“*groups*”) of size G and then applies a *pure* predicate function f to decide whether each group is retained. Formally, for $n = 1, 2, \dots, \frac{N}{G}$, define the n -th group as $g_n = (x_{(n-1)G+1}, \dots, x_{nG})$. The output includes g_n only if $f(g_n) = \text{true}$. This

selective mechanism extends the group data-parallel pattern, maintaining data-parallel independence across groups while filtering out those that do *not* satisfy the predicate.

- **window+group+filter**: the window+group+filter pattern extends the window+group pattern by selectively retaining only those results that satisfy a *pure* predicate. As in window+group, the input vector is divided into contiguous sub-vectors of size G , with each sub-vector allowed to read up to W additional elements beyond its boundary. A *pure* function f then produces an output from each extended sub-vector. Formally, for the n -th sub-vector, we consider $(x_{(n-1)G+1}, \dots, x_{nG+W})$, and compute $y_n = f(x_{(n-1)G+1}, \dots, x_{nG+W})$. A separate *pure* predicate p then determines whether y_n is kept in the output: include y_n if and only if $p(y_n) = \text{true}$. Because f and p are both pure, each sub-vector can be processed independently, preserving the data-parallel benefits of the underlying window+group pattern while allowing for filtering of results.

7.3.2 Dataflow Programming Interface

DaPPA allows the programmer to use the data-parallel pattern APIs to implement a given task or application. To do so, DaPPA exposes to the user a *dataflow programming interface*, which Figure 7.2 illustrates. The *key idea* behind DaPPA’s dataflow programming interface is to allow the programmer to *implicitly* describe the data movement between data-dependent sub-tasks in the target task/application. At a high-level, the *dataflow programming interface* has three main components: (i) a Pipeline (❶ in Figure 7.2), which defines a collection of transformations over the input data; (ii) one or more stages (❷), which composes the Pipeline while each stage represents an unique data-parallel pattern from DaPPA’s data-parallel pattern APIs; (iii) implicit dataflow (❸), where data moves sequentially, in a pipeline-fashion, across each stage.

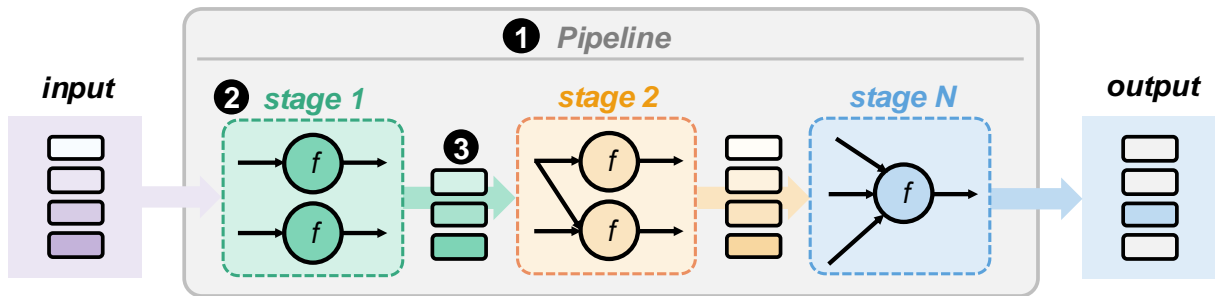


Figure 7.2: DaPPA’s dataflow programming interface.

Concretely, the dataflow programming interface exposes to the programmer one main C++ class, the Pipeline class, which represents a sequence of data-parallel patterns that will be executed on PIM cores. The Pipeline class has a set data vector size to guarantee length compatibility between all inputs, which can only be reduced or divided by filter and group data-

parallel patterns. A given Pipeline has one or more stages, and works in three main steps. First, the input data is transformed within each stage using a *stage-specific function*, based on a given data-parallel pattern, producing an output data. The output produced by a stage i can be used as input data for any subsequent stage $i + 1$. Second, after the user specifies all needed data transformations that the PIM cores will execute across the different stages, they can specify the final output data that will be fetched from the PIM cores to the CPU. Third, the user initiates the execution of the stages specified for a given Pipeline across the PIM cores. Note that, while defining each stage and its equivalent stage-specific function, the user does *not* need to define *any* PIM-specific command, including those related to data orchestration and parallelism distribution. This happens because DaPPA abstracts the underlying hardware characteristics from the user, allowing the programmer to focus only on implementing the functionality of the target application.

The Pipeline Class: Implementation

The primary interface DaPPA exposes to the user is the Pipeline class. We explain the main components of the Pipeline class using a vector dot product example in Listing 7.1. The Pipeline class has five main methods, which we describe next.

Class Constructor. Creates a new Pipeline object that will be used for any subsequent in-memory operations. The class construction takes an integer length as parameter, which determines the length of the input and output vectors that will be processed by the instantiated Pipeline.

```
Pipeline::Pipeline(length);
```

Stage Creation. The stage method adds a new stage to the Pipeline. It takes as input: (i) a macro string `str` that represents the stage data-parallel pattern; (ii) a function pointer `func`, which defines the computation that will be executed by a PIM thread within a PIM core; (iii) a tuple `argsTuple` composed of `<data type, array pointer>`, which lists the input/output vectors for the given stage; (iv) an extra output array output, which is used in case the produced output array needs to be replicated; and (v) the number of elements that will be used for a window (overlap) or a group (`groupSize`). For the tuple `argsTuple`, the user needs to define the *type* (i.e., `ArgTypes`) of each *array pointer*, which can be either an input array, an output array, an array used as *both* input and output, a scalar parameters, a scalar reduction output, or a combination function (used to combine partial results across PIM cores). The stage method returns *true* in case the stage was successfully added to the Pipeline.

Fetch Output from PIM Memory. The fetch method is used to *explicitly* mark an output vector (or scalar value) that needs to be copied from the PIM memory to the CPU main mem-

```

// Map / Window / Group
template<typename... ArgTypes>
bool stage(const std::string &str, std::function<void(ArgTypes*...)> func, std::tuple<ArgTyped
    ↳ <ArgTypes>...> argsTuple, uint32_t overlap, uint32_t groupSize);

// Filter (Input/Output)
template<typename FilterType, typename... ArgTypes>
bool stage(const std::string &str, std::function<bool(FilterType*, ArgTypes*...)> func,
    ↳ ArgTyped<FilterType> output, std::tuple<ArgTyped<FilterType>, ArgTyped<ArgTypes>...>
    ↳ argsTuple, uint32_t overlap, uint32_t groupSize);

// Filter (InOut)
template<typename FilterType, typename... ArgTypes>
bool stage(const std::string &str, std::function<bool(FilterType*, ArgTypes*...)> func,
    ↳ ArgTyped<FilterType> inout, std::tuple<ArgTyped<ArgTypes>...> argsTuple, uint32_t
    ↳ overlap, uint32_t groupSize);

// Reduce
template<typename... ArgTypes>
bool stage(const std::string &str, std::function<void(ArgTypes*...)> func, std::tuple<ArgTyped
    ↳ <ArgTypes>...> argsTuple);

```

ory after the Pipeline is executed. This means that the marked vector will *not* be treated as intermediate data (the default behavior for output vectors and scalar values within Pipeline).

```
Pipeline::fetch(vector);
```

Start PIM Execution. The execute method processes all stages that have been added to the Pipeline, and once each stage finishes its execution, writes all fetched outputs (from PIM memory) to their respective vectors or scalar values (to the CPU main memory).

```
Pipeline::execute();
```

Get Result Length. The getLength method retrieves the resulting length of an output vector after the PIM execution has finished. This is only needed if the Pipeline includes a filter data-parallel pattern, as the resulting length of all other data-parallel patterns can be known or calculated *a priori*.

```
Pipeline::getLength(vector);
```

Implementing a Pipeline

The user follows 5 main steps to implement an application using DaPPA's dataflow programming interface. We reference the simple vector dot-product example in Listing 7.1 to illustrate each step. First, the user needs to allocate the input arrays that will be processed by the Pipeline (line 2–6). DaPPA accepts as input arrays either `std::vectors` or a raw pointer. Second, the user creates a Pipeline object (line 8). This object will be used to construct the

dot-product algorithm. The user needs to specify the length of the input and output data vectors in this step. A key requirement for a given Pipeline is that the vector length should be the same across all stages. In case different vector lengths are required, the user can combine several different-length Pipelines. Third, the user adds the stages to the Pipeline (lines 9–21), where each stage represents a part of dot-product algorithm. Each stage contains the kernel that a PIM thread will execute, and a set of inputs and outputs. In this example, the user uses a map data-parallel pattern to implement a vector multiplication in arrays *a* and *b* (line 10), and a reduce data-parallel pattern to implement a scalar reduction of vector *c* (line 18). An important point is that the user does *not* need to fetch to the CPU memory the vector *c* during the Pipeline execution, since it is used as the intermediate result between the map and reduce stages. As long as an array is *only* used for intermediate data, it does *not* need to be allocated in the host CPU main memory, allowing DaPPA to save host CPU memory space. Fourth, the user marks all of the outputs that need to be fetched from the PIM cores after computation (line 23). As described above, this is done so that DaPPA can avoid fetching intermediate results from PIM cores. Fifth, the user triggers the execution of the Pipeline (line 24). Only at this point DaPPA will allocate PIM cores and run each stage in the Pipeline. After the execution is finished, the fetched result data (i.e., *sum*) can be accessed by the host CPU.

```

1 uint32_t dataLength = 1048576;
2 std::vector<uint32_t> a(dataLength);
3 std::vector<uint32_t> b(dataLength);
4 uint32_t c; // Not fetched, no buffer needed
5 uint32_t sum = 0;
6 // Fill a and b with data here
7
8 Upmem::Pipeline p(dataLength);
9 p.stage(MAP(([] (uint32_t *c, uint32_t *a, uint32_t *b){
10     *c = *a * *b;
11 })),
12     OUTPUT(uint32_t, &c),
13     INPUT(uint32_t, a),
14     INPUT(uint32_t, b));
15
16 // REDUCE_OUT because it's a scalar and not a vector
17 p.stage(REDUCE(([] (uint32_t *sum, uint32_t *c){
18     *sum += *c;
19 })),
20     REDUCE_OUT(uint32_t, &sum),
21     INPUT(uint32_t, &c));
22
23 p.fetch(&sum);
24 p.execute();

```

Listing 7.1: DaPPA’s implementation of a vector dot-product using its dataflow programming interface.

7.3.3 Dynamic Template-Based Compilation

After the user implements the target computation using the data-parallel pattern APIs and the dataflow programming interface, DaPPA generates the appropriate PIM binary using a *dynamic template-based compilation*. To do so, DaPPA uses two main components. First, it makes use of *template-based coding*, where the PIM code is created based on an initial skeleton of a PIM application. Second, DaPPA *dynamically* generates and compiles the target PIM code by applying three key optimizations, i.e., stringification, type removal, and memory arrangement, through four code transformations that (i) extract the required information from the user's implemented Pipeline to feed the PIM code skeleton; (ii) calculate the appropriate offsets used to manage data across PIM banks and local PIM scratchpad memory; and (iii) divide computation between CPU and PIM cores. Figure 7.3 gives an overview of DaPPA's code transformations targeting the UPMEM PIM system. It takes as user input a C++ code (implementing a given Pipeline) and generates as output a UPMEM binary. This process is dynamically repeated per Pipeline.

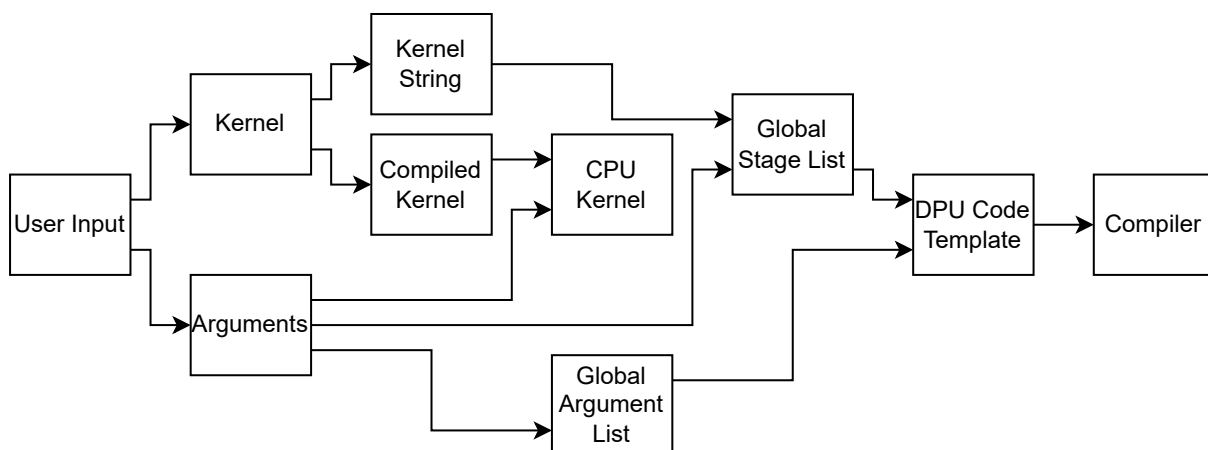


Figure 7.3: DaPPA's template-based compilation flow.

Next, we give an overview of each transformation that DaPPA performs to generate PIM code. In our current implementation, we make use of the Inja [1337] template engine to manage and populate the UPMEM code skeleton.

First Transformation. In the first transformation, DaPPA extracts information regarding the function kernels (i.e., func) specified within stages across a Pipeline, and its associated input/output arguments (stringification). Kernel information is added to a *global stage list*, while input/output arguments are added to a *global argument list*. After this, most of the argument type information is stripped, apart from the type size and its string representation (type removal). In this way, we can reduce the amount of templating required, which reduces overall

complexity and compilation time. Once all stages have been processed and added to the *global state list*, DaPPA moves to the second transformation.

Second Transformation. In the second transformation, DaPPA finalizes some parameter calculations that depends on having a global view of the application, and consequently, complete information about all stages. This includes memory parameters, such as how to arrange the data in MRAM and WRAM (memory arrangement). Thus, the second transformation is crucial to orchestrate data movement in the DPU system. In order to manage MRAM space, the second transformation sets parameters related to MRAM data allocation depending on the stages and their arguments, while respecting the following approach. When the data is copied to the DPUs, DaPPA splits its total size *evenly* across all DPUs while respecting the 8-byte alignment requirement. Within a DPU, DaPPA further divides the data evenly between all tasklets so that they can independently perform their calculations. DaPPA also directly arranges the data in MRAM by calculating offsets from the MRAM base address (see Section 7.3.3). The data for all stages are copied simultaneously before starting the DPU process. If the data does *not* fit in MRAM, DaPPA performs multiple execution rounds until the entire dataset is processed. Any intermediate results that have to propagate through the Pipeline (i.e., outputs of one stage that become input of subsequent stages) also have their dedicated MRAM space.

Likewise, the second transformation also generates the appropriate parameters to manage WRAM using the following approach. Once the DPU starts execution, it needs to first initialize its memory space and set up the WRAM. It then iterates over each stage, in order. Each stage loops over WRAM blocks (i.e., data segments that are small enough to fit into WRAM). In the UPMEM system, the kernel needs to transfer the data from MRAM to the WRAM prior to execution, by passing pointers to the appropriate WRAM location as its arguments. After the computation is finished, it copies the results back to MRAM. Hence, the second transformation sets (i) the required pointers by casting them to the correct type first using the type information present in each stage argument; and (ii) WRAM block index for a given WRAM access.

Third Transformation. In the third transformation, DaPPA deals with the case where the Pipeline data size does *not* respect the 8-byte alignment requirement of the UPMEM system. In this case, DaPPA decides to execute the remaining part of the computation at the CPU. The third transformation is responsible to identify such computation and to generate CPU code to execute it. To do so, DaPPA creates a separate CPU thread that will process some elements on the CPU while the DPU is processing the portion of the data that is 8-byte aligned. The amount of data processed on the CPU can be manually increased so that the CPU does *not* have to idle while the DPUs are processing the data, which can lead to performance improvements.

Fourth Transformation. In the fourth transformation, DaPPA deals with the need of post-

processing required for some stages, in particular these that implement a filter or reduce data-parallel pattern. For a filter, the results of each tasklet have to be compressed to make the data contiguous again. Since parallel data transfers usually achieves higher throughput in the UPMEM system [476], we have to copy the same amount of data from every DPU, even if the number of elements passing the filters of each DPU might differ. This will leave holes in the data, which we must remove in the CPU. Similarly, a reduce also needs further processing by combining the partial results of each DPU in the host CPU.

After the four transformations are performed, all of the parameters and kernels are inserted into the UPMEM code skeleton, and the UPMEM code is compiled.

Managing DPU Memory

In order to manage the DPU memory, DaPPA tries to allocate as much data as possible across the total memory space of the DPUs. In case the data cannot all fit into the combined MRAM of the DPUs, we need to perform multiple execution rounds to process all of the data. For this, we transfer as much data to the DPUs as possible, run the entire Pipeline on that part of the data, and then repeat this process until we have processed all of the data. To this end, DaPPA performs different element count calculations, which we describe next.

Element Count Calculations: General Case. DaPPA must determine how many elements of the input/output vectors, passed as arguments to function kernels, can be processed simultaneously across stages of a Pipeline. We describe how DaPPA handles this process for the general case, i.e., where the target data-parallel patterns lead to *homogeneous* WRAM and MRAM accesses.

1. Calculating WRAM Parameters. We first compute the WRAM cache element count, which defines how many elements a stage's WRAM cache can hold per argument. This count is uniform across all arguments within a stage unless a group data-parallel pattern partitions it. The WRAM cache element count also determines how many function kernel invocations can occur before requiring a data reload. To maximize WRAM utilization, we compute the count per stage, considering its specific number of arguments. The process begins by summing the element type sizes of all arguments in a stage and dividing the total available WRAM space by this sum to obtain a preliminary count. However, since MRAM–WRAM transfers require 8-byte alignment, adjustments are necessary. We iterate over the arguments, computing the total required space, including padding. If the padded size exceeds WRAM capacity, we decrement the element count until alignment constraints are met. Finally, we determine the cache offsets for each argument by sequentially placing them in WRAM.

2. Calculating MRAM Parameters. Next, we determine the maximum number of elements

a DPU can hold in MRAM for the entire Pipeline. Unlike WRAM, where each stage is considered independently, MRAM capacity must accommodate all arguments across all stages simultaneously. The calculation follows the same method as WRAM, adhering to 8-byte alignment constraints but encompassing all arguments rather than a single stage.

3. Calculating Leftover Parameters. Finally, we determine the number of elements processed on the CPU. Due to UPMEM’s 8-byte alignment requirements, some data may not fit into DPUs without violating alignment rules. These excess elements are handled by the CPU. The number of DPU-processed elements follows from the elements-per-round computation: $\text{CPU elements} = \text{total_length} - (\text{elements_per_round} \times \text{nr_rounds})$.

Element Count Calculations: Special Cases. DaPPA accounts for special cases when managing DPU memory, depending on the stage’s target parallel pattern. We describe these cases below.

window Data-Parallel Pattern. The window data-parallel pattern requires overlapping input data between DPUs, as each DPU processes elements while looking ahead at data handled by the next DPU. At the end of the dataset, however, no additional elements remain for lookahead. To address this, one approach is to reduce the output length by the overlap size, but this complicates subsequent stages that rely on a consistent output size and may *not* align with user expectations. Instead, DaPPA allows users to provide a small vector of overlap data, which is appended to the original input to maintain the expected output size. Users preferring the first approach can manually discard excess results.

filter Data-Parallel Pattern. Implementing the filter data-parallel pattern on the DPU is straightforward: the kernel function processes each element, appending those that satisfy the filter condition to the output vector. However, managing WRAM–MRAM transfers introduces complexity. There are two possible strategies for output transfers: (i) transferring *all* available output elements *after* processing a full input WRAM block, or (ii) waiting until a full output WRAM block is accumulated *before* transferring. The latter is more efficient due to larger batch transfers but requires frequent checks for a full WRAM block, which is costly. To avoid this overhead, DaPPA implements the first approach. A challenge in this method is ensuring 8-byte alignment, as the number of retained elements is unpredictable. To address this, we round up the transfer size to the nearest valid alignment, ensuring that no overwrites occur. Since the maximum possible output length (where all elements are retained) is always aligned by design, this guarantees safe memory handling. During transfers, the last 8-byte section of each output WRAM block contains both valid data and padding. Since subsequent transfers cannot create gaps, the base MRAM destination must remain unchanged. To handle this, we copy the last

8 bytes of the previous WRAM block to the start of the next one, adjusting the offset so that new elements seamlessly append to the existing data.

7.3.4 Handling Invalid Pipeline Implementations

Certain stage combinations cannot be processed within a single Pipeline as described so far. Specifically, the outputs of `filter` and `reduce` cannot be directly used by subsequent stages except for additional filtering or reduction. For `filter`, a `map` operation cannot process its output since each PIM core lacks knowledge of how many elements preceding PIM cores retained. Without this information, a PIM core cannot determine the correct position of its filtered results in the global output vector, making it impossible to align multiple inputs in a `map` operation when one of them is a `filter` output. Similarly, for `reduce`, each PIM core only has a partial result, meaning further stages would receive incomplete or incorrect data.

To resolve this, filtered or reduced results *must* be copied back to the CPU and combined before further processing. This effectively splits execution into two separate Pipelines: one handling operations up to the `filter` or `reduce` stages, and another processing the aggregated results.

To assist in such cases, DaPPA provides the `PipelineFull` class, which automatically detects invalid stage combinations and partitions execution into multiple sub-pipelines. This ensures that all stage configurations can be handled correctly. The class is separate from `Pipeline` to highlight its potential performance impact, encouraging users to make an informed choice. Its interface remains identical to that of a regular `Pipeline`.

7.4 Methodology

7.4.1 Implementation

As a case study, we implement DaPPA targeting a UPMEM PIM system that includes a 2-socket Intel Xeon Silver 4110 CPU at 2.10 GHz (host CPU), standard main memory (DDR4-2400) of 128 GB, and 20 UPMEM PIM DIMMs with 160 GB PIM-capable memory and 2,560 DPUs [474]. We implemented DaPPA in C++, and compiled it as a shared library, therefore it can be distributed independently from the user application, if needed. To use DaPPA, we link our target application implementation to the shared library.

7.4.2 Workloads

We evaluate DaPPA using six PIM-friendly applications from the PrIM benchmark suite [6, 476]: vector addition (VA), select (SEL), unique (UNI), reduction (RED), general matrix-vector multiplication (GEMV), and image histogram small (HST-S). We use the hand-tuned implemen-

tations of such workloads from the PRIM benchmark suite as our baseline. Below, we describe the data-parallel patterns we use to implement each one of the six PRIM workloads. If not otherwise specified, we use 1M 32-bit integer elements per UPMEM core as input dataset for each workload.

Vector Addition (VA). Element-wise addition of two arrays. We implement VA using a map data-parallel pattern.

Select (SEL). Selects elements from the input vector based on a predicate. We implement SEL using a filter data-parallel pattern.

Unique (UNI). Removes duplicates from a sorted vector. We implement UNI using a window+filter data-parallel pattern, with a window of two. Thus, our implementation accesses two consecutive elements, keeping an element if it differs from the next one.

Reduction (RED). Adds all elements of an input array into a scalar value. We implement RED using a reduce data-parallel pattern.

General Matrix-Vector Multiplication (GEMV). Standard matrix-vector multiplication. We implement GEMV using a group data-parallel pattern by (i) setting the group size equal to the vector size, (ii) treating the vector as a scalar, and (iii) manually iterating over rows to perform multiplication and summation. While this approach requires the user to explicitly write the loop, it is necessary because DaPPA does *not* inherently recognize non-vector data structures such as matrices. Additionally, this method requires the entire vector to fit within WRAM. This constraint is also present in the PRIM benchmark. We evaluate the runtime of GEMV for matrices with 4096 rows and 256 columns per UPMEM core.

Image Histogram Small (HST-S). Counts the number of times each value appears in a vector input. We implement HST-S using a reduce data-parallel pattern. In our HST-S implementation, the reduction variable is a vector, whose size depends on the amount of unique values that appear in the input vector. We evaluate the runtime of HST-S for 1M 32-bit integer elements per UPMEM core, with the number of histogram bins set to 256 [6, 476].

7.5 Evaluation

We first describe how DaPPA improves programming productivity. Second, we provide a performance analysis of DaPPA compared to hand-tuned reference implementations of our six evaluated workloads. Third, we discuss DaPPA's overheads.

7.5.1 Productivity Improvement

We evaluate how DaPPA can improve programming productivity compared to the hand-tune PRIM workloads, and a prior framework for UPMEM programmability called SimplePIM [390].

Similar to DaPPA, SimplePIM provides a series of high-level APIs that allow the user to abstract low-level implementation details when writing code for the UPMEM system. However, different than DaPPA, in SimplePIM, the user is still responsible to *explicitly* handle CPU-DPU and DPU-DPU data communication. We use lines-of-code (LOC) as a productivity metric [1338–1340]. To do so, we manually count the lines of *effective* UPMEM-programming related code for each one of the six workloads, which excludes lines of code for data loading from a file to the host main memory, host memory allocation, variable definition, and time measurements.

Table 7.1 summarizes the lines of effective code saved by using DaPPA for the six workloads compared to the hand-tuned PrIM implementation and SimplePIM. Note that there is no available reference implementation of SimplePIM for three of our workloads (i.e., SEL, UNI, and GEMV). We make two observations from the table. First, compared to the hand-tuned PrIM implementations, DaPPA *significantly* reduces LOC. On average across all six workloads, DaPPA reduces LOC by 94% compared to the PrIM implementations. This is possible since DaPPA *significantly* raises the abstraction level when implementing UPMEM workloads, allowing the user to mainly focus the target kernel function. Second, compared to SimplePIM, DaPPA further improves productivity by 59%. This is due to the fact that in DaPPA, the user does *not* need to write code for data communication or metadata bookkeeping, as in SimplePIM. We conclude that DaPPA is an efficient framework to ease UPMEM programmability.

Table 7.1: Lines-of-code (LOC) comparison.

Workload	LOC PrIM [241]	LOC SimplePIM [390]	LOC DaPPA	LOC Red. (vs. PrIM)	LOC Red. (vs. SimplePIM)
VA	78	14	6	92%	57%
SEL	120	-	6	95%	-
UNI	155	-	6	96%	-
RED	123	14	6	95%	57%
GEMV	180	-	9	95%	-
HST-S	113	21	8	93%	62%
GMean	124	16	7	94%	59%

7.5.2 Performance Analysis

We compare DaPPA’s performance for our six workloads in comparison to their PrIM hand-tuned implementations. We conduct our analysis in a real UPMEM-based system (described in Section 7.4). In our analysis, we configure the DPUs to use 11 tasklets (for both DaPPA and PrIM workloads), which is the minimum number of tasklets in order to fill the DPU instruction pipeline [6, 476]. We report the average execution time across 10 execution runs.

End-to-End Execution Time. Figure 7.4 shows the average end-to-end execution time to execute each one of our six workloads using PrIM and DaPPA implementations. In this analy-

sis, we measure both the time it takes for CPU–DPU/DPU–CPU data transfer, inter-DPU data movement, and DPU kernel execution time. We make four observations from the figure. First, as expected, the CPU–DPU and DPU–CPU transfer times comprise the vast majority of the processing time for both PrIM and DaPPA implementations. Second, for four workloads (i.e., VA, RED, GEMV, and HST–S), DaPPA achieves performance on par with the hand-tuned PrIM implementations. Third, for two workloads (i.e., SEL and UNI), DaPPA performs *significantly* better than PrIM implementations. On average across these two workloads, DaPPA achieves 10× the performance of PrIM implementations. This is due to the fact that PrIM implementations for such workloads use slower serial data transfers instead of faster parallel data transfer when copying data back from the DPUs to the CPU main memory. As these workloads have undefined output sizes (since they include filtering operations), PrIM transfers the output data back from each DPU *individually*, one after another, after communicating the correct result size to the CPU. In contrast, DaPPA copies back from DPUs to the CPU *all* the output data, and only compresses the data to remove the ‘holes’ after we transferred it back to the CPU, hence improving transfer time. Fourth, on average across all six workloads, DaPPA achieves 2.1× the end-to-end performance of the hand-tuned PrIM implementations. We conclude that DaPPA *consistently* achieves performance comparable to the PrIM hand-tune reference implementations.

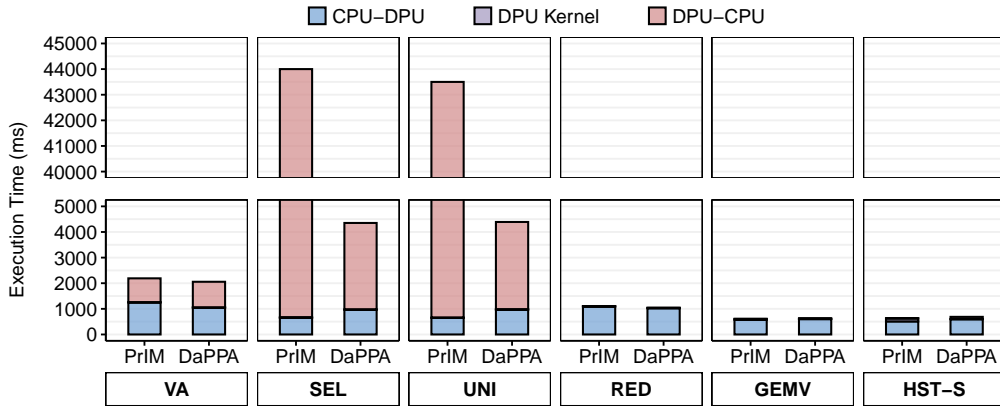


Figure 7.4: End-to-end execution time for six workloads using PrIM [6] hand-tuned and DaPPA implementations.

DPU Kernel Execution Time. Figure 7.5 shows the DPU kernel execution time (i.e., the execution time *excluding* memory transfer times) for our six workloads using both PrIM and DaPPA implementations. We make two observations from the figure. First, for most workloads, DaPPA either achieves on par performance or outperforms their PrIM implementations. On average across all workloads, DaPPA achieves 1.4× the performance of the PrIM implementations (and up to 3.5×). Second, for some workloads (i.e., SEL and HST–S), there is a large per-

formance gap between DaPPA and PrIM implementations, in favor of DaPPA. This is because different amounts of work are performed in the DPU in these cases: the PrIM implementations performs part of the compression/combination after the filter/reduction already in the DPU, which counts towards the DPU time, whereas DaPPA perform such operations within the host CPU, which counts towards the memory transfer time presented in Figure 7.4.

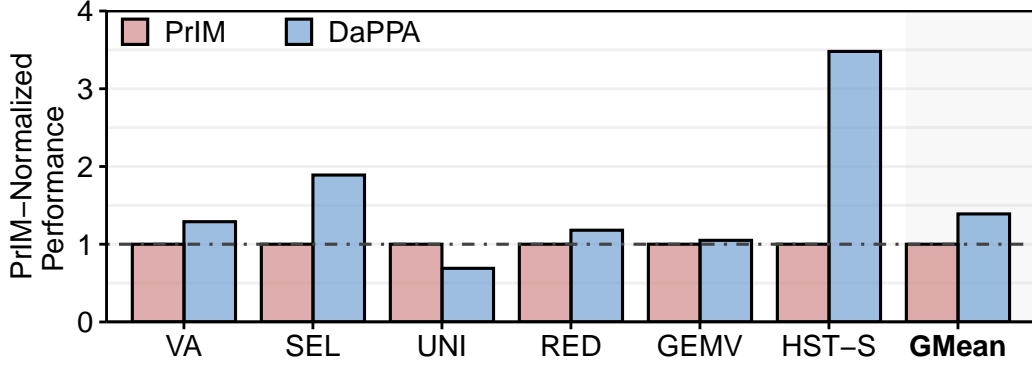


Figure 7.5: DPU kernel performance comparison for six workloads using PrIM [6] and DaPPA implementations.

7.5.3 DaPPA Execution Time Overheads

DaPPA induces some additional execution overheads due to its dynamic template-based compilation. We measured such overheads for our six workload implementations, and we observe that DaPPA execution time overheads are of (i) 1 ms for substituting values into the DPU code skeleton; (ii) 150 ms for compiling the DPU binary (recall that in DaPPA, the DPU binary has to be compile at runtime for each Pipeline); (iii) 1–150 ms for other various operations (e.g., element count calculations). Such execution overheads are negligible in comparison to the time the UPMEM SDK takes to allocate DPUs (1200 ms) and end-to-end DPU execution time (Figure 7.4).

7.6 Summary

We introduce DaPPA (data-parallel processing-in-memory architecture), a data-parallel programming framework that simplifies programming in general-purpose PNM systems. By abstracting hardware complexities through high-level data-parallel patterns, DaPPA enables efficient PIM execution without manual optimizations. DaPPA is comprised of three main components, a set of data-parallel pattern APIs, a dataflow programming interface, and a dynamic template-based compilation scheme. Our evaluation shows that DaPPA improves performance while reducing programming complexity for different PIM workloads. DaPPA bridges the gap between ease of use and efficiency in PIM architectures, fostering broader adoption for general-purpose PNM systems.

Chapter 8

Conclusions and Future Directions

In summary, the goal of this dissertation is to provide tools and system support for PIM architectures (with a focus on DRAM-based solutions), to ease the adoption of such architectures in current and future systems. To achieve this goal, we conduct a set of research projects based on the thesis statement that “*We can effectively exploit the inherent parallelism of PIM architectures and facilitate their adoption across a broad spectrum of workloads through end-to-end design of hardware and software support for PIM, including benchmark suites and workload analysis methodologies, compiler/programming frameworks, and data-aware runtime systems, thereby enabling large (e.g., factors or orders of magnitude) improvements in performance and energy efficiency.*” To this end, we combine workload analyses, hardware/software co-designed mechanisms, and software-level frameworks.

First, we build a comprehensive understanding of data movement bottlenecks in modern systems. To this end, we conduct the first large-scale characterization of data movement across 77K functions from 345 applications, identifying key sources of data movement and evaluating the effectiveness of compute-centric (e.g., caching, prefetching) and memory-centric (e.g., PIM) mitigation techniques (Chapter 4). We develop the DAMOV benchmark suite, selecting 144 diverse functions that capture different types of data movement across various domains. Using DAMOV, we conduct four case studies on PIM systems, analyzing load balance, inter-PIM communication, core model impacts, and the utility of simple PIM instructions. We conclude that DAMOV enables rigorous study of data movement and provides a valuable tool for developing and evaluating PIM architectures. We open-source DAMOV and the complete source code for our new characterization methodology at <https://github.com/CMU-SAFARI/DAMOV>.

Second, we enable efficient and flexible PIM execution by overcoming the limitations of PUD with MIMDRAM, a hardware/software co-designed system (Chapter 5). MIMDRAM leverages fine-grained DRAM access to support SIMD/MIMD execution at a DRAM subarray, improving utilization and programmability. It introduces lightweight hardware exten-

sions and memory controller modifications to enable independent execution of PUD instructions and in-memory vector-to-scalar reduction operations. On the software side, MIMDRAM implements compiler passes to identify PUD-friendly code regions, determine appropriate SIMD granularity, and schedule operations across DRAM mats. Our evaluation on twelve applications and 495 workload mixes shows that MIMDRAM provides $34\times$ performance and $14.3\times$ energy efficiency improvements over state-of-the-art PUD, while incurring small area cost. We open-source MIMDRAM workloads and evaluation framework at <https://github.com/CMU-SAFARI/MIMDRAM>.

Third, we introduce *Proteus*, a hardware framework that improves PUD execution efficiency by dynamically adapting to workload characteristics (Chapter 6). *Proteus* addresses the limitations of static data representation and throughput-only execution in bit-serial PUD architectures by exploiting narrow data values and DRAM internal parallelism. It automatically selects the best data formats, bit-precision, and arithmetic algorithms (bit-serial or bit-parallel) for high-performance PUD execution. Compared to CPU, GPU, and SIMDRAM, *Proteus* achieves up to $90.3\times$ energy savings and $17\times$ higher performance per area across twelve applications, while adding only 1.6% DRAM and 0.03% CPU area overhead. *Proteus* demonstrates the importance of data-aware execution in PIM systems. We open-source *Proteus* workloads and evaluation framework at <https://github.com/CMU-SAFARI/Proteus>.

Fourth, we ease PIM programmability with DaPPA, a software framework for general-purpose PNM systems (Chapter 7). DaPPA abstracts low-level hardware management using high-level data-parallel patterns and a dataflow programming interface. It automates data movement, allocation, and workload distribution, allowing efficient programming without requiring detailed hardware knowledge. DaPPA comprises pattern APIs, a dataflow model, and a dynamic compilation backend. Evaluated on six PrIM workloads [479], DaPPA improves performance by $2.1\times$ and reduces code complexity by 94% compared to manual implementations. Our results highlight DaPPA’s potential in making PIM programming more accessible and productive.

8.1 Future Research Directions

Although this dissertation focuses on enabling system support for PIM systems, proposing several new ideas for efficient and programmer-oblivious PIM execution, we believe that this work is applicable in a more general sense and opens up new research directions. This section reviews promising directions for future work.

8.1.1 Extending the DAMOV Methodology & Benchmark Suite

Evaluating Data Movement Bottlenecks in Other Processor-Centric Systems. First, our DAMOV methodology can be extended to evaluate data movement bottlenecks in processor-centric systems beyond general-purpose CPUs. Modern computing platforms increasingly incorporate heterogeneous components such as GPUs, custom accelerators, and FPGAs, each with distinct memory subsystem characteristics and bottlenecks. Applying DAMOV methodology to these platforms would require adapting its instrumentation and profiling tools to capture low-level data movement behavior in these architectures. For example, GPUs exhibit high main memory throughput but suffer from memory coalescing and bank conflicts, while FPGAs and accelerators often rely on statically defined memory hierarchies. Characterizing how data movement bottlenecks manifest across these systems can provide deeper insight into their performance limitations and guide the development of architecture-specific data movement mitigation mechanisms, including platform-tailored PIM solutions.

Evaluating the Impact of Data Bottlenecks Caused by Storage & Network. Second, the DAMOV methodology can be extended to account for data movement bottlenecks arising from the storage and networking subsystems, which are increasingly critical in data-intensive and distributed applications. Today's systems rely heavily on high-speed storage devices (e.g., NVMe SSDs) and fast network interconnects (e.g., RDMA) that move data across devices and distributed nodes. Incorporating these components into DAMOV requires modifying the methodology to be able to gather profiling information regarding I/O and network traffic, enabling a holistic view of data movement across the entire system. Such an extension would facilitate the identification of data movement bottlenecks that span multiple layers of the system stack, such as data ingestion pipelines, checkpointing, or remote memory access, and guide the design of new hardware/software optimizations, including in-storage or in-network processing approaches.

Identifying PUM Suitability. Third, DAMOV can be extended to evaluate the suitability of PUM techniques, which perform computation directly within the memory arrays. Unlike PIM solutions that rely on integrating compute units near memory, PUM exploits the analog properties of DRAM to perform operations such as copy, initialization, or bitwise logic. Extending DAMOV to model and evaluate PUM requires new characterization dimensions that capture the access patterns, data types, and computational primitives amenable to in-DRAM execution. DAMOV could be used to build a classification framework that identifies code regions likely to benefit from PUM, complementing existing PIM-focused analysis. By integrating PUM fea-

sibility studies into its benchmark suite, DAMOV can serve as a comprehensive platform to explore the full spectrum of memory-centric computation paradigms.

8.1.2 Improving MIMDRAM & *Proteus* Execution Model

Reducing the Cost of Inter-Lane Communication. A key performance bottleneck in MIMDRAM and *Proteus* arises from the costly inter-lane communication within DRAM, particularly during reduction operations. Due to the narrow interconnect between DRAM columns, transferring partial results across lanes requires multiple DRAM commands, significantly increasing latency and energy consumption. Future work can explore low-cost, high-bandwidth intra-subarray interconnects that enable more efficient broadcast and aggregation of DRAM columns. Such improvements could allow more efficient in-memory reductions execution, enabling broader applicability of PUM for workloads with reduction-heavy computations.

Avoiding Data Layout Transformations. Both MIMDRAM and *Proteus* require data transposition to convert data from a row-major (horizontal) layout to a column-major (vertical) layout suitable for bit-serial operations. This data layout transformation incurs overheads in terms of performance, energy, and code complexity. One promising direction is to develop fine-grained inter-lane interconnects within the DRAM mat, reducing the need for full data transposition. Alternatively, future work could explore compiler- and OS-level data placement strategies that lay out data vertically across DRAM mats by construction, allowing in-place execution of vertical PUM operations. A pipelined execution model, inspired by recent works like RACER [338], could further reduce the need for global transpositions by overlapping horizontal and vertical operations across DRAM mats.

Smarter Offloading Decisions. The current MIMDRAM compiler lacks a cost model to decide whether offloading a computation to PUM will be beneficial, leading to the possibility of offloading instructions that are better suited for CPU execution due to cache locality. Incorporating a hybrid compiler/runtime system that integrates compile-time static analysis with runtime profiling can improve offloading decisions. For example, the compiler could annotate code regions with potential memory access footprints, while a lightweight runtime system monitors cache behavior and dynamically chooses whether to execute the region in PUM or CPU. Such hybrid schemes would reduce performance regressions and improve the robustness of PUM-enabled systems across diverse workloads.

Generalizing the Execution Model. MIMDRAM's compiler currently limits auto-vectorization to inner loops, restricting the opportunity to extract data parallelism from outer-loop structures. An improved programming model could adopt a SMT-style approach, mapping outer loop iterations to independent threads running on different DRAM subarrays, while

retaining SIMD execution within inner loops. This hierarchical execution model would allow MIMDRAM to exploit both coarse- and fine-grained parallelism across DRAM, increasing the utilization of available compute substrates. Compiler support for loop tiling and cross-subarray synchronization primitives will be necessary to efficiently orchestrate such SIMT-like PUM execution.

Enabling Efficient In-DRAM Multiplication. While PUM enables efficient in-DRAM execution of bitwise and simple arithmetic operations, multiplication remains a costly primitive in current designs. Stochastic computing offers one possible approximation-based solution, but it introduces significant accuracy and convergence challenges. Future research should explore new algorithms that decompose multiplication into simpler DRAM-friendly primitives, or leverage emerging non-volatile memory technologies that support native multiply-accumulate operations. Additionally, PUM-specific approximate multiplication techniques could be tuned based on application-level tolerance to inaccuracy, enabling trade-offs between precision and efficiency in domains such as machine learning and signal processing.

Combining PUM and PNM Execution. MIMDRAM and *Proteus* currently focus exclusively on PUM execution and do *not* explore the potential synergies with processing-near-memory (PNM) designs. A combined PUM–PNM execution model could address several current limitations. For instance, expensive operations such as multiplication and reduction could be delegated to lightweight near-bank ALU engines, while inexpensive vector-wide operations are executed within the DRAM arrays. Such a hybrid model allows each operation to be executed where it is most efficient, reducing the burden on the DRAM mat and improving overall system throughput. Developing orchestration mechanisms between PUM and PNM execution units, as well as compiler/runtime frameworks to partition code accordingly, presents a promising avenue for future work.

8.1.3 Enhancing the DaPPA Programming Framework

Supporting Multi-Dimensional Data Structures. DaPPA currently supports operations primarily over one-dimensional vectors, limiting its expressiveness for applications that naturally operate on higher-dimensional data structures such as matrices, tensors, or multidimensional grids. Many real-world applications in scientific computing, image processing, and machine learning rely on native support for multi-dimensional arrays. Future work can extend DaPPA’s programming model to support multi-dimensional abstractions, allowing the programmer to express computation over multi-dimensional domains more naturally. This extension would also require enhancing the underlying memory allocation and scheduling in-

frastructure to support multi-dimensional data decomposition and distribution across the PIM cores efficiently.

Extending the Set of Data-Parallel Patterns. DaPPA currently focuses on five core data-parallel patterns—map, reduce, filter, window, and group—which, while powerful, limit its applicability to a subset of data-parallel workloads. Many applications rely on more complex patterns, such as stencil, commonly used in scientific simulations, or farm, used in embarrassingly parallel workloads. Extending DaPPA to support a richer set of patterns would enable it to target a wider range of workloads and allow more programmers to express their computation within the framework. Incorporating new patterns would also open opportunities for pattern-specific compiler optimizations and hardware-aware scheduling strategies.

Raising the Level of Abstraction with Automatic Pattern Detection. While DaPPA simplifies programming by abstracting away hardware-specific details, the programmer is still responsible for manually identifying and selecting the appropriate data-parallel pattern for each computation. Prior works [1341–1344] show that it is possible to automatically detect data-parallel patterns in imperative code written in C/C++ through static and dynamic analysis. Integrating such pattern detection capabilities into DaPPA would raise the level of abstraction further, enabling legacy applications to be ported to PIM with minimal programmer intervention. This automation would reduce programming effort, lower the barrier to adoption, and allow more developers to leverage the performance benefits of PIM architectures.

Enabling Portability Across PIM Architectures. Currently, DaPPA is tightly coupled to the UPMEM PIM architecture and does *not* support other real-world PIM platforms. Supporting multiple backends would significantly broaden DaPPA’s applicability and facilitate comparative studies across diverse PIM systems. Future work can focus on decoupling DaPPA’s intermediate representation from its hardware-specific backend, enabling portability to alternative PIM architectures such as HBM-based PIM systems or hybrid PUM/PNM platforms. This backend modularity would position DaPPA as a general-purpose PIM programming framework, serving both research and industry use cases across heterogeneous computing environments.

8.2 Concluding Remarks

In this dissertation, we investigate the tools, system, and programming support required to enable PIM architectures in current future systems efficiently. We first build a comprehensive understanding of data movement bottlenecks by characterizing 77K functions across 345 applications, leading to the DAMOV methodology and benchmark suite (Chapter 4). We then propose two PUM systems: (i) MIMDRAM (Chapter 5), which enables flexible in-DRAM SIMD/MIMD execution through fine-grained DRAM access alongside a holistic system support design to au-

tomatically generate and execute PUD-capable code in a system; and (ii) *Proteus* (Chapter 6), which dynamically adapts the data representation, precision, and arithmetic PUD implementation for efficient in-DRAM computation. Finally, we introduce DaPPA (Chapter 7), a high-level programming framework for general-purpose PNM systems, which simplifies programmability and improves performance of PIM code through data-parallel patterns.

As applications continue to grow in complexity and scale, data movement is rapidly emerging as a fundamental bottleneck in modern computing systems, significantly impacting performance, energy efficiency, and system reliability. Existing processor-centric architectures are increasingly constrained by this bottleneck, and it is becoming clear that incremental improvements to traditional processor-centric designs are insufficient. This dissertation advocates for a paradigm shift towards processing-in-memory (PIM), an approach that *fundamentally* mitigates data movement by moving computation to where the data resides.

Although the core idea of PIM is not new, recent technological advances have made it feasible to manufacture and prototype PIM architectures that aim to accommodate the computational demands of data-intensive workloads. At the same time, fully embracing PIM requires overcoming significant system-level challenges due to the entrenched assumptions and abstractions imposed by decades of processor-centric designs. Through the contributions of this dissertation, which span workload characterization, hardware/software co-design, and programming support, we take meaningful steps toward enabling practical, efficient, and programmable PIM systems. However, the road to widespread adoption of PIM remains long. Continued effort is required across the entire computing stack to fully realize the promise of PIM and enable a future where systems are designed from the ground up with data movement as a *first-class* design concern. We remain optimistic that such a future is within reach and that PIM will play a central role in shaping the next generation of high-performance, energy-efficient, and sustainable computing platforms.

Appendix A

Other Works of the Author

In this chapter, we first summarize other works led by the author but that are not included in this dissertation, and second, we briefly discuss other works co-lead by the author.

A.1 Other Works Lead by the Author

A.1.1 Extending Memory Capacity in Modern Consumer Systems with Emerging Non-Volatile Memory: Experimental Analysis and Characterization Using the Intel Optane SSD

In our IEEE Access paper [1345], we provide the *first* analysis of the impact of extending the main memory space of consumer devices using off-the-shelf non-volatile memories (NVMs). We *extensively* examine system performance and energy consumption when the NVM device is used as swap space for DRAM main memory to effectively extend the main memory capacity. Our empirical analyses lead us to several observations and insights that can be useful for the design of future systems and NVMs.

For our experimental evaluation, we equip real web-based Chromebook computers [1346] with the Intel Optane SSD [1347]. Our target workloads are interactive applications, with a focus on the Google Chrome [872] web browser. We choose such workloads for two reasons. First, in interactive applications, the system needs to respond to user inputs at a target output latency to provide a satisfactory user experience. Second, in Chromebooks, the Chrome browser serves as the main interface to execute services for the user. We compare the performance and energy consumption of interactive workloads running on our Chromebook with NVM-based swap space, where the Intel Optane SSD capacity is used as swap space to extend main memory capacity, against two state-of-the-art systems: (i) a baseline system with double the amount of DRAM than the system with the NVM-based swap space, which resembles cur-

rent consumer devices but has high manufacturing cost due to the large DRAM capacity and relatively high cost-per-bit of DRAM; and (ii) a system where the Intel Optane SSD is naively replaced with a state-of-the-art (yet slower) off-the-shelf NAND-flash-based SSD, which we use as a swap space of equivalent size as the NVM-based swap space. The NAND-flash-based SSD provides a cheap alternative to extend the main memory space, but it can penalize system performance due to its high access latency. We use a memory capacity pressure test [1348] to measure the impact of the new NVM swap space on user tasks that consist of loading, scrolling, and switching between Chrome browser tabs. We measure how the NVM device increases the 99th-percentile latency (i.e., tail latency) of each task and the total number of Chrome tabs that the user can open without discarding old tabs.

To summarize, our experimental analysis reveals that extending the main memory space by using the Intel Optane SSD as NVM-based swap space for DRAM provides a cost-effective way to alleviate DRAM scalability issues. However, naively integrating the Intel Optane SSD into the system leads to several system-level overheads that can negatively impact overall performance and energy efficiency. We mitigate such overheads by examining and evaluating system optimizations driven by our analyses.

We provide the following six key takeaways from our empirical analyses:

1. *Effect of Intel Optane SSD as swap space.* Reducing DRAM size and extending the main memory space with the Intel Optane SSD as swap space provides benefits for the Chrome browser, since it can (i) increase the number of open tabs, and (ii) reduce system cost. However, it also leads to an increase in the number of tab switches with high latency compared to the baseline.
2. *Reducing tail latency by enabling Zswap.* Zswap [1349] is a good mechanism to reduce I/O traffic introduced by the Intel Optane SSD, at the cost of a small increase in tab switch latency at large tab counts. The Zswap cache reduces system energy by $2\times$ (compared to the Intel Optane SSDc3 without Zswap enabled), at the cost of increasing the high-latency tab switches by 4% and reducing the number of open tabs by 12%.
3. *Effect of using different NVM devices.* A state-of-the-art NAND-flash-based SSD provides benefits over both the baseline and the Intel Optane SSD. Importantly, it enables more Chrome tabs to be open. These benefits come due to the larger effective main memory capacity provided by the state-of-the-art NAND-flash-based SSD over the baseline configuration. Unfortunately, these benefits come at the cost of higher tab switch latencies, compared to both the baseline and Optane configurations, due to the much longer device latencies of NAND flash memory. These large tab switch latencies degrade user experience. Taking both performance and user experience into account, emerging NVM-based SSDs such as the Intel Optane SSD are quite promising to employ in consumer devices, provid-

ing performance benefits without the undesirable user experience trade-offs incurred by NAND-flash-based SSDs.

4. *System bottlenecks caused by NVMs.* The Linux block I/O layer [1350, 1351] is a key system bottleneck when the Intel Optane SSD is used as swap space. We can mitigate some of the overheads caused by the block I/O layer by (i) employing an I/O scheduler that meets the requirements of the application’s access pattern and (ii) using different I/O request completion mechanisms.
5. *Optimization 1: block I/O schedulers.* We can reduce tab switch latency by changing the default budget-fair queuing (BFQ) [1350] I/O scheduler in the system that uses the Intel Optane SSD as swap space. We reduce 95th- and 99th-percentile latencies by employing the None [1352] and the Kyber [1353] I/O schedulers, respectively, as those I/O schedulers reduce I/O scheduling overheads and fit the I/O access pattern of the Chrome web browser.
6. *Optimization 2: interrupt- vs. polling-based I/O request completion.* On average, the interrupt-based I/O request completion mechanism provides the best performance for the system with the Intel Optane SSD device. However, the Hybrid I/O request completion mechanism can help reduce 99th-percentile latency for block I/O requests.

Based on our analysis, we conclude that there is a large optimization space to be explore in order to *efficiently* adopt emerging NVMs in consumer devices. For example, we believe that one of the main issues the system suffers from when executing interactive workloads is that scheduling decisions made by the OS do not consider the response time expected by the workload. Exposing such information to the OS could reduce tail latency and allow the scheduler to take action according to the needs of a particular workload (e.g., by prioritizing the workload with the shorter or more urgent response deadlines). We leave the design, implementation, and evaluation of such ideas for future work.

A.1.2 Surveys & Summary Works on PIM

Accelerating Neural Network Inference With Processing-in-DRAM: From the Edge to the Cloud. In our IEEE Micro paper [384], we conduct a comprehensive analysis of three state-of-the-art DRAM-based PIM architectures, i.e., UPMEM PIM [474, 475], Mensa [14], and SIMD RAM [378], to evaluate their effectiveness in accelerating neural network (NN) inference workloads. We show that traditional compute-centric accelerators often suffer from high under-utilization and energy inefficiency for memory-bound NN models. In contrast, the three evaluated PIM architectures can alleviate memory bottlenecks and significantly improve both performance and energy efficiency. We make three key observations. First, the UPMEM PIM architecture can outperform high-end GPUs under memory oversubscription for general matrix-vector product (GEMV) workloads. Second, Mensa achieves higher throughput and lower en-

ergy usage than the Google Edge TPU by specializing accelerators for different NN layer types. Third, SIMDRAM can significantly accelerate binary NNs, outperforming CPUs and GPUs while maintaining compatibility with standard DRAM infrastructure. We conclude that no single PIM architecture fits all NN models, highlighting the need for heterogeneous PIM systems with unified programming models to fully harness the benefits of multiple PIM approaches.

Methodologies, Workloads, and Tools for Processing-in-Memory: Enabling the Adoption of Data-Centric Architectures. In our ISVLSI paper [387], we contextualize our DAMOV methodology [24] and SIMDRAM framework [378] as means to facilitate the adoption of PIM architectures. Together, DAMOV and SIMDRAM provide practical tools and system-level support to guide the design, programming, and integration of PIM systems into modern computing platforms.

Heterogeneous Data-Centric Architectures for Modern Data-Intensive Applications: Case Studies in Machine Learning and Databases. In our second ISVLSI paper [388], we demonstrate the performance and energy benefits that can be achieved through hardware/software co-design tailored for PIM architectures. Using two case studies, i.e., Mensa [14], a composable framework for accelerating machine learning inference on edge devices, and Polynesia [278], a specialized system for hybrid transactional/analytical database processing, we show that aligning architectural design with application-specific characteristics enables efficient use of limited memory-side compute resources. Both systems achieve significant improvements over state-of-the-art platforms by customizing hardware accelerators and execution strategies to the underlying application behavior, highlighting co-design as a key enabler for realizing the full potential of memory-centric computing.

A.2 Other Works the Author Contributed to as Co-Author

Besides the works presented in this dissertation, I had the opportunity to contribute on several different areas during my doctoral studies in collaboration with researchers from ETH Zürich, Carnegie Mellon University, University of Illinois Urbana-Champaign, Galicia Supercomputing Center, University of Toronto, Barcelona Supercomputing Center, TOBB University of Economics and Technology, Intel, NVIDIA, and Google. In this chapter, I acknowledge these works in six categories.

New PIM Architectures. In collaboration with Amirali Boroumand, we design: (i) Mensa [14], a new acceleration framework for edge NN inference models that incorporates multiple heterogeneous edge machine learning (ML) accelerators (including both on-chip and near-data accelerators), each of which caters to the characteristics of a particular subset of NN models and layers; (ii) Polynesia [278], a hardware–software co-designed system

for in-memory hybrid transactional and analytical processing (HTAP) databases that avoids the large throughput losses of traditional HTAP systems.

In collaboration with Gagandeep Singh, we design NAPEL [282], a high-level performance and energy estimation framework for PIM architectures. In collaboration with Nika Mansouri Ghiasi, we design ALP [876], a new programmer-transparent technique to leverage the performance benefits of PIM by alleviating the performance impact of inter-segment data movement between host and memory and enabling efficient partitioning of applications between host and PIM cores. In collaboration with João Dinis Ferreira, we design pLUTo [333], a DRAM-based PUM architecture that leverages the high storage density of DRAM to enable the massively parallel storing and querying of lookup tables. In collaboration with Jisung Park, we design Flash-Cosmos [336], a new in-flash processing technique that significantly increases the performance and energy efficiency of bulk bitwise operations while providing high reliability. In collaboration with Alain Denzler, we design Casper [250], a near-cache accelerator consisting of specialized stencil computation units connected to the LLC of a traditional CPU.

Understanding & Exploiting Real-World PIM Architectures. In collaboration with Juan Gómez-Luna, we (i) conduct an experimental characterization of the UPMEM-based PIM system using microbenchmarks to assess various architecture limits such as compute throughput and memory bandwidth, yielding new insights, and present PrIM (Processing-In-Memory benchmarks), a benchmark suite of 16 workloads from different application domains designed for the UPMEM-based PIM system [242]; and (ii) study the potential of general-purpose PIM architectures to accelerate ML training [392, 720].

In collaboration with Maurus Item, we design TransPimLib [393], a library that provides CORDIC-based and LUT-based methods for transcendental (and other hard-to-calculate) functions in general-purpose PIM systems.

PIM on commodity off-the-shelf (COTS) DRAM Chips. In collaboration with Ismail Emir Yuksel, we experimentally demonstrate that COTS DRAM chips are capable of (i) performing functionally-complete bulk-bitwise Boolean operations: NOT, NAND, and NOR [894], (ii) executing up to 16-input AND, NAND, OR, and NOR operations [894], and (iii) copying the contents of a DRAM row (concurrently) into up to 31 other DRAM rows with >99.98% reliability [895].

Novel DRAM Architectures. In collaboration with Ataberk Olgun, we design Sectored DRAM [454], a new, low-overhead DRAM substrate that reduces wasted energy by enabling fine-grained DRAM data transfer and DRAM row activation.

DRAM Reliability & Read Disturbance. In collaboration with Minesh Patel, we design HARP [591], a new error profiling algorithm that rapidly achieves full coverage of at-risk bits. In collaboration with Abdullah Giray Yağlıkçı, we (i) experimentally demonstrate on 272 real

DRAM chips that lowering DRAM's wordline voltage reduces a DRAM chip's RowHammer vulnerability [1258]; and (ii) design Sv rd [191], a new RowHammer mitigation mechanism that dynamically adapts the aggressiveness of existing solutions based on the row-level read disturbance profile.

In collaboration with Ataberk Olgun, we (i) design ABACuS [192], a new low-cost hardware-counter-based RowHammer mitigation technique that performance-, energy-, and area-efficiently scales with worsening RowHammer vulnerability; and (ii) experimentally demonstrate for the first time that the read disturbance threshold of a DRAM row significantly and unpredictably changes over time.

In collaboration with O uzhan Canpolat, we design Chronus [198], a new on-DRAM-die RowHammer mitigation mechanism that (i) updates row activation counters concurrently while serving accesses by separating counters from the data and (ii) prevents the wave attack by dynamically controlling the number of preventive refreshes performed.

Virtual Memory. In collaboration with Nastaran Hajinazar, we design VBI [1354], a new virtual memory framework that delegates memory management duties to hardware to reduce the overheads and software complexity associated with virtual memory.

Appendix B

Complete List of the Author's Contributions

This section lists the author's contributions to the literature in reverse chronological order under two categories: (i) major contributions that the author led (§B.1), and (ii) other contributions (§B.2).

B.1 Major Contributions Led by the Author

1. Geraldo F. Oliveira, Mayank Kabra, Yuxin Guo, Kangqi Chen, A. Giray Yağlıkçı, Melina Soysal, Mohammad Sadrosadati, Joaquin Olivares Bueno, Saugata Ghose, Juan Gómez-Luna, Onur Mutlu, “*Proteus: Achieving High-Performance Processing-Using-DRAM with Dynamic Bit-Precision, Adaptive Data Representation, and Flexible Arithmetic*,” in ICS, 2025.
2. Geraldo F. Oliveira, Ataberk Olgun, Abdullah Giray Yağlıkçı, F. Nisa Bostanci, Juan Gómez-Luna, Saugata Ghose, and Onur Mutlu, “*MIMDRAM: An End-to-End Processing-Using-DRAM System for High-Throughput, Energy-Efficient and Programmer-Transparent Multiple-Instruction Multiple-Data Processing*,” in HPCA, 2024.
3. Geraldo F. Oliveira, Saugata Ghose, Juan Gómez-Luna, Amirali Boroumand, Alexis Savery, Sonny Rao, Salman Qazi, Gwendal Grignou, Rahul Thakur, Eric Shiu, and Onur Mutlu, “*Extending Memory Capacity in Modern Consumer Systems With Emerging Non-Volatile Memory: Experimental Analysis and Characterization Using the Intel Optane SSD*.” IEEE Access, September 2023.
4. Geraldo F. Oliveira, Juan Gómez-Luna, Saugata Ghose, Amirali Boroumand, and Onur

Mutlu, “Accelerating Neural Network Inference With Processing-in-DRAM: From the Edge to the Cloud.” IEEE Micro, 2022.

5. Geraldo F. Oliveira, Amirali Boroumand, Saugata Ghose, Juan Gómez-Luna, Onur Mutlu, “Heterogeneous Data-Centric Architectures for Modern Data-Intensive Applications: Case Studies in Machine Learning and Databases,” in IVLSI, 2022.
6. Geraldo F. Oliveira, Juan Gómez-Luna, Saugata Ghose, Onur Mutlu, “Methodologies, Workloads, and Tools for Processing-in-Memory: Enabling the Adoption of Data-Centric Architectures,” in IVLSI, 2022.
7. Geraldo F. Oliveira, Nastaran Hajinazar, Sven Gregorio, Joao Dinis Ferreira, Nika Mansouri Ghiasi, Minesh Patel, Mohammed Alser, Saugata Ghose, Juan Gomez-Luna, and Onur Mutlu, “SIMDRAM: An End-to-End Framework for Bit-Serial SIMD Computing in DRAM,” in ASPLOS, 2021.
8. Geraldo F. Oliveira, Juan Gómez-Luna, Lois Orosa, Saugata Ghose, Nandita Vijaykumar, Ivan fernandez, Mohammad Sadrosadati, and Onur Mutlu, “DAMOV: A New Methodology and Benchmark Suite for Evaluating Data Movement Bottlenecks.” IEEE Access, 2021.
9. Geraldo F. Oliveira, Larissa Rozales Gonçalves, Marcelo Brandalero, Antonio Carlos S. Beck, and Luigi Carro, “Employing Classification-based Algorithms for General-Purpose Approximate Computing,” in DAC, 2019.
10. Geraldo F. Oliveira, Paulo C. Santos, Marco A. Z. Alves , and Luigi Carro, “A Generic Processing-in-Memory Cycle Accurate Simulator under Hybrid Memory Cube Architecture,” in SAMOS, 2017.
11. Geraldo F. Oliveira, Paulo C. Santos, Marco A. Z. Alves, and Luigi Carro, “NIM: An HMC-Based Machine for Neuron Computation,” in ARC, 2017.

B.2 Other Contributions

1. Melina Soysal, Konstantina Koliogeorgi, Can Firtina, Nika Mansouri Ghiasi, Rakesh Nadig, Haiyu Mao, Geraldo F. Oliveira, Yu Liang, Klea Zambaku, Mohammad Sadrosadati, and Onur Mutlu, “MARS: Processing-In-Memory Acceleration of Raw Signal Genome Analysis Inside the Storage Subsystem,” in ICS, 2025.
2. Oguzhan Canpolat, Abdullah Giray Yağlıkçı, Geraldo Francisco de Oliveira, Ataberk Olgun, Nisa Bostanci, Ismail Emir Yuksel, Haocong Luo, Oguz Ergin, and Onur Mutlu,

- “Chronus: Understanding and Securing the Cutting-Edge Industry Solutions to DRAM Read Disturbance,”* in HPCA, 2025.
3. Ataberk Olgun, Nisa Bostanci, Ismail Emir Yuksel, Abdullah Giray Yağlıkçı, Geraldo Francisco de Oliveira, Haocong Luo, Oguzhan Canpolat, Minesh Patel, and Onur Mutlu, *“Variable Read Disturbance: An Experimental Analysis of Temporal Variation in DRAM Read Disturbance,”* in HPCA, 2025.
 4. Ataberk Olgun, Yahya Can Tugrul, Nisa Bostanci, Ismail Emir Yuksel, Haocong Luo, Steve Rhyner, Abdullah Giray Yağlıkçı, Geraldo F. Oliveira, and Onur Mutlu, *“ABACuS: All-Bank Activation Counters for Scalable and Low Overhead RowHammer Mitigation,”* in USENIX Security, 2024.
 5. Abdullah Giray Yağlıkçı, Geraldo F. Oliveira, Yahya Can Tugrul, Ismail Yuksel, Ataberk Olgun, Haocong Luo, and Onur Mutlu, *“Spatial Variation-Aware Read Disturbance Defenses: Experimental Analysis of Real DRAM Chips and Implications on Future Solutions,”* in HPCA, 2024.
 6. Ismail Emir Yuksel, Yahya Can Tugrul, Ataberk Olgun, F. Nisa Bostanci, A. Giray Yağlıkçı, Geraldo F. Oliveira, Haocong Luo, Juan Gomez-Luna, Mohammad Sadrosadati, and Onur Mutlu, *“Functionally-Complete Boolean Logic in Real DRAM Chips: Experimental Characterization and Analysis,”* in HPCA, 2024.
 7. Ismail Emir Yuksel, Yahya Can Tugrul, F. Nisa Bostanci, Geraldo F. Oliveira, A. Giray Yağlıkçı, Ataberk Olgun, Melina Soysal, Haocong Luo, Juan Gomez-Luna, Mohammad Sadrosadati, and Onur Mutlu, *“Simultaneous Many-Row Activation in Off-the-Shelf DRAM Chips: Experimental Characterization and Analysis,”* in DSN, 2024.
 8. Onur Mutlu, Ataberk Olgun, İsmail Emir Yüksel, and Geraldo F. Oliveira, *“Memory-Centric Computing: Recent Advances in Processing-in-DRAM,”* Invited Paper in IEDM, 2024.
 9. Alain Denzler, Rahul Bera, Nastaran Hajinazar, Gagandeep Singh, Geraldo F. Oliveira, Juan Gómez-Luna, and Onur Mutlu, *“Casper: Accelerating Stencil Computation using Near-Cache Processing.”* IEEE Access, 2023.
 10. Juan Gómez Luna, Yuxin Guo, Sylvan Brocard, Julien Legriel, Remy Cimadomo, Geraldo F. Oliveira, Gagandeep Singh, and Onur Mutlu, *“Evaluating Machine Learning Workloads on Memory-Centric Computing Systems,”* in ISPASS, 2023.

11. Maurus Item, Juan Gómez Luna, Yuxin Guo, Geraldo F. Oliveira, Mohammad Sadrosadati, and Onur Mutlu, “*TransPimLib: Efficient Transcendental Functions for Processing-in-Memory Systems*,” in ISPASS, 2023.
12. A. Giray Yağlıkçı, Haocong Luo, Geraldo F. de Oliveira, Ataberk Olgun, Minesh Patel, Jisung Park, Hasan Hassan, Jeremie S. Kim, Lois Orosa, and Onur Mutlu, “*Understanding RowHammer Under Reduced Wordline Voltage: An Experimental Study Using Real DRAM Devices*,” in DSN, 2022.
13. Jisung Park, Roknoddin Azizi, Geraldo F. Oliveira, Mohammad Sadrosadati, Rakesh Nadig, David Novo, Juan Gómez-Luna, Myungsuk Kim, and Onur Mutlu, “*Flash-Cosmos: In-Flash Bulk Bitwise Operations Using Inherent Computation Capability of NAND Flash Memory*,” in MICRO, 2022.
14. João Dinis Ferreira, Gabriel Falcao, Juan Gómez-Luna, Mohammed Alser, Lois Orosa, Mohammad Sadrosadati, Jeremie S. Kim, Geraldo F. Oliveira, Taha Shahroodi, Anant Nori, and Onur Mutlu, “*pLUTo: Enabling Massively Parallel Computation in DRAM via Lookup Tables*,” in MICRO, 2022.
15. Nika Mansouri Ghiasi, Nandita Vijaykumar, Geraldo F. Oliveira, Lois Orosa, Ivan Fernandez, Mohammad Sadrosadati, Konstantinos Kanellopoulos, Nastaran Hajinazar, Juan Gómez Luna, and Onur Mutlu, “*ALP: Alleviating CPU-Memory Data Movement Overheads in Memory-Centric Systems*.” IEEE Transactions on Emerging Topics in Computing (TETC), 2022.
16. Juan Gomez-Luna, Izzat El Hajj, Ivan Fernandez, Christina Giannoula, Geraldo F. Oliveira, and Onur Mutlu, “*Benchmarking a New Paradigm: Experimental Analysis and Characterization of a Real Processing-in-Memory System*.” IEEE Access, 2022.
17. Juan Gómez-Luna, Yuxin Guo, Sylvan Brocard, Julien Legriel, Remy Cimadomo, Geraldo F. Oliveira, Gagandeep Singh, Onur Mutlu, “*Machine Learning Training on a Real Processing-in-Memory System*,” in ISVLSI, 2022.
18. Amirali Boroumand, Saugata Ghose, Geraldo F. Oliveira, and Onur Mutlu, “*Polynesia: Enabling High-Performance and Energy-Efficient Hybrid Transactional/Analytical Databases with Hardware/Software Co-Design*,” in ICDE, 2022.
19. Minesh Patel, Geraldo F. de Oliveira, and Onur Mutlu, “*HARP: Practically and Effectively Identifying Uncorrectable Errors in Memory Chips That Use On-Die Error-Correcting Codes*,” in MICRO, 2021.

20. Amirali Boroumand, Saugata Ghose, Berkin Akin, Ravi Narayanaswami, Geraldo F. Oliveira, Xiaoyu Ma, Eric Shiu, and Onur Mutlu, “*Google Neural Network Models for Edge Devices: Analyzing and Mitigating Machine Learning Inference Bottlenecks*,” in PACT, 2021.
21. Nastaran Hajinazar, Pratyush Patel, Minesh Patel, Konstantinos Kanellopoulos, Saugata Ghose, Rachata Ausavarungnirun, Geraldo F. Oliveira, Jonathan Appavoo, Vivek Seshadri, and Onur Mutlu, “*The Virtual Block Interface: A Flexible Alternative to the Conventional Virtual Memory Framework*,” in ISCA, 2020.
22. Gagandeep Singh, Juan Gomez-Luna, Giovanni Mariani, Geraldo F. Oliveira, Stefano Corda, Sander Stujik, Onur Mutlu, and Henk Corporaal, “*NAPEL: Near-Memory Computing Application Performance Prediction via Ensemble Learning*,” in DAC, 2019.
23. Michael G Jordan, Marcelo Brandalero, Guilherme M Malfatti, Geraldo F. Oliveira, Arthur F Lorenzon, Bruno C da Silva, Luigi Carro, Mateus B Rutzig, and Antonio C. S. Beck, “*Data Clustering for Efficient Approximate Computing*,” Design Automation for Embedded Systems, 2019.
24. Marcelo Brandalero, Guilherme Meneguzzi Malfatti, Geraldo F. Oliveira, Leonardo Almeida Da Silveira, Larissa Rozales Gonçalves, Bruno Castro Da Silva, Luigi Carro, and Antonio C. S. Beck, “*Efficient Local Memory Support for Approximate Computing*,” in SBESC, 2018.
25. Paulo C Santos, Geraldo F. Oliveira, João P. Lima, Marco AZ Alves, Luigi Carro, and Antonio C. S. Beck, “*Processing in 3D Memories to Speed Up Operations on Complex Data Structures*,” in DATE, 2018.
26. Paulo C Santos, Geraldo F. Oliveira, Diego G Tomé, Marco AZ Alves, Eduardo C Almeida, and Luigi Carro, “*Operand Size Reconfiguration for Big Data Processing-in-Memory*,” in DATE, 2017.

Appendix C

Complete List of Application Functions, Representative Functions, and Evaluated Applications in DAMOV

C.1 Application Functions in the DAMOV Benchmark Suite

We present the list of application functions in each one of the six classes of data movement bottlenecks we identify using our new methodology.

Our benchmark suite is composed of 144 different application functions, collected from 74 different applications. These applications belong to a different set of previously published and widely used benchmark suites. In total, we collect applications from 16 benchmark suites, including: BWA [1355], Chai [1139], Darknet [1154], GASE [1148], Hardware Effects [1356], Hashjoin [1149], HPCC [1146], HPCG [1147], Ligra [1152], PARSEC [1075], Parboil [1141], PolyBench [1268], Phoenix [4], Rodinia [1142], SPLASH-2 [1144], STREAM [1145]. The 144 application functions that are part of DAMOV are listed across six tables, each designating one of the six classes we identify in Section 4.3.3:

- Table C.1 lists application functions in Class 1a, i.e., that are DRAM bandwidth-bound (characterized in Section 4.3.3);
- Table C.2 lists application functions in Class 1b, i.e., that are DRAM latency-bound (characterized in Section 4.3.3);
- Table C.3 lists application functions in Class 1c, i.e., that are bottlenecked by the available L1/L2 cache capacity (characterized in Section 4.3.3);

- Table C.4 lists application functions in Class 2a, i.e., that are bottlenecked by L3 cache contention (characterized in Section 4.3.3);
- Table C.5 lists application functions in Class 2b, i.e., that are bottlenecked by L1 cache size (characterized in Section 4.3.3);
- Table C.6 lists application functions in Class 2c, i.e., that are compute-bound (characterized in Section 4.3.3).

In each table we list the benchmark suite, the application name, and the function name. We also list the input size/problem size we use to evaluate each application function.

Table C.1: List of application functions in Class 1a.

Class	Suite	Benchmark	Function	Input Set/ Problem Size	Representative Function?
1a	Chai [1139]	Transpose	cpu	-m 1024 -n 524288	No
1a	Chai [1139]	Vector Pack	run_cpu_threads	-m 268435456 -n 16777216	No
1a	Chai [1139]	Vector Unpack	run_cpu_threads	-m 268435456 -n 16777216	No
1a	Darknet [1154]	Yolo	gemm	ref	Yes
1a	Hardware Effects [1356]	Bandwidth Saturation - Non Temporal	main	ref	No
1a	Hardware Effects [1356]	Bandwidth Saturation - Temporal	main	ref	No
1a	Hashjoin [1149]	NPO	knuth	-r 12800000 -s 12000000 -x 12345 -y 54321	No
1a	Hashjoin [1149]	NPO	ProbeHashTable	-r 12800000 -s 12000000 -x 12345 -y 54321	Yes
1a	Hashjoin [1149]	PRH	knuth	-r 12800000 -s 12000000 -x 12345 -y 54321	No
1a	Hashjoin [1149]	PRH	lock	-r 12800000 -s 12000000 -x 12345 -y 54321	No
1a	Hashjoin [1149]	PRHO	knuth	-r 12800000 -s 12000000 -x 12345 -y 54321	No
1a	Hashjoin [1149]	PRHO	radix	-r 12800000 -s 12000000 -x 12345 -y 54321	No
1a	Hashjoin [1149]	PRO	knuth	-r 12800000 -s 12000000 -x 12345 -y 54321	No
1a	Hashjoin [1149]	PRO	parallel	-r 12800000 -s 12000000 -x 12345 -y 54321	No
1a	Hashjoin [1149]	PRO	radix	-r 12800000 -s 12000000 -x 12345 -y 54321	No
1a	Hashjoin [1149]	RJ	knuth	-r 12800000 -s 12000000 -x 12345 -y 54321	No
1a	Ligra [1152]	Betweenness Centrality	edgeMapSparse	rMat	No
1a	Ligra [1152]	Breadth-First Search	edgeMapSparse	rMat	No
1a	Ligra [1152]	Connected Components	compute	rMat	No
1a	Ligra [1152]	Connected Components	compute	USA	No
1a	Ligra [1152]	Connected Components	edgeMapDense	USA	No
1a	Ligra [1152]	Connected Components	edgeMapSparse	USA	Yes
1a	Ligra [1152]	K-Core Decomposition	compute	rMat	No
1a	Ligra [1152]	K-Core Decomposition	compute	USA	No
1a	Ligra [1152]	K-Core Decomposition	edgeMapDense	USA	No
1a	Ligra [1152]	K-Core Decomposition	edgeMapSparse	rMat	No
1a	Ligra [1152]	Maximal Independent Set	compute	rMat	No
1a	Ligra [1152]	Maximal Independent Set	compute	USA	No
1a	Ligra [1152]	Maximal Independent Set	edgeMapDense	USA	No
1a	Ligra [1152]	Maximal Independent Set	edgeMapSparse	rMat	No
1a	Ligra [1152]	Maximal Independent Set	edgeMapSparse	USA	No
1a	Ligra [1152]	PageRank	compute	rMat	No
1a	Ligra [1152]	PageRank	compute	USA	No
1a	Ligra [1152]	PageRank	edgeMapDense	USA	Yes
1a	Ligra [1152]	Radii	compute	rMat	No
1a	Ligra [1152]	Radii	compute	USA	No
1a	Ligra [1152]	Radii	edgeMapSparse	USA	No
1a	Ligra [1152]	Triangle Count	edgeMapDense	rMat	Yes
1a	SPLASH-2 [1144]	Oceancp	relax	simlarge	No
1a	SPLASH-2 [1144]	Oceanncp	relax	simlarge	No
1a	STREAM [1145]	Add	Add	50000000	Yes
1a	STREAM [1145]	Copy	Copy	50000000	Yes
1a	STREAM [1145]	Scale	Scale	50000000	Yes
1a	STREAM [1145]	Triad	Triad	50000000	Yes

Table C.2: List of application functions in Class 1b.

Class	Suite	Benchmark	Function	Input Set/ Problem Size	Representative Function?
1b	Chai [1139]	Canny Edge Detection	gaussian	ref	No
1b	Chai [1139]	Canny Edge Detection	supression	ref	No
1b	Chai [1139]	Histogram - input partition	run_cpu_threads	ref	Yes
1b	Chai [1139]	Select	run_cpu_threads	-n 67108864	No
1b	GASE [1148]	FastMap	2occ4	Wg2	No
1b	GASE [1148]	FastMap	occ4	Wg2	No
1b	Hashjoin [1149]	PRH	HistogramJoin	-r 12800000 -s 12000000 -x 12345 -y 54321	Yes
1b	Phoenix [4]	Linear Regression	linear_regression_map	key_file_500MB	No
1b	Phoenix [4]	PCA	main	ref	No
1b	Phoenix [4]	String Match	string_match_map	key_file_500MB	Yes
1b	PolyBench [1268]	linear-algebra	lu	LARGE_DATASET	Yes
1b	Rodinia [1142]	Kmeans	euclidDist	819200.txt	No
1b	Rodinia [1142]	Kmeans	find	819200.txt	No
1b	Rodinia [1142]	Kmeans	main	819200.txt	No
1b	Rodinia [1142]	Streamcluster	pengain	ref	No
1b	SPLASH-2 [1144]	Oceanpcp	slave2	simlarge	Yes

Table C.3: List of application functions in Class 1c.

Class	Suite	Benchmark	Function	Input Set/ Problem Size	Representative Function?
1c	BWA [1355]	Align	bwa_aln_core	Wg1	No
1c	Chai [1139]	Breadth-First Search	comp	USA-road-d	No
1c	Chai [1139]	Breadth-First Search	fetch	USA-road-d	No
1c	Chai [1139]	Breadth-First Search	load	USA-road-d	No
1c	Chai [1139]	Breadth-First Search	run_cpu_threads	USA-road-d	No
1c	Chai [1139]	Canny Edge Detection	hystresis	ref	No
1c	Chai [1139]	Canny Edge Detection	sobel	ref	No
1c	Chai [1139]	Histogram - output partition	run_cpu_threads	ref	No
1c	Chai [1139]	Padding	run_cpu_threads	-m 10000 -n 9999	Yes
1c	Chai [1139]	Select	fetch	-n 67108864	No
1c	Chai [1139]	Stream Compaction	run_cpu_threads	ref	No
1c	Darknet [1154]	Resnet	gemm	ref	Yes
1c	Hashjoin [1149]	NPO	lock	-r 12800000 -s 12000000 -x 12345 -y 54321	No
1c	Ligra [1152]	BFS-Connected Components	edgeMapSparse	rMat	No
1c	Ligra [1152]	Triangle Count	compute	rMat	No
1c	Ligra [1152]	Triangle Count	compute	USA	No
1c	Ligra [1152]	Triangle Count	edgeMapDense	USA	No
1c	PARSEC [1075]	Blackscholes	BlkSchlsEqEuroNoDiv	simlarge	No
1c	PARSEC [1075]	Fluidaminate	ProcessCollision2MT	simlarge	Yes
1c	PARSEC [1075]	Streamcluster	DistL2Float	simlarge	No
1c	Rodinia [1142]	Myocyte	find	1000000	No
1c	Rodinia [1142]	Myocyte	master	1000000	No

Table C.4: List of application functions in Class 2a.

Class	Suite	Benchmark	Function	Input Set/ Problem Size	Representative Function?
2a	HPCC [1146]	RandomAccess	main	ref	No
2a	HPCC [1146]	RandomAccess	update	ref	No
2a	Ligra [1152]	Betweenness Centrality	Compute	rMat	No
2a	Ligra [1152]	Betweenness Centrality	Compute	USA	No
2a	Ligra [1152]	Betweenness Centrality	edgeMapDense	rMat	No
2a	Ligra [1152]	Betweenness Centrality	*edgeMapSparse	USA	Yes
2a	Ligra [1152]	BFS-Connected Components	Compute	rMat	No
2a	Ligra [1152]	BFS-Connected Components	Compute	USA	No
2a	Ligra [1152]	BFS-Connected Components	edgeMapSparse	USA	Yes
2a	Ligra [1152]	Breadth-First Search	compute	rMat	No
2a	Ligra [1152]	Breadth-First Search	compute	USA	No
2a	Ligra [1152]	Breadth-First Search	edgeMapDense	rMat	No
2a	Ligra [1152]	Breadth-First Search	edgeMapSparse	USA	Yes
2a	Ligra [1152]	Connected Components	edgeMapDense	rMat	No
2a	Ligra [1152]	Maximal Independent Set	edgeMapDense	rMat	No
2a	Ligra [1152]	PageRank	edgeMapDense(Rmat)	rMat	No
2a	Phoenix [4]	WordCount	main	word_100MB	No
2a	PolyBench [1268]	linear-algebra	gramschmidt	LARGE_DATASET	Yes
2a	Rodinia [1142]	CFD Solver	main	fvcorr.donn.193K	No
2a	SPLASH-2 [1144]	FFT2	Reverse	simlarge	Yes
2a	SPLASH-2 [1144]	FFT2	Transpose	simlarge	Yes
2a	SPLASH-2 [1144]	Oceanncp	jacobcalc	simlarge	No
2a	SPLASH-2 [1144]	Oceanncp	laplaccalc	simlarge	No
2a	SPLASH-2 [1144]	Oceanncp	jacobcalc	simlarge	Yes
2a	SPLASH-2 [1144]	Oceanncp	laplaccalc	simlarge	Yes
2a	SPLASH-2 [1144]	Oceanncp	slave2	simlarge	No

Table C.5: List of application functions in Class 2b.

Class	Suite	Benchmark	Function	Input Set/ Problem Size	Representative Function?
2b	Chai [1139]	Bezier Surface	main_thread	ref	Yes
2b	Hardware Effects [1356]	False Sharing - Isolated	main	ref	No
2b	PolyBench [1268]	convolution	convolution-2d	LARGE_DATASET	No
2b	PolyBench [1268]	linear-algebra	gemver	LARGE_DATASET	Yes
2b	SPLASH-2 [1144]	Lucb	Bmod	simlarge	Yes
2b	SPLASH-2 [1144]	Radix	slave2	simlarge	Yes

Table C.6: List of application functions in Class 2c.

Class	Suite	Benchmark	Function	Input Set/ Problem Size	Representative Function?
2c	BWA [1355]	Align	bwa_aln_core	Wg2	No
2c	Chai [1139]	Transpose	run_cpu_threads	-m 1024 -n 524288	No
2c	Darknet [1154]	Alexnet	gemm	ref	No
2c	Darknet [1154]	vgg16	gemm	ref	No
2c	Hardware Effects [1356]	False Sharing - Shared	main	ref	No
2c	HPCG [1147]	HPCG	ComputePrologation	ref	Yes
2c	HPCG [1147]	HPCG	ComputeRestriction	ref	Yes
2c	HPCG [1147]	HPCG	ComputeSPMV	ref	Yes
2c	HPCG [1147]	HPCG	ComputeSYMGS	ref	Yes
2c	Ligra [1152]	K-Core Decomposition	edgeMapDense	rMat	No
2c	Ligra [1152]	Radii	edgeMapSparse	rMat	No
2c	Parboil [1141]	Breadth-First Search	BFS_CPU	ref	No
2c	Parboil [1141]	MRI-Gridding	CPU_kernels	ref	No
2c	Parboil [1141]	Stencil	cpu_stencil	ref	No
2c	Parboil [1141]	Two Point Angular Correlation Function	doCompute	ref	No
2c	PARSEC [1075]	Bodytrack	FilterRow	ref	No
2c	PARSEC [1075]	Ferret	DistL2Float	ref	Yes
2c	Phoenix [4]	Kmeans	main	ref	No
2c	PolyBench [1268]	linear-algebra	3mm	LARGE_DATASET	Yes
2c	PolyBench [1268]	linear-algebra	doitgen	LARGE_DATASET	Yes
2c	PolyBench [1268]	linear-algebra	gemm	LARGE_DATASET	Yes
2c	PolyBench [1268]	linear-algebra	symm	LARGE_DATASET	Yes
2c	PolyBench [1268]	stencil	fdtd-apml	LARGE_DATASET	Yes
2c	Rodinia [1142]	Back Propagation	adjustweights	134217728	No
2c	Rodinia [1142]	Back Propagation	layerfoward	134217728	No
2c	Rodinia [1142]	Breadth-First Search	main	graph1M_6	Yes
2c	Rodinia [1142]	Needleman-Wunsch	main	32768	Yes
2c	Rodinia [1142]a	Srad	FIN	ref	No
2c	SPLASH-2 [1144]	Barnes	computeForces	simlarge	No
2c	SPLASH-2 [1144]	Barnes	gravsub	simlarge	No

C.2 Representative Application Functions

Table C.7: 44 representative application functions studied in detail in this work.

Suite	Benchmark	Function	Short Name	Class	%
Chai [1139]	Bezier Surface	Bezier	CHABsBez	2b	100
	Histogram	Histogram	CHAHsti	1b	100
	Padding	Padding	CHAOpad	1c	75.1
Darknet [1154]	Resnet 152	gemm_nn	DRKRes	1c	95.2
	Yolo	gemm_nn	DRKYolo	1a	97.1
Hashjoin [1149]	NPO	ProbeHashTable	HSJNPO	1a	47.8
	PRH	HistogramJoin	HSJPRH	1b	53.1
HPCG [1147]	HPCG	ComputeProlongation	HPGProl	2c	34.3
	HPCG	ComputeRestriction	HPGRes	2c	42.1
	HPCG	ComputeSPMV	HPGSpm	2c	30.5
	HPCG	ComputeSYMGS	HPGSyms	2c	63.6
Ligra [1152]	Betweenness Centrality	EdgeMapSparse (USA [1156])	LIGBcEms	2a	78.9
	Breadth-First Search	EdgeMapSparse (USA)	LIGBfsEms	2a	67.0
	BFS-Connected Components	EdgeMapSparse (USA)	LIGBfscEms	2a	68.3
	Connected Components	EdgeMapSparse (USA)	LIGCompEms	1a	25.6
	PageRank	EdgeMapDense (USA [1156])	LIGPrkEmd	1a	57.2
	Radii	EdgeMapSparse (USA)	LIGRadiEms	1a	67.0
	Triangle	EdgeMapDense (Rmat)	LIGTriEmd	1a	26.7
PARSEC [1075]	Ferret	DistL2Float	PRSFerr	2c	18.6
	Fluidaminate	ProcessCollision2MT	PRSFlu	1c	23.9
Phoenix [4]	Linear Regression	linear_regression_map	PHELinReg	1b	76.2
	String Matching	string_match_map	PHEStrMat	1b	38.3
PolyBench [1268]	Linear Algebra	3 Matrix Multiplications	PLY3mm	2c	100.0
	Linear Algebra	Multi-resolution analysis kernel	PLYDoitgen	2c	98.3
	Linear Algebra	Matrix-multiply $C=\alpha.A.B+\beta.C$	PLYgemm	2c	99.7
	Linear Algebra	Vector Mult. and Matrix Addition	PLYgemver	2b	44.4
	Linear Algebra	Gram-Schmidt decomposition	PLYGramSch	2a	100.0
	Linear Algebra	LU decomposition	PLYalu	1b	100.0
	Linear Algebra	Symmetric matrix-multiply	PLYSymm	2c	99.9
	Stencil	2D Convolution	PLYcon2d	2b	100.0
	Stencil	2-D Finite Different Time Domain	PLYdtd	2c	39.8
Rodinia [1357]	BFS	BFSGraph	RODBfs	2c	100.0
	Needleman-Wunsch	runTest	RODNw	2c	84.9
SPLASH-2 [1144]	FFT	Reverse	SPLFftRev	2a	12.7
	FFT	Transpose	SPLFftTra	2a	8.0
	Lucb	Bmod	SPLLucb	2b	77.6
	Oceanncp	jacobcalc	SPLOcnpJac	2a	30.7
	Oceanncp	laplacalc	SPLOcnpLap	2a	23.4
	Oceancp	slave2	SPLOcpSlave	1b	24.4
	Radix	slave_sort	SPLRad	2b	41.1
	Add	Add	STRAdd	1a	98.4
STREAM [1145]	Copy	Copy	STRCpy	1a	98.3
	Scale	Scale	STRSca	1a	97.5
	Triad	Triad	STRTriad	1a	99.1

* Short names are encoded as XXXYyyZzz, where XXX is the source application suite, Yyy is the application name, and Zzz is the function (if more than one per benchmark). For graph processing applications from Ligra, we test two different input graphs, so we append the graph name to the short benchmark name as well. The % column indicates the percentage of clock cycles that the function consumes as a fraction of the execution time of the entire benchmark.

C.3 Complete List of Evaluated Applications

Table C.8: List of the evaluated 345 applications.

Benchmark Suite	Application	Benchmark Suite	Application	Benchmark Suite	Application
ArtraCFD [1358]	ArtraCFD	HPCG [1147]	Global Dot Product	SD-VBS - Vision [1359]	disparity
blasr [1360]	Long read aligner		Multigrid preconditione		localization
BWA [1361]	aln		Sparse Matrix Vector Multiplication (SpMV)		mser
	fastmap		Symmetric Gauss-Seidel smoother (SymGS)		multi_ncut
Chai [1139]	BFS	IMPICA Workloads [155]	Vector Update		pca
	BS		btree		sift
	CEDD		hashtable		stitch
	HSTI		llubenchmark		svm
	HSTO	libvpx [1362]	VP8		texture_synthesis
	OOPPAD		VP9		tracking
	OOPTRNS		BC	sort-merge-joins [1363]	m-pass
	SC		BellmanFord		m-way
	SELECT	Ligra [1152]	BFS		400.perlbenc
	TRNS		BFS-Bitvector		401.bzip2
	VPACK		BFS-CC		403.gcc
	VUPACK		CF		410.bwaves
clstm [1364]	clstm		Components		416.gamess
CombBLAS [1365]	BetwCent		KCore		429.mcf
	BipartiteMatchings		MIS		433.milc
	CC		PageRank		434.zeusmp
	DirOptBFS		PageRankDelta		435.gromacs
	FilteredBFS	Metagraph [1366]	Radii		436.cactusADM
	FilteredMIS		Triangle		437.leslie3d
	MCL3D		annotate		444.namd
	Ordering/RCM		classify		445.gobmk
	TopDownBFS	MKL [1367]	ASUM	SPEC CPU2006 [1267]	447.dealll
	AMG2013		AXPY		450.soplex
CORAL [1140]	CAM-SE		DOT		453.povray
	Graph500		GEMM		454.calculix
	HACC		GEMV		456.hmmer
	Hash	Parboil [1141]	mri-q		458.sjeng
	homme1_3_6		BFS		459.GemsFDTD
	Integer Sort		cutcp		462.libquantum
	KMI		histo		464.h264ref
	LSMS		lbn		465.tonto
	LULESH		mri-gridding		470.lbm
	MCB		sad		471.omnetpp
	miniFE		sgemm		473.astar
	Nekbone	PARSEC [1075]	spmv		481.wrf
	QBOX		stencil		482.sphinx3
	SNAP		tpacf		483.xalancbmk
	SPECint2006*peak*		blackscholes		500.perlbenc_r
	UMT2013		bodytrack		502.gcc_r
Darknet [1154]	AlexNet		canneal		503.bwaves_r
	Darknet19		dedup		505.mcf_r
	Darknet53		facesim		507.cactuBSSN_r
	Densenet 201		ferret		508.namd_r
	Extraction		fluidanimate		510.parest_r
	Resnet 101		fraqmine		511.povray_r
	Resnet 152		raytrace		519.lbm_r
	Resnet 18		streamcluster		520.omnetpp_r
	Resnet 34		swaptions		521.wrf_r
	Resnet 50		vips		523.xalancbmk_r
	ResNeXt 101	Phoenix [4]	x264		525.x264_r
	ResNext 152		histogram		526.blender_r
	ResNeXt50		kmeans		527.cam4_r
	VGG-16		linear-regression		531.deepsjeng_r
DBT-5 [1368]	Yolo		matrix multiply		538.imagick_r
	TPC-E		pca		541.leela_r
DBx1000 [1369]	TPCC DL_DETECT	SPEC CPU2017 [5]	string_match		544.nab_r
	TPCC HEKATON		word_count		548.exchange2_r
	TPCC NO_WAIT		2mm		549.fotonik3d_r
	TPCC SILO		3mm		554.roms_r
	TPCC TICTOC		atax		557.xz_r
	YCSB DL_DETECT		bigc		600.perlbenc_s
	YCSB HEKATON		cholesky		602.gcc_s
	YCSB NO_WAIT		convolution-2d		603.bwaves_s
	YCSB SILO		convolution-3d		605.mcf_s
	YCSB TICTOC		correlation		607.cactuBSSN_s
DLRM [796]	RM1-large [595]	PolyBench [1268]	covariance		619.lbm_s
	RM1-small [595]		doitgen		620.omnetpp_s
	RM2-large [595]		durbin		621.wrf_s
	RM2-small [595]		fdtd-apm		623.xalancbmk_s
GASE [1148]	FastMap		gemm		625.x264_s
	gale_aln		gemver		627.cam4_s
GraphMat [1151]	BFS		gramschmidt		628.pop2_s
	DeltaStepping		gramschmidt		631.deepsjeng_s
	Incremental PageRank		lu		638.imagick_s
	LDA		lu		641.leela_s
	PageRank		mvt		644.nab_s
	SDG		symm		648.exchange2_s
	SSSP		syr2k		649.fotonik3d_s
	Topological Sort		syrk		654.roms_s
	Triangle Counting		trmm		657.xz_s

Benchmark Suite	Application	Benchmark Suite	Application	Benchmark Suite	Application	
Hardware Effects [1356]	4k aliasing	resectionvolume [1370]	resectionvolume	SPLASH-2 [1144]	barnes	
	bandwidth saturation non-temporal		b+tree		cholesky	
	bandwidth saturation temporal		backprop		fft	
	branch misprediction sort		bfs		fmm	
	branch misprediction unsort		cfid		lu_cb	
	branch target misprediction		heartwall		lu_ncb	
	cache conflicts		hotspot		ocean_cp	
	cache/memory hierarchy bandwidth		hotspot3D		ocean_ncp	
	data dependencies		kmeans		radiosity	
	denormal floating point numbers		lavaMD		radix	
	denormal floating point numbers flush		leukocyte		raytrace	
	DRAM refresh interval		lud		volrend	
	false sharing		mummergepu		water_nsquared	
	hardware prefetching		myocyte		water_spatial	
	hardware prefetching shuffle		nn	Tailbench [1371]	img-dnn	
	hardware store elimination		nw		masstree	
	memory-bound program		particlefilter		moses	
	misaligned accesses		pathfinder		shore	
	non-temporal stores		srad		silo	
	software prefetching		streamcluster		specjbb	
	store buffer capacity		lda		sphinx	
	write combining		libl		xapian	
Hashjoin [1149]	NPO	SD-VBS- Cortex [1359]	me	WHISPER [1372]	ctree	
	PRH		pca		echo	
	PRHO		rbm		exim	
	PRO		sphinx		hashmap	
	RJ		srr		memcached	
HPCC [1146]	RandomAccesses		svd		nfs	
					redis	
					sql	
					tpcc	
					vacation	
					ycsb	
				ZipML [1373]	SGD	
				Stream [1145]	STREAM	

Bibliography

- [1] Kevin K Chang, “Understanding and Improving the Latency of DRAM-Based Memory Systems,” Ph.D. dissertation, Carnegie Mellon University, 2017.
- [2] Andrew D Booth, “A Signed Binary mMultiplication Technique,” *The Quarterly Journal of Mechanics and Applied Mathematics*, 1951.
- [3] Anatolii Alekseevich Karatsuba and Yu P Ofman, “Multiplication of Many-Digital Numbers by Automatic Computers,” in *USSR Academy of Sciences*, 1962.
- [4] R. M. Yoo, A. Romano, and C. Kozyrakis, “Phoenix Rebirth: Scalable MapReduce on a Large-Scale Shared-Memory System,” in *IISWC*, 2009.
- [5] Standard Performance Evaluation Corp., “SPEC CPU2017 Benchmarks,” <http://www.spec.org/cpu2017/>.
- [6] Juan Gómez-Luna, Izzat El Hajj, Ivan Fernandez, Christina Giannoula, Geraldo F Oliveira, and Onur Mutlu, “Benchmarking a New Paradigm: Experimental Analysis and Characterization of a Real Processing-in-Memory System,” *IEEE Access*, 2022.
- [7] Onur Mutlu, “Memory Scaling: A Systems Architecture Perspective,” in *IMW*, 2013.
- [8] Onur Mutlu and Lavanya Subramanian, “Research Problems and Opportunities in Memory Systems,” *SUPERFRI*, 2014.
- [9] Jeffrey Dean and Luiz André Barroso, “The Tail at Scale,” *CACM*, 2013.
- [10] Svilen Kanev, Juan Pablo Darago, Kim Hazelwood, Parthasarathy Ranganathan, Tipp Moseley, Gu-Yeon Wei, and David Brooks, “Profiling a Warehouse-Scale Computer,” in *ISCA*, 2015.
- [11] Michael Ferdman, Almutaz Adileh, Onur Kocberber, Stavros Volos, Mohammad Alisafae, Djordje Jevdjic, Cansu Kaynak, Adrian Daniel Popescu, Anastasia Ailamaki, and Babak Falsafi, “Clearing the Clouds: A Study of Emerging Scale-Out Workloads on Modern Hardware,” in *ASPLOS*, 2012.
- [12] Lei Wang, Jianfeng Zhan, Chunjie Luo, Yuqing Zhu, Qiang Yang, Yongqiang He, Wanling Gao, Zhen Jia, Yingjie Shi, Shujie Zhang *et al.*, “BigDataBench: A Big Data Benchmark Suite from Internet Services,” in *HPCA*, 2014.

- [13] Amirali Boroumand, Saugata Ghose, Youngsok Kim, Rachata Ausavarungnirun, Eric Shiu, Rahul Thakur, Daehyun Kim, Aki Kuusela, Allan Knies, Parthasarathy Ranganathan *et al.*, “Google Workloads for Consumer Devices: Mitigating Data Movement Bottlenecks,” in *ASPLOS*, 2018.
- [14] Amirali Boroumand, Saugata Ghose, Berkin Akin, Ravi Narayanaswami, Geraldo F Oliveira, Xiaoyu Ma, Eric Shiu, and Onur Mutlu, “Google Neural Network Models for Edge Devices: Analyzing and Mitigating Machine Learning Inference Bottlenecks,” in *PACT*, 2021.
- [15] Amirali Boroumand, Saugata Ghose, Berkin Akin, Ravi Narayanaswami, Geraldo F Oliveira, Xiaoyu Ma, Eric Shiu, and Onur Mutlu, “Google Neural Network Models for Edge Devices: Analyzing and Mitigating Machine Learning Inference Bottlenecks,” arXiv:2109.14320 [cs.AR], 2021.
- [16] Onur Mutlu, Saugata Ghose, Juan Gómez-Luna, and Rachata Ausavarungnirun, “Enabling Practical Processing in and Near Memory for Data-Intensive Computing,” in *DAC*, 2019.
- [17] Onur Mutlu, Saugata Ghose, Juan Gómez-Luna, and Rachata Ausavarungnirun, “Processing Data Where It Makes Sense: Enabling In-Memory Computation,” *MicPro*, 2019.
- [18] Onur Mutlu, “Intelligent Architectures for Intelligent Machines,” in *VLSI-DAT*, 2020.
- [19] Saugata Ghose, Amirali Boroumand, Jeremie S Kim, Juan Gómez-Luna, and Onur Mutlu, “Processing-in-Memory: A Workload-Driven Perspective,” *IBM JRD*, 2019.
- [20] Mohammed Alser, Zülal Bingöl, Damla Senol Cali, Jeremie Kim, Saugata Ghose, Can Alkan, and Onur Mutlu, “Accelerating Genome Analysis: A Primer on an Ongoing Journey,” *IEEE Micro*, 2020.
- [21] Damla Senol Cali, Gurpreet S Kalsi, Zülal Bingöl, Can Firtina, Lavanya Subramanian, Jeremie S Kim, Rachata Ausavarungnirun, Mohammed Alser, Juan Gomez-Luna, Amirali Boroumand *et al.*, “GenASM: A High-Performance, Low-Power Approximate String Matching Acceleration Framework for Genome Sequence Analysis,” in *MICRO*, 2020.
- [22] Skanda Koppula, Lois Orosa, A Giray Yağlıkçı, Roknoddin Azizi, Taha Shahroodi, Konstantinos Kanellopoulos, and Onur Mutlu, “EDEN: Enabling Energy-Efficient, High-Performance Deep Neural Network Inference Using Approximate DRAM,” in *MICRO*, 2019.
- [23] Konstantinos Kanellopoulos, Nandita Vijaykumar, Christina Giannoula, Roknoddin Azizi, Skanda Koppula, Nika Mansouri Ghiasi, Taha Shahroodi, Juan Gomez-Luna, and Onur Mutlu, “SMASH: Co-Designing Software Compression and Hardware-Accelerated Indexing for Efficient Sparse Matrix Operations,” in *MICRO*, 2019.
- [24] Geraldo F. Oliveira, Juan Gómez-Luna, Lois Orosa, Saugata Ghose, Nandita Vijaykumar, Ivan Fernandez, Mohammad Sadrosadati, and Onur Mutlu, “DAMOV: A New Methodology and Benchmark Suite for Evaluating Data Movement Bottlenecks,” *IEEE Access*, 2021.

- [25] Geraldo F. Oliveira, Juan Gómez-Luna, Lois Orosa, Saugata Ghose, Nandita Vijaykumar, Ivan Fernandez, Mohammad Sadrosadati, and Onur Mutlu, “DAMOV: A New Methodology and Benchmark Suite for Evaluating Data Movement Bottlenecks,” arXiv:2105.03725 [cs.AR], 2021.
- [26] Geraldo F. Oliveira, “DAMOV: A New Methodology and Benchmark Suite for Evaluating Data Movement Bottlenecks,” https://people.inf.ethz.ch/omutlu/pub/DAMOV-Bottleneck-Analysis-and-DataMovement-Benchmarks_arxiv21-talk.pptx, video available at <https://youtu.be/GWideVyo0nM>, 2021, SAFARI Live Seminar, 22 July 2021.
- [27] O. Mutlu, “Processing Data Where It Makes Sense: Enabling In-Memory Computation,” <https://people.inf.ethz.ch/omutlu/pub/onur-MST-Keynote-EnablingInMemoryComputation-October-27-2017-unrolled-FINAL.pptx>, 2017, Keynote talk at MST.
- [28] O. Mutlu, “Processing Data Where It Makes Sense in Modern Computing Systems: Enabling In-Memory Computation,” <https://people.inf.ethz.ch/omutlu/pub/onur-GWU-EnablingInMemoryComputation-February-15-2019-unrolled-FINAL.pptx>, video available at <https://www.youtube.com/watch?v=oHqsNbxgdzM>, 2019, distinguished lecture at George Washington University.
- [29] O. Mutlu, “Processing Data Where It Makes Sense in Modern Computing Systems: Enabling In-Memory Computation,” <https://people.inf.ethz.ch/omutlu/pub/onur-ISSCC2019-talk.pptx>, 2019, Invited Talk at ISSCC Special Forum on “Intelligence at the Edge: How Can We Make Machine Learning More Energy Efficient?”, as part of the 2019 International Solid State Circuits Conference (ISSCC), San Francisco, CA, USA, February 2019.
- [30] O. Mutlu, “Processing Data Where It Makes Sense in Modern Computing Systems: Enabling In-Memory Computation,” <https://people.inf.ethz.ch/omutlu/pub/onur-GLSVLSI-KeynoteTalk-EnablingInMemoryComputation-May-10-2019-unrolled.pptx>, 2019, Keynote Talk at 29th ACM Great Lakes Symposium on VLSI (GLSVLSI), Washington, DC, USA, May 2019.
- [31] O. Mutlu, “Processing Data Where It Makes Sense in Modern Computing Systems: Enabling In-Memory Computation,” <https://people.inf.ethz.ch/omutlu/pub/onur-A-PPT-Keynote-EnablingInMemoryComputation-August-16-2019-unrolled.pptx>, video available at <https://www.youtube.com/watch?v=K0OcJxVhEw>, 2019, Keynote talk at International Symposium on Advanced Parallel Processing Technology (APPT), Tianjin, China, 16 August 2019.
- [32] O. Mutlu, “Processing Data Where It Makes Sense in Modern Computing Systems: Enabling In-Memory Computation,” <https://people.inf.ethz.ch/omutlu/pub/onur-ICC2019-Keynote-EnablingInMemoryComputation-November-19-2019-unrolled.pptx>, video available at https://www.youtube.com/watch?v=njX_14584Jw, 2019, Keynote talk at 37th IEEE International Conference on Computer Design (ICCD), Abu Dhabi, UAE, 19 November 2019.
- [33] G Narancic, Patrick Judd, D Wu, Islam Atta, M Elnacouzi, Jason Zebchuk, Jorge Albericio, N Enright Jerger, Andreas Moshovos, K Kutulakos *et al.*, “Evaluating the Memory System Behavior of Smartphone Workloads,” in *SAMOS*, 2014.

- [34] Grant Ayers, Jung Ho Ahn, Christos Kozyrakis, and Parthasarathy Ranganathan, "Memory Hierarchy for Web Search," in *HPCA*, 2018.
- [35] Zhen Jia, Jianfeng Zhan, Lei Wang, Chunjie Luo, Wanling Gao, Yi Jin, Rui Han, and Lixin Zhang, "Understanding Big Data Analytics Workloads on Modern Processors," *TPDS*, 2016.
- [36] S. Manegold, P. A. Boncz, and M. L. Kersten, "Optimizing database architecture for the new bottleneck: Memory access," *The VLDB Journal*, vol. 9, no. 3, December 2000.
- [37] Amir Gholami, Zhewei Yao, Sehoon Kim, Coleman Hooper, Michael W Mahoney, and Kurt Keutzer, "AI and Memory Wall," *IEEE Micro*, 2024.
- [38] Holger Stengel, Jan Treibig, Georg Hager, and Gerhard Wellein, "Quantifying Performance Bottlenecks of Stencil Computations Using the Execution-Cache-Memory Model," in *ISC*, 2015.
- [39] Zeshan Chishti and Berkin Akin, "Memory System Characterization of Deep Learning Workloads," in *MEMSYS*, 2019.
- [40] Douglas C Burger, James R Goodman, and Alain Kagi, "The Declining Effectiveness of Dynamic Caching for General-Purpose Microprocessors," University of Wisconsin-Madison, Tech. Rep. 1261, 1995.
- [41] Udit Gupta, Carole-Jean Wu, Xiaodong Wang, Maxim Naumov, Brandon Reagen, David Brooks, Bradford Cottel, Kim Hazelwood, Mark Hempstead, Bill Jia *et al.*, "The Architectural Implications of Facebook's DNN-based Personalized Recommendation," in *HPCA*, 2020.
- [42] Akshitha Sriraman, Abhishek Dhanotia, and Thomas F Wenisch, "SoftSKU: Optimizing Server Architectures for Microservice Diversity @Scale," in *ISCA*, 2019.
- [43] Mark Zhao, Niket Agarwal, Aarti Basant, Buğra Gedik, Satadru Pan, Mustafa Ozdal, Rakesh Komuravelli, Jerry Pan, Tianshu Bao, Haowei Lu *et al.*, "Understanding Data Storage and Ingestion for Large-Scale Deep Recommendation Model Training: Industrial Product," in *ISCA*, 2022.
- [44] Zhenyuan Ruan, Tong He, and Jason Cong, "{INSIDER}: Designing {In-Storage} Computing System for Emerging {High-Performance} Drive," in *ATC*, 2019.
- [45] Yu Gan and Christina Delimitrou, "The Architectural Implications of Cloud Microservices," *CAL*, 2018.
- [46] Akshitha Sriraman and Abhishek Dhanotia, "Accelerometer: Understanding Acceleration Opportunities for Data Center Overheads at Hyperscale," in *ASPLOS*, 2020.
- [47] Yifan Yuan, Jinghan Huang, Yan Sun, Tianchen Wang, Jacob Nelson, Dan RK Ports, Yipeng Wang, Ren Wang, Charlie Tai, and Nam Sung Kim, "RAMBDA: RDMA-Driven Acceleration Framework for Memory-Intensive μ s-Scale Datacenter Applications," in *HPCA*, 2023.

- [48] Christina Delimitrou and Christos Kozyrakis, “Amdahl’s Law for Tail Latency,” *CACM*, 2018.
- [49] Samuel Hsia, Udit Gupta, Mark Wilkening, Carole-Jean Wu, Gu-Yeon Wei, and David Brooks, “Cross-Stack Workload Characterization of Deep Recommendation Systems,” in *IISWC*, 2020.
- [50] Andrea Lottarini, Alex Ramirez, Joel Coburn, Martha A Kim, Parthasarathy Ranganathan, Daniel Stodolsky, and Mark Wachsler, “vbench: Benchmarking Video Transcoding in the Cloud,” in *ASPLOS*, 2018.
- [51] Kangjin Wang, Ying Li, Cheng Wang, Tong Jia, Kingsum Chow, Yang Wen, Yaoyong Dou, Guoyao Xu, Chuanjia Hou, Jie Yao *et al.*, “Characterizing Job Microarchitectural Profiles at Scale: Dataset and Analysis,” in *ICPP*, 2022.
- [52] Daniel Richins, Dharmisha Doshi, Matthew Blackmore, Aswathy Thulaseedharan Nair, Neha Pathapati, Ankit Patel, Brainard Daguman, Daniel Dobrijalowski, Ramesh Illickal, Kevin Long *et al.*, “Missing the Forest for the Trees: End-to-End AI Application Performance in Edge Data Centers,” in *HPCA*, 2020.
- [53] Sally A McKee, “Reflections on the Memory Wall,” in *CF*, 2004.
- [54] Milad Hashemi, Eiman Ebrahimi, Onur Mutlu, Yale N Patt *et al.*, “Accelerating Dependent Cache Misses with an Enhanced Memory Controller,” in *ISCA*, 2016.
- [55] Milad Hashemi, Onur Mutlu, and Yale N Patt, “Continuous Runahead: Transparent Hardware Acceleration for Memory Intensive Workloads,” in *MICRO*, 2016.
- [56] Junwhan Ahn, Sungpack Hong, Sungjoo Yoo, Onur Mutlu, and Kiyoun Choi, “A Scalable Processing-in-Memory Accelerator for Parallel Graph Processing,” in *ISCA*, 2015.
- [57] Junwhan Ahn, Sungjoo Yoo, Onur Mutlu, and Kiyoun Choi, “PIM-Enabled Instructions: A Low-Overhead, Locality-Aware Processing-in-Memory Architecture,” in *ISCA*, 2015.
- [58] Stephen W Keckler, William J Dally, Brucek Khailany, Michael Garland, and David Glasco, “GPUs and the Future of Parallel Computing,” *Micro, IEEE*, 2011.
- [59] M. V. Wilkes, “Slave Memories and Dynamic Storage Allocation,” *TEC*, 1965.
- [60] Norman P Jouppi, 1990.
- [61] Mark D Hill, “A Case for Direct-Mapped Caches,” *Computer*, 1988.
- [62] Gurindar S Sohi and Manoj Franklin, “High-Bandwidth Data Memory Systems for Superscalar Processors,” in *ASPLOS*, 1991.
- [63] Darrell Boggs, Aravindh Baktha, Jason Hawkins, Deborah T Marr, J Alan Miller, Patrice Roussel, Ronak Singhal, Bret Toll, and KS Venkatraman, “The Microarchitecture of the Intel Pentium 4 Processor on 90nm Technology,” *Intel Technology Journal*, 2004.
- [64] David B Papworth, “Tuning the Pentium Pro Microarchitecture,” *IEEE Micro*, 1996.

- [65] Ron Kalla, Balaram Sinharoy, William J Starke, and Michael Floyd, "POWER7: IBM's Next-Generation Server Processor," *IEEE Micro*, 2010.
- [66] Balaram Sinharoy, Ron Kalla, William J Starke, Hung Q Le, Robert Cargnoni, James A Van Norstrand, Bruce J Ronchetti, Jeffrey Stuecheli, Jens Leenstra, Guy L Guthrie *et al.*, "IBM POWER7 Multicore Server Processor," *IJRD*, 2011.
- [67] Balaram Sinharoy, JA Van Norstrand, Richard J Eickemeyer, Hung Q Le, Jens Leenstra, Dung Q Nguyen, B Konigsburg, K Ward, MD Brown, José E Moreira *et al.*, "IBM POWER8 Processor Core Microarchitecture," *IJRD*, 2015.
- [68] Dave Christie, "Developing the AMD-K5 Architecture," *IEEE Micro*, 1996.
- [69] Robert Cooksey, "Content-Sensitive Data Prefetching," Ph.D. dissertation, 2002.
- [70] Xiaotong Zhuang and Hsien-Hsin S. Lee, "A Hardware-Based Cache Pollution Filtering Mechanism for Aggressive Prefetches," in *ICPP-32*, 2003.
- [71] Sorin Iacobovici, Lawrence Spracklen, Sudarshan Kadamby, Yuan Chou, and Santosh G. Abraham, "Effective Stream-Based and Execution-Based Data Prefetching," in *ICS*, 2004.
- [72] Kyle J. Nesbit, Ashutosh S. Dhodapkar, and James E. Smith, "AC/DC: An Adaptive Data Cache Prefetcher," in *PACT*, 2004.
- [73] Ibrahim Hur and Calvin Lin, "Memory Prefetching Using Adaptive Stream Detection," in *MICRO*, 2006.
- [74] Rahul Bera, Konstantinos Kanellopoulos, Anant Nori, Taha Shahroodi, Sreenivas Subramoney, and Onur Mutlu, "Pythia: A Customizable Hardware Prefetching Framework using Online Reinforcement Learning," in *MICRO*, 2021.
- [75] Yasuo Ishii, Mary Inaba, and Kei Hiraki, "Access Map Pattern Matching for Data Cache Prefetch," in *ISC*, 2009.
- [76] John WC Fu, Janak H Patel, and Bob L Janssens, "Stride Directed Prefetching in Scalar Processors," in *MICRO*, 1992.
- [77] Tien-Fu Chen and Jean-Loup Baer, "Effective Hardware-Based Data Prefetching for High-Performance Processors," *TC*, 1995.
- [78] Mohammad Bakhshalipour, Pejman Lotfi-Kamran, and Hamid Sarbazi-Azad, "Domino Temporal Data Prefetcher," in *HPCA*, 2018.
- [79] Rahul Bera, Anant V Nori, Onur Mutlu, and Sreenivas Subramoney, "DSPatch: Dual Spatial Pattern Prefetcher," in *MICRO*, 2019.
- [80] José González and Antonio González, "Speculative Execution via Address Prediction and Data Prefetching," in *ICS*, 1997.
- [81] Eiman Ebrahimi, Onur Mutlu, Chang Joo Lee, and Yale N Patt, "Coordinated Control of Multiple Prefetchers in Multi-Core Systems," in *MICRO*, 2009.

- [82] Pei Cao, Edward W Felten, Anna R Karlin, and Kai Li, "A Study of Integrated Prefetching and Caching Strategies," in *SIGMETRICS*, 1995.
- [83] Mark J. Charney and Anthony P. Reeves, "Generalized Correlation-Based Hardware Prefetching," Cornell Univ., Tech. Rep., 1995.
- [84] Amir Roth and Gurindar S Sohi, "Effective Jump-Pointer Prefetching for Linked Data Structures," in *ISCA*, 1999.
- [85] Murali Annavaram, Jignesh M Patel, and Edward S Davidson, "Data Prefetching by Dependence Graph Precomputation," in *ISCA*, 2001.
- [86] Sam Ainsworth and Timothy M Jones, "Graph Prefetching Using Data Structure Knowledge," in *ICS*, 2016.
- [87] Anirudh Mohan Kaushik, Gennady Pekhimenko, and Hiren Patel, "Gretch: A Hardware Prefetcher for Graph Analytics," *TACO*, 2021.
- [88] Karthik Nilakant, Valentin Dalibard, Amitabha Roy, and Eiko Yoneki, "PrefEdge: SSD Prefetcher for Large-Scale Graph Traversal," in *SYSTOR*, 2014.
- [89] Mark Charney, "Correlation-Based Hardware Prefetching," Ph.D. dissertation, Cornell University, 1995.
- [90] Robert Cooksey, Stephan Jourdan, and Dirk Grunwald, "A Stateless, Content-Directed Data Prefetching Mechanism," in *ASPLOS*, 2002.
- [91] Doug Joseph and Dirk Grunwald, "Prefetching Using Markov Predictors," in *ISCA*, 1997.
- [92] Santhosh Srinath, Onur Mutlu, Hyesoon Kim, and Yale N Patt, "Feedback Directed Prefetching: Improving the Performance and Bandwidth-Efficiency of Hardware Prefetchers," in *HPCA*, 2007.
- [93] Eiman Ebrahimi, Onur Mutlu, and Yale N Patt, "Techniques for Bandwidth-Efficient Prefetching of Linked Data Structures in Hybrid Prefetching Systems," in *HPCA*, 2009.
- [94] Jamison D Collins, Hong Wang, Dean M Tullsen, Christopher Hughes, Yong-Fong Lee, Dan Lavery, and John P Shen, "Speculative Precomputation: Long-Range Prefetching of Delinquent Loads," in *ISCA*, 2001.
- [95] Mohammad Sadrosadati, Amirhossein Mirhosseini, Seyed Borna Ehsani, Hamid Sarbazi-Azad, Mario Drumond, Babak Falsafi, Rachata Ausavarungnirun, and Onur Mutlu, "LTRF: Enabling High-Capacity Register Files for GPUs via Hardware/Software Cooperative Register Prefetching," in *ASPLOS*, 2018.
- [96] Amir Roth, Andreas Moshovos, and Gurindar S. Sohi, "Dependence Based Prefetching for Linked Data Structures," in *ASPLOS*, 1998.
- [97] Mikko H. Lipasti, William J. Schmidt, Steven R. Kunkel, and Robert R. Roediger, "SPaid: Software Prefetching in Pointer- and Call-Intensive Environments," in *MICRO*, 1995.

- [98] Magnus Karlsson, Fredrik Dahlgren, and Per Stenström, "A Prefetching Technique for Irregular Accesses to Linked Data Structures," in *HPCA*, 2000.
- [99] Jamison D. Collins, Suleyman Sair, Brad Calder, and Dean M. Tullsen, "Pointer Cache Assisted Prefetching," in *MICRO*, 2002.
- [100] Zhigang Hu, Margaret Martonosi, and Stefanos Kaxiras, "TCP: Tag Correlating Prefetchers," in *HPCA*, 2003.
- [101] Xiangyao Yu, Christopher J. Hughes, Nadathur Satish, and Srinivas Devadas, "IMP: Indirect Memory Prefetcher," in *MICRO*, 2015.
- [102] Alan Jay Smith, "Sequential Program Prefetching in Memory Hierarchies," *Computer*, 1978.
- [103] David Kroft, "Lockup-Free Instruction Fetch/Prefetch Cache Organization," in *ISCA*, 1981.
- [104] R. L. Lee, P.-C. Yew, and D. H. Lawrie, "Data Prefetching in Shared Memory Multiprocessors," in *ICPP*, 1987.
- [105] William Y. Chen, Roger A. Bringmann, Scott A. Mahlke, Richard E. Hank, and James E. Siculo, "An Efficient Architecture for Loop Based Data Prefetching," in *MICRO*, 1992.
- [106] James E. Smith and W.-C. Hsu, "Prefetching in Supercomputer Instruction Caches," in *SC*, 1992.
- [107] Fredrik Dahlgren, Michel Dubois, and Per Stenström, "Sequential Hardware Prefetching in Shared-Memory Multiprocessors," *IPDS*, 1995.
- [108] Jim Pierce and Trevor Mudge, "Wrong-Path Instruction Prefetching," in *MICRO*, 1996.
- [109] Chun Xia and Josep Torrellas, "Instruction Prefetching of System Codes With Layout Optimized for Reduced Cache Misses," in *ISCA*, 1996.
- [110] Ando Ki and Alan E. Knowles, "Adaptive Data Prefetching Using Cache Information," in *SC*, 1997.
- [111] Chi-Keung Luk and Todd C. Mowry, "Cooperative Prefetching: Compiler and Hardware Support for Effective Instruction Prefetching in Modern Processors," in *MICRO*, 1998.
- [112] C. Zhang and S. A. McKee, "Hardware-Only Stream Prefetching and Dynamic Access Ordering," in *ICS*, 2000.
- [113] Onur Mutlu, Jared Stark, Chris Wilkerson, and Yale N Patt, "Runahead Execution: An Effective Alternative to Large Instruction Windows," *IEEE Micro*, 2003.
- [114] Onur Mutlu, Hyesoon Kim, and Yale N Patt, "Efficient Runahead Execution: Power-Efficient Memory Latency Tolerance," *IEEE Micro*, 2006.

- [115] Onur Mutlu, Hyesoon Kim, and Yale N Patt, "Techniques for Efficient Processing in Runahead Execution Engines," in *ISCA*, 2005.
- [116] Onur Mutlu, Jared Stark, Chris Wilkerson, and Yale N Patt, "Runahead Execution: An Alternative to Very Large Instruction Windows for Out-of-Order Processors," in *HPCA*, 2003.
- [117] Y. N. Patt, S. W. Melvin, W.-M. Hwu, and M. C. Shebanow, "Critical Issues Regarding HPS, a High Performance Microarchitecture," in *MICRO*, 1985.
- [118] Y. N. Patt, W.-M. Hwu, and M. Shebanow, "HPS, a New Microarchitecture: Rationale and Introduction," in *MICRO*, 1985.
- [119] R. M. Tomasulo, "An Efficient Algorithm for Exploiting Multiple Arithmetic Units," *IBM JRD*, 1967.
- [120] Ron Kalla, Balaram Sinharoy, and Joel M Tendler, "IBM Power5 Chip: A Dual-Core Multithreaded Processor," *IEEE Micro*, 2004.
- [121] Joel Tendler, Steve Dodson, Steve Fields, Hung Le, and Balaram Sinharoy, "POWER4 System Microarchitecture," *IBM JRD*, 2001.
- [122] Kenneth C. Yeager, "The MIPS R10000 Superscalar Microprocessor," *IEEE Micro*, 1996.
- [123] Glenn Hinton, Dave Sager, Mike Upton, Darrell Boggs, Doug Carmean, Alan Kyker, and Patrice Roussel, "The Microarchitecture of the Pentium 4 Processor," *Intel Technology Journal*, 2001.
- [124] Richard E. Kessler, "The Alpha 21264 Microprocessor," *IEEE Micro*, 1999.
- [125] James E Thornton, "Parallel Operation in the Control Data 6600," in *AFIPS*, 1964.
- [126] Burton J Smith, "A Pipelined, Shared Resource MIMD Computer," in *ICPP*, 1978.
- [127] Poonacha Kongetira, Kathirgamar Aingaran, and Kunle Olukotun, "Niagara: A 32-Way Multithreaded SPARC Processor," *IEEE Micro*, 2005.
- [128] Burton J Smith, "Architecture and Applications of the HEP Multiprocessor Computer System," in *Real-Time Signal Processing IV*, 1982.
- [129] Gregory M. Papadopoulos and Kenneth R. Traub, "Multithreading: A Revisionist View of Dataflow Architectures," in *ISCA*, 1991.
- [130] Dean M. Tullsen, Susan J. Eggers, and Henry M. Levy, "Simultaneous Multithreading: Maximizing On-Chip Parallelism," in *ISCA*, 1995.
- [131] Haitham Akkary and Michael A. Driscoll, "A Dynamic Multithreading Processor," in *MICRO*, 1998.
- [132] Amir Roth and Gurindar S. Sohi, "Speculative Data-Driven Multithreading," in *HPCA*, 2001.

- [133] Lawrence Spracklen and Santosh G. Abraham, “Chip Multithreading: Opportunities and Challenges,” in *HPCA*, 2005.
- [134] Sara S. Baghsorkhi, Isaac Gelado, Matthieu Delahaye, and Wen-mei W. Hwu, “Efficient performance evaluation of memory hierarchy for highly multithreaded graphics processors,” in *PPoPP*, 2012.
- [135] Kenzo Van Craeynest, Stijn Eyerman, and Lieven Eeckhout, “MLP-Aware Runahead Threads in a Simultaneous Multithreading Processor,” in *HiPEAC*, 2009.
- [136] José A Joao, M Aater Suleman, Onur Mutlu, and Yale N Patt, “Bottleneck Identification and Scheduling in Multithreaded Applications,” in *ASPLOS*, 2012.
- [137] Rakesh Kumar, Dean M Tullsen, Parthasarathy Ranganathan, Norman P Jouppi, and Keith I Farkas, “Single-ISA Heterogeneous Multi-Core Architectures for Multithreaded Workload Performance,” in *ISCA*, 2004.
- [138] José A Joao, M Aater Suleman, Onur Mutlu, and Yale N Patt, “Utility-Based Acceleration of Multithreaded Applications on Asymmetric CMPs,” in *ISCA*, 2013.
- [139] Chi-Keung Luk, “Tolerating Memory Latency Through Software-Controlled Pre-Execution in Simultaneous Multithreading Processors,” in *ISCA*, 2001.
- [140] R. Kumar and G. Hinton, “A Family of 45nm IA Processors,” in *ISSCC*, 2009.
- [141] J. Howard, S. Dighe, Y. Hoskote, S. Vangal, D. Finan, G. Ruhl, D. Jenkins, H. Wilson, N. Borkar, G. Schrom, F. Paillet, S. Jain, T. Jacob, S. Yada, S. Marella, P. Salihundam, V. Erraguntla, M. Konow, M. Riepen, G. Droege, J. Lindemann, M. Gries, T. Apel, K. Henriss, T. Lund-Larsen, S. Steibl, S. Borkar, V. De, R. V. D. Wijngaart, and T. Mattson, “A 48-Core IA-32 Message-Passing Processor with DVFS in 45nm CMOS,” in *ISSCC*, 2010.
- [142] R. Jotwani, S. Sundaram, S. Kosonocky, A. Schaefer, V. Andrade, G. Constant, A. Novak, and S. Naffziger, “An x86-64 Core Implemented in 32nm SOI CMOS,” in *ISSCC*, 2010.
- [143] K. Gillespie, H. R. Fair, C. Henrion, R. Jotwani, S. Kosonocky, R. S. Orefice, D. A. Priore, J. White, and K. Wilcox, “5.5 Steamroller: An x86-64 Core Implemented in 28nm Bulk CMOS,” in *ISSCC*, 2014.
- [144] T. Singh, S. Rangarajan, D. John, C. Henrion, S. Southard, H. McIntyre, A. Novak, S. Kosonocky, R. Jotwani, A. Schaefer, E. Chang, J. Bell, and M. Co, “3.2 Zen: A Next-Generation High-Performance x86 Core,” in *ISSCC*, 2017.
- [145] Onur Mutlu, “Memory-Centric Computing,” arXiv:2305.20000 [cs.AR], 2023.
- [146] Robert H. Dennard, “Field-Effect Transistor Memory,” U.S. Patent 3,387,286, 1968.
- [147] Robert H Dennard, Fritz H Gaensslen, Hwa-Nien Yu, V Leo Rideout, Ernest Bassous, and Andre R LeBlanc, “Design of Ion-Implanted MOSFET’s with Very Small Physical Dimensions,” *JSSC*, 1974.

- [148] John Markoff, “IBM’s Robert H. Dennard and the Chip That Changed the World,” <https://www.ibm.com/blogs/think/2019/11/ibms-robert-h-dennard-and-the-chip-that-changed-the-world/>, 2019.
- [149] Nature Electronics, “Memory Lane,” 2018.
- [150] Po-An Tsai, Changping Chen, and Daniel Sanchez, “Adaptive Scheduling for Systems with Asymmetric Memory Hierarchies,” in *MICRO*, 2018.
- [151] Richard Sites, “It’s the Memory, Stupid!” *MPR*, 1996.
- [152] S. Ghose, T. Li, N. Hajinazar, D. Senol Cali, and O. Mutlu, “Demystifying Complex Workload–DRAM Interactions: An Experimental Study,” in *SIGMETRICS*, 2020.
- [153] Vivek Seshadri, Thomas Mullins, Amirali Boroumand, Onur Mutlu, Phillip B Gibbons, Michael A Kozuch, and Todd C Mowry, “Gather-Scatter DRAM: In-DRAM Address Translation to Improve the Spatial Locality of Non-Unit Strided Accesses,” in *MICRO*, 2015.
- [154] Lifeng Nai, Ramyad Hadidi, Jaewoong Sim, Hyojong Kim, Pranith Kumar, and Hye-soon Kim, “GraphPIM: Enabling Instruction-Level PIM Offloading in Graph Computing Frameworks,” in *HPCA*, 2017.
- [155] Kevin Hsieh, Samira Khan, Nandita Vijaykumar, Kevin K Chang, Amirali Boroumand, Saugata Ghose, and Onur Mutlu, “Accelerating Pointer Chasing in 3D-Stacked Memory: Challenges, Mechanisms, Evaluation,” in *ICCD*, 2016.
- [156] Jeremie S Kim, Damla Senol Cali, Hongyi Xin, Donghyuk Lee, Saugata Ghose, Mohammed Alser, Hasan Hassan, Oguz Ergin, Can Alkan, and Onur Mutlu, “GRIM-Filter: Fast Seed Location Filtering in DNA Read Mapping Using Processing-in-Memory Technologies,” *BMC Genomics*, 2018.
- [157] Amirali Boroumand, “Practical Mechanisms for Reducing Processor-Memory Data Movement in Modern Workloads,” Ph.D. dissertation, Carnegie Mellon University, 2020.
- [158] Uksong Kang, Hak-Soo Yu, Churoo Park, Hongzhong Zheng, John Halbert, Kuljit Bains, S Jang, and Joo Sun Choi, “Co-Architecting Controllers and DRAM to Enhance DRAM Process Scaling,” in *The Memory Forum*, 2014.
- [159] Maurice V Wilkes, “The Memory Gap and the Future of High Performance Memories,” *CAN*, 2001.
- [160] Yoongu Kim, Ross Daly, Jeremie Kim, Chris Fallin, Ji Hye Lee, Donghyuk Lee, Chris Wilkerson, Konrad Lai, and Onur Mutlu, “Flipping Bits in Memory Without Accessing Them: An Experimental Study of DRAM Disturbance Errors,” in *ISCA*, 2014.
- [161] Yoongu Kim, Vivek Seshadri, Donghyuk Lee, Jamie Liu, and Onur Mutlu, “A Case for Exploiting Subarray-Level Parallelism (SALP) in DRAM,” in *ISCA*, 2012.

- [162] Yoongu Kim, “Architectural Techniques to Enhance DRAM Scaling,” Ph.D. dissertation, Carnegie Mellon University, 2015.
- [163] Jamie Liu, Ben Jaiyen, Richard Veras, and Onur Mutlu, “RAIDR: Retention-Aware Intelligent DRAM Refresh,” in *ISCA*, 2012.
- [164] Onur Mutlu, “The RowHammer Problem and Other Issues We May Face as Memory Becomes Denser,” in *DATE*, 2017.
- [165] Donghyuk Lee, Lavanya Subramanian, Rachata Ausavarungnirun, Jongmoo Choi, and Onur Mutlu, “Decoupled Direct Memory Access: Isolating CPU and IO Traffic by Leveraging a Dual-Data-Port DRAM,” in *PACT*, 2015.
- [166] Benjamin C. Lee, Engin Ipek, Onur Mutlu, and Doug Burger, “Architecting Phase Change Memory as a Scalable DRAM Alternative,” in *ISCA*, 2009.
- [167] HanBin Yoon, Justin Meza, Rachata Ausavarungnirun, Rachael A Harding, and Onur Mutlu, “Row Buffer Locality Aware Caching Policies for Hybrid Memories,” in *ICCD*, 2012.
- [168] Hanbin Yoon, Justin Meza, Naveen Muralimanohar, Norman P. Jouppi, and Onur Mutlu, “Efficient Data Mapping and Buffering Techniques for Multilevel Cell Phase-Change Memories,” *ACM TACO*, 2014.
- [169] Kevin Lim, Jichuan Chang, Trevor Mudge, Parthasarathy Ranganathan, Steven K. Reinhardt, and Thomas F. Wenisch, “Disaggregated Memory for Expansion and Sharing in Blade Servers,” in *ISCA*, 2009.
- [170] Wm A Wulf and Sally A McKee, “Hitting the Memory Wall: Implications of the Obvious,” *CAN*, 1995.
- [171] Kevin K. Chang, Abhijith Kashyap, Hasan Hassan, Saugata Ghose, Kevin Hsieh, Donghyuk Lee, Tianshi Li, Gennady Pekhimenko, Samira Khan, and Onur Mutlu, “Understanding Latency Variation in Modern DRAM Chips: Experimental Characterization, Analysis, and Optimization,” in *SIGMETRICS*, 2016.
- [172] Donghyuk Lee, Yoongu Kim, Vivek Seshadri, Jamie Liu, Lavanya Subramanian, and Onur Mutlu, “Tiered-Latency DRAM: A Low Latency and Low Cost DRAM Architecture,” in *HPCA*, 2013.
- [173] Donghyuk Lee, Yoongu Kim, Gennady Pekhimenko, Samira Khan, Vivek Seshadri, Kevin Chang, and Onur Mutlu, “Adaptive-Latency DRAM: Optimizing DRAM Timing for the Common-Case,” in *HPCA*, 2015.
- [174] Kevin K Chang, A Giray Yağlıkçı, Saugata Ghose, Aditya Agrawal, Niladri Chatterjee, Abhijith Kashyap, Donghyuk Lee, Mike O’Connor, Hasan Hassan, and Onur Mutlu, “Understanding Reduced-Voltage Operation in Modern DRAM Devices: Experimental Characterization, Analysis, and Mechanisms,” in *SIGMETRICS*, 2017.

- [175] Donghyuk Lee, Samira Khan, Lavanya Subramanian, Saugata Ghose, Rachata Ausavarungnirun, Gennady Pekhimenko, Vivek Seshadri, and Onur Mutlu, “Design-Induced Latency Variation in Modern DRAM Chips: Characterization, Analysis, and Latency Reduction Mechanisms,” in *SIGMETRICS*, 2017.
- [176] Yixin Luo, Sriram Govindan, Bikash Sharma, Mark Santaniello, Justin Meza, Aman Kansal, Jie Liu, Badriddine Khessib, Kushagra Vaid, and Onur Mutlu, “Characterizing Application Memory Error Vulnerability to Optimize Datacenter Cost via Heterogeneous-Reliability Memory,” in *DSN*, 2014.
- [177] Yixin Luo, Saugata Ghose, Tianshi Li, Sriram Govindan, Bikash Sharma, Bryan Kelly, Amirali Boroumand, and Onur Mutlu, “Using ECC DRAM to Adaptively Increase Memory Capacity,” arXiv:1706.08870 [cs:AR], 2017.
- [178] Hasan Hassan, Nandita Vijaykumar, Samira Khan, Saugata Ghose, Kevin Chang, Gennady Pekhimenko, Donghyuk Lee, Oguz Ergin, and Onur Mutlu, “SoftMC: A Flexible and Practical Open-Source Infrastructure for Enabling Experimental DRAM Studies,” in *HPCA*, 2017.
- [179] Hasan Hassan, Gennady Pekhimenko, Nandita Vijaykumar, Vivek Seshadri, Donghyuk Lee, Oguz Ergin, and Onur Mutlu, “ChargeCache: Reducing DRAM Latency by Exploiting Row Access Locality,” in *HPCA*, 2016.
- [180] Minesh Patel, Jeremie S Kim, and Onur Mutlu, “The Reach Profiler (REAPER): Enabling the Mitigation of DRAM Retention Failures via Profiling at Aggressive Conditions,” in *ISCA*, 2017.
- [181] Hasan Hassan, Minesh Patel, Jeremie S Kim, A Giray Yaglikci, Nandita Vijaykumar, Nika Mansouri Ghiasi, Saugata Ghose, and Onur Mutlu, “CROW: A Low-Cost Substrate for Improving DRAM Performance, Energy Efficiency, and Reliability,” in *ISCA*, 2019.
- [182] Saugata Ghose, Abdullah Giray Yaglikçi, Raghav Gupta, Donghyuk Lee, Kais Kudrolli, William X Liu, Hasan Hassan, Kevin K Chang, Niladrish Chatterjee, Aditya Agrawal *et al.*, “What Your DRAM Power Models Are Not Telling You: Lessons from a Detailed Experimental Study,” in *SIGMETRICS*, 2018.
- [183] Jeremie Kim, Minesh Patel, Hasan Hassan, and Onur Mutlu, “Solar-DRAM: Reducing DRAM Access Latency by Exploiting the Variation in Local Bitlines,” in *ICCD*, 2018.
- [184] Jeremie S Kim, Minesh Patel, A Giray Yağlıkçı, Hasan Hassan, Roknoddin Azizi, Lois Orosa, and Onur Mutlu, “Revisiting RowHammer: An Experimental Analysis of Modern DRAM Devices and Mitigation Techniques,” in *ISCA*, 2020.
- [185] Onur Mutlu and Jeremie S Kim, “RowHammer: A Retrospective,” *TCAD*, 2019.
- [186] Yaohua Wang, Arash Tavakkol, Lois Orosa, Saugata Ghose, Nika Mansouri Ghiasi, Minesh Patel, Jeremie S Kim, Hasan Hassan, Mohammad Sadrosadati, and Onur Mutlu, “Reducing DRAM Latency via Charge-Level-Aware Look-Ahead Partial Restoration,” in *MICRO*, 2018.

- [187] Onur Mutlu, Saugata Ghose, and Rachata Ausavarungnirun, “Recent Advances in DRAM and Flash Memory Architectures,” *Invited Journal Issue IPSI Transactions on Internet Research*, 2018.
- [188] Onur Mutlu, “Main Memory Scaling: Challenges and Solution Directions,” in *More Than Moore Technologies for Next Generation Computer Design*. Springer-Verlag, 2015.
- [189] Sungjoo Hong, “Memory Technology Trend and Future Challenges,” in *IEDM*, 2010.
- [190] Haocong Luo, Ataberk Olgun, Abdullah Giray Yağlıkçı, Yahya Can Tuğrul, Steve Rhyner, Meryem Banu Cavlak, Joël Lindegger, Mohammad Sadrosadati, and Onur Mutlu, “RowPress: Amplifying Read Disturbance in Modern DRAM Chips,” in *ISCA*, 2023.
- [191] A. Giray Yağlıkçı, Yahya Can Tuğrul, Geraldo F De Oliviera, Ismail Emir Yüksel, Ataberk Olgun, Haocong Luo, and Onur Mutlu, “Spatial Variation-Aware Read Disturbance Defenses: Experimental Analysis of Real DRAM Chips and Implications on Future Solutions,” in *HPCA*, 2024.
- [192] Ataberk Olgun, Yahya Can Tugrul, F. Nisa Bostancı, Ismail Emir Yüksel, Haocong Luo, Steve Rhyner, A. Giray Yaglıkçı, Geraldo F. Oliveira, and Onur Mutlu, “ABACuS: All-Bank Activation Counters for Scalable and Low Overhead RowHammer Mitigation,” in *USENIX Security*, 2024.
- [193] F. Nisa Bostancı, Ismail Emir Yüksel, Ataberk Olgun, Konstantinos Kanellopoulos, Yahya Can Tugrul, A. Giray Yaglıkçı, Mohammad Sadrosadati, and Onur Mutlu, “CoMeT: Count-Min-Sketch-Based Row Tracking to Mitigate RowHammer at Low Cost,” in *HPCA*, 2024.
- [194] A Giray Yağlıkçı, Ataberk Olgun, Minesh Patel, Haocong Luo, Hasan Hassan, Lois Orosa, Oğuz Ergin, and Onur Mutlu, “HiRA: Hidden Row Activation for Reducing Refresh Latency of Off-the-Shelf DRAM Chips,” in *MICRO*, 2022.
- [195] Abdullah Giray Yağlıkçı, “Enabling Efficient and Scalable DRAM Read Disturbance Mitigation via New Experimental Insights into Modern DRAM Chips,” Ph.D. dissertation, ETH Zürich, 2024.
- [196] F Bostancı, Oğuzhan Canpolat, Ataberk Olgun, İsmail Emir Yüksel, Konstantinos Kanellopoulos, Mohammad Sadrosadati, A Giray Yağlıkçı, and Onur Mutlu, “Understanding and Mitigating Side and Covert Channel Vulnerabilities Introduced by RowHammer Defenses,” arXiv:2503.17891 [cs.CR], 2025.
- [197] Haocong Luo, İsmail Emir Yüksel, Ataberk Olgun, A Giray Yağlıkçı, and Onur Mutlu, “Revisiting DRAM Read Disturbance: Identifying Inconsistencies Between Experimental Characterization and Device-Level Studies,” in *VTS*, 2025.
- [198] Oğuzhan Canpolat, A. Giray Yağlıkçı, Geraldo F. Oliveira, Ataberk Olgun, F. Nisa Bostancı, Ismail E. Yüksel, Haocong Luo, Oğuz Ergin, and Onur Mutlu, “Chronus: Understanding and Securing the Cutting-Edge Industry Solutions to DRAM Read Disturbance,” in *HPCA*, 2025.

- [199] Yahya Can Tuğrul, A Giray Yağlıkçı, İsmail Emir Yüksel, Ataberk Olgun, Oğuzhan Canpolat, Nisa Bostancı, Mohammad Sadrosadati, Oğuz Ergin, and Onur Mutlu, “Understanding RowHammer Under Reduced Refresh Latency: Experimental Analysis of Real DRAM Chips and Implications on Future Solutions,” in *HPCA*, 2025.
- [200] Song Liu, Karthik Pattabiraman, Thomas Moscibroda, and Benjamin G. Zorn, “Flicker: Saving DRAM Refresh-Power through Critical Data Partitioning,” in *ASPLOS*, 2011.
- [201] Chung-Hsiang Lin, De-Yu Shen, Yi-Jung Chen, Chia-Lin Yang, and Michael Wang, “SECRET: Selective Error Correction for Refresh Energy Reduction in DRAMs,” in *ICCD*, 2012.
- [202] Seungjae Baek, Sangyeun Cho, and Rami Melhem, “Refresh Now and Then,” *IEEE TC*, 2013.
- [203] Ishwar Bhati, Zeshan Chishti, and Bruce Jacob, “Coordinated Refresh: Energy Efficient Techniques for DRAM Refresh Scheduling,” in *ISPLED*, 2013.
- [204] Prashant Nair, Chia-Chen Chou, and Moinuddin K Qureshi, “A Case for Refresh Pausing in DRAM Memory Systems,” in *HPCA*, 2013.
- [205] Amir Rahmati, Matthew Hicks, Daniel Holcomb, and Kevin Fu, “Refreshing Thoughts on DRAM: Power Saving vs. Data Integrity,” in *WACAS*, 2014.
- [206] Ishwar Singh Bhati, “Scalable and Energy Efficient DRAM Refresh Techniques,” Ph.D. dissertation, 2014.
- [207] Zehan Cui, Sally A McKee, Zhongbin Zha, Yungang Bao, and Mingyu Chen, “DTail: A Flexible Approach to DRAM Refresh Management,” in *SC*, 2014.
- [208] Yinhe Han, Ying Wang, Huawei Li, and Xiaowei Li, “Data-Aware DRAM Refresh to Squeeze the Margin of Retention Time in Hybrid Memory Cube,” in *ICCAD*, 2014.
- [209] Matthias Jung, Christian Weis, Norbert Wehn, Mohammadsadegh Sadri, and Luca Benini, “Optimized Active and Power-Down Mode Refresh Control in 3D-DRAMs,” in *VLSI-SoC*, 2014.
- [210] Prashant J Nair, Chia-Chen Chou, and Moinuddin K Qureshi, “Refresh Pausing in DRAM Memory Systems,” *TACO*, 2014.
- [211] Tao Zhang, Matt Poremba, Cong Xu, Guangyu Sun, and Yuan Xie, “CREAM: A Concurrent-Refresh-Aware DRAM Memory Architecture,” in *HPCA*, 2014.
- [212] Ishwar Bhati, Zeshan Chishti, Shih-Lien Lu, and Bruce Jacob, “Flexible Auto-Refresh: Enabling Scalable and Energy-Efficient DRAM Refresh Reductions,” in *ISCA*, 2015.
- [213] Matthias Jung, Éder Zulian, Deepak M. Mathew, Matthias Herrmann, Christian Brugger, Christian Weis, and Norbert Wehn, “Omitting Refresh: A Case Study for Commodity and Wide I/O DRAMs,” in *MEMSYS*, 2015.
- [214] Ishwar Bhati, Mu-Tien Chang, Zeshan Chishti, Shih-Lien Lu, and Bruce Jacob, “DRAM Refresh Mechanisms, Penalties, and Trade-Offs,” in *TC*, 2016.

- [215] Jagadish B Kotra, Narges Shahidi, Zeshan A Chishti, and Mahmut T Kandemir, "Hardware-Software Co-Design to Mitigate DRAM Refresh Overheads: A Case for Refresh-Aware Process Scheduling," *ASPLOS*, 2017.
- [216] Kate Nguyen, Kehan Lyu, Xianze Meng, Vilas Sridharan, and Xun Jian, "Nonblocking Memory Refresh," in *ISCA*, 2018.
- [217] Shibo Wang, Mahdi Nazm Bojnordi, Xiaochen Guo, and Engin Ipek, "Content Aware Refresh: Exploiting the Asymmetry of DRAM Retention Errors to Reduce the Refresh Frequency of Less Vulnerable Data," *IEEE TC*, 2018.
- [218] Xing Pan and Frank Mueller, "Hiding DRAM Refresh Overhead in Real-Time Cyclic Executives," in *RTSS*, 2019.
- [219] Xing Pan and Frank Mueller, "The Colored Refresh Server for DRAM," in *ISORC*, 2019.
- [220] Haerang Choi, Dosun Hong, Jaesung Lee, and Sungjoo Yoo, "Reducing DRAM Refresh Power Consumption by Runtime Profiling of Retention Time and Dual-Row Activation," *MICPRO*, 2020.
- [221] Seikwon Kim, Wonsang Kwak, Changdae Kim, Daehyeon Baek, and Jaehyuk Huh, "Charge-Aware DRAM Refresh Reduction with Value Transformation," in *HPCA*, 2020.
- [222] Moinuddin K Qureshi, DaeHyun Kim, Samira Khan, Prashant J Nair, and Onur Mutlu, "AVATAR: A Variable-Retention-Time (VRT) Aware Refresh for DRAM Systems," in *DSN*, 2015.
- [223] Chiachen Chou, Prashant Nair, and Moinuddin K Qureshi, "Reducing Refresh Power in Mobile Devices with Morphable ECC," in *DSN*, 2015.
- [224] Kevin Kai-Wei Chang, Donghyuk Lee, Zeshan Chishti, Alaa R Alameldeen, Chris Wilkerson, Yoongu Kim, and Onur Mutlu, "Improving DRAM Performance by Parallelizing Refreshes with Accesses," in *HPCA*, 2014.
- [225] Anup Das, Hasan Hassan, and Onur Mutlu, "VRL-DRAM: Improving DRAM Performance via Variable Refresh Latency," in *DAC*, 2018.
- [226] J. Mukundan, H. Hunter, K. H. Kim, J. Stuecheli, and J. F. Martínez, "Understanding and Mitigating Refresh Overheads in High-Density DDR4 DRAM Systems," in *ISCA*, 2013.
- [227] Mrinmoy Ghosh and Hsien-Hsin S Lee, "Smart Refresh: An Enhanced Memory Controller Design for Reducing Energy in Conventional and 3D Die-Stacked DRAMs," in *MICRO*, 2007.
- [228] Riichiro Takemura, Kiyoo Itoh, Tomonori Sekiguchi, Satoru Akiyama, Satoru Hanzawa, Kazuhiko Kajigaya, and Takayuki Kawahara, "Long-Retention-Time, High-Speed DRAM Array with 12-F 2 Twin Cell for Sub 1-V Operation," *TOE*, 2007.
- [229] Wei Kong, Paul C Parries, G Wang, and Subramanian S Iyer, "Analysis of Retention Time Distribution of Embedded DRAM-A New Method to Characterize Across-Chip Threshold Voltage Variation," in *ITC*, 2008.

- [230] Heesang Kim, Byoungchan Oh, Younghwan Son, Kyungdo Kim, Seon-Yong Cha, Jae-Goan Jeong, Sung-Joo Hong, and Hyungcheol Shin, "Characterization of the Variable Retention Time in Dynamic Random Access Memory," *TED*, 2011.
- [231] Heesang Kim, Byoungchan Oh, Younghwan Son, Kyungdo Kim, Seon-Yong Cha, Jae-Goan Jeong, Sung-Joo Hong, and Hyungcheol Shin, "Study of Trap Models Related to the Variable Retention Time Phenomenon in DRAM," *TED*, 2011.
- [232] Angelo Bacchini, Marco Rovatti, Gianluca Furano, and Marco Ottavi, "Characterization of Data Retention Faults in DRAM Devices," in *DFT*, 2014.
- [233] Angelo Bacchini, Gianluca Furano, Marco Rovatti, and Marco Ottavi, "Total Ionizing Dose Effects On DRAM Data Retention Time," *IEEE Trans. Nucl. Sci.*, 2014.
- [234] Jue Wang, Xiangyu Dong, and Yuan Xie, "ProactiveDRAM: A DRAM-Initiated Retention Management Scheme," in *ICCD*, 2014.
- [235] Ying Wang, Yinhe Han, Cheng Wang, Huawei Li, and Xiaowei Li, "RADAR: A Case for Retention-Aware DRAM Assembly and Repair in Future FGR DRAM Memory," in *DAC*, 2015.
- [236] Christian Weis, Matthias Jung, Peter Ehses, Cristiano Santos, Pascal Vivet, Sven Goossens, Martijn Koedam, and Norbert Wehn, "Retention Time Measurements and Modelling of Bit Error Rates of Wide I/O DRAM in MPSoCs," in *DATE*, 2015.
- [237] Amin Farmahini-Farahani, Jung Ho Ahn, Katherine Morrow, and Nam Sung Kim, "NDA: Near-DRAM Acceleration Architecture Leveraging Commodity DRAM Devices and Standard Memory Modules," in *HPCA*, 2015.
- [238] Oreoluwatomiwa O Babarinsa and Stratos Idreos, "JAFAR: Near-Data Processing for Databases," in *SIGMOD*, 2015.
- [239] Fabrice Devaux, "The True Processing in Memory Accelerator," in *Hot Chips*, 2019.
- [240] Nika Mansouri Ghiasi, Jisung Park, Harun Mustafa, Jeremie Kim, Ataberk Olgun, Arvid Gollwitzer, Damla Senol Cali, Can Firtina, Haiyu Mao, Nour Almadhoun Alserr *et al.*, "GenStore: A High-Performance and Energy-Efficient In-Storage Computing System for Genome Sequence Analysis," in *ASPLOS*, 2022.
- [241] Juan Gómez-Luna, Izzat El Hajj, Ivan Fernandez, Christina Giannoula, Geraldo F Oliveira, and Onur Mutlu, "Benchmarking Memory-Centric Computing Systems: Analysis of Real Processing-in-Memory Hardware," in *CUT*, 2021.
- [242] Juan Gómez-Luna, Izzat El Hajj, Ivan Fernández, Christina Giannoula, Geraldo F. Oliveira, and Onur Mutlu, "Benchmarking a New Paradigm: An Experimental Analysis of a Real Processing-in-Memory Architecture," arXiv:2105.03814 [cs.AR], 2021.
- [243] Christina Giannoula, Nandita Vijaykumar, Nikela Papadopoulou, Vasileios Karakostas, Ivan Fernandez, Juan Gómez-Luna, Lois Orosa, Nectarios Koziris, Georgios Goumas, and Onur Mutlu, "SynCron: Efficient Synchronization Support for Near-Data-Processing Architectures," in *HPCA*, 2021.

- [244] Gagandeep Singh, Dionysios Diamantopoulos, Christoph Hagleitner, Juan Gomez-Luna, Sander Stuijk, Onur Mutlu, and Henk Corporaal, “NERO: A Near High-Bandwidth Memory Stencil Accelerator for Weather Prediction Modeling,” in *FPL*, 2020.
- [245] S. Lee, K. Kim, S. Oh, J. Park, G. Hong, D. Ka, K. Hwang, J. Park, K. Kang, J. Kim, J. Jeon, N. Kim, Y. Kwon, K. Vladimir, W. Shin, J. Won, M. Lee, H. Joo *et al.*, “A 1ynm 1.25V 8Gb, 16Gb/s/pin GDDR6-based Accelerator-in-Memory Supporting 1TFLOPS MAC Operation and Various Activation Functions for Deep-Learning Applications,” in *ISSCC*, 2022.
- [246] Liu Ke, Xuan Zhang, Jinin So, Jong-Geon Lee, Shin-Haeng Kang, Sukhan Lee, Songyi Han, Yeongon Cho, Jin Hyun Kim, Yongsuk Kwon *et al.*, “Near-Memory Processing in Action: Accelerating Personalized Recommendation with AxDIMM,” *IEEE Micro*, 2021.
- [247] Christina Giannoula, Ivan Fernandez, Juan Gómez Luna, Nectarios Koziris, Georgios Goumas, and Onur Mutlu, “SparseP: Towards Efficient Sparse Matrix Vector Multiplication on Real Processing-in-Memory Architectures,” in *SIGMETRICS*, 2022.
- [248] Hyunsung Shin, Dongyoung Kim, Eunhyeok Park, Sungho Park, Yongsik Park, and Sungjoo Yoo, “McDRAM: Low Latency and Energy-Efficient Matrix Computations in DRAM,” *IEEE TCADICS*, 2018.
- [249] Seunghwan Cho, Haerang Choi, Eunhyeok Park, Hyunsung Shin, and Sungjoo Yoo, “McDRAM v2: In-Dynamic Random Access Memory Systolic Array Accelerator to Address the Large Model Problem in Deep Neural Networks on the Edge,” *IEEE Access*, 2020.
- [250] Alain Denzler, Rahul Bera, Nastaran Hajinazar, Gagandeep Singh, Geraldo F Oliveira, Juan Gómez-Luna, and Onur Mutlu, “Casper: Accelerating Stencil Computation using Near-Cache Processing,” arXiv:2112.14216 [cs.AR], 2021.
- [251] Hadi Asghari-Moghaddam, Young Hoon Son, Jung Ho Ahn, and Nam Sung Kim, “Chameleon: Versatile and Practical Near-DRAM Acceleration Architecture for Large Memory Systems,” in *MICRO*, 2016.
- [252] D. Patterson, T. Anderson, N. Cardwell *et al.*, “A Case for Intelligent RAM,” *IEEE Micro*, 1997.
- [253] D. G. Elliott, M. Stumm, W. M. Snelgrove *et al.*, “Computational RAM: Implementing Processors in Memory,” *Design and Test of Computers*, 1999.
- [254] M. A. Z. Alves, P. C. Santos, F. B. Moreira, and others, “Saving Memory Movements Through Vector Processing in the DRAM,” in *CASES*, 2015.
- [255] S. L. Xi, O. Babarinsa, M. Athanassoulis, and S. Idreos, “Beyond the Wall: Near-Data Processing for Databases,” in *DaMoN*, 2015.
- [256] Weiyi Sun, Zhaoshi Li, Shouyi Yin, Shaojun Wei, and Leibo Liu, “ABC-DIMM: Alleviating the Bottleneck of Communication in DIMM-Based Near-Memory Processing with Inter-DIMM Broadcast,” in *ISCA*, 2021.

- [257] Kiran Kumar Matam, Gunjae Koo, Haipeng Zha, Hung-Wei Tseng, and Murali Annavaram, "GraphSSD: Graph Semantics Aware SSD," in *ISCA*, 2019.
- [258] Maya Gokhale, Bill Holmes, and Ken Iobst, "Processing in Memory: The Terasys Massively Parallel PIM Array," *Computer*, 1995.
- [259] Mary Hall, Peter Kogge, Jeff Koller, Pedro Diniz, Jacqueline Chame, Jeff Draper, Jeff LaCoss, John Granacki, Jay Brockman, Apoorv Srivastava *et al.*, "Mapping Irregular Applications to DIVA, a PIM-Based Data-Intensive Architecture," in *SC*, 1999.
- [260] Marco A. Z. Alves, Paulo C. Santos, Matthias Diener, and Luigi Carro, "Opportunities and Challenges of Performing Vector Operations Inside the DRAM," in *MEMSYS*, 2015.
- [261] Elliot Lockerman, Axel Feldmann, Mohammad Bakhshalipour, Alexandru Stanescu, Shashwat Gupta, Daniel Sanchez, and Nathan Beckmann, "Livia: Data-Centric Computing Throughout the Memory Hierarchy," in *ASPLOS*, 2020.
- [262] Amirali Boroumand, Saugata Ghose, Brandon Lucia, Kevin Hsieh, Krishna Malladi, Hongzhong Zheng, and Onur Mutlu, "LazyPIM: An Efficient Cache Coherence Mechanism for Processing-in-Memory," *CAL*, 2017.
- [263] Dongping Zhang, Nuwan Jayasena, Alexander Lyashevsky, Joseph L Greathouse, Lifan Xu, and Michael Ignatowski, "TOP-PIM: Throughput-Oriented Programmable Processing in Memory," in *HPDC*, 2014.
- [264] Mingyu Gao and Christos Kozyrakis, "HRL: Efficient and Flexible Reconfigurable Logic for Near-Data Processing," in *HPCA*, 2016.
- [265] Mario Drumond, Alexandros Daglis, Nooshin Mirzadeh, Dmitrii Ustiugov, Javier Picorel, Babak Falsafi, Boris Grot, and Dionisios Pnevmatikatos, "The Mondrian Data Engine," in *ISCA*, 2017.
- [266] P. C. Santos, G. F. Oliveira, D. G. Tomé, M. A. Z. Alves, E. C. Almeida, and L. Carro, "Operand Size Reconfiguration for Big Data Processing in Memory," in *DATE*, 2017.
- [267] Geraldo F Oliveira, Paulo C Santos, Marco AZ Alves, and Luigi Carro, "NIM: An HMC-Based Machine for Neuron Computation," in *ARC*, 2017.
- [268] Mingyu Gao, Jing Pu, Xuan Yang, Mark Horowitz, and Christos Kozyrakis, "TETRIS: Scalable and Efficient Neural Network Acceleration with 3D Memory," in *ASPLOS*, 2017.
- [269] Duckhwan Kim, Jaeha Kung, Sek Chai, Sudhakar Yalamanchili, and Saibal Mukhopadhyay, "Neurocube: A Programmable Digital Neuromorphic Architecture with High-Density 3D Memory," in *ISCA*, 2016.
- [270] Peng Gu, Shuangchen Li, Dylan Stow, Russell Barnes, Liu Liu, Yuan Xie, and Eren Kursun, "Leveraging 3D Technologies for Hardware Security: Opportunities and Challenges," in *GLSVLSI*, 2016.

- [271] Amirali Boroumand, Saugata Ghose, Minesh Patel, Hasan Hassan, Brandon Lucia, Rachata Ausavarungnirun, Kevin Hsieh, Nastaran Hajinazar, Krishna T Malladi, Hongzhong Zheng *et al.*, “CoNDA: Efficient Cache Coherence Support for Near-Data Accelerators,” in *ISCA*, 2019.
- [272] Kevin Hsieh, Eiman Ebrahimi, Gwangsun Kim, Niladrish Chatterjee, Mike O’Connor, Nandita Vijaykumar, Onur Mutlu, and Stephen W Keckler, “Transparent Offloading and Mapping (TOM) Enabling Programmer-Transparent Near-Data Processing in GPU Systems,” in *ISCA*, 2016.
- [273] S. H. Pugsley, J. Jestes, H. Zhang, R. Balasubramonian *et al.*, “NDC: Analyzing the Impact of 3D-Stacked Memory+Logic Devices on MapReduce Workloads,” in *ISPASS*, 2014.
- [274] Ashutosh Pattnaik, Xulong Tang, Adwait Jog, Onur Kayiran, Asit K Mishra, Mahmut T Kandemir, Onur Mutlu, and Chita R Das, “Scheduling Techniques for GPU Architectures with Processing-in-Memory Capabilities,” in *PACT*, 2016.
- [275] Berkin Akin, Franz Franchetti, and James C Hoe, “Data Reorganization in Memory Using 3D-Stacked DRAM,” in *ISCA*, 2015.
- [276] Joo Hwan Lee, Jaewoong Sim, and Hyesoon Kim, “BSSync: Processing Near Memory for Machine Learning Workloads with Bounded Staleness Consistency Models,” in *PACT*, 2015.
- [277] Amirali Boroumand, Saugata Ghose, Berkin Akin, Ravi Narayanaswami, Geraldo F Oliveira, Xiaoyu Ma, Eric Shiu, and Onur Mutlu, “Mitigating Edge Machine Learning Inference Bottlenecks: An Empirical Study on Accelerating Google Edge Models,” arXiv:2103.00768 [cs.AR], 2021.
- [278] Amirali Boroumand, Saugata Ghose, Geraldo F Oliveira, and Onur Mutlu, “Polynesia: Enabling High-Performance and Energy-Efficient Hybrid Transactional/Analytical Databases with Hardware/Software Co-Design,” in *ICDE*, 2022.
- [279] Amirali Boroumand, Saugata Ghose, Geraldo F Oliveira, and Onur Mutlu, “Polynesia: Enabling Effective Hybrid Transactional/Analytical Databases with Specialized Hardware/Software Co-Design,” arXiv:2103.00798 [cs.AR], 2021.
- [280] Maciej Besta, Raghavendra Kanakagiri, Grzegorz Kwasniewski, Rachata Ausavarungnirun, Jakub Beránek, Konstantinos Kanellopoulos, Kacper Janda, Zur Vonarburg-Shmaria, Lukas Gianinazzi, Ioana Stefan *et al.*, “SISA: Set-Centric Instruction Set Architecture for Graph Mining on Processing-in-Memory Systems,” in *MICRO*, 2021.
- [281] Ivan Fernandez, Ricardo Quisilant, Eladio Gutiérrez, Oscar Plata, Christina Giannoula, Mohammed Alser, Juan Gómez-Luna, and Onur Mutlu, “NATSA: A Near-Data Processing Accelerator for Time Series Analysis,” in *ICCD*, 2020.
- [282] Gagandeep Singh, Giovanni , Geraldo F Oliveira, Stefano Corda, Sander Stuijk, Onur Mutlu, and Henk Corporaal, “NAPEL: Near-Memory Computing Application Performance Prediction via Ensemble Learning,” in *DAC*, 2019.

- [283] Young-Cheon Kwon, Suk Han Lee, Jaehoon Lee, Sang-Hyuk Kwon, Je Min Ryu, Jong-Pil Son, O Seongil, Hak-Soo Yu, Haesuk Lee, Soo Young Kim *et al.*, “A 20nm 6GB Function-in-Memory DRAM, Based on HBM2 with a 1.2 TFLOPS Programmable Computing Unit using Bank-Level Parallelism, for Machine Learning Applications,” in *ISSCC*, 2021.
- [284] Sukhan Lee, Shin-haeng Kang, Jaehoon Lee, Hyeonsu Kim, Eojin Lee, Seungwoo Seo, Hosang Yoon, Seungwon Lee, Kyoungwan Lim, Hyunsung Shin *et al.*, “Hardware Architecture and Software Stack for PIM Based on Commercial DRAM Technology: Industrial Product,” in *ISCA*, 2021.
- [285] Dimin Niu, Shuangchen Li, Yuhao Wang, Wei Han, Zhe Zhang, Yijin Guan, Tianchan Guan, Fei Sun, Fei Xue, Lide Duan *et al.*, “184QPS/W 64Mb/mm² 3D Logic-to-DRAM Hybrid Bonding with Process-Near-Memory Engine for Recommendation System,” in *ISSCC*, 2022.
- [286] Q. Zhu, T. Graf, H. E. Sumbul, L. Pileggi, and F. Franchetti, “Accelerating Sparse Matrix-Matrix Multiplication with 3D-Stacked Logic-in-Memory Hardware,” in *HPEC*, 2013.
- [287] Erfan Azarkhish, Christoph Pfister, Davide Rossi, Igor Loi, and Luca Benini, “Logic-Base Interconnect Design for Near Memory Computing in the Smart Memory Cube,” *IEEE VLSI*, 2016.
- [288] Erfan Azarkhish, Davide Rossi, Igor Loi, and Luca Benini, “Neurostream: Scalable and Energy Efficient Deep Learning with Smart Memory Cubes,” *TPDS*, 2018.
- [289] Qi Guo, Nikolaos Alachiotis, Berkin Akin, Fazle Sadi, Guanglin Xu, Tze Meng Low, Larry Pileggi, James C Hoe, and Franz Franchetti, “3D-Stacked Memory-Side Acceleration: Accelerator and System Design,” in *WoNDP*, 2014.
- [290] Jo textasciitilde ao Paulo C de Lima, Paulo Cesar Santos, Marco AZ Alves, Antonio Beck, and Luigi Carro, “Design Space Exploration for PIM Architectures in 3D-Stacked Memories,” in *CF*, 2018.
- [291] Berkin Akin, James C Hoe, and Franz Franchetti, “HAMLeT: Hardware Accelerated Memory Layout Transform within 3D-Stacked DRAM,” in *HPEC*, 2014.
- [292] Yu Huang, Long Zheng, Pengcheng Yao, Jieshan Zhao, Xiaofei Liao, Hai Jin, and Jingling Xue, “A Heterogeneous PIM Hardware-Software Co-Design for Energy-Efficient Graph Processing,” in *IPDPS*, 2020.
- [293] Guohao Dai, Tianhao Huang, Yuze Chi, Jishen Zhao, Guangyu Sun, Yongpan Liu, Yu Wang, Yuan Xie, and Huazhong Yang, “GraphH: A Processing-in-Memory Architecture for Large-Scale Graph Processing,” *TCAD*, 2018.
- [294] Jiawen Liu, Hengyu Zhao, Matheus A Ogleari, Dong Li, and Jishen Zhao, “Processing-in-Memory for Energy-Efficient Neural Network Training: A Heterogeneous Approach,” in *MICRO*, 2018.

- [295] Peng Gu, Xinfeng Xie, Yufei Ding, Guoyang Chen, Weifeng Zhang, Dimin Niu, and Yuan Xie, “iPIM: Programmable In-Memory Image Processing Accelerator using Near-Bank Architecture,” in *ISCA*, 2020.
- [296] A. Farmahini-Farahani, J. H. Ahn, K. Compton, and N. S. Kim, “DRAMA: An Architecture for Accelerated Processing Near Memory,” *Computer Architecture Letters*, 2014.
- [297] H. Asghari-Moghaddam, A. Farmahini-Farahani, K. Morrow *et al.*, “Near-DRAM Acceleration with Single-ISA Heterogeneous Processing in Standard Memory Modules,” *IEEE Micro*, 2016.
- [298] Jiayi Huang, Ramprakash Reddy Puli, Pritam Majumder, Sungkeun Kim, Rahul Boyapati, Ki Hwan Yum, and Eun Jung Kim, “Active-Routing: Compute on the Way for Near-Data Processing,” in *HPCA*, 2019.
- [299] Chad D Kersey, Hyesoon Kim, and Sudhakar Yalamanchili, “Lightweight SIMT Core Designs for Intelligent 3D Stacked DRAM,” in *MEMSYS*, 2017.
- [300] Jie Li, Xi Wang, Antonino Tumeo, Brody Williams, John D Leidel, and Yong Chen, “PIMS: A Lightweight Processing-in-Memory Accelerator for Stencil Computations,” in *MEMSYS*, 2019.
- [301] Jeremie S Kim, Damla Senol, Hongyi Xin, Donghyuk Lee, Saugata Ghose, Mohammed Alser, Hasan Hassan, Oguz Ergin, Can Alkan, and Onur Mutlu, “GRIM-Filter: Fast Seed Filtering in Read Mapping using Emerging Memory Technologies,” arXiv:1708.04329 [q-bio.GN], 2017.
- [302] Amirali Boroumand, Saugata Ghose, Minesh Patel, Hasan Hassan, Brandon Lucia, Nataran Hajinazar, Kevin Hsieh, Krishna T Malladi, Hongzhong Zheng, and Onur Mutlu, “LazyPIM: Efficient Support for Cache Coherence in Processing-in-Memory Architectures,” arXiv:1706.03162 [cs.AR], 2017.
- [303] Youwei Zhuo, Chao Wang, Mingxing Zhang, Rui Wang, Dimin Niu, Yanzhi Wang, and Xuehai Qian, “GraphQ: Scalable PIM-Based Graph Processing,” in *MICRO*, 2019.
- [304] Mingxing Zhang, Youwei Zhuo, Chao Wang, Mingyu Gao, Yongwei Wu, Kang Chen, Christos Kozyrakis, and Xuehai Qian, “GraphP: Reducing Communication for PIM-Based Graph Processing with Efficient Data Partition,” in *HPCA*, 2018.
- [305] Hongyeol Lim and Giho Park, “Triple Engine Processor (TEP): A Heterogeneous Near-Memory Processor for Diverse Kernel Operations,” *TACO*, 2017.
- [306] Erfan Azarkhish, Davide Rossi, Igor Loi, and Luca Benini, “A Case for Near Memory Computation Inside the Smart Memory Cube,” in *EMS*, 2016.
- [307] M. A. Z. Alves, M. Diener, P. C. Santos, and L. Carro, “Large Vector Extensions Inside the HMC,” in *DATE*, 2016.
- [308] Jaeyoung Jang, Jun Heo, Yejin Lee, Jaeyeon Won, Seonghak Kim, Sung Jun Jung, Hakbeom Jang, Tae Jun Ham, and Jae W Lee, “Charon: Specialized Near-Memory Processing Architecture for Clearing Dead Objects in Memory,” in *MICRO*, 2019.

- [309] R. Nair, S. F. Antao, C. Bertolli, P. Bose *et al.*, “Active Memory Cube: A Processing-in-Memory Architecture for Exascale Systems,” *IBM JRD*, 2015.
- [310] Ramyad Hadidi, Lifeng Nai, Hyojong Kim, and Hyesoon Kim, “CAIRO: A Compiler-Assisted Technique for Enabling Instruction-Level Offloading of Processing-in-Memory,” *TACO*, 2017.
- [311] Paulo C Santos, Geraldo F Oliveira, Jo textasciitilde ao P Lima, Marco AZ Alves, Luigi Carro, and Antonio CS Beck, “Processing in 3D Memories to Speed Up Operations on Complex Data Structures,” in *DATE*, 2018.
- [312] Ping Chi, Shuangchen Li, Cong Xu, Tao Zhang, Jishen Zhao, Yongpan Liu, Yu Wang, and Yuan Xie, “PRIME: A Novel Processing-in-Memory Architecture for Neural Network Computation in ReRAM-Based Main Memory,” in *ISCA*, 2016.
- [313] Ali Shafiee, Anirban Nag, Naveen Muralimanohar, Rajeev Balasubramonian, John Paul Strachan, Miao Hu, R. Stanley Williams, and Vivek Srikumar, “ISAAC: A Convolutional Neural Network Accelerator with In-Situ Analog Arithmetic in Crossbars,” in *ISCA*, 2016.
- [314] Vivek Seshadri, Donghyuk Lee, Thomas Mullins, Hasan Hassan, Amirali Boroumand, Jeremie Kim, Michael A Kozuch, Onur Mutlu, Phillip B Gibbons, and Todd C Mowry, “Ambit: In-Memory Accelerator for Bulk Bitwise Operations Using Commodity DRAM Technology,” in *MICRO*, 2017.
- [315] Vivek Seshadri and Onur Mutlu, “In-DRAM Bulk Bitwise Execution Engine,” arXiv:1905.09822 [cs.AR], 2019.
- [316] Shuangchen Li, Dimin Niu, Krishna T Malladi, Hongzhong Zheng, Bob Brennan, and Yuan Xie, “DRISA: A DRAM-Based Reconfigurable In-Situ Accelerator,” in *MICRO*, 2017.
- [317] Vivek Seshadri, Yoongu Kim, Chris Fallin, Donghyuk Lee, Rachata Ausavarungnirun, Gennady Pekhimenko, Yixin Luo, Onur Mutlu, Phillip B Gibbons, Michael A Kozuch *et al.*, “RowClone: Fast and Energy-Efficient In-DRAM Bulk Data Copy and Initialization,” in *MICRO*, 2013.
- [318] Vivek Seshadri and Onur Mutlu, “The Processing Using Memory Paradigm: In-DRAM Bulk Copy, Initialization, Bitwise AND and OR,” arXiv:1610.09603 [cs.AR], 2016.
- [319] Quan Deng, Lei Jiang, Youtao Zhang, Minxuan Zhang, and Jun Yang, “DrAcc: A DRAM Based Accelerator for Accurate CNN Inference,” in *DAC*, 2018.
- [320] Xin Xin, Youtao Zhang, and Jun Yang, “ELP2IM: Efficient and Low Power Bitwise Operation Processing in DRAM,” in *HPCA*, 2020.
- [321] Linghao Song, Youwei Zhuo, Xuehai Qian, Hai Li, and Yiran Chen, “GraphR: Accelerating Graph Processing Using ReRAM,” in *HPCA*, 2018.

- [322] Linghao Song, Xuehai Qian, Hai Li, and Yiran Chen, “PipeLayer: A Pipelined ReRAM-Based Accelerator for Deep Learning,” in *HPCA*, 2017.
- [323] Fei Gao, Georgios Tziantzioulis, and David Wentzlaff, “ComputeDRAM: In-Memory Compute Using Off-the-Shelf DRAMs,” in *MICRO*, 2019.
- [324] Charles Eckert, Xiaowei Wang, Jingcheng Wang, Arun Subramaniyan, Ravi Iyer, Dennis Sylvester, David Blaauw, and Reetuparna Das, “Neural Cache: Bit-Serial In-Cache Acceleration of Deep Neural Networks,” in *ISCA*, 2018.
- [325] Shaizeen Aga, Supreet Jeloka, Arun Subramaniyan, Satish Narayanasamy, David Blaauw, and Reetuparna Das, “Compute Caches,” in *HPCA*, 2017.
- [326] Daichi Fujiki, Scott Mahlke, and Reetuparna Das, “Duality Cache for Data Parallel Acceleration,” in *ISCA*, 2019.
- [327] Vivek Seshadri, Donghyuk Lee, Thomas Mullins, Hasan Hassan, Amirali Boroumand, Jeremie Kim, Michael A Kozuch, Onur Mutlu, Phillip B Gibbons, and Todd C Mowry, “Buddy-RAM: Improving the Performance and Efficiency of Bulk Bitwise Operations Using DRAM,” arXiv:1611.09988 [cs.AR], 2016.
- [328] Vivek Seshadri and Onur Mutlu, “Simple Operations in Memory to Reduce Data Movement,” in *Advances in Computers, Volume 106*, 2017.
- [329] Vivek Seshadri, Yoongu Kim, Chris Fallin, Donghyuk Lee, Rachata Ausavarungnirun, Gennady Pekhimenko, Yixin Luo, Onur Mutlu, Phillip B Gibbons, Michael A Kozuch *et al.*, “RowClone: Accelerating Data Movement and Initialization Using DRAM,” arXiv:1805.03502 [cs.AR], 2018.
- [330] Vivek Seshadri, Kevin Hsieh, Amirali Boroum, Donghyuk Lee, Michael A Kozuch, Onur Mutlu, Phillip B Gibbons, and Todd C Mowry, “Fast Bulk Bitwise AND and OR in DRAM,” *CAL*, 2015.
- [331] Shuangchen Li, Cong Xu, Qiaosha Zou, Jishen Zhao, Yu Lu, and Yuan Xie, “Pinatubo: A Processing-in-Memory Architecture for Bulk Bitwise Operations in Emerging Non-Volatile Memories,” in *DAC*, 2016.
- [332] Jo textasciitilde ao Dinis Ferreira, Gabriel Falcao, Juan Gómez-Luna, Mohammed Alser, Lois Orosa, Mohammad Sadrosadati, Jeremie S Kim, Geraldo F Oliveira, Taha Shahroodi, Anant Nori *et al.*, “pLUTo: In-DRAM Lookup Tables to Enable Massively Parallel General-Purpose Computation,” arXiv:2104.07699 [cs.AR], 2021.
- [333] Jo textasciitilde ao Dinis Ferreira, Gabriel Falcao, Juan Gómez-Luna, Mohammed Alser, Lois Orosa, Mohammad Sadrosadati, Jeremie S Kim, Geraldo F Oliveira, Taha Shahroodi, Anant Nori *et al.*, “pLUTo: Enabling Massively Parallel Computation in DRAM via Lookup Tables,” in *MICRO*, 2022.

- [334] Mohsen Imani, Saransh Gupta, Yeseong Kim, and Tajana Rosing, "FloatPIM: In-Memory Acceleration of Deep Neural Network Training with High Precision," in *ISCA*, 2019.
- [335] Zhezhi He, Li Yang, Shaahin Angizi, Adnan Siraj Rakin, and Deliang Fan, "Sparse BD-Net: A Multiplication-Less DNN with Sparse Binarized Depth-Wise Separable Convolution," *JETC*, 2020.
- [336] Jisung Park, Roknoddin Azizi, Geraldo F. Oliveira, Mohammad Sadrosadati, Rakesh Nadig, David Novo, Juan Gómez-Luna, Myungsuk Kim, and Onur Mutlu, "Flash-Cosmos: In-Flash Bulk Bitwise Operations Using Inherent Computation Capability of NAND Flash Memory," in *MICRO*, 2022.
- [337] Minh SQ Truong, Liting Shen, Alexander Glass, Alison Hoffmann, L Richard Carley, James A Bain, and Saugata Ghose, "Adapting the RACER Architecture to Integrate Improved In-ReRAM Logic Primitives," *JETCAS*, 2022.
- [338] Minh SQ Truong, Eric Chen, Deanyone Su, Liting Shen, Alexander Glass, L Richard Carley, James A Bain, and Saugata Ghose, "RACER: Bit-Pipelined Processing Using Resistive Memory," in *MICRO*, 2021.
- [339] Ataberk Olgun, Minesh Patel, Abdullah Giray Yağlıkçı, Haocong Luo, Jeremie S. Kim, F. Nisa Bostancı, Nandita Vijaykumar, Oğuz Ergin, and Onur Mutlu, "QUAC-TRNG: High-Throughput True Random Number Generation Using Quadruple Row Activation in Commodity DRAMs," in *ISCA*, 2021.
- [340] Jeremie S Kim, Minesh Patel, Hasan Hassan, Lois Orosa, and Onur Mutlu, "D-RaNGe: Using Commodity DRAM Devices to Generate True Random Numbers With Low Latency and High Throughput," in *HPCA*, 2019.
- [341] Jeremie S Kim, Minesh Patel, Hasan Hassan, and Onur Mutlu, "The DRAM Latency PUF: Quickly Evaluating Physical Unclonable Functions by Exploiting the Latency-Reliability Tradeoff in Modern Commodity DRAM Devices," in *HPCA*, 2018.
- [342] F Nisa Bostancı, Ataberk Olgun, Lois Orosa, A Giray Yağlıkçı, Jeremie S Kim, Hasan Hassan, Oğuz Ergin, and Onur Mutlu, "DR-STRaNGe: End-to-End System Design for DRAM-Based True Random Number Generators," in *HPCA*, 2022.
- [343] Ataberk Olgun, Juan Gomez Luna, Konstantinos Kanellopoulos, Behzad Salami, Hasan Hassan, Oguz Ergin, and Onur Mutlu, "PiDRAM: A Holistic End-to-End FPGA-Based Framework for Processing-in-DRAM," *TACO*, 2022.
- [344] Mustafa F Ali, Akhilesh Jaiswal, and Kaushik Roy, "In-Memory Low-Cost Bit-Serial Addition Using Commodity DRAM Technology," in *TCAS-I*, 2019.
- [345] Shaahin Angizi and Deliang Fan, "GraphiDe: A Graph Processing Accelerator Leveraging In-DRAM-Computing," in *GLSVLSI*, 2019.
- [346] Shuangchen Li, Alvin Oliver Glova, Xing Hu, Peng Gu, Dimin Niu, Krishna T Malladi, Hongzhong Zheng, Bob Brennan, and Yuan Xie, "SCOPE: A Stochastic Computing Engine for DRAM-Based In-Situ Accelerator," in *MICRO*, 2018.

- [347] Arun Subramaniyan and Reetuparna Das, "Parallel Automata Processor," in *ISCA*, 2017.
- [348] Yue Zha and Jing Li, "Hyper-AP: Enhancing Associative Processing Through A Full-Stack Optimization," in *ISCA*, 2020.
- [349] Daichi Fujiki, Scott Mahlke, and Reetuparna Das, "In-Memory Data Parallel Processor," in *ASPLOS*, 2018.
- [350] Lois Orosa, Yaohua Wang, Mohammad Sadrosadati, Jeremie Kim, Minesh Patel, Ivan Puddu, Haocong Luo, Kaveh Razavi, Juan Gómez-Luna, Hasan Hassan, Nika Mansouri Ghiasi, Saugata Ghose, and Onur Mutlu, "CODIC: A Low-Cost Substrate for Enabling Custom In-DRAM Functionalities and Optimizations," in *ISCA*, 2021.
- [351] Mrigank Sharad, Deliang Fan, and Kaushik Roy, "Ultra Low Power Associative Computing with Spin Neurons and Resistive Crossbar Memory," in *DAC*, 2013.
- [352] Seyyed Hossein SeyyedAghaei Rezaei, Mehdi Modarressi, Rachata Ausavarungnirun, Mohammad Sadrosadati, Onur Mutlu, and Masoud Daneshtalab, "NoM: Network-on-Memory for Inter-Bank Data Transfer in Highly-Banked Memories," *CAL*, 2020.
- [353] Congming Gao, Xin Xin, Youyou Lu, Youtao Zhang, Jun Yang, and Jiwu Shu, "Para-Bit: Processing Parallel Bitwise Operations in NAND Flash Memory Based SSDs," in *MICRO*, 2021.
- [354] Won Ho Choi, Pi-Feng Chiu, Wen Ma, Gertjan Hemink, Tung Thanh Hoang, Martin Lueker-Boden, and Zvonimir Bandic, "An In-Flash Binary Neural Network Accelerator with SLC NAND Flash Array," in *ISCAS*, 2020.
- [355] Runze Han, Peng Huang, Yachen Xiang, Chen Liu, Zhen Dong, Zhiqiang Su, Yongbo Liu, Lu Liu, Xiaoyan Liu, and Jinfeng Kang, "A Novel Convolution Computing Paradigm Based on NOR Flash Array with High Computing Speed and Energy Efficiency," *TCAS-I*, 2019.
- [356] Farnood Merrikh-Bayat, Xinjie Guo, Michael Klachko, Mirko Prezioso, Konstantin K Likharev, and Dmitri B Strukov, "High-Performance Mixed-Signal Neurocomputing with Nanoscale Floating-Gate Memory Cell Arrays," *TNNLS*, 2017.
- [357] Panni Wang, Feng Xu, Bo Wang, Bin Gao, Huaqiang Wu, He Qian, and Shimeng Yu, "Three-Dimensional NAND Flash for Vector-Matrix Multiplication," *TVLSI*, 2018.
- [358] Hang-Ting Lue, Po-Kai Hsu, Ming-Liang Wei, Teng-Hao Yeh, Pei-Ying Du, Wei-Chen Chen, Keh-Chung Wang, and Chih-Yuan Lu, "Optimal Design Methods to Transform 3D NAND Flash into a High-Density, High-Bandwidth and Low-Power Non-volatile Computing in Memory (nvCIM) Accelerator for Deep-Learning Neural Networks (DNN)," in *IEDM*, 2019.
- [359] Shine Kim, Yunho Jin, Gina Sohn, Jonghyun Bae, Tae Jun Ham, and Jae W Lee, "Behemoth: A Flash-Centric Training Accelerator for Extreme-Scale {DNNs}," in *FAST*, 2021.

- [360] Shaodi Wang, “MemCore: Computing-in-Flash Design for Deep Neural Network Acceleration,” in *EDTM*, 2022.
- [361] Runze Han, Yachen Xiang, Peng Huang, Yihao Shan, Xiaoyan Liu, and Jinfeng Kang, “Flash Memory Array for Efficient Implementation of Deep Neural Networks,” *Adv. Intell. Syst.*, 2021.
- [362] Myeonggu Kang, Hyeonuk Kim, Hyein Shin, Jaehyeong Sim, Kyeonghan Kim, and Lee-Sup Kim, “S-FLASH: A NAND Flash-Based Deep Neural Network Accelerator Exploiting Bit-Level Sparsity,” *TC*, 2021.
- [363] Sung-Tae Lee and Jong-Ho Lee, “Neuromorphic Computing Using NAND Flash Memory Architecture with Pulse Width Modulation Scheme,” *Front. Neurosci.*, 2020.
- [364] Hunjun Lee, Minseop Kim, Dongmoon Min, Joonsung Kim, Jongwon Back, Honam Yoo, Jong-Ho Lee, and Jangwoo Kim, “3D-FPIM: An Extreme Energy-Efficient DNN Acceleration System Using 3D NAND Flash-Based In-Situ PIM Unit,” in *MICRO*, 2022.
- [365] Xin Si, Win-San Khwa, Jia-Jing Chen, Jia-Fang Li, Xiaoyu Sun, Rui Liu, Shimeng Yu, Hiroyuki Yamauchi, Qiang Li, and Meng-Fan Chang, “A Dual-Split 6T SRAM-Based Computing-in-Memory Unit-Macro with Fully Parallel Product-Sum Operation for Binarized DNN Edge Processors,” *TCAS-I*, 2019.
- [366] William Andrew Simon, Yasir Mahmood Qureshi, Marco Rios, Alexandre Levisse, Marina Zapater, and David Atienza, “BLADE: An In-Cache Computing Architecture for Edge Devices,” *Trans. on Comp.*, 2020.
- [367] Anirban Nag, CN Ramachandra, Rajeev Balasubramonian, Ryan Stutsman, Edouard Giacomin, Hari Kambalasubramanyam, and Pierre-Emmanuel Gaillardon, “GenCache: Leveraging In-Cache Operators for Efficient Sequence Alignment,” in *MICRO*, 2019.
- [368] Xiaowei Wang, Jiecao Yu, Charles Augustine, Ravi Iyer, and Reetuparna Das, “Bit Prudent In-Cache Acceleration of Deep Convolutional Neural Networks,” in *HPCA*, 2019.
- [369] Khalid Al-Hawaj, Olalekan Afuye, Shady Agwa, Alyssa Apsel, and Christopher Batten, “Towards a Reconfigurable Bit-Serial/Bit-Parallel Vector Accelerator Using In-Situ Processing-in-SRAM,” in *ISCAS*, 2020.
- [370] Mingu Kang, Min-Sun Keel, Naresh R Shanbhag, Sean Eilert, and Ken Curewitz, “An Energy-Efficient VLSI Architecture for Pattern Recognition via Deep Embedding of Computation in SRAM,” in *ICASSP*, 2014.
- [371] Hyunjoon Kim, Taegeun Yoo, Tony Tae-Hyoung Kim, and Bongjin Kim, “Colonnade: A Reconfigurable SRAM-Based Digital Bit-Serial Compute-in-Memory Macro for Processing Neural Networks,” *JSSC*, 2021.
- [372] Zhewei Jiang, Shihui Yin, Jae-Sun Seo, and Mingoo Seok, “C3SRAM: An In-Memory-Computing SRAM Macro Based on Robust Capacitive Coupling Computing Mechanism,” *JSSC*, 2020.

- [373] Supreet Jeloka, Naveen Bharathwaj Akesh, Dennis Sylvester, and David Blaauw, “A 28 nm Configurable Memory (TCAM/BCAM/SRAM) Using Push-Rule 6T Bit Cell Enabling Logic-in-Memory,” *JSSC*, 2016.
- [374] Zhengrong Wang, Christopher Liu, Aman Arora, Lizy John, and Tony Nowatzki, “Infinity Stream: Portable and Programmer-Friendly In-/Near-Memory Fusion,” in *ASPLOS*, 2023.
- [375] Mingu Kang, Eric P Kim, Min-sun Keel, and Naresh R Shanbhag, “Energy-Efficient and High Throughput Sparse Distributed Memory Architecture,” in *ISCAS*, 2015.
- [376] Mohsen Imani, Saikishan Pampana, Saransh Gupta, Minxuan Zhou, Yeseong Kim, and Tajana Rosing, “DUAL: Acceleration of Clustering Algorithms Using Digital-Based Processing in-Memory,” in *MICRO*, 2020.
- [377] Kevin K Chang, Prashant J Nair, Donghyuk Lee, Saugata Ghose, Moinuddin K Qureshi, and Onur Mutlu, “Low-Cost Inter-Linked Subarrays (LISA): Enabling Fast Inter-Subarray Data Movement in DRAM,” in *HPCA*, 2016.
- [378] Geraldo F Oliveira, Nastaran Hajinazar, Sven Gregorio, Jo textasciitilde ao Dinis Ferreira, Nika Mansouri Ghiasi, Minesh Patel, Mohammed Alser, Saugata Ghose, Juan Gómez-Luna, and Onur Mutlu, “SIMDRAM: A Framework for Bit-Serial SIMD Processing Using DRAM,” in *ASPLOS*, 2021.
- [379] Quan Deng, Youtao Zhang, Minxuan Zhang, and Jun Yang, “LAcc: Exploiting Lookup Table-Based Fast and Accurate Vector Multiplication in DRAM-Based CNN Accelerator,” in *DAC*, 2019.
- [380] Purab Ranjan Sutradhar, Sathwika Bavikadi, Mark Connolly, Savankumar Prajapati, Mark A Indovina, Sai Manoj Pudukotai Dinakarrao, and Amlan Ganguly, “Look-Up-Table Based Processing-in-Memory Architecture with Programmable Precision-Scaling for Deep Learning Applications,” *TPDS*, 2021.
- [381] Purab Ranjan Sutradhar, Mark Connolly, Sathwika Bavikadi, Sai Manoj Pudukotai Dinakarrao, Mark A Indovina, and Amlan Ganguly, “pPIM: A Programmable Processor-in-Memory Architecture with Precision-Scaling for Deep Learning,” *CAL*, 2020.
- [382] Marzieh Lenjani, Patricia Gonzalez, Elaheh Sadredini, Shuangchen Li, Yuan Xie, Ameen Akel, Sean Eilert, Mircea R Stan, and Kevin Skadron, “Fulcrum: A Simplified Control and Access Mechanism Toward Flexible and Practical In-Situ Accelerators,” in *HPCA*, 2020.
- [383] Xiangjun Peng, Yaohua Wang, and Ming-Chang Yang, “CHOPPER: A Compiler Infrastructure for Programmable Bit-Serial SIMD Processing Using Memory In DRAM,” in *HPCA*, 2023.
- [384] Geraldo F Oliveira, Juan Gómez-Luna, Saugata Ghose, Amirali Boroumand, and Onur Mutlu, “Accelerating Neural Network Inference with Processing-in-DRAM: From the Edge to the Cloud,” *IEEE Micro*, 2022.

- [385] Gagandeep Singh, Mohammed Alser, Damla Senol Cali, Dionysios Diamantopoulos, Juan Gómez-Luna, Henk Corporaal, and Onur Mutlu, “FPGA-Based Near-Memory Acceleration of Modern Data-Intensive Applications,” *IEEE Micro*, 2021.
- [386] Geraldo F Oliveira, Alain Kohli, David Novo, Juan Gómez-Luna, and Onur Mutlu, “DaPPA: A Data-Parallel Framework for Processing-in-Memory Architectures,” arXiv:2310.10168 [cs.AR], 2023.
- [387] Geraldo F Oliveira, Juan Gómez-Luna, Saugata Ghose, and Onur Mutlu, “Methodologies, Workloads, and Tools for Processing-in-Memory: Enabling the Adoption of Data-Centric Architectures,” in *ISVLSI*, 2022.
- [388] Geraldo F Oliveira, Amirali Boroumand, Saugata Ghose, Juan Gómez-Luna, and Onur Mutlu, “Heterogeneous Data-Centric Architectures for Modern Data-Intensive Applications: Case Studies in Machine Learning and Databases,” in *ISVLSI*, 2022.
- [389] Taha Shahroodi, Gagandeep Singh, Mahdi Zahedi, Haiyu Mao, Joel Lindegger, Can Firtina, Stephan Wong, Onur Mutlu, and Said Hamdioui, “Swordfish: A Framework for Evaluating Deep Neural Network-Based Basecalling Using Computation-In-Memory with Non-Ideal Memristors,” in *MICRO*, 2023.
- [390] Jinfan Chen, Juan Gómez-Luna, Izzat El Hajj, Yuxin Guo, and Onur Mutlu, “SimplePIM: A Software Framework for Productive and Efficient Processing-in-Memory,” in *PACT*, 2023.
- [391] Harshita Gupta, Mayank Kabra, Juan Gómez-Luna, Konstantinos Kanellopoulos, and Onur Mutlu, “Evaluating Homomorphic Operations on a Real-World Processing-In-Memory System,” in *IISWC*, 2023.
- [392] Juan Gómez-Luna, Yuxin Guo, Sylvan Brocard, Julien Legriel, Remy Cimadomo, Geraldo F Oliveira, Gagandeep Singh, and Onur Mutlu, “Evaluating Machine Learning Workloads on Memory-Centric Computing Systems,” in *ISPASS*, 2023.
- [393] Maurus Item, Juan Gómez-Luna, Yuxin Guo, Geraldo F. Oliveira, Mohammad Sadrosadati, and Onur Mutlu, “TransPimLib: Efficient Transcendental Functions for Processing-in-Memory Systems,” in *ISPASS*, 2023.
- [394] Safaa Diab, Amir Nassereldine, Mohammed Alser, Juan Gómez Luna, Onur Mutlu, and Izzat El Hajj, “A Framework for High-Throughput Sequence Alignment Using Real Processing-In-Memory Systems,” *Bioinformatics*, 2023.
- [395] Haiyu Mao, Mohammed Alser, Mohammad Sadrosadati, Can Firtina, Akanksha Baranwal, Damla Senol Cali, Aditya Manglik, Nour Almadhoun Alser, and Onur Mutlu, “GenPIP: In-Memory Acceleration of Genome Analysis via Tight Integration of Basecalling and Read Mapping,” in *MICRO*, 2022.
- [396] Gagandeep Singh, Dionysios Diamantopoulos, Juan Gómez-Luna, Christoph Hagleitner, Sander Stuijk, Henk Corporaal, and Onur Mutlu, “Accelerating Weather Prediction Using Near-Memory Reconfigurable Fabric,” *TRETS*, 2022.

- [397] Sang-Soo Park, KyungSoo Kim, Jinin So, Jin Jung, Jonggeon Lee, Kyoungwan Woo, Nayeon Kim, Younghyun Lee, Hyungyo Kim, Yongsuk Kwon *et al.*, “An LPDDR-based CXL-PNM Platform for TCO-efficient Inference of Transformer-based Large Language Models,” in *HPCA*, 2024.
- [398] Donghun Lee, Jinin So, MINSEON AHN, Jong-Geon Lee, Jungmin Kim, Jeonghyeon Cho, Rebholz Oliver, Vishnu Charan Thummala, Ravi shankar JV, Sachin Suresh Upadhyaya *et al.*, “Improving In-Memory Database Operations with Acceleration DIMM (AxDIMM),” in *DaMoN*, 2022.
- [399] Jin Hyun Kim, Shin-haeng Kang, Sukhan Lee, Hyeonsu Kim, Woongjae Song, Yuhwan Ro, Seungwon Lee, David Wang, Hyunsung Shin, Bengseng Phuah *et al.*, “Aquabolt-XL: Samsung HBM2-PIM with In-Memory Processing for ML Accelerators and Beyond,” in *Hot Chips*, 2021.
- [400] Jin Hyun Kim, Yuhwan Ro, Jinin So, Sukhan Lee, Shin-haeng Kang, YeonGon Cho, Hyeonsu Kim, Byeongho Kim, Kyungsoo Kim, Sangsoo Park, Jin-Seong Kim, Sanghoon Cha, Won-Jo Lee, Jin Jung, Jong-Geon Lee, Jieun Lee, JoonHo Song, Seungwon Lee, Jeonghyeon Cho, Jaehoon Yu, and Kyomin Sohn, “Samsung PIM/PNM for Transformer Based AI: Energy Efficiency on PIM/PNM Cluster,” in *HotChips*, 2023.
- [401] Joonseop Sim, Soohong Ahn, Taeyoung Ahn, Seungyong Lee, Myunghyun Rhee, Jooyoung Kim, Kwangsik Shin, Donguk Moon, Euseok Kim, and Kyoung Park, “Computational CXL-Memory Solution for Accelerating Memory-Intensive Applications,” *CAL*, 2022.
- [402] Chirag Sudarshan, Mohammad Hassani Sadi, Lukas Steiner, Christian Weis, and Norbert Wehn, “A Critical Assessment of DRAM-PIM Architectures-Trends, Challenges and Solutions,” in *SAMOS*, 2022.
- [403] Kangqi Chen, Rakesh Nadig, Manos Frouzakis, Nika Mansouri Ghiasi, Yu Liang, Haiyu Mao, Jisung Park, Mohammad Sadrosadati, and Onur Mutlu, “REIS: A High-Performance and Energy-Efficient Retrieval System with In-Storage Processing,” in *ISCA*, 2025.
- [404] Ismail Emir Yuksel, Akash Sood, Ataberk Olgun, Oğuzhan Canpolat, Haocong Luo, Nisa Bostanci, Mohammad Sadrosadati, Giray Yaglikci, and Onur Mutlu, “PuDHammer: Experimental Analysis of Read Disturbance Effects of Processing-using-DRAM in Real DRAM Chips,” in *ISCA*, 2025.
- [405] Melina Soysal, Konstantina Koliogeorgi, Can Firtina, Nika Mansouri Ghiasi, Rakesh Nadig, Haiyu Mao, Geraldo F Oliveira, Yu Liang, Klea Zambaku, Mohammad Sadrosadati *et al.*, “MARS: Processing-In-Memory Acceleration of Raw Signal Genome Analysis Inside the Storage Subsystem,” in *ICS*, 2025.
- [406] Oğuzhan Canpolat, Ataberk Olgun, David Novo, Oğuz Ergin, and Onur Mutlu, “Easy-DRAM: An FPGA-Based Infrastructure for Fast and Accurate End-to-End Evaluation of Emerging DRAM Techniques,” in *DSN*, 2025.

- [407] William Andrew Simon, Leonid Yavits, Konstantina Koliogeorgi, Yann Falevoz, Yoshihiro Shibuya, Dominique Lavenier, Irem Boybat, Klea Zambaku, Berkan Şahin, Mohammad Sadrosadati *et al.*, “Processing-in-Memory for Genomics Workloads,” arXiv:2506.00597 [q-bio.GN], 2025.
- [408] Lorenzo Asquini, Manos Frouzakis, Juan Gómez-Luna, Mohammad Sadrosadati, Onur Mutlu, and Francesco Silvestri, “Accelerating Triangle Counting with Real Processing-in-Memory Systems,” arXiv:2505.04269 [cs.AR], 2025.
- [409] Onur Mutlu, Ataberk Olgun, and İsmail Emir Yüksel, “Memory-Centric Computing: Solving Computing’s Memory Problem,” in *IMW*, 2025.
- [410] William Andrew Simon, Irem Boybat, Riselda Kodra, Elena Ferro, Gagandeep Singh, Mohammed Alser, Shubham Jain, Hsinyu Tsai, Geoffrey W Burr, Onur Mutlu *et al.*, “CiMBA: Accelerating Genome Sequencing Through On-Device Basecalling via Compute-in-Memory,” *TPDS*, 2025.
- [411] Manos Frouzakis, Juan Gómez-Luna, Geraldo F Oliveira, Mohammad Sadrosadati, and Onur Mutlu, “PIMDAL: Mitigating the Memory Bottleneck in Data Analytics using a Real Processing-in-Memory System,” arXiv:2504.01948 [cs.AR], 2025.
- [412] Mayank Kabra, Rakesh Nadig, Harshita Gupta, Rahul Bera, Manos Frouzakis, Vaman Arulchelvan, Yu Liang, Haiyu Mao, Mohammad Sadrosadati, and Onur Mutlu, “CIPHERMATCH: Accelerating Homomorphic Encryption-Based String Matching via Memory-Efficient Data Packing and In-Flash Processing,” in *ASPLOS*, 2025.
- [413] Yintao He, Haiyu Mao, Christina Giannoula, Mohammad Sadrosadati, Juan Gómez-Luna, Huawei Li, Xiaowei Li, Ying Wang, and Onur Mutlu, “PAPI: Exploiting Dynamic Parallelism in Large Language Model Decoding with a Processing-In-Memory-Enabled Computing System,” in *ASPLOS*, 2025.
- [414] Yufeng Gu, Alireza Khadem, Sumanth Umesh, Ning Liang, Xavier Servot, Onur Mutlu, Ravi Iyer, and Reetuparna Das, “PIM is All You Need: A CXL-Enabled GPU-Free System for Large Language Model Inference,” in *ASPLOS*, 2025.
- [415] F Nisa Bostancı, Konstantinos Kanellopoulos, Ataberk Olgun, A Giray Yağlıkçı, İsmail Emir Yüksel, Nika Mansouri Ghiasi, Zülal Bingöl, Mohammad Sadrosadati, and Onur Mutlu, “Revisiting Main Memory-Based Covert and Side Channel Attacks in the Context of Processing-in-Memory,” in *DSN*, 2025.
- [416] Onur Mutlu, Saugata Ghose, Juan Gómez-Luna, and Rachata Ausavarungnirun, “A Modern Primer on Processing in Memory,” in *Emerging Computing: From Devices to Systems — Looking Beyond Moore and Von Neumann*. Springer, 2021.
- [417] S. Ghose, K. Hsieh, A. Boroumand, R. Ausavarungnirun, and O. Mutlu, “The Processing-in-Memory Paradigm: Mechanisms to Enable Adoption,” in *Beyond-CMOS Technologies for Next Generation Computer Design*, 2019.
- [418] Gabriel H Loh, Nuwan Jayasena, M Oskin, Mark Nutter, David Roberts, Mitesh Meswani, Dong Ping Zhang, and Mike Ignatowski, “A Processing in Memory Taxonomy and a Case for Studying Fixed-Function PIM,” in *WoNDP*, 2013.

- [419] R. Balasubramonian, J. Chang, T. Manning *et al.*, “Near-Data Processing: Insights from a MICRO-46 Workshop,” *IEEE Micro*, 2014.
- [420] Harold S Stone, “A Logic-in-Memory Computer,” *IEEE TC*, 1970.
- [421] Ashley Saulsbury, Fong Pong, and Andreas Nowatzky, “Missing the Memory Wall: The Case for Processor/Memory Integration,” in *ISCA*, 1996.
- [422] Onur Mutlu, Ataberk Olgun, Geraldo F. Oliveira, and Ismail Emir Yuksel, “Memory-Centric Computing: Recent Advances in Processing-in-DRAM,” arXiv:2412.19275 [cs.AR], 2024.
- [423] Hybrid Memory Cube Consortium, “Hybrid Memory Cube Specification Rev. 2.0,” <http://www.hybridmemorycube.org/>.
- [424] Dong Uk Lee, Kyung Whan Kim, Kwan Weon Kim, Hongjung Kim, Ju Young Kim, Young Jun Park, Jae Hwan Kim, Dae Suk Kim, Heat Bit Park, Jin Wook Shin *et al.*, “A 1.2V 8Gb 8-Channel 128GB/s High-Bandwidth Memory (HBM) Stacked DRAM with Effective Microbump I/O Test Methods Using 29nm Process and TSV,” in *ISSCC*, 2014.
- [425] Donghyuk Lee, Saugata Ghose, Gennady Pekhimenko, Samira Khan, and Onur Mutlu, “Simultaneous Multi-Layer Access: Improving 3D-Stacked Memory Bandwidth at Low Cost,” *TACO*, 2016.
- [426] Chirag Sudarshan, Taha Soliman, Thomas Kämpfe, Christian Weis, and Norbert Wehn, “FeFET versus DRAM Based PIM Architectures: A Comparative Study,” in *VLSI-SoC*, 2022.
- [427] Chirag Sudarshan, Taha Soliman, Jan Lappas, Christian Weis, Mohammad Hassani Sadi, Matthias Jung, Andre Guntoro, and Norbert Wehn, “A Weighted Current Summation Based Mixed Signal DRAM-PIM Architecture for Deep Neural Network Inference,” *JETCAS*, 2022.
- [428] Chirag Sudarshan, Mohammad Hassani Sadi, Christian Weis, and Norbert Wehn, “Optimization of DRAM Based PIM Architecture for Energy-Efficient Deep Neural Network Training,” in *ISCAS*, 2022.
- [429] Chirag Sudarshan, Taha Soliman, Cecilia De la Parra, Christian Weis, Leonardo Ecco, Matthias Jung, Norbert Wehn, and Andre Guntoro, “A Novel DRAM-Based Process-in-Memory Architecture and Its Implementation for CNNs,” in *ASP-DAC*, 2021.
- [430] Benjamin Y Cho, Yongkee Kwon, Sangkug Lym, and Mattan Erez, “Near Ddata Acceleration with Concurrent Host Access,” in *ICA*, 2020.
- [431] Changmin Shin, Jaeyong Song, Hongsun Jang, Dogeun Kim, Jun Sung, Taehee Kwon, Jae Hyung Ju, Frank Liu, Yeonkyu Choi, and Jinho Lee, “Piccolo: Large-Scale Graph Processing with Fine-Grained in-Memory Scatter-Gather,” in *HPCA*, 2025.
- [432] Seong Hoon Seo, Junghoon Kim, Donghyun Lee, Seonah Yoo, Seokwon Moon, Yeonhong Park, and Jae W Lee, “FACIL: Flexible DRAM Address Mapping for SoC-PIM Cooperative On-device LLM Inference,” in *HPCA*, 2025.

- [433] Tatsuya Kubo, Daichi Tokuda, Tomoya Nagatani, Masayuki Usui, Lei Qu, Ting Cao, and Shinya Takamaeda-Yamazaki, “MVDRAM: Enabling GeMV Execution in Unmodified DRAM for Low-Bit LLM Acceleration,” arXiv:2503.23817 [cs.AR], 2025.
- [434] Tatsuya Kubo, Daichi Tokuda, Lei Qu, Ting Cao, and Shinya Takamaeda-Yamazaki, “PUdTune: Multi-Level Charging for High-Precision Calibration in Processing-Using-DRAM,” *IEEE CAL*, 2025.
- [435] Mingxuan He, Choungki Song, Ilkon Kim, Chunseok Jeong, Seho Kim, Il Park, Mithuna Thottethodi, and TN Vijaykumar, “Newton: A DRAM-Maker’s Accelerator-in-Memory (AiM) Architecture for Machine Learning,” in *MICRO*, 2020.
- [436] Maurice Peemen, Arnaud AA Setio, Bart Mesman, and Henk Corporaal, “Memory-Centric Accelerator Design for Convolutional Neural Networks,” in *ICCD*, 2013.
- [437] Christina Giannoula, Peiming Yang, Ivan Fernandez, Jiacheng Yang, Sankeerth Durvasula, Yu Xin Li, Mohammad Sadrosadati, Juan Gomez Luna, Onur Mutlu, and Gennady Pekhimenko, “PyGim: An Efficient Graph Neural Network Library for Real Processing-In-Memory Architectures,” in *SIGMETRICS*, 2024.
- [438] Chuhan Min, Jiachen Mao, Hai Li, and Yiran Chen, “NeuralHMC: An Efficient HMC-Based Accelerator for Deep Neural Networks,” in *ASP-DAC*, 2019.
- [439] Minxuan Zhou, Weihong Xu, Jaeyoung Kang, and Tajana Rosing, “TransPIM: A Memory-Based Acceleration via Software-Hardware Co-Design for Transformer,” in *HPCA*, 2022.
- [440] Pei Liu, Ahmed Hemani, Kolin Paul, Christian Weis, Matthias Jung, and Norbert Wehn, “3D-Stacked Many-Core Architecture for Biological Sequence Analysis Problems,” *IJPP*, 2017.
- [441] Helena Caminal, Yannis Chronis, Tianshu Wu, Jignesh M Patel, and José F Martínez, “Accelerating Database Analytic Query Workloads Using an Associative Processor,” in *ISCA*, 2022.
- [442] Lifeng Nai and Hyesoon Kim, “Instruction Offloading with HMC 2.0 Standard: A Case Study for Graph Traversals,” in *MEMSYS*, 2015.
- [443] Shaahin Angizi, Jiao Sun, Wei Zhang, and Deliang Fan, “GraphS: A Graph Processing Accelerator Leveraging SOT-MRAM,” in *DATE*, 2019.
- [444] Hyojong Kim, Hyesoon Kim, Sudhakar Yalamanchili, and Arun F Rodrigues, “Understanding Energy Aspects of Processing-Near-Memory for HPC Workloads,” in *MEMSYS*, 2015.
- [445] Wooyoung Jo, Sangjin Kim, Juhyoung Lee, Donghyeon Han, Sangyeob Kim, Seungyoon Choi, and Hoi-Jun Yoo, “NeRPIM: A 4.2 mJ/Frame Neural Rendering Processing-in-Memory Processor with Space Encoding Block-Wise Mapping for Mobile Devices,” in *VLSI Technology and Circuits*, 2023.

- [446] Xiaoyu Sun, Weidong Cao, Brian Crafton, Kerem Akarvardar, Haruki Mori, Hidehiro Fujiwara, Hiroki Noguchi, Yu-Der Chih, Meng-Fan Chang, Yih Wang *et al.*, “Efficient Processing of MLPerf Mobile Workloads Using Digital Compute-in-Memory Macros,” *TCAD*, 2023.
- [447] Dufy Teguia, Jiaxuan Chen, Stella Bitchebe, Oana Balmau, and Alain Tchana, “vPIM: Processing-in-Memory Virtualization,” in *Middleware*, 2024.
- [448] Shuang Chen, Yi Jiang, Christina Delimitrou, and José F Martínez, “PIMCloud: QoS-Aware Resource Management of Latency-Critical Applications in Clouds with Processing-in-Memory,” in *HPCA*, 2022.
- [449] Elliott Cooper-Balis and Bruce Jacob, “Fine-Grained Activation for Power Reduction in DRAM,” *IEEE Micro*, 2010.
- [450] Aniruddha N Udipi, Naveen Muralimanohar, Niladrish Chatterjee, Rajeev Balasubramonian, Al Davis, and Norman P Jouppi, “Rethinking DRAM Design and Organization for Energy-Constrained Multi-Cores,” in *ISCA*, 2010.
- [451] Tao Zhang, Ke Chen, Cong Xu, Guangyu Sun, Tao Wang, and Yuan Xie, “Half-DRAM: A High-Bandwidth and Low-Power DRAM Architecture from the Rethinking of Fine-Grained Activation,” in *ISCA*, 2014.
- [452] Heonjae Ha, Ardavan Pedram, Stephen Richardson, Shahar Kvatinsky, and Mark Horowitz, “Improving Energy Efficiency of DRAM by Exploiting Half Page Row Access,” in *MICRO*, 2016.
- [453] Yebin Lee, Hyeonggyu Kim, Seokin Hong, and Soontae Kim, “Partial Row Activation for Low-Power DRAM System,” in *HPCA*, 2017.
- [454] Ataberk Olgun, F Bostanci, Geraldo F Oliveira, Yahya Can Tugrul, Rahul Bera, A Giray Yaglikci, Hasan Hassan, Oguz Ergin, and Onur Mutlu, “Sectored DRAM: An Energy-Efficient High-Throughput and Practical Fine-Grained DRAM Architecture,” arXiv:2207.13795 [cs.AR], 2022.
- [455] James Michael O’Connor, “Energy Efficient High Bandwidth DRAM for Throughput Processors,” Ph.D. dissertation, The University of Texas at Austin, 2021.
- [456] Mike O’Connor, Niladrish Chatterjee, Donghyuk Lee, John Wilson, Aditya Agrawal, Stephen W Keckler, and William J Dally, “Fine-Grained DRAM: Energy-Efficient DRAM for Extreme Bandwidth Systems,” in *MICRO*, 2017.
- [457] Ataberk Olgun, F Bostanci, Geraldo F Oliveira, Yahya Can Tugrul, Rahul Bera, A Giray Yaglikci, Hasan Hassan, Oguz Ergin, and Onur Mutlu, “Sectored DRAM: A Practical Energy-Efficient and High-Performance Fine-Grained DRAM Architecture,” *TACO*, 2024.
- [458] Intel Corp., “6th Generation Intel Core Processor Family Datasheet,” <http://www.intel.com/content/www/us/en/processors/core/>.

- [459] NVIDIA, “NVIDIA A100 Tensor Core GPU Architecture. White Paper,” <https://tinyurl.com/53a8easc>, 2020.
- [460] Gennady Pekhimenko, Vivek Seshadri, Onur Mutlu, Michael A Kozuch, Phillip B Gibbons, and Todd C Mowry, “Base-Delta-Immediate Compression: Practical Data Compression for On-Chip Caches,” in *PACT*, 2012.
- [461] Alaa R Alameldeen and David A Wood, “Adaptive Cache Compression for High-Performance Processors,” in *ISCA*, 2004.
- [462] Mafijul Md Islam and Per Stenstrom, “Characterization and Exploitation of Narrow-Width Loads: The Narrow-Width Cache Approach,” in *CASES*, 2010.
- [463] Oguz Ergin, Osman Unsal, Xavier Vera, and Antonio Gonzalez, “Exploiting Narrow Values for Soft Error Tolerance,” *Comp. Arch. Lett.*, 2006.
- [464] David Brooks and Margaret Martonosi, “Dynamically Exploiting Narrow Width Operands to Improve Processor Power and Performance,” in *HPCA*, 1999.
- [465] Oguz Ergin, Deniz Balkan, Kanad Ghose, and Dmitry Ponomarev, “Register Packing: Exploiting Narrow-Width Operands for Reducing Register File Pressure,” in *MICRO*, 2004.
- [466] Mihai Budiu, Majd Sakr, Kip Walker, and Seth C Goldstein, “BitValue Inference: Detecting and Exploiting Narrow Bitwidth Computations,” in *Euro-Par*, 2000.
- [467] Paul R Wilson, Scott F Kaplan, and Yannis Smaragdakis, “The Case for Compressed Caching in Virtual Memory Systems,” in *USENIX ATC*, 1999.
- [468] CC Guest and Thomas K Gaylord, “Truth-Table Look-Up Optical Processing Utilizing Binary and Residue Arithmetic,” *Applied Optics*, 1980.
- [469] Dhananjay S. Phatak and Israel Koren, “Hybrid Signed-Digit Number Systems: A Unified Framework for Redundant Number Representations with Bounded Carry Propagation Chains,” *TC*, 1994.
- [470] Marcel Lapointe, Huu Tue Huynh, and Paul Fortier, “Systematic Design of Pipelined Recursive Filters,” *TC*, 1993.
- [471] Joaquín Olivares, Javier Hormigo, Julio Villalba, Ignacio Benavides, and Emilio L Zapata, “SAD Computation based on Online Arithmetic for Motion Estimation,” *Microprocessors and Microsystems*, 2006.
- [472] Joaquín Olivares, Javier Hormigo, Julio Villalba, and Ignacio Benavides, “Minimum Sum of Absolute Differences Implementation in a Single FPGA Device,” in *FPL*, 2004.
- [473] Mary D Brown and Yale N Patt, “Using Internal Redundant Representations and Limited Bypass to Support Pipelined Adders and Register Files,” in *HPCA*, 2002.
- [474] UPMEM, “UPMEM Website,” <https://www.upmem.com>, 2020.

- [475] UPMEM, “Introduction to UPMEM PIM. Processing-in-memory (PIM) on DRAM Accelerator (White Paper),” 2018.
- [476] Juan Gómez-Luna, Izzat El Hajj, Ivan Fernandez, Christina Giannoula, Geraldo F Oliveira, and Onur Mutlu, “Benchmarking a New Paradigm: An Experimental Analysis of a Real Processing-in-Memory Architecture,” arXiv:2105.03814 [cs.AR], 2021.
- [477] Murray I Cole, *Algorithmic Skeletons: Structured Management of Parallel Computation*. Pitman London, 1989.
- [478] Murray Cole, “Bringing Skeletons Out of the Closet: A Pragmatic Manifesto for Skeletal Parallel Programming,” *Parallel Computing*, 2004.
- [479] SAFARI Research Group, “PrIM Benchmark Suite,” <https://github.com/CMU-SAFARI/prim-benchmarks>.
- [480] Esteban Garzón, Robert Hanhan, Marco Lanuzza, Adam Teman, and Leonid Yavits, “FASTA: Revisiting Fully Associative Memories in Computer Microarchitecture,” *IEEE Access*, 2024.
- [481] Jaewon Kwon, Yongju Lee, Hongju Kal, Minjae Kim, Youngsok Kim, and Won Woo Ro, “McCore: A Holistic Management of High-Performance Heterogeneous Multicores,” in *MICRO*, 2023.
- [482] Veronia Iskandar, Mohamed A Abd El Ghany, and Diana Goehringer, “NDP-RANK: Prediction and Ranking of NDP Systems Performance using Machine Learning,” *Microprocessors and Microsystems*, 2023.
- [483] Berk Saglam, Nam Ho, Carlos Falquez, Antoni Portero, Fabian Schätzle, Estela Suarez, and Dirk Pleiter, “Data Prefetching on Processors with Heterogeneous Memory,” in *MEMSYS*, 2024.
- [484] Kazi Asifuzzaman, Mohammad Alaul Haque Monil, Frank Liu, and Jeffrey S Vetter, “Evaluating HPC Kernels for Processing in Memory,” in *MEMSYS*, 2022.
- [485] Inseong Hwang, Jihoon Jang, and Hyun Kim, “Optimizing Deep Neural Network Precision for Processing-in-Memory: A Memory Bottleneck Perspective,” in *ICEIC*, 2025.
- [486] Veronia Iskandar, Mohamed A Abd El Ghany, and Diana Goehringer, “Auto-DOK: Compiler-Assisted Automatic Detection of Offload Kernels for FPGA-HBM Architectures,” in *DSD*, 2023.
- [487] Dimitrios Papalekas, Athanasios Tziouvaras, George Floros, Georgios Dimitriou, Michael Dossis, and Georgios Stamoulis, “Near Data Processing Performance Improvement Prediction via Metric-Based Workload Classification,” in *MOCAS*T, 2022.
- [488] Tom Glint, Chandan Kumar Jha, Manu Awasthi, and Joyce Mekie, “A Fresh Perspective on DNN Accelerators by Performing Holistic Analysis Across Paradigms,” arXiv:2208.05294 [cs.AR], 2022.

- [489] Parker Hao Tian, “Novel Affinity-Based Data Placement Mechanism for Processing-in-Memory Architectures,” Master’s thesis, 2023.
- [490] Changkyu Kim, Doug Burger, and Stephen W Keckler, “An Adaptive, Non-Uniform Cache Structure for Wire-Delay Dominated On-Chip Caches,” in *ASPLOS*, 2002.
- [491] Kyu-Nam Lim, Woong-Ju Jang, Hyung-Sik Won, Kang-Yeol Lee, Hyungsoo Kim, Dong-Whee Kim, Mi-Hyun Cho, Seung-Lo Kim, Jong-Ho Kang, Keun-Woo Park *et al.*, “A 1.2 V 23nm 6F2 4Gb DDR3 SDRAM with Local-Bitline Sense Amplifier, Hybrid LIO Sense Amplifier and Dummy-Less Array Architecture,” in *ISSCC*, 2012.
- [492] Tsugio Takahashi, Tomonori Sekiguchi, Riichiro Takemura, Seiji Narui, Hiroki Fujisawa, Shinichi Miyatake, Makoto Morino, Koji Arai, Satoru Yamada, Shoji Shukuri *et al.*, “A Multigigabit DRAM Technology with 6F2 Open-Bitline Cell, Distributed Over-driven Sensing, and Stacked-Flash Fuse,” *JSSC*, 2001.
- [493] Haocong Luo, Taha Shahroodi, Hasan Hassan, Minesh Patel, A Giray Yağlıkçı, Lois Orosa, Jisung Park, and Onur Mutlu, “CLR-DRAM: A Low-Cost DRAM Architecture Enabling Dynamic Capacity-Latency Trade-Off,” in *ISCA*, 2020.
- [494] Yoongu Kim, Weikun Yang, and Onur Mutlu, “Ramulator: A Fast and Extensible DRAM Simulator,” *CAL*, 2016.
- [495] Donghyuk Lee, Samira Khan, Lavanya Subramanian, Rachata Ausavarungnirun, Genady Pekhimenko, Vivek Seshadri, Saugata Ghose, and Onur Mutlu, “Reducing DRAM Latency by Exploiting Design-Induced Latency Variation in Modern DRAM Chips,” in *SIGMETRICS*, 2017.
- [496] Donghyuk Lee, “Reducing DRAM Latency at Low Cost by Exploiting Heterogeneity,” Ph.D. dissertation, Carnegie Mellon University, 2016.
- [497] Jamie Liu, Ben Jaiyen, Yoongu Kim, Chris Wilkerson, Onur Mutlu, J Liu, B Jaiyen, Y Kim, C Wilkerson, and O Mutlu, “An Experimental Study of Data Retention Behavior in Modern DRAM Devices: Implications for Retention Time Profiling Mechanisms,” in *ISCA*, 2013.
- [498] Engin Ipek, Onur Mutlu, José F Martínez, and Rich Caruana, “Self-Optimizing Memory Controllers: A Reinforcement Learning Approach,” in *ISCA*, 2008.
- [499] Brent Keeth, R Jacob Baker, Brian Johnson, and Feng Lin, *DRAM Circuit Design: Fundamental and High-Speed Topics*. John Wiley & Sons, 2007.
- [500] Minesh Patel, “Enabling Effective Error Mitigation In Memory Chips That Use On-Die Error-Correcting Codes,” Ph.D. dissertation, ETH Zürich, 2022.
- [501] Hasan Hassan, “Improving DRAM Performance, Reliability, and Security by Rigorously Understanding Intrinsic DRAM Operation,” Ph.D. dissertation, ETH Zürich, 2022.
- [502] Brent Keeth and R Jacob Baker, *DRAM Circuit Design: A Tutorial*, 2001.

- [503] Pietro Frigo, Emanuele Vannacc, Hasan Hassan, Victor Van Der Veen, Onur Mutlu, Cristiano Giuffrida, Herbert Bos, and Kaveh Razavi, “TRRespass: Exploiting the Many Sides of Target Row Refresh,” in *SP*, 2020.
- [504] Bruce Jacob, Spencer Ng, and David Wang, *Memory systems: cache, DRAM, disk*. Morgan Kaufmann, 2008.
- [505] Bruce Jacob, “The memory system: You can’t avoid it, you can’t ignore it, you can’t fake it,” *Synthesis Lectures on Computer Architecture*, vol. 4, no. 1, pp. 1–77, 2009.
- [506] Vinodh Cuppu, Bruce Jacob, Brian Davis, and Trevor Mudge, “A Performance Comparison of Contemporary DRAM Architectures,” in *ISCA*, 1999.
- [507] Kinam Kim, Chang-Gyu Hwang, and Jong Gil Lee, “DRAM Technology Perspective for Gigabit Era,” *T-ED*, 1998.
- [508] Minesh Patel, Taha Shahroodi, Aditya Manglik, Abdullah Giray Yağlıkçı, Ataberk Olgun, Haocong Luo, and Onur Mutlu, “Rethinking the Producer-Consumer Relationship in Modern DRAM-Based Systems,” *IEEE Access*, 2024.
- [509] JEDEC, *DDR3 SDRAM Specification*, 2008.
- [510] JEDEC, “JEDEC Standard: DDR4 SDRAM,” *JESD79-4C*, June, 2012.
- [511] JEDEC, *JESD79-5: DDR5 SDRAM Standard*, 2020.
- [512] Apple Inc., “About the Security Content of Mac EFI Security Update 2015-001,” <https://support.apple.com/en-us/HT204934>, 2015.
- [513] Hewlett-Packard Enterprise, “HP Moonshot Component Pack Version 2015.05.0,” <http://h17007.www1.hp.com/us/en/enterprise/servers/products/moonshot/component-pack/index.aspx>, 2015.
- [514] Lenovo, “Row Hammer Privilege Escalation,” https://support.lenovo.com/us/en/product_security/row_hammer, 2015.
- [515] Zvika Greenfield and Tomer Levy, “Throttling Support for Row-Hammer Counters,” U.S. Patent 925,188,5B2, 2012.
- [516] Dae-Hyun Kim, Prashant J Nair, and Moinuddin K Qureshi, “Architectural Support for Mitigating Row Hammering in DRAM Memories,” *IEEE CAL*, 2014.
- [517] Kuljit S Bains, John B Halbert, Suneeta Sah, and Zvika Greenfield, “Method, Apparatus and System for Providing a Memory Refresh,” U.S. Patent 9,030,903, 2015.
- [518] Kuljit S Bains and John B Halbert, “Row Hammer Monitoring Based on Stored Row Hammer Threshold Value,” U.S. Patent 10,083,737, 2016.
- [519] Kuljit S Bains and John B Halbert, “Distributed Row Hammer Tracking,” U.S. Patent 9,299,400, 2016.
- [520] Barbara Aichinger, “DDR Memory Errors Caused by Row Hammer,” in *HPEC*, 2015.

- [521] Zelalem Birhanu Aweke, Salessawi Ferede Yitbarek, Rui Qiao, Reetuparna Das, Matthew Hicks, Yossi Oren, and Todd Austin, “ANVIL: Software-Based Protection Against Next-Generation Rowhammer Attacks,” in *ASPLOS*, 2016.
- [522] Hector Gomez, Andres Amaya, and Elkim Roa, “DRAM Row-Hammer Attack Reduction using Dummy Cells,” in *NORCAS*, 2016.
- [523] Chia Yang, Chen Kang Wei, Yu Jing Chang, Tieh Chiang Wu, Hsiu Pin Chen, and Chao Sung Lai, “Suppression of RowHammer Effect by Doping Profile Modification in Saddle-Fin Array Devices for Sub-30-nm DRAM Technology,” *TDMR*, 2016.
- [524] Mungyu Son, Hyunsun Park, Junwhan Ahn, and Sungjoo Yoo, “Making DRAM Stronger Against Row Hammering,” in *DAC*, 2017.
- [525] Seyed Mohammad Seyedzadeh, Alex K. Jones, and Rami Melhem, “Counter-Based Tree Structure for Row Hammering Mitigation in DRAM,” *IEEE CAL*, 2017.
- [526] Seyed Mohammad Seyedzadeh, Donald Kline Jr, Alex K Jones, and Rami Melhem, “Mitigating Bitline Crosstalk Noise in DRAM Memories,” in *MEMSYS*, 2017.
- [527] S. M. Seyedzadeh, A. K. Jones, and R. Melhem, “Mitigating Wordline Crosstalk Using Adaptive Trees of Counters,” in *ISCA*, 2018.
- [528] Gorka Irazoqui, Thomas Eisenbarth, and Berk Sunar, “MASCAT: Stopping Microarchitectural Attacks Before Execution,” *IACR Cryptology*, 2016.
- [529] Seong-Wan Ryu, Kyungkyu Min, Jungho Shin, Heimi Kwon, Donghoon Nam, Taekyung Oh, Tae-Su Jang, Minsoo Yoo, Yongtaik Kim, and Sungjoo Hong, “Overcoming the Reliability Limitation in the Ultimately Scaled DRAM using Silicon Migration Technique by Hydrogen Annealing,” in *IEDM*, 2017.
- [530] Chia-Ming Yang, Chen-Kang Wei, Hsiu-Pin Chen, Jian-Shing Luo, Yu Jing Chang, Tieh-Chiang Wu, and Chao-Sung Lai, “Scanning Spreading Resistance Microscopy for Doping Profile in Saddle-Fin Devices,” *IEEE Transactions on Nanotechnology*, 2017.
- [531] Jung Min You and Joon-Sung Yang, “MRLoc: Mitigating Row-Hammering Based on Memory Locality,” in *DAC*, 2019.
- [532] Eojin Lee, Ingab Kang, Sukhan Lee, G. Edward Suh, and Jung Ho Ahn, “TWiCe: Preventing Row-Hammering by Exploiting Time Window Counters,” in *ISCA*, 2019.
- [533] Yeonhong Park, Woosuk Kwon, Eojin Lee, Tae Jun Ham, Jung Ho Ahn, and Jae W Lee, “Graphene: Strong yet Lightweight Row Hammer Protection,” in *MICRO*, 2020.
- [534] A. Giray Yağlıkcı, Jeremie S. Kim, Fabrice Devaux, and Onur Mutlu, “Security Analysis of the Silver Bullet Technique for RowHammer Prevention,” arXiv:2106.07084 [cs.CR], 2021.
- [535] A Giray Yağlıkcı, Minesh Patel, Jeremie S Kim, Roknoddin Azizi, Ataberk Olgun, Lois Orosa, Hasan Hassan, Jisung Park, Konstantinos Kanellopoulos, Taha Shahroodi *et al.*, “BlockHammer: Preventing RowHammer at Low Cost by Blacklisting Rapidly-Accessed DRAM Rows,” in *HPCA*, 2021.

- [536] Oğuzhan Canpolat, A. Giray Yağlıkçı, Ataberk Olgun, Ismail Emir Yüksel, Yahya Can Tuğrul, Konstantinos Kanellopoulos, Oğuz Ergin, and Onur Mutlu, “BreakHammer: Enabling Scalable and Low Overhead RowHammer Mitigations via Throttling Preventive Action Triggering Threads,” in *MICRO*, 2024.
- [537] Ingab Kang, Eojin Lee, and Jung Ho Ahn, “CAT-TWO: Counter-Based Adaptive Tree, Time Window Optimized for DRAM Row-Hammer Prevention,” *IEEE Access*, 2020.
- [538] Hasan Hassan, Yahya Can Tugrul, Jeremie S Kim, Victor Van der Veen, Kaveh Razavi, and Onur Mutlu, “Uncovering In-DRAM RowHammer Protection Mechanisms: A New Methodology, Custom RowHammer Patterns, and Implications,” in *MICRO*, 2021.
- [539] Moinuddin Qureshi, Aditya Rohan, Gururaj Saileshwar, and Prashant J Nair, “Hydra: Enabling Low-Overhead Mitigation of Row-Hammer at Ultra-Low Thresholds via Hybrid Tracking,” in *ISCA*, 2022.
- [540] Gururaj Saileshwar, Bolin Wang, Moinuddin Qureshi, and Prashant J Nair, “Randomized Row-Swap: Mitigating Row Hammer by Breaking Spatial Correlation Between Aggressor and Victim Rows,” in *ASPLOS*, 2022.
- [541] Ferdinand Brasser, Lucas Davi, David Gens, Christopher Liebchen, and Ahmad-Reza Sadeghi, “Can’t Touch This: Software-Only Mitigation Against Rowhammer Attacks Targeting Kernel Memory,” in *USENIX Security*, 2017.
- [542] Radhesh Krishnan Konoth, Marco Oliverio, Andrei Tatar, Dennis Andriesse, Herbert Bos, Cristiano Giuffrida, and Kaveh Razavi, “ZebRAM: Comprehensive and Compatible Software Protection Against Rowhammer Attacks,” in *OSDI*, 2018.
- [543] Victor van der Veen, Martina Lindorfer, Yanick Fratantonio, Harikrishnan Padmanabha Pillai, Giovanni Vigna, Christopher Kruegel, Herbert Bos, and Kaveh Razavi, “GuardION: Practical Mitigation of DMA-Based Rowhammer Attacks on ARM,” in *DIMVA*, 2018.
- [544] Saru Vig, Sarani Bhattacharya, Debdeep Mukhopadhyay, and Siew-Kei Lam, “Rapid Detection of Rowhammer Attacks Using Dynamic Skewed Hash Tree,” in *HASP*, 2018.
- [545] S. K. Gautam, S. K. Manhas, Arvind Kumar, Mahendra Pakala, and Yiehm Ellie, “Row Hammering Mitigation Using Metal Nanowire in Saddle Fin DRAM,” *IEEE TED*, 2019.
- [546] Michael Jaemin Kim, Jaehyun Park, Yeonhong Park, Wanju Doh, Namhoon Kim, Tae Jun Ham, Jae W Lee, and Jung Ho Ahn, “Mithril: Cooperative Row Hammer Protection on Commodity DRAM Leveraging Managed Refresh,” in *HPCA*, 2022.
- [547] Gyu-Hyeon Lee, Seongmin Na, Ilkwon Byun, Dongmoon Min, and Jangwoo Kim, “CryoGuard: A Near Refresh-Free Robust DRAM Design for Cryogenic Computing,” in *ISCA*, 2021.
- [548] Michele Marazzi, Flavien Solt, Patrick Jattke, Kubo Takashi, and Kaveh Razavi, “Pro-TRR: Principled yet Optimal In-DRAM Target Row Refresh,” in *IEEE S&P*, 2023.

- [549] Zhi Zhang, Yueqiang Cheng, Minghua Wang, Wei He, Wenhao Wang, Surya Nepal, Yansong Gao, Kang Li, Zhe Wang, and Chenggang Wu, “SoftTRR: Protect Page Tables against Rowhammer Attacks using Software-only Target Row Refresh,” in *USENIX ATC*, 2022.
- [550] Biresh Kumar Joardar, Tyler K Bletsch, and Krishnendu Chakrabarty, “Learning to Mitigate RowHammer Attacks,” in *DATE*, 2022.
- [551] Jonas Juffinger, Lukas Lamster, Andreas Kogler, Maria Eichlseder, Moritz Lipp, and Daniel Gruss, “CSI: Rowhammer–Cryptographic Security and Integrity against Rowhammer,” in *IEEE S&P*, 2023.
- [552] Anish Saxena, Gururaj Saileshwar, Prashant J. Nair, and Moinuddin Qureshi, “AQUA: Scalable Rowhammer Mitigation by Quarantining Aggressor Rows at Runtime,” in *MICRO*, 2022.
- [553] Evgeny Manzhosov, Adam Hastings, Meghna Pancholi, Ryan Piersma, Mohamed Tarek Ibn Ziad, and Simha Sethumadhavan, “Revisiting Residue Codes for Modern Memories,” in *MICRO*, 2022.
- [554] Samira Mirbagher Ajorpaz, Daniel Moghimi, Jeffrey Neal Collins, Gilles Pokam, Nael Abu-Ghazaleh, and Dean Tullsen, “EVAX: Towards a Practical, Pro-active & Adaptive Architecture for High Performance & Security,” in *MICRO*, 2022.
- [555] Amir Naseredini, Martin Berger, Matteo Sammartino, and Shale Xiong, “ALARM: Active LeArning of Rowhammer Mitigations,” <https://users.sussex.ac.uk/~mfb21/rh-draft.pdf>, 2022.
- [556] Biresh Kumar Joardar, Tyler K. Bletsch, and Krishnendu Chakrabarty, “Machine Learning-Based Rowhammer Mitigation,” *TCAD*, 2022.
- [557] Hasan Hassan, Ataberk Olgun, A Giray Yaglikci, Haocong Luo, and Onur Mutlu, “A Case for Self-Managing DRAM Chips: Improving Performance, Efficiency, Reliability, and Security via Autonomous in-DRAM Maintenance Operations,” arXiv:2207.13358 [cs.AR], 2022.
- [558] Zhenkai Zhang, Zihao Zhan, Daniel Balasubramanian, Bo Li, Peter Volgyesi, and Xenofon Koutsoukos, “Leveraging EM Side-Channel Information to Detect Rowhammer Attacks,” in *IEEE S&P*, 2020.
- [559] Kevin Loughlin, Stefan Saroiu, Alec Wolman, and Baris Kasikci, “Stop! Hammer Time: Rethinking Our Approach to Rowhammer Mitigations,” in *HotOS*, 2021.
- [560] Fabrice Devaux and Renaud Ayrignac, “Method and Circuit for Protecting a DRAM Memory Device from the Row Hammer Effect,” U.S. Patent 10,885,966, 2021.
- [561] Jin-Woo Han, Jungsik Kim, Dafna Beery, K. Deniz Bozdog, Peter Cuevas, Amitay Levi, Irwin Tain, Khai Tran, Andrew J. Walker, Senthil Vadakupudhu Palayam, Antonio Arreghini, Arnaud Furnémont, and M. Meyyappan, “Surround Gate Transistor With Epitaxially Grown Si Pillar and Simulation Study on Soft Error and Rowhammer Tolerance for DRAM,” *IEEE TED*, 2021.

- [562] Ali Fakhrzadehgan, Yale N. Patt, Prashant J. Nair, and Moinuddin K. Qureshi, “Safe-Guard: Reducing the Security Risk from Row-Hammer via Low-Cost Integrity Protection,” in *HPCA*, 2022.
- [563] Stefan Saroiu, Alec Wolman, and Lucian Cojocar, “The Price of Secrecy: How Hiding Internal DRAM Topologies Hurts Rowhammer Defenses,” in *IRPS*, 2022.
- [564] Stefan Saroiu and Alec Wolman, “How to Configure Row-Sampling-Based Rowhammer Defenses,” *DRAMSec*, 2022.
- [565] Kevin Loughlin, Stefan Saroiu, Alec Wolman, Yatin A. Manerkar, and Baris Kasikci, “MOESI-Prime: Preventing Coherence-Induced Hammering in Commodity Workloads,” in *ISCA*, 2022.
- [566] Ranyang Zhou, Sepehr Tabrizchi, Arman Roohi, and Shaahin Angizi, “LT-PIM: An LUT-Based Processing-in-DRAM Architecture with RowHammer Self-Tracking,” *IEEE CAL*, 2022.
- [567] Seungki Hong, Dongha Kim, Jaehyung Lee, Reum Oh, Changsik Yoo, Sangjoon Hwang, and Jooyoung Lee, “DSAC: Low-Cost Rowhammer Mitigation Using In-DRAM Stochastic and Approximate Counting Algorithm,” arXiv:2302.03591 [cs.CR], 2023.
- [568] Onur Mutlu, Ataberk Olgun, and A. Giray Yaglikci, “Fundamentally Understanding and Solving RowHammer,” in *ASP-DAC*, 2023.
- [569] Michele Marazzi, Patrick Jattke, Flavien Solt, and Kaveh Razavi, “REGA: Scalable Rowhammer Mitigation with Refresh-Generating Activations,” in *IEEE S&P*, 2022.
- [570] Andrea Di Dio, Koen Koning, Herbert Bos, and Cristiano Giuffrida, “Copy-on-Flip: Hardening ECC Memory Against Rowhammer Attacks,” in *NDSS*, 2023.
- [571] Sonia Sharma, Debdeep Sanyal, Arpit Mukhopadhyay, and Ramij Hasan Shaik, “A Review on Study of Defects of DRAM-RowHammer and Its Mitigation,” *Journal For Basic Sciences*, 2022.
- [572] Jeonghyun Woo, Gururaj Saileshwar, and Prashant J Nair, “Scalable and Secure Row-Swap: Efficient and Safe Row Hammer Mitigation in Memory Systems,” in *HPCA*, 2023.
- [573] Jin Hyo Park, Su Yeon Kim, Dong Young Kim, Geon Kim, Je Won Park, Sunyong Yoo, Young-Woo Lee, and Myoung Jin Lee, “RowHammer Reduction Using a Buried Insulator in a Buried Channel Array Transistor,” *IEEE Transactions on Electron Devices*, 2022.
- [574] Minbok Wi, Jaehyun Park, Seoyoung Ko, Michael Jaemin Kim, Nam Sung Kim, Eojin Lee, and Jung Ho Ahn, “SHADOW: Preventing Row Hammer in DRAM with Intra-Subarray Row Shuffling,” in *HPCA*, 2023.
- [575] Woongrae Kim, Chulmoon Jung, Seongnyuh Yoo, Duckhwa Hong, Jeongjin Hwang, Jungmin Yoon, Ohyoung Jung, Joonwoo Choi, Sanga Hyun, Mankeun Kang *et al.*, “A 1.1 V 16Gb DDR5 DRAM with Probabilistic-Aggressor Tracking, Refresh-Management Functionality, Per-Row Hammer Tracking, a Multi-Step Precharge, and Core-Bias Modulation for Security and Reliability Enhancement,” in *ISSCC*, 2023.

- [576] C Gude Ramarao, K Tejesh Kumar, G Ujjinappa, and B Vasu Deva Naidu, “Defending SoCs with FPGAs from Rowhammer Attacks,” *Material Science*, 2023.
- [577] Krishnendu Guha and Amlan Chakrabarti, “Criticality Based Reliability from Rowhammer Attacks in Multi-User-Multi-FPGA Platform,” in *VLSID*, 2022.
- [578] Loïc France, Florent Bruguier, Maria Mushtaq, David Novo, and Pascal Benoit, “Modeling Rowhammer in the gem5 Simulator,” in *CHES*, 2022.
- [579] Loïc France, Florent Bruguier, David Novo, Maria Mushtaq, and Pascal Benoit, “Reducing the Silicon Area Overhead of Counter-Based Rowhammer Mitigations,” in *18th CryptArch Workshop*, 2022.
- [580] Tanj Bennett, Stefan Saroiu, Alec Wolman, and Lucian Cojocar, “Panopticon: A Complete In-DRAM Rowhammer Mitigation,” in *DRAMSec*, 2021.
- [581] Shuhei Enomoto, Hiroki Kuzuno, and Hiroshi Yamada, “Efficient Protection Mechanism for CPU Cache Flush Instruction Based Attacks,” *IEICE Transactions on Information and Systems*, 2022.
- [582] Kerem Arıkan, Alessandro Palumbo, Luca Cassano, Pedro Reviriego, Salvatore Pontarelli, Giuseppe Bianchi, Oğuz Ergin, and Marco Ottavi, “Processor Security: Detecting Microarchitectural Attacks via Count-Min Sketches,” *VLSI*, 2022.
- [583] Chihiro Tomita, Makoto Takita, Kazuhide Fukushima, Yuto Nakano, Yoshiaki Shiraishi, and Masakatu Morii, “Extracting the Secrets of OpenSSL with RAMBleed,” *Sensors*, 2022.
- [584] Anish Saxena, Gururaj Saileshwar, Jonas Juffinger, Andreas Kogler, Daniel Gruss, and Moinuddin Qureshi, “PT-Guard: Integrity-Protected Page Tables to Defend Against Breakthrough Rowhammer Attacks,” in *DSN*, 2023.
- [585] Ranyang Zhou, Sabbir Ahmed, Adnan Siraj Rakin, and Shaahin Angizi, “DNN-Defender: An In-DRAM Deep Neural Network Defense Mechanism for Adversarial Weight Attack,” arXiv:2305.08034 [cs.CR], 2023.
- [586] Minesh Patel, Jeremie S Kim, Taha Shahroodi, Hasan Hassan, and Onur Mutlu, “Bit-Exact ECC Recovery (BEER): Determining DRAM On-Die ECC Functions by Exploiting DRAM Data Retention Characteristics,” in *MICRO*, 2020.
- [587] Samira Khan, Donghyuk Lee, Yoongu Kim, Alaa R Alameldeen, Chris Wilkerson, and Onur Mutlu, “The Efficacy of Error Mitigation Techniques for DRAM Retention Failures: A Comparative Experimental Study,” in *SIGMETRICS*, 2014.
- [588] Samira Khan, Donghyuk Lee, and Onur Mutlu, “PARBOR: An Efficient System-Level Technique to Detect Data-Dependent Failures in DRAM,” in *DSN*, 2016.
- [589] Samira Khan, Chris Wilkerson, Donghyuk Lee, Alaa R Alameldeen, and Onur Mutlu, “A Case for Memory Content-Based Detection and Mitigation of Data-Dependent Failures in DRAM,” *CAL*, 2016.

- [590] Samira Khan, Chris Wilkerson, Zhe Wang, Alaa R Alameldeen, Donghyuk Lee, and Onur Mutlu, “Detecting and Mitigating Data-Dependent DRAM Failures by Exploiting Current Memory Content,” in *MICRO*, 2017.
- [591] Minesh Patel, Geraldo Francisco de Oliveira, and Onur Mutlu, “HARP: Practically and Effectively Identifying Uncorrectable Errors in Memory Chips That Use On-Die Error-Correcting Codes,” in *MICRO*, 2021.
- [592] Minesh Patel, Jeremie S Kim, Hasan Hassan, and Onur Mutlu, “Understanding and Modeling On-Die Error Correction in Modern DRAM: An Experimental Study Using Real Devices,” in *DSN*, 2019.
- [593] Minesh Patel, Taha Shahroodi, Aditya Manglik, Abdullah Giray Yağlıkçı, Ataberk Olgun, Haocong Luo, and Onur Mutlu, “Rethinking the Producer-Consumer Relationship in Modern DRAM-Based Systems,” arXiv:2401.16279 [cs.AR], 2024.
- [594] Xiaowu Zhang, Jong Kai Lin, Sunil Wickramanayaka, Songbai Zhang, Roshan Weerasekera, Rahul Dutta, Ka Fai Chang, King-Jien Chui, Hong Yu Li, David Soon Wee Ho *et al.*, “Heterogeneous 2.5 D Integration on Through Silicon Interposer,” *Applied Physics Reviews*, 2015.
- [595] Liu Ke, Udit Gupta, Benjamin Youngjae Cho, David Brooks, Vikas Chandra, Utku Diril, Amin Firoozshahian, Kim Hazelwood, Bill Jia, Hsien-Hsin S Lee *et al.*, “RecNMP: Accelerating Personalized Recommendation with Near-Memory Processing,” in *ISCA*, 2020.
- [596] Gabriel H. Loh, “3D-Stacked Memory Architectures for Multi-Core Processors,” in *ISCA*, 2008.
- [597] JEDEC Solid State Technology Assn., “JESD23-5D: High Bandwidth Memory (HBM) DRAM Standard,” March 2021.
- [598] JEDEC, “Wide I/O Single Data Rate (Wide I/O SDR),” Standard No. JESD229, 2011.
- [599] JEDEC, “Wide I/O 2 (WideIO2),” Standard No. JESD229-2, 2014.
- [600] Hybrid Memory Cube Consortium, “HMC Specification 2.0,” 2014.
- [601] Y Kagawa, N Fujii, K Aoyagi, Y Kobayashi, S Nishi, N Todaka, S Takeshita, J Taura, H Takahashi, Y Nishimura *et al.*, “Novel Stacked CMOS Image Sensor with Advanced Cu2Cu Hybrid Bonding,” in *IEDM*, 2016.
- [602] Dimin Niu, Shuangchen Li, Yuhao Wang, Wei Han, Zhe Zhang, Yijin Guan, Tianchan Guan, Fei Sun, Fei Xue, Lide Duan *et al.*, “184QPS/W 64Mb/mm² 3D Logic-to-DRAM Hybrid Bonding with Process-Near-Memory Engine for Recommendation System,” in *ISSCC*, 2022.
- [603] Martin A Schmidt, “Wafer-to-Wafer Bonding for Microstructure Formation,” *Proc. IEEE*, 1998.
- [604] B. Gopireddy and J. Torrellas, “Designing Vertical Processors in Monolithic 3D,” in *ISCA*, 2019.

- [605] S. Mitra, “Abundant-Data Computing: The N3XT 1,000X,” in *VLSI-TSA*, 2018.
- [606] W. Hwang, W. Wan, S. Mitra, and H. . P. Wong, “Coming Up N3XT, After 2D Scaling of Si CMOS,” in *ISCAS*, 2018.
- [607] S. Mitra, “From Nanodevices to Nanosystems: The N3XT Information Technology,” in *E3S*, 2015.
- [608] Dennis Rich, Andrew Bartolo, Carlo Gilardo, Binh Le, Haitong Li, Rebecca Park, Robert M. Radway, Mohamed M. Sabry Aly, H.-S. Philip Wong, and Subhasish Mitra, *Heterogeneous 3D Nano-Systems: The N3XT Approach?* Springer, 2020.
- [609] M. M. Sabry Aly, M. Gao, G. Hills, C. Lee, G. Pitner, M. M. Shulaker, T. F. Wu, M. Asheghi, J. Bokor, F. Franchetti, K. E. Goodson, C. Kozyrakis, I. Markov, K. Olukotun, L. Pileggi, E. Pop, J. Rabaey, C. Ré, H. . P. Wong, and S. Mitra, “Energy-Efficient Abundant-Data Computing: The N3XT 1,000x,” *Computer*, 2015.
- [610] M. M. Sabry Aly, T. F. Wu, A. Bartolo, Y. H. Malviya, W. Hwang, G. Hills, I. Markov, M. Wootters, M. M. Shulaker, H. . Philip Wong, and S. Mitra, “The N3XT Approach to Energy-Efficient Abundant-Data Computing,” *Proc. IEEE*, 2019.
- [611] Nika Mansouri Ghiasi, Mohammad Sadrosadati, Geraldo F Oliveira, Konstantinos Kanellopoulos, Rachata Ausavarungnirun, Juan Gómez Luna, Aditya Manglik, Jo textasciitilde ao Ferreira, Jeremie S Kim, Christina Giannoula *et al.*, “RevaMp3D: Architecting the Processor Core and Cache Hierarchy for Systems with Monolithically-Integrated Logic and Memory,” arXiv:2210.08508 [cs.AR], 2022.
- [612] John H Lau, “Recent Advances and Trends in Cu–Cu Hybrid Bonding,” *IEEE Trans. Compon. Packag. Manuf. Technol.*, 2023.
- [613] Mohammad Sadegh Ebrahimi, Gage Hills, Mohamed M Sabry, Max M Shulaker, Hai Wei, Tony F Wu, Subhasish Mitra, and H-S Philip Wong, “Monolithic 3D Integration Advances and Challenges: From Technology to System Levels,” in *S3S*, 2014.
- [614] Jun-young Kim, Xin Ju, Kah-Wee Ang, and Dongzhi Chi, “Van der Waals Layer Transfer of 2D Materials for Monolithic 3D Electronic System Integration: Review and Outlook,” *ACS Nano*, 2023.
- [615] Amirali Boroumand, Saugata Ghose, Minesh Patel, Hasan Hassan, Brandon Lucia, Kevin Hsieh, Krishna T. Malladi, Hongzhong Zheng, and Onur Mutlu, “CoNDA: Enabling Efficient Near-Data Accelerator Communication by Optimizing Data Movement,” *ISCA*, 2019.
- [616] Q. Zhu, B. Akin, H. E. Sumbul *et al.*, “A 3D-Stacked Logic-in-Memory Accelerator for Application-Specific Data Intensive Computing,” in *3DIC*, 2013.
- [617] W. H. Kautz, “Cellular Logic-in-Memory Arrays,” *IEEE TC*, 1969.
- [618] Raschid, Fei, and Lam, “A Special-Function Unit for Sorting and Sort-Based Satabase Operations,” *IEEE TC*, 1986.

- [619] David Elliot Shaw, "The non-von supercomputer," Columbia University, Tech. Rep., 1982. [Online]. Available: <https://academiccommons.columbia.edu/doi/10.7916/D8PV6TC0>
- [620] David Elliot Shaw, "NON-VON's Applicability to Three AI Task Areas," in *IJCAI*, 1985.
- [621] N Takagi and C-K Wong, "A Hardware Sort-Merge System," *IJRD*, 1985.
- [622] Emam and Lipovski, "The Architectural Features and Implementation Techniques of the Multicell CASSM," *IEEE TC*, 1979.
- [623] David K Hsiao, Krishnamurthi Kannan, and Douglas S Kerr, "Structure Memory Designs for a Database Computer," in *ACM*, 1977.
- [624] Casper R DeFiore and P Bruce Berra, "A Data Management System Utilizing an Associative Memory," in *AFIPS*, 1973.
- [625] Chyuan Shiun Lin and Diane CP Smith, "The Design of a Rotating Associative Array Memory for a Relational Data Base Management Application," in *VLDB*, 1975.
- [626] Stanley YW Su, George P Copeland, and G Jack Lipovski, "Retrieval Operations and Data Representations in a Context-Addressed Disc System," in *SIGIR*, 1973.
- [627] James Lawrence Parker, "A Logic Per Track Information Retrieval System," Ph.D. dissertation, University of Illinois at Urbana-Champaign, 1971.
- [628] NAFTALY Minsky, "Rotating Storage devices as Partially Associative Memories," in *SIGFIDET*, 1972.
- [629] Mario Jino and Jane W. S. Liu, "Intelligent Magnetic Bubble Memories," in *ISCA*, 1978.
- [630] Doty, Greenblatt, and Stanley Y.W. Su, "Magnetic Bubble Memory Architectures for Supporting Associative Searching of Relational Databases," *IEEE TC*, 1980.
- [631] Bongiovanni and Luccio, "Maintaining Sorted Files in a Magnetic Bubble Memory," *IEEE TC*, 1980.
- [632] David Elliot Shaw, Salvatore J. Stolfo, Hussein Ibrahim, Bruce Hillyer, Gio Wiederhold, and JA Andrews, "The NON-VON Database Machine: A Brief Overview," *IEEE Database Eng. Bull.*, 1981.
- [633] Mark Oskin, Frederic T Chong, and Timothy Sherwood, "Active Pages: A Computation Model for Intelligent Memory," in *ISCA*, 1998.
- [634] Yi Kang, Wei Huang, Seung-Moon Yoo, Diana Keen, Zhenzhou Ge, Vinh Lam, Pratap Pattanaik, and Josep Torrellas, "FlexRAM: Toward an Advanced Intelligent Memory System," in *ICCD*, 1999.
- [635] Ngeci Bowman, Neal Cardwell, C Kozyrakis *et al.*, "Evaluation of existing architectures in iram systems," in *Int. Symp. Computer Architecture - Workshop on Mixing Logic and DRAM*, 1997.

- [636] Kimberly Keeton, David A. Patterson, and Joseph M. Hellerstein, “A Case for Intelligent Disks (IDISKs),” *SIGMOD Rec.*, 1998.
- [637] Peter M Kogge, “EXECUBE—A New Architecture for Scaleable MPPs,” in *ICPP*, 1994.
- [638] Duncan G Elliott, W Martin Snelgrove, and Michael Stumm, “Computational RAM: A Memory-SIMD Hybrid and Its Application to DSP,” in *CICC*, 1992.
- [639] Ytong-Bin Kim and Tom W Chen, “Assessing Merged DRAM/Logic Technology,” *Integration*, 1999.
- [640] Ytong-Bin Kim and Tom W Chen, “Assessing Merged DRAM/Logic Technology,” in *ISCA*, 1996.
- [641] Taeho Kgil, Shaun D’Souza, Ali Saidi, Nathan Binkert, Ronald Dreslinski, Trevor Mudge, Steven Reinhardt, and Krisztian Flautner, “PicoServer: Using 3D Stacking Technology to Enable a Compact Energy Efficient Chip Multiprocessor,” in *ASPLOS*, 2006.
- [642] Hybrid Memory Cube Consortium, “HMC Specification 1.1,” 2013.
- [643] Maya Gokhale, Scott Lloyd, and Chris Macaraeg, “Hybrid Memory Cube Performance Characterization on Data-Centric Workloads,” in *IA³*, 2015.
- [644] Damla Senol, Jeremie Kim, Saugata Ghose, Can Alkan, and Onur Mutlu, “Nanopore Sequencing Technology and Tools for Genome Assembly: Computational Analysis of the Current State, Bottlenecks and Future Directions,” in *Briefings in Bioinformatics (BIB)*, 2018.
- [645] Mohammed Alser, Hasan Hassan, Hongyi Xin, Oğuz Ergin, Onur Mutlu, and Can Alkan, “GateKeeper: A New Hardware Architecture for Accelerating Pre-Alignment in DNA Short Read Mapping,” *Bioinformatics*, 2017.
- [646] Mohammed Alser, Taha Shahroodi, Juan Gomez-Luna, Can Alkan, and Onur Mutlu, “SneakySnake: A Fast and Accurate Universal Genome Pre-Alignment Filter for CPUs, GPUs, and FPGAs,” arXiv:1910.09020 [q-bio.GN], 2020.
- [647] Mohammed Alser, Hasan Hassan, Akash Kumar, Onur Mutlu, and Can Alkan, “Shouji: A Fast and Efficient Pre-Alignment Filter for Sequence Alignment,” *Bioinformatics*, 2019.
- [648] Thomas Moscibroda and Onur Mutlu, “Memory Performance Attacks: Denial of Memory Service in Multi-Core Systems,” in *USENIX Security*, 2007.
- [649] Onur Mutlu and Thomas Moscibroda, “Stall-Time Fair Memory Access Scheduling for Chip Multiprocessors,” in *MICRO*, 2007.
- [650] Onur Mutlu and Thomas Moscibroda, “Parallelism-Aware Batch Scheduling: Enhancing Both Performance and Fairness of Shared DRAM Systems,” in *ISCA*, 2008.
- [651] Lavanya Subramanian, “Providing High and Controllable Performance in Multicore Systems Through Shared Resource Management,” Ph.D. dissertation, Carnegie Mellon University, 2015.

- [652] Lavanya Subramanian, Vivek Seshadri, Yoongu Kim, Ben Jaiyen, and Onur Mutlu, "MISE: Providing Performance Predictability and Improving Fairness in Shared Main Memory Systems," in *HPCA*, 2013.
- [653] Hiroyuki Usui, Lavanya Subramanian, Kevin Kai-Wei Chang, and Onur Mutlu, "DASH: Deadline-Aware High-Performance Memory Scheduler for Heterogeneous Systems With Hardware Accelerators," *TACO*, 2016.
- [654] Lavanya Subramanian, Vivek Seshadri, Arnab Ghosh, Samira Khan, and Onur Mutlu, "The Application Slowdown Model: Quantifying and Controlling the Impact of Inter-Application Interference at Shared Caches and Main Memory," in *MICRO*, 2015.
- [655] Yoongu Kim, Michael Papamichael, Onur Mutlu, and Mor Harchol-Balter, "Thread Cluster Memory Scheduling: Exploiting Differences in Memory Access Behavior," in *MICRO*, 2010.
- [656] Hyoseung Kim, Dionisio De Niz, Björn Andersson, Mark Klein, Onur Mutlu, and Ragu-nathan Rajkumar, "Bounding Memory Interference Delay in COTS-Based Multi-Core Systems," in *RTAS*, 2014.
- [657] Hyoseung Kim, Dionisio De Niz, Björn Andersson, Mark Klein, Onur Mutlu, and Ra-gunathan Rajkumar, "Bounding and Reducing Memory Interference in COTS-Based Multi-Core Systems," *Real-Time Systems*, 2016.
- [658] G. Pekhimenko, T. C. Mowry, and O. Mutlu, "Linearly Compressed Pages: A Main Memory Compression Framework with Low Complexity and Low Latency," in *PACT*, 2012.
- [659] Gennady Pekhimenko, Vivek Seshadri, Yoongu Kim, Hongyi Xin, Onur Mutlu, Phillip B Gibbons, Michael A Kozuch, and Todd C Mowry, "Linearly Compressed Pages: A Low-Complexity, Low-Latency Main Memory Compression Framework," in *MICRO*, 2013.
- [660] I.N Churin and A Georgiev, "A CAMAC Crate Controller for the IBM PC/XT Family Computers with Built-In Selftest Features," *MicPro*, 1988.
- [661] B. Abali, H. Franke, D. E. Poff, R. A. Saccone, C. O. Schulz, L. M. Herger, and T. B. Smith, "Memory Expansion Technology (MXT): Software Support and Performance," *IBM JRD*, 2001.
- [662] J. Friedrich, H. Le, W. Starke, J. Stuechli, B. Sinharoy, E. J. Fluhr, D. Dreps, V. Zyuban, G. Still, C. Gonzalez, D. Hogenmiller, F. Malgioglio, R. Nett, R. Puri, P. Restle, D. Shan, Z. T. Deniz, D. Wendel, M. Ziegler, and D. Victor, "The POWER8™ Processor: De-signed for Big Data, Analytics, and Cloud Environments," in *ICICDT*, 2014.
- [663] Lois Orosa, Abdullah Giray Yaglikci, Haocong Luo, Ataberk Olgun, Jisung Park, Hasan Hassan, Minesh Patel, Jeremie S Kim, and Onur Mutlu, "A Deeper Look into RowHam-mer's Sensitivities: Experimental Analysis of Real DRAM Chips and Implications on Future Attacks and Defenses," in *MICRO*, 2021.

- [664] Saugata Ghose, Tianshi Li, Nastaran Hajinazar, Damla Senol Cali, and Onur Mutlu, “Demystifying Complex Workload-DRAM Interactions: An Experimental Study,” in *SIGMETRICS*, 2019.
- [665] Lucian Cojocar, Jeremie Kim, Minesh Patel, Lillian Tsai, Stefan Saroiu, Alec Wolman, and Onur Mutlu, “Are We Susceptible to Rowhammer? An End-to-End Methodology for Cloud Providers,” in *S&P*, 2020.
- [666] Misiker Tadesse Aga, Zelalem Birhanu Aweke, and Todd Austin, “When Good Protections Go Bad: Exploiting Anti-DoS Measures to Accelerate Rowhammer Attacks,” in *HOST*, 2017.
- [667] E. Bosman, K. Razavi, H. Bos, and C. Giuffrida, “Dedup Est Machina: Memory Deduplication as an Advanced Exploitation Vector,” in *S&P*, 2016.
- [668] Lucian Cojocar, Kaveh Razavi, Cristiano Giuffrida, and Herbert Bos, “Exploiting Correcting Codes: On the Effectiveness of ECC Memory Against RowHammer Attacks,” in *S&P*, 2019.
- [669] Daniel Gruss, Clémentine Maurice, and Stefan Mangard, “Rowhammer.js: A Remote Software-Induced Fault Attack in Javascript,” in *DIMVA*, 2016.
- [670] D. Gruss *et al.*, “Another Flip in the Wall of Rowhammer Defenses,” in *S&P*, 2018.
- [671] Rui Qiao and Mark Seaborn, “A New Approach for Rowhammer Attacks,” in *HOST*, 2016.
- [672] Andrei Tatar, Cristiano Giuffrida, Herbert Bos, and Kaveh Razavi, “Defeating Software Mitigations Against Rowhammer: A Surgical Precision Hammer,” in *RAID*, 2018.
- [673] Victor van der Veen, Yanick Fratantonio, Martina Lindorfer, Daniel Gruss, Clementine Maurice, Giovanni Vigna, Herbert Bos, Kaveh Razavi, and Cristiano Giuffrida, “Drammer: Deterministic Rowhammer Attacks on Mobile Platforms,” in *CCS*, 2016.
- [674] Zhi Zhang, Yueqiang Cheng, Dongxi Liu, Surya Nepal, Zhi Wang, and Yuval Yarom, “PTHammer: Cross-User-Kernel-Boundary Rowhammer Through Implicit Accesses,” in *MICRO*, 2020.
- [675] Jianxin Wang, Hongke Xu, Chaoen Xiao, Lei Zhang, and Yuzheng Zheng, “Research and Implementation of Rowhammer Attack Method Based on Domestic NeoKylin Operating System,” in *ICFTIC*, 2022.
- [676] Anil Kurmus, Nikolas Ioannou, Matthias Neugschwandtner, Nikolaos Papandreou, and Thomas Parnell, “From Random Block Corruption to Privilege Escalation: A Filesystem Attack Vector for RowHammer-like Attacks,” in *USENIX WOOT*, 2017.
- [677] M. Seaborn and T. Dullien, “Exploiting the DRAM Rowhammer Bug to Gain Kernel Privileges,” <http://googleprojectzero.blogspot.com.tr/2015/03/exploiting-dram-rowhammer-bug-to-gain.html>.

- [678] M. Seaborn and T. Dullien, “Exploiting the DRAM Rowhammer Bug to Gain Kernel Privileges,” <https://www.blackhat.com/docs/us-15/materials/us-15-Seaborn-Exploiting-The-DRAM-Rowhammer-Bug-To-Gain-Kernel-Privileges.pdf>, 2016.
- [679] Daniel Gruss, Clémentine Maurice, and Stefan Mangard, “Rowhammer.js: A Remote Software-Induced Fault Attack in JavaScript,” *CoRR*, 2015.
- [680] P. Frigo *et al.*, “Grand Pwning Unit: Accelerating Microarchitectural Attacks with the GPU,” in *S&P*, 2018.
- [681] M. Lipp *et al.*, “Nethammer: Inducing Rowhammer Faults through Network Requests,” arXiv:1805.04956v1 [cs.CR], 2018.
- [682] A. Tatar *et al.*, “Throwhammer: Rowhammer Attacks over the Network and Defenses,” in *USENIX ATC*, 2018.
- [683] Sebastien Carre, Matthieu Desjardins, Adrien Facon, and Sylvain Guilley, “OpenSSL Bellcore’s Protection Helps Fault Attack,” in *DSD*, 2018.
- [684] Yaakov Cohen, Kevin Sam Tharayil, Arie Haenel, Daniel Genkin, Angelos D Keromytis, Yossi Oren, and Yuval Yarom, “HammerScope: Observing DRAM Power Consumption Using Rowhammer,” in *CCS*, 2022.
- [685] Sangwoo Ji, Youngjoo Ko, Saeyoung Oh, and Jong Kim, “Pinpoint Rowhammer: Suppressing Unwanted Bit Flips on Rowhammer Attacks,” in *ASIACCS*, 2019.
- [686] Andrew Kwong, Daniel Genkin, Daniel Gruss, and Yuval Yarom, “RAMBleed: Reading Bits in Memory Without Accessing Them,” in *IEEE S&P*, 2020.
- [687] Youssef Tobah, Andrew Kwong, Ingab Kang, Daniel Genkin, and Kang G. Shin, “SpecHammer: Combining Spectre and Rowhammer for New Speculative Attacks,” in *IEEE S&P*, 2022.
- [688] Anandpreet Kaur, Pravin Srivastav, and Bibhas Ghoshal, “Work-in-Progress: DRAM-MaUT: DRAM Address Mapping Unveiling Tool for ARM Devices,” in *CASES*, 2022.
- [689] Dawei Li, Di Liu, Yangkun Ren, Ziyi Wang, Yu Sun, Zhenyu Guan, Qianhong Wu, and Jianwei Liu, “FPHammer: A Device Identification Framework based on DRAM Fingerprinting,” in *TrustCom*, 2023.
- [690] Kaveh Razavi, Ben Gras, Erik Bosman, Bart Preneel, Cristiano Giuffrida, and Herbert Bos, “Flip Feng Shui: Hammering a Needle in the Software Stack,” in *USENIX Security*, 2016.
- [691] Y. Xiao *et al.*, “One Bit Flips, One Cloud Flops: Cross-VM Row Hammer Attacks and Privilege Escalation,” in *USENIX Sec.*, 2016.
- [692] Fan Yao, Adnan Siraj Rakin, and Deliang Fan, “Deephhammer: Depleting the Intelligence of Deep Neural Networks Through Targeted Chain of Bit Flips,” in *USENIX Security*, 2020.

- [693] M Caner Tol, Saad Islam, Andrew J Adiletta, Berk Sunar, and Ziming Zhang, “Don’t Knock! Rowhammer at the Backdoor of DNN Models,” in *DSN*, 2023.
- [694] Sanghyun Hong, Pietro Frigo, Yiğitcan Kaya, Cristiano Giuffrida, and Tudor Dumitras, “Terminal Brain Damage: Exposing the Graceless Degradation in Deep Neural Networks Under Hardware Fault Attacks,” in *USENIX Security*, 2019.
- [695] Finn de Ridder, Pietro Frigo, Emanuele Vannacci, Herbert Bos, Cristiano Giuffrida, and Kaveh Razavi, “SMASH: Synchronized Many-Sided Rowhammer Attacks from JavaScript,” in *USENIX Security*, 2021.
- [696] Patrick Jattke, Victor van der Veen, Pietro Frigo, Stijn Gunter, and Kaveh Razavi, “Blacksmith: Scalable Rowhammering in the Frequency Domain,” in *IEEE S&P*, 2022.
- [697] Andreas Kogler, Jonas Juffinger, Salman Qazi, Yoongu Kim, Moritz Lipp, Nicolas Boichat, Eric Shiu, Mattias Nissler, and Daniel Gruss, “Half-Double: Hammering From the Next Row Over,” in *USENIX Security*, 2022.
- [698] Peter Pessl, Daniel Gruss, Clémentine Maurice, Michael Schwarz, and Stefan Mangard, “DRAMA: Exploiting DRAM Addressing for Cross-CPU Attacks,” in *USENIX Security*, 2016.
- [699] Zhenkai Zhang, Zihao Zhan, Daniel Balasubramanian, Xenofon Koutsoukos, and Gabor Karsai, “Triggering Rowhammer Hardware Faults on ARM: A Revisit,” in *ASHES*, 2018.
- [700] Sarani Bhattacharya and Debdeep Mukhopadhyay, “Curious Case of RowHammer: Flipping Secret Exponent Bits using Timing Analysis,” in *CHES*, 2016.
- [701] Sarani Bhattacharya and Debdeep Mukhopadhyay, “Advanced Fault Attacks in Software: Exploiting the Rowhammer Bug,” in *Fault Tolerant Architectures for Cryptography and Hardware Security*, 2018.
- [702] Michael Fahr Jr, Hunter Kippen, Andrew Kwong, Thinh Dang, Jacob Lichtinger, Dana Dachman-Soled, Daniel Genkin, Alexander Nelson, Ray Perlner, Arkady Yerukhimovich *et al.*, “When Frodo Flips: End-to-End Key Recovery on FrodoKEM via Rowhammer,” *CCS*, 2022.
- [703] Damian Poddebniak, Juraj Somorovsky, Sebastian Schinzel, Manfred Lochter, and Paul Rösler, “Attacking Deterministic Signature Schemes using Fault Attacks,” in *EuroS&P*, 2018.
- [704] Zane Weissman, Thore Tiemann, Daniel Moghimi, Evan Custodio, Thomas Eisenbarth, and Berk Sunar, “JackHammer: Efficient Rowhammer on Heterogeneous FPGA–CPU Platforms,” arXiv:1912.11523 [cs.CR], 2020.
- [705] Koksai Mus, Yarkin Doröz, M Caner Tol, Kristi Rahman, and Berk Sunar, “Jolt: Recovering TLS Signing Keys via Rowhammer Faults,” *Cryptology ePrint Archive*, 2022.

- [706] Michael Jacob Fahr, “The Effects of Side-Channel Attacks on Post-Quantum Cryptography: Influencing FrodoKEM Key Generation Using the Rowhammer Exploit,” Master’s thesis, University of Arkansas, Fayetteville, 2022.
- [707] Saad Islam, Koksai Mus, Richa Singh, Patrick Schaumont, and Berk Sunar, “Signature Correction Attack on Dilithium Signature Scheme,” in *Euro S&P*, 2022.
- [708] Liang Liu, Yanan Guo, Yueqiang Cheng, Youtao Zhang, and Jun Yang, “Generating Robust DNN with Resistance to Bit-Flip Based Adversarial Weight Attack,” *IEEE TC*, 2022.
- [709] Adnan Siraj Rakin, Md Hafizul Islam Chowdhuryy, Fan Yao, and Deliang Fan, “Deep-Steal: Advanced Model Extractions Leveraging Efficient Weight Stealing in Memories,” in *IEEE S&P*, 2022.
- [710] Mengxin Zheng, Qian Lou, and Lei Jiang, “TrojViT: Trojan Insertion in Vision Transformers,” arXiv:2208.13049 [cs.LG], 2022.
- [711] Kunbei Cai, Zhenkai Zhang, and Fan Yao, “On the Feasibility of Training-Time Trojan Attacks through Hardware-Based Faults in Memory,” in *HOST*, 2022.
- [712] Arman Roohi and Shaahin Angizi, “Efficient Targeted Bit-Flip Attack Against the Local Binary Pattern Network,” in *HOST*, 2022.
- [713] Felix Staudigl, Hazem Al Indari, Daniel Schön, Dominik Sisejkovic, Farhad Merchant, Jan Moritz Joseph, Vikas Rana, Stephan Menzel, and Rainer Leupers, “NeuroHammer: Inducing Bit-Flips in Memristive Crossbar Memories,” in *DATE*, 2022.
- [714] Li-Hsing Yang, Shin-Shan Huang, Tsai-Ling Cheng, Yi-Ching Kuo, and Jian-Jhih Kuo, “Socially-Aware Collaborative Defense System against Bit-Flip Attack in Social Internet of Things and Its Online Assignment Optimization,” in *ICCCN*, 2022.
- [715] Adnan Siraj Rakin, Zhezhi He, and Deliang Fan, “Bit-Flip Attack: Crushing Neural Network with Progressive Bit Search,” in *ICCV*, 2019.
- [716] Christina Giannoula, Ivan Fernandez, Juan Gómez-Luna, Nectarios Koziris, Georgios Goumas, and Onur Mutlu, “Towards Efficient Sparse Matrix Vector Multiplication on Real Processing-In-Memory Systems,” arXiv:2204.00900 [cs.AR], 2022.
- [717] SAFARI Research Group, “SparseP – GitHub Repository,” <https://github.com/CMU-SAFARI/SparseP>.
- [718] Safaa Diab, Amir Nassereldine, Mohammed Alser, Juan Gómez-Luna, Onur Mutlu, and Izzat El Hajj, “High-Throughput Pairwise Alignment with the Wavefront Algorithm Using Processing-in-Memory,” arXiv:2204.02085 [cs.AR], 2022.
- [719] SAFARI Research Group, “AIM – GitHub Repository,” <https://github.com/CMU-SAFARI/alignment-in-memory>.
- [720] Juan Gómez-Luna, Yuxin Guo, Sylvan Brocard, Julien Legriel, Remy Cimadomo, Geraldo F. Oliveira, Gagandeep Singh, and Onur Mutlu, “Machine Learning Training on a Real Processing-in-Memory System,” in *ISVLSI*, 2022.

- [721] Steve Rhyner, Haocong Luo, Juan Gomez-Luna, Mohammad Sadrosadati, Jiawei Jiang, Ataberk Olgun, Harshita Gupta, Ce Zhang, and Onur Mutlu, “PIM-Opt: Demystifying Distributed Optimization Algorithms on a Real-World Processing-In-Memory System,” in *PACT*, 2024.
- [722] Kailash Gogineni, Sai Santosh Dayapule, Juan Gómez-Luna, Karthikeya Gogineni, Peng Wei, Tian Lan, Mohammad Sadrosadati, Onur Mutlu, and Guru Venkataramani, “SwiftRL: Towards Efficient Reinforcement Learning on Real Processing-In-Memory Systems,” in *ISPASS*, 2024.
- [723] Liang-Chi Chen, Chien-Chung Ho, and Yuan-Hao Chang, “UpPipe: A Novel Pipeline Management on In-Memory Processors for RNA-seq Quantification,” in *DAC*, 2023.
- [724] Dominique Lavenier, Remy Cimadomo, and Romaric Jodin, “Variant Calling Parallelization on Processor-in-Memory Architecture,” in *BIBM*, 2020.
- [725] Dominique Lavenier, Charles Deltel, David Furodet, and Jean-François Roy, “BLAST on UPMEM,” INRIA Rennes-Bretagne Atlantique, Tech. Rep. 8878, 2016.
- [726] Hongbo Kang, Yiwei Zhao, Guy E Blelloch, Laxman Dhulipala, Yan Gu, Charles McGuffey, and Phillip B Gibbons, “PIM-trie: A Skew-Resistant Trie for Processing-in-Memory,” in *SPAA*, 2023.
- [727] Alexander Baumstark, Muhammad Attahir Jibril, and Kai-Uwe Sattler, “Accelerating Large Table Scan Using Processing-in-Memory Technology,” *BTW*, 2023.
- [728] Alexander Baumstark, Muhammad Attahir Jibril, and Kai-Uwe Sattler, “Adaptive Query Compilation with Processing-in-Memory,” in *ICDEW*, 2023.
- [729] Chaemin Lim, Suhyun Lee, Jinwoo Choi, Jounghoo Lee, Seongyeon Park, Hanjun Kim, Jinho Lee, and Youngsok Kim, “Design and Analysis of a Processing-in-DIMM Join Algorithm: A Case Study with UPMEM DIMMs,” *SIGMOD*, 2023.
- [730] Arthur Bernhardt, Andreas Koch, and Ilia Petrov, “pimDB: From Main-Memory DBMS to Processing-In-Memory DBMS-Engines on Intelligent Memories,” in *DaMoN*, 2023.
- [731] Suhyun Lee, Chaemin Lim, Jinwoo Choi, Heelim Choi, Chan Lee, Yongjun Park, Kwanghyun Park, Hanjun Kim, and Youngsok Kim, “SPID-Join: A Skew-Resistant Processing-in-DIMM Join Algorithm Exploiting the Bank-and Rank-level Parallelisms of DIMMs,” *SIGMOD*, 2024.
- [732] Joel Nider, Jackson Dagger, Niloo Gharavi, Daniel Ng, and Alexandra Fedorova, “Bulk JPEG Decoding on In-Memory Processors,” in *SYSTOR*, 2022.
- [733] Prangon Das, Purab Ranjan Sutradhar, Mark Indovina, Sai Manoj Pudukotai Dinakarrao, and Amlan Ganguly, “Implementation and Evaluation of Deep Neural Networks in Commercially Available Processing in Memory Hardware,” in *SOCC*, 2022.
- [734] Niloofar Zarif, “Offloading Embedding Lookups to Processing-in-Memory for Deep Learning Recommender Models,” Master’s thesis, University of British Columbia, 2023.

- [735] Hyeoncheol Kim, Taehoon Kim, Taehyeong Park, Donghyeon Kim, Yongseung Yu, Hanjun Kim, and Yongjun Park, “Accelerating LLMs using an Efficient GEMM Library and Target-Aware Optimizations on Real-World PIM Devices,” in *CGO*, 2025.
- [736] Saul B Needleman and Christian D Wunsch, “A General Method Applicable to the Search for Similarities in the Amino Acid Sequence of Two Proteins,” *Journal of Molecular Biology*, 1970.
- [737] Osamu Gotoh, “An Improved Algorithm for Matching Biological Sequences,” *Journal of Molecular Biology*, 1982.
- [738] Santiago Marco-Sola, Juan Carlos Moure, Miquel Moreto, and Antonio Espinosa, “Fast Gap-Affine Pairwise Alignment using the Wavefront Algorithm,” *Bioinformatics*, 2021.
- [739] Adrien Marie Legendre, *Nouvelles Méthodes Pour la Détermination des Orbites des Comètes*. Courcier, 1805.
- [740] Carl Friedrich Gauss, *Theoria Motus Corporum Coelestium in Sectionibus Conicis Solem Ambientium*. Perthes & Besser, 1809.
- [741] Joseph Berkson, “Application of the Logistic Function to Bio-Assay,” *JASA*, 1944.
- [742] James N Morgan and John A Sonquist, “Problems in the Analysis of Survey Data, and a Proposal,” *JASA*, 1963.
- [743] Stuart Lloyd, “Least Squares Quantization in PCM,” *IEEE Trans. Inf. Theory*, 1982.
- [744] James MacQueen, “Some Methods for Classification and Analysis of Multivariate Observations,” in *Fifth Berkeley Symposium on Mathematical Statistics and Probability*, 1967.
- [745] Herbert Robbins and Sutton Monro, “A Stochastic Approximation Method,” *Ann. Math. Statist.*, 1951.
- [746] Will Hamilton, Zhitao Ying, and Jure Leskovec, “Inductive Representation Learning on Large Graphs,” *NIPS*, 2017.
- [747] Thomas N Kipf and Max Welling, “Semi-Supervised Classification with Graph Convolutional Networks,” arXiv:1609.02907 [cs.LG], 2016.
- [748] Keyulu Xu, Weihua Hu, Jure Leskovec, and Stefanie Jegelka, “How Powerful Are Graph Neural Networks?” arXiv:1810.00826 [cs.LG], 2018.
- [749] Da Zheng, Chao Ma, Minjie Wang, Jinjing Zhou, Qidong Su, Xiang Song, Quan Gan, Zheng Zhang, and George Karypis, “DistDGL: Distributed Graph Neural Network Training for Billion-Scale Graphs,” in *IA3*, 2020.
- [750] Richard S Sutton and Andrew G Barto, *Reinforcement Learning: An Introduction*. Bradford Books, 2018.

- [751] Dongjae Lee, Bongjoon Hyun, Taehun Kim, and Minsoo Rhu, "PIM-MMU: A Memory Management Unit for Accelerating Data Transfers in Commercial PIM Systems," in *MICRO*, 2024.
- [752] Bongjoon Hyun, Taehun Kim, Dongjae Lee, and Minsoo Rhu, "Pathfinding Future PIM Architectures by Demystifying a Commercial PIM Technology," in *HPCA*, 2024.
- [753] Si Ung Noh, Junguk Hong, Chaemin Lim, Seongyeon Park, Jeehyun Kim, Hanjun Kim, Youngsok Kim, and Jinho Lee, "PID-Comm: A Fast and Flexible Collective Communication Framework for Commodity Processing-in-DIMM Devices," in *ISCA*, 2024.
- [754] Donghyeon Kim, Taehoon Kim, Inyong Hwang, Taehyeong Park, Hanjun Kim, Youngsok Kim, and Yongjun Park, "Virtual PIM: Resource-Aware Dynamic DPU Allocation and Workload Scheduling Framework for Multi-DPU PIM Architecture," in *PACT*, 2023.
- [755] Ian Goodfellow, Jean Pouget-Abadie, Mehdi Mirza, Bing Xu, David Warde-Farley, Sherjil Ozair, Aaron Courville, and Yoshua Bengio, "Generative Adversarial Networks," in *NIPS*, 2014.
- [756] Diederik P Kingma, "Auto-Encoding Variational Bayes," arXiv:1312.6114 [stat.ML], 2013.
- [757] Ashish Vaswani, Noam Shazeer, Niki Parmar, Jakob Uszkoreit, Llion Jones, Aidan N Gomez, Lukasz Kaiser, and Illia Polosukhin, "Attention Is All You Need," in *NIPS*, 2017.
- [758] Josh Achiam, Steven Adler, Sandhini Agarwal, Lama Ahmad, Ilge Akkaya, Florencia Leoni Aleman, Diogo Almeida, Janko Altschmidt, Sam Altman, Shyamal Anadkat *et al.*, "GPT-4 Technical Report," arXiv:2303.08774 [cs.CL], 2023.
- [759] Ben Wang, "Mesh-Transformer-JAX: Model-Parallel Implementation of Transformer Language Model with JAX," <https://github.com/kingoflolz/mesh-transformer-jax>, 2021.
- [760] Colin Raffel, Noam Shazeer, Adam Roberts, Katherine Lee, Sharan Narang, Michael Matena, Yanqi Zhou, Wei Li, and Peter J Liu, "Exploring the Limits of Transfer Learning with a Unified Text-to-Text Transformer," *JMLR*, 2020.
- [761] Jacob Devlin, Ming-Wei Chang, Kenton Lee, and Kristina Toutanova, "BERT: Pre-Training of Deep Bidirectional Transformers for Language Understanding," in *naacl-HLT*, 2019.
- [762] Jacob Devlin, Ming-Wei Chang, Kenton Lee, and Kristina Toutanova, "BERT: Pre-Training of Deep Bidirectional Transformers for Language Understanding," arXiv:1810.04805 [cs.CL], 2018.
- [763] Hugo Touvron, Louis Martin, Kevin Stone, Peter Albert, Amjad Almahairi, Yasmine Babaei, Nikolay Bashlykov, Soumya Batra, Prajjwal Bhargava, Shruti Bhosale *et al.*, "Llama 2: Open Foundation and Fine-Tuned Chat Models," arXiv:2307.09288 [cs.CL], 2023.

- [764] JEDEC Solid State Technology Assn., “JESD209-4C: Low Power Double Data Rate 4 (LPDDR4) Standard,” January 2020.
- [765] Stephen Van Doren, “Compute Express Link,” in *HOTI*, 2019.
- [766] JEDEC Solid State Technology Assn., “DDR4 SDRAM Registered DIMM Design Specification,” September 2014.
- [767] JEDEC Solid State Technology Assn., “DDR5 Registering Clock Driver Definition (DDR5RCD04),” June 2024.
- [768] JEDEC Solid State Technology Assn., “LRDIMM DDR3 Memory Buffer (MB),” January 2023.
- [769] Doe Hyun Yoon and Mattan Erez, “Virtualized and Flexible ECC for Main Memory,” in *ASPLOS*, 2010.
- [770] Youngeun Kwon, Yunjae Lee, and Minsoo Rhu, “TensorDIMM: A Practical Near-Memory Processing Architecture for Embeddings and Tensor Operations in Deep Learning,” in *MICRO*, 2019.
- [771] Zhe Zhou, Cong Li, Xuechao Wei, and Guangyu Sun, “GCNear: A Hybrid Architecture for Efficient GCN Training with Near-Memory Processing,” arXiv:2111.00680 [cs.LG], 2021.
- [772] Teng Tian, Xiaotian Wang, Letian Zhao, Wei Wu, Xuechang Zhang, Fangmin Lu, Tianqi Wang, and Xi Jin, “G-NMP: Accelerating Graph Neural Networks with DIMM-Based Near-Memory Processing,” *JSA*, 2022.
- [773] Haechan Kim, Jinmoo Heo, Seongjoo Lee, and Yunho Jung, “SARDIMM: High-Speed Near-Memory Processing Architecture for Synthetic Aperture Radar Imaging,” *Applied Sciences*, 2024.
- [774] Shiyan Yi, Yudi Qiu, Lingfei Lu, Guohao Xu, Yong Gong, Xiaoyang Zeng, and Yibo Fan, “GATe: Streamlining Memory Access and Communication to Accelerate Graph Attention Network with Near-Memory Processing,” *CAL*, 2024.
- [775] Sungmin Yun, Hwayong Nam, Jaehyun Park, Byeongho Kim, Jung Ho Ahn, and Eojin Lee, “GraNDe: Efficient Near-Data Processing Architecture for Graph Neural Networks,” *TC*, 2023.
- [776] Guohao Dai, Zhenhua Zhu, Tianyu Fu, Chiyue Wei, Bangyan Wang, Xiangyu Li, Yuan Xie, Huazhong Yang, and Yu Wang, “DIMMining: Pruning-Efficient and Parallel Graph Mining on Near-Memory-Computing,” in *ISCA*, 2022.
- [777] Jaehyun Park, Byeongho Kim, Sungmin Yun, Eojin Lee, Minsoo Rhu, and Jung Ho Ahn, “TRiM: Enhancing Processor-Memory Interfaces with Scalable Tensor Reduction in Memory,” in *MICRO*, 2021.
- [778] Dan Chen, Haiheng He, Hai Jin, Long Zheng, Yu Huang, Xinyang Shen, and Xiaofei Liao, “MetaNMP: Leveraging Cartesian-Like Product to Accelerate HGNNs with Near-Memory Processing,” in *MICRO*, 2023.

- [779] Zhe Zhou, Cong Li, Fan Yang, and Guangyu Sun, “DIMM-Link: Enabling Efficient Inter-DIMM Communication for Near-Memory Processing,” in *HPCA*, 2023.
- [780] Wenqin Huangfu, Xueqi Li, Shuangchen Li, Xing Hu, Peng Gu, and Yuan Xie, “MEDAL: Scalable DIMM Based Near Data Processing Accelerator for DNA Seeding Algorithm,” in *MICRO*, 2019.
- [781] Haifeng Liu, Long Zheng, Yu Huang, Chaoqiang Liu, Xiangyu Ye, Jingrui Yuan, Xiaofei Liao, Hai Jin, and Jingling Xue, “Accelerating Personalized Recommendation with Cross-Level Near-Memory Processing,” in *ISCA*, 2023.
- [782] Youngeun Kwon, Yunjae Lee, and Minsoo Rhu, “Tensor Casting: Co-Designing Algorithm-Architecture for Personalized Recommendation Training,” in *HPCA*, 2021.
- [783] Siying Feng, Xin He, Kuan-Yu Chen, Liu Ke, Xuan Zhang, David Blaauw, Trevor Mudge, and Ronald Dreslinski, “MeNDA: A Near-Memory Multi-Way Merge Solution for Sparse Transposition and Dataflows,” in *ISCA*, 2022.
- [784] B. Tian, Y. Li, L. Jiang, S. Cai, and M. Gao, “NDPBridge: Enabling Cross-Bank Coordination in Near-DRAM-Bank Processing Architectures,” in *ISCA*, 2024.
- [785] Mohammad Alian, Seung Won Min, Hadi Asgharimoghaddam, Ashutosh Dhar, Dong Kai Wang, Thomas Roewer, Adam McPadden, Oliver O’Halloran, Deming Chen, Jinjun Xiong *et al.*, “Application-Transparent Near-Memory Processing Architecture with Memory Channel Network,” in *MICRO*, 2018.
- [786] Benjamin Y Cho, Jeageun Jung, and Mattan Erez, “Accelerating Bandwidth-Bound Deep Learning Inference with Main-Memory Accelerators,” in *SC*, 2021.
- [787] Nam Sung Kim, Deming Chen, Jinjun Xiong, and W Hwu Wen-mei, “Heterogeneous Computing Meets Near-Memory Acceleration and High-Level Synthesis in the Post-Moore Era,” *IEEE Micro*, 2017.
- [788] Wenjie Xiong, Liu Ke, Dimitrije Jankov, Michael Kounavis, Xiaochen Wang, Eric Northup, Jie Amy Yang, Bilge Acun, Carole-Jean Wu, Ping Tak Peter Tang *et al.*, “Sec-NDP: Secure Near-Data Processing with Untrusted Memory,” in *HPCA*, 2022.
- [789] Liu Liu, Jilan Lin, Zheng Qu, Yufei Ding, and Yuan Xie, “ENMC: Extreme Near-Memory Classification via Approximate Screening,” in *MICRO*, 2021.
- [790] Lian Liu, Shixin Zhao, Bing Li, Haimeng Ren, Zhaohui Xu, Mengdi Wang, Xiaowei Li, Yinhe Han, and Ying Wang, “Make LLM Inference Affordable to Everyone: Augmenting GPU Memory with NDP-DIMM,” in *HPCA*, 2025.
- [791] Liyan Chen, Dongxu Lyu, Jianfei Jiang, Qin Wang, Zhigang Mao, and Naifeng Jing, “AsyncDIMM: Achieving Asynchronous Execution in DIMM-Based Near-Memory Processing,” in *HPCA*, 2025.
- [792] Liyan Chen, Jianfei Jiang, Qin Wang, Zhigang Mao, and Naifeng Jing, “Bridge-NDP: Achieving Efficient Communication-Computation Overlap in Near Data Processing with Bridge Architecture,” in *ASP-DAC*, 2024.

- [793] Liyan Chen, Pengyu Liu, Dongxu Lyu, Jianfei Jiang, Qin Wang, Zhigang Mao, and Naifeng Jing, “Bridge-NDP: Efficient Communication-Computation Overlap in Near Data Processing System,” *TCAD*, 2025.
- [794] Liyan Chen, Jianfei Jiang, Qin Wang, Zhigang Mao, and Naifeng Jing, “MDNMP: Metapath-Driven Software-Hardware Co-Design for HGNN Acceleration with Near-Memory Processing,” in *ASP-DAC*, 2025.
- [795] Minkyu Lee, Sang-Seol Lee, Kyungho Kim, Eunchong Lee, and Sung-Joon Jang, “HAIL-DIMM: Host Access Interleaved with Near-Data Processing on DIMM-Based Memory System,” in *DAC*, 2024.
- [796] Maxim Naumov, Dheevatsa Mudigere, Hao-Jun Michael Shi, Jianyu Huang, Narayanan Sundaraman, Jongsoo Park, Xiaodong Wang, Udit Gupta, Carole-Jean Wu, Alisson G. Azzolini, Dmytro Dzhulgakov, Andrey Mallevich, Ilia Cherniavskii, Yinghai Lu, Raghuraman Krishnamoorthi, Ansha Yu, Volodymyr Kondratenko, Stephanie Pereira, Xianjie Chen, Wenlin Chen, Vijay Rao, Bill Jia, Liang Xiong, and Misha Smelyanskiy, “Deep Learning Recommendation Model for Personalization and Recommendation Systems,” arXiv:1906.00091 [cs.IR], 2019.
- [797] Udit Gupta, Xiaodong Wang, Maxim Naumov, Carole-Jean Wu, Brandon Reagen, David Brooks, Bradford Cottel, Kim Hazelwood, Bill Jia, Hsien-Hsin S Lee *et al.*, “The Architectural Implications of Facebook’s DNN-Based Personalized Recommendation,” in *HPCA*, 2020.
- [798] JEDEC, “Graphics Double Data Rate (GDDR6) SGRAM Standard,” *JEDEC Standard JESD250C*, 2021.
- [799] Xilinx, “Alveo U250 Data Center Accelerator Card,” <https://www.xilinx.com/products/boards-and-kits/alveo/u250.html#documentation>.
- [800] Yaohua Wang, Lois Orosa, Xiangjun Peng, Yang Guo, Saugata Ghose, Minesh Patel, Jeremie S Kim, Juan Gómez Luna, Mohammad Sadrosadati, Nika Mansouri Ghiasi *et al.*, “FIGARO: Improving System Performance via Fine-Grained In-DRAM Data Relocation and Caching,” in *MICRO*, 2020.
- [801] Kiyoo Itoh, *VLSI Memory Chip Design*. Springer Science & Business Media, 2013.
- [802] Zhengrong Wang, Christopher Liu, Nathan Beckmann, and Tony Nowatzki, “Affinity Alloc: Taming Not-So Near-Data Computing,” in *MICRO*, 2023.
- [803] Brian C Schwedock and Nathan Beckmann, “Leviathan: A Unified System for General-Purpose Near-Data Computing,” in *MICRO*, 2024.
- [804] Brian C Schwedock, Piratach Yoovidhya, Jennifer Seibert, and Nathan Beckmann, “Tākō: A Polymorphic Cache Hierarchy for General-Purpose Optimization of Data Movement,” in *ISCA*, 2022.
- [805] Zhengrong Wang, Jian Weng, Sihao Liu, and Tony Nowatzki, “Near-Stream Computing: General and Transparent Near-Cache Acceleration,” in *HPCA*, 2022.

- [806] Anant V Nori, Rahul Bera, Shankar Balachandran, Joydeep Rakshit, Om J Omer, Avishai Abuhatzera, Belliappa Kuttanna, and Sreenivas Subramoney, "REDUCT: Keep It Close, Keep It Cool!: Efficient Scaling of DNN Inference on Multi-Core CPUs with Near-Cache Compute," in *ISCA*, 2021.
- [807] Alain Denzler, Rahul Bera, Nastaran Hajinazar, Gagandeep Singh, Geraldo F Oliveira, Juan Gómez-Luna, and Onur Mutlu, "Casper: Accelerating Stencil Computation Using Near-Cache Processing," *IEEE Access*, 2023.
- [808] Joao Vieira, Nuno Roma, Gabriel Falcao, and Pedro Tomás, "A Compute Cache System for Signal Processing Applications," *JSPS*, 2021.
- [809] Grégoire Eggermann, Marco Rios, Giovanni Ansaloni, Sani Nassif, and David Atienza, "A 16-Bit Floating-Point Near-SRAM Architecture for Low-Power Sparse Matrix-Vector Multiplication," in *VLSI-SoC*, 2023.
- [810] Ofer Shacham, Zain Asgar, Han Chen, Amin Firoozshahian, Rehan Hameed, Christos Kozyrakis, Wajahat Qadeer, Stephen Richardson, Alex Solomatnikov, Don Stark *et al.*, "Smart Memories Polymorphic Chip Multiprocessor," in *DAC*, 2009.
- [811] Dan Zhang, Xiaoyu Ma, Michael Thomson, and Derek Chiou, "Minnow: Lightweight Offload Engines for Worklist Management and Worklist-Directed Prefetching," *ASPLOS*, 2018.
- [812] Nika Mansouri Ghiasi, Jisung Park, Harun Mustafa, Jeremie Kim, Ataberk Olgun, Arvid Gollwitzer, Damla Senol Cali, Can Firtina, Haiyu Mao, Nour Almadhoun Alserr *et al.*, "GenStore: A High-Performance In-Storage Processing System for Genome Sequence Analysis," in *ASPLOS*, 2022.
- [813] Shuyi Pei, Jing Yang, and Qing Yang, "REGISTOR: A Platform for Unstructured Data Processing inside SSD Storage," *ACM TOS*, 2019.
- [814] Sang-Woo Jun, Andy Wright, Sizhuo Zhang, Shuotao Xu *et al.*, "GraFBoost: Using Accelerated Flash Storage for External Graph Analytics," in *ISCA*, 2018.
- [815] Jaeyoung Do, Yang-Suk Kee, Jignesh M Patel, Chanik Park, Kwanghyun Park, and David J DeWitt, "Query Processing on Smart SSDs: Opportunities and Challenges," in *ACM SIGMOD*, 2013.
- [816] Sudharsan Seshadri, Mark Gahagan, Sundaram Bhaskaran, Trevor Bunker, Arup De, Yanqin Jin, Yang Liu, and Steven Swanson, "Willow: A User-Programmable SSD," in *USENIX OSDI*, 2014.
- [817] Sungchan Kim, Hyunok Oh, Chanik Park, Sangyeun Cho, Sang-Won Lee, and Bongki Moon, "In-Storage Processing of Database Scans and Joins," *Information Sciences*, 2016.
- [818] Boncheol Gu, A. S. Yoon, D.-H. Bae, I. Jo, J. Lee, J. Yoon, J.-U. Kang, M. Kwon, C. Yoon, S. Cho, J. Jeong, and D. Chang, "Biscuit: A Framework for Near-Data Processing of Big Data Workloads," in *ISCA*, 2016.

- [819] Yangwook Kang, Yang-suk Kee, Ethan L Miller, and Chanik Park, “Enabling Cost-effective Data Processing with Smart SSD,” in *MSST*, 2013.
- [820] Xiaohao Wang, Yifan Yuan, You Zhou, Chance C Coats, and Jian Huang, “Project Almanac: A Time-Traveling Solid-State Drive,” in *EuroSys*, 2019.
- [821] Sang-Woo Jun, Ming Liu, Sungjin Lee, Jamey Hicks, John Ankcorn, Myron King, Shuotao Xu *et al.*, “BlueDBM: An Appliance for Big Data Analytics,” in *ISCA*, 2015.
- [822] Sang-Woo Jun, Ming Liu, Sungjin Lee, Jamey Hicks, John Ankcorn, Myron King, and Shuotao Xu, “BlueDBM: Distributed Flash Storage for Big Data Analytics,” *ACM TOCS*, 2016.
- [823] Mahdi Torabzadehkashi, Siavash Rezaei, Ali Heydarigorji, Hosein Bobarshad, Vladimir Alves, and Nader Bagherzadeh, “Catalina: In-Storage Processing Acceleration for Scalable Big Data Analytics,” in *Euromicro PDP*, 2019.
- [824] Joo Hwan Lee, Hui Zhang, Veronica Lagrange, Praveen Krishnamoorthy, Xiaodong Zhao, and Yang Seok Ki, “SmartSSD: FPGA Accelerated Near-Storage Data Analytics on SSD,” *IEEE CAL*, 2020.
- [825] Mohammadamin Ajdari, Pyeongsu Park, Joonsung Kim, Dongup Kwon, and Jangwoo Kim, “CIDR: A Cost-Effective In-Line Data Reduction System for Terabit-per-Second Scale SSD Arrays,” in *HPCA*, 2019.
- [826] Gunjae Koo, Kiran Kumar Matam, Te I, HV Krishna Giri Narra, Jing Li, Hung-Wei Tseng, Steven Swanson, and Murali Annavaram, “Summarizer: Trading Communication with Computing Near Storage,” in *MICRO*, 2017.
- [827] C. Y. Cho, W. S. Jeong, O. Doohwan, and W. W. Ro, “XSD: Accelerating Mapreduce by Harnessing the GPU Inside an SSD,” in *Workshop on Near-Data*, 2013.
- [828] Won Seob Jeong, Changmin Lee, Keunsoo Kim, Myung Kuk Yoon, Won Jeon, Myoung-soo Jung, and Won Woo Ro, “REACT: Scalable and High-Performance Regular Expression Pattern Matching Accelerator for In-Storage Processing,” *IEEE TPDS*, 2019.
- [829] Sang-Woo Jun, Huy T Nguyen, Vijay Gadepally *et al.*, “In-Storage Embedded Accelerator for Sparse Pattern Processing,” in *HPEC*, 2016.
- [830] N. Ghiasi, M. Sadrosadati, H. Mustafa, A. Gollwitzer, C. Firtina, J. Eudine, H. Mao, J. Lindegger, M. Cavlak, M. Alser, J. Park, and O. Mutlu, “MegIS: High-Performance, Energy-Efficient, and Low-Cost Metagenomic Analysis with In-Storage Processing,” in *ISCA*, 2024.
- [831] Devesh Tiwari, Simona Boboila, Sudharshan Vazhkudai, Youngjae Kim, Xiaosong Ma, Peter Desnoyers, and Yan Solihin, “Active Flash: Towards {Energy-Efficient},{In-Situ} Data Analytics on {Extreme-Scale} Machines,” in *FAST*, 2013.
- [832] Sangyeun Cho, Chanik Park, Hyunok Oh, Sungchan Kim, Youngmin Yi, and Gregory R Ganger, “Active Disk Meets Flash: A Case for Intelligent SSDs,” in *ICS*, 2013.

- [833] Jianguo Wang, Dongchul Park, Yang-Suk Kee, Yannis Papakonstantinou, and Steven Swanson, "SSD In-Storage Computing for List Intersection," in *DaMoN*, 2016.
- [834] Yangwook Kang, Rekha Pitchumani, Pratik Mishra, Yang-suk Kee, Francisco Londono, Sangyoon Oh, Jongyeol Lee, and Daniel DG Lee, "Towards Building a High-Performance, Scale-In Key-Value Storage System," in *SYSTOR*, 2019.
- [835] Sahand Salamat, Armin Haj Aboutalebi, Behnam Khaleghi, Joo Hwan Lee, Yang Seok Ki, and Tajana Rosing, "NASCENT: Near-Storage Acceleration of Database Sort on SmartSSD," in *FPGA*, 2021.
- [836] Mohammadreza Soltaniyeh, Veronica Lagrange Moutinho Dos Reis, Matt Bryson, Xuebin Yao, Richard P Martin, and Santosh Nagarakatte, "Near-Storage Processing for Solid State Drive Based Recommendation Inference with SmartSSDs®," in *ICPE*, 2022.
- [837] Erik Riedel, Christos Faloutsos, Garth A Gibson, and David Nagle, "Active Disks for Large-Scale Data Processing," *Computer*, 2001.
- [838] Anurag Acharya, Mustafa Uysal, and Joel Saltz, "Active Disks: Programming Model, Algorithms and Evaluation," in *ASPLOS*, 1998.
- [839] Erik Riedel, Garth Gibson, and Christos Faloutsos, "Active Storage for Large-scale Data Mining and Multimedia Applications," in *VLDB*, 1998.
- [840] Myungsuk Kim, Jisung Park, Genhee Cho, Yoona Kim, Lois Orosa, Onur Mutlu, and Jihong Kim, "Evanesco: Architectural Support for Efficient Data Sanitization in Modern Flash-Based Storage Systems," in *ASPLOS*, 2020.
- [841] Yixin Luo, Saugata Ghose, Yu Cai, Erich F Haratsch, and Onur Mutlu, "Improving 3D NAND Flash Memory Lifetime by Tolerating Early Retention Loss and Process Variation," in *SIGMETRICS*, 2018.
- [842] Yixin Luo, Saugata Ghose, Yu Cai, Erich F Haratsch, and Onur Mutlu, "HeatWatch: Improving 3D NAND Flash Memory Device Reliability by Exploiting Self-Recovery and Temperature Awareness," in *HPCA*, 2018.
- [843] Yixin Luo, Yu Cai, Saugata Ghose, Jongmoo Choi, and Onur Mutlu, "WARM: Improving NAND Flash Memory Lifetime with Write-Hotness Aware Retention Management," in *MSST*, 2015.
- [844] Yu Cai, Gulay Yalcin, Onur Mutlu, Erich F Haratsch, Adrian Crista, Osman S Unsal, and Ken Mai, "Error Analysis and Retention-Aware Error Management for NAND Flash Memory," *Intel Technology Journal*, 2013.
- [845] Yu Cai, Erich F Haratsch, Onur Mutlu, and Ken Mai, "Error Patterns in MLC NAND Flash Memory: Measurement, Characterization, and Analysis," in *DATE*, 2012.
- [846] Yu Cai, Gulay Yalcin, Onur Mutlu, Erich F Haratsch, Adrian Cristal, Osman S Unsal, and Ken Mai, "Flash Correct-and-Refresh: Retention-Aware Error Management for Increased Flash Memory Lifetime," in *ICCD*, 2012.

- [847] Y. Cai, S. Ghose, E. F. Haratsch, Y. Luo, and O. Mutlu, “Reliability Issues in Flash-Memory-Based Solid-State Drives: Experimental Analysis, Mitigation, Recovery,” in *Inside Solid State Drives (SSDs)*, 2018.
- [848] Y. Cai, S. Ghose, E. F. Haratsch, Y. Luo, and O. Mutlu, “Errors in Flash-Memory-Based Solid-State Drives: Analysis, Mitigation, and Recovery,” arXiv:1711.11427 [cs.AR], 2018.
- [849] Yu Cai, “NAND Flash Memory: Characterization, Analysis, Modeling, and Mechanisms,” Ph.D. dissertation, Carnegie Mellon University, 2013.
- [850] Yixin Luo, “Architectural Techniques for Improving NAND Flash Memory Reliability,” Ph.D. dissertation, Carnegie Mellon University, 2018.
- [851] Y. Cai, S. Ghose, E. F. Haratsch, Y. Luo, and O. Mutlu, “Error Characterization, Mitigation, and Recovery in Flash-Memory-Based Solid-State Drives,” *Proc. IEEE*, Sep. 2017.
- [852] Jie Zhang and Myoungsoo Jung, “FlashAbacus: A Self-Governing Flash-Based Accelerator for Low-Power Systems,” in *EuroSys*, 2018.
- [853] A. De, M. Gokhale, R. Gupta, and S. Swanson, “Minerva: Accelerating Data Analysis in Next-Generation SSDs,” in *FCCM*, 2013.
- [854] T. Hamamoto, S. Sugiura, and S. Sawada, “On the Retention Time Distribution of Dynamic Random Access Memory (DRAM),” *IEEE TED*, 1998.
- [855] Dan Chen, Hai Jin, Long Zheng, Yu Huang, Pengcheng Yao, Chuangyi Gui, Qinggang Wang, Haifeng Liu, Haiheng He, Xiaofei Liao *et al.*, “A General Offloading Approach for Near-DRAM Processing-in-Memory Architectures,” in *IPDPS*, 2022.
- [856] Lifeng Nai, Ramyad Hadidi, He Xiao, Hyojong Kim, Jaewoong Sim, and Hyesoon Kim, “Thermal-Aware Processing-in-Memory Instruction Offloading,” *JPDC*, 2019.
- [857] Rodrigo M Sokulski, Paulo C Santos, Sairo R dos Santos, and Marco AZ Alves, “SAPIVE: Simple AVX to PIM Vectorizer,” in *SBESC*, 2022.
- [858] Rodrigo M Sokulski, Sairo R dos Santos, and Marco AZ Alves, “On the SPEC-CPU 2017 Opportunities for Dynamic Vectorization Possibilities on PIM Architectures,” in *WSCAD*, 2022.
- [859] Paulo C Santos, Joao PC de Lima, Rafael F de Moura, Marco AZ Alves, Antonio CS Beck, and Luigi Carro, “Enabling Near-Data Accelerators Adoption by Through Investigation of Datapath Solutions,” *IJPP*, 2021.
- [860] Lifeng Nai, Ramyad Hadidi, He Xiao, Hyojong Kim, Jaewoong Sim, and Hyesoon Kim, “CoolPIM: Thermal-Aware Source Throttling for Efficient PIM Instruction Offloading,” in *IPDPS*, 2018.
- [861] Hameeza Ahmed, Paulo C Santos, Joao PC Lima, Rafael F Moura, Marco AZ Alves, Antônio CS Beck, and Luigi Carro, “A Compiler for Automatic Selection of Suitable Processing-in-Memory Instructions,” in *DATE*, 2019.

- [862] Damla Senol Cali, Konstantinos Kanellopoulos, Joel Lindegger, Zülal Bingöl, Gurpreet S Kalsi, Ziyi Zuo, Can Firtina, Meryem Banu Cavlak, Jeremie Kim, Nika Mansouri Ghiasi *et al.*, “SeGraM: A Universal Hardware Accelerator for Genomic Sequence-to-Graph and Sequence-to-Sequence Mapping,” in *ISCA*, 2022.
- [863] Bahar Asgari, Saibal Mukhopadhyay, and Sudhakar Yalamanchili, “MAHASIM: Machine-Learning Hardware Acceleration Using a Software-Defined Intelligent Memory System,” *J. Signal Process Syst.*, 2020.
- [864] Namhyung Kim, Jeongseob Ahn, Sungpack Hong, Hassan Chafi, and Kiyoun Choi, “How Much Computation Power Do You Need for Near-Data Processing in Cloud?” in *ASBD*, 2017.
- [865] Shengwen Liang, Ying Wang, Cheng Liu, Huawei Li, and Xiaowei Li, “InS-DLA: An In-SSD Deep Learning Accelerator for Near-Data Processing,” in *FPL*, 2019.
- [866] Alvin Oliver Glova, Itir Akgun, Shuangchen Li, Xing Hu, and Yuan Xie, “Near-Data Acceleration of Privacy-Preserving Biomarker Search with 3D-Stacked Memory,” in *DATE*, 2019.
- [867] Peng Gu, Xinfeng Xie, Shuangchen Li, Dimin Niu, Hongzhong Zheng, Krishna T Malladi, and Yuan Xie, “DLUX: A LUT-Based Near-Bank Accelerator for Data Center Deep Learning Training Workloads,” *TCAD*, 2020.
- [868] Milan Radulovic, Darko Zivanovic, Daniel Ruiz, Bronis R de Supinski, Sally A McKee, Petar Radojković, and Eduard Ayguadé, “Another Trip to the Wall: How Much Will Stacked DRAM Benefit HPC?” in *MEMSYS*, 2015.
- [869] Leonid Yavits, Roman Kaplan, and Ran Ginosar, “GIRAF: General Purpose In-Storage Resistive Associative Framework,” *TPDS*, 2021.
- [870] Jose M Herruzo, Ivan Fernandez, Sonia González-Navarro, and Oscar Plata, “Enabling Fast and Energy-Efficient FM-Index Exact Matching Using Processing-Near-Memory,” *The Journal of Supercomputing*, 2021.
- [871] Bahar Asgari, Ramyad Hadidi, Jiashen Cao, Da Eun Shim, Sung-Kyu Lim, and Hye-soon Kim, “FAFNIR: Accelerating Sparse Gathering by Using Efficient Near-Memory Intelligent Reduction,” in *HPCA*, 2021.
- [872] Google LLC, “Chrome Browser,” <https://www.google.com/chrome/browser/>.
- [873] Google LLC, “TensorFlow: Mobile,” <https://www.tensorflow.org/mobile/>.
- [874] Google LLC, “YouTube,” <https://www.youtube.com/>.
- [875] Google LLC, “Google Hangouts,” <https://hangouts.google.com/>.
- [876] Nika Mansouri Ghiasi, Nandita Vijaykumar, Geraldo F Oliveira, Lois Orosa, Ivan Fernandez, Mohammad Sadrosadati, Konstantinos Kanellopoulos, Nastaran Hajinazar, Juan Gómez Luna, and Onur Mutlu, “ALP: Alleviating CPU-Memory Data Movement Overheads in Memory-Centric Systems,” *IEEE TETC*, 2022.

- [877] G. Kim, N. Chatterjee, M. O'Connor, and K. Hsieh, "Toward Standardized Near-Data Processing with Unrestricted Data Placement for GPUs," in *SC*, 2017.
- [878] Kanishkan Vadivel, Lorenzo Chelini, Ali BanaGozar, Gagandeep Singh, Stefano Corda, Roel Jordans, and Henk Corporaal, "TDO-CIM: Transparent Detection and Offloading for Computation In-Memory," in *DATE*, 2020.
- [879] Sheng Xu, Chun Li, Le Luo, Wu Zhou, Liang Yan, and Xiaoming Chen, "Identifying Optimal Workload Offloading Partitions for CPU-PIM Graph Processing Accelerators," *VLSI*, 2025.
- [880] Satanu Maity, Manojit Ghose, and Sudeep Pasricha, "A Framework for Near Memory Processing with Computation Offloading and Load Balancing," *TCAD*, 2025.
- [881] Qingcai Jiang, Shaojie Tan, Junshi Chen, and Hong An, "A3PIM: An Automated, Analytic and Accurate Processing-in-Memory Offloader," in *DATE*, 2024.
- [882] Asif Ali Khan, Hamid Farzaneh, Karl FA Friebe, Clément Fournier, Lorenzo Chelini, and Jeronimo Castrillon, "CINM (Cinnamon): A Compilation Infrastructure for Heterogeneous Compute In-Memory and Compute Near-Memory Paradigms," arXiv:2301.07486 [cs.AR], 2022.
- [883] Yizhou Wei, Minxuan Zhou, Sihang Liu, Korakit Seemakhupt, Tajana Rosing, and Samira Khan, "PIMProf: An Automated Program Profiler for Processing-in-Memory Offloading Decisions," in *DATE*, 2022.
- [884] M Aater Suleman, Onur Mutlu, José A Joao, and Yale N Patt, "Data Marshaling for Multi-Core Architectures," in *ISCA*, 2010.
- [885] M. A. Suleman, Onur Mutlu, Jose A. Joao, Khubaib, and Y. N. Patt, "Data Marshaling for Multi-core Systems," *IEEE Micro (TOP PICKS Issue)*, 2011.
- [886] James R Goodman, "Using Cache Memory to Reduce Processor-memory Traffic," in *ISCA*, 1983.
- [887] Mark S Papamarcos and Janak H Patel, "A Low-Overhead Coherence Solution for Multiprocessors with Private Cache Memories," in *ISCA*, 1984.
- [888] Junwhan Ahn, Sungpack Hong, Sungjoo Yoo, Onur Mutlu, and Kiyoun Choi, "Retrospective: A Scalable Processing-in-Memory Accelerator for Parallel Graph Processing," *Retrospective Issue for ISCA-50*, 2023.
- [889] Amirali Boroumand, Saugata Ghose, Geraldo F Oliveira, and Onur Mutlu, "Polynesia: Enabling Effective Hybrid Transactional Analytical Databases with Specialized Hardware Software Co-Design," in *ICDE*, 2022.
- [890] Amir Yazdanbakhsh, Choungki Song, Jacob Sacks, Pejman Lotfi-Kamran, Hadi Esmaeilzadeh, and Nam Sung Kim, "In-DRAM Near-Data Approximate Acceleration for GPUs," in *PACT*, 2018.

- [891] Juan Gómez-Luna, Yuxin Guo, Sylvan Brocard, Julien Legriel, Remy Cimadomo, Geraldo F Oliveira, Gagandeep Singh, and Onur Mutlu, “Machine Learning Training on a Real Processing-in-Memory System,” arXiv:2206.06022 [cs.AR], 2022.
- [892] Alexandar Devic, Siddhartha Balakrishna Rai, Anand Sivasubramaniam, Ameen Akel, Sean Eilert, and Justin Eno, “To PIM or Not for Emerging General Purpose Processing in DDR Memory Systems,” in *ISCA*, 2022.
- [893] Geraldo F Oliveira, Ataberk Olgun, A. Giray Gregorio Yaglikçi, Nisa Bostanci, Juan Gómez-Luna, Saugata Ghose, and Onur Mutlu, “MIMDRAM: An End-to-End Processing-Using-DRAM System for High-Throughput, Energy-Efficient and Programmer-Transparent Multiple-Instruction Multiple-Data Computing,” in *HPCA*, 2024.
- [894] Ismail Emir Yuksel, Yahya Can Tuğrul, Ataberk Olgun, F. Nisa Bostanci, A. Giray Yaglikçi, Geraldo F. Oliveira, Haocong Luo, Juan Gómez-Luna, Mohammad Sadrosadati, and Onur Mutlu, “Functionally-Complete Boolean Logic in Real DRAM Chips: Experimental Characterization and Analysis,” in *HPCA*, 2024.
- [895] Ismail Emir Yuksel, Yahya Can Tugrul, F Bostanci, Geraldo F Oliveira, A Giray Yaglikci, Ataberk Olgun, Melina Soysal, Haocong Luo, Juan Gómez-Luna, Mohammad Sadrosadati *et al.*, “Simultaneous Many-Row Activation in Off-the-Shelf DRAM Chips: Experimental Characterization and Analysis,” in *DSN*, 2024.
- [896] S. Angizi, Z. He, and D. Fan, “PIMA-Logic: A Novel Processing-in-Memory Architecture for Highly Flexible and Energy-Efficient Logic Computation,” in *DAC*, 2018.
- [897] S. Angizi, A. S. Rakin, and D. Fan, “CMP-PIM: An Energy-Efficient Comparator-Based Processing-in-Memory Neural Network Accelerator,” in *DAC*, 2018.
- [898] S. Angizi, J. Sun, W. Zhang, and D. Fan, “AlignS: A Processing-in-Memory Accelerator for DNA Short Read Alignment Leveraging SOT-MRAM,” in *DAC*, 2019.
- [899] Yifat Levy, Jehoshua Bruck, Yuval Cassuto, Eby G. Friedman, Avinoam Kolodny, Eitan Yaakobi, and Shahar Kvatinsky, “Logic Operations in Memory Using a Memristive Akers Array,” *Microelectronics Journal*, 2014.
- [900] S. Kvatinsky, D. Belousov, S. Liman, G. Satat, N. Wald, E. G. Friedman, A. Kolodny, and U. C. Weiser, “MAGIC—Memristor-Aided Logic,” *IEEE TCAS II: Express Briefs*, 2014.
- [901] S. Kvatinsky, A. Kolodny, U. C. Weiser, and E. G. Friedman, “Memristor-Based IMPLY Logic Design Procedure,” in *ICCD*, 2011.
- [902] S. Kvatinsky, G. Satat, N. Wald, E. G. Friedman, A. Kolodny, and U. C. Weiser, “Memristor-Based Material Implication (IMPLY) Logic: Design Principles and Methodologies,” *TVLSI*, 2014.
- [903] P.-E. Gaillardon, L. Amaru, A. Siemon, and et al., “The Programmable Logic-in-Memory (PLiM) Computer,” in *DATE*, 2016.

- [904] D. Bhattacharjee, R. Devadoss, and A. Chattopadhyay, “ReVAMP: ReRAM Based VLIW Architecture for In-Memory Computing,” in *DATE*, 2017.
- [905] S. Hamdioui, L. Xie, H. A. D. Nguyen, and et al., “Memristor Based Computation-in-Memory Architecture for Data-Intensive Applications,” in *DATE*, 2015.
- [906] L. Xie, H. A. D. Nguyen, M. Taouil, and et al., “Fast Boolean Logic Papped on Memristor Crossbar,” in *ICCD*, 2015.
- [907] S. Hamdioui, S. Kvatinisky, and et al. G. Cauwenberghs, “Memristor for Computing: Myth or Reality?” in *DATE*, 2017.
- [908] J. Yu, H. A. D. Nguyen, L. Xie, and et al., “Memristive Devices for Computation-in-Memory,” in *DATE*, 2018.
- [909] Yue Xi, Bin Gao, Jianshi Tang, An Chen, Meng-Fan Chang, Xiaobo Sharon Hu, Jan Van Der Spiegel, He Qian, and Huaqiang Wu, “In-Memory Learning With Analog Resistive Switching Memory: A Review and Perspective,” *Proc. IEEE*, 2020.
- [910] Le Zheng, Sangho Shin, Scott Lloyd, Maya Gokhale, Kyungmin Kim, and Sung-Mo Kang, “RRAM-Based TCAMs for Pattern Search,” in *ISCAS*, 2016.
- [911] Xiaoyang Ma, Shan Deng, Juejian Wu, Zijian Zhao, David Lehninger, Tarek Ali, Konrad Seidel, Sourav De, Xiyu He, Yiming Chen *et al.*, “A 2-Transistor-2-Capacitor Ferroelectric Edge Compute-in-Memory Scheme with Disturb-Free Inference and High Endurance,” *EDL*, 2023.
- [912] Stefan Slesazeck, Taras Ravsher, Viktor Havel, Evelyn T Breyer, Halid Mulaosmanovic, and Thomas Mikolajick, “A 2TnC Ferroelectric Memory Gain Cell Suitable for Compute-in-Memory and Neuromorphic Application,” in *IEDM*, 2019.
- [913] Qiao Wang, Donglin Zhang, Yulin Zhao, Chao Liu, Qiao Hu, Xuanzhi Liu, Jianguo Yang, and Hangbing Lv, “A 1T2C FeCAP-Based In-Situ Bitwise X(N)OR Logic Operation with Two-Step Write-Back Circuit for Accelerating Compute-in-Memory,” *Micromachines*, 2021.
- [914] Jack A Mandelman, Robert H Dennard, Gary B Bronner, John K DeBrosse, Rama Divakaruni, Yujun Li, and Carl J Radens, “Challenges and Future Directions for the Scaling of Dynamic Random-Access Memory (DRAM),” *IBM JRD*, 2002.
- [915] Ataberk Olgun, Juan Gómez-Luna, Konstantinos Kanellopoulos, Behzad Salami, Hassan Hassan, Oğuz Ergin, and Onur Mutlu, “PiDRAM: A Holistic End-to-End FPGA-Based Framework for Processing-in-DRAM,” arXiv:2111.00082 [cs.AR], 2021.
- [916] National Institute of Standards and Technology, “180-2: Secure Hash Standard (SHS),” *US Department of Commerce, National Institute of Standards and Technology (NIST)*, 2012.
- [917] Amogh Agrawal, Akhilesh Jaiswal, Chankyu Lee, and Kaushik Roy, “X-SRAM: Enabling In-Memory Boolean Computations in CMOS Static Random Access Memories,” *TCAS-I*, 2018.

- [918] Jack E Volder, “The CORDIC Trigonometric Computing Technique,” *IRE Transactions on Electronic Computers*, 1959.
- [919] John Stephen Walther, “A Unified Algorithm for Elementary Functions,” in *FIPS*, 1971.
- [920] Jieui Kang, Soeun Choi, Eunjin Lee, and Jaehyeong Sim, “SpDRAM: Efficient In-DRAM Acceleration of Sparse Matrix-Vector Multiplication,” *IEEE Access*, 2024.
- [921] Salma Afifi, Ishan Thakkar, and Sudeep Pasricha, “ARTEMIS: A Mixed Analog-Stochastic In-DRAM Accelerator for Transformer Neural Networks,” *TCAD*, 2024.
- [922] Shaahin Angizi and Deliang Fan, “ReDRAM: A Reconfigurable Processing-in-DRAM Platform for Accelerating Bulk Bit-Wise Operations,” in *ICCAD*, 2019.
- [923] Ranyang Zhou, Arman Roohi, Durga Misra, and Shaahin Angizi, “FlexiDRAM: A Flexible In-DRAM Framework to Enable Parallel General-Purpose Computation,” in *ISLPED*, 2022.
- [924] Lingxi Wu, Rasool Sharifi, Marzieh Lenjani, Kevin Skadron, and Ashish Venkat, “Sieve: Scalable In-Situ DRAM-Based Accelerator Designs for Massively Parallel k-Mer Matching,” in *ISCA*, 2021.
- [925] Xin Xin, Youtao Zhang, and Jun Yang, “ROC: DRAM-Based Processing with Reduced Operation Cycles,” in *DAC*, 2019.
- [926] J. Kim, M. Patel, H. Hassan, and O. Mutlu, “The DRAM Latency PUF: Quickly Evaluating Physical Unclonable Functions by Exploiting the Latency-Reliability Tradeoff in Modern DRAM Devices,” in *HPCA*, 2018.
- [927] Ranyang Zhou, Arman Roohi, Durga Misra, and Shaahin Angizi, “ReD-LUT: Reconfigurable In-DRAM LUTs Enabling Massive Parallel Computation,” in *ICCAD*, 2022.
- [928] Purab Ranjan Sutradhar, Sathwika Bavikadi, Mark Indovina, Sai Manoj Pudukotai Dinakarrao, and Amlan Ganguly, “FlutPIM:: A Look-up Table-based Processing in Memory Architecture with Floating-point Computation Support for Deep Learning Applications,” in *GLVSLI*, 2023.
- [929] Purab Ranjan Sutradhar, Sathwika Bavikadi, Sai Manoj Pudukotai Dinakarrao, Mark A Indovina, and Amlan Ganguly, “3DL-PIM: A Look-Up Table Oriented Programmable Processing in Memory Architecture Based on the 3-D Stacked Memory for Data-Intensive Applications,” *TETC*, 2023.
- [930] Mingyu Gao, Christina Delimitrou, Dimin Niu, Krishna T Malladi, Hongzhong Zheng, Bob Brennan, and Christos Kozyrakis, “DRAF: A Low-Power DRAM-Based Reconfigurable Acceleration Fabric,” in *ISCA*, 2016.
- [931] SAFARI Research Group, “SoftMC v1.0 – GitHub Repository,” <https://github.com/CMU-SAFARI/SoftMC/>.

- [932] Ataberk Olgun, Hasan Hassan, A. Giray Yağlıkcı, Yahya Can Tuğrul, Lois Orosa, Haocong Luo, Minesh Patel, Ergin Oğuz, and Onur Mutlu, “DRAM Bender: An Extensible and Versatile FPGA-Based Infrastructure to Easily Test State-of-the-Art DRAM Chips,” *TCAD*, 2023.
- [933] SAFARI Research Group, “DRAM Bender – GitHub Repository,” <https://github.com/CMU-SAFARI/DRAM-Bender>, 2022.
- [934] Julien Borghetti, Gregory S Snider, Philip J Kuekes, J Joshua Yang, Duncan R Stewart, and R Stanley Williams, “‘Memristive’ Switches Enable ‘Stateful’ Logic Operations via Material Implication,” *Nature*, 2010.
- [935] Eike Linn, R Rosezin, Stefan Tappertzhofen, U Böttger, and Rainer Waser, “Beyond Von Neumann—Logic Operations in Passive Crossbar Arrays Alongside Memory Operations,” *Nanotechnology*, 2012.
- [936] Eero Lehtonen and Mika Laiho, “Stateful Implication Logic with Memristors,” in *NANOARCH*, 2009.
- [937] Kyosun Kim, Sangho Shin, and Sung-Mo Kang, “Field Programmable Stateful Logic Array,” *TCAD*, 2011.
- [938] Eero Lehtonen, Jussi H Poikonen, and Mika Laiho, “Applications and Limitations of Memristive Implication Logic,” in *CNNA*, 2012.
- [939] Hiwa Mahmoudi, Thomas Windbacher, Viktor Sverdlov, and Siegfried Selberherr, “Implication Logic Gates Using Spin-Transfer-Torque-Operated Magnetic Tunnel Junctions for Intrinsic Logic-in-Memory,” *Solid-State Electron.*, 2013.
- [940] Kyung Min Kim, Nuo Xu, Xinglong Shao, Kyung Jean Yoon, Hae Jin Kim, R Stanley Williams, and Cheol Seong Hwang, “Single-Cell Stateful Logic Using a Dual-Bit Memristor,” *Phys. Status Solidi Rapid Res. Lett.*, 2019.
- [941] Lei Xie, Hoang Anh Du Nguyen, Jintao Yu, Ali Kaichouhi, Mottaqiallah Taouil, Mohammad AlFailakawi, and Said Hamdioui, “Scouting Logic: A Novel Memristor-Based Logic Design for Resistive Computing,” in *ISVLSI*, 2017.
- [942] Ivan Fernandez, Christina Giannoula, Aditya Manglik, Ricardo Quisilant, Nika Mansouri Ghiasi, Juan Gómez-Luna, Eladio Gutierrez, Oscar Plata, and Onur Mutlu, “MATSA: An MRAM-Based Energy-Efficient Accelerator for Time Series Analysis,” *IEEE Access*, 2024.
- [943] Huai Lin, Xi Luo, Long Liu, Di Wang, Xuefeng Zhao, Ziwei Wang, Xiaoyong Xue, Feng Zhang, and Guozhong Xing, “All-Electrical Control of Compact SOT-MRAM: Toward Highly Efficient and Reliable Non-Volatile In-Memory Computing,” *Micromachines*, 2022.
- [944] Farhana Parveen, Shaahin Angizi, Zhezhi He, and Deliang Fan, “Low Power In-Memory Computing Based on Dual-Mode SOT-MRAM,” in *ISLPED*, 2017.

- [945] Shaahin Angizi, Wei Zhang, and Deliang Fan, “Exploring DNA Alignment-in-Memory Leveraging Emerging SOT-MRAM,” in *GLSVLSI*, 2020.
- [946] Orian Leitersdorf, Dean Leitersdorf, Jonathan Gal, Mor Dahan, Ronny Ronen, and Shahr Kvatinsky, “AritPIM: High-Throughput In-Memory Arithmetic,” *IEEE Trans. Emerg. Topics Comput.*, 2023.
- [947] Philippe Esling and Carlos Agon, “Time-Series Data Mining,” *ACM Computing Surveys (CSUR)*, 2012.
- [948] Nagadastagiri Challapalle, Sahithi Rampalli, Linghao Song, Nandhini Chandramoorthy, Karthik Swaminathan, John Sampson, Yiran Chen, and Vijaykrishnan Narayanan, “GaaS-X: Graph Analytics Accelerator Supporting Sparse Data Representation Using Crossbar Architectures,” in *ISCA*, 2020.
- [949] Mahdi Nazm Bojnordi and Engin Ipek, “Memristive Boltzmann Machine: A Hardware Accelerator for Combinatorial Optimization and Deep Learning,” in *HPCA*, 2016.
- [950] Ben Feinberg, Uday Kumar Reddy Vengalam, Nathan Whitehair, Shibo Wang, and Engin Ipek, “Enabling scientific computing on memristive accelerators,” in *2018 ACM/IEEE 45th Annual International Symposium on Computer Architecture (ISCA)*. IEEE, 2018, pp. 367–382.
- [951] Daniele Ielmini and H-S Philip Wong, “In-Memory Computing with Resistive Switching Devices,” *Nature Electronics*, 2018.
- [952] Weier Wan, Rajkumar Kubendran, Clemens Schaefer, Sukru Burc Eryilmaz, Wenqiang Zhang, Dabin Wu, Stephen Deiss, Priyanka Raina, He Qian, Bin Gao *et al.*, “A Compute-in-Memory Chip Based on Resistive Random-Access Memory,” *Nature*, 2022.
- [953] Seungchul Jung, Hyungwoo Lee, Sungmeen Myung, Hyunsoo Kim, Seung Keun Yoon, Soon-Wan Kwon, Yongmin Ju, Minje Kim, Wooseok Yi, Shinhee Han *et al.*, “A Crossbar Array of Magnetoresistive Memory Devices for In-Memory Computing,” *Nature*, 2022.
- [954] Abu Sebastian, Manuel Le Gallo, Riduan Khaddam-Aljameh, and Evangelos Eleftheriou, “Memory Devices and Applications for In-Memory Computing,” *Nature Nanotechnology*, 2020.
- [955] Manuel Le Gallo, Riduan Khaddam-Aljameh, Milos Stanisavljevic, Athanasios Vasilopoulos, Benedikt Kersting, Martino Dazzi, Geethan Karunaratne, Matthias Brändli, Abhairaj Singh, Silvia M Mueller *et al.*, “A 64-Core Mixed-Signal In-Memory Compute Chip Based on Phase-Change Memory for Deep Neural Network Inference,” *Nature Electronics*, 2023.
- [956] Aayush Ankit, Izzat El Hajj, Sai Rahul Chalamalasetti, Geoffrey Ndu, Martin Foltin, R. Stanley Williams, Paolo Faraboschi, Wen-mei W Hwu, John Paul Strachan, Kaushik Roy, and Dejan S. Milojevic, “PUMA: A Programmable Ultra-Efficient Memristor-Based Accelerator for Machine Learning Inference,” in *ASPLOS*, 2019.

- [957] Vinay Joshi, Manuel Le Gallo, Simon Haefeli, Irem Boybat, Sasidharan Rajalekshmi Nandakumar, Christophe Piveteau, Martino Dazzi, Bipin Rajendran, Abu Sebastian, and Evangelos Eleftheriou, "Accurate Deep Neural Network Inference Using Computational Phase-Change Memory," *Nature Communications*, 2020.
- [958] Can Li, Zhongrui Wang, Mingyi Rao, Daniel Belkin, Wenhao Song, Hao Jiang, Peng Yan, Yunning Li, Peng Lin, Miao Hu *et al.*, "Long Short-Term Memory Networks in Memristor Crossbar Arrays," *Nature Machine Intelligence*, 2019.
- [959] Hossein Valavi, Peter J Ramadge, Eric Nestler, and Naveen Verma, "A 64-Tile 2.4-Mb In-Memory-Computing CNN Accelerator Employing Charge-Domain Compute," *JSSC*, 2019.
- [960] Manuel Le Gallo, Abu Sebastian, Roland Mathis, Matteo Manica, Heiner Giefers, Tomas Tuma, Costas Bekas, Alessandro Curioni, and Evangelos Eleftheriou, "Mixed-Precision In-Memory Computing," *Nature Electronics*, 2018.
- [961] Tzu-Hsien Yang, Hsiang-Yun Cheng, Chia-Lin Yang, I-Ching Tseng, Han-Wen Hu, Hung-Sheng Chang, and Hsiang-Pang Li, "Sparse ReRAM Engine: Joint Exploration of Activation and Weight Sparsity in Compressed Neural Networks," in *ISCA*, 2019.
- [962] Hongyang Jia, Hossein Valavi, Yinqi Tang, Jintao Zhang, and Naveen Verma, "A Programmable Heterogeneous Microprocessor Based on Bit-Scalable In-Memory Computing," *JSSC*, 2020.
- [963] Tianqi Tang, Lixue Xia, Boxun Li, Yu Wang, and Huazhong Yang, "Binary Convolutional Neural Network on RRAM," in *ASP-DAC*, 2017.
- [964] Matthew J Marinella, Sapan Agarwal, Alexander Hsia, Isaac Richter, Robin Jacobs-Gedrim, John Niroula, Steven J Plimpton, Engin Ipek, and Conrad D James, "Multi-scale Co-Design Analysis of Energy, Latency, Area, and Accuracy of a ReRAM Analog Neural Training Accelerator," *JETCAS*, 2018.
- [965] Geng Yuan, Payman Behnam, Zhengang Li, Ali Shafiee, Sheng Lin, Xiaolong Ma, Hang Liu, Xuehai Qian, Mahdi Nazm Bojnordi, Yanzhi Wang *et al.*, "FORMS: Fine-Grained Polarized ReRAM-Based In-Situ Computation for Mixed-Signal DNN Accelerator," in *ISCA*, 2021.
- [966] Shiping Wen, Jiadong Chen, Yingcheng Wu, Zheng Yan, Yuting Cao, Yin Yang, and Tingwen Huang, "CKFO: Convolution Kernel First Operated Algorithm with Applications in Memristor-Based Convolutional Neural Network," *TCAD*, 2020.
- [967] Aayush Ankit, Izzat El Hajj, Sai Rahul Chalamalasetti, Sapan Agarwal, Matthew Marinella, Martin Foltin, John Paul Strachan, Dejan Milojicic, Wen-Mei Hwu, and Kaushik Roy, "Panther: A Programmable Architecture for Neural Network Training Harnessing Energy-Efficient ReRAM," *TC*, 2020.
- [968] Shiping Wen, Huaqiang Wei, Zheng Yan, Zhenyuan Guo, Yin Yang, Tingwen Huang, and Yiran Chen, "Memristor-Based Design of Sparse Compact Convolutional Neural Network," *TNSE*, 2019.

- [969] Y. Long, T. Na, and S. Mukhopadhyay, “ReRAM-Based Processing-in-Memory Architecture for Recurrent Neural Network Acceleration,” in *TVLSI*, 2018.
- [970] Teyuh Chou, Wei Tang, Jacob Botimer, and Zhengya Zhang, “Cascade: Connecting RRAMs to Extend Analog Dataflow in an End-to-End In-Memory Processing Paradigm,” in *MICRO*, 2019.
- [971] Ben Feinberg, Shibo Wang, and Engin Ipek, “Making Memristive Neural Network Accelerators Reliable,” in *HPCA*, 2018.
- [972] Weitao Li, Pengfei Xu, Yang Zhao, Haitong Li, Yuan Xie, and Yingyan Lin, “Timely: Pushing Data Movements and Interfaces in PIM Accelerators Towards Local and in Time Domain,” in *ISCA*, 2020.
- [973] Shaahin Angizi, Zhezhi He, Amro Awad, and Deliang Fan, “MRIMA: An MRAM-Based In-Memory Accelerator,” *TCAD*, 2019.
- [974] Peiqi Wang, Yu Ji, Chi Hong, Yongqiang Lyu, Dongsheng Wang, and Yuan Xie, “SNram: An Efficient Sparse Neural Network Computation Architecture Based on Resistive Random-Access Memory,” in *DAC*, 2018.
- [975] Zhenhua Zhu, Hanbo Sun, Yujun Lin, Guohao Dai, Lixue Xia, Song Han, Yu Wang, and Huazhong Yang, “A Configurable Multi-Precision CNN Computing Framework Based on Single Bit RRAM,” in *DAC*, 2019.
- [976] Xiaoxuan Yang, Bonan Yan, Hai Li, and Yiran Chen, “ReTransformer: ReRAM-Based Processing-in-Memory Architecture for Transformer Acceleration,” in *ICCAD*, 2020.
- [977] Shibin Tang, Shouyi Yin, Shixuan Zheng, Peng Ouyang, Fengbin Tu, Leiyue Yao, JinZhou Wu, Wenming Cheng, Leibo Liu, and Shaojun Wei, “AEPE: An Area and Power Efficient RRAM Crossbar-Based Accelerator for Deep CNNs,” in *NVMSA*, 2017.
- [978] Lixue Xia, Tianqi Tang, Wenqin Huangfu, Ming Cheng, Xiling Yin, Boxun Li, Yu Wang, and Huazhong Yang, “Switched by Input: Power Efficient Structure for RRAM-Based Convolutional Neural Network,” in *DAC*, 2016.
- [979] Lixue Xia, Mengyun Liu, Xuefei Ning, Krishnendu Chakrabarty, and Yu Wang, “Fault-Tolerant Training with On-Line Fault Detection for RRAM-Based Neural Computing Systems,” in *DAC*, 2017.
- [980] Hantao Huang, Leibin Ni, Kanwen Wang, Yuangang Wang, and Hao Yu, “A Highly Parallel and Energy Efficient Three-Dimensional Multilayer CMOS-RRAM Accelerator for Tensorized Neural Network,” *IEEE Trans. Nanotechnol.*, 2017.
- [981] Ming Cheng, Lixue Xia, Zhenhua Zhu, Yi Cai, Yuan Xie, Yu Wang, and Huazhong Yang, “TIME: A Training-in-Memory Architecture for Memristor-Based Deep Neural Networks,” in *DAC*, 2017.
- [982] Fan Chen, Linghao Song, and Yiran Chen, “ReGAN: A Pipelined ReRAM-Based Accelerator for Generative Adversarial Networks,” in *ASP-DAC*, 2018.

- [983] Yi Cai, Tianqi Tang, Lixue Xia, Ming Cheng, Zhenhua Zhu, Yu Wang, and Huazhong Yang, "Training Low Bitwidth Convolutional Neural Network on RRAM," in *ASP-DAC*, 2018.
- [984] Haiyu Mao, Mingcong Song, Tao Li, Yuting Dai, and Jiwu Shu, "LerGAN: A Zero-free, Low Data Movement and PIM-based GAN Architecture," in *MICRO*, 2018.
- [985] Anirban Nag, Rajeev Balasubramonian, Vivek Srikumar, Ross Walker, Ali Shafiee, John Paul Strachan, and Naveen Muralimanohar, "Newton: Gravitating Towards the Physical Limits of Crossbar Acceleration," *IEEE Micro*, 2018.
- [986] Gustav Kirchhoff, "Über den Zusammenhang zwischen Emission und Absorption von Licht und. Wärme," *Monatsberichte der Akademie der Wissenschaften zu Berlin*, 1859.
- [987] Gustav Kirchhoff, "Über das Verhältnis zwischen dem Emissionsvermögen und dem Absorptionsvermögen der Körper für Wärme und Licht," *Von Kirchhoff bis Planck: Theorie der Wärmestrahlung in Historisch-kritischer Darstellung*, 1978.
- [988] Gustav Kirchhoff, "On the Relation between the Radiating and Absorbing Powers of Different Bodies for Light and Heat," *The London, Edinburgh, and Dublin Philosophical Magazine and Journal of Science*, 1860.
- [989] Fabien Alibart, Ligang Gao, Brian D Hoskins, and Dmitri B Strukov, "High Precision Tuning of State for Memristive Devices by Adaptable Variation-Tolerant Algorithm," *Nanotechnology*, 2012.
- [990] AJ Holmes, RAG Gibson, J Hajto, AF Murray, AE Owen, MJ Rose, and AJ Snell, "Use of a-Si: H Memory Devices for Non-Volatile Weight Storage in Artificial Neural Networks," *Journal of Non-Crystalline Solids*, 1993.
- [991] Miao Hu, Hai Li, Qing Wu, and Garrett S Rose, "Hardware Realization of BSB Recall Function Using Memristor Crossbar Arrays," in *DAC*, 2012.
- [992] Yu Wang, Boxun Li, Rong Luo, Yiran Chen, Ningyi Xu, and Huazhong Yang, "Energy Efficient Neural Networks for Big Data Analytics," in *DATE*, 2014.
- [993] Boxun Li, Yi Shan, Miao Hu, Yu Wang, Yiran Chen, and Huazhong Yang, "Memristor-Based Approximated Computation," in *ISLPED*, 2013.
- [994] Mirko Prezioso, Farnood Merrikh-Bayat, BD Hoskins, Gina C Adam, Konstantin K Likharev, and Dmitri B Strukov, "Training and operation of an integrated neuromorphic network based on metal-oxide memristors," *Nature*, vol. 521, no. 7550, p. 61, 2015.
- [995] Yongtae Kim, Yong Zhang, and Peng Li, "A Reconfigurable Digital Neuromorphic Processor with Memristive Synaptic Crossbar for Cognitive Computing," *JETC*, 2015.
- [996] Zhe Chen, Bin Gao, Zheng Zhou, Peng Huang, Haitong Li, Wenjia Ma, Dongbin Zhu, Lifeng Liu, Xiaoyan Liu, Jinfeng Kang *et al.*, "Optimized Learning Scheme for Grayscale Image Recognition in a RRAM Based Analog Neuromorphic System," in *IEDM*, 2015.

- [997] Geoffrey W Burr, Pritish Narayanan, Robert M Shelby, Severin Sidler, Irem Boybat, Carmelo Di Nolfo, and Yusuf Leblebici, “Large-Scale Neural Networks Implemented with Non-Volatile Memory as the Synaptic Weight Element: Comparative Performance Analysis (Accuracy, Speed, and Power),” in *IEDM*, 2015.
- [998] Qian Lou, Sarath Chandra Janga, and Lei Jiang, “Helix: Algorithm/Architecture Co-Design for Accelerating Nanopore Genome Base-Calling,” in *PACT*, 2020.
- [999] Fan Chen, Linghao Song, Yiran Chen *et al.*, “PARC: A Processing-in-CAM Architecture for Genomic Long Read Pairwise Alignment using ReRAM,” in *ASP-DAC*, 2020.
- [1000] Yu Cai, Onur Mutlu, Erich F Haratsch, and Ken Mai, “Program Interference in MLC NAND Flash Memory: Characterization, Modeling, and Mitigation,” in *ICCD*, 2013.
- [1001] Yu Cai, Saugata Ghose, Yixin Luo, Ken Mai, Onur Mutlu, and Erich F Haratsch, “Vulnerabilities in MLC NAND Flash Memory Programming: Experimental Analysis, Exploits, and Mitigation Techniques,” in *HPCA*, 2017.
- [1002] Jisung Park, Jaeyong Jeong, Sungjin Lee, Youngsun Song, and Jihong Kim, “Improving Performance and Lifetime of NAND Storage Systems Using Relaxed Program Sequence,” in *DAC*, 2016.
- [1003] Yu Cai, Yixin Luo, Erich F Haratsch, Ken Mai, and Onur Mutlu, “Data Retention in MLC NAND Flash Memory: Characterization, Optimization, and Recovery,” in *HPCA*, 2015.
- [1004] Yu Cai, Yixin Luo, Saugata Ghose, and Onur Mutlu, “Read Disturb Errors in MLC NAND Flash Memory: Characterization, Mitigation, and Recovery,” in *DSN*, 2015.
- [1005] Keonsoo Ha, Jaeyong Jeong, and Jihong Kim, “An Integrated Approach for Managing Read Disturbs in High-density NAND Flash Memory,” *IEEE TCAD*, 2015.
- [1006] Sungjin Lee, Keonsoo Ha, Kangwon Zhang, Jihong Kim, and Junghwan Kim, “FlexFS: A Flexible Flash File System for MLC NAND Flash Memory,” in *USENIX ATC*, 2009.
- [1007] Yu Cai, Erich F Haratsch, Onur Mutlu, and Ken Mai, “Threshold Voltage Distribution in MLC NAND Flash Memory: Characterization, Analysis, and Modeling,” in *DATE*, 2013.
- [1008] Yu Cai, Gulay Yalcin, Onur Mutlu, Erich F Haratsch, Osman Unsal, Adrian Cristal, and Ken Mai, “Neighbor-Cell Assisted Error Correction for MLC NAND Flash Memories,” in *SIGMETRICS*, 2014.
- [1009] Rakesh Nadig, Mohammad Sadrosadati, Haiyu Mao, Nika Mansouri Ghiasi, Arash Tavakkol, Jisung Park, Hamid Sarbazi-Azad, Juan Gómez Luna, and Onur Mutlu, “Venice: Improving Solid-State Drive Parallelism at Low Cost via Conflict-Free Accesses,” in *ISCA*, 2023.
- [1010] Milad Hashemi, Kevin Swersky, Jamie A Smith, Grant Ayers, Heiner Litz, Jichuan Chang, Christos Kozyrakis, and Parthasarathy Ranganathan, “Learning Memory Access Patterns,” in *ICML*, 2018.

- [1011] Lois Orosa, Rodolfo Azevedo, and Onur Mutlu, “AVPP: Address-First Value-Next Predictor with Value Prefetching for Improving the Efficiency of Load Value Prediction,” *TACO*, 2018.
- [1012] Adwait Jog, Onur Kayiran, Asit K Mishra, Mahmut T Kandemir, Onur Mutlu, Ravishankar Iyer, and Chita R Das, “Orchestrated Scheduling and Prefetching for GPGPUs,” in *ISCA*, 2013.
- [1013] Chang Joo Lee, Onur Mutlu, Veynu Narasiman, and Yale N Patt, “Prefetch-Aware Memory Controllers,” *TC*, 2011.
- [1014] Todd M Austin and Gurindar S Sohi, “Zero-Cycle Loads: Microarchitecture Support for Reducing Load Latency,” in *MICRO*, 1995.
- [1015] Luis Ceze, Karin Strauss, James Tuck, Josep Torrellas, and Jose Renau, “CAVA: Using Checkpoint-Assisted Value Prediction to Hide L2 Misses,” *TACO*, 2006.
- [1016] David Kadjo, Jinchun Kim, Prabal Sharma, Reena Panda, Paul Gratz, and Daniel Jimenez, “B-Fetch: Branch Prediction Directed Prefetching for Chip-Multiprocessors,” in *MICRO*, 2014.
- [1017] Nevin Kirman, Meyrem Kirman, Mainak Chaudhuri, and Jose F Martinez, “Checkpointed Early Load Retirement,” in *HPCA*, 2005.
- [1018] Eiman Ebrahimi, Chang Joo Lee, Onur Mutlu, and Yale N Patt, “Prefetch-Aware Shared Resource Management for Multi-Core Systems,” in *ISCA*, 2011.
- [1019] Chang Joo Lee, Veynu Narasiman, Onur Mutlu, and Yale N Patt, “Improving Memory Bank-Level Parallelism in the Presence of Prefetching,” in *MICRO*, 2009.
- [1020] Chang Joo Lee, O. Mutlu, V. Narasiman, and Y.N. Patt, “Prefetch-Aware DRAM Controllers,” in *MICRO*, 2008.
- [1021] Onur Mutlu, Hyesoon Kim, David N Armstrong, and Yale N Patt, “Using the First-Level Caches as Filters to Reduce the Pollution Caused by Speculative Memory References,” *IJPP*, 2005.
- [1022] Amir Yazdanbakhsh, Gennady Pekhimenko, Bradley Thwaites, Hadi Esmaeilzadeh, Onur Mutlu, and Todd C Mowry, “RFVP: Rollback-Free Value Prediction with Safe-to-Approximate Loads,” *TACO*, 2016.
- [1023] Richard J Eickemeyer and Stamatis Vassiliadis, “A Load-Instruction Unit for Pipelined Processors,” *IBM JRD*, 1993.
- [1024] Fernando A Endo, Arthur Perais, and André Seznec, “On the Interactions Between Value Prediction and Compiler Optimizations in the Context of EOLE,” *TACO*, 2017.
- [1025] Mikko H Lipasti and John Paul Shen, “Exceeding the Dataflow Limit via Value Prediction,” in *MICRO*, 1996.
- [1026] Mikko H Lipasti, Christopher B Wilkerson, and John Paul Shen, “Value Locality and Load Value Prediction,” in *ASPLOS*, 1996.

- [1027] Brad Calder, Glenn Reinman, and Dean M Tullsen, "Selective Value Prediction," in *ISCA*, 1999.
- [1028] Kai Wang and Manoj Franklin, "Highly Accurate Data Value Prediction Using Hybrid Predictors," in *MICRO*, 1997.
- [1029] Freddy Gabbay and Avi Mendelson, "Speculative Execution Based on Value Prediction," Technion — Israel Institute of Technology, Tech. Rep. 1080, 1996.
- [1030] Martin Burtscher and Benjamin G Zorn, "Exploring Last N Value Prediction," in *PACT*, 1999.
- [1031] Chao-Ying Fu, Matthew D Jennings, Sergei Y Larin, and Thomas M Conte, "Value Speculation Scheduling for High Performance Processors," in *ASPLOS*, 1998.
- [1032] Bart Goeman, Hans Vandierendonck, and Koenraad De Bosschere, "Differential FCM: Increasing Value Prediction Accuracy by Improving Table Usage Efficiency," in *HPCA*, 2001.
- [1033] Tarun Nakra, Rajiv Gupta, and Mary Lou Soffa, "Global Context-Based Value Prediction," in *HPCA*, 1999.
- [1034] Toshinori Sato and Itsujiro Arita, "Low-Cost Value Predictors Using Frequent Value Locality," in *HPCA*, 2002.
- [1035] Yiannakis Sazeides and James E Smith, "The Predictability of Data Values," in *MICRO*, 1997.
- [1036] Nathan Tuck and Dean M Tullsen, "Multithreaded Value Prediction," in *HPCA*, 2005.
- [1037] Dean M Tullsen and John S Seng, "Storageless Value Prediction Using Prior Register Values," in *ISCA*, 1999.
- [1038] Eric S Tune, Dean M Tullsen, and Brad Calder, "Quantifying Instruction Criticality," in *PACT*, 2002.
- [1039] Julien Dusser, Thomas Piquet, and André Seznec, "Zero-Vontent Augmented Caches," in *ICS*, 2009.
- [1040] Jun Yang, Youtao Zhang, and Rajiv Gupta, "Frequent Value Compression in Data Caches," in *MICRO*, 2000.
- [1041] Youtao Zhang, Jun Yang, and Rajiv Gupta, "Frequent Value Locality and Value-Centric Data Cache Design," in *ASPLOS*, 2000.
- [1042] Gennady Pekhimenko, Evgeny Bolotin, Nandita Vijaykumar, Onur Mutlu, Todd C Mowry, and Stephen W Keckler, "A Case for Toggle-Aware Compression for GPU Systems," in *HPCA*, 2016.
- [1043] Gennady Pekhimenko, Evgeny Bolotin, Mike O'Connor, Onur Mutlu, Todd C Mowry, and Stephen W Keckler, "Toggle-Aware Compression for GPUs," *CAL*, 2015.

- [1044] Gennady Pekhimenko, Evgeny Bolotin, Mike O'Connor, Onur Mutlu, Todd C Mowry, and Stephen W Keckler, "Energy-Efficient Data Compression for GPU Memory Systems," in *ASPLOS*, 2015.
- [1045] Gennady Pekhimenko, Tyler Huberty, Rui Cai, Onur Mutlu, Phillip B Gibbons, Michael A Kozuch, and Todd C Mowry, "Exploiting Compressed Block Size as an Indicator of Future Reuse," in *HPCA*, 2015.
- [1046] Xi Chen, Lei Yang, Robert P Dick, Li Shang, and Haris Lekatsas, "C-Pack: A High-Performance Microprocessor Cache Compression Algorithm," *TVLSI*, 2009.
- [1047] Erik G Hallnor and Steven K Reinhardt, "A Unified Compressed Memory Hierarchy," in *HPCA*, 2005.
- [1048] Dan W Hammerstrom and Edward S Davidson, "Information Content of CPU Memory Referencing Behavior," in *ISCA*, 1977.
- [1049] Mafijul Md Islam and Per Stenstrom, "Zero-Value Caches: Cancelling Loads That Return Zero," in *PACT*, 2009.
- [1050] Angelos Arelakis and Per Stenstrom, "SC2: A Statistical Compression Cache Scheme," in *ISCA*, 2014.
- [1051] Magnus Ekman and Per Stenstrom, "A Robust Main-Memory Compression Scheme," in *ISCA*, 2005.
- [1052] Nandita Vijaykumar, Gennady Pekhimenko, Adwait Jog, Abhishek Bhowmick, Rachata Ausavarungnirun, Chita Das, Mahmut Kandemir, Todd C Mowry, and Onur Mutlu, "A Case for Core-Assisted Bottleneck Acceleration in GPUs: Enabling Flexible Data Compression with Assist Warps," in *ISCA*, 2015.
- [1053] Jayesh Gaur, Alaa R Alameldeen, and Sreenivas Subramoney, "Base-Victim Compression: An Opportunistic Cache Compression Architecture," in *ISCA*, 2016.
- [1054] Joshua San Miguel, Jorge Albericio, Andreas Moshovos, and Natalie Enright Jerger, "Doppelgänger: A Cache for Approximate Computing," in *ISCA*, 2015.
- [1055] Geraldo F Oliveira, Larissa Rozales Gonçalves, Marcelo Brandalero, Antonio Carlos S Beck, and Luigi Carro, "Employing Classification-Based Algorithms for General-Purpose Approximate Computing," in *DAC*, 2018.
- [1056] Nandita Vijaykumar, Abhilasha Jain, Diptesh Majumdar, Kevin Hsieh, Gennady Pekhimenko, Eiman Ebrahimi, Nastaran Hajinazar, Phillip B Gibbons, and Onur Mutlu, "A Case for Richer Cross-Layer Abstractions: Bridging the Semantic Gap with Expressive Memory," in *ISCA*, 2018.
- [1057] Amir Yazdanbakhsh, Bradley Thwaites, Hadi Esmaeilzadeh, Gennady Pekhimenko, Onur Mutlu, and Todd C Mowry, "Mitigating the Memory Bottleneck with Approximate Load Value Prediction," *IEEE Design & Test*, 2016.

- [1058] Po-An Tsai, Yee Ling Gan, and Daniel Sanchez, “Rethinking the Memory Hierarchy for Modern Languages,” in *MICRO*, 2018.
- [1059] Andreas Sembrant, Erik Hagersten, and David Black-Schaffer, “The Direct-to-Data (D2D) Cache: Navigating the Cache Hierarchy with a Single Lookup,” in *ISCA*, 2014.
- [1060] Zehra Sura, Arpith Jacob, Tong Chen, Bryan Rosenberg, Olivier Sallenave, Carlo Bertolli, Samuel Antao, Jose Brunheroto, Yoonho Park, Kevin O’Brien *et al.*, “Data Access Optimization in a Processing-in-Memory System,” in *CF*, 2015.
- [1061] D. P. Zhang, N. Jayasena, A. Lyashevsky *et al.*, “A New Perspective on Processing-in-Memory Architecture Design,” in *MSPC*, 2013.
- [1062] Seth Pugsley, Rajeev Balasubramonian, Jeffrey Jestes, Feifei Li, Al Davis, Vijayalakshmi Srinivasan, and Alper Buyuktosunoglu, “Comparing Different Implementations of Near Data Computing with In-Memory MapReduce Workloads,” *IEEE Micro*, 2014.
- [1063] Erfan Azarkhish, “Memory Hierarchy Design for Next Generation Scalable Many-Core Platforms,” Ph.D. dissertation, Università di Bologna, 2016.
- [1064] Po-An Tsai, Nathan Beckmann, and Daniel Sanchez, “Jenga: Software-Defined Cache Hierarchies,” in *ISCA*, 2017.
- [1065] Po-An Tsai and Daniel Sanchez, “Compress Objects, Not Cache Lines: An Object-Based Compressed Memory Hierarchy,” in *ASPLOS*, 2019.
- [1066] Nandita Vijaykumar, Eiman Ebrahimi, Kevin Hsieh, Phillip B Gibbons, and Onur Mutlu, “The Locality Descriptor: A Holistic Cross-Layer Abstraction to Express Data Locality in GPUs,” in *ISCA*, 2018.
- [1067] Onur Mutlu, “Intelligent Architectures for Intelligent Computing Systems,” in *DATE*, 2020.
- [1068] Dhinakaran Pandiyan and Carole-Jean Wu, “Quantifying the Energy Cost of Data Movement for Emerging Smart Phone Workloads on Mobile Platforms,” in *IISWC*, 2014.
- [1069] Kaige Yan, Xingyao Zhang, and Xin Fu, “Characterizing, Modeling, and Improving the QoE of Mobile Devices with Low Battery Level,” in *MICRO*, 2015.
- [1070] Daves Shingari, Akhil Arunkumar, and Carole-Jean Wu, “Characterization and Throttling-Based Mitigation of Memory Interference for Heterogeneous Smartphones,” in *IISWC*, 2015.
- [1071] Christos Kozyrakis, Aman Kansal, Sriram Sankar, and Kushagra Vaid, “Server Engineering Insights for Large-Scale Online Services,” *IEEE Micro*, 2010.
- [1072] Ahmad Yasin, Yosi Ben-Asher, and Avi Mendelson, “Deep-Dive Analysis of the Data Analytics Workload in CloudSuite,” in *IISWC*, 2014.
- [1073] Richard C Murphy, Peter M Kogge, and Arun Rodrigues, “The Characterization of Data Intensive Memory Workloads on Distributed PIM Systems,” in *Intelligent Memory Systems*. Springer-Verlag, 2001.

- [1074] Ankur Limaye and Tosiron Adegbiya, “A Workload Characterization of the SPEC CPU2017 Benchmark Suite,” in *ISPASS*, 2018.
- [1075] Christian Bienia, Sanjeev Kumar, Jaswinder Pal Singh, and Kai Li, “The PARSEC Benchmark Suite: Characterization and Architectural Implications,” in *PACT*, 2008.
- [1076] Stefano Corda, Gagandeep Singh, Ahsan Javed Awan, Roel Jordans, and Henk Corporaal, “Memory and Parallelism Analysis Using a Platform-Independent Approach,” in *SCOPES*, 2019.
- [1077] Samuel Williams, Andrew Waterman, and David Patterson, “Roofline: An Insightful Visual Performance Model for Multicore Architectures,” *CACM*, 2009.
- [1078] Hyojong Kim, Ramyad Hadidi, Lifeng Nai, Hyesoon Kim, Nuwan Jayasena, Yasuko Eckert, Onur Kayiran, and Gabriel Loh, “CODA: Enabling Co-Location of Computation and Data for Multiple GPU Systems,” *TACO*, 2018.
- [1079] Byungchul Hong, Gwangsun Kim, Jung Ho Ahn, Yongkee Kwon, Hongsik Kim, and John Kim, “Accelerating Linked-List Traversal Through Near-Data Processing,” in *PACT*, 2016.
- [1080] Matthias Gries, Pau Cabré, and Julio Gago, “Performance Evaluation and Feasibility Study of Near-Data Processing on DRAM Modules (DIMM-NDP) for Scientific Applications,” *Technical Report*, 2019.
- [1081] Juan Gómez-Luna, Yuxin Guo, Sylvan Brocard, Julien Legriel, Remy Cimadomo, Geraldo F Oliveira, Gagandeep Singh, and Onur Mutlu, “An Experimental Evaluation of Machine Learning Training on a Real Processing-in-Memory System,” arXiv:2207.07886 [cs.AR], 2022.
- [1082] Joël Lindegger, Damla Senol Cali, Mohammed Alser, Juan Gómez-Luna, Nika Mansouri Ghiasi, and Onur Mutlu, “Scrooge: A Fast and Memory-Frugal Genomic Sequence Aligner for CPUs, GPUs, and ASICs,” *Bioinformatics*, 2023.
- [1083] Cong Li, Zhe Zhou, Yang Wang, Fan Yang, Ting Cao, Mao Yang, Yun Liang, and Guangyu Sun, “PIM-DL: Expanding the Applicability of Commodity DRAM-PIMs for Deep Learning via Algorithm-System Co-Optimization,” in *ASPLOS*, 2024.
- [1084] Xuan-Jun Chen, Han-Ping Chen, and Chia-Lin Yang, “PointCIM: A Computing-in-Memory Architecture for Accelerating Deep Point Cloud Analytics,” in *MICRO*, 2024.
- [1085] Jaehyun Park, Jaewan Choi, Kwanhee Kyung, Michael Jaemin Kim, Yongsuk Kwon, Nam Sung Kim, and Jung Ho Ahn, “AttAcc! Unleashing the Power of PIM for Batched Transformer-Based Generative Model Inference,” in *ASPLOS*, 2024.
- [1086] Satanu Maity, Mayank Goel, and Manojit Ghose, “CoaT: Compiler-Assisted Two-Stage Offloading Approach for Data-Intensive Applications Under NMP Framework,” *TETC*, 2024.
- [1087] Saambhavi Baskaran and Jack Sampson, “Decentralized Offload-Based Execution on Memory-Centric Compute Cores,” in *MEMSYS*, 2020.

- [1088] Satanu Maity, Mayank Goel, and Manojit Ghose, “Data Locality Aware Computation Offloading in Near Memory Processing Architecture for Big Data Applications,” in *HiPC*, 2023.
- [1089] Yoongu Kim, Dongsu Han, Onur Mutlu, and Mor Harchol-Balter, “ATLAS: A Scalable and High-Performance Scheduling Algorithm for Multiple Memory Controllers,” in *HPCA*, 2010.
- [1090] Sai Prashanth Muralidhara, Lavanya Subramanian, Onur Mutlu, Mahmut Kandemir, and Thomas Moscibroda, “Reducing Memory Interference in Multicore Systems via Application-Aware Memory Channel Partitioning,” in *MICRO*, 2011.
- [1091] John Cheng, Max Grossman, and Ty McKercher, *Professional CUDA C Programming*. John Wiley & Sons, 2014.
- [1092] OpenACC Organization, “The OpenACC®~Application Programming Interface, Version 3.1,” 2020.
- [1093] Socrates S Wong, Cecilio C Tamarit, and José F Martínez, “PUMICE: Processing-using-Memory Integration with a Scalar Pipeline for Symbiotic Execution,” in *DAC*, 2023.
- [1094] Chris Lattner, Mehdi Amini, Uday Bondhugula, Albert Cohen, Andy Davis, Jacques Pienaar, River Riddle, Tatiana Shpeisman, Nicolas Vasilache, and Oleksandr Zinenko, “MLIR: Scaling Compiler Infrastructure for Domain Specific Computation,” in *CGO*, 2021.
- [1095] Konstantinos Kanellopoulos, Hong Chul Nam, Nisa Bostanci, Rahul Bera, Mohammad Sadrosadati, Rakesh Kumar, Davide Basilio Bartolini, and Onur Mutlu, “Victima: Drastically Increasing Address Translation Reach by Leveraging Underutilized Cache Resources,” in *MICRO*, 2023.
- [1096] Konstantinos Kanellopoulos, Rahul Bera, Kosta Stojiljkovic, F Nisa Bostanci, Can Firtina, Rachata Ausavarungnirun, Rakesh Kumar, Nastaran Hajinazar, Mohammad Sadrosadati, Nandita Vijaykumar *et al.*, “Utopia: Fast and Efficient Address Translation via Hybrid Restrictive & Flexible Virtual-to-Physical Address Mappings,” in *MICRO*, 2023.
- [1097] Arkaprava Basu, Jayneel Gandhi, Jichuan Chang, Mark D Hill, and Michael M Swift, “Efficient Virtual Memory for Big Memory Servers,” in *ISCA*, 2013.
- [1098] Vasileios Karakostas, Osman S Unsal, Mario Nemirovsky, Adrian Cristal, and Michael Swift, “Performance Analysis of the Memory Management Unit Under Scale-Out Workloads,” in *IISWC*, 2014.
- [1099] Konstantinos Kanellopoulos, Konstantinos Sgouras, and Onur Mutlu, “Virtuoso: An Open-Source, Comprehensive and Modular Simulation Framework for Virtual Memory Research,” arXiv:2403.04635 [cs.AR], 2024.
- [1100] Chen Li, Rachata Ausavarungnirun, Christopher J Rossbach, Youtao Zhang, Onur Mutlu, Yang Guo, and Jun Yang, “A Framework for Memory Oversubscription Management in Graphics Processing Units,” in *ASPLOS*, 2019.

- [1101] Rachata Ausavarungnirun, Joshua Landgraf, Vance Miller, Saugata Ghose, Jayneel Gandhi, Christopher J. Rossbach, and Onur Mutlu, “Mosaic: Enabling Application-Transparent Support for Multiple Page Sizes in Throughput Processors,” *OSR*, 2018.
- [1102] Rachata Ausavarungnirun, Vance Miller, Joshua Landgraf, Saugata Ghose, Jayneel Gandhi, Adwait Jog, Christopher J Rossbach, and Onur Mutlu, “MASK: Redesigning the GPU Memory Hierarchy to Support Multi-Application Concurrency,” in *ASPLOS*, 2018.
- [1103] Rachata Ausavarungnirun, Joshua Landgraf, Vance Miller, Saugata Ghose, Jayneel Gandhi, Christopher J Rossbach, and Onur Mutlu, “Mosaic: A GPU Memory Manager with Application-Transparent Support for Multiple Page Sizes,” in *MICRO*, 2017.
- [1104] Shuai Che, Arkaprava Basu, and Jonathan Gallmeier, “Challenges of Programming a System with Heterogeneous Memories and Heterogeneous Processors: A Programmer’s View,” in *MEMSYS*, 2016.
- [1105] Mary Hall and Craig Steele, “Memory Management in a PIM-Based Architecture,” in *IMS*, 2000.
- [1106] Javier Picorel, Djordje Jevdjic, and Babak Falsafi, “Near-Memory Address Translation,” in *PACT*, 2017.
- [1107] Wei Jiang, Vignesh T Ravi, and Gagan Agrawal, “A Map-Reduce System with an Alternate API for Multi-Core Environments,” in *CCGRID*, 2010.
- [1108] Lavanya Subramanian, Donghyuk Lee, Vivek Seshadri, Harsha Rastogi, and Onur Mutlu, “BLISS: Balancing Performance, Fairness and Complexity in Memory Access Scheduling,” *TPDS*, 2016.
- [1109] SAFARI Research Group, “DAMOV Benchmark Suite and Simulation Framework,” <https://github.com/CMU-SAFARI/DAMOV>.
- [1110] Daniel Sanchez and Christos Kozyrakis, “ZSim: Fast and Accurate Microarchitectural Simulation of Thousand-Core Systems,” in *ISCA*, 2013.
- [1111] Intel Corp., “Intel VTune Profiler User Guide,” <https://software.intel.com/content/www/us/en/develop/documentation/vtune-help/>, 2021.
- [1112] A. Yasin, “A Top-Down Method for Performance Analysis and Counters Architecture,” in *ISPASS*, 2014.
- [1113] Intel Corp., “Intel VTune Profiler User Guide,” <https://software.intel.com/content/www/us/en/develop/documentation/vtune-help/top/reference/cpu-metrics-reference/memory-bound.html>.
- [1114] Thomas M. Conte and Wen-mei W Hwu, “Benchmark Characterization,” *IEEE Computer*, 1991.
- [1115] Mark S Johnstone and Paul R Wilson, “The Memory Fragmentation Problem: Solved?” in *ISMM*, 1998.

- [1116] Jonathan Weinberg, Michael O McCracken, Erich Strohmaier, and Allan Snavely, "Quantifying Locality in the Memory Access Patterns of HPC Applications," in *SC*, 2005.
- [1117] Y. S. Shao and D. Brooks, "ISA-Independent Workload Characterization and Its Implications for Specialized Architectures," in *ISPASS*, 2013.
- [1118] Yutao Zhong, Xipeng Shen, and Chen Ding, "Program Locality Analysis Using Reuse Distance," *TOPLAS*, 2009.
- [1119] Xiaoming Gu, Ian Christopher, Tongxin Bai, Chengliang Zhang, and Chen Ding, "A Component Model of Spatial Locality," in *ISMM*, 2009.
- [1120] Jonathan C Beard and Joshua Randall, "Eliminating Dark Bandwidth: A Data-Centric View of Scalable, Efficient Performance, Post-Moore," in *HiPC*, 2017.
- [1121] Scott Lloyd and Maya Gokhale, "In-Memory Data Rearrangement for Irregular, Data-Intensive Computing," *IEEE Computer*, 2015.
- [1122] Thomas M Conte and Wen-mei W Hwu, "A Brief Survey of Benchmark Usage in the Architecture Community," *CAN*, 1991.
- [1123] Thomas M Conte and Wen-mei W Hwu, "Advances in Benchmarking Techniques: New Standards and Quantitative Metrics," in *Advances in Computers*, 1995.
- [1124] Douglas Doerfler, Jack Deslippe, Samuel Williams, Leonid Oliker, Brandon Cook, Thorsten Kurth, Mathieu Lobet, Tareq Malas, Jean-Luc Vay, and Henri Vincenti, "Applying the Roofline Performance Model to the Intel Xeon Phi Knights Landing Processor," in *HiPC*, 2016.
- [1125] Eiman Ebrahimi, Chang Joo Lee, Onur Mutlu, and Yale N Patt, "Fairness via Source Throttling: A Configurable and High-Performance Fairness Substrate for Multi-Core Memory Systems," in *ASPLOS*, 2010.
- [1126] Subbarao Palacharla and Richard E Kessler, "Evaluating Stream Buffers as a Secondary Cache Replacement," in *ISCA*, 1994.
- [1127] Paulo C Santos, Marco AZ Alves, Matthias Diener, Luigi Carro, and Philippe OA Navaux, "Exploring Cache Size and Core Count Tradeoffs in Systems with Reduced Memory Access Latency," in *PDP*, 2016.
- [1128] Andrew Glew, "MLP Yes! ILP No!" in *ASPLOS WACI*, 1998.
- [1129] Moinuddin K Qureshi, Daniel N Lynch, Onur Mutlu, and Yale N Patt, "A Case for MLP-Aware Cache Replacement," in *ISCA*, 2006.
- [1130] Tse-Yu Yeh and Yale N Patt, "Two-Level Adaptive Training Branch Prediction," in *MICRO*, 1991.
- [1131] Naveen Muralimanohar, Rajeev Balasubramonian, and Norm Jouppi, "Optimizing NUCA Organizations and Wiring Alternatives for Large Caches with CACTI 6.0," in *MICRO*, 2007.

- [1132] Rachata Ausavarungnirun, Chris Fallin, Xiangyao Yu, Kevin Kai-Wei Chang, Greg Nazario, Reetuparna Das, Gabriel H Loh, and Onur Mutlu, “Design and Evaluation of Hierarchical Rings with Deflection Routing,” in *SBAC-PAD*, 2014.
- [1133] Mingyu Gao, Grant Ayers, and Christos Kozyrakis, “Practical Near-Data Processing for in-Memory Analytics Frameworks,” in *PACT*, 2015.
- [1134] Gwangsun Kim, John Kim, Jung Ho Ahn, and Jaeha Kim, “Memory-Centric System Interconnect Design with Hybrid Memory Cubes,” in *PACT*, 2013.
- [1135] Utku Sirin, Ahmad Yasin, and Anastasia Ailamaki, “A Methodology for OLTP Micro-Architectural Analysis,” in *DAMON*, 2017.
- [1136] R. Appuswamy, J. Fellay, and N. Chaturvedi, “Sequence Alignment Through the Looking Glass,” in *IPDPSW*, 2018.
- [1137] Intel Corp., “Intel Xeon Processor E3-1240,” <http://ark.intel.com/products/52273/>, 2011.
- [1138] Intel Corp., “Understanding How General Exploration Works in Intel VTune Amplifier,” <https://software.intel.com/en-us/articles/understanding-how-general-exploration-works-in-intel-vtune-amplifier-xe>, 2018.
- [1139] Juan Gómez-Luna, Izzat El Hajj, Victor Chang, Li-Wen Garcia-Flores, Simon Garcia de Gonzalo, Thomas Jablin, Antonio J Pena, and Wen-mei Hwu, “Chai: Collaborative Heterogeneous Applications for Integrated-Architectures,” in *ISPASS*, 2017.
- [1140] United States Department of Energy, “CORAL Benchmark Codes,” <https://asc.llnl.gov/CORAL-benchmarks/>, 2014.
- [1141] John A Stratton, Christopher Rodrigues, I-Jui Sung, Nady Obeid, Li-Wen Chang, Nasser Anssari, Geng Daniel Liu, and Wen-mei W Hwu, “Parboil: A Revised Benchmark Suite for Scientific and Commercial Throughput Computing,” Univ. of Illinois at Urbana-Champaign, IMPACT Research Group, Tech. Rep. IMPACT-12-01, 2012.
- [1142] S. Che, M. Boyer, J. Meng, D. Tarjan, J. W. Sheaffer, S. Lee, and K. Skadron, “Rodinia: A Benchmark Suite for Heterogeneous Computing,” in *IISWC*, 2009.
- [1143] S. K. Venkata, I. Ahn, D. Jeon, A. Gupta, C. Louie, S. Garcia, S. Belongie, and M. B. Taylor, “SD-VBS: The San Diego Vision Benchmark Suite,” in *IISWC*, 2009.
- [1144] Steven Cameron Woo, Moriyoshi Ohara, Evan Torrie, Jaswinder Pal Singh, and Anoop Gupta, “The SPLASH-2 Programs: Characterization and Methodological Considerations,” in *ISCA*, 1995.
- [1145] John D McCalpin *et al.*, “Memory Bandwidth and Machine Balance in Current High Performance Computers,” *IEEE TCCA Newsletter*, 1995.
- [1146] Piotr R Luszczek, David H Bailey, Jack J Dongarra, Jeremy Kepner, Robert F Lucas, Rolf Rabenseifner, and Daisuke Takahashi, “The HPC Challenge (HPCC) Benchmark Suite,” in *SC*, 2006.

- [1147] Jack Dongarra, Michael A Heroux, and Piotr Luszczek, “HPCG Benchmark: A New Metric for Ranking High Performance Computing Systems,” Univ. of Tennessee Dept. of Electrical Engg. and Computer Sci., Tech. Rep. UT-EECS-15-736, 2015.
- [1148] Nauman Ahmed, Koen Bertels, and Zaid Al-Ars, “A Comparison of Seed-and-Extend Techniques in Modern DNA Read Alignment Algorithms,” in *BIBM*, 2016.
- [1149] C. Balkesen, J. Teubner, G. Alonso, and M. T. Oszu, “Main-Memory Hash Joins on Modern Processor Architectures,” *TKDE*, 2015.
- [1150] J. Gómez-Luna, L. Chang, I. Sung, W. Hwu, and N. Guil, “In-Place Data Sliding Algorithms for Many-Core Architectures,” in *ICPP*, 2015.
- [1151] Narayanan Sundaram, Nadathur Satish, Md Mostofa Ali Patwary, Subramanya R. Dulloor, Michael J. Anderson, Satya Gautam Vadlamudi, Dipankar Das, and Pradeep Dubey, “GraphMat: High Performance Graph Analytics Made Productive,” *PVLDB*, 2015.
- [1152] Julian Shun and Guy E. Blelloch, “Ligra: A Lightweight Graph Processing Framework for Shared Memory,” in *PPoPP*, 2013.
- [1153] Alex Krizhevsky, Ilya Sutskever, and Geoffrey E Hinton, “ImageNet Classification with Deep Convolutional Neural Networks,” in *NIPS*, 2012.
- [1154] Joseph Redmon, “Darknet: Open Source Neural Networks in C,” <http://pjreddie.com/darknet>.
- [1155] Deepayan Chakrabarti, Yiping Zhan, and Christos Faloutsos, “R-MAT: A Recursive Model for Graph Mining,” in *SDM*, 2004.
- [1156] Center for Discrete Mathematics & Theoretical Computer Science, “9th DIMACS Implementation Challenge,” <http://www.dis.uniroma1.it/challenge9/>, 2014.
- [1157] Ramyad Hadidi, Bahar Asgari, Burhan Ahmad Mudassar, Saibal Mukhopadhyay, Sudhakar Yalamanchili, and Hyesoon Kim, “Demystifying the Characteristics of 3D-Stacked Memories: A Case Study for Hybrid Memory Cube,” in *IISWC*, 2017.
- [1158] John A Hartigan and Manchek A Wong, “Algorithm AS 136: A K-Means Clustering Algorithm,” *J. R. Stat. Soc. C-Appl.*, 1979.
- [1159] Yuan Chou, Brian Fahs, and Santosh Abraham, “Microarchitecture Optimizations for Exploiting Memory-Level Parallelism,” in *ISCA*, 2004.
- [1160] James Tuck, Luis Ceze, and Josep Torrellas, “Scalable Cache Miss Handling for High Memory-Level Parallelism,” in *MICRO*, 2006.
- [1161] Sujay Phadke and Satish Narayanasamy, “MLP Aware Heterogeneous Memory System,” in *DATE*, 2011.
- [1162] Stijn Everman and Lieven Eeckhout, “A Memory-Level Parallelism Aware Fetch Policy for SMT Processors,” in *HPCA*, 2007.

- [1163] George Patsilaras, Niket K Choudhary, and James Tuck, “Efficiently Exploiting Memory Level Parallelism on Asymmetric Coupled Cores in the Dark Silicon Era,” *TACO*, 2012.
- [1164] Y. Eckert, N. Jayasena, and G. H. Loh, “Thermal Feasibility of Die-Stacked Processing in Memory,” in *WoNDP*, 2014.
- [1165] Abanti Basak, Shuangchen Li, Xing Hu, Sang Min Oh, Xinfeng Xie, Li Zhao, Xiaowei Jiang, and Yuan Xie, “Analysis and Optimization of the Memory Hierarchy for Graph Processing Workloads,” in *HPCA*, 2019.
- [1166] Mingyu Yan, Xing Hu, Shuangchen Li, Abanti Basak, Han Li, Xin Ma, Itir Akgun, Yujing Feng, Peng Gu, Lei Deng *et al.*, “Alleviating Irregularity in Graph Analytics Acceleration: A Hardware/Software Co-Design Approach,” in *MICRO*, 2019.
- [1167] Srikanth T Srinivasan, Ravi Rajwar, Haitham Akkary, Amit Gandhi, and Mike Upton, “Continual Flow Pipelines,” in *ASPLOS*, 2004.
- [1168] Jamison D Collins, Dean M Tullsen, Hong Wang, and John Paul Shen, “Dynamic Speculative Precomputation,” in *MICRO*, 2001.
- [1169] James Dundas and Trevor Mudge, “Improving Data Cache Performance by Pre-Executing Instructions Under a Cache Miss,” in *ICS*, 1997.
- [1170] Tanausu Ramirez, Alex Pajuelo, Oliverio J Santana, and Mateo Valero, “Runahead Threads to Improve SMT Performance,” in *HPCA*, 2008.
- [1171] Tanausú Ramírez, Alex Pajuelo, Oliverio J Santana, Onur Mutlu, and Mateo Valero, “Efficient Runahead Threads,” in *PACT*, 2010.
- [1172] Weifeng Zhang, Dean M Tullsen, and Brad Calder, “Accelerating and Adapting Pre-computation Threads for Efficient Prefetching,” in *HPCA*, 2007.
- [1173] S. Ghose, H. Lee, and J. F. Martínez, “Improving Memory Scheduling via Processor-Side Load Criticality Information,” in *ISCA*, 2013.
- [1174] Onur Mutlu, “Lecture Notes for 18-447 Computer Architecture – Lecture 17: Memory Hierarchy and Caches,” <https://course.ece.cmu.edu/~ece447/s15/lib/exe/fetch.php?media=onur-447-spring15-lecture17-memoryhierarchyandcaches-afterlecture.pdf>, 2015.
- [1175] Teresa L Johnson, Daniel A Connors, Matthew C Merten, and Wen-mei W. Hwu, “Run-Time Cache Bypassing,” *TC*, 1999.
- [1176] Vivek Seshadri, Abhishek Bhowmick, Onur Mutlu, Phillip B Gibbons, Michael A Kozuch, and Todd C Mowry, “The Dirty-Block Index,” in *ISCA*, 2014.
- [1177] Vivek Seshadri, Samihan Yedkar, Hongyi Xin, Onur Mutlu, Phillip B Gibbons, Michael A Kozuch, and Todd C Mowry, “Mitigating Prefetcher-Caused Pollution Using Informed Caching Policies for Prefetched Blocks,” *TACO*, 2015.
- [1178] Teresa L Johnson and Wen-Mei W Hwu, “Run-Time Adaptive Cache Hierarchy Management via Reference Analysis,” in *ISCA*, 1997.

- [1179] Gary Tyson, Matthew Farrens, John Matthews, and Andrew R Pleszkun, "A Modified Approach to Data Cache Management," in *MICRO*, 1995.
- [1180] Gokhan Memik, Glenn Reinman, and William H Mangione-Smith, "Just Say No: Benefits of Early Cache Miss Determination," in *HPCA*, 2003.
- [1181] Mazen Kharbutli and Yan Solihin, "Counter-Based Cache Replacement and Bypassing Algorithms," *TC*, 2008.
- [1182] Saurabh Gupta, Hongliang Gao, and Huiyang Zhou, "Adaptive Cache Bypassing for Inclusive Last Level Caches," in *IPDPS*, 2013.
- [1183] Lingda Li, Dong Tong, Zichao Xie, Junlin Lu, and Xu Cheng, "Optimal Bypass Monitor for High Performance Last-Level Caches," in *PACT*, 2012.
- [1184] Aswinkumar Sridharan and André Seznec, "Discrete Cache Insertion Policies for Shared Last Level Cache Management on Large Multicores," in *IPDPS*, 2016.
- [1185] Jungwhan Choi, Wongyu Shin, Jaemin Jang, Jinwoong Suh, Yongkee Kwon, Youngsuk Moon, and Lee-Sup Kim, "Multiple Clone Row DRAM: A Low Latency and Area Optimized DRAM," in *ISCA*, 2015.
- [1186] Young Hoon Son, O Seongil, Yuhwan Ro, Jae W Lee, and Jung Ho Ahn, "Reducing Memory Access Latency with Asymmetric DRAM Bank Organizations," in *ISCA*, 2013.
- [1187] Micron, "RLDRAM 2 and 3 Specifications," <https://www.micron.com/products/dram/rldram-memory>.
- [1188] Yasuharu Sato, Takaaki Suzuki, Tadao Aikawa, SY Fujioka, Waichiro Fujieda, Hiroyuki Kobayashi, Hitoshi Ikeda, Takayuki Nagasawa, Akihiro Funyu, Y Fuji *et al.*, "Fast Cycle RAM (FCRAM); A 20-ns Random Row Access, Pipe-Lined Operating DRAM," in *VLSIC*, 1998.
- [1189] O Seongil, Young Hoon Son, Nam Sung Kim, and Jung Ho Ahn, "Row-Buffer Decoupling: A Case for Low-Latency DRAM Microarchitecture," in *ISCA*, 2014.
- [1190] Rachata Ausavarungnirun, Kevin Kai-Wei Chang, Lavanya Subramanian, Gabriel H Loh, and Onur Mutlu, "Staged Memory Scheduling: Achieving High Performance and Scalability in Heterogeneous Systems," in *ISCA*, 2012.
- [1191] Lavanya Subramanian, Donghyuk Lee, Vivek Seshadri, Harsha Rastogi, and Onur Mutlu, "The Blacklisting Memory Scheduler: Achieving High Performance and Fairness at Low Cost," in *ICCD*, 2014.
- [1192] Scott Rixner, "Memory Controller Optimizations for Web Servers," in *MICRO*, 2004.
- [1193] Scott Rixner, William J Dally, Ujval J Kapasi, Peter Mattson, and John D Owens, "Memory Access Scheduling," in *ISCA*, 2000.
- [1194] William K Zuravleff and Timothy Robinson, "Controller for a Synchronous DRAM That Maximizes Throughput by Allowing Memory Requests and Commands to Be Issued Out of Order," U.S. Patent 5 630 096, 1997.

- [1195] Thomas Moscibroda and Onur Mutlu, “Distributed Order Scheduling and Its Application to Multi-Core DRAM Controllers,” in *PODC*, 2008.
- [1196] Eiman Ebrahimi, Rustam Miftakhutdinov, Chris Fallin, Chang Joo Lee, José A Joao, Onur Mutlu, and Yale N Patt, “Parallel Application Memory Scheduling,” in *MICRO*, 2011.
- [1197] Ibrahim Hur and Calvin Lin, “Adaptive History-Based Memory Schedulers,” in *MICRO*, 2004.
- [1198] Mingli Xie, Dong Tong, Kan Huang, and Xu Cheng, “Improving System Throughput and Fairness Simultaneously in Shared Memory CMP Systems via Dynamic Bank Partitioning,” in *HPCA*, 2014.
- [1199] George L Yuan, Ali Bakhoda, and Tor M Aamodt, “Complexity Effective Memory Access Scheduling for Many-Core Accelerator Architectures,” in *MICRO*, 2009.
- [1200] Hao Wang, Ripudaman Singh, Michael J Schulte, and Nam Sung Kim, “Memory Scheduling Towards High-Throughput Cooperative Heterogeneous Computing,” in *PACT*, 2014.
- [1201] Thomas Moscibroda and Onur Mutlu, “A Case for Bufferless Routing in On-Chip Networks,” in *ISCA*, 2009.
- [1202] Reetuparna Das, Onur Mutlu, Thomas Moscibroda, and Chita R Das, “Application-Aware Prioritization Mechanisms for On-Chip Networks,” in *MICRO*, 2009.
- [1203] Reetuparna Das, Onur Mutlu, Thomas Moscibroda, and Chita R Das, “Aergia: Exploiting Packet Latency Slack in On-Chip Networks,” in *ISCA*, 2010.
- [1204] George P Nychis, Chris Fallin, Thomas Moscibroda, Onur Mutlu, and Srinivasan Seshan, “On-Chip Networks from a Networking Perspective: Congestion and Scalability in Many-Core Interconnects,” in *SIGCOMM*, 2012.
- [1205] Maciej Besta, Syed Minhaj Hassan, Sudhakar Yalamanchili, Rachata Ausavarungnirun, Onur Mutlu, and Torsten Hoefler, “Slim NoC: A Low-Diameter On-Chip Network Topology for High Energy Efficiency and Scalability,” in *ASPLOS*, 2018.
- [1206] Chris Fallin, Chris Craik, and Onur Mutlu, “CHIPPER: A Low-Complexity Bufferless Deflection Router,” in *HPCA*, 2011.
- [1207] Boris Grot, Joel Hestness, Stephen W Keckler, and Onur Mutlu, “Kilo-NOC: A Heterogeneous Network-on-Chip Architecture for Scalability and Service Guarantees,” in *ISCA*, 2011.
- [1208] Luca Benini and Giovanni De Micheli, “Networks on Chip: A New Paradigm for Systems on Chip Design,” in *DATE*, 2002.
- [1209] Dan Zhang, “ZSim++,” <https://github.com/dzhang50/zsim-plusplus>.

- [1210] Onur Mutlu, “Lecture Notes for Digital Design and Computer Architecture – Lecture 15a: Out-of-Order Execution,” <https://safari.ethz.ch/digitaltechnik/spring2020/lib/exe/fetch.php?media=onur-digitaldesign-2020-lecture15a-out-of-order-execution-before-lecture.pdf>, 2020.
- [1211] Marco AZ Alves, Matthias Diener, Paulo C Santos, and Luigi Carro, “Large Vector Extensions Inside the HMC,” in *DATE*, 2016.
- [1212] Erfan Azarkhish, Davide Rossi, Igor Loi, and Luca Benini, “Design and Evaluation of a Processing-in-Memory Architecture for the Smart Memory Cube,” in *ARC*, 2016.
- [1213] Zhiyu Liu, Irina Calciu, Maurice Herlihy, and Onur Mutlu, “Concurrent Data Structures for Near-Memory Computing,” in *SPAA*, 2017.
- [1214] Jerome Friedman, Trevor Hastie, and Robert Tibshirani, *The Elements of Statistical Learning*, 2nd ed. Springer-Verlag, 2008.
- [1215] E. Azarkhish, D. Ross, I. Loi, and L. Benini, “High Performance AXI-4.0 Based Interconnect for Extensible Smart Memory Cubes,” in *DATE*, 2015.
- [1216] Ramyad Hadidi, Bahar Asgari, Jeffrey Young, Burhan Ahmad Mudassar, Kartikay Garg, Tushar Krishna, and Hyesoon Kim, “Performance Implications of NoCs on 3D-Stacked Memories: Insights from the Hybrid Memory Cube,” in *ISPASS*, 2018.
- [1217] Yakun Sophia Shao, Brandon Reagen, Gu-Yeon Wei, and David Brooks, “Aladdin: A Pre-RTL, Power-Performance Accelerator Simulator Enabling Large Design Space Exploration of Customized Architectures,” in *ISCA*, 2014.
- [1218] Chenhao Xie, Shuaiwen Leon Song, Jing Wang, Weigong Zhang, and Xin Fu, “Processing-in-Memory Enabled Graphics Processors for 3D Rendering,” in *HPCA*, 2017.
- [1219] Syed Minhaj Hassan, Sudhakar Yalamanchili, and Saibal Mukhopadhyay, “Near Data Processing: Impact and Optimization of 3D Memory System Architecture on the Uncore,” in *MEMSYS*, 2015.
- [1220] Shruti Padmanabha, Andrew Lukefahr, Reetuparna Das, and Scott Mahlke, “Mirage Cores: The Illusion of Many Out-of-Order Cores Using In-Order Hardware,” in *MICRO*, 2017.
- [1221] Chris Fallin, Chris Wilkerson, and Onur Mutlu, “The Heterogeneous Block Architecture,” in *ICCD*, 2014.
- [1222] Carlos Villavieja, Jose A Joao, Rustam Miftakhutdinov, and Yale N Patt, “Yoga: A Hybrid Dynamic VLIW/OoO Processor,” Univ. of Texas at Austin, High Performance Systems Group, Tech. Rep. TR-HPS-2014-001, 2014.
- [1223] M Aater Suleman, Milad Hashemi, Chris Wilkerson, Yale N Patt *et al.*, “Morphcore: An Energy-Efficient Microarchitecture for High Performance ILP and High Throughput TLP,” in *MICRO*, 2012.

- [1224] Engin Ipek, Meyrem Kirman, Nevin Kirman, and Jose F Martinez, "Core Fusion: Accommodating Software Diversity in Chip Multiprocessors," in *ISCA*, 2007.
- [1225] Paula Petrica, Adam M Izraelevitz, David H Albonesi, and Christine A Shoemaker, "Flicker: A Dynamically Adaptive Architecture for Power Limited Multicore Systems," in *ISCA*, 2013.
- [1226] Changkyu Kim, Simha Sethumadhavan, Madhu S Govindan, Nitya Ranganathan, Divya Gulati, Doug Burger, and Stephen W Keckler, "Composable Lightweight Processors," in *MICRO*, 2007.
- [1227] Andrew Lukefahr, Shruti Padmanabha, Reetuparna Das, Faissal M Sleiman, Ronald Dreslinski, Thomas F Wenisch, and Scott Mahlke, "Composite Cores: Pushing Heterogeneity Into a Core," in *MICRO*, 2012.
- [1228] M Aater Suleman, Onur Mutlu, Moinuddin K Qureshi, and Yale N Patt, "Accelerating Critical Section Execution with Asymmetric Multi-Core Architectures," in *ASPLOS*, 2009.
- [1229] Shailender Chaudhry, Robert Cypher, Magnus Ekman, Martin Karlsson, Anders Landin, Sherman Yip, Håkan Zeffer, and Marc Tremblay, "Simultaneous Speculative Threading: A Novel Pipeline Architecture Implemented in Sun's ROCK Processor," in *ISCA*, 2009.
- [1230] David Tarjan, Michael Boyer, and Kevin Skadron, "Federation: Repurposing Scalar Cores for Out-of-Order Instruction Issue," in *DAC*, 2008.
- [1231] Mehdi Alipour, Stefanos Kaxiras, David Black-Schaffer, and Rakesh Kumar, "Delay and Bypass: Ready and Criticality Aware Instruction Scheduling in Out-of-Order Processors," in *HPCA*, 2020.
- [1232] Rakesh Kumar, Mehdi Alipour, and David Black-Schaffer, "Freeway: Maximizing MLP for Slice-Out-of-Order Execution," in *HPCA*, 2019.
- [1233] Mehdi Alipour, Rakesh Kumar, Stefanos Kaxiras, and David Black-Schaffer, "FIFOOrder MicroArchitecture: Ready-Aware Instruction Scheduling for OoO Processors," in *DATE*, 2019.
- [1234] Rakesh Kumar, Keith I Farkas, Norman P Jouppi, Parthasarathy Ranganathan, and Dean M Tullsen, "Single-ISA Heterogeneous Multi-Core Architectures: The Potential for Processor Power Reduction," in *MICRO*, 2003.
- [1235] Grant Ayers, Heiner Litz, Christos Kozyrakis, and Parthasarathy Ranganathan, "Classifying Memory Access Patterns for Prefetching," in *ASPLOS*, 2020.
- [1236] Angela Pohl, Biagio Cosenza, and Ben Juurlink, "Cost Modelling for Vectorization on ARM," in *CLUSTER*, 2018.
- [1237] Konrad Trifunovic, Dorit Nuzman, Albert Cohen, Ayal Zaks, and Ira Rosen, "Polyhedral-Model Guided Loop-Nest Auto-Vectorization," in *PACT*, 2009.

- [1238] Chris Lattner, “LLVM and Clang: Next Generation Compiler Technology,” in *BSDCan*, 2008.
- [1239] Suyog Sarda and Mayur Pandey, *LLVM Essentials*. Packt Publishing Ltd, 2015.
- [1240] Bruno Cardoso Lopes and Rafael Auler, *Getting Started with LLVM Core Libraries*. Packt Publishing Ltd, 2014.
- [1241] Adrian Sampson, “LLVM for Grad Students,” <https://tinyurl.com/y3tyb7z2>.
- [1242] IITH-Compilers, “LLVM-Loop-Profiler,” <https://github.com/IITH-Compilers/LLVM-Loop-Profiler>.
- [1243] Seunghak Lee, Ki-Dong Kang, Hwanjun Lee, Hyungwon Park, Younghoon Son, Nam Sung Kim, and Daehoon Kim, “GreenDIMM: OS-Assisted DRAM Power Management for DRAM with a Sub-array Granularity Power-Down State,” in *MICRO*, 2021.
- [1244] Michael R Garey, Ronald L Graham, and Jeffrey D Ullman, “Worst-Case Analysis of Memory Allocation Algorithms,” in *STOC*, 1972.
- [1245] LLVM Project, “Auto-Vectorization in LLVM,” <https://llvm.org/docs/Vectorizers.html>.
- [1246] Thomas H Cormen, Charles E Leiserson, Ronald L Rivest, and Clifford Stein, *Introduction to Algorithms*. MIT Press, 2022.
- [1247] Robert Endre Tarjan, “Edge-Disjoint Spanning Trees and Depth-First Search,” *Acta Informatica*, 1976.
- [1248] Leonardo Dagum and Ramesh Menon, “OpenMP: An Industry Standard API for Shared-Memory Programming,” *IEEE CSE*, 1998.
- [1249] Erik Lindholm, John Nickolls, Stuart Oberman, and John Montrym, “NVIDIA Tesla: A Unified Graphics and Computing Architecture,” *IEEE Micro*, 2008.
- [1250] NVIDIA, “NVIDIA’s Next Generation CUDA Compute Architecture: Fermi,” White Paper, 2009.
- [1251] Bruno Lopes, Rafael Auler, Rodolfo Azevedo, and Edson Borin, “ISA Aging: A X86 Case Study,” in *WIVOSCA*, 2013.
- [1252] Bruno Cardoso Lopes, Rafael Auler, Luiz Ramos, Edson Borin, and Rodolfo Azevedo, “SHRINK: Reducing the ISA Complexity via Instruction Recycling,” in *ISCA*, 2015.
- [1253] Max Doblás, Oscar Lostes-Cazorla, Quim Aguado-Puig, Nick Cebry, Pau Fontova-Musté, Christopher Frances Batten, Santiago Marco-Sola, and Miquel Moretó, “GMX: Instruction Set Extensions for Fast, Scalable, and Efficient Genome Sequence Alignment,” in *MICRO*, 2023.
- [1254] Rahul Razdan and Michael D Smith, “A High-Performance Microarchitecture with Hardware-Programmable Functional Units,” in *MICRO*, 1994.
- [1255] Intel Corp., *Intel® 64 and IA-32 Architectures Software Developer’s Manual, Vol. 3*, 2016.

- [1256] ARM Ltd., *Cortex-A8 Technical Reference Manual*, 2010.
- [1257] "The Kernel Development Community", "Linux and the Devicetree — The Linux Kernel Documentation," <https://www.kernel.org/doc/html/latest/devicetree/usage-model.html>.
- [1258] A Giray Yağlıkçı, Haocong Luo, Geraldo F De Oliviera, Ataberk Olgun, Minesh Patel, Jisung Park, Hasan Hassan, Jeremie S Kim, Lois Orosa, and Onur Mutlu, "Understanding RowHammer Under Reduced Wordline Voltage: An Experimental Study Using Real DRAM Devices," in *DSN*, 2022.
- [1259] Kevin Loughlin, Jonah Rosenblum, Stefan Saroiu, Alec Wolman, Dimitrios Skarlatos, and Baris Kasikci, "Siloz: Leveraging DRAM Isolation Domains to Prevent Inter-VM Rowhammer," in *SOSP*, 2023.
- [1260] David S Johnson, "Near-Optimal Bin Packing Algorithms," Ph.D. dissertation, Massachusetts Institute of Technology, 1973.
- [1261] Kenneth C Knowlton, "A Programmer's Description of L6," *CACM*, 1966.
- [1262] Nathan Binkert, Bradford Beckmann, Gabriel Black, Steven K. Reinhardt, Ali Saidi, Arkaprava Basu, Joel Hestness, Derek R. Hower, Tushar Krishna, Somayeh Sardashti, Rathijit Sen, Korey Sewell, Muhammad Shoaib, Nilay Vaish, Mark D. Hill, and David A. Wood, "The gem5 Simulator," *Comput. Archit. News*, 2011.
- [1263] Nadeem Firasta, Mark Buxton, Paula Jinbo, Kaveh Nasri, and Shihjong Kuo, "Intel AVX: New Frontiers in Performance Improvements and Energy Efficiency," Intel Corp., 2008, white paper.
- [1264] Marcus Hähnel, Björn Döbel, Marcus Völz, and Hermann Härtig, "Measuring Energy Consumption for Short Code Paths Using RAPL," *SIGMETRICS*, 2012.
- [1265] NVIDIA Corp., "NVIDIA Management Library (NVML)," <https://developer.nvidia.com/nvidia-management-library-nvml>.
- [1266] Premkishore Shivakumar and Norman P Jouppi, "CACTI 3.0: An Integrated Cache Timing, Power, and Area Model," Compaq Computer Corporation, Tech. Rep. 2001/2, 2001.
- [1267] Standard Performance Evaluation Corp., "SPEC CPU2006 Benchmarks," <http://www.spec.org/cpu2006/>.
- [1268] Louis-Noël Pouchet, "PolyBench: The Polyhedral Benchmark Suite," <https://www.cs.colostate.edu/~pouchet/software/polybench/>.
- [1269] Amir Yazdanbakhsh, Divya Mahajan, Hadi Esmaeilzadeh, and Pejman Lotfi-Kamran, "AxBench: A Multiplatform Benchmark Suite for Approximate Computing," *IEEE Design & Test*, 2016.
- [1270] Nhut-Minh Ho, Elavarasi Manogaran, Weng-Fai Wong, and Asha Anoosheh, "Efficient Floating Point Precision Tuning for Approximate Computing," in *ASP-DAC*, 2017.

- [1271] Allan Snively and Dean M Tullsen, "Symbiotic Jobscheduling for A Simultaneous Multithreaded Processor," in *ASPLOS*, 2000.
- [1272] Stijn Eyerman and Lieven Eeckhout, "System-Level Performance Metrics for Multiprogram Workloads," *IEEE Micro*, 2008.
- [1273] Pierre Michaud, "Demystifying Multicore Throughput Metrics," *CAL*, 2012.
- [1274] Kun Luo, Jayanth Gummaraju, and Manoj Franklin, "Balancing Throughput and Fairness in SMT Processors," in *ISPASS*, 2001.
- [1275] Reetuparna Das, Rachata Ausavarungnirun, Onur Mutlu, Akhilesh Kumar, and Mani Azimi, "Application-to-Core Mapping Policies to Reduce Memory System Interference in Multi-Core Systems," in *HPCA*, 2013.
- [1276] Synopsys, Inc., "Design Compiler." [Online]. Available: <https://www.synopsys.com/implementation-and-signoff/rtl-synthesis-test/design-compiler-graphical.html>
- [1277] Aaron Stillmaker and Bevan Baas, "Scaling Equations for the Accurate Prediction of CMOS Device Performance from 180 Nm to 7 Nm," *Integration*, 2017.
- [1278] Yaqi Zhang, Nathan Zhang, Tian Zhao, Matt Vilim, Muhammad Shahbaz, and Kunle Olukotun, "SARA: Scaling a Reconfigurable Dataflow Accelerator," in *ISCA*, 2021.
- [1279] Guangshan Duan and Shuai Wang, "Exploiting Narrow-Width Values for Improving Non-Volatile Cache Lifetime," in *DATE*, 2014.
- [1280] Carlos Molina, Carles Aliagas, Montse García, Antonio González, and Jordi Tubella, "Non Redundant Data Cache," in *ISLPEL*, 2003.
- [1281] Joonho Kong and Sung Woo Chung, "Exploiting Narrow-Width Values for Process Variation-Tolerant 3-D Microprocessors," in *DAC*, 2012.
- [1282] Gennady Pekhimenko, "Practical Data Compression for Modern Memory Hierarchies," Ph.D. dissertation, Carnegie Mellon University, 2016.
- [1283] Xin Wang and Wei Zhang, "GPU Register Packing: Dynamically Exploiting Narrow-Width Operands to Improve Performance," in *TrustCom*, 2017.
- [1284] Jie Hu, Shuai Wang, and Sotirios G Ziavras, "In-Register Duplication: Exploiting Narrow-Width Value for Improving Register File Reliability," in *DSN*, 2006.
- [1285] Shuai Wang, Jie Hu, Sotirios G Ziavras, and Sung Woo Chung, "Exploiting Narrow-Width Values for Thermal-Aware Register File Designs," in *DATE*, 2009.
- [1286] Meltem Özsoy, Y Onur Koçberber, Mehmet Kayaalp, and Oğuz Ergin, "Dynamic Register File Partitioning in Superscalar Microprocessors for Energy Efficiency," in *ICCD*, 2010.
- [1287] Sparsh Mittal, Haonan Wang, Adwait Jog, and Jeffrey S Vetter, "Design and Analysis of Soft-Error Resilience Mechanisms for GPU Register File," in *VLSID*, 2017.

- [1288] Oğuz Ergin, “Exploiting Narrow Values for Energy Efficiency in the Register Files of Superscalar Microprocessors,” in *PATMOS*, 2006.
- [1289] Michael Canesche, Ricardo Ferreira, José Augusto Nacif, and Fernando Magno Quintao Pereira, “A Polynomial Time Exact Solution to the Bit-Aware Register Binding Problem,” in *CC*, 2022.
- [1290] Andrew Canis, Jongsok Choi, Blair Fort, Ruolong Lian, Qijing Huang, Nazanin Calagar, Marcel Gort, Jia Jun Qin, Mark Aldham, Tomasz Czajkowski *et al.*, “From Software to Accelerators with LegUp High-Level Synthesis,” in *CASES*, 2013.
- [1291] Christian Pilato and Fabrizio Ferrandi, “Bambu: A Modular Framework for the High Level Synthesis of Memory-Intensive Applications,” in *FPL*, 2013.
- [1292] Yusuf Onur Koçberber, Yusuf Osmanlioğlu, and Oğuz Ergin, “Exploiting Narrow Values for Faster Parity Generation,” *Microelectronics International*, 2009.
- [1293] Yusuf Osmanlioglu, Y Onur Koçberber, and Oguz Ergin, “Reducing Parity Generation Latency Through Input Value Aware Circuits,” in *GLSVLSI*, 2009.
- [1294] Myeongjae Jang, Jinkwon Kim, Jesung Kim, and Soontae Kim, “ENCORE Compression: Exploiting Narrow-width Values for Quantized Deep Neural Networks,” in *DATE*, 2022.
- [1295] Jorge Albericio, Alberto Delmás, Patrick Judd, Sayeh Sharify, Gerard O’Leary, Roman Genov, and Andreas Moshovos, “Bit-Pragmatic Deep Neural Network Computing,” in *MICRO*, 2017.
- [1296] I Burak Karsli, Pedro Reviriego, M Fatih Balli, Oguz Ergin, and Juan Antonio Maestro, “Enhanced Duplication: A Technique to Correct Soft Errors in Narrow Values,” *CAL*, 2012.
- [1297] Oguz Ergin, Osman Unsal, Xavier Vera, and Antonio Gonzalez, “Reducing Soft Errors Through Operand Width Aware Policies,” *TDSC*, 2008.
- [1298] Mikko H Lipasti, Brian R Mestan, and Erika Gunadi, “Physical Register Inlining,” in *ISCA*, 2004.
- [1299] Gabriel H Loh, “Exploiting Data-Width Locality to Increase Superscalar Execution Bandwidth,” in *MICRO*, 2002.
- [1300] Mark Stephenson, Jonathan Babb, and Saman Amarasinghe, “Bidwidth Analysis with Application to Silicon Compilation,” in *PLDI*, 2000.
- [1301] Raphael Ernani Rodrigues, Victor Hugo Sperle Campos, and Fernando Magno Quintao Pereira, “A Fast and Low-Overhead Technique to Secure Programs Against Integer Overflows,” in *CGO*, 2013.
- [1302] Victor Hugo Sperle Campos, Raphael Ernani Rodrigues, Igor Rafael de Assis Costa, and Fernando Magno Quintao Pereira, “Speed and Precision in Range Analysis,” in *SBLP*, 2012.

- [1303] Jason Cong, Yiping Fan, Guoling Han, Yizhou Lin, Junjuan Xu, Zhiru Zhang, and Xu Cheng, “Bitwidth-Aware Scheduling and Binding in High-level Synthesis,” in *ASP-DAC*, 2005.
- [1304] DDR4 SDRAM STANDARD, “Jesd79-4,” *Joint Electron Device Engineering Council*, 2012.
- [1305] SAFARI Research Group, “Proteus Simulation Framework,” <https://github.com/CMU-SAFARI/Proteus>.
- [1306] Orest J Bedrij, “Carry-Select Adder,” *IEEE TC*, 1962.
- [1307] Peter M Kogge and Harold S Stone, “A Parallel Algorithm for the Efficient Solution of a General Class of Recurrence Equations,” *IEEE TC*, 1973.
- [1308] Richard E Ladner and Michael J Fischer, “Parallel Prefix Computation,” *JACM*, 1980.
- [1309] Brent and Kung, “A Regular Layout for Parallel Adders,” *IEEE TC*, 1982.
- [1310] Hiroshi Makino, Yasunobu Nakase, Hiroaki Suzuki, Hiroyuki Morinaka, Hirofumi Shinohara, and Koichiro Mashiko, “An 8.8-ns 54/SPL Times/54-bit Multiplier with High Speed Redundant Binary Architecture,” *JSSC*, 1996.
- [1311] Ian Goodfellow, Yoshua Bengio, and Aaron Courville, *Deep Learning*. MIT Press, 2016.
- [1312] Song Han, Xingyu Liu, Huizi Mao, Jing Pu, Ardavan Pedram, Mark A Horowitz, and William J Dally, “EIE: Efficient Inference Engine on Compressed Deep Neural Network,” in *ISCA*, 2016.
- [1313] JEDEC, “DDR3 SDRAM Standard,” *JEDEC Standard*, no. 79-3F, 2012.
- [1314] JEDEC, “JEDEC Standard: DDR4 SDRAM,” *JESD79-4*, Sep, 2012.
- [1315] Micron, “Micron Collaborates with Broadcom to Solve DRAM Timing Challenge, Delivering Improved Performance for Networking Customers,” <https://bit.ly/3RmxI0L>, 2013.
- [1316] SAFARI Research Group, “MIMDRAM Simulation Framework,” <https://github.com/CMU-SAFARI/MIMDRAM>.
- [1317] Intel Corp., “10th Generation Intel Core Processor Family Datasheet,” <https://tinyurl.com/4fh5ze38>.
- [1318] Ranyang Zhou, Sepehr Tabrizchi, Mehrdad Morsali, Arman Roohi, and Shaahin Angizi, “P-PIM: A Parallel Processing-in-DRAM Framework Enabling Row Hammer Protection,” in *DATE*, 2023.
- [1319] NVIDIA Corp., “NVIDIA/cutlass: CUDA Templates for Linear Algebra Subroutines,” <https://github.com/NVIDIA/cutlass>.
- [1320] UPMEM, “UPMEM User Manual. Version 2021.1.0,” 2021.
- [1321] Michael McCool, James Reinders, and Arch Robison, *Structured Parallel Programming: Patterns for Efficient Computation*. Elsevier, 2012.

- [1322] Michael D McCool, “Structured Parallel Programming with Deterministic Patterns,” in *HotPar*, 2010.
- [1323] T Rauber and G Rünger, *Parallel Programming: For Multicore and Cluster Systems*. Springer, 2013.
- [1324] Georg Hager and Gerhard Wellein, *Introduction to High Performance Computing for Scientists and Engineers*. CRC Press, 2010.
- [1325] Steffen Ernsting and Herbert Kuchen, “Data Parallel Algorithmic Skeletons with Accelerator Support,” *IJPP*, 2017.
- [1326] Steffen Ernsting and Herbert Kuchen, “Algorithmic Skeletons for Multi-Core, Multi-GPU Systems and Clusters,” *IJHPCN*, 2012.
- [1327] Marco Aldinucci, Marco Danelutto, Peter Kilpatrick, and Massimo Torquati, “Fastflow: High-Level and Efficient Streaming on Multicore,” *Programming Multi-Core and Many-Core Computing Systems*, 2017.
- [1328] Johan Enmyren and Christoph W Kessler, “SkePU: A Multi-Backend Skeleton Programming Library for Multi-GPU Systems,” in *HLPP*, 2010.
- [1329] Mehrzad Samadi, Davoud Anoushe Jamshidi, Janghaeng Lee, and Scott Mahlke, “Paraprox: Pattern-Based Approximation for Data Parallel Applications,” in *ASPLOS*, 2014.
- [1330] Marco Aldinucci, Sonia Campa, Marco Danelutto, Peter Kilpatrick, and Massimo Torquati, “Targeting Distributed Systems in FastFlow,” in *Euro-Par*, 2013.
- [1331] Mario Leyton and José M Piquer, “Skandium: Multi-Core Programming with Algorithmic Skeletons,” in *PDP*, 2010.
- [1332] Philipp Ciechanowicz, Michael Poldner, and Herbert Kuchen, “The Münster Skeleton Library Muesli: A Comprehensive Overview,” *ERCIS Working Paper*, 2009.
- [1333] Aaftab Munshi, “The OpenCL Specification,” in *HCS*, 2009.
- [1334] Chuck Pheatt, “Intel® Threading Building Blocks,” *J. Comput. Sci. Coll.*, 2008.
- [1335] Matei Zaharia, Mosharaf Chowdhury, Michael J Franklin, Scott Shenker, and Ion Stoica, “Spark: Cluster Computing with Working Sets,” in *HotCloud*, 2010.
- [1336] Matei Zaharia, Reynold S Xin, Patrick Wendell, Tathagata Das, Michael Armbrust, Ankur Dave, Xiangrui Meng, Josh Rosen, Shivaram Venkataraman, Michael J Franklin *et al.*, “Apache Spark: A Unified Engine for Big Data Processing,” *CACM*, 2016.
- [1337] pantor, “GitHub - pantor/inja: A Template Engine for Modern C++.” [Online]. Available: <https://github.com/pantor/inja>
- [1338] Barry W Boehm, “Software Engineering Economics,” *TSE*, 1984.
- [1339] Capers Jones, *Programming Productivity*. McGraw-Hill, Inc., 1985.

- [1340] Tom DeMarco, *Controlling Software Projects: Management, Measurement, and Estimates*. Prentice Hall PTR, 1986.
- [1341] David del Rio Astorga, Manuel F Dolz, Luis Miguel Sánchez, J Daniel García, Marco Danelutto, and Massimo Torquati, “Finding Parallel Patterns Through Static Analysis in C++ Applications,” *Int. J. High Perform. Comput. Appl.*, 2018.
- [1342] Sean Rul, Hans Vandierendonck, and Koen De Bosschere, “A Profile-Based Tool for Finding Pipeline Parallelism in Sequential Programs,” *Parallel Computing*, 2010.
- [1343] Korbinian Molitorisz, Tobias Müller, and Walter F Tichy, “Patty: A Pattern-Based Parallelization Tool for the Multicore Age,” in *PMAM*, 2015.
- [1344] Georgios Tournavitis and Björn Franke, “Semi-Automatic Extraction and Exploitation of Hierarchical Pipeline Parallelism using Profiling Information,” in *PACT*, 2010.
- [1345] Geraldo F Oliveira, Saugata Ghose, Juan Gómez-Luna, Amirali Boroumand, Alexis Savery, Sonny Rao, Salman Qazi, Gwendal Grignou, Rahul Thakur, Eric Shiu *et al.*, “Extending Memory Capacity in Modern Consumer Systems With Emerging Non-Volatile Memory: Experimental Analysis and Characterization Using the Intel Optane SSD,” *IEEE Access*, 2023.
- [1346] Google LLC, “Chromebook,” <https://www.google.com/chromebook/>.
- [1347] Intel Corp., “Intel® Optane™ Memory H10 with Solid State Storage,” <https://rb.gy/f682j>.
- [1348] Chromium Project, “MemoryPressure Tast Test,” <https://rb.gy/j1ft7>.
- [1349] Bartłomiej Zolnierkiewicz, “Efficient Memory Management on Mobile Devices,” *LinuxCon*, 2013.
- [1350] Daniel P Bovet and Marco Cesati, *Understanding the Linux Kernel: From I/O Ports to Process Management*, 3rd ed. O’Reilly Media, Inc., 2005.
- [1351] Jie Chen, Ron C Chiang, H Howie Huang, and Guru Venkataramani, “Energy-Aware Writes to Non-Volatile Main Memory,” *OSR*, 2012.
- [1352] Matias Bjørling, Jens Axboe, David Nellans, and Philippe Bonnet, “Linux Block IO: Introducing Multi-Queue SSD Access on Multi-Core Systems,” in *SYSTOR*, 2013.
- [1353] Omar Sandoval, “Kyber MQ I/O Scheduler,” <https://rb.gy/6azue>, 2017.
- [1354] Nastaran Hajinazar, Pratyush Patel, Minesh Patel, Konstantinos Kanellopoulos, Saugata Ghose, Rachata Ausavarungnirun, Geraldo Francisco de Oliveira Jr, Jonathan Appavoo, Vivek Seshadri, and Onur Mutlu, “The Virtual Block Interface: A Flexible Alternative to the Conventional Virtual Memory Framework,” in *ISCA*, 2020.
- [1355] Heng Li and Richard Durbin, “Fast and Accurate Short Read Alignment with Burrows–Wheeler Transform,” *Bioinformatics*, 2009.
- [1356] Jakub Beranek, “Hardware Effects,” <https://github.com/Kobzol/hardware-effects>.

- [1357] Min Chen, Shiwen Mao, and Yunhao Liu, “Big Data: A Survey,” *Mobile Networks and Applications*, 2014.
- [1358] Huangrui Mo, “Mesoscale Modeling and Direct Simulation of Explosively Dispersed Granular Materials,” Ph.D. dissertation, University of Waterloo, 2019.
- [1359] Shelby Thomas, Chetan Gohkale, Enrico Tanuwidjaja, Tony Chong, David Lau, Saturnino Garcia, and Michael Bedford Taylor, “CortexSuite: A Synthetic Brain Benchmark Suite,” in *IISWC*, 2014.
- [1360] Mark J Chaisson and Glenn Tesler, “Mapping Single Molecule Sequencing Reads Using Basic Local Alignment with Successive Refinement (BLASR): Application and Theory,” *Bioinformatics*, 2012.
- [1361] Heng Li, “Aligning Sequence Reads, Clone Sequences and Assembly Contigs with BWA-MEM,” arXiv:1303.3997 [q-bio.GN], 2013.
- [1362] WebM, “VP8/VP9 Codec SDK,” <https://github.com/ittiamvpx/libvpx>.
- [1363] Cagri Balkesen, Gustavo Alonso, Jens Teubner, and M Tamer Özsu, “Multi-Core, Main-Memory Joins: Sort vs. Hash Revisited,” *VLDB*, 2013.
- [1364] Shalini Ghosh, Oriol Vinyals, Brian Strope, Scott Roy, Tom Dean, and Larry Heck, “Contextual LSTM (CLSTM) Models for Large Scale NLP Tasks,” arXiv:1602.06291 [cs.CL], 2016.
- [1365] Aydın Buluç and John R Gilbert, “The Combinatorial BLAS: Design, Implementation, and Applications,” *IJHPCA*, 2011.
- [1366] Mikhail Karasikov, Harun Mustafa, Daniel Danciu, Marc Zimmermann, Christopher Barber, Gunnar Ratsch, and André Kahles, “Metagraph: Indexing and Analysing Nucleotide Archives at Petabase-Scale,” bioRxiv 2020.10.01.322164, 2020.
- [1367] Intel Corp., “Accelerate Fast Math with Intel oneAPI Math Kernel Library,” <https://software.intel.com/content/www/us/en/develop/tools/oneapi/components/onemkl.html>.
- [1368] Rilson O Nascimento and Paulo RM Maciel, “DBT-5: An Open-Source TPC-E Implementation for Global Performance Measurement of Computer Systems,” *Computing and Informatics*, 2010.
- [1369] Xiangyao Yu, George Bezerra, Andrew Pavlo, Srinivas Devadas, and Michael Stonebraker, “Staring Into the Abyss: An Evaluation of Concurrency Control with One Thousand Cores,” *VLDB*, 2014.
- [1370] Rafael Palomar, Juan Gómez-Luna, Faouzi A Cheikh, Joaquín Olivares-Bueno, and Ole J Elle, “High-Performance Computation of Bézier Surfaces on Parallel and Heterogeneous Platforms,” *IJPP*, 2018.
- [1371] Harshad Kasture and Daniel Sanchez, “Tailbench: A Benchmark Suite and Evaluation Methodology for Latency-Critical Applications,” in *IISWC*, 2016.

- [1372] Sanketh Nalli, Swapnil Haria, Mark D Hill, Michael M Swift, Haris Volos, and Kimberly Keeton, “An Analysis of Persistent Memory Use with WHISPER,” in *ASPLOS*, 2017.
- [1373] Kaan Kara, Dan Alistarh, Gustavo Alonso, Onur Mutlu, and Ce Zhang, “FPGA-Accelerated Dense Linear Machine Learning: A Precision-Convergence Trade-Off,” in *FCCM*, 2017.